



Conception de vecteurs polymères pour l'imagerie moléculaire et le traitement ciblé de la thrombose

Maya Juenet

► To cite this version:

Maya Juenet. Conception de vecteurs polymères pour l'imagerie moléculaire et le traitement ciblé de la thrombose. Biologie moléculaire. Université Sorbonne Paris Cité, 2017. Français. NNT : 2017USPCD036 . tel-01912771

HAL Id: tel-01912771

<https://theses.hal.science/tel-01912771>

Submitted on 5 Nov 2018

HAL is a multi-disciplinary open access archive for the deposit and dissemination of scientific research documents, whether they are published or not. The documents may come from teaching and research institutions in France or abroad, or from public or private research centers.

L'archive ouverte pluridisciplinaire **HAL**, est destinée au dépôt et à la diffusion de documents scientifiques de niveau recherche, publiés ou non, émanant des établissements d'enseignement et de recherche français ou étrangers, des laboratoires publics ou privés.

UNIVERSITÉ SORBONNE PARIS CITÉ – UNIVERSITÉ PARIS 13
ÉCOLE DOCTORALE MTCI 563

DOCTORAT

Discipline : Sciences pour l'Ingénieur

Mention : Génie Biologique et Médical

Maya JUENET

Conception de vecteurs polymères pour l'imagerie moléculaire
et le traitement ciblé de la thrombose

Thèse dirigée par le Docteur Cédric CHAUVIERRE

Soutenue publiquement le 2 juin 2017

Devant le jury composé de

Docteur Ruxandra GREF
Professeur Denis VIVIEN
Professeur Laurence MOTTE
Monsieur Bertrand LOUBATON
Docteur Cédric CHAUVIERRE

Rapporteur
Rapporteur
Examinateur
Examinateur
Directeur de thèse

Laboratory for Vascular Translational Science (LVTS) – INSERM U1148
Hôpital Bichat – Claude Bernard, Paris, France

Remerciements

Je tiens tout d'abord à remercier Ruxandra Gref et Denis Vivien pour avoir accepté de revoir mon mémoire de thèse, ainsi que Laurence Motte et Bertrand Loubaton pour avoir accepté de juger mon travail.

Je remercie très chaleureusement Cédric Chauvierre, mon directeur de thèse, pour sa disponibilité et ses conseils toujours bienveillants, ainsi que pour la confiance qu'il m'a témoignée tout au long de ce projet. Je souhaite exprimer ma profonde gratitude à Didier Letourneur pour m'avoir engagée au sein de son laboratoire et de son équipe et pour m'avoir entraînée dans l'aventure *NanoAthero*. Merci à tous les deux d'avoir toujours pris le temps de partager leur expertise et de m'avoir permis de progresser.

J'adresse mes plus vifs remerciements à l'INSERM et à la commission européenne qui ont financé ce travail par le programme FP7 *NanoAthero*. Je remercie les membres du consortium *NanoAthero* auprès desquels j'ai eu la chance d'apprendre beaucoup sur le monde de la nanomédecine.

Je souhaite remercier l'ensemble des membres du *LVTS* pour leur accueil. En particulier, je remercie vivement Véronique Ollivier pour sa rigueur et son écoute. J'ai pris beaucoup de plaisir à apprendre à ses côtés. Merci également à Frédéric Chaubet, Martine Jandrot-Perrus, Benoît Ho-Tin-Noé, Stéphane Loyau, Liliane Louedec, Murielle Maire, Anne Pellé et Graciela Pavon-Djavid pour leurs conseils scientifiques et pratiques. Merci également à Corinne Legrand et à Asma Tighouart pour leur aide et leur patience.

Je tiens à adresser mes plus sincères remerciements aux membres de l'équipe 3, et tout particulièrement aux membres de "l'étage", pour leur soutien technique et amical et pour leurs mots d'encouragement. Je remercie chaleureusement Rachida et Bo avec qui j'ai eu la chance de travailler au quotidien. Merci pour nos discussions scientifiques et moins scientifiques et pour leur présence. Je remercie également Mariana et Joana pour leur aide au cours de ce projet. Un grand merci aussi à Pierre et à Jessica pour m'avoir fait partager leur expérience de thésard, et à Marisol pour ces années de thèses partagées. Je remercie très sincèrement les autres doctorants et post-doctorants de l'équipe, qui ont su rendre le travail agréable quel que soit le résultat, notamment : Thomas, Cécilia, Louis, Fred, Sophie, Nicolas, Lucas, Teresa, Soraya et Marie-Noëlle. Je remercie aussi les étudiants avec lesquels j'ai eu la chance de travailler et qui m'ont beaucoup appris : Alice, Pierre, Antoine, Nina et Clara.

Je remercie mes amis, qui m'ont motivée. En particulier, merci à Claire, Marine, Pauline et Perrine de m'entourer et de me comprendre. Merci aussi aux autres PCéens pour leur soutien : notamment à François, Celia et Victor. Je tiens également à remercier Claire et Gwennaël pour leur amitié de longue date et leur écoute.

Je remercie chaleureusement mes frères, Tom et Jacques, ainsi que Maud et Constance, de m'avoir constamment encouragée. Merci Constance et Jacques de m'avoir hébergée et d'avoir pris soin de moi pendant les dernières semaines de rédaction. Je remercie affectueusement mes parents. Grâce à eux, j'ai pu étudier et m'épanouir dans les meilleures conditions. Je les remercie pour leur soutien indéfectible et pour leur aide précieuse, surtout en fin de thèse. Un merci particulier à ma mère pour s'être si bien occupée de moi pendant la période d'écriture. Enfin, je souhaite remercier Hugo de m'avoir écoutée, guidée et motivée avec patience jour après jour pendant ces quelques années.

Pour finir, je tiens à remercier les personnes qui m'ont aidée à relire ce manuscrit : Pauline, Hugo, Marie-Noëlle et Joana.

Table des matières

Introduction générale	7
CONTEXTE ET OBJECTIFS	7
PLAN DU MANUSCRIT	11
État de l'art	13
1. LA THROMBOSE ARTÉRIELLE	14
1.1. Physiologie de l'artère	14
1.2. Causes de la thrombose	15
1.2.1. L'athérosclérose	15
1.2.2. L'anévrisme	19
1.3. Mécanismes de la thrombose	20
1.3.1. Rôle de l'endothélium activé	20
1.3.2. Exposition des éléments sous-endothéliaux	21
1.4. Diagnostic	23
1.4.1. Diagnostic anatomique	23
1.4.2. Vers un diagnostic moléculaire.....	28
1.5. Traitement	31
1.5.1. Les agents thrombolytiques	32
1.5.2. Utilisation dans le cadre de l'AVC ischémique.....	34
1.5.3. Vers un traitement plus sûr et plus efficace.....	37
2. NANOMÉDECINE ET VECTORISATION	41
2.1. Principe	41
2.2. Matériaux	42
2.2.1. Lipidiques	43
2.2.2. Inorganiques.....	43
2.2.3. Polymères	44
2.2.4. Microbulles	45
2.3. Biomarqueurs et ligands	46
2.3.1. Les plaquettes activées	46
2.3.2. La fibrine	50
3. VECTEURS TESTÉS EN PRÉCLINIQUE	51
3.1. Vecteurs pour l'imagerie moléculaire de la thrombose.....	52
3.2. Vecteurs pour la thrombolyse	55
3.2.1. Sans ciblage	56

3.2.2. Ciblage physique	58
3.2.3. Ciblage moléculaire.....	59
3.2.4. Association à des ultrasons	60
3.3. Vecteurs théranostiques	60
4. STRATÉGIE DU PROJET	61
4.1. Biomarqueur	62
4.2. Ligand	62
4.3. Vecteurs	63
4.3.1. Polymérisation radicalaire en milieu oxydo-réducteur	64
4.3.2. Réticulation chimique.....	66
Résultats expérimentaux	69
1. MICROCAPSULES POLYMÈRES POUR CIBLER LA P-SÉLECTINE	71
2. NANOParticules COPOLYMÈRES POUR LA THROMBOLYSE CIBLÉE	105
3. FORMULATION DE NANOGELS POLYSACCHARIDES.....	137
Discussion et perspectives	159
Conclusion générale	173
Bibliographie	175
Annexe A - Chapitre de livre et revues	187
A.1. NANOTHERANOSTICS IN CARDIOVASCULAR DISEASES	187
A.2. NANOMEDICINE FOR THE MOLECULAR DIAGNOSIS OF CARDIOVASCULAR PATHOLOGIES ...	187
A.3. NANOMEDICINE AS A STRATEGY TO FIGHT THROMBOTIC DISEASES	187
A.4. POLYSACCHARIDE-BASED STRATEGIES FOR HEART TISSUE ENGINEERING	187
Publication dans le cadre du consortium NanoAthero	243
NANOPARTICLES FOR INTRAVASCULAR APPLICATIONS: PHYSICOCHEMICAL CHARACTERIZATION AND CYTOTOXICITY TESTING	243

Liste des abréviations

SCA	Syndrome Coronarien Aigu
IM	Infarctus du Myocarde
AVC	Accident Vasculaire Cérébral
CE	Cellule Endothéliale
CML	Cellule Musculaire Lisse
LDL	Lipoprotéine de basse densité
ox-LDL	Lipoprotéine de basse densité oxydée
MMP	Métalloprotéase matricielle
PSGL-1	P-sélectine glycoprotéine ligand-1
AAA	Anévrisme de l'Aorte Abdominale
IRM	Imagerie par Résonance Magnétique
CT	Tomodensitométrie
TEMP	Tomographie à Emission Monophotonique
TEP	Tomographie à Emission de Positons
IV	Intraveineux
FDA	Food & Drug Administration
EMA	European Medicines Agency
tPA	Activateur tissulaire du plasminogène
rt-PA	Forme recombinante de l'activateur tissulaire du plasminogène
UK	Urokinase
SK	Streptokinase
Rpa	Reteplase
TNKase	Tenecteplase
PEG	Polyéthylène glycol
PLGA	Poly(acide lactique-co-glycolique)
PVA	Alcool polyvinyle
RGD	Séquence L-Arginine/Glycine/Acid L-aspartique
PACA	Poly(cyanoacrylate d'alkyle)
IBCA	Cyanoacrylate d'isobutyle
PIBCA	Poly(cyanoacrylate d'isobutyle)
RREP	Réaction d'émulsion polymérisation en milieu redox
STMP	Trimétaphosphate de sodium

Liste des figures

Figure 1. Structure schématique d'une artère	14
Figure 2. Représentation schématique du développement d'une plaque d'athérosclérose.	18
Figure 3. Schéma simplifié du recrutement plaquettaire A) par les cellules endothéliales activées et B) à la suite d'une exposition du sous-endothélium.	21
Figure 4. Schéma simplifié de la cascade de coagulation menant à la formation d'un réseau de fibrine.....	22
Figure 5. Exemples d'images standards d'occlusion carotidienne ou cérébrale.....	25
Figure 6. Exemples illustrant l'optimisation des séquences d'IRM pour la visualisation directe du thrombus et de la plaque vulnérable.	28
Figure 7. Exemples de systèmes en imagerie moléculaire préclinique ou clinique de la thrombose.	30
Figure 8. Approches thérapeutiques médicamenteuses des thromboses artérielles.	31
Figure 9. Schéma de la fibrinolyse par les activateurs du plasminogène.	33
Figure 10. Action de l'activateur tissulaire du plasminogène sur un réseau de fibrine et effets délétères....	36
Figure 11. Structure et fonctions du rt-PA.....	38
Figure 12. Principe de la vectorisation pour le diagnostic et le traitement de la thrombose.	41
Figure 13. Principaux types de nanovecteurs mis au point pour la thrombolyse.	42
Figure 14. Structures du pullulane et du dextrane.....	45
Figure 15. Spécificité des ligands des différentes sélectines.	47
Figure 16. Structure simplifiée du fucoidane.	50
Figure 17. Formulations utilisant du fucoidane testées dans des modèles précliniques d'anévrisme de l'aorte abdominale pour l'imagerie moléculaire.....	63
Figure 18. Réaction de polymérisation radicalaire en milieu redox et structure associée.....	65
Figure 19. Réticulation chimique des polysaccharides par le STMP.....	66
Figure 20. Schéma du dispositif d'interaction en flux.	74
Figure 21. Protocoles pour tester l'interaction des microcapsules avec les sélectines et avec les agrégats plaquettaires activés.	75
Figure 22. Modèle préclinique pour l'évaluation des nanoparticules copolymères.....	108

Liste des tableaux

Tableau 1. Agents thrombolytiques autorisés par la FDA et l'EMA pour les pathologies artérielles.	32
Tableau 2. Ligands potentiels de la P-sélectine.	49
Tableau 3. Exemples de vecteurs testés dans des modèles précliniques pour l'imagerie de la thrombose et classés selon leur cible moléculaire.	54
Tableau 4. Exemples de vecteurs testés dans des modèles précliniques pour la thrombolyse et classés selon les stratégies de ciblage.	57
Tableau 5. Exemples de vecteurs testés dans des modèles précliniques pour la thrombolyse ciblé et l'imagerie moléculaire de la thrombose.	61
Tableau 6. Rétention de l'activité amidolytique du rt-PA au contact de différentes compositions de nanoparticules copolymères.....	165

Introduction générale

Contexte et objectifs

Les pathologies de la paroi artérielle, et notamment l'athérosclérose, sont responsables de plus de 25% des décès dans le monde. L'athérosclérose désigne la formation de plaques riches en lipides dans les artères de gros et de moyen calibres. C'est un processus physiopathologique qui est initié dès l'enfance et évolue en fonction de facteurs génétiques et environnementaux. Le risque majeur est une rupture ou une érosion de la plaque, qui expose son contenu à la circulation. Les plaques à risque de rupture sont dites vulnérables. En réponse à l'exposition des éléments de la plaque, il y a formation locale d'un thrombus, plus communément appelé caillot, composé majoritairement d'un agrégat de plaquettes activées consolidé par un réseau de longues chaînes de fibrine. Le processus de formation du thrombus est appelé thrombose. Un thrombus peut évoluer de différentes manières ; i) se résorber naturellement par dégradation du réseau de fibrine, appelée fibrinolyse, ii) s'incruster dans la paroi artérielle où il subira des transformations et participera à la formation d'une lésion vulnérable, iii) provoquer une occlusion de la lumière vasculaire. Cette occlusion peut être locale ou survenir à un autre endroit de l'arbre vasculaire suite à la fragmentation du thrombus et à sa migration dans d'autres artères. Il en résulte un défaut d'irrigation des tissus en aval ; c'est l'ischémie. Sans recanalisation, une ischémie conduit rapidement et de façon irréversible à une nécrose des tissus.

Selon l'endroit du corps où le thrombus se forme et selon qu'il occlut partiellement ou totalement la lumière vasculaire, il engendre différentes pathologies. Par exemple, un syndrome coronarien aigu (SCA) se produit lorsqu'une artère coronaire est affectée. En particulier, l'infarctus du myocarde (IM) correspond à une occlusion totale d'une artère coronaire suivie d'une nécrose d'une partie du cœur. Les SCA sont à l'origine de plus de 7 millions de morts par an. Lorsque l'occlusion se produit dans une carotide ou une artère cérébrale, il s'agit d'un Accident Vasculaire Cérébral (AVC) ischémique. Parmi les formes d'AVC, plus de 80% sont d'origine ischémique. Ils causent plus de 6 millions de morts par an et représentent la cause majeure de handicap soudainement acquis chez l'adulte. La thrombose est ainsi la première forme de mortalité mondiale.

L'évaluation des facteurs de risque, les campagnes de prévention associées et une médication préventive des personnes vulnérables à l'aide de traitements anticoagulants et antiagrégants plaquettaires ont permis de réduire le nombre d'évènements thrombotiques aigus dans les pays développés. De nombreuses pistes sont également explorées afin de mieux évaluer l'état des plaques d'athérosclérose et de les traiter de façon à éviter la rupture. Néanmoins, la majorité des patients à risque ne sont identifiés qu'à la suite d'un premier accident ischémique et la prise en charge de ces évènements cliniques aigus reste un problème majeur, comme l'indiquent les forts taux de mortalité et de morbidité associés.

Lorsqu'un accident ischémique survient, la priorité est de rétablir la circulation sanguine. Il existe cependant très peu de méthodes non invasives pour y parvenir. Dans le cas particulier des AVC ischémiques, l'injection intraveineuse (IV) d'une forme recombinante de l'activateur tissulaire du plasminogène est l'unique traitement approuvé pour provoquer la dégradation du thrombus. Il demeure l'approche thérapeutique recommandée depuis les années 1990. Pourtant, cet actif présente une efficacité modérée avec un taux de recanalisation inférieur à 50%. De plus, son utilisation est très restreinte car elle est associée à des risques hémorragiques sévères.

L'évaluation du ratio bénéfice/risque pour choisir d'injecter ou non ce traitement repose en partie sur l'imagerie de la zone ischémique. Les techniques d'imagerie

standards, comme la tomodensitométrie ou l'imagerie par résonance magnétique, permettent de visualiser rapidement et avec précision la perfusion des tissus. Toutefois, il n'existe actuellement pas d'imagerie directe du thrombus qui pourrait renseigner les cliniciens sur la composition de ce dernier. Pourtant, avoir des informations sur les éléments du thrombus pourrait guider le dosage de l'actif. Ainsi, l'activateur tissulaire du plasminogène agit sur le réseau de fibrine et son efficacité dépend donc entre autres de la densité de fibrine du thrombus.

La compréhension des mécanismes cellulaires et moléculaires menant à la thrombose permet d'envisager la mise en œuvre d'une médecine moléculaire et personnalisée. Un biomarqueur désigne une molécule exprimée spécifiquement dans une pathologie donnée. Des ligands de certains biomarqueurs ont été identifiés. L'imagerie moléculaire consiste à associer ces ligands à des agents de contraste pour visualiser non plus l'anatomie des vaisseaux mais les processus biologiques les affectant. Un couplage entre ces ligands et un actif thérapeutique favoriserait aussi l'accumulation de l'actif dans la zone souhaitée pour augmenter son efficacité locale et diminuer ses effets secondaires. La mise en place d'une imagerie moléculaire et d'un traitement ciblé semble donc prometteuse, à condition de créer des outils capables d'associer les actifs aux ligands.

La nanomedecine s'est développée dans le but de répondre à cette problématique. Elle a pour objectif, par l'utilisation de "nanovecteurs", d'offrir un nouveau mode de transport des actifs thérapeutiques et des agents de contraste et ainsi de modifier leurs propriétés physico-chimiques et biologiques. Le terme "vecteur" désigne dans ce manuscrit un objet complexe développé dans l'intention de charger et de véhiculer un ou plusieurs agents. Le qualificatif de "nano" et le terme de "nanoparticule" qualifient ici des structures qui ont une taille inférieure d'au moins un ordre de grandeur à l'échelle cellulaire, soit globalement $< 1 \mu\text{m}$. La nanomedecine a connu un véritable essor ces deux dernières décennies, d'abord en oncologie puis dans le domaine cardiovasculaire, et des nanoparticules très diverses ont été synthétisées. Les nanoparticules ont deux rôles principaux. Premièrement, elles servent de plateformes pour le transport des actifs afin de les charger en masse et d'optimiser des propriétés, telles que leur temps de circulation et leur pénétration dans les cellules. En particulier, un système contenant à la fois un agent

de contraste et un principe actif est qualifié de “théranostique”. Deuxièmement, des ligands peuvent être greffés à leur surface pour favoriser leur interaction spécifique avec le biomarqueur ciblé. Les nanoparticules assurent ainsi la vectorisation des actifs au thrombus. Du fait de leur taille, elles ont l'avantage de présenter une très grande surface spécifique d'interaction.

Ce travail de thèse s'inscrit dans un projet visant à développer un traitement de la thrombose plus efficace à base de nanoparticules polymères. En parallèle de ce thème de recherche principal, deux autres types de particules sont étudiés comme outils potentiels pour l'imagerie moléculaire des pathologies thrombotiques. Pour les trois plateformes décrites, la stratégie de ciblage moléculaire reste la même et consiste à cibler la P-sélectine par le fucoïdane. Lors de la formation d'un thrombus, un large panel de récepteurs entre en jeu engendrant l'adhésion, l'activation et l'agrégation des plaquettes ainsi que la génération d'un réseau de fibrine subséquent. Les plaquettes activées et la fibrine sont donc les cibles d'intérêts pour développer des stratégies moléculaires. Parmi les biomarqueurs potentiels, la P-sélectine est une glycoprotéine exprimée par les cellules de la paroi artérielle en souffrance et par les plaquettes activées. Le fucoïdane, un polysaccharide extrait d'algues brunes, montre une forte affinité pour la P-sélectine. Charger en fucoïdane des nanoparticules associées à des actifs ou à des agents de contraste favoriserait leur accumulation spécifique au thrombus et améliorerait ainsi le traitement local et la détection de la thrombose.

Cette thèse, réalisée dans l'équipe de *Bio-ingénierie Cardiovasculaire* du *Laboratoire de Science Vasculaire Translationnelle*, a été menée dans le cadre du projet européen FP7 *NanoAthero*. Ce consortium a pour objectif de développer des méthodes de thérapie et de diagnostic innovantes de l'athérosclérose et de la thrombose à partir de nanovecteurs. Il regroupe 16 partenaires privés ou publics qui travaillent vers un but commun pendant 5 ans (2013-2018) en étudiant plusieurs formulations de nanoparticules, plusieurs couples ligand-biomarqueur et plusieurs actifs thérapeutiques et diagnostiques. Entre autres, un essai clinique pour le traitement de la plaque a été mené aux Pays-Bas et un autre pour l'imagerie du thrombus va être mis en place à l'hôpital Bichat dans le cadre de ce consortium.

Plan du manuscrit

Ce manuscrit débute par un état de l'art sur l'utilisation de la nanomédecine pour le traitement et le diagnostic de la thrombose artérielle. Après une description des mécanismes impliqués dans la thrombose, les outils diagnostiques et thérapeutiques disponibles en clinique sont décrits. Enfin, les vecteurs mis au point pour les pathologies thrombotiques sont passés en revue. Les travaux de thèse se divisent ensuite en trois parties présentées sous forme d'article. Chaque article est précédé d'une introduction, qui situe la stratégie développée dans le contexte de l'état de l'art, et d'un résumé.

Dans la première partie, un test *in vitro* d'adhésion en conditions de flux est développé pour étudier l'interaction de microcapsules polymères présentant du fucoïdane en surface avec la P-sélectine et les plaquettes activées. Ces expériences valident l'affinité et la spécificité des microcapsules-fucoïdane pour leur cible moléculaire et cellulaire. Ces résultats sont intégrés à la présentation d'un nouveau mode de synthèse de microcapsules polymères développé par un autre doctorant. Ces données ont fait l'objet d'une publication et d'une couverture dans le journal *Advanced Healthcare Materials*.

La deuxième partie détaille la synthèse et la caractérisation de nanoparticules copolymères fonctionnalisées avec du fucoïdane et chargées avec l'actif fibrinolytique de référence. L'affinité des nanoparticules-fucoïdane pour la P-sélectine et les agrégats plaquettaires activés est d'abord validée sous flux avec le modèle d'adhésion décrit dans la première partie. Le potentiel des nanoparticules-fucoïdane chargées avec l'actif pour augmenter l'efficacité de la thrombolyse est démontré dans un modèle murin de thrombose. Ces résultats ont été soumis dans le journal *Theranostics* et sont en révisions à la date d'envoi du manuscrit.

Enfin, la dernière partie décrit la mise au point de nanoparticules composées exclusivement de polysaccharides pour une biocompatibilité améliorée. Un nouveau mode de synthèse par précipitation suivie d'une réticulation est détaillé. Des tests sur leur potentielle utilisation pour l'imagerie de la thrombose sont exposés.

Chaque article est suivi d'une courte conclusion. Une discussion développant les perspectives envisagées sur la base de ces résultats clôt la présentation de ces travaux.

État de l'art

Les pathologies de la paroi artérielle, et notamment l'athérosclérose, sont responsables de plus de 25% des décès dans le monde selon l'Organisation Mondiale de la Santé [1]. Ces pathologies sont à l'origine d'évènements cliniques aigus caractérisés par l'occlusion d'une artère par un thrombus. La première partie de ce chapitre détaille les causes et les mécanismes de la thrombose. Les outils de diagnostic et de traitement utilisés en clinique ainsi que leurs limitations sont ensuite décrits.

1. La thrombose artérielle

La thrombose artérielle fait principalement référence à trois types de pathologies selon l'endroit du corps où le thrombus se forme : les syndromes coronariens aigus (SCA) dont l'infarctus du myocarde (IM), l'AVC ischémique et les maladies artérielles des membres, ou périphériques. Elle provoque une ischémie des tissus, qui conduit à leur nécrose. Cette section débute par un court rappel de la structure d'une artère, essentiel pour comprendre les phénomènes cellulaires associés à ces pathologies.

1.1. Physiologie de l'artère

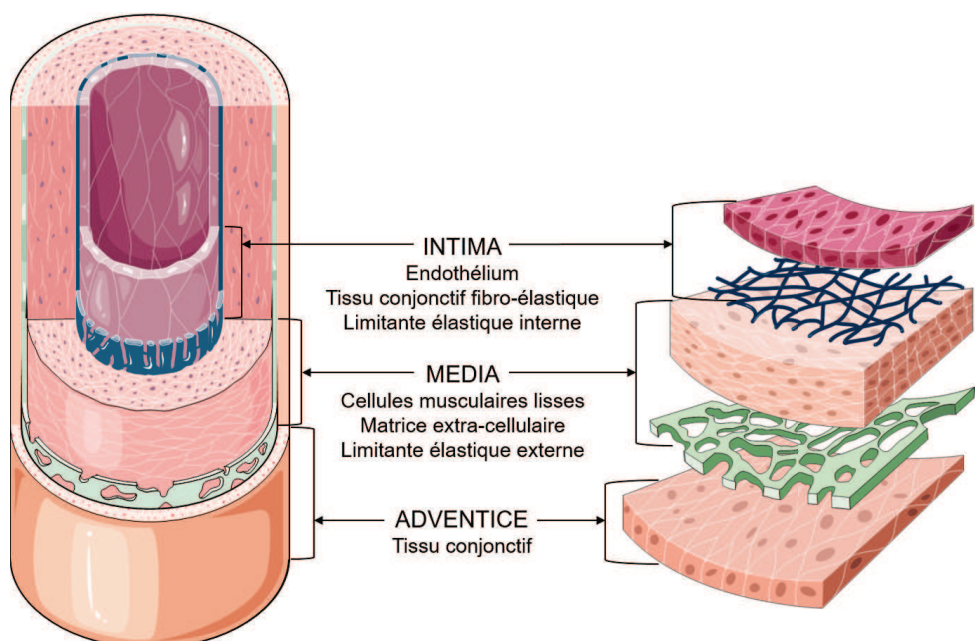


Figure 1. Structure schématique d'une artère.

Les composants principaux des trois tuniques sont détaillés. *Servier Medical Art.*

La paroi des artères de moyen et de gros calibres se compose de trois tuniques (**Figure 1**) qui sont, de l'intérieur vers l'extérieur :

- *L'intima* : est composée d'une monocouche de cellules endothéliales (CE) reposant sur une membrane basale, et d'une couche sous-endothéliale de tissu conjonctif contenant notamment des fibres de collagène, des fibres musculaires lisses et des fibroblastes. La membrane basale renferme plusieurs types de collagène. L'intima est séparée de la media par une lame de fibres élastiques constituées d'élastine ; la limitante élastique interne.
- *La media* : consiste en l'empilement concentrique d'unités lamellaires formées de cellules musculaires lisses (CML). Les CML sont entourées d'une matrice extracellulaire contenant du collagène et de l'élastine. Elle est la tunique la plus épaisse et est séparée de l'aventice par la limitante élastique externe.
- *L'aventice* : est formée essentiellement de tissu conjonctif riche en collagène et en fibres élastiques, elle contient des fibroblastes et des adipocytes. Elle permet entre autres l'ancre aux tissus environnant et assure l'apport nutritif des cellules de la paroi par un réseau de micro-vaisseaux, le *vasa-vasorum*.

1.2. Causes de la thrombose

La cause principale est le développement de plaques d'athérosclérose vulnérables [2]. D'autres pathologies, tels que les anévrismes, sont également associées à un état thrombotique [3]. Il existe d'autres causes, affectant par exemple les facteurs de la coagulation, qui ne seront pas décrites dans ce manuscrit.

1.2.1. L'athérosclérose

L'athérosclérose est une maladie silencieuse évoluant sur des décennies qui provoque un remodelage progressif de l'intima des artères. Elle désigne l'apparition de zones riches en lipides communément appelées plaques. C'est un processus multifactoriel qui se développe préférentiellement aux bifurcations artérielles où le flux est le plus

perturbé [4]. De nombreuses études réalisées avant les années 1990 sur des échantillons humains ont permis d'appréhender l'évolution des plaques au cours de la vie et de les classifier [5, 6]. Toutefois les mécanismes impliqués ne sont pas encore tous élucidés. La description suivante, illustrée par la **Figure 2**, résume de façon simplifiée les principaux phénomènes identifiés dans le développement de lésions athérosclérotiques. Cette description a été établie à partir de plusieurs revues [4, 7-9].

1.2.1.a. Initiation

Une plaque d'athérosclérose est initiée par la diffusion de lipoprotéines de basse densité (Low Density Lipoproteins LDL) dans l'intima. Les LDL, composées d'une monocouche de phospholipides et d'une molécule d'apolipoprotéine B, assurent normalement le transport du cholestérol et des triglycérides dans la circulation. Dans l'intima, les LDL subissent plusieurs modifications et sont notamment oxydées (ox-LDL) par des radicaux libres générés par les cellulaires vasculaires activées. Des facteurs de risque, tels que l'hypercholestérolémie, l'hypertension, le diabète, l'obésité, une alimentation riche en matières grasses, le stress et le tabagisme, influent entre autres sur la concentration plasmatique en LDL et sur l'état d'activation des cellules vasculaires.

Les ox-LDL stimulent le phénotype pro-inflammatoire des CE. Celles-ci expriment alors des molécules d'adhésion et initient le recrutement et la pénétration de lymphocytes et de monocytes dans l'espace sous-endothélial. En particulier, les monocytes infiltrés se différencient en macrophages et s'accumulent dans la plaque participant au maintien de l'inflammation (**Figure 2-A**). Les macrophages internalisent les ox-LDL hautement oxydées. Les CML prolifèrent dans l'intima et sont également capables d'internaliser les ox-LDL. Les macrophages et les CML chargées en lipides se transforment en cellules spumeuses. L'accumulation de cellules spumeuses s'organise sous forme de stries lipidiques. Ces phénomènes initient un épaissement de la paroi et un rétrécissement du lumen (sténose) (**Figure 2-B**). Ces processus apparaissent dès l'adolescence et des plaques peuvent rester sous cette forme pendant des années.

1.2.1.b. Développement

Dans certaines lésions, une zone riche en lipides et en débris cellulaires provenant de l'apoptose des cellules spumeuses et des CML apparaît et participe à la formation d'un cœur nécrotique (**Figure 2-C**). L'intima peut s'épaissir vers la media et non plus vers la lumière. Ce phénomène est qualifié de remodelage positif [10]. Ainsi une plaque qui évolue très rapidement n'induit pas nécessairement une sténose conséquente.

Les CML migrent au contact de l'endothélium et perdent leur phénotype de contractilité. Elles prolifèrent et sécrètent de la matrice extracellulaire contribuant à la formation d'une chape fibreuse riche en collagène (**Figure 2-C**). Des foyers de calcifications, potentiellement générés par le cœur nécrotique, peuvent apparaître et engendrer une calcification quasi-complète de la plaque. Des plaques présentant une épaisse chape fibreuse et/ou calcifiées sont considérées comme « stables » ; elles sont associées à un risque faible d'épisode thrombotique. Néanmoins, elles peuvent provoquer une sténose conséquente et d'autres complications.

1.2.1.c. Fragilisation

Certaines plaques évoluent au contraire vers un phénotype dit fragile, et deviennent vulnérables ; elles sont associées à un risque fort de générer une thrombose (**Figure 2-D**). Entre autres, une forte densité de macrophages, une fine chape fibreuse et un large cœur nécrotique ont été identifiés comme des indicateurs de vulnérabilité [11-13]. Ces caractéristiques sont liées à plusieurs mécanismes.

Au cours de la progression de l'athérosclérose, un réseau de micro-vaisseaux se développe depuis l'aventice (angiogenèse) et peut causer des hémorragies intra-plaque. Ces hémorragies participent au maintien de l'inflammation locale et au grossissement du cœur nécrotique [14, 15]. La chape fibreuse peut subir une dégradation, notamment suite à l'apoptose des CML et à la dégradation de la matrice extracellulaire par les métalloprotéases matricielles (matrix metalloprotease MMP) secrétées par les macrophages [16, 17].

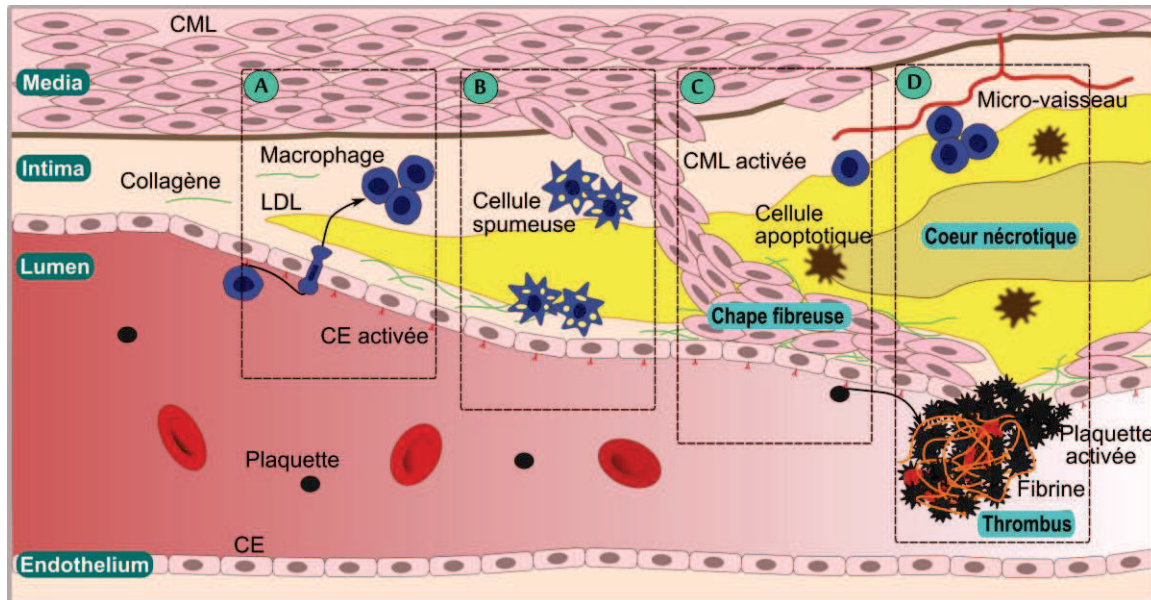


Figure 2. Représentation schématique du développement d'une plaque d'athérosclérose.

A) L'accumulation de LDL dans l'intima stimule l'activation des cellules endothéliales (CE). Les monocytes s'infiltrent, s'accumulent et se différencient en macrophages. **B)** Une zone riche en lipides grandit. Les LDL sont oxydées et internalisées par les macrophages qui se transforment en cellules spumeuses. **C)** Des événements apoptotiques provoquent la formation d'un noyau nécrotique. Les cellules musculaires lisses (CML) migrent dans l'intima et deviennent activées, perdant leur phénotype de contractilité. Elles produisent de la matrice extracellulaire et forment une chape fibreuse riche en collagène. **D)** Un remodelage positif affecte la taille de l'intima vers la media. L'apparition de micro-vaisseaux et l'accumulation de macrophages fragilisent la plaque. En cas de rupture ou d'érosion, l'espace sous-endothélial est exposé à la circulation. Les plaquettes adhèrent, s'activent et s'agrègent au site de rupture. Un réseau de fibrine se forme.

1.2.1.d. Thrombose

La thrombose, ou athérothrombose lorsqu'elle est initiée par une plaque d'athérosclérose, survient lorsque les éléments sous-endothéliaux sont exposés à la circulation (**Figure 2-D**). La majorité des événements cliniques aigus font suite à deux mécanismes ; une rupture de la chape fibreuse (60 à 80% des cas) ou une érosion de l'endothélium [18]. Dans les deux cas, des substances pro-coagulantes sont libérées induisant dans un premier temps l'adhésion et l'activation des plaquettes à l'endothélium et la formation d'un thrombus mural riche en plaquettes, dit “blanc”. Les plaquettes continuent de s'agrèger et un réseau de fibrine se forme en un thrombus dit “rouge” [19]. Ces mécanismes seront décrits dans la **section 1.3**.

Le thrombus peut générer une occlusion locale, transitoire ou totale. Il peut également migrer et entraîner l'occlusion d'une autre artère. Lorsqu'une artère coronaire est occluse, il s'agit d'un SCA. En particulier, un IM est diagnostiqué si une ischémie

d'une partie du myocarde est observée pouvant aller jusqu'à la nécrose. Si une carotide ou une artère cérébrale est occluse, la thrombose est à l'origine d'un AVC ischémique.

Toutefois, toutes les thromboses ne sont pas nécessairement symptomatiques. Certaines peuvent rester silencieuses avec une stabilisation temporaire de la plaque et une reformation superficielle de l'endothélium. La présence de plusieurs zones de rupture est communément considérée comme un phénomène accélérant la survenue d'un accident aigu [2, 20]. De plus, des zones matures de plusieurs heures voire plusieurs jours avant l'accident clinique aigu ont été observées dans des thrombus retirés de patients souffrant d'IM et de mort cardiaque subite [21, 22]. Lorsqu'une plaque entre dans ce processus intermittent de rupture ou d'érosion, c'est alors le patient qui est qualifié de "vulnérable" [23].

1.2.2. L'anévrisme

Un anévrisme est une dilatation définitive d'une paroi artérielle amincie. Il se développe principalement à la suite de processus athéromateux ayant fragilisé la paroi. Toutes les artères peuvent être concernées, néanmoins l'anévrisme de l'aorte abdominal (AAA) représente 85% des cas d'anévrisme. La complication majeure est la rupture d'anévrisme correspondant au déchirement de l'artère et causant une hémorragie conséquente. La rupture est associée à une mortalité extrêmement élevée (>75%) [24].

Les mécanismes conduisant à l'AAA sont complexes. Entre autres, l'accumulation de cellules inflammatoires dans l'intima augmente fortement l'activité protéolytique locale des MMP, qui dégradent l'élastine et le collagène de la media [25, 26]. La dilatation progressive de l'artère est également corrélée à l'apoptose des CML. Le développement de micro-vaisseaux dans la paroi contribue aussi à sa fragilisation.

Un thrombus intra-luminal est généré par une modification voire une stase du flux au niveau de la dilatation. Il est amplifié par la libération de substances pro-coagulantes au site d'inflammation [3]. Il a été montré que ce thrombus intra-luminal avait également un rôle dans l'accélération de la pathologie [27, 28]. De plus, sa croissance pourrait être directement corrélée au risque de rupture [29].

1.3. Mécanismes de la thrombose

Le thrombus artériel est majoritairement provoqué par la perte d'intégrité de l'endothélium exposant le sous-endothélium fortement thrombogène. Avant l'exposition des éléments sous-endothéliaux, une plaque d'athérosclérose favorise déjà le recrutement et l'activation des plaquettes circulantes via l'endothélium activé [30]. L'exposition des éléments sous-endothéliaux va ensuite causer deux phénomènes concomitants : la formation d'un agrégat plaquettaire activé et celle d'un réseau réticulé de fibrine. Ces deux voies sont imbriquées.

1.3.1. Rôle de l'endothélium activé

L'endothélium quiescent présente une surface thromborésistante et a des effets anti-thrombotiques, par exemple par la libération d'inhibiteurs plaquettaires comme l'oxyde nitrique [31]. Les CE activées deviennent pro-thrombotiques. D'une part, elles sécrètent des molécules qui augmentent le phénotype d'agrégabilité plaquettaire, comme la Thromboxane A2 [32]. D'autre part, elles expriment des molécules qui favorisent l'adhésion des plaquettes à leur surface. Ainsi, l'activation des CE génère l'exocytose des corps de Weibel-Palade, granules de stockage présentes dans leur cytoplasme. Les corps de Weibel-Palade contiennent deux composants principaux : le Facteur de von Willebrand (FW) et la P-sélectine (ou CD62P) [33]. Le FW est relargué dans l'espace sous-endothélial et dans la circulation. La P-sélectine se retrouve exprimée à la surface des CE. Ces deux molécules ont un rôle majeur dans la thrombose.

Le complexe GPIb/IX/V des plaquettes interagit avec le FW. Cette interaction initie le recrutement des plaquettes à la surface des CE activées (**Figure 3-A**). Les plaquettes interagissent également avec la P-sélectine endothéliale par deux récepteurs : le complexe GPIb/IX/V et la P-sélectine glycoprotéine ligand-1 (PSGL-1) plaquettaire. Ces liaisons participent conséutivement au “rolling” des plaquettes à la surface de l'endothélium (**Figure 3-A**) [34].

1.3.2. Exposition des éléments sous-endothéliaux

1.3.2.a. Formation d'un agrégat plaquettaire activé

Après rupture ou érosion, le collagène se retrouve exposé à la circulation. Au contact du collagène, le FW libéré dans l'espace sous-endothélial permet l'adhésion des plaquettes toujours au niveau du complexe GPIb/IX/V. Les plaquettes forment aussi des liaisons directes avec les fibres de collagène notamment via la glycoprotéine GpVI (**Figure 3-B**) [35, 36].

L'adhésion des plaquettes induit leur activation. Les plaquettes subissent des modifications morphologiques et biochimiques. Elles sécrètent des substances pro-thrombotiques qui vont favoriser le recrutement et l'activation d'autres plaquettes [2]. Leur activation modifie également le panel de molécules exprimées à leur surface ; entre autres la glycoprotéine GpIIb/IIIa change de conformation et la P-sélectine se retrouve exprimée [30]. Le changement de conformation du complexe GpIIb/IIIa permet tout d'abord la stabilisation de l'adhésion des plaquettes au FW lié au collagène. De plus, la GpIIb/IIIa assure l'interaction inter-plaquettaire en liant le fibrinogène circulant. Les plaquettes s'agrègent et des ponts de fibrinogène se forment (**Figure 3-B**). La P-sélectine stabilise l'interaction GpIIb/IIIa-fibrinogène et favorise l'ancrage du thrombus [37].

Dans les zones de contraintes de cisaillement élevées comme les artères, ces phénomènes s'enclenchent dès la première minute et prédominent dans un premier temps donnant lieu à un thrombus mural formé en grande partie de plaquettes [18].

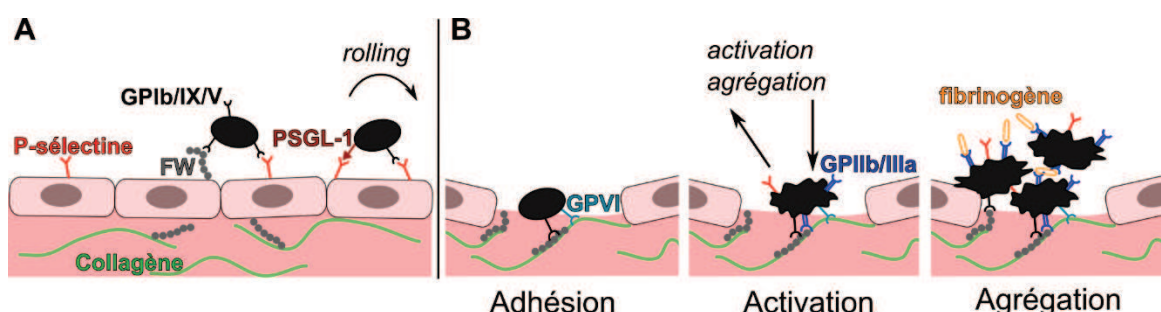


Figure 3. Schéma simplifié du recrutement plaquettaire A) par les cellules endothéliales activées et B) à la suite d'une exposition du sous-endothélium.

A) La P-sélectine et le FW initient le recrutement des plaquettes. B) Les plaquettes se fixent au collagène directement ou par le FW. Elles sont activées et favorisent l'activation et l'agrégation d'autres plaquettes. Un agrégat plaquettaire se forme avec des ponts de fibrinogène.

1.3.2.b. Formation d'un réseau réticulé de fibrine

La rupture de l'endothélium déclenche en parallèle la cascade de la coagulation. Le facteur tissulaire (FT), protéine transmembranaire des cellules de la media et de l'adventice, est mis au contact du sang et provoque une cascade d'activation enzymatique de laquelle résulte la génération de thrombine. Cette enzyme assure la transformation du fibrinogène circulant en monomères de fibrine [18]. La fibrine est ensuite stabilisée par le facteur XIII qui est aussi activé par la thrombine. Le facteur XIII activé (FXIIIa) permet la création de liaisons covalentes entre les monomères de fibrine et la formation d'un réseau réticulé qui s'arrange en longues chaînes fibreuses (**Figure 4**). La thrombine stimule également l'activation des plaquettes.

Les plaquettes elles-mêmes sont à l'origine d'une seconde source locale de FT. Les monocytes circulants produisent des microparticules qui portent du FT. Ces microparticules expriment le PSGL-1. Il est démontré que les microparticules interagissent par ce récepteur avec la P-sélectine plaquettaire et que cette interaction conduit au relargage de FT directement au sein du thrombus [38].

La stabilisation de l'agrégat plaquétaire par un réseau réticulé de fibrine intervient dans les minutes qui suivent la formation du thrombus mural [2].

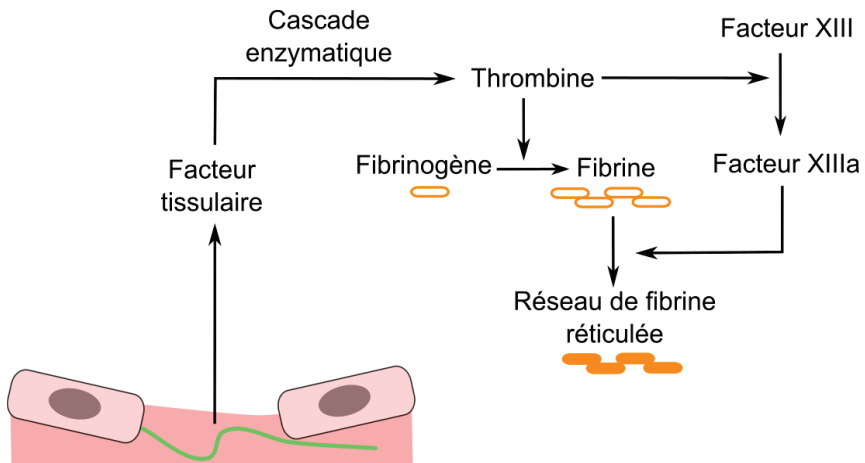


Figure 4. Schéma simplifié de la cascade de coagulation menant à la formation d'un réseau de fibrine. Le facteur tissulaire est le point de départ d'une cascade enzymatique à l'origine de la thrombine. Le fibrinogène soluble va être transformé en un réseau de fibrine insoluble réticulée par le Facteur XIII activé.

Les plaquettes et la fibrine sont les composants majoritaires du thrombus, mais des érythrocytes et des leucocytes en font également partie. À titre d'exemple, une étude réalisée sur des thrombi retirés de patients souffrant d'IM a quantifié que la fibrine comptait en moyenne pour 55% en masse, les plaquettes pour 17%, les érythrocytes pour 12% et les leucocytes pour 1% [39]. Des débris de plaques peuvent également s'y trouver. La composition du thrombus dépend de son origine (rupture ou érosion) [22]. Elle varie grandement avec les conditions de flux locales et le temps d'ischémie [39]. Il est démontré que la composition du thrombus et la pathologie qu'il induit sont corrélés. Par exemple, lors d'un IM, le thrombus se forme dans des conditions spécifiques et aura donc une composition particulière par rapport aux autres types de SCA [40].

Connaître la composition du thrombus par des méthodes non invasives permettrait d'avoir des indications sur l'origine de la thrombose et ainsi de choisir le traitement adéquat. Aujourd'hui les méthodes d'imagerie utilisées pour confirmer le diagnostic d'un évènement clinique aigu reposent en grande partie sur des outils anatomiques. Les méthodes d'imagerie et les challenges associés sont détaillés dans la section suivante.

1.4. Diagnostic

Valider l'occlusion et trouver la plaque vulnérable à son origine pour prévenir une récidive reposent en grande partie sur une visualisation de la lumière des vaisseaux. Les méthodes d'imagerie consistent à visualiser la morphologie des vaisseaux et la perfusion des organes. Néanmoins, les avancées technologiques dans ce domaine et une meilleure connaissance des mécanismes biologiques permettent aujourd'hui d'envisager une médecine personnalisée.

1.4.1. Diagnostic anatomique

1.4.1.a. Pratique clinique standard

Les modalités sont détaillées dans cette section dans le cadre de leur utilisation pour le diagnostic d'un patient montrant les symptômes d'un AVC. La suspicion d'une occlusion dans une carotide ou dans une artère cérébrale est prise ici comme exemple.

- L'échographie repose sur la différence d'impédance entre les tissus et fournit un moyen rapide, peu coûteux et entièrement sûr d'imager la paroi artérielle. Elle permet de déterminer avec précision la présence d'une sténose ou d'une occlusion dans une carotide, artère peu profonde. De plus, *l'échographie doppler* offre une image simultanée des perturbations de flux locales (**Figure 5-A**).

- La tomodensitométrie (computed tomographie CT) repose sur la différence d'absorption des rayons X des tissus. La CT possède une bonne résolution spatiale (<100 µm) et présente l'avantage d'être un examen rapide. Néanmoins elle expose le patient à des radiations. Une imagerie CT sans agent de contraste est l'examen standard pour valider l'état d'ischémie cérébral (**Figure 5-D**).

Des composés à base d'iode fortement radio-opaques sont utilisés comme agents de contraste. Une *angiographie CT assistée par cathéter* (ou *artériographie*) est une méthode invasive qui consiste à injecter l'agent de contraste dans la zone à imager après l'y avoir amené par microcathéter. Elle est la méthode de référence pour visualiser avec une grande précision la lumière vasculaire et les modifications morphologiques des parois mais présente des risques de part son caractère invasif (**Figure 5-B**) [41]. Elle permet de déterminer la taille de l'occlusion et donc indirectement celle du thrombus.

Ces mêmes agents de contraste peuvent être injectés en IV pour réaliser une *CT de perfusion*. L'état de perfusion des tissus va donner des informations sur les potentiels bénéfices d'un traitement (voir **section 1.5.2.a**) (**Figure 5-E**).

Enfin, ces agents de contraste peuvent également être utilisés pour réaliser une *angiographie CT (angioscanner ou CTA)*. Une CTA permet de visualiser le réseau des artères principales (**Figure 5-F**) [42].

- L'imagerie par résonance magnétique (IRM) repose sur la résonance magnétique des atomes d'hydrogène des molécules d'eau présentes en quantités variables dans les tissus. Elle fournit une image morphologique de l'organe et/ou de l'artère avec une bonne

résolution ($25 \mu\text{m}$ à 1 mm). De même qu'avec la CT, plusieurs séquences peuvent être mises en place pour faire ressortir les zones ischémiques (imageries de diffusion et de perfusion). *L'angiographie par résonance magnétique (angioIRM ou MRA)* permet, comme la CTA, de visualiser rapidement (<15 minutes) le pool sanguin et un possible site d'occlusion ou de sténose (**Figure 5-C**) [43]. Une MRA peut être réalisée avec ou sans agent de contraste. Les agents de contraste utilisés pour l'IRM sont des chélates de Gadolinium. Globalement, l'IRM est une modalité moins accessible et plus coûteuse que la CT mais peut fournir des informations complémentaires, comme la visualisation de micro-hémorragies dans la paroi [44]. Ces méthodes d'angiographies peu invasives (CTA ou MRA) sont de plus en plus utilisées [42].

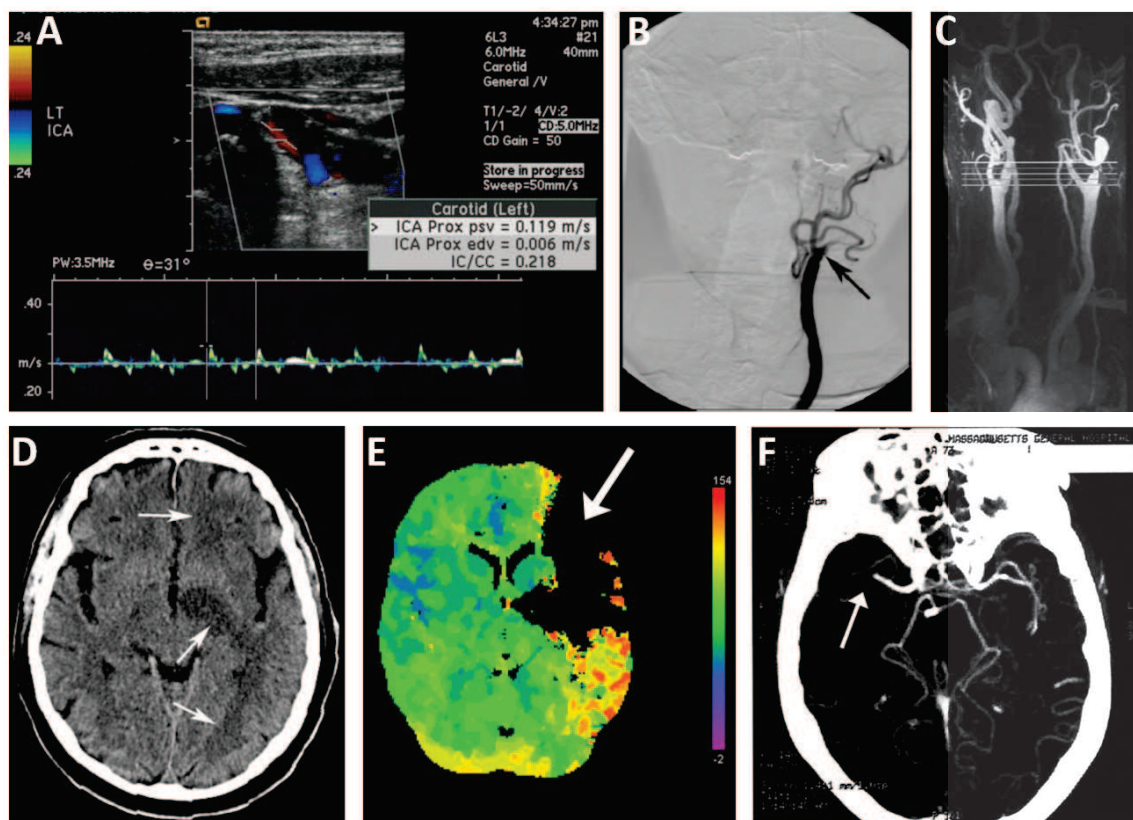


Figure 5. Exemples d'images standards d'occlusion carotidiennes ou cérébrales.

A), B) et C) Occlusion carotidiennes ; A) Echographie doppler montrant un flux pulsatile minimal au niveau d'une sténose ; B) Angiographie CT par cathéter révélant une occlusion (flèche) ; C) MRA soulignant une sténose conséquente de la carotide droite. D), E) et F) Occlusion cérébrale ; D) Imagerie CT sans agent de contraste discriminant le type d'AVC (ischémies pointées par les flèches) ; E) Imagerie CT de perfusion avec injection d'agent de contraste permettant de définir la sévérité de l'ischémie (arrêt du flux au niveau de la flèche) ; F) Angiographie CT montrant un site d'occlusion (flèche). *Images adaptées de [41, 43, 45].*

Après la phase aiguë, des examens complémentaires sont menés sur les différentes artères pour déterminer si possible l'origine de l'accident, et la présence d'autres plaques vulnérables. De nombreuses études montrent que les patients ayant souffert d'un accident ischémique courent un risque élevé de récidive à court terme (48 heures) et à long terme (plusieurs années) soulignant la nécessité de diagnostiquer la cause sous-jacente [46, 47]. Ces observations peuvent être corrélées au fait qu'une plaque ayant généré un premier évènement ischémique reste hautement à risque à court terme. De plus, l'athérosclérose étant un processus multi-sites, une plaque vulnérable sous-tend généralement l'existence d'autres plaques qui peuvent s'avérer à risque à plus long terme.

En résumé, des techniques qui permettent de visualiser le pool sanguin sont majoritairement utilisées pour évaluer une sténose ou une occlusion. Des méthodes d'angiographies moins invasives se développent. Des techniques qui permettent de visualiser la perfusion des tissus sont utilisées pour quantifier une ischémie et prendre les décisions relatives au traitement d'urgence.

1.4.1.b. Limitations

La principale limitation de ces méthodes anatomiques standards est qu'elles ne fournissent pas d'informations directes sur le thrombus mais uniquement sur les effets que la thrombose provoque sur la circulation. Actuellement, le traitement standard non invasif est l'injection d'un actif qui dégrade la fibrine, dit fibrinolytique (voir **section 1.5**). Il est montré que cet actif n'a pas d'efficacité sur des thrombi dont la taille est supérieure à 8 mm [48]. Aussi, de part son mode de fonctionnement, cet actif n'a pas la même efficacité selon la composition du thrombus [49]. Davantage d'informations sur la nature du thrombus (densité plaquettaire et fibrineuse, thrombus jeune ou mature, ...) pourraient donc être décisives pour le choix du traitement [50]. Avoir une visualisation directe du thrombus permettrait également de déterminer l'efficacité de ce traitement.

De plus, lors de la suspicion d'un accident thrombotique, plusieurs imageries sont réalisées car les modalités ne sont pas toutes adaptées aux différentes parties du corps impliquées, comme la tête, le cou ou le thorax. Des examens multiples sont nécessaires

pour dresser une cartographie des sites d'ischémie et de la vulnérabilité des différentes artères. Pouvoir dresser une imagerie corps entier des sites de thrombose serait un gain de temps précieux dans la prise en charge des patients vulnérables [51].

Enfin, les pathologies à l'origine de la thrombose n'ont pas forcément une évolution anatomique représentative de leur état de vulnérabilité. Une plaque à haut risque n'engendre pas nécessairement un rétrécissement conséquent de la lumière et n'est donc pas forcément visible par les méthodes anatomiques classiques (voir **section 1.2.1.b)** [13]. Certains éléments de la plaque, comme une fine chape fibreuse et une forte accumulation de macrophages, ont été identifiés comme de meilleurs indicateurs du risque de rupture [11-13]. De plus, comme décrit **section 1.2.1**, une thrombose silencieuse peut être initiée plusieurs jours voire plusieurs semaines avant l'accident. Des ruptures multiples pourraient être caractéristiques des plaques vulnérables [2]. Des indications sur la présence d'un thrombus mural pourraient donc donner des indices sur la vulnérabilité d'une plaque.

En prenant maintenant l'exemple des AAA, la taille de la dilatation de la paroi reste le facteur standard pour évaluer le risque de rupture. Or, plusieurs études démontrent que la présence et la composition du thrombus intraluminal peuvent fournir davantage d'outils pour prédire la rupture [27, 28].

1.4.1.c. Amélioration des outils d'imagerie

Des techniques d'imagerie émergent pour évaluer directement la taille du thrombus et son architecture avec des moyens moins invasifs que l'artériographie. En particulier, des séquences d'IRM optimisées permettent d'imager des thrombi formés dans de larges artères cérébrales comme celui illustré sur la **Figure 6-A** [52, 53].

L'IRM permet également d'identifier certaines caractéristiques des plaques vulnérables telles que : un épais cœur nécrotique, des hémorragies intra-plaque, un remodelage positif et un thrombus mural [54-56] (**Figure 6-B**). L'imagerie CT peut quant à elle être utilisée pour connaître le taux de calcification des plaques. D'autres modalités d'imageries, invasives ou non, comme l'OCT (*optical coherence tomography*) ou l'IVUS

(*Intra-Vascular Ultrasonography*) fournissent des informations complémentaires sur la structure et la composition des artères [57].

Le développement de ces technologies modernes permet donc de passer d'une imagerie uniquement anatomique à une imagerie structurelle qui fournit des informations sur la composition cellulaire des parois.

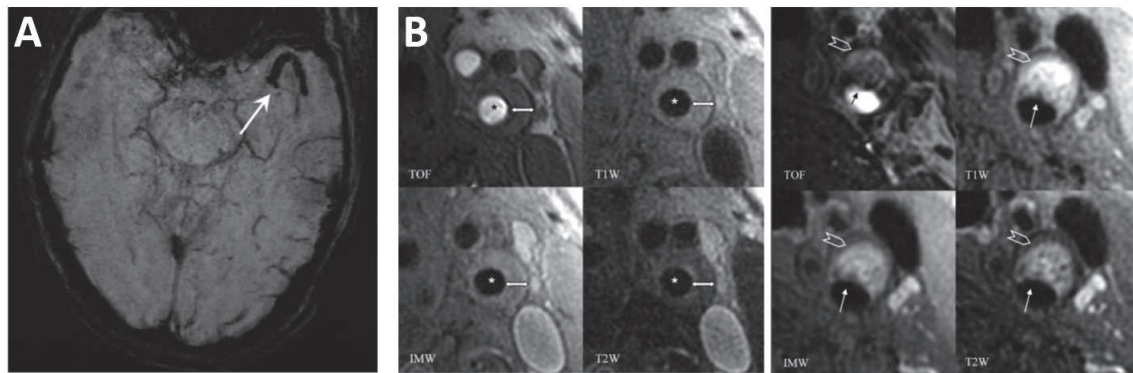


Figure 6. Exemples illustrant l'optimisation des séquences d'IRM pour la visualisation directe du thrombus et de la plaque vulnérable.

A) Thrombus cérébral (flèche) [52], B) Coupes transverses de carotides montrant une sténose ; Gauche : plaque homogène et probablement stable ; Droite : plaque hétérogène et probablement vulnérable avec ulcération superficielle (flèche) suggérant la présence d'un thrombus mural [55].

1.4.2. Vers un diagnostic moléculaire

1.4.2.a. Principe

En parallèle, la notion d'imagerie moléculaire s'est développée. Il s'agit non plus d'imager la structure des tissus mais d'utiliser les mécanismes moléculaires pour obtenir une image fonctionnelle et “quantitative” de leur activité. Cette notion est fortement liée à l'implantation d'une autre modalité d'imagerie :

- *La scintigraphie* comprend la *tomographie par émission monophotonique (TEMP)* et la *tomographie par émission de positrons (TEP)*. Ces techniques apportent une imagerie fonctionnelle des tissus après injection d'un radioisotope. Du fait de sa grande sensibilité et de l'utilisation de radioisotopes, l'imagerie nucléaire est la première modalité à avoir été utilisée en routine clinique pour l'imagerie moléculaire. Les

radioisotopes sont associés à des petites molécules. Celles-ci ont généralement une fonction biologique précise. Ils forment ensemble les radio-pharmaceutiques. Le plus courant est le ^{18}F -fluorodésoxyglucose (^{18}F -FDG) utilisé pour l'imagerie TEP [58]. Cet analogue du glucose est piégé dans les macrophages métaboliquement actifs où il s'accumule. Dans le domaine cardiovasculaire, l'imagerie ^{18}F -FDG a démontré son efficacité pour la détection des plaques à haut risque riches en macrophages. Le ^{18}F -FDG est employé dans les essais cliniques menés depuis plus d'une dizaine d'années pour évaluer l'efficacité de nouveaux traitements contre l'athérosclérose [59].

1.4.2.b. Implantation clinique de l'imagerie moléculaire de la thrombose

L'imagerie moléculaire requiert une grande sensibilité du mode de détection. C'est pourquoi la scintigraphie reste la modalité la plus utilisée. A la fin des années 1990, un peptide dirigé contre le récepteur GpIIb/IIIa des plaquettes activées et radiomarqué au Technétium 99m ($^{99\text{m}}\text{Tc}$) a été testé en clinique sur des cas de thrombose veineuse [60].

D'autres structures sont à l'étude pour la scintigraphie. L'Annexin-A5 radiomarquée au $^{99\text{m}}\text{Tc}$ vient d'entrer en évaluation clinique (Phases I et II) à l'hôpital Bichat (*équipe 4 du LVTS*) pour le diagnostic de l'endocardite (inflammation d'une valve) et de la thrombose atriale (thrombus qui se forme par stase suite à un trouble du rythme cardiaque) [61]. Le fucoïdane radiomarqué au $^{99\text{m}}\text{Tc}$ va également être testé dans un essai clinique de phases I et II dans le cadre du consortium *NanoAthero* (le fucoïdane est détaillé en **section 2.3.1.b**). Sa capacité à s'accumuler au niveau des sites thrombotiques a été validée dans plusieurs modèles précliniques (**Figure 7-A&B**) [62, 63]. La $^{99\text{m}}\text{Tc}$ -Annexin-A5 et le $^{99\text{m}}\text{Tc}$ -fucoïdane sont dirigés respectivement contre la phosphatidylsérine et la P-sélectine. Ces deux molécules sont exprimées à la surface des plaquettes dans leur état activé [64].

L'IRM a aussi été utilisée pour l'imagerie moléculaire de la thrombose chez l'Homme. Ainsi, des chélates de Gadolinium ont été liés de manière covalente à un peptide spécifique de la fibrine. La preuve de concept de l'utilisation de cette sonde, nommée EP-2104R (EPIX Pharmaceuticals, Inc.), pour la visualisation directe du

thrombus a été obtenue dans un essai clinique de phase II sur 52 patients souffrant de thromboses veineuses et/ou artérielles [65]. Les résultats sont illustrés **Figure 7-C,D&E** [66].

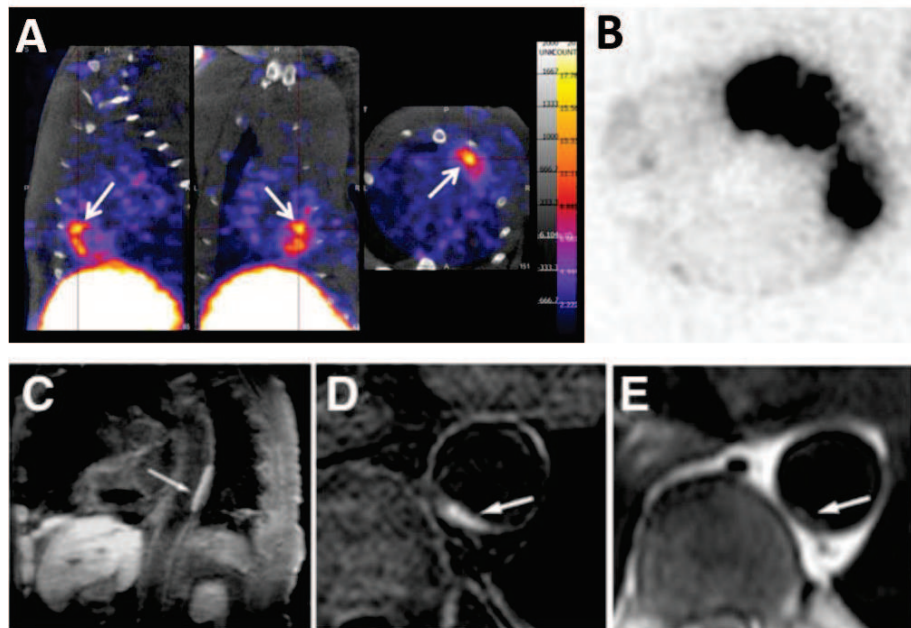


Figure 7. Exemples de systèmes en imagerie moléculaire préclinique ou clinique de la thrombose.
A) Imagerie TEMP après injection de ^{99m}Tc -Fucoïdane dans un modèle d’ischémie du myocarde suivie d’une reperfusion chez le rat. L’ischémie-reperfusion engendre une forte zone d’activation endothéliale et plaquettaire. B) Autoradiographie correspondante du myocarde. La zone en noir correspond à l’accumulation du radioisotope [63]. C) D) E) Imageries IRM après injection de la sonde EP-2104R chez des patients souffrant de thrombose artérielle [66, 67].

Actuellement, les systèmes développés pour l'imagerie moléculaire de la thrombose consistent donc en de petites molécules solubles directement liées par un agent de contraste. Plusieurs autres systèmes similaires sont en étude préclinique [50, 68]. Ces molécules présentent l'avantage de pouvoir être facilement utilisable en clinique, toutefois elles encourrent les risques : i) d'être trop rapidement éliminées par l'organisme et ii) de ne pas être détectable car la densité en agent de contraste par ligand est faible. La **section 2** de ce chapitre explique comment la nanomédecine propose de répondre à ces problématiques. Avant, les challenges liés au traitement de la thrombose sont exposés.

1.5. Traitement

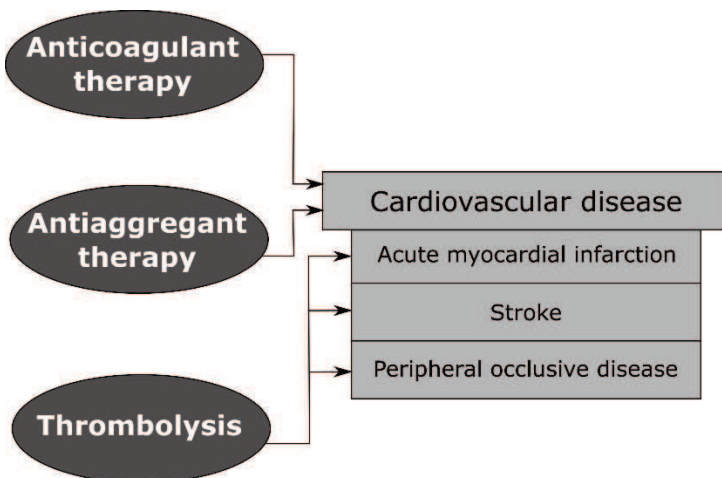


Figure 8. Approches thérapeutiques médicamenteuses des thromboses artérielles.
Adapté de [69].

Le traitement de la thrombose dépend de sa sévérité (occlusion partielle ou totale) et de sa localisation. Deux approches sont envisagées ; la chirurgie et/ou les médicaments. Cette section s'intéresse uniquement aux approches médicamenteuses et plus particulièrement à la thrombolyse.

Si l’occlusion n’est pas totale, le traitement priviliege l’administration de médicaments qui empêchent la croissance du thrombus et favorisent sa disparition ; les anticoagulants et les antiagrégants plaquettaires (**Figure 8**). Les anticoagulants consistent surtout en des inhibiteurs des différents facteurs impliqués dans la cascade de la coagulation. Les antiagrégants visent quant à eux à réduire le potentiel d’agrégabilité plaquette en inhibant des récepteurs tels que le complexe GpIIb/IIIa [69].

Lors de l'occlusion totale d'une artère, un troisième type de traitement entre en jeu ; les agents fibrinolytiques ou agents thrombolytiques. Ces agents ont une action directe sur le thrombus en stimulant la dégradation du réseau de fibrine. L'objectif est d'induire une reperfusion rapide de l'artère pour éviter la mort des tissus.

1.5.1. Les agents thrombolytiques

Les agents thrombolytiques approuvés par la U.S. Food & Drug Administration (FDA) et l'European Medicines Agency (EMA) sont : la streptokinase (SK), l'urokinase (UK) et des formes recombinantes de l'activateur tissulaire du plasminogène (tPA). Les premières autorisations chez l'Homme pour les pathologies artérielles ont eu lieu dans les années 1980 (**Tableau 1**).

Type	Agents	Abbrev.	Mw (kDa)	Demi-vie (min)	Fibrino-sélectif	Date	Indication
Activateur indirect : actif après formation d'un complexe avec le plasminogène	Streptokinase Streptofactor®, Biofactor GmbH, Germany	SK	47	Seul : 18 Complexé : 80	Non	1987	IM
Activateur du plasminogène de type urokinase	Urokinase Kinlytic®, Microbix Biosystems Inc., Canada	UK	31	13	Non	1999	IM*
	Alteplase Activase®, Genentech Inc., US Actilyse®, Boehringer Ingelheim, Germany	rt-PA	65	5	Oui +++	1987 1996	IM AVC
Formes recombinantes de l'activateur tissulaire du plasminogène (tPA)	Reteplase Retavase®, Chiesi, Italy Rapilysin®, Actavis, US	rPA	40	15	Oui +	1996	IM
	Tenecteplase TNKase®, Genentech Inc., US Metalysé®, Boehringer Ingelheim, Germany	TNKase	59	24	Oui ++++	2000	IM

Tableau 1. Agents thrombolytiques autorisés par la FDA et l'EMA pour les pathologies artérielles.
 AVC = Accident Vasculaire Cérébral ischémique ; IM = infarctus du myocarde. *Données issues du site de la U.S. Food & Drug Administration (FDA), de l'electronic Medicines Compendium (eMC, Datapharm Communications Limited) et des sites web des industriels. Date = date de première autorisation par la FDA pour l'injection IV pour les indications citées. *L'UK n'est plus utilisée actuellement dans le cadre de l'IM.*

1.5.1.a. Modes d'action

L'UK et le tPA sont des enzymes protéolytiques naturellement sécrétées par l'organisme. Ces enzymes provoquent la transformation de plasminogène en plasmine. La plasmine dégrade ensuite le réseau de fibrine. Ces deux types d'activateurs du plasminogène sont rapidement inhibés dans la circulation, notamment par l'inhibiteur de l'activateur du plasminogène 1 (PAI-1) (**Figure 9**) [70]. Ils présentent un temps de demi-vie relativement court de l'ordre de quelques minutes, du fait de leur élimination rapide par voie hépatique (5 minutes pour l'Alteplase et 13 minutes pour l'Urokinase) (**Tableau 1**). La SK est inactive sous sa forme injectée, mais devient active après avoir formé un complexe avec le plasminogène [71].

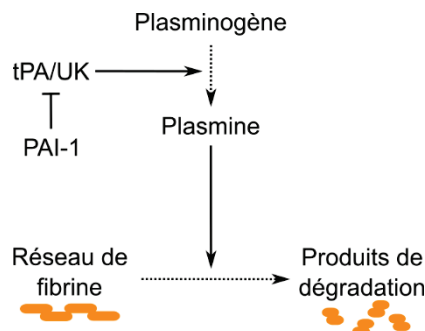


Figure 9. Schéma de la fibrinolyse par les activateurs du plasminogène.

Le tPA et l'UK agissent de façon similaire en générant la plasmine à partir du plasminogène. La plasmine dégrade le réseau de fibrine.

Une différence majeure entre le tPA et les autres types d'agents thrombolytiques est que le tPA est fibrino-sélectif. Au contact de la fibrine, son activité protéolytique est fortement stimulée. La constante de réaction sur le plasminogène lié à la fibrine est jusqu'à 500 fois plus élevée que sur le plasminogène circulant [72]. Cet aspect est intéressant pour deux raisons. Premièrement, le tPA génère donc la production de plasmine directement dans le thrombus où elle doit agir. Deuxièmement, il évite la production de plasmine dans la circulation. Celle-ci entraîne en effet une baisse du taux de fibrinogène circulant (fibrinogénolyse) ce qui perturbe les acteurs de la cascade de la coagulation. Cet effet peut avoir une action délétère sur l'hémostase ; ensemble des mécanismes qui participent au maintien de l'intégrité vasculaire, et provoquer des saignements (voir **section 1.5.2.b**) [73].

Une autre caractéristique propre au tPA est qu'il présente une forte affinité de liaison pour la fibrine. Il s'y lie et forme un complexe ternaire cyclique avec le plasminogène lié [74] (**Figure 10**).

1.5.1.b. Développement historique et utilisation actuelle

La SK a été le premier agent testé chez l'Homme pour le traitement IV de l'IM dès 1958 [71, 75]. Les premiers essais ont validé le bénéfice d'utiliser un agent fibrinolytique. Néanmoins, la SK présente des risques immunogènes. Le tPA a été produit sous une forme recombinante (alteplase ou rt-PA) à partir de cellules mammifères (Chinese Hamster Ovary) au début des années 1980 par Collen *et al.*, ce qui a participé à son implémentation à grande échelle [74]. La molécule de rt-PA est identique à celle du tPA endogène, notamment en termes d'activité protéolytique [76]. En raison de son accessibilité et de sa fibrino-sélectivité, le rt-PA a ensuite été privilégié dans les études cliniques des années 1990 pour le traitement des IM et des AVC ischémiques [71]. Il a notamment montré sa supériorité par rapport à la SK pour les IM [77]. Ces études en font aujourd'hui le traitement de référence. Jusqu'à maintenant, le rt-PA (ou Alteplase) reste le seul actif à être autorisé pour le traitement thrombolytique des AVC ischémiques (injection IV). Les bénéfices et les risques liés à son injection dans le cadre de cette pathologie vont être détaillés pour illustrer les challenges cliniques actuels.

1.5.2. Utilisation dans le cadre de l'AVC ischémique

1.5.2.a. Bénéfices

L'occlusion d'une artère cérébrale par un thrombus provoque une ischémie d'une partie du cerveau. Les tissus entourant le thrombus forment le *cœur* de l'ischémie et sont généralement nécrosés de manière irréversible. Ils sont entourés de tissus sous-perfusés qui peuvent potentiellement récupérer leurs fonctions lorsqu'ils seront de nouveau irrigués ; ceux-ci constituent la *pénombre*. Les déficits neurologiques qui suivent l'accident sont fonctions de la zone et de la taille de l'ischémie. Plus le thrombus est

dégradé rapidement et efficacement, moins les tissus restent en souffrance. Il a ainsi été montré que les bénéfices en termes de récupération des fonctions neurologiques étaient directement corrélés ; i) au temps de l'injection du rt-PA après l'apparition des premiers symptômes [78] et ii) à l'efficacité de la thrombolyse (taux de recanalisation) [79].

En pratique, la dose approuvée de rt-PA est de 0,9 mg/kg avec un maximum de 90 mg. Un bolus de 10% de la dose est administré sur une période de 1 minute. Le reste est perfusé sur 60 minutes à cause du temps de demi-vie court du rt-PA. Des méta-analyses portant sur plusieurs milliers de patients et mises à jour régulièrement concluent aux bénéfices de l'injection du rt-PA jusqu'à 6h après l'apparition des premiers symptômes. Dans ces analyses, le pourcentage de patients en vie et indépendants à 3 mois est de 46,3% avec le rt-PA contre 42,1% dans le groupe non traité par thrombolytique [80, 81]. Toutes les études ne sont toutefois pas homogènes en termes de dose, de types de patients (âge, antécédents, ...) et de temps de prise en charge. Ces chiffres peuvent varier légèrement d'une étude à l'autre mais valident l'utilisation du rt-PA.

1.5.2.b. Risques

Le risque majeur associé à l'utilisation du rt-PA est la survenue de complications hémorragiques. Les hémorragies intracrâniennes sont particulièrement redoutées. Dans les études citées précédemment, 7,7% des patients recevant le rt-PA ont développé une hémorragie intracrânienne symptomatiques (HIS), contre 1,8% dans le groupe non traité par thrombolytique [80, 81]. Le nombre de décès à 7 jours post-admission est de ce fait plus élevé dans le groupe traité (8,9% contre 6,4%), néanmoins le bénéfice à 3 mois reste positif [82].

Ce risque existe aussi avec les autres agents thrombolytiques. L'augmentation de la tendance aux saignements est liée en partie à la transformation du plasminogène systémique qui perturbe l'hémostase (**Figure 10**). C'est une des raisons pour lesquels le rt-PA avait été privilégié [73]. Ainsi, son caractère fibrino-sélectif fait qu'il engendre moins de plasmine dans la circulation que les actifs non fibrino-sélectifs.

Toutefois, les mécanismes à l'origine des HIS sont plus complexes. Des HIS sont également observées après injection d'actif thrombolytique à des patients souffrant d'IM, bien que dans une moindre mesure (de 1 à 2% des patients traités). Des études cliniques réalisées dans le cadre des IM n'ont pas montré une diminution du taux de HIS avec l'utilisation du rt-PA fibrino-sélectif par rapport à la SK non fibrino-sélective [77].

Les processus qui expliquent l'apparition d'HIS ne sont pas encore totalement élucidés. Entre autres, le rt-PA a un effet délétère sur l'intégrité de la barrière hémato encéphalique (BHE) en augmentant l'activité de certaines MMP [83]. La BHE endommagée et les mécanismes déclenchés par l'ischémie favorisent cette action. En effet, la majorité des HIS surviennent au niveau de la zone ischémique (**Figure 10**) [84]. De part sa liaison avec la fibrine, le rt-PA pourrait également être retenu sur site et entraîner la lyse de thrombus hémostatiques formés post-accident. Enfin, le rt-PA présente des effets excitotoxiques (type de neurotoxicité induisant la mort neuronale), qui peuvent être fonction de sa concentration locale [85].

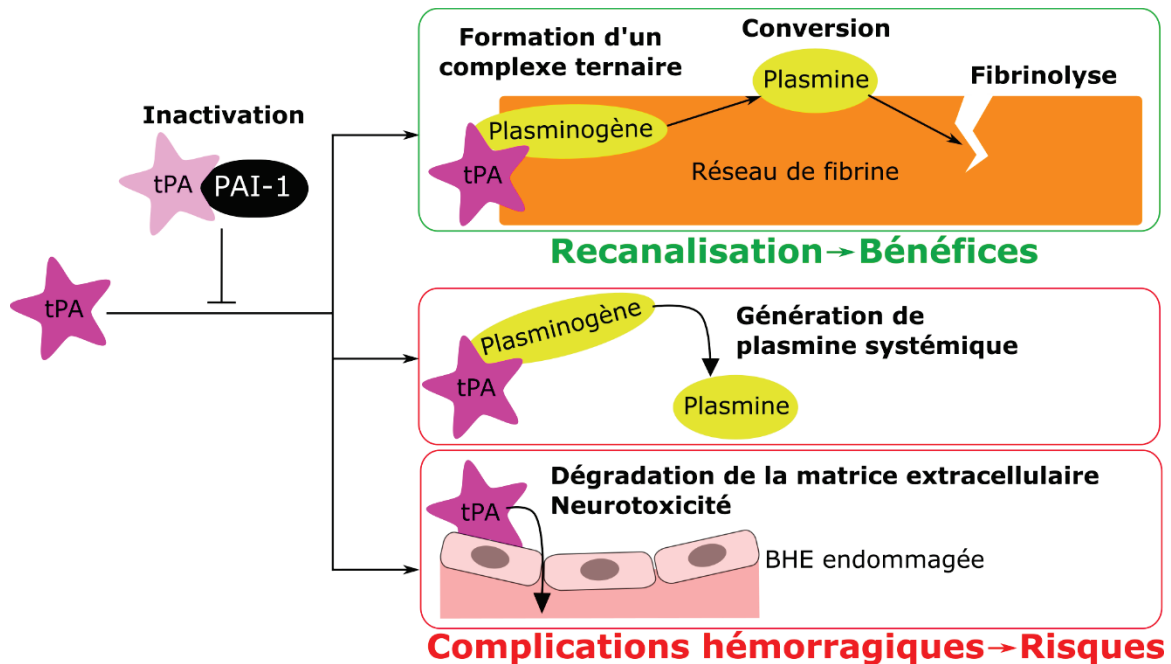


Figure 10. Action de l'activateur tissulaire du plasminogène sur un réseau de fibrine et effets délétères.

Le tPA forme un complexe cyclique ternaire avec le plasminogène lié et la fibrine ce qui permet la génération locale de plasmine. Le tPA peut générer, dans une moindre mesure, de la plasmine systémique, ce qui favorise les saignements. Les transformations hémorragiques intracrâniennes sont en partie liées à l'interaction du tPA avec les cellules de la BHE endommagée.

1.5.2.c. Évaluation du ratio bénéfices/risques

À cause du risque d’HIS, de nombreux critères sont analysés avant l’injection du rt-PA. L’hypertension artérielle, la concentration plaquettaire, des antécédents d’AVC ou de IM doivent être entre autres contrôlés avant de prendre la décision d’injecter l’actif [86]. L’imagerie du cerveau pour définir l’étendue du cœur et de la pénombre est un paramètre important. Le cœur s’étend en quelques heures seulement. Au vu des risques pris pour un bénéfice incertain, les recommandations préconisent donc de ne pas procéder à l’injection de rt-PA au-delà de 4 heures 30 après l’apparition des premiers symptômes en Europe (3 heures aux États-Unis) [78]. Finalement, le rt-PA est injecté à moins de 10% des patients [87]. Bien que les bénéfices soient directement corrélés au taux de recanalisation, le rt-PA présente de plus une efficacité limitée avec un taux de recanalisation < 50% [79, 88].

1.5.3. Vers un traitement plus sûr et plus efficace

La priorité clinique est de trouver des critères diagnostiques qui soient robustes pour prédire le ratio bénéfices/risques. Cette approche passe par l’amélioration des méthodes d’imagerie [83, 89]. En parallèle, des recherches portent sur la mise au point d’agents thrombolytiques plus sûrs et plus efficaces pour pouvoir agir vite et sur un grand nombre de patients. D’autres techniques de recanalisation sont également à l’étude.

1.5.3.a. Amélioration des actifs thrombolytiques

L’agent thrombolytique “idéal” devrait ; i) être facile à administrer, ii) présenter une grande efficacité locale, iii) n’être actif qu’au contact de la fibrine (fibrino-spécificité) donc ne pas perturber l’hémostase, iv) n’avoir aucun effet délétère sur la BHE et les neurones (n’avoir aucun effet toxique en général). Trois pistes ont été étudiées : modifier la structure des actifs existants, fonctionnaliser les actifs existants ou enfin développer de nouveaux actifs.

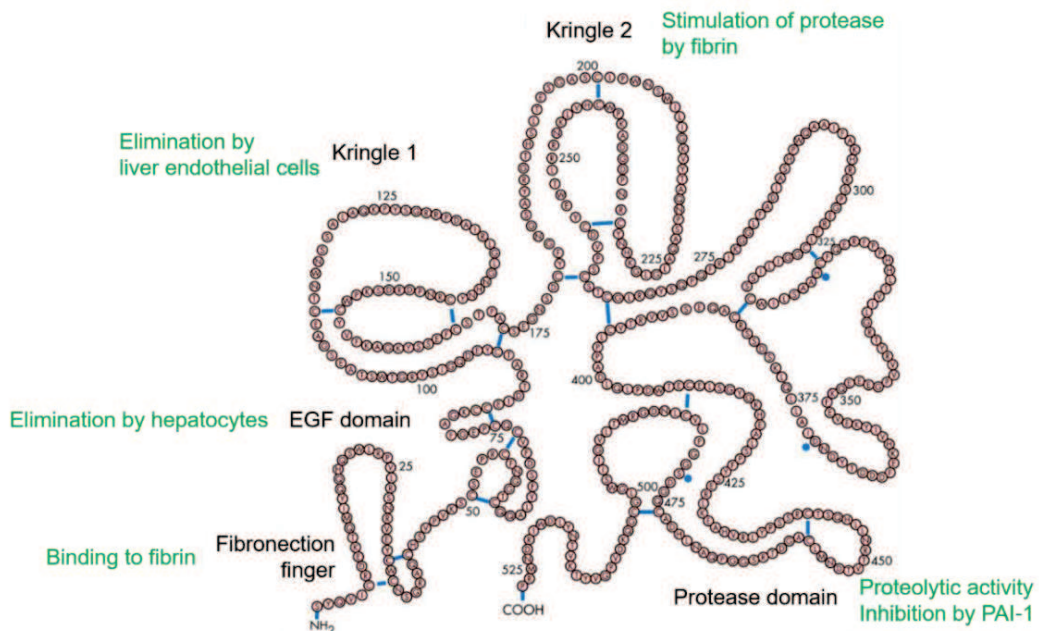


Figure 11. Structure et fonctions du rt-PA.

Le rt-PA est composé de 527 acides aminés subdivisés en 5 domaines (en noir). Leurs fonctions principales sont indiquées en vert. Notamment, le domaine fibronectine assure sa liaison avec la fibrine. Le domaine Kringle 2 participe à la stimulation de son activité enzymatique au contact de la fibrine. Adapté de [90, 91].

C'est dans cette optique que des formes tronquées ou modifiées du rt-PA, comme le Reteplase (rPA) et le Tenecteplase (TNKase), ont été mises au point. L'étude du lien entre la structure du rt-PA et certaines de ses fonctions a permis de synthétiser ces nouvelles formes [76, 90, 91]. Le rt-PA se compose de 5 domaines. Une illustration de ces domaines et de leurs fonctions dans le cadre de la fibrinolyse est présentée **Figure 11**. Le rPA et la TNKase présentent des temps de demi-vie plus longs que le rt-PA (15 et 24 minutes respectivement ; **Tableau 1**). Cette caractéristique permet leur administration en un ou deux bolus uniquement, contrairement au rt-PA injecté en un premier bolus suivi d'une perfusion. Ils répondent donc tous deux au premier critère car leur administration est simplifiée. Ils se différencient sur les autres critères. Le rPA et la TNKase n'ont pas la même affinité pour la fibrine ni la même réactivité. Le rPA n'a pas d'affinité de liaison pour la fibrine car il n'a pas de domaine fibronectine. Son activité protéolytique au contact de la fibrine est elle aussi altérée [90]. À l'inverse, la TNKase est légèrement plus fibrino-sélective que le rt-PA [92]. Concrètement, le rPA et la TNKase ont montré des résultats équivalents au rt-PA dans la prise en charge des IM en termes de mortalité à 30 jours [90]. La TNKase donne également des résultats préliminaires prometteurs pour la prise en charge des AVC ischémiques [93].

Une deuxième approche consiste à fonctionnaliser les actifs déjà existants. Une équipe a mené des études précliniques dès la fin des années 1980 en greffant sur le rt-PA ou sur l'UK des anticorps monoclonaux dirigés contre la fibrine ou contre les plaquettes [94-96]. Ce ciblage “moléculaire” a pour objectif d’augmenter l’efficacité thrombolytique en favorisant l’accumulation spécifique du rt-PA au thrombus. Ces études ont montré que de tels systèmes augmentaient l’efficacité thrombolytique dans des modèles de thrombose veineuse. De plus, le taux de fibrinogène plasmatique et les temps de saignements étaient moins affectés qu’avec l’injection de l’actif seul. Développer de telles stratégies de ciblage semble donc prometteur pour répondre aux problèmes d’efficacité. L’apport doit néanmoins être évalué en fonction des probables effets secondaires associés à une augmentation locale de l’actif au contact de la BHE.

Enfin, un autre agent extrait de salive de chauve-souris, le desmoteplase, a également été étudié. Il a une structure très proche de celle du rt-PA. Sa demi-vie est de 138 minutes [92]. Il présente une très forte fibrino-sélectivité et n’a pas d’effet excitotoxique [97]. Il répond ainsi à tous les critères du cahier des charges de l’agent thrombolytique “idéal”. Concrètement, après de premiers essais cliniques prometteurs, deux essais de phase III ont montré une augmentation du taux de recanalisation mais pas de bénéfice à 3 mois par rapport au groupe placebo [98]. Toutefois, l’administration pouvait avoir lieu jusqu’à 9 heures après les premiers symptômes, or les bénéfices potentiels diminuent rapidement au cours de l’ischémie. Il est à noter que dans ces essais la survenue d’HIS était équivalente au groupe placebo, ce qui est intéressant pour développer des traitements plus sûrs.

1.5.3.b. Autres méthodes de recanalisation

Méthodes endovasculaires

Après plusieurs essais cliniques, le retrait mécanique du thrombus, ou thrombectomie, est désormais recommandé pour les patients non éligibles au rt-PA ou en complément de l’injection de rt-PA pour les occlusions majeures des larges vaisseaux jusqu’à 6 heures après l’apparition des premiers symptômes [99].

Sonothrombolyse

Plusieurs essais menés depuis une dizaine années et revus par Rubiera et Alexandrov ont montré que l'application d'ultrasons associée ou non à l'injection de rt-PA et/ou de microbulles pouvaient être bénéfiques [100]. À certaines fréquences, les ultrasons fragiliseraient le thrombus et favoriseraient la pénétration du rt-PA. Les microbulles pourraient potentialiser ce phénomène par des méthodes de cavitation ; oscillation de la microstructure puis destruction sous ultrasons [101]. Les microbulles sont décrites en **section 2.2.4.**

Cette première partie a montré que la thrombose artérielle est majoritairement d'origine athérothrombotique. Le thrombus se développe d'abord sur la paroi suite à l'érosion ou, plus fréquemment, à la rupture d'une plaque. Ce processus peut également être influencé par des facteurs hémodynamiques (cas de l'AAA). Le thrombus peut provoquer une ischémie locale ou migrer dans une autre artère. Un large panel de récepteurs entre en jeu engendrant l'adhésion, l'activation et l'agrégation des plaquettes ainsi que la génération d'un réseau de fibrine subséquent. Malgré les progrès réalisés dans les techniques d'imagerie, la visualisation directe du thrombus reste un challenge. Pourtant, elle pourrait fournir des indications précieuses pour l'évaluation du ratio bénéfices/risques. L'injection IV de rt-PA reste la méthode standard pour le traitement non invasif de l'IM et de l'AVC ischémique dans les premières heures qui suivent l'accident, bien qu'elle soit associée à de forts risques hémorragiques. Mettre au point un traitement plus sûr et plus efficace est donc nécessaire. Les connaissances actuelles des mécanismes biologiques de la thrombose permettent d'envisager des stratégies personnalisées à la fois pour l'imagerie et pour le traitement. Une approche intéressante est de réaliser un ciblage moléculaire. Cette stratégie consiste à : i) identifier des molécules spécifiques de la pathologie, dites "biomarqueurs", ii) développer des ligands qui soient capables de les reconnaître et de s'y lier, iii) associer ces ligands à des agents de contraste ou des agents thrombolytiques. La nanomédecine permet de fournir les outils nécessaires pour y parvenir. La deuxième partie de l'état de l'art décrit les outils disponibles pour mettre au point des vecteurs fonctionnels.

2. Nanomédecine et vectorisation

2.1. Principe

La nanomédecine a émergé comme une solution pour concentrer, protéger et véhiculer les principes actifs à l'organe cible, autrement dit les “vectoriser”, en utilisant des nanoparticules comme vecteurs. Les preuves de concept ont d'abord été faites dans le domaine de l'oncologie, avec notamment l'autorisation du Doxil® par la FDA en 1995 [102]. L'utilisation de nanovecteurs a depuis connu un essor considérable dans le domaine cardiovasculaire [103, 104]. Les avantages des nanoparticules, illustrés **Figure 12**, sont principalement de :

- prévenir la dégradation des actifs par leurs inhibiteurs présents dans la circulation → *augmenter l'efficacité du traitement*,
- améliorer les caractéristiques physico-chimiques d'actifs toxiques ou mal acceptés → *limiter les effets systémiques et modifier les interactions avec la BHE*,
- combiner des agents de contraste et des agents thérapeutiques pour développer des plateformes dites “théranostiques” → *développer une médecine personnalisée*,
- favoriser l'accumulation des actifs sur un site spécifique en les associant par exemple à des ligands et profiter de la grande surface spécifique des nanoparticules → *augmenter l'efficacité et la spécificité du traitement*.

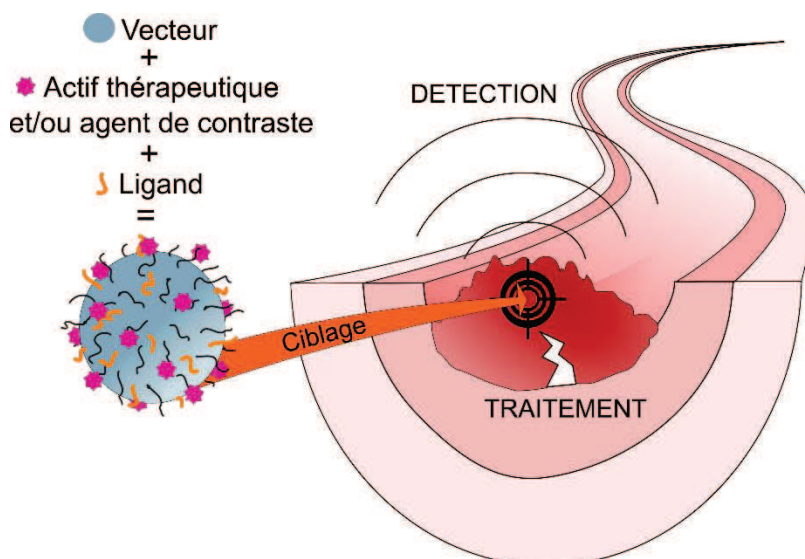


Figure 12. Principe de la vectorisation pour le diagnostic et le traitement de la thrombose.

2.2. Matériaux

De nombreux types de nanoparticules ont été synthétisés. La majorité des nanovecteurs publiés dans le cadre de la thrombose sont formulés à partir de nanoparticules lipidiques, inorganiques et polymères (**Figure 13**). Un autre type de structure, les microbulles, sera également détaillé, du fait de son potentiel theranostique.

Les matériaux qui forment ces nanoparticules doivent respecter plusieurs critères : i) être acceptés par l'organisme (biocompatibles), ii) être éliminés par voie naturelle (biodégradables) et iii) pouvoir être facilement modifiables avec des principes actifs ou des ligands pour acquérir des fonctions biologiques spécifiques (“fonctionnalisables”). Selon leur composition, des actifs hydrophobes ou hydrophiles peuvent y être incorporés ou associés en surface. Les propriétés physico-chimiques des vecteurs (taille, charge de surface, présence d'un revêtement...) vont affecter leur clairance et leur distribution dans l'organisme. Lors de l'injection d'un nanovecteur dans la circulation, la première voie d'élimination est l'assimilation par les macrophages. Un revêtement de polyéthylène glycol (PEG) a été largement utilisé sur les trois types de vecteurs afin de retarder ce processus et d'améliorer les propriétés pharmacocinétiques des matériaux [105, 106]. Le PEG est un composé hydrophile biocompatible et éliminé par les reins.

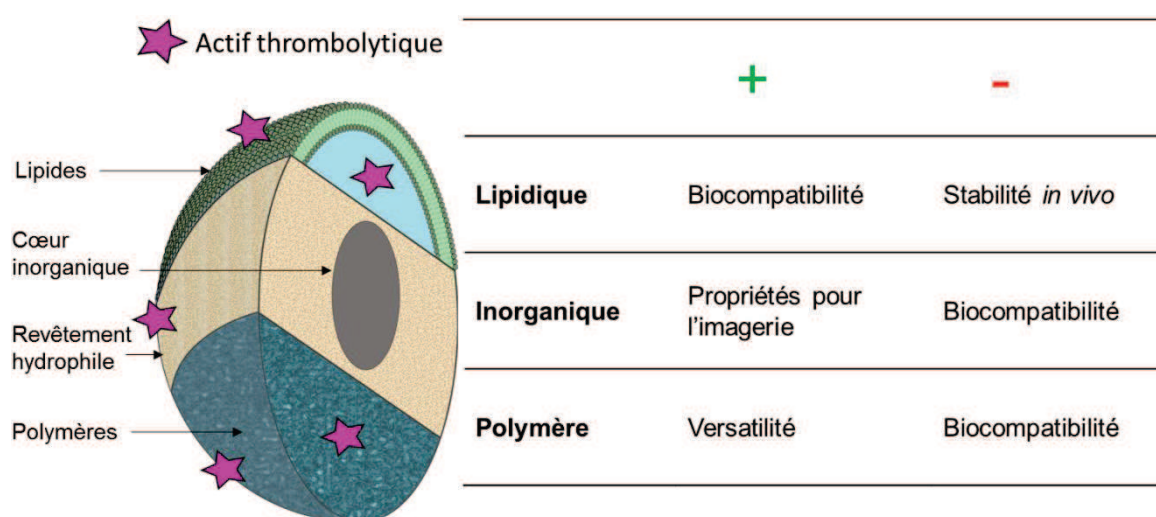


Figure 13. Principaux types de nanovecteurs mis au point pour la thrombolyse.
Les méthodes standards de chargement d'un actif thrombolytique, au cœur ou en surface de la nanoparticule, sont illustrées sur le schéma. Les matériaux sont décrits dans cette section. Des exemples de chaque type de vecteurs chargés en actif sont détaillés dans la **section 3.2**. Le tableau résume les principaux avantages et inconvénients liés aux trois types de nanoparticules.

2.2.1. Lipidiques

Les nanoparticules à base de lipides sont composées de molécules amphiphiles ; les phospholipides. Sous condition aqueuse, ces molécules s'organisent en structures telles que des micelles, des liposomes et des microémulsions [107]. Les liposomes présentent un cœur aqueux entouré d'une bicouche phospholipidique. Ils ont été les premières formulations approuvées en clinique ; avec le Doxil®, liposome PEGylé. Les nanoparticules lipidiques représentent un avantage significatif pour leur utilisation dans le domaine cardiovasculaire car elles sont non toxiques [108]. Toutefois certaines structures peuvent être fragiles et rapidement déstabilisées *in vivo* [109]. Selon le caractère hydrophobe ou hydrophile de l'agent thérapeutique ou de l'agent de contraste à charger, celui-ci peut par exemple être incorporé dans le cœur aqueux du liposome, ou dans sa bicouche phospholipidique (**Figure 13**).

2.2.2. Inorganiques

Ces nanoparticules sont composées d'un cœur inorganique, pouvant avoir des propriétés intéressantes pour l'imagerie, généralement revêtu d'une enveloppe polymère pour améliorer leur stabilité colloïdale et leur biocompatibilité (**Figure 13**).

En particulier, les nanoparticules magnétiques sont composées d'un cœur d'oxyde de fer paramagnétique. Le dextrane, un polysaccharide naturel, est un revêtement très utilisé pour la formulation des particules magnétiques [110]. Selon leur taille, les nanoparticules magnétiques sont divisées en deux catégories : les particules “ultrasmall” superparamagnétiques d’oxydes de fer (USPIO), de taille hydrodynamique inférieure à 50 nm et les particules superparamagnétiques d’oxydes de fer (SPIO), de taille hydrodynamique de 50 à quelques centaines de nanomètres. Elles ont la capacité d'influer sur leur environnement magnétique et peuvent ainsi être utilisées comme agent de contraste en IRM. Plusieurs générations d'USPIO ont été approuvées et testées en clinique depuis plus d'une quinzaine d'années. Les USPIO sont naturellement assimilés par les macrophages présents en nombre dans les plaques et dans les anévrismes [111, 112]. Leur utilisation dans le domaine de l'imagerie est détaillée par Cicha *et al.* [104] et dans l'**Annexe A-1**. Leurs capacités magnétiques peuvent également être mises à profit

pour la délivrance ciblée d'actif : l'application externe d'un aimant au niveau d'un vaisseau thrombosé peut promouvoir leur accumulation locale.

Les nanoparticules à cœur métallique, et notamment en or, constituent un second type de nanoparticules inorganiques utilisées pour l'imagerie de la thrombose. Elles sont particulièrement intéressantes pour l'imagerie CT car elles offrent des coefficients d'absorption des rayons X bien meilleurs que les composés à base d'iode utilisés en clinique [113]. Toutefois, leur toxicité est encore à l'étude et dépend de leurs caractéristiques physico-chimiques, comme leur taille et leur revêtement [114, 115].

Dans le cadre de leur utilisation pour du ciblage thérapeutique, les actifs sont en général greffés sur la couche externe des vecteurs inorganiques (**Figure 13**).

2.2.3. Polymères

Des monomères ainsi que des chaînes polymères synthétiques et naturelles ont également été utilisés dans la conception de nanostructures pour le traitement et le diagnostic de la thrombose. Selon le type de polymères, différentes techniques, telles que la nanoprecipitation, l'émulsion-polymérisation ou encore la gélification ionique permettent d'obtenir des nanoparticules [116]. Les caractéristiques de ces particules polymères, comme la taille, la porosité, l'hydrophobicité, la rigidité ou encore la présence de groupements fonctionnels peuvent être contrôlées par le type de polymère utilisé et par les paramètres de la synthèse. Elles sont extrêmement versatiles. L'utilisation de polymères biocompatibles et biodégradables doit être privilégiée (**Figure 13**). Le poly(acide lactique-co-glycolique) (PLGA), copolymère approuvé par la FDA et l'EMA pour des utilisations orales et sous-cutanées, et l'alcool polyvinyle (PVA) sont des polymères biodégradables largement étudiés pour la recherche nanomédicale [117].

Parmi les polymères naturels, les polysaccharides sont des polymères carbohydrates globalement composés d'unités monosaccharidiques (sucres) variées. Ces monosaccharides sont liés entre eux par des liaisons glycosidiques qui se forment entre 2 groupements hydroxyles. Ils sont abondamment présents à l'état naturel, par exemple dans la matrice extracellulaire. Du fait de leur biocompatibilité et de leur biodégradabilité, ils sont très utilisés dans la conception de biomatériaux et peuvent être

formulés sous forme de nanoparticules (**Annexe A-4**) [118]. Une structure de ces deux polysaccharides est montrée sur la figure **Figure 14**. Le dextrane est approuvé par la FDA et l'EMA pour son utilisation comme substitut plasmatique. Le pullulan, approuvé pour l'administration orale, est un additif alimentaire. Certains polysaccharides possèdent à la fois des propriétés structurelles et fonctionnelles. C'est le cas du chitosane et du fucoïdane qui présentent une affinité pour la fibrine et la P-selectine respectivement (**section 2.3**).

Dans les vecteurs polymères, les actifs peuvent être piégés dans la matrice polymère pendant la synthèse ou chargés en surface après synthèse (**Figure 13**).

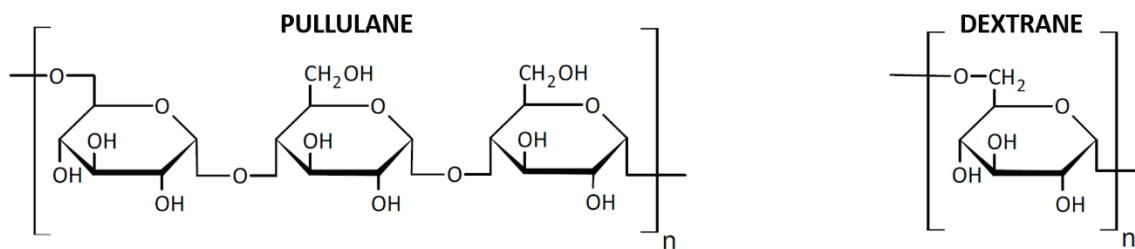


Figure 14. Structures du pullulan et du dextrane.

2.2.4. Microbulles

L'échographie de contraste a été développée dans les années 1990. Des microbulles gazeuses (1 - 5 µm) sont apparues comme de très bons agents de contraste en raison de leur forte différence d'impédance avec le sang et les tissus environnents. Des bulles d'air qui se dissolvent rapidement dans le sang ont d'abord été utilisées (première génération). Des microbulles de perfluorocarbone (PFC) gazeux plus stables ont été mises au point afin d'accroître le temps de circulation (deuxième génération) [119]. Ces types de systèmes sont stabilisés par une coque faite de lipides, de protéines ou de polymères. Aujourd'hui, au moins trois types de microbulles sont approuvés par la FDA : SonoVue® (Bracco), Definity® (Lantheus Medical Imaging) et Optison™ (GE Healthcare). Leur principale application est l'échocardiographie de contraste pour visualiser les frontières endocardiques du ventricule gauche et quantifier la perfusion myocardique. Certains PFC, comme le bromure de perfluorooctyle (PFOB), montrent également des propriétés échogènes ainsi qu'une grande stabilité sous leur forme liquide [120].

2.3. Biomarqueurs et ligands

La section précédente donne un aperçu des matériaux existants pour la formulation de nanoparticules. Ces nanoparticules servent de plateformes pour charger un agent de contraste et/ou un agent thrombolytique. Une des stratégies pour ensuite vectoriser ces agents est de charger les particules en ligands. Les plaquettes et la fibrine, qui sont les composants majoritaires du thrombus, sont les cibles à privilégier pour définir les biomarqueurs d'intérêt et leurs ligands.

2.3.1. Les plaquettes activées

Deux biomarqueurs vont être détaillés dans cette section : le complexe GpIIb/IIIa et la P-sélectine. Ils sont tous les deux exprimés sur les plaquettes uniquement dans leur état activé (voir **section 1.3.2**).

2.3.1.a. Le complexe GpIIb/IIIa

Expression dans le thrombus

La glycoprotéine GpIIb/IIIa, ou intégrine α IIb β III, est exprimée exclusivement par les plaquettes et change de conformation sur les plaquettes activées. Une plaquette présente environ 80 000 de ces molécules à sa surface [121].

Ligands

Le fibrinogène est le principal ligand de cette intégrine. Cette dernière fait partie d'une famille d'intégrines qui possèdent un site de reconnaissance du motif tripeptidiques RGD (L-Arginine/Glycine/Acide L-aspartique) [122]. La séquence RGD peut être modifiée pour être spécifique de l'intégrine cible, notamment par cyclisation (RGD cyclique) [123]. De cette façon, des antagonistes du complexe GpIIb/IIIa ont été mis au point et sont utilisés en clinique depuis de nombreuses années pour diminuer l'agrégabilité plaquettaire [124]. Les stratégies thérapeutiques élaborées à partir de peptides RGD modifiés sont nombreuses dans le domaine de la nanomédecine et des biomatériaux [125]. Des anticorps ont également été mis au point pour reconnaître et lier le complexe GpIIb/IIIa [126].

2.3.1.b. La P-sélectine plaquettaire

Expression dans le thrombus

La P-sélectine plaquettaire est fortement exprimée dans le thrombus, d'abord à l'interface endothélium-plaquettes puis dans le thrombus lui-même au fur et à mesure du recrutement plaquettaire (**Figure 3**). La P-sélectine est également exprimée par les cellules endothéliales. La densité plaquettaire est 10 fois plus élevée que la densité endothéliale avec environ 10 000 molécules de P-sélectine par plaquette stimulée [127].

Ligands

Pour comprendre les différents ligands possibles de la P-sélectine, il est nécessaire de donner quelques informations sur la famille des sélectines. La P-sélectine appartient à une famille de trois glycoprotéines transmembranaires ; la E-, la L- et la P-sélectine (E pour endothélium, L pour leucocyte et P pour plaquettes). La E-sélectine est exprimée par les cellules endothéliales activées, plusieurs heures après leur stimulation. La L-sélectine est exprimée sur tous les granulocytes et monocytes et sur la plupart des lymphocytes. Le site de liaison entre ces trois sélectines et leurs ligands naturels est le Sialyl Lewis X (SLex). Le SLex est un tétrasaccharide carbohydrate qui contient notamment des fucoses et des groupements sulfates [128]. D'autres groupements schématisés sur la **Figure 15** assurent la spécificité des interactions entre les sélectines et leurs ligands [129].

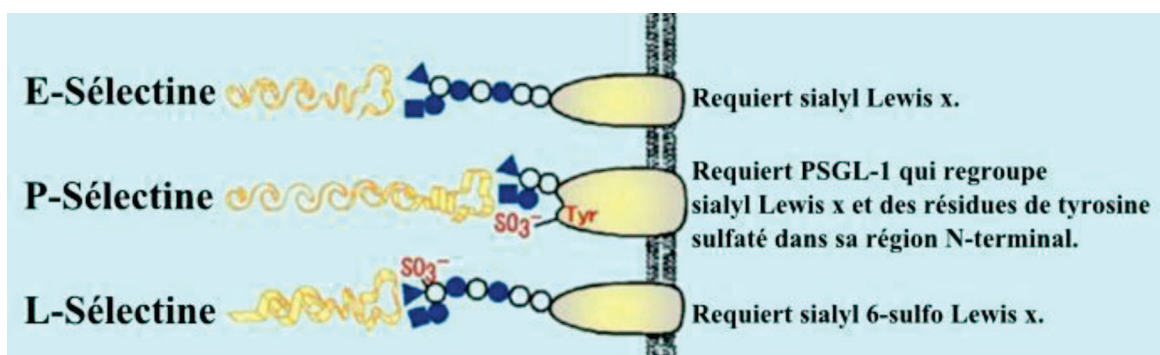


Figure 15. Spécificité des ligands des différentes sélectines.
Le site commun de liaison des trois sélectines sur leurs ligands est le Sialyl Lewis X. Adapté de [130].

Deux types de ligands de la P-sélectine ont été développés :

- *les ligands protéiques* (anticorps, peptides ou fragments peptidiques). En particulier un anticorps monoclonal, l'*inlacumab*, a été testé avec succès en essai clinique pour diminuer le risque de thrombose et d'inflammation après les interventions coronariennes invasives [131]. Son affinité pour la P-sélectine est de l'ordre du nanomolaire et est 3 000 fois plus importante que pour les sélectines E- et L- [132] (**Tableau 2**).

- *les ligands saccharidiques naturels ou synthétiques*. Le ligand principal de la P-sélectine est la glycoprotéine PSGL-1 exprimée sur la membrane des leucocytes. La reconnaissance implique le SLex et trois résidus de tyrosine sulfatés dans le squelette de la protéine [133] (**Figure 15**). Le PSGL-1 peut également lié la E-sélectine [133]. Outre le PSGL-1, des études ont montré que des composés synthétiques qui miment le SLex, ainsi que des oligosaccharides sulfatés et des polysaccharides sulfatés sont capables d'interagir avec la P-sélectine [134]. Dans le cadre de précédents travaux de l'équipe *Bio-ingénierie cardiovasculaire* du *LVTS*, les interactions de différents polysaccharides sulfatés de bas poids moléculaire (fucoïdane, héparine et dextrane sulfate) avec la P-sélectine ont été comparées. Il a ainsi été démontré par résonance plasmonique de surface que le fucoïdane : i) empêche la liaison de la P-sélectine au Sialyl Lewis X avec un IC₅₀ de 20 nM (contre 400 nM pour l'héparine et > 25 000 nM pour le dextrane sulfate), ii) présente une grande affinité de liaison pour la P-sélectine immobilisée avec une constante d'association de 1,2 nM, iii) forme un complexe avec la P-sélectine. De plus, il est démontré que le fucoïdane entre en compétition avec un anticorps anti-P-sélectine lors de l'interaction avec des plaquettes activées et que cette interaction dépend du niveau d'activation plaquettaire [135] (**Tableau 2**). Le fucoïdane interagit donc avec les plaquettes activées spécifiquement par la P-sélectine.

Ligand	Constante d'affinité	Avantages	Inconvénients	Réf.
Anticorps	~1 nM	Forte affinité Spécificité	Coût Risque immunogène	[132]
SLeX et analogues	~100 µM	Structure simple	Peu sélectif	[128]
PSGL-1	~300 nM	Bonne affinité Sélectivité	Coût Risque immunogène	[135]
Fucoïdane	~1 nM	Forte affinité Faible coût Sans risque immunogène	Sources multiples : relation structure-fonction non établie Spécificité	[135]

Tableau 2. Ligands potentiels de la P-sélectine.

De part sa constante d'affinité et son faible coût, le fucoïdane est donc un ligand très intéressant. Toutefois, deux paramètres majeurs sont à contrôler. Premièrement, il est difficile d'obtenir un fucoïdane standard et d'établir un lien structure-fonction en raison de la multiplicité des sources de fucoïdane. Ainsi, cette molécule peut être extraite de plus de 70 espèces d'algues brunes dont : *ascophyllum nodosum* et *fucus vesiculosus*. Elle se retrouve également chez des animaux marins invertébrés tels que les concombres de mer et les oursins [136]. Sa composition et sa structure chimique sont extrêmement variables d'une espèce à l'autre et dépendent même des conditions de croissance de l'espèce [137]. Une structure commune à tous les fucoïdanes est toutefois identifiée : ils sont composés de 50 à 90% de L-fucose, de 35 à 45% de sulfates et de moins de 8% d'acide uronique [138]. D'autres monosaccharides ont également été mis en évidence, comme le galactose et le mannose. Une structure simplifiée du fucoïdane est représentée sur la **Figure 16**. Outre la présence de fucoses et de sulfates, qui miment la structure du SLeX, l'incidence de sa composition en monosaccharides sur son affinité avec la P-sélectine n'est pas élucidée. Il a été démontré que modifier les proportions des différents composés a une influence sur son affinité pour la P-sélectine et sa biodistribution [63]. Il est donc important de connaître la source et les méthodes d'extraction du fucoïdane avant de l'utiliser. Deuxièmement, il a été rapporté que certains fucoïdanes interagissent également avec la L-sélectine [139]. La sélectivité de l'interaction fucoïdane/P-sélectine est donc à évaluer avant la conception de systèmes dirigés contre la P-sélectine.

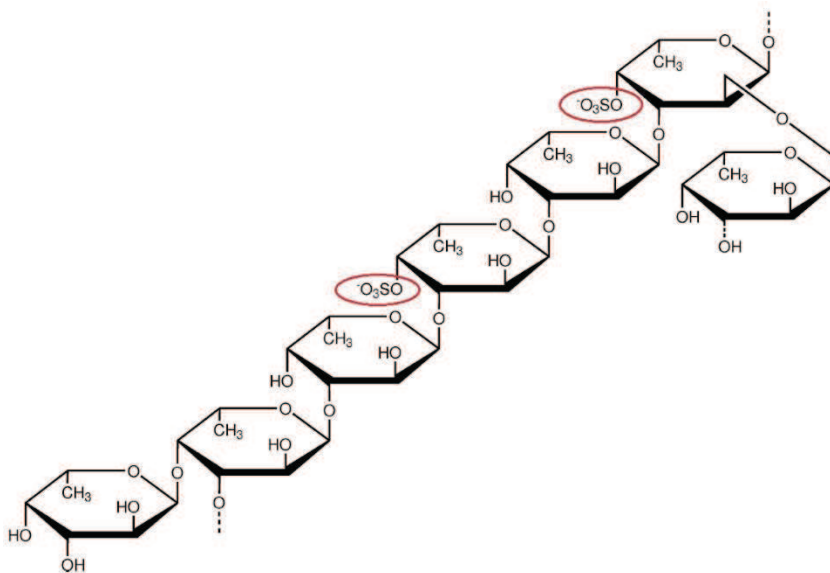


Figure 16. Structure simplifiée du fucoïdane.

Cette molécule est composée d'un enchaînement linéaire d'unités fucoses dont certaines présentent des groupements sulfates substitués (entourés en rouge). Des ramifications d'unité fucoses sont également décrites.

2.3.2. La fibrine

Les stratégies utilisées pour développer des systèmes dirigés contre la fibrine reposent principalement sur l'utilisation d'anticorps. Des composés naturels, comme la gélatine et le chitosane présentent également une affinité pour la fibrine et peuvent être intéressants dans la conception de nanosystèmes [118].

En conclusion, des ligands ont été mis en évidence pour cibler le complexe GpIIb/IIIa, la P-sélectine ou directement la fibrine. Ils peuvent être utilisés pour fonctionnaliser les vecteurs. Des nanovecteurs synthétisés à partir des matériaux décrits en **section 2.2** et ciblant les biomarqueurs détaillés en **section 2.3** ont été testé en préclinique. Ils vont maintenant être revus selon leur fonction : diagnostique, thérapeutique et théranostique.

3. Vecteurs testés en préclinique

Les modèles animaux les plus couramment utilisés pour évaluer la capacité des vecteurs pour l'imagerie moléculaire et le traitement de la thrombose sont :

- *des modèles de thrombose* :

La thrombose peut être induite chimiquement par apposition de thrombine ou de FeCl₃. Le FeCl₃ dénature l'endothélium entraînant une activation locale très importante. Elle peut également être obtenue mécaniquement, par exemple par ligature ou pincement [140].

Des modèles avec insertion d'un thrombus pré-formé *in vitro* à partir de sang humain ont aussi été décrits. Ces modèles sont en particulier utilisés pour tester l'efficacité des actifs thrombolytiques. Ce choix s'explique par le fait que chez les rongeurs le plasminogène est 10 fois moins sensible aux activateurs du plasminogène humain [141].

- *des modèles de pathologies dans lesquels une activation et une agrégation plaquettaire sont observées* :

- Ischémie-reperfusion du myocarde chez le rat: la perfusion myocardique est temporairement réduite pendant une période donnée par ligature. Ce modèle est surtout utilisé pour son aspect hautement inflammatoire, mais une activation endothéiale et plaquettaire est observée [142].
- AAA chez le rat : ce modèle est obtenu par perfusion d'élastase dans l'aorte. L'élastase dégrade l'élastine et un anévrisme se développe sur plusieurs semaines. Dans les modèles précliniques, l'injection régulière de la bactérie *Porphyromonas gingivalis* par IV permet de favoriser le développement d'un thrombus intraluminal [143].
- Souris ApoE-/- : les souris ApoE-/- sont des lignées déficientes en apolipoprotéine E qui développent des plaques riches en lipides. Une agrégation plaquettaire a été observée aux stades avancés [144].

3.1. Vecteurs pour l'imagerie moléculaire de la thrombose

Les systèmes développés pour l'imagerie moléculaire de l'athérosclérose et de la thrombose ont fait l'objet d'un chapitre de livre et d'une revue co-écrite et publiées pendant ma thèse :

- Annexe A-1 : Nanotheranostics in cardiovascular diseases, Chapitre du livre : Nanotheranostics for Personalized Medicine, 2016 Jan. World Scientific Publishing, Singapore, and Imperial College Press, London. Couvreur P, Mura S
Juenet M, Varna M, Chauvierre C, Letourneur D

Ce chapitre de livre décrit le fonctionnement des différentes modalités d'imageries et les agents de contraste associés. Il détaille ensuite les nano et micro vecteurs développés pour l'imagerie moléculaire de la plaque et du thrombus. Les systèmes y sont classés par type : lipidique, inorganique et polymère.

- Annexe A-2 : Nanomedicine for the molecular diagnosis of cardiovascular pathologies. Biochem Biophys Res Commun. 2015 Dec; 468(3)
Juenet M, Varna M, Aid-Launais R, Chauvierre C, Letourneur D

Cette revue détaille les nanovecteurs mis au point pour le diagnostic moléculaire de la plaque et du thrombus par IRM, scintigraphie et CT. Les systèmes y sont classés par type d'agents de contraste incorporé.

Le **Tableau 3** propose un récapitulatif des systèmes développés pour les biomarqueurs identifiés précédemment.

Les systèmes mis au point pour cibler la fibrine sont fonctionnalisés avec des séquences peptidiques ou des anticorps monoclonaux. L'équipe de Kim *et al.* a notamment synthétisé des particules d'or recouvertes de chitosane glycol et les a fonctionnalisées en surface avec un peptide [145]. Dès 5 minutes après injection, une prise de contraste locale est visible par micro-CT. Ce signal est corrélé avec le contenu en fibrine du thrombus. Néanmoins, la cytotoxicité de ces systèmes reste importante. Ainsi, des tests *in vitro* démontrent que ces particules ont un effet délétère sur la viabilité de cellules en culture à partir de 50 µg/mL. La concentration d'injection nécessaire pour une

prise de contraste est de 120 mg Au/kg, correspondant à une concentration de 1500 µg/mL dans la circulation, donc bien supérieure à la valeur seuil définie *in vitro* (estimation pour une souris de 25 g et un volume sanguin de 2 mL).

Les systèmes développés pour l'imagerie moléculaire du récepteur GpIIb/IIIa consistent en des microbulles chargées en surface avec des séquences peptidiques ou des anticorps pour l'échographie de contraste. L'équipe de Bin *et al.* a testé de tels systèmes dans plusieurs modèles [144, 146, 147], et a notamment démontré une corrélation entre la sévérité de la lésion d'athérome et l'expression de GpIIb/IIIa chez les souris ApoE-/- [144].

Enfin, plusieurs systèmes ont été développés contre la P-sélectine pour l'IRM, l'échographie de contraste (US) et la TEMP. Les moyens de ciblage sont variés : anticorps, PSGL-1 ou Sialyl Lewis X, et fucoïdane [148-154]. Des modèles qui présentent à la fois une activation endothéliale et une activation plaquettaire, comme l'AAA chez le rat ou le modèle d'ischémie-reperfusion myocardique, ont été utilisés. En particulier, les systèmes développés à partir de fucoïdane sont illustrés en **Figure 17**. Une prise de contraste au niveau d'un AAA est visible en IRM dès 15 minutes après l'injection d'USPIO recouverts de dextrane sur lequel est greffé du fucoïdane [152]. Des microparticules dextrane-pullulane contenant du fucoïdane et renfermant des USPIO montrent des résultats similaires [153]. Ces microparticules permettent également de détecter l'AAA par TEMP dès 30 minutes après injection. La structure polymère est dans ce cas marquée au ^{99m}Tc [154]. Dans ces trois études, la colocalisation entre l'accumulation des systèmes et le thrombus intraluminal exprimant la P-sélectine est validée par des coupes histologiques après explantation de l'anévrisme [152-154].

Ces études précliniques démontrent la faisabilité de l'utilisation de la nanomédecine pour détecter la pathologie thrombotique dans des modèles variés. De tels systèmes sont prometteurs pour quantifier l'état d'avancement de la pathologie et son contenu en fibrine et/ou en plaquettes et ainsi fournir des informations complémentaires aux méthodes d'imagerie standards.

Cible	Agent de ciblage	Vecteur <i>Revêtement</i>	Modalité d'imagerie	Modèle animal	Réf.
Fibrine	Anticorps monoclonal	Émulsion PFC	IRM	Thrombus induit par thrombine	[145]
	Peptide	Cœur magnétique <i>Dextrane</i>	IRM	Ischémie/reperfusion	[155]
	Peptide	Or <i>Chitosane glycol</i>	CT	Thrombus induit au FeCl ₃ ou pré-formé <i>in vitro</i>	[156, 157]
GpIIb/IIIa	Peptide RGD	Microbulle <i>Lipides</i>	US	Thrombus induit à l'acide arachidonique	[146]
	Peptide RGD	Microbulle <i>Lipides</i>	US	AAA	[147]
	Peptide RGD	Microbulle <i>Lipides</i>	US	Souris ApoE-/-	[144]
P-sélectine	Anticorps	Cœur magnétique <i>Polyuréthane</i>	IRM	Souris ApoE-/-	[148]
	Anticorps	Microbulle <i>Lipides</i>	US	Souris ApoE-/-	[149]
	SLeX	Microbulle <i>Lipides</i>	US	Ischémie/reperfusion	[150]
	PSGL-1 et anticorps	Microbulle <i>Lipides</i>	US	Ischémie/reperfusion	[151]
	Fucoïdane	Cœur magnétique <i>Dextrane</i>	IRM	AAA	[152]
	Fucoïdane	Dextrane-Pullulane	IRM	AAA	[153]
	Fucoïdane	Dextrane-Pullulane	TEMP	AAA	[154]

Tableau 3. Exemples de vecteurs testés dans des modèles précliniques pour l'imagerie de la thrombose et classés selon leur cible moléculaire.

Type de plateforme : jaune = lipidique ; vert = inorganique ; bleu = polymère.
US = échographie de contraste.

3.2. Vecteurs pour la thrombolyse

Les nanovecteurs mis au point pour la thrombolyse ont fait l'objet d'un article de revue co-écrit et publié pendant ma thèse :

- Annexe A-3 : Nanomedicine as a strategy to fight thrombotic diseases. Future Science OA, 2015 Nov. 1;1(4)

Varna M, Juenet M, Bayles R, Mazighi M, Chauvierre C, Letourneur D

Réédité comme chapitre du livre : Handbook of Clinical Nanomedicine: From Bench to Bedside, 2016. Pan Stanford Publishing, Singapore. Bawa R, Audette G and Rubinstein I

Les systèmes y sont classés par type d'agent thrombolytique chargé : SK, UK et tPA.

Ces systèmes sont également décrits dans la deuxième partie de l'Annexe A-1 et classés par type ; lipidique, inorganique et polymère.

Le **Tableau 4** offre un récapitulatif des systèmes incorporant un actif thrombolytique en fonction de la stratégie de ciblage. Quatre stratégies principales y sont décrites :

- *sans ciblage* : systèmes synthétisés dans le but d'augmenter le temps de circulation des actifs sans ciblage actif.
- *ciblage physique* : par application externe d'un aimant.
- *ciblage moléculaire* : avec fonctionnalisation par un ligand.
- *combinaison avec l'application locale d'ultrasons* : pour perturber la structure du thrombus et/ou du vecteur.

Ces études sont assez difficiles à homogénéiser du fait de la multiplicité des modèles et des différents actifs utilisés. La dose de vecteur injectée est normalisée en termes de masse d'actif thrombolytique chargé ou d'activité protéolytique chargée exprimée en unité internationale (UI). L'activité protéolytique de l'enzyme est généralement mesurée *in vitro* par une méthode chromogénique où l'actif est mis au contact d'un substrat qu'il est capable de cliver. Le produit de clivage est coloré et/ou fluorescent. La cinétique de formation de ce produit renseigne sur l'activité enzymatique de l'actif thrombolytique, appelée activité amidolytique.

3.2.1. Sans ciblage

Les premières études ont consisté à encapsuler un agent thrombolytique dans des nanostructures, pour la plupart recouvertes de PEG, dans le but d'augmenter le temps de circulation de l'actif dans l'organisme (première partie **Tableau 4**) [158-161]. Leach *et al.* ont encapsulé de la SK dans un mélange PVA-PEG et ont testé cette formulation dans plusieurs modèles [158-160]. Dans ces études, le temps de reperfusion est significativement diminué dans un modèle de thrombose artérielle coronarienne chez le chien par rapport à l'injection de SK seule et une réduction de la taille de l'infarctus est observée [159]. Une autre étude a montré que le temps de demi-vie du rtPA chargé dans les liposomes-PEG est multiplié par 21 par rapport à l'actif seul [161]. Plus récemment, Jin *et al.* ont piégé de l'UK dans des nanoparticules de chitosane réticulé avec une efficacité d'encapsulation de 95%. *In vivo*, l'activité de l'UK dans le sang décroît rapidement, tandis que celle de l'UK associée aux NPs est retrouvée jusqu'à plusieurs heures après injection [162]. Ces études justifient le rationnel de l'association de l'actif avec un nanovecteur furtif pour augmenter son temps de circulation et ainsi permettre son injection en bolus.

Une approche originale est celle de Korin *et al.* qui ont formulé des nanoparticules de PLGA de 180 nm assemblées en microagrégats ($3,8 \pm 1,6 \mu\text{m}$) sur lesquelles ils ont greffé du rt-PA par liaison biotine-streptavidine [163]. Au niveau d'un thrombus, la contrainte de cisaillement peut être plus de 100 fois plus élevée que dans une artère saine. Cette observation est mise à profit pour contraindre les microagrégats à se désolidariser au niveau du thrombus et permettre au rt-PA d'agir localement. Cette hypothèse est testée dans un modèle de thrombose occlusive au FeCl_3 sur une artère mésentérique. Les microagrégats sont injectés pendant la formation du thrombus (8 minutes après induction). Une dissociation locale des microagrégats sous contraintes de cisaillement élevées et une interaction des nanoparticules avec le thrombus sont effectivement observées. Ce procédé permet d'augmenter significativement le temps à l'occlusion par rapport au rt-PA seul ou à l'injection de nanoparticules PLGA chargées en rt-PA mais pré-dissociées.

Stratégie	Vecteur Revêtement	Actif	Chargement	Thrombus	Dose	Temps	Réf.
Sans ciblage	PVA PEG	SK	Piégeage	Induit par thrombine	240 000 UI	240 min	[158-160]
	Liposomes PEG	rt-PA	Encapsulation	-	-	-	[161]
	PLGA	rt-PA	Lien covalent	Induit par FeCl ₃	0,02 mg/kg	Temps jusqu'à l'occlusion	[163]
	Chitosane	UK	Piégeage	Induit par thrombine	100 000 UI	-	[162]
Ciblage physique	Cœur magnétique différents polymères	rt-PA	Lien covalent	Pré-formé <i>in vitro</i>	0,2 mg/kg	75 min 120 min 25 min 60 min	[164] [165] [166] [167]
	Cœur magnétique PEG	rt-PA	Lien covalent	Insertion d'un stent	0,38 mg /porc	-	[168]
	Cœur magnétique Dextrane	UK	Lien covalent	Induction mécanique	50 000 – 15 000 UI	30 min	[169]
Ciblage moléculaire de :							
Fibrine	Émulsion PFC	UK	Lien covalent	Induction électrique	NC	120 min	[170]
FXIIIa	Cœur magnétique Dextrane/PEG	rt-PA	Lien covalent	Pré-formé <i>in vitro</i>	0,1 – 0,5 mg/kg	60 min	[171]
GpIIb/IIIa	Liposome	SK	Encapsulation	Pré-formé <i>in vitro</i>	15 000 UI/kg	30 min 60 min	[172]
	Liposome PEG	rt-PA	Encapsulation	Induit par FeCl ₃	1 mg/kg	480 min	[173]
Combinaison à des ultrasons	Liposomes	rt-PA	Encapsulation	Induction mécanique + thrombine	0,2 mg /lapin	16 min	[174, 175]
	Émulsion PFC	rt-PA	Encapsulation	Induction mécanique + électrique	27 500 UI/kg	0 → 90 min	[176]
	Gélatine PEG	rt-PA	Piégeage	Induction mécanique	0,45 – 0,22 mg/kg	30 min 60 min	[177, 178]

Tableau 4. Exemples de vecteurs testés dans des modèles précliniques pour la thrombolyse et classés selon les stratégies de ciblage.

Type de plateforme : bleu = polymères ; jaune = lipidiques ; vert = inorganique. NC = non communiqué. Le critère La colonne Temps indique le temps auquel la quantification de l'efficacité de thrombolyse a été effectuée après injection.

3.2.2. Ciblage physique

Plusieurs équipes ont travaillé sur des nanoparticules magnétiques fonctionnalisées en surface avec un actif thrombolytique greffé de manière covalente (deuxième partie **Tableau 4**). L'application d'un aimant le long du vaisseau occlus a pour objectif d'accumuler les nanoparticules à l'endroit de la thrombose et de réduire ainsi considérablement les effets secondaires liés à l'actif. Le lien covalent se fait en général par la réaction classique d'EDC/NHS par le groupement terminal NH₂ du rt-PA et des groupements carboxyles à la surface des nanoparticules (EDC = 1-éthyl-3-(3-diméthylaminopropyl)carbodiimide, NHS = N-hydroxysuccinimide) [179]. Ce couplage covalent est plus sûr que le couplage biotine/streptavidine du fait de l'immunogénicité de la streptavidine [180]. Toutefois, une liaison covalente par le NH₂ terminal du domaine fibronectine du rt-PA pourrait affecter son affinité pour la fibrine et potentiellement diminuer son activité protéolytique au contact du thrombus (voir **section 1.5.3.a** et **Figure 11**). Dans le but de greffer covalemment l'actif thrombolytique, une équipe a formulé des nanoparticules magnétiques avec différents revêtement de polymères dont du chitosane [164-167]. Ces nanoparticules ont ensuite été testées dans un même modèle. Le thrombus y est pré-formé *in vitro* à partir de sang humain et inséré dans l'artère iliaque. Les nanoparticules induisent une réduction significative de la thrombose et une recanalisation à environ 20% de la dose recommandée chez l'Homme, ce sur des temps relativement courts : de 25 à 120 minutes après injection.

Cette stratégie permet donc ; i) d'accumuler l'actif au thrombus et ainsi de diminuer la dose injectée, ii) d'éviter un possible effet de l'actif sur des thrombus hémostatiques localisés à un autre endroit du corps. En revanche, cette méthode semble complexe à implémenter en clinique au vu des contraintes liées à la pénétration du champ magnétique dans le corps pour atteindre des artères profondes comme les artères cérébrales. Elle implique également de connaître avec précision la localisation de l'occlusion. De plus dans le cadre des AVC, l'application du champ externe pourrait favoriser la pénétration des nanoparticules à travers la BHE.

3.2.3. Ciblage moléculaire

À notre connaissance, toutes les stratégies de ciblage moléculaire qui ont été développées utilisent des anticorps ou des peptides greffés à la surface des nanoparticules (troisième partie **Tableau 4**). Des nanovecteurs dirigés contre des éléments de la coagulation (fibrine et FXIIIa) et associés à un agent thrombolytique ont été mis au point. Des observations par microscopie intravitaire après injection de ces nanoparticules fluorescentes ont démontré que les nanoparticules ciblées s'accumulent davantage au niveau du thrombus, et en particulier à sa périphérie, en comparaison aux mêmes nanoparticules non ciblées [170, 171]. La microscopie intravitaire est une méthode de microscopie à fluorescence où des fluorophores sont directement injectés dans la circulation pour marquer certaines cellules (plaquettes, leucocytes, ...). Les vaisseaux sont ensuite exposés et visualisés en temps réel sous le microscope. L'efficacité thrombolytique des nanoparticules dirigées contre le FXIIIa a été évaluée comme équivalente à celle du rt-PA seul [171]. Ces études confirment la possibilité de réaliser un ciblage moléculaire du réseau de fibrine pour favoriser l'accumulation locale des actifs. Des expériences complémentaires sur l'efficacité de ces nanoparticules doivent être menées.

D'autres particules ont été synthétisées avec des peptides RGD ou des anticorps en surface pour lier les plaquettes via leur récepteur GpIIb/IIIa [172, 173, 181, 182]. L'encapsulation de rt-PA dans des liposomes fonctionnalisés a par exemple permis d'augmenter son efficacité. L'affinité des liposomes-RGD pour les plaquettes activées a au préalable été comparée à celle des mêmes liposomes non ciblés en incubant ces systèmes marqués en fluorescence avec des thrombus formés *in vitro* puis en mesurant la fluorescence liée au thrombus [173].

Ces études montrent que les systèmes fonctionnalisés avec un agent de ciblage et un actif peuvent induire une meilleure recanalisation en s'accumulant sur le thrombus. La P-sélectine n'a pas été étudiée dans le cadre de la thrombolyse ciblée.

3.2.4. Association à des ultrasons

L'injection simultanée de rt-PA et de microbulles est déjà à l'étude en clinique (**section 1.5.3.b**). Plusieurs équipes ont mis au point des systèmes chargés en rt-PA et ont observé leurs effets associés à l'application locale d'ultrasons dans des modèles précliniques. Les ultrasons ne sont pas utilisés ici pour l'imagerie mais à des fréquences spécifiques afin d'induire une détérioration des vecteurs et du thrombus. En particulier, des liposomes échogènes constitués d'une bicouche phospholipidique renfermant à la fois du gaz et du liquide ont été étudiés. Combiner les liposomes chargés de rt-PA aux ultrasons a permis d'augmenter le taux recanalisation par rapport aux liposomes chargés mais sans ultrasons [174, 175]. Uesugi *et al.* ont chargé du rt-PA dans un réseau de gélatine réticulée ioniquement. Ce mode de chargement a permis d'augmenter environ 3 fois la demi-vie de l'actif. Afin d'induire la thrombolyse, des ultrasons ont été appliqués pendant 60 minutes. Une recanalisation complète a été observée, potentiellement liée à la dissociation de la gélatine et aux effets des ultrasons sur le thrombus. Des résultats similaires ont été obtenus chez le porc après occlusion d'une artère coronaire [177, 178].

3.3. Vecteurs théranostiques

L'échographie est également une modalité intéressante pour le développement de systèmes théranostiques afin de visualiser en temps réel l'efficacité de la thrombolyse. Wang *et al.* ont ainsi greffé du rt-PA à la surface de microbulles-RGD échogènes (**Tableau 5**) [181]. Ils ont d'abord montré *in vitro* que les microbulles-RGD interagissent avec des agrégats plaquettaires activés. Une prise de contraste est observée avec les microbulles ciblées dans un modèle de thrombus carotidien chez la souris. Ce contraste diminue sur 45 minutes lorsque les microbulles ciblées sont chargées en rt-PA. La diminution du contraste est corrélée à la lyse du thrombus.

Un autre exemple de vecteur consiste en une nanoparticule magnétique renfermant du rt-PA et sur laquelle sont greffés des peptides RGD. L'effet du rt-PA vectorisé sur le thrombus est imposé par IRM. Les images confirment que les nanoparticules s'accumulent aux bords du thrombus et que le rt-PA est capable de lyser ce dernier [182].

Cible	Vecteur <i>Revêtement</i>	Modalité d'imagerie	Actif	Modèle animal	Réf.
GpIIb/IIIa	Microbulles <i>Lipides</i>	US	UK	Thrombus induit par FeCl ₃	[126, 181]
	Cœur magnétique <i>PLGA/Chitosane</i>	IRM	rt-PA	Thrombus induit par FeCl ₃	[182]

Tableau 5. Exemples de vecteurs testés dans des modèles précliniques pour la thrombolyse ciblé et l'imagerie moléculaire de la thrombose.

Type de plateforme : bleu = polymères ; jaune = lipidiques ; vert = inorganique.

Peu de systèmes théranostiques ont été testés *in vivo* jusqu'à présent. Cet aspect va sans nul doute être de plus en plus étudié au vu de la multiplicité et de la versatilité des vecteurs proposés dans la littérature.

4. Stratégie du projet

L'objectif principal de cette thèse est de développer un vecteur pour la thrombolyse. Dans le but de réaliser une injection simple sans avoir besoin de l'application d'un aimant ou d'un échographe, la stratégie par ciblage moléculaire semble la plus prometteuse. De plus, elle permet potentiellement d'associer un agent de contraste aux vecteurs développés pour en faire des systèmes théranostiques. Cette approche a donc été choisie dans ce projet. La stratégie a été établie en tenant compte des trois paramètres suivants :

- Le *biomarqueur* doit être fortement exprimé et spécifique de la pathologie,
- Le *ligand* choisi doit présenter une affinité très importante pour le biomarqueur et en être spécifique,
- Le *vecteur* doit être biocompatible, biodégradable, fonctionnalisable avec un ligand et des actifs.

4.1. Biomarqueur

La P-sélectine. En particulier, le couple P-sélectine/fucoïdane est choisi du fait des avantages décrits dans la **section 2.3.1.b.** Le choix de cibler la P-sélectine peut être discutable du fait qu'elle soit aussi exprimée par les cellules endothéliales activées et n'est donc pas spécifique du thrombus. Néanmoins ces cellules endothéliales activées vont justement se trouver au niveau des plaques vulnérables et des zones ischémiques qui sont susceptibles d'être le foyer de thrombose. De plus, comme souligné précédemment, la densité de P-sélectine plaquettaire est supérieure à la densité endothéliale. Enfin, le ciblage de la P-sélectine n'a pas, à notre connaissance, été exploré pour améliorer l'efficacité thrombolytique.

4.2. Ligand

Le fucoïdane. De précédents travaux menés au sein de l'équipe *Bioingénierie cardiovasculaire* ont déjà montré le potentiel du fucoïdane seul ou inclus dans des nano ou microstructures pour l'imagerie moléculaire de pathologies thrombotiques *in vivo*. Les résultats ont été détaillés en **section 1.4.2.b** et **section 3.1/Tableau 3** et sont illustrés sur la **Figure 17**. Une attention particulière est portée au sein de notre laboratoire pour utiliser des lots de fucoïdane caractérisés au mieux et proches les uns des autres. L'équipe *Bio-ingénierie cardiovasculaire* a monté un laboratoire commun *FucoChem* avec la société Algues&Mer qui exploite l'espèce d'algues brunes *Aschophyllum nodosum* et assure l'extraction et la purification du fucoïdane. Afin d'évaluer l'affinité des vecteurs développés pour les sélectines, un test d'adhésion en flux est mis en place. Il est décrit dans le **projet expérimental 1** présenté dans ce manuscrit.

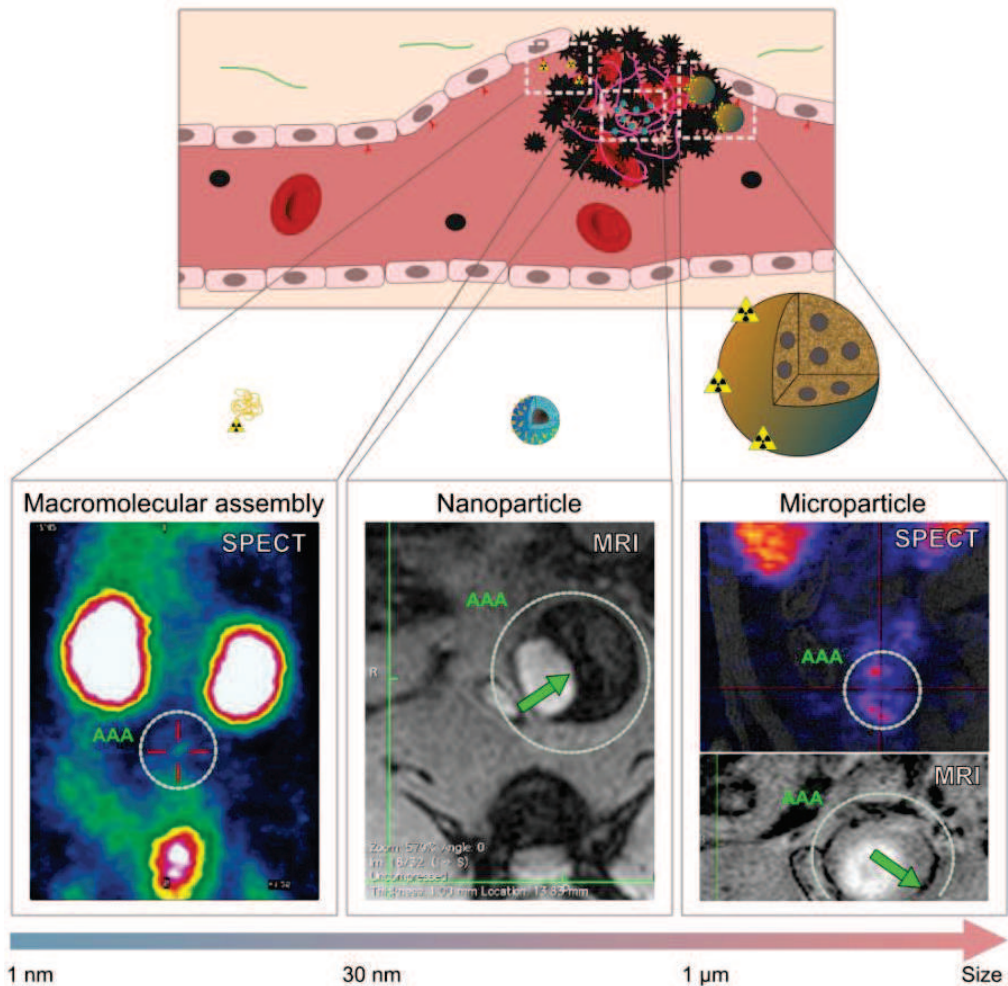


Figure 17. Formulations utilisant du fucoidane testées dans des modèles précliniques d'anévrisme de l'aorte abdominale pour l'imagerie moléculaire.

Toutes les images ont été prises dans des modèles d'AAA chez le rat. De gauche à droite ; système macromoléculaire composé de ^{99m}Tc -fucoidane pour la TEMP ; USPIO revêtu de dextrane et fonctionnalisé en surface avec du fucoidane pour l'IRM ; microparticules pullulane-dextrane incorporant du fucoidane radiomarquée avec du ^{99m}Tc pour la TEMP ou renfermant des USPIOS pour l'IRM.

4.3. Vecteurs

Vecteurs polymères, à condition de privilégier des matériaux biocompatibles et biodégradables. Le choix se porte sur des particules polymères pour leur versatilité et pour leur capacité à intégrer le fucoidane, qui est un polysaccharide. Plusieurs méthodes ont été décrites pour formuler des particules qui présentent des polysaccharides en surface [118, 183]. Ces méthodes de synthèse sont intéressantes pour favoriser le rôle du fucoidane. Deux d'entre elles vont être étudiées.

4.3.1. Polymérisation radicalaire en milieu oxydo-réducteur

Des nanoparticules copolymères formées d'un cœur de poly(cyanoacrylate d'alkyle) (PACA) et d'une couronne de polysaccharides ont été formulées par une méthode de copolymérisation radicalaire en milieu redox et apparaissent comme de bons vecteurs potentiels [184]. Les PACA sont des polymères obtenus à partir de monomères de cyanoacrylate d'alkyle. Certains monomères de cette famille sont utilisés comme colle chirurgicale. Des nanoparticules formulées à partir de monomères à longue chaîne alkyle, comme le cyanoacrylate d'isobutyle (IBCA), ont été étudiées depuis les années 1980 [185]. Une formulation basée sur un monomère proche est actuellement en essai clinique de phase III pour le traitement de l'hépatocarcinome [186].

D'un point de vue physico-chimique, les nanoparticules cœur-couronne présentent les avantages ; i) d'être bien caractérisées, ii) d'avoir une couronne hydrophile de polysaccharide pour le chargement de l'actif thrombolytique, iii) de pouvoir incorporer le fucoïdane dans cette couronne, iv) d'avoir un cœur hydrophobe qui peut être chargé avec un agent de contraste pour créer un système théranostique. D'un point de vue biologique, la compatibilité et la dégradabilité de tels systèmes doivent être discutées. La principale voie de dégradation *in vivo* est la dégradation enzymatique par des estérases en acide poly(cyanoacrylique) soluble qui peut être éliminé par voie rénale [185]. Ces phénomènes se produisent en quelques heures [187]. Les PACA ont donc été qualifiés de « bioérodibles » et seraient compatibles avec une utilisation pour le domaine cardiovasculaire [184]. Certaines formulations de nanoparticules cœur-couronne peuvent toutefois présenter une cytocompatibilité limitée et un temps de circulation court. Le mécanisme d'émulsion-polymérisation radicalaire en conditions oxydantes (redox radical emulsion polymerization RREP) est justement privilégié dans l'optique d'augmenter la compatibilité et la furtivité des nanoparticules. Ce mécanisme repose sur la création d'un radical libre à une extrémité de la chaîne polysaccharidique par oxydation avec des ions de cérium (IV) dans des conditions acides (pH 1). Le couple polysaccharide-cérium (IV) initie une polymérisation en chaîne du monomère en créant un copolymère di-bloc amphiphile linéaire [183]. Dans des conditions aqueuses, les copolymères s'assemblent en nanoparticules avec un noyau PACA hydrophobe recouvert d'une coque de

polysaccharide (**Figure 18**). Des études ont montré que, parmi les différentes méthodes de synthèse existantes, le RREP favorisait l'obtention de nanoparticules associées à une faible activation du complément et un long temps de circulation [188]. De plus, les polysaccharides adoptent une configuration en peigne [189].

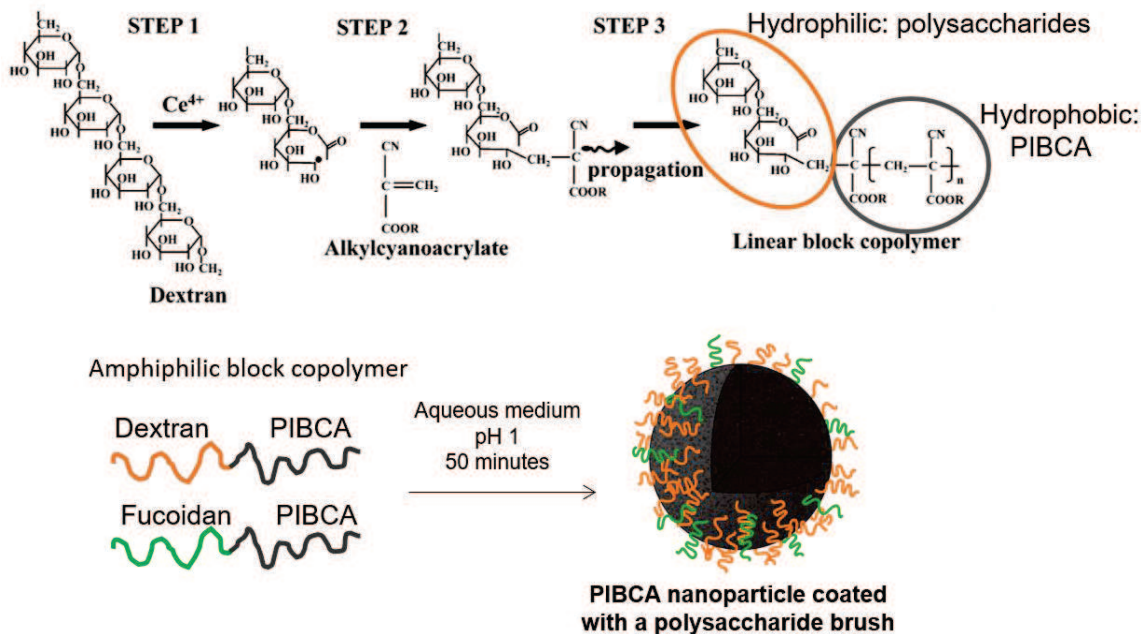


Figure 18. Réaction de polymérisation radicalaire en milieu redox et structure associée. Un radical libre est créé par oxydation des polysaccharides par les ions Cerium (IV) (step 1). Il initie la réaction de polymérisation en chaîne des monomères d'IBCA (step 2). Un copolymère dibloc amphiphile est formé (step 3). Il s'assemble en structure cœur-couronne. Schéma de la réaction adapté de [183].

Ce type de structure facilite l'adsorption des protéines. Ainsi l'hémoglobine peut facilement être chargée sur une couronne d'héparine [189, 190]. Dans un tel système, l'activité antithrombotique de l'héparine mesurée *in vitro* est conservée à 78% et l'affinité de l'héparine pour le FW n'est pas affectée. Formuler des nanoparticules avec une couronne contenant du fucoïdane pourrait permettre d'adsorber l'actif thrombolytique sans affecter son activité fibrinolytique et de préserver la capacité de ciblage du fucoïdane. Ces nanoparticules copolymères bien référencées sont donc intéressantes pour favoriser le rôle du fucoïdane et charger un agent thrombolytique en surface. Elles vont être étudiées dans ce but dans le **projet expérimental 2**.

4.3.2. Réticulation chimique

Des vecteurs composés uniquement de polysaccharides ont également été décrits. En particulier, des microparticules polysaccharides réticulées par du trimétaphosphate de sodium (STMP) ont été développées au sein de l'équipe *Bio-ingénierie cardiovasculaire* [153, 154]. Le procédé de réticulation chimique par STMP est illustré sur la **Figure 19**. En conditions basiques, les groupements hydroxyles des polysaccharides réagissent avec le STMP et forment des ponts phosphates. En pratique, les microparticules sont obtenues après émulsion d'une solution basique concentrée de polysaccharides et de STMP dans une phase d'huile en présence de surfactants. Les polysaccharides réticulent au sein des gouttes d'eau émulsionnées dans l'huile puis les structures sont extraites en phase aqueuse et purifiées. Ces microparticules ont été fonctionnalisées pour l'imagerie moléculaire de la P-selectine. Les résultats pour l'imagerie moléculaire ont ainsi été exposés sur la **Figure 17** et dans la **section 3.1**. Cette méthode de synthèse de vecteurs polysaccharides par réticulation présente les avantages ; i) d'avoir lieu en solution aqueuse, ii) d'offrir des structures hydrophiles de type hydrogel intéressantes pour le chargement de principes actifs hydrophiles, iii) de pouvoir incorporer du fucoïdane. Toutefois, le procédé d'émulsion-réticulation engendre des populations polydispersées avec des tailles de 300 nm à 10 µm au sein d'une même synthèse. Cette polydispersité provient notamment du fait que les polysaccharides doivent être suffisamment concentrés pour réagir, ce qui engendre une viscosité importante de la phase aqueuse et la rend plus difficile à émulsionner. Aussi, créer des émulsions plus fines et homogènes requiert dans ce cas un apport d'énergie considérable et/ou la présence de surfactants en grande quantité [191, 192].

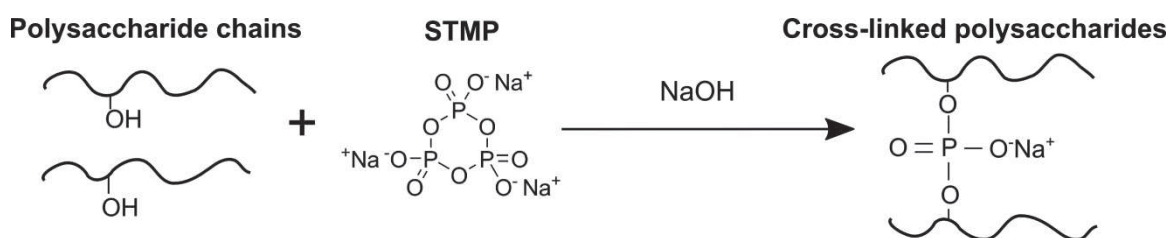


Figure 19. Réticulation chimique des polysaccharides par le STMP.
La réaction a lieu en conditions basiques. Des ponts phosphates se forment entre les chaînes de polysaccharides.

Ces structures présentent donc un fort potentiel d'un point de vue biologique mais nécessitent encore des phases d'optimisation pour obtenir des populations mieux définies. Le **projet expérimental 3** décrit un nouveau procédé d'obtention de nanoparticules homogènes faites de polysaccharides réticulés par le STMP.

Les vecteurs polymères décrits dans la partie expérimentale qui suit sont tous mis au point dans le but de cibler la P-sélectine par le fucoïdane. Les méthodes de chargement en actif thrombolytique ou en agent de contraste sont détaillées et justifiées en fonction du type de vecteurs.

Résultats expérimentaux

1. Microcapsules polymères pour cibler la P-sélectine

Publication:

Development of fucoidan functionalized polymer microcapsules to target P-selectin overexpressed in cardiovascular diseases

Bo Li, Maya Juenet, Rachida Aid-Launais, Murielle Maire, Véronique

Ollivier, Didier Letourneur, Cédric Chauvierre

Advanced Healthcare Materials, 2017, in press

doi: 10.1002/adhm.201601200

Keywords: microcapsules, fucoidan, P-selectin, thrombosis, targeting

Introduction

Le projet de thèse de Bo Li dirigé par le Docteur Cédric Chauvierre s'est déroulé en parallèle de cette thèse et a consisté à développer des nano et microsystèmes pour le diagnostic de l'AAA. L'échographie est une modalité largement implantée. Avoir accès à une imagerie moléculaire de la P-sélectine par échographie constituerait un moyen rapide d'obtenir des informations sur l'état d'activation des AAA. Dans ce contexte, Bo Li a mis au point un nouveau mode de synthèse de microcapsules composées de PIBCA, chargées en PFOB et fonctionnalisées avec du fucoïdane. Le PFOB peut en effet être utilisé comme agent de contraste pour l'échographie et sa forme liquide présente un avantage de stabilité par rapport aux microbulles gazeuses commercialisées. Le PFOB est aussi utilisé dans ce contexte comme un agent hydrophobe modèle pour la conception d'une plateforme diagnostique versatile. Des vecteurs développés au LVTS et fonctionnalisés avec du fucoïdane ont déjà démontré leur capacité à atteindre leur cible *in vivo* (**Figure 17**). Toutefois, une collaboration a depuis été initiée pour travailler sur des lots de fucoïdane spécifiques, extraits par la société Algues&Mer. Une grande variété de fucoïdanes existe et leur capacité à lier spécifiquement la P-sélectine peut dépendre de leur provenance. De plus, cette capacité peut être altérée par le mode de chargement du fucoïdane sur le vecteur. Pour valider l'interaction des microcapsules ciblées avec la P-sélectine avant leur évaluation *in vivo*, une méthode *in vitro* d'adhésion en flux artériel est implémentée.

Résumé de l'article

Les références *en italique* désignent les figures et les tableaux de l'article qui suit.

Les microcapsules sont synthétisées par polymérisation de monomères d'IBCA en présence de PFOB et de polysaccharides, en conditions neutres ou basiques. Deux types de microcapsules sont synthétisés avec les proportions suivantes en polysaccharides : 10% fucoïdane et 90% dextrane (Fuco-MCs) et 100% dextrane (MCs). Après optimisation des paramètres de synthèse, des microcapsules sphériques de 2 à 6 µm contenant 42% de PFOB en poids sont obtenues (*Figures 1 & 4, Tableaux 1 & 2*). Pour obtenir des coques fluorescentes, du Nile Red ou du dextrane-FITC sont incorporés au cours de la synthèse. Des images en microscopie confocale montrent que les polysaccharides sont incorporés dans une coque de PIBCA (*Figure 2*). La présence de fucoïdane est validée par colocalisation de fucoïdane-FITC avec les microcapsules par cytométrie en flux (*Figure 3*). Leur charge de surface est grandement influencée par le type de polysaccharide incorporé. Ainsi l'ajout de 10% de fucoïdane, polysaccharide anionique, fait décroître le potentiel zéta de - 9 mV (MCs) à - 52 mV (Fuco-MCs) suggérant qu'une partie au moins du fucoïdane est localisée en surface (*Tableau 2*).

Afin de valider l'interaction des Fuco-MCs avec les plaquettes activées via la P-sélectine, les microcapsules sont mises en contact avec du plasma riche en plaquettes (PRP) humain dans trois conditions différentes : 1) plaquettes non activées, 2) plaquettes activées, 3) plaquettes activées et préalablement mélangées avec un anticorps anti-P-sélectine (anti-CD62P). La colocalisation des microcapsules fluorescentes incubées durant 20 minutes avec les plaquettes met ainsi en évidence par cytométrie en flux que les Fuco-MCs montrent une très forte affinité avec les plaquettes activées. L'intensité de fluorescence moyenne est plus de 30 fois supérieure à celle détectée au contact des plaquettes non activées. Cette intensité moyenne est réduite par un facteur 11 en présence d'anti-CD62P (*Figure 6*). Les MCs ne montrent quant à elles d'affinité avec aucun des groupes. Cette expérience valide que le fucoïdane à la surface interagit avec la P-sélectine exprimée par les plaquettes activées. Néanmoins, les contraintes de cisaillement dans la circulation *in vivo* peuvent interférer sur ces interactions et ne sont pas prises en compte dans ce type d'expériences.

Un test *in vitro* en flux est mis en place dans ce projet pour :

- évaluer l'interaction des microcapsules avec la P-sélectine recombinante,
- la comparer à l'interaction des microcapsules pour les autres sélectines (E- et L-),
- évaluer l'interaction des microcapsules avec des agrégats plaquettaires activés.

Des micro-canaux (100 µm x 400 µm x 28 mm) sont recouverts de sélectines recombinantes ou de fibres de collagène et sont directement visualisés sous microscope. Une pompe connectée permet de faire passer les suspensions de microcapsules ou du sang total à des contraintes fixées pouvant aller jusqu'aux contraintes artérielles (**Figure 20**).

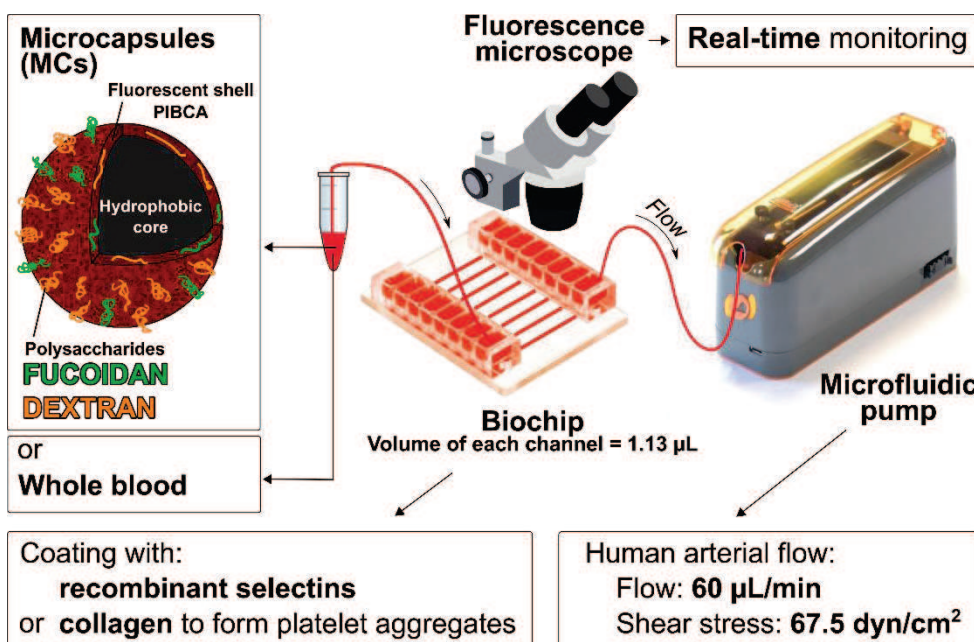


Figure 20. Schéma du dispositif d'interaction en flux.

Dans une première expérience, les microcapsules sont passées directement sur un coating de sélectine (**Figure 21**). Les Fuco-MCs interagissent fortement avec la P-sélectine et adhèrent 10 fois plus que les MCs (**Figure 7**). Cette adhésion est dépendante de la concentration en P-sélectine et peut être inhibée par une injection préalable de fucoïdane seul. De plus, l'interaction des Fuco-MCs avec les sélectines E- et L- est moindre. Une seconde expérience permet de montrer que les Fuco-MCs adhèrent en nombre aux agrégats plaquettaires activés formés à partir de sang total passé au contact du collagène (**Figure 8**). Les MCs ne présentent pas d'affinité pour les agrégats.

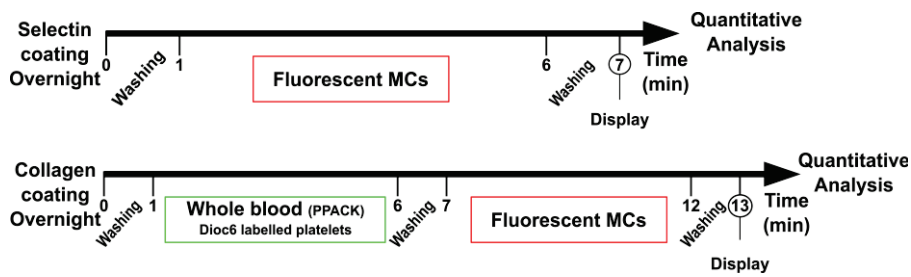
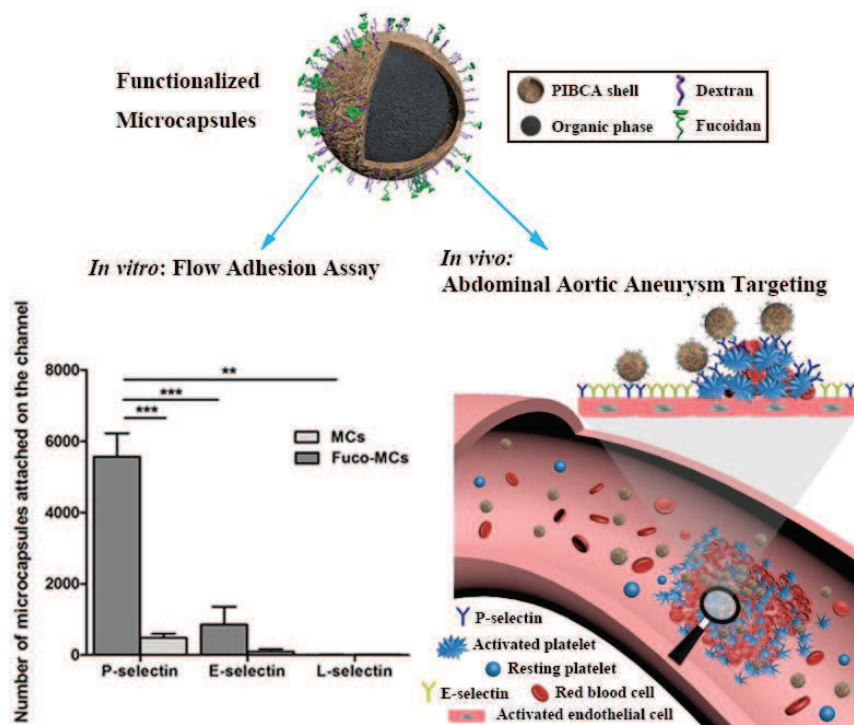


Figure 21. Protocoles pour tester l'interaction des microcapsules avec les sélectines et avec les agrégats plaquettaires activés.

Il est ensuite démontré par des tests *in vitro* que les microcapsules ne présentent pas de cytotoxicité à 24 heures (*Figure 9*). Enfin, pour valider leur interaction *in vivo* avec la P-sélectine, les microcapsules sont injectées à des rats sains ou présentant un AAA. La colocalisation des Fuco-MCs avec la paroi anévrismale dans un modèle d'AAA chez le rat est validée par analyse histologique (*Figure 10*). À l'inverse, les MCs ne se retrouvent pas dans la paroi malade, ce qui confirme le rôle du fucoïdane.

Development of fucoidan functionalized polymer microcapsules to target P-selectin overexpressed in cardiovascular diseases



Abstract

New tools for molecular imaging and targeted therapy for cardiovascular diseases are still required. Herein, biodegradable microcapsules (MCs) made of polycyanoacrylate and polysaccharide and functionalized with fucoidan (Fuco-MCs) were designed as new carriers to target arterial thrombi overexpressing P-selectin. Physico-chemical characterizations demonstrated that microcapsules have a core-shell structure and that fucoidan was present onto the surface of Fuco-MCs. Furthermore, their size ranged from 2 to 6 μm and they were stable on storage over 30 days at 4°C. Flow cytometry experiments evidenced the binding of Fuco-MCs for human activated platelets as compared to MCs (MFI: 12,008 vs 9, $P < 0.001$) and its absence for non-activated platelets (432). An *in vitro* flow adhesion assay showed high specific binding efficiency of Fuco-MCs to P-selectin and to activated platelet aggregates under arterial shear stress conditions. Moreover, both types of microcapsules revealed excellent compatibility with 3T3 cells in cytotoxicity assay. One hour after intravenous injection of microcapsules,

histological analysis revealed that Fuco-MCs were localized in the rat Abdominal Aortic Aneurysm thrombotic wall and that the binding in the healthy aorta was low. In conclusion, these microcapsules appear as promising carriers for targeting of tissues characterized by P-selectin overexpression and for their molecular imaging or treatment.

Introduction

P-selectin, an adhesion molecule, is expressed at the surface of activated platelets and injured vascular endothelium. Therefore, P-selectin is a marker of biologically active arterial thrombi and expansion of Abdominal Aortic Aneurysms (AAA).[1, 2] In recent studies, P-selectin was described as a molecular imaging target for AAA early detection, dilatation and rupture risk assessment. Some authors have developed nano/micro-contrast agents for imaging of P-selectin using ultrasound or magnetic resonance.[3-7] Limitations are related to the low binding efficiency in high blood shear rate of nano/microspheres to P-selectin on the area of AAA leading to not sufficient detectable contrast signals for predicting AAA rupture risk. Moreover, microspheres as compared to nanospheres showed higher margination efficiency in recirculating blood flow and thus may be an advantage for treatment of arterial thrombi.[8] New carrier systems with strong P-selectin binding are still needed for vascular-targeted imaging or drug delivery.

Fucoidan, a seaweed-derived polysaccharide with sulfated chains, was proved to be an efficient glycosidic ligand of P-selectin.[9] Our group previously demonstrated its ability to bind P-selectin and developed a radiotracer by combining Technetium (^{99m}Tc) to fucoidan to enable detection of activated endothelium and thrombosis.[10] Recently, we developed fucoidan functionalized iron oxide nanoparticles and polysaccharide microparticle radiolabeled with ^{99m}Tc , for MRI or SPECT imaging respectively.[11-13]

The aim of the present study was to produce by an easy way injectable polymer microcapsules able to target P-selectin. The first design of biodegradable poly(alkylcyanoacrylate) (PACA) nanoparticles prepared by emulsion polymerization as *in vivo* drug delivery carrier was described in 1979.[14] The classical approach for the preparation of PACA nanoparticles is the emulsion polymerization by either anionic or

redox radical mechanisms.[15-17] Different types of PACA nanosystems have been developed in the past decades such as polymer nanoparticles,[18] core-shell polymer nanoparticles[19] and polymer nanocapsules.[20] Moreover, a great variety of bioactive compounds have been loaded on these different types of PACA nanosystems[21] such as antioxidant agents,[22] anticancer drugs,[23] antibiotics,[24, 25] proteins,[26] peptides[27] and nucleic acids.[20, 28] However, issues still exist such as the initiation of the polymerization reaction of alkylcyanoacrylates by the chosen reactive drug instead of by the hydroxyl ions for anionic mechanism or by free radicals for redox radical mechanism. To overcome these limitations, Yordanov G. et al recently reported the preparation of poly (butylcyanoacrylate) (PBCA) homopolymer nanospheres by the nanoprecipitation method using a pre-synthesized polymer and colloidal stabilizers.[29-33] Nevertheless, this method requires multiple steps for obtaining PACA nanospheres. We report here a new process to obtain microcapsules that are assembled from polymerization of isobutyl cyanoacrylate (IBCA) in presence of perfluorooctyl bromide (PFOB), coated by polysaccharides and functionalized with fucoidan. The choice of perfluorooctylbromide was based on two main reasons. Firstly, perfluorooctylbromide can be used as a contrast agent for ultrasonography and 19F Magnetic Resonance Imaging (MRI). Perfluorooctylbromide microcapsules functionalized with fucoidan could therefore be used as contrast agents for the molecular imaging of cardiovascular diseases. Secondly it was used here as a model carrier for loading active agents with regard to its hydrophobic property, some hydrophobic drugs (e.g. curcumin) could be considered to be loaded into the hydrophobic core of the microcapsules by following the same synthesis method. The thickness of the microcapsules can be adjusted by simply modifying the pH value of the water phase prior to emulsification. Flow cytometry and flow chamber experiments were performed to evaluate the specificity of the interaction between activated platelets and microcapsules functionalized with fucoidan (Fuco-MCs). In addition, *in vivo* experiments performed in an elastase-induced AAA rat model showed that Fuco-MCs were located in the thrombotic abdominal aorta and not in healthy rats which confirms the ability of these microcapsules to target specifically P-selectin. These microcapsules appear as new tools to image at molecular level or to treat cardiovascular pathologies in which P-selectin is overexpressed.

Methods and Materials

Materials

Methylene chloride (CH_2Cl_2) RPE-ACS 99.5% and Acetone 99.8% were provided by Carlo Erba Reactifs (Peypin, France). 1-Bromoheptadecafluorooctane (PFOB), CDCl_3 (99.96 atom % D), isopropanol, MTT solution and Nile Red were provided by Sigma Aldrich (Saint Quentin Fallavier, France). Dextran 20 and FITC-Dextran 20 were obtained from TdB Consultancy (Uppsala, Sweden). Fucoidan was a gift from Algues & Mer (Ouessant, France). Perfluoro-15-crown-5-ether (PFCE) was purchased from Fluorochem (Hadfield, UK). Isobutyl cyanoacrylate (IBCA) was provided by ORAPI (Saint Vulbas, France). TRAP (thrombin receptor-activating-peptide) was obtained from PolyPeptide laboratories (Strasbourg, France). PE-CyTM5 mouse anti-human CD41a and PE-CyTM5 mouse IgG1,κ Isotype Control were provided by BD Pharmingen, (Le Pont-de-Claix, France), mouse anti-human CD62P, mouse anti-human CD62P-FITC and mouse IgG1-FITC Isotype Control were obtained from Beckman Coulter (Villepinte, France). Recombinant human E-selectin, L-selectin and P-selectin were provided by R&D Systems (Lille, France). Flow chambers (Vena8Fluoro+) were obtained from Cellix Ltd (Dublin, Ireland).

Synthesis of core-shell microcapsules

Dextran 20 coated poly(isobutyl cyanoacrylate) (PIBCA) microcapsules (MCs) with 1-Bromoheptadecafluorooctane (PFOB) core as a reference loaded agent were prepared by modification of the emulsion-evaporation process described by Pisani.[45] Briefly, 100 μL of IBCA was dissolved into 4 mL of methylene chloride along with 60 μL of PFOB. The organic solution was mixed to ensure full miscibility of the PFOB. Subsequently, the whole organic phase was slowly injected into 20 mL of a cold aqueous solution containing 300 mg of dextran (1.5% (w/v)) adjusted to the desired pH conditions (pH 3, 7 or 10), and dispersed at 30,000 rpm for 2 min with a homogenizer (Polytron PT 3100, dispersing aggregate PT-DA 07/2 EC-B101, Kinematica, Luzern, Switzerland). To

prepare fucoidan-functionalized microcapsules (Fuco-MCs), 30 mg of fucoidan was blended into 270 mg of dextran. They were dissolved into an aqueous solution at pH 10. Emulsification was performed in a 50 mL beaker placed in ice. Methylene chloride was then evaporated by magnetic stirring for about 4 h at room temperature or 3 h in a thermostated bath (30°C). After full evaporation of the solvents, samples were centrifuged at 600 g for 30 min (5702RH centrifuge Beckman Coulter, Villepinte, France), supernatants were discarded and precipitates were washed by deionized water. The centrifugation and washing steps were repeated three times. For fluorescent and confocal microscopy studies, 10 µL (0.57 mg/ml) of Nile red were added to the organic solution and 3 mg of FITC-dextran were added to the aqueous solution before emulsification. The fluorescence intensity of microcapsules was analyzed by Image J software. Finally, the precipitate was resuspended into 3 mL of deionized water for storage at 4°C until use or for freeze-drying.

For freeze-drying, the purified suspensions were frozen at -18°C and freeze-dried during 48-72 hours without using any cryo-protecting agent (Lyovac, SRK Systemtechnik, Riedstadt, Germany).

The mass yield (%) was calculated as follows:

$$Yield = \frac{m_{\text{Microcapsules}}^{\text{mass}}}{m_{\text{Polysaccharides}}^{\text{feed}} + m_{\text{polymer}}^{\text{feed}} + m_{\text{PFOB}}^{\text{feed}}} \quad (1)$$

Where $m_{\text{Polysaccharides}}^{\text{feed}}$, $m_{\text{polymer}}^{\text{feed}}$, $m_{\text{PFOB}}^{\text{feed}}$ are the initial masses of the components introduced in the reaction solution, $m_{\text{Microcapsules}}^{\text{mass}}$ corresponds to the final mass of microcapsules evaluated after the freeze-drying process.

Physico-chemical characterization

Size and zeta potential determination

The size distribution of microcapsules was quantitatively obtained using a laser dynamic scattering granulometry at 25°C (Mastersizer 3000, Malvern Instruments, Orsay, France). Zeta potential (ζ) of the microcapsules was measured to evaluate their stability in suspension and to identify the presence of the polysaccharides onto the surface.

Samples were diluted in 1 mM KCl. Measurements were performed at 25°C using quasi-elastic light scattering apparatus (Nano ZS, Malvern Instruments, Orsay, France). All the measurements were performed in triplicate and the results were expressed as mean ± standard deviation.

Scanning Electron Microscopy and Transmission Electron Microscopy

The surface morphology of microcapsules was imaged using a Scanning Electron Microscopy (SEM) apparatus (Philips XL 30 ESEM-FEG, Amsterdam, Netherlands) on dried samples coated with a thin gold layer. Transmission Electron Microscopy (TEM) was performed using a Philips EM208 apparatus (Amsterdam, Netherlands) operating at 80 kV.

Determination of PFOB content

Microcapsules were freeze-dried for 24-48 hours. Subsequently, freeze-dried microcapsules were dissolved into CDCl₃ along with PFCE as an internal standard ([PFCE] = 0.76 mmol/L). The ¹⁹F NMR (Nuclear Magnetic Resonance) spectra were recorded on a Bruker (400 MHz) Spectrometer (Billerica, USA). The amount of PFOB was obtained after integration of the peak at -80.7 ppm, corresponding to the CF₃ group and normalization by the area of the PFCE peak at -89.5 ppm. Mass fraction was calculated as follows:

$$C_{PFOB} = \frac{m_{PFOB}^{\text{NMR}}}{m_{MC}} \quad (2)$$

Where m_{MC} is the quantity of freeze-dried microcapsules, and m_{PFOB}^{NMR} corresponds to the mass of PFOB recovered after the freeze-drying process.

Sulfate and fucoidan quantitative analysis

Sulfate quantification was conducted according to Gustaffson.[46] Briefly, a certain amount of fucoidan functionalized microcapsules was freeze-dried. Subsequently,

the sample was exposed to nitrogen (100 mL/min) while boiled in iodohydric acid for 20 min. Released hydrogen sulfur reacted with zinc acetate (0.2 M) to form zinc sulfur. Then 8 mL of ammonium iron sulfate at 16 mM and 2 mL of 3.7 mM diamine were added into the sample. Following 15 min of agitation, absorbance at 675 nm and 745 nm was measured using a spectrophotometer (PerkinElmer®). Sulfate content was calculated from a standard curve obtained with a potassium sulfate reference solution. Finally, sulfate content was measured and fucoidan content of the microcapsules was calculated.

Affinity for activated platelets in static conditions

The interaction between three groups of PE-Cy5 labeled platelets (non-activated platelets (PRP), activated platelets (PRP + TRAP) and P-selectin blocked activated platelets (PRP + TRAP + CD62P) and two groups of microcapsules with FITC-dextran (MCs, Fuco-MCs) were measured by flow cytometry. 5 mL of blood from healthy adult volunteers were collected in sodium citrate 3.8% (w/v). Platelet-rich plasma (PRP) was obtained by centrifugation at 200 g for 15 min (5702RH centrifuge Beckman Coulter, Villepinte, France) and platelet concentration was adjusted to 2×10^8 ml⁻¹ with autologous platelet-poor plasma (PPP). Activated PRP was obtained by stimulation of PRP with 20 µM TRAP (thrombin receptor-activating-peptide). In some experiments, activated then P-selectin-blocked PRP were obtained by incubation with a non-labeled anti-human CD62P at high concentration (0.04 g.L⁻¹). Before assessing the interaction with microcapsules, P-selectin expression level at the platelet surface was assessed using an anti-human CD62P-FITC. An additional tube of PRP was also incubated with a mouse IgG1/FITC to verify that the FITC signal was not due to non-specific binding to the platelets. In addition, MCs and Fuco-MCs were incubated with anti-human PE-Cy5 at a similar concentration to prove that microcapsules could not be labeled by antibody. Thus, for each test, we measured the FITC signal by flow cytometry and confirmed that P-selectin was expressed by platelets from PRP + TRAP batches and that low level of P-selectin was detected on PRP and PRP + TRAP + CD62P batches. To evaluate the binding ability of microcapsules to P-selectin expressed onto platelets, 5 µL of non-activated PRP, of activated PRP with TRAP or of anti P-selectin-treated activated PRP

were incubated for 20 min with 5 µl of MCs and of Fuco-MCs (50 mg/ml), together with 5 µL of PE-Cy5 mouse anti-human CD41a to label platelets. In addition, each PRP sample was incubated with an isotype-matched control antibody. Samples were analyzed on a LSRII flow cytometer (BD Biosciences, Le Pont de Claix, France), 50,000 PE-Cy5 positive platelets collected per samples, and the mean fluorescence intensity (MFI) was measured in these platelets.

***In vitro* flow adhesion assay**

Adhesion on recombinant selectins

Flow chamber experiments: Channels were coated either with a solution of P-selectin, L-selectin or E-selectin at 100 µg/mL (PBS). Some channels were coated with different concentrations of P-selectin (from 5 µg/mL to 100 µg/mL) to confirm that the affinity of Fuco-MCs for P-selectin was dependent on the concentration of P-selectin. The selectin solutions were left in the channels overnight at 4°C in a wet chamber. Channels were then washed with NaCl 0.9%. A suspension of fluorescent MCs or Fuco-MCs at 50 mg/mL in sterile saline was passed through the channels for 5 minutes at a shear rate of 1,500 s⁻¹. For competitive binding experiment, fucoidan solution (10 mg/ml) was injected at the same rate 5 min before microcapsules were injected. After microcapsules injection, all the channels were washed with NaCl 0.9% for 1 minute at the same flow. Images of the bottom surface were taken along each channel. Fluorescence microscopy images were further analyzed with HistoLab software (Microvision, Evry, France) to quantify the number of attached particles.

Adhesion on activated platelet aggregates

For platelet dynamic binding experiments, channels were coated with collagen at 50 µg/mL. The collagen solution was left in the channels overnight at 4°C in a wet chamber. Channels were then washed with NaCl 0.9%. Collagen fibers covering the channels wall were visualized by phase contrast microscopy. Human whole blood was passed through the channels for 3.5 minutes on average at 1,500 s⁻¹. Platelets

aggregations through contact with collagen were visualized in real time with phase contrast microscopy (Axio Observer, Carl Zeiss Microscopy, Oberkochen, Germany). The channels were washed for 1 minute with NaCl 0.9%. On one channel FITC anti-CD62P antibody was infused at 20 µg/mL in NaCl 0.9% for a few minutes to confirm P-selectin expression on platelets membrane. One channel was used as a control for a control isotype-matched FITC-IgG at the same concentration. In the other channels, the platelets were labeled with DIOC₆ (0.15 mM) before their injection. After their aggregation, fluorescent microcapsules (MCs or Fuco-MCs) were injected through the channels at 50 mg/mL for 5 minutes. Channels were finally washed for 1 minute with NaCl 0.9%. Images in phase contrast and in fluorescence microscopy were taken along each channel. Quantitative analysis was performed on at least three channels per type of microcapsules. The mean fluorescence intensity of the red fluorescence channel of several aggregates was measured using Zen 2012 Software (Carl Zeiss, Oberkochen, Germany). The red fluorescence background was measured on aggregates only and subtracted from the results.

Cytocompatibility assay

To evaluate the cytotoxicity of the microcapsules and fucoidan functionalized microcapsules, MTT colorimetric assay was used on mouse fibroblasts 3T3 line. The cells were cultured in DMEM supplemented with 10% (v/v) fetal bovine serum (FBS), 4 mmol of L-glutamine, 100 units/mL of penicillin, and 100 µg/mL of streptomycin. The cells were kept in an incubator at 37°C in a humidified atmosphere of 5% CO₂, 95% air. 3T3 cells were seeded (at the density of 10⁴ cells per well) in 96-well plates (Costar) and incubated for 24 hours. After that, the cell culture medium was removed and 200 µL of series of dilution (0.625, 1.25, 2.5 and 5 g/L) of microcapsules in the medium were added to the plate. Culture medium were used as the positive controls. After 24 hour of incubation, the supernatant was removed and 10 µL (5 mg/mL) of MTT solution was added to the medium in each well and the plates were incubated for 4 hours at 37°C and 5% CO₂. Then, the medium with MTT was removed and 100 µL per well of isopropanol solution was added to each well to dissolve the formazan crystals. The plates were read

immediately in Tecan (Infinite@ M200 PRO) at 490 nm. The relative cell viability was expressed as Abs microcapsules/Abs control × 100%, where Abs control was obtained in the absence of the microcapsules.

In vivo study on rat model of Abdominal Aortic Aneurysm

AAA model

Animal studies were done in accordance with principles of laboratory animal care and with approval of the animal care and use committee of the Claude Bernard Institute (N°2012-15/698-0100) (Paris, France). The ability of the functionalized microcapsules to target P-selectin expression *in vivo* was assessed in an abdominal aortic aneurysm (AAA) experimental model in rats. The elastase model was performed on 8 male adult Wistar rats (7 weeks, Janvier Labs, Le Genest-Saint-Isle, France). Animals were anesthetized with intra-peritoneal injection of pentobarbital (1 µL/g body weight, Ceva Santé Animale SA, La Ballastiere, France). Porcine pancreatic elastase (2.7 mg/mL, Sigma Aldrich, Saint Quentin Fallavier, France) was perfused into the lumen of an isolated segment of the infrarenal abdominal aorta for 15 minutes at a rate of 2.5 mL/h. Delbosc *et al.* reported that repeated intravenous injection of *Porphyromonas gingivalis* (Pg) in a rat model of AAA led to enhanced aortic dilation associated with neutrophil retention and persistence of a non-healing luminal thrombus.[47] In this study, *Porphyromonas gingivalis* suspension (107 CFU in 500 µL 0.9% saline), a gift from La Pitié Salpétrière Hospital, was injected to the rats once a week via the penis vein for 4 weeks. Two days after the fourth injection, rats were anaesthetized by sodium pentobarbital intra-peritoneal injection (1 µL/g,) and 200 µl of MCs or Fuco-MCs (50 mg/mL) in sterile saline were injected slowly via the penis vein. Healthy rats were injected as controls.

Histological analysis

Animals were sacrificed with pentobarbital overdose 60 minutes after injection of MCs or Fuco-MCs. Abdominal aorta aneurysms of rats and healthy aorta of normal control rats were removed, washed in 0.9 % saline, fixed in paraformaldehyde (PFA) 4%

(w/v) and then frozen. The aorta samples were cryo-sectioned at 10 µm thicknesses for standard histology evaluations. The cell nucleus of arterial vascular wall were labeled with DAPI, microcapsules expressed red fluorescence. The 20x magnified images of region of interest (ROI) were used for semi-quantitative analysis. The red and blue fluorescence areas were measured using ImageJ image analysis software.

Biodistribution study

Biodistribution of microcapsules were studies in a similar way. Briefly, liver, spleen, lungs and kidneys were excised and washed at 1 hour or 24 hours after injection of MCs or Fuco-MCs. The samples were cryo-sectioned and cell nuclei were labeled with DAPI, the whole area of tissue slice of samples were used for semi-quantitative analysis.

Statistical Analysis

Data are presented as mean ± SEM ($n \geq 3$). Each experiment was performed using Student t test for paired data. Flow cytometry results were analyzed statistically with a one-way ANOVA with Bonferroni post-tests to compare data obtained with MCs and Fuco-MCs. A difference of $P < 0.05$ was considered significant.

Results

Preparation and characterization of microcapsules

New polymer microcapsules coated with polysaccharides and loaded with PFOB were prepared by modification of the commonly used emulsion-evaporation polymerization process (Figure 1). According to previous studies,[9, 16, 34, 35] PACA nanoparticles are synthesized at low pH values to avoid anionic homopolymerization occurring spontaneously due to the rapid initiation by the hydroxyl groups of water. However, it was impossible to form microcapsules at a pH value lower than 3 (Table 1). In contrast, when the pH value was either set to 7 or 10 at 30°C, the microcapsule mass yield reached 9% or 30% respectively, whereas the weight percent fraction of PFOB represented 69% or 43% of the total microcapsule weight. The mean sizes were $41.50 \pm 0.68 \mu\text{m}$ and $6.41 \pm 0.02 \mu\text{m}$ respectively. The D90 value (90% of the particles are smaller than this diameter) was significantly lower for the microcapsules synthesized at basic pH than for the ones synthesized at neutral pH, indicating a narrower distribution of the microcapsule size. Additionally, the yield of microcapsules decreased when reducing the temperature from 30°C to 20°C.

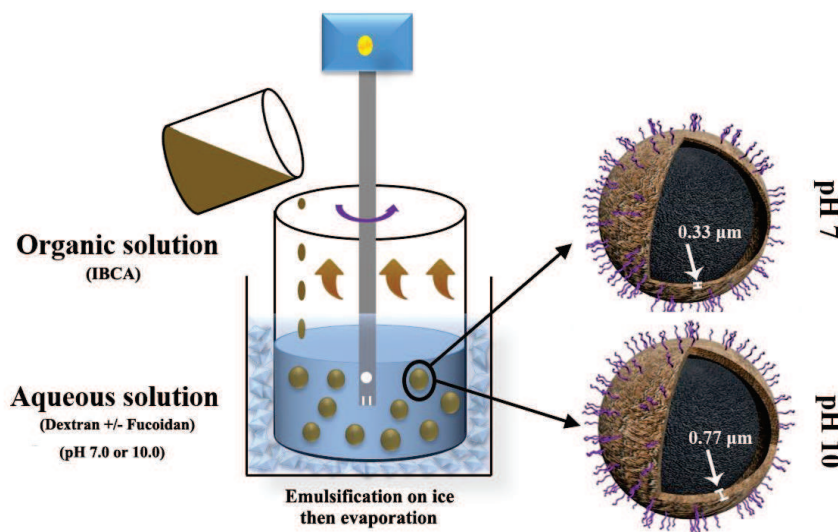
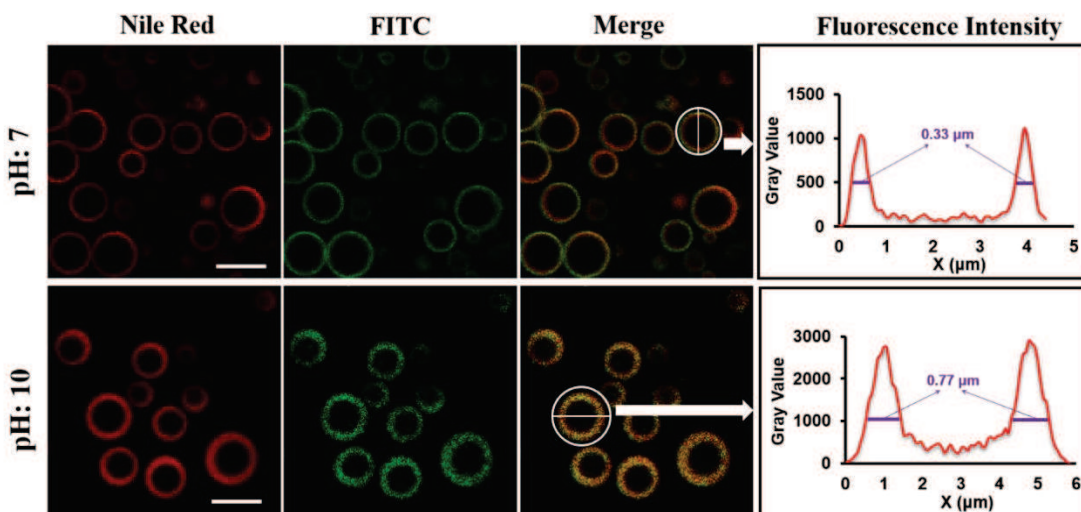


Figure 1. Overall scheme of one-step protocol for microcapsules synthesis.

pH	T (°C)	Polysaccharide	Stability in water	Size distributions			Zeta potential (mV)	Yield (% w/w)	PFOB content (% w/w)
				D ₁₀ (μm)	D ₅₀ (μm)	D ₉₀ (μm)			
3	30	Dextran	No product	-	-	-	-	-	-
7	30	Dextran	Stable	1.57±0.01	5.68±0.04	41.50±0.68	-16.83±0.31	9.00±2.15	69.02±3.44
10	30	Dextran	Stable	2.40±0.01	4.07±0.01	6.41±0.02	-12.10±0.59	30.03±1.98	42.54±2.16
10	20	Dextran	Stable	2.31±0.04	4.03±0.05	6.50±0.10	-16.25±0.42	25.88±2.70	42.50±1.68

Table 1. Characteristics of non-functionalized microcapsules.

To further visualize the polysaccharide presence in microcapsules, a portion of dextran (1% w/w) was substituted during the emulsion process by FITC-dextran, and Nile red was added in the organic phase to stain in red the hydrophobic poly (isobutyl cyanoacrylate) (PIBCA). Microcapsule suspensions were observed by confocal microscopy (Figure 2 Left). The core–shell structure of the microcapsules was perfectly visible; the core composed of liquid appeared in dark and the fluorescent shell was well defined.

**Figure 2. Confocal microscopy images of microcapsules.**

Polymers appeared in color and the liquid content appeared in dark. Red fluorescence channel: PIBCA (left), green fluorescence channel: FITC-Dextran (center) and merging of both channels (right), pH 7 (top), pH 10 (bottom) (Scale bar = 5 μm). Fluorescence Intensity graph profile (X: distance measurement) (Right). Determination of the shell thickness, pH 7 (top) and pH 10 (bottom). (n=3)

Surprisingly, polysaccharides were not preferentially localized at the polymer/water interface. In fact, the green fluorescence was homogeneously distributed in the whole shell thickness, the polysaccharides being therefore mixed with the polymer shell. The scanning of focused equatorial slice of Nile red-labeled microcapsule shells was performed and the fluorescence intensity profiles were measured (Figure 2 Right). Confocal images showed that microcapsules had a thickness of $0.33 \pm 0.08 \mu\text{m}$ and $0.77 \pm 0.13 \mu\text{m}$ for reaction medium pH of 7 and 10 respectively.

To obtain functionalized particles, fucoidan was introduced into the polymerization medium, as 10% w/w of the total polysaccharide mass. As indicated in Table 2, stable microcapsules functionalized with fucoidan (Fuco-MCs) had a mean size of $7.09 \pm 0.14 \mu\text{m}$. The zeta potential of Fuco-MCs decreased compared to MCs ($-50.88 \pm 0.52 \text{ mV}$ vs $-12.10 \pm 0.59 \text{ mV}$ for MCs). This result indicated that at least a part of the anionic fucoidan was present at the surface of the microcapsules, a property already observed with fucoidan coated nanoparticles[35]. To further evidence the presence of fucoidan in Fuco-MCs, FITC-fucoidan (1% w/w of the total fucoidan mass) was incorporated during their synthesis. The co-localization of FITC-fucoidan and the microcapsules was evaluated by flow cytometry. Non-fluorescent Fuco-MCs were used as a control to adjust their autofluorescence level. A noticeable difference in the fluorescent signal was detected between FITC-Fuco-MCs and Fuco-MCs, indicating that almost all microcapsules in contact with FITC-fucoidan were functionalized by FITC-fucoidan (Figure 3).

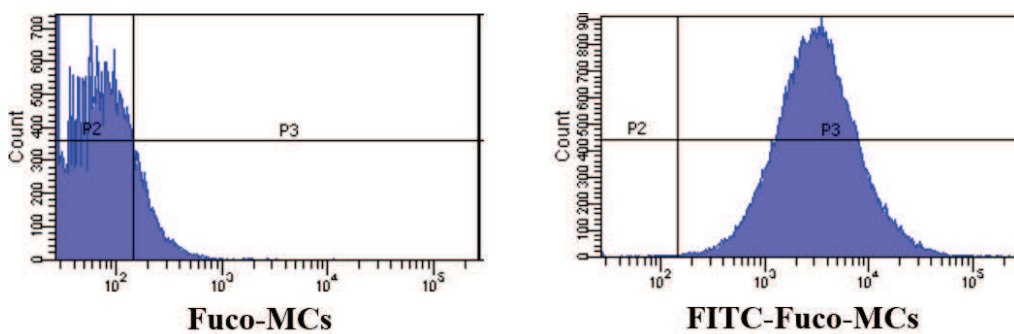


Figure 3. Flow cytometry evaluation of the co-localization of FITC-Fucoidan with microcapsules. 1% w/w of FITC-fucoidan was introduced during the synthesis of Fuco-MCs. The green fluorescence signal associated to the fucoidan functionalized microcapsules was analyzed by flow cytometry in presence or not of FITC-fucoidan.

Microcapsules	Stability in water	Size distributions			Zeta potential ζ (mV)	Yield (%, w/w)	PFOB content (%, w/w)
		D ₁₀ (μm)	D ₅₀ (μm)	D ₉₀ (μm)			
Non-functionalized (MCs)	Stable	After preparation	2.40±0.01	4.07±0.01	6.41±0.02	-12.10±0.59	30.03±2.12
		After purification	2.24±0.02	3.79±0.03	5.90±0.10	-8.86±0.88	29.25±3.48
Functionalized with fucoidan (Fuco-MCs)	Stable	After preparation	2.30±0.01	4.19±0.05	7.09±0.14	-50.88±0.52	28.51±2.61
		After purification	2.19±0.02	3.69±0.02	5.84±0.05	-51.76±1.33	24.56±3.11

Table 2. Characteristics of non-functionalized and functionalized microcapsules.

The size distribution of each type of microcapsules decreased after purification. After purification, both MCs and Fuco-MCs had similar size distribution (from 2.2 μm to 5.9 μm for MCs and from 2.2 μm to 5.8 μm for Fuco-MCs) and the mass percent of loaded agent was similar (42% and 41% respectively) (Table 2).

The morphology of obtained microcapsules was analyzed by Scanning Electron Microscopy (SEM) and Transmission Electron Microscopy (TEM) (Figure 4). Both MCs and Fuco-MCs showed a typical well-defined spherical capsule structure.

Quantitative analysis showed that Fuco-MCs contained 0.10 μmol/g of sulfur. Since the fucoidan used in this study was determined to contain 1,550 μmol/g of sulfur, we calculated the fucoidan content of Fuco-MCs to be 0.008 % (w/w) right after synthesis. Long-term stability in distilled water was assessed upon storage of the suspensions at 4°C. Size and zeta potential remained stable at least one month for both types (Figure. 5). Moreover, the content of fucoidan in Fuco-MCs did not obviously change with time (0.006 % (w/w) at 1 month).

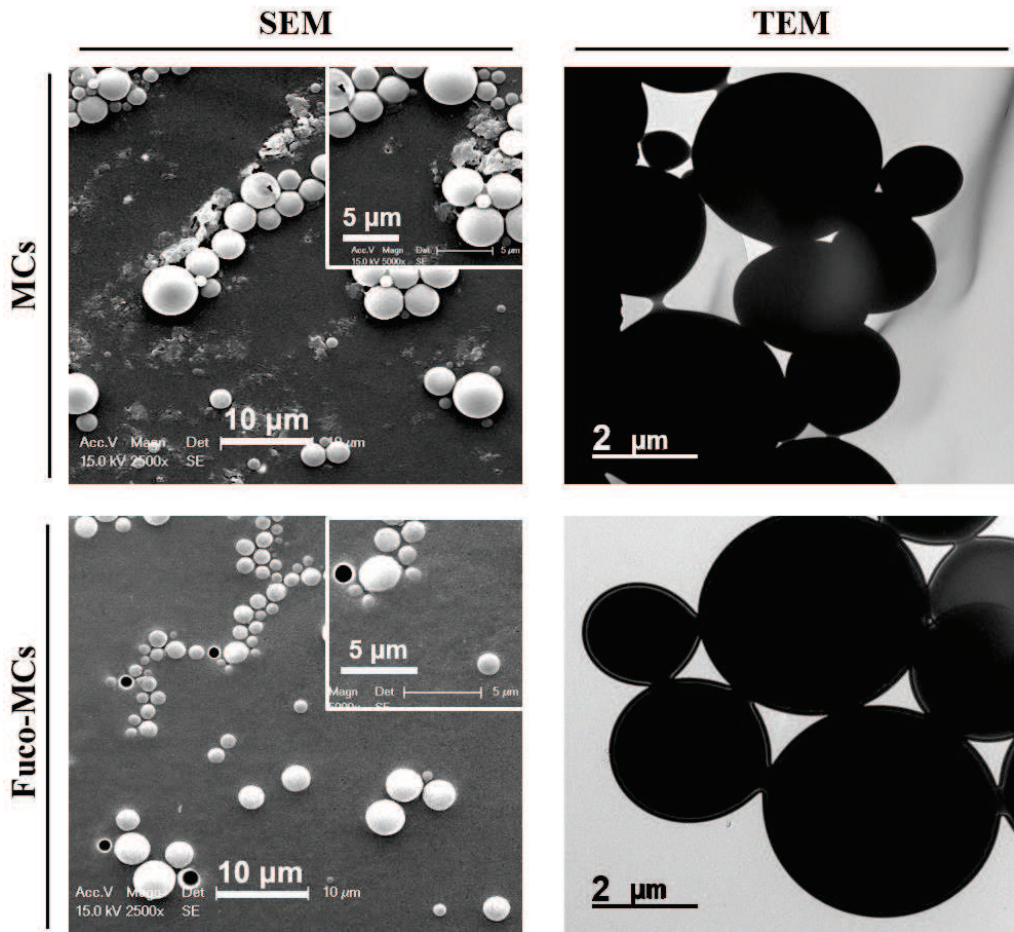


Figure 4. Scanning and Transmission Electron Microscopy images of microcapsules.
Top: MCs. Bottom: Fuco-MCs. Left: SEM images with zooms. Right: TEM images.

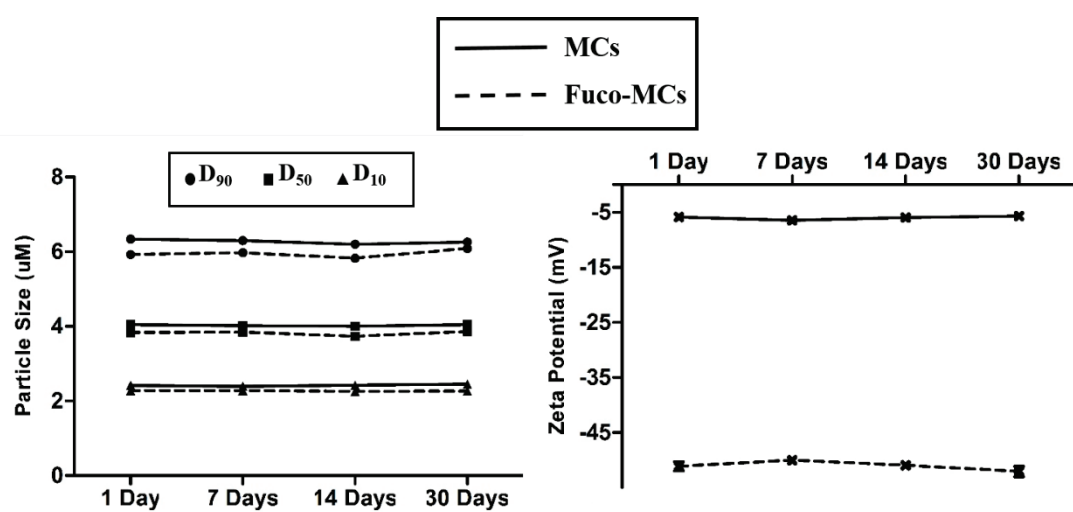


Figure 5. Stability at 4°C in distilled water of MCs and Fuco-MCs suspensions according to size and zeta potential measurements.

Affinity for activated platelets in static conditions

To evaluate the affinity of MCs and Fuco-MCs for P-selectin expressed onto the surface of human activated platelets, flow cytometry experiments were performed. Interactions were assessed between microcapsules and three groups respectively composed of: human Plasma-Rich Platelets (PRP), human Plasma-Rich Platelets where platelets were activated with TRAP (PRP+TRAP), and human Plasma-Rich Platelets where platelets were activated with TRAP and P-selectin blocked by a specific blocking antibody (PRP + TRAP + anti-CD62P). As shown on Figure 6, non-functionalized microcapsules (MCs) barely or only minimally bound to the three groups of platelets, as shown by low values of the mean fluorescence intensity (MFI) (9.75 ± 2.11 ; 9.00 ± 0.87 ; 6.50 ± 1.77 , respectively). In contrast, Fuco-MCs exhibited an important binding to activated platelets (MFI = $12\,008 \pm 2\,359$) compared to PRP (MFI = 432.4 ± 212.8) or to PRP + TRAP + anti-CD62P (MFI = 1093 ± 419.2).

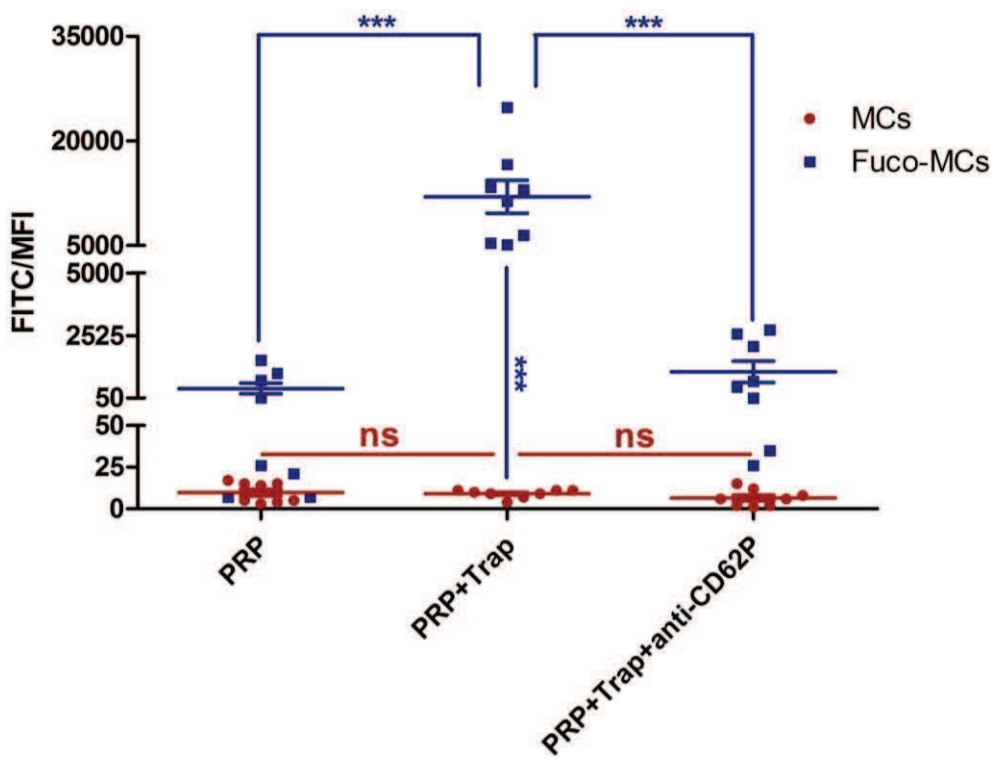


Figure 6. Flow cytometry assessment of microcapsule affinity for activated platelets.

Flow cytometry assessment of interactions of FITC-labeled MCs and FITC-labeled Fuco-MCs with either non-activated platelet-rich plasma (PRP), platelet-rich plasma activated with TRAP (PRP+Trap) and platelet-rich plasma activated plus P-selectin antibody (PRP+Trap+anti-CD62P). The mean fluorescence intensity (MFI) on the FITC channel was measured for 50,000 events of PE-Cy5 labeled platelets, and at a microcapsule concentration of 50 g/L (n=8; ***p<0.001).

***In vitro* flow adhesion assay**

Adhesion on recombinant selectins

To evaluate the ability of MCs and Fuco-MCs to target selectins under arterial blood flow conditions, flow chamber experiments with selectins coating were performed. Under arterial blood flow, FITC-Fuco-MCs showed a significantly higher adhesion to P-selectin than FITC-MCs (5565 ± 662 adhered Fuco-MCs versus 482 ± 113 adhered MCs, $p<0.001$) (Figures 7 A&D). Fuco-MCs adhered to the chamber immediately after their injection and remained attached for the whole duration of the experiment. On the contrary, only few MCs were seen to adhere. Washing with NaCl 0.9% at the end of the experiment did not significantly affect the adhesion of both types of microcapsules. The number of adhered Fuco-MCs after 5 min was significantly lower to E-selectin (854 ± 502) or L-selectin (10 ± 8) than to P-selectin (5565 ± 662) (Figure 7A). Adhesion of Fuco-MCs was comparable to that of MCs on E-selectin or L-selectin.

The Fuco-MCs adhesion dependence on P-selectin concentration was investigated (Figure 7B). The number of attached Fuco-MCs was normalized over the mean number of attached microcapsules for a P-selectin concentration of $100 \mu\text{g/mL}$. Results indicated a dose-dependent relation between the concentration of P-selectin and Fuco-MCs ($r^2 = 0.965$) (Figure 7B). The competitive inhibition experiments showed that the injection of a free fucoidan solution (10 mg/ml) before the injection of Fuco-MCs suspension inhibited the binding of Fuco-MCs to P-selectin (486 ± 75 versus 3048 ± 565 , respectively, $p<0.05$) (Figure 7C).

Adhesion on activated platelet aggregates

To mimic the interaction of microcapsules and P-selectin under physiological conditions, human platelets from whole blood were activated and aggregated on collagen at high shear stress (67.5 dyn/cm^2). Aggregating platelets were visualized in real time under phase contrast microscopy and expression of P-selectin was evidenced by the green fluorescence uptake after injection of a FITC anti-CD62P antibody through the channel (Figure 8A). No signal was detected after injection of the FITC-IgG control (Data not shown). When passed at arterial flow on the platelets aggregates, Fuco-MCs bound to the

aggregates and remained attached, whereas MCs showed almost no binding (Figure 8A). Quantitative analysis after 5 minutes confirmed that the mean fluorescence intensity of fluorescent microcapsules was significantly higher for Fuco-MCs than for MCs (2275 ± 188 MFI versus 305 ± 69 MFI, respectively, $P < 0.001$) (Figure 8B).

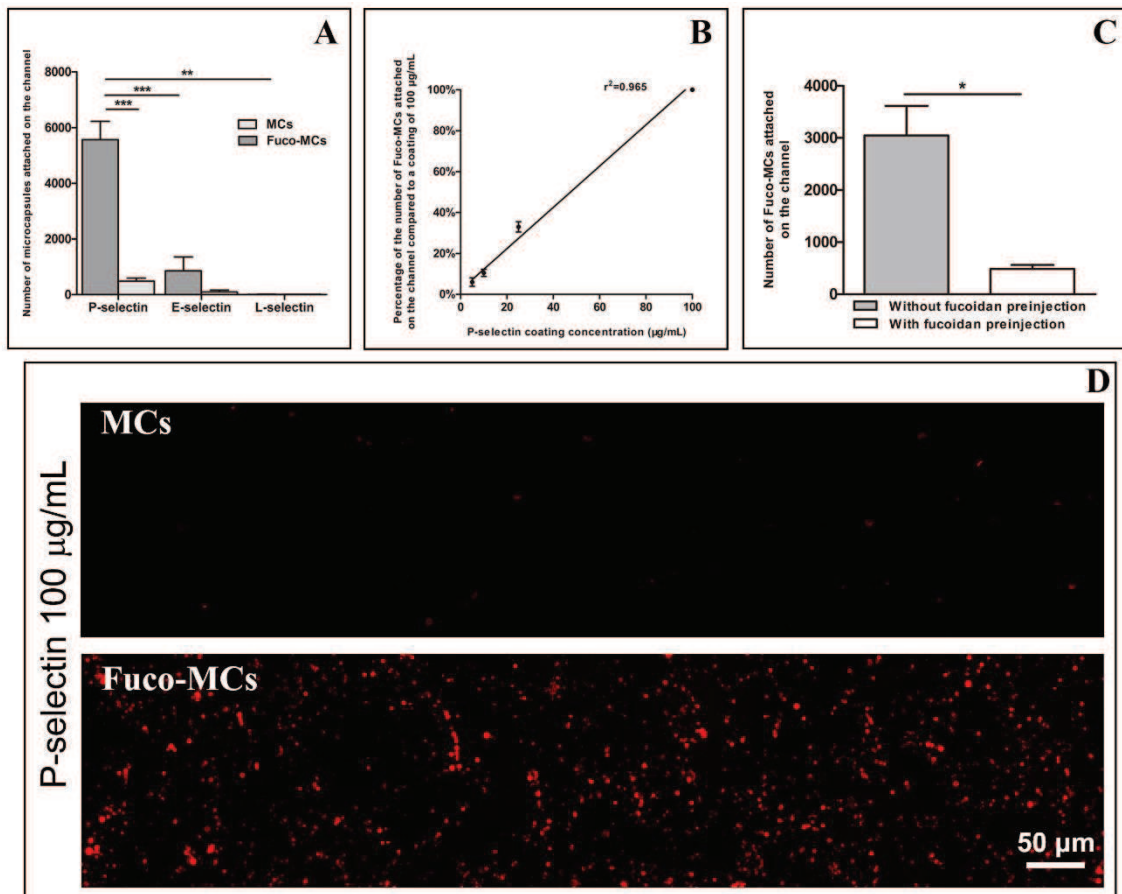


Figure 7. Evaluation of microcapsule interactions with recombinant selectins in an *in vitro* arterial flow assay.

A) Adhesion of microcapsules on selectins. Channels were coated at an E, L, P-selectin concentration of 100 µg/mL. MCs and Fuco-MCs were injected over 5 minutes under arterial flow conditions (shear rate: 1,500 s⁻¹). After 5 minutes, channels were washed with 0.9% NaCl. The number of fluorescent microcapsules attached along each channel was quantified with Histolab (Microvision) ($n > 3$, ** $p < 0.01$, *** $p < 0.001$). **B)** Number of attached microcapsules as a function of the P-selectin concentration from 5 µg/mL to 100 µg/mL. The number of microcapsules was normalized over the average number of microcapsules attached for a P-selectin concentration of 100 µg/mL. **C)** Fucoidan pre-injection inhibits Fuco-MCs binding. Channels were coated at a P-selectin concentration of 100 µg/mL. After washing with 0.9% NaCl, fucoidan solution (10 mg/ml) was injected or not over 5 min, then microcapsules were injected during 5 minutes. Channels were washed and the number of microcapsules was quantified (* $p < 0.05$). **D)** Macroscopic view of MCs or Fuco-MCs adhesion over a P-selectin coating of 100 µg/mL. ($n = 10$ for MCs and $n = 11$ for Fuco-MCs; Scale bar = 50 µm).

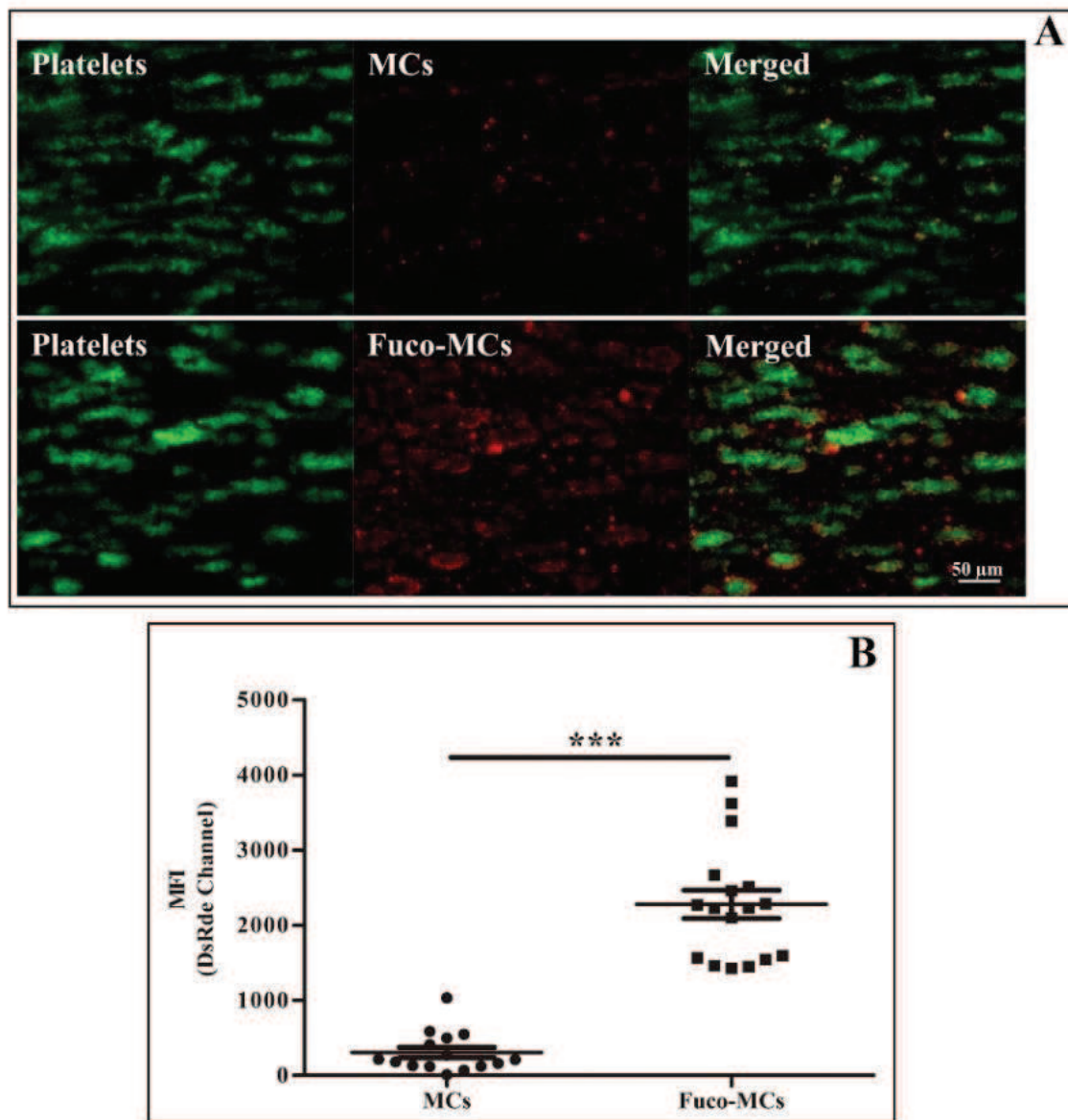


Figure 8. Microcapsule adhesion over platelet aggregates.

A) Whole blood labeled with DIOC₆ was injected onto channels coated with collagen at 50 $\mu\text{g}/\text{mL}$. Under arterial flow conditions, platelets adhered onto the channel wall forming aggregates expressing P-selectin (Left) and FITC-MCs or FITC-Fuco-MCs were then injected for 5 minutes (Middle panel). Channels were washed with 0.9% NaCl. Microcapsules and aggregates co-localization was assessed by merged fluorescence microscopy (Right). B) Quantitative analysis of the mean fluorescence intensity of platelet aggregates (n=15 for MCs and n=17 for Fuco-MCs; ***p<0.001).

Cell viability

The cytotoxicity of microcapsules was evaluated by MTT assay. As shown in Figure 9, the results demonstrated that MCs and Fuco-MCs did not significantly affect the mean viability of mouse fibroblasts 3T3 cells at concentrations of 0.625, 1.25, 2.5 and 5 g/L, there were no obvious difference between MCs and Fuco-MCs.

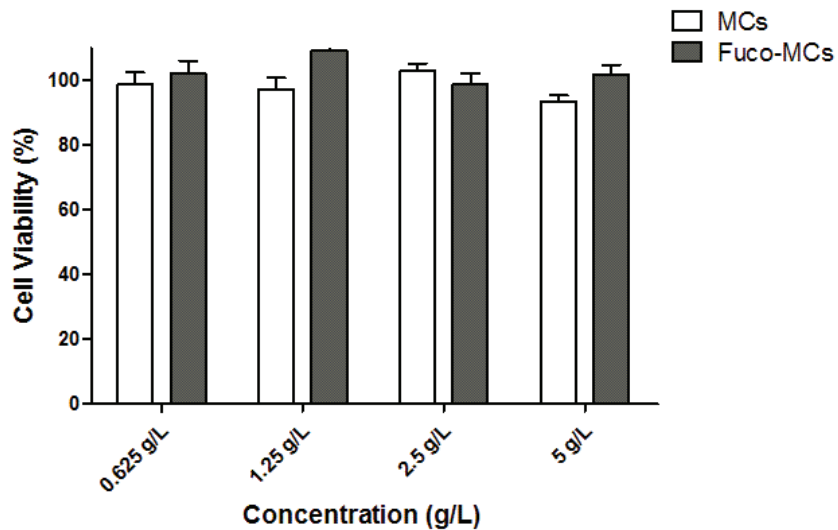


Figure 9. Cytocompatibility assay.

MTT assay performed on 3T3 cells after 24 h of incubation in the presence of MCs and Fuco-MCs at different concentrations. (n=6)

Localization of microcapsules within the thrombotic Abdominal Aortic Aneurysm wall of rats and biodistribution

To assess whether Fuco-MCs accumulated *in vivo* within an AAA, histological staining of both AAA and healthy aorta samples were performed 1 hour after the injection of FITC-MCs and FITC-Fuco-MCs. On histological stained sections, smooth muscle cells from connective tissues and several layers of the aneurysmal wall were distinguished (Figure 10A). Many Fuco-MCs (red spheres) were localized in the arterial wall, between the thrombus and the media layer compared to MCs (Figure 10A). On the other hand, only few Fuco-MCs were found in arterial wall of healthy rats (Figure 10A). Semi-quantitative analysis confirmed that the fluorescence in the AAA wall was higher for Fuco-MCs than for MCs, and the binding of Fuco-MCs or MCs in healthy aorta was low (Figure 10B).

To evaluate the biodistribution, the presence of MCs and Fuco-MCs in four organs (liver, spleen, lungs and kidneys) was assessed at 1 hour and 24 hours after injection by histological analysis of several sections of each organ. At 1 hour, both types of microcapsules were mainly found in lungs, (although no respiratory problems were noted), then in liver, in spleen and finally in kidneys. At 24 hours, the number of microcapsules decreased in a similar way in the four organs.

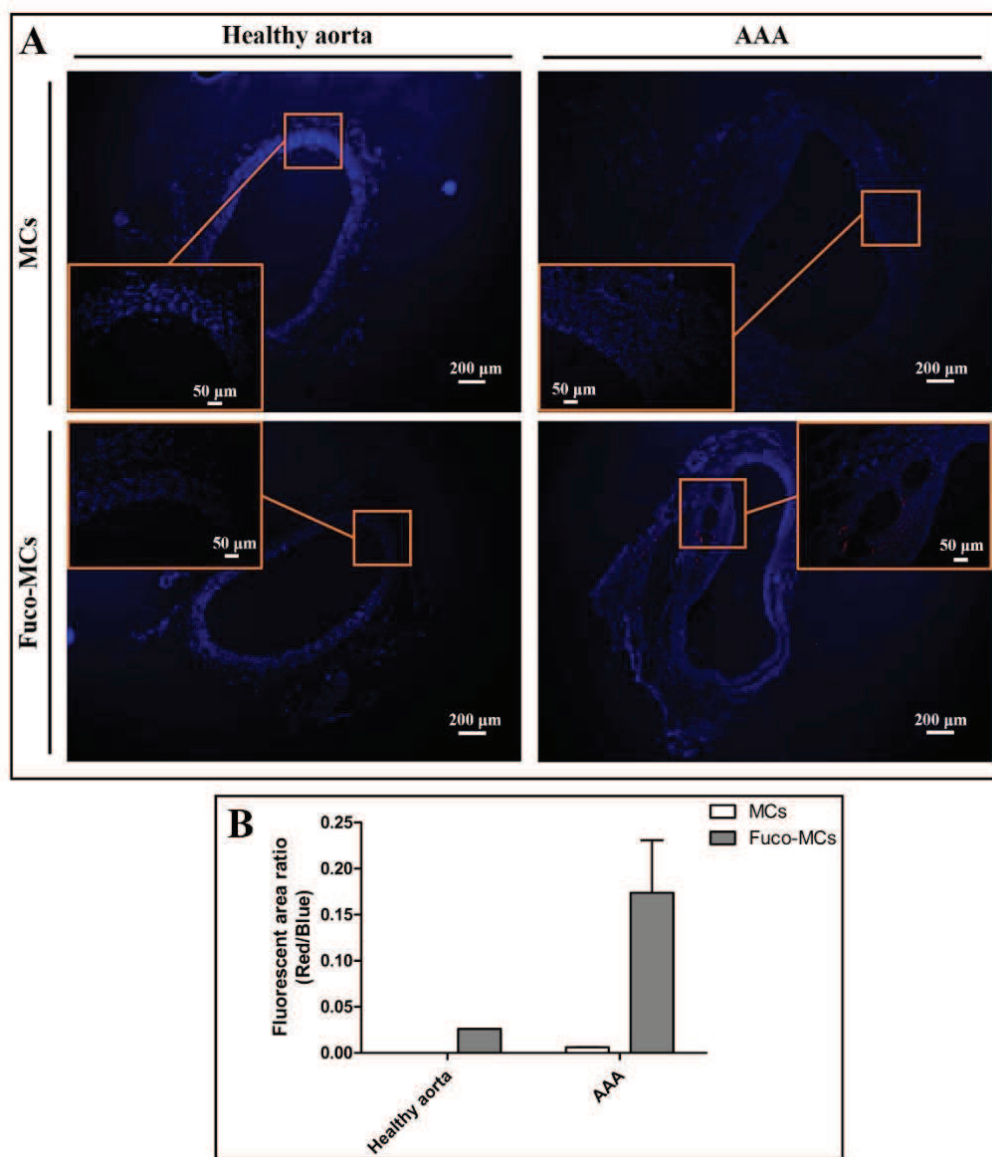


Figure 10. Histological analysis of abdominal aorta sections and corresponding semi-quantitative analysis.

A) Healthy rats (left) and rat Abdominal Aorta Aneurysms (right). Inserts are magnification of Regions of Interest. Muscle cells appear in blue fluorescence and MCs or Fuco-MCs appear in red. **B)** Data are expressed as the proportion of red fluorescent area to blue fluorescent area ($\times 20$) on healthy rats or rats with AAA injected with MCs or Fuco-MCs.

Discussion

In this study, injectable core-shell polymer microcapsules functionalized with fucoidan were developed as a carrier tool to target P-selectin overexpressed in cardiovascular diseases.

Nanoparticle made of PACA and coated with polysaccharides are promising substrates because of their biodegradability and biocompatibility.[17, 36] We developed here microcapsules composed of a lipophilic liquid core and a PIBCA-polysaccharide mixed membrane. This microcapsule structure was prepared by a new emulsion-evaporation polymerization process performed either in neutral or alkaline conditions. Using this method, the rate of polymerization was controlled by the evaporation rate. This technique allowed for the first time the polymerization of IBCA in emulsion under neutral and alkaline conditions leading to reproducible polymer microcapsules that can be functionalized with polysaccharides such as fucoidan.

Two key conditions must be fulfilled to form stable core-shell microcapsules. First, the water phase should contain water-soluble colloidal stabilizers, such as polysaccharides, making microcapsules more hydrophilic and avoiding particle aggregation. Second, the pH of the polymerization medium should be well controlled. Acidic condition reduced the initial polymerization rate resulting in insufficient polymer film thickness which did not provide enough surface tension to make droplets. Under neutral or alkaline conditions, the hydroxyl ions in the solution could accelerate the polymerization reaction to form stable shell encapsulating a hydrophobic agent.

For the use as drug carriers, the shell thickness-to-radius ratio (T/R) strongly influenced the embedded drug release behavior. Jiao et al. showed that the amount and rate of doxorubicin release in hollow mesoporous silica nanoparticles exhibited shell thickness dependence, decreasing with the increase of the shell thickness.[37] Furthermore, compare to undesired burst effect, drug controlled release prolongs the time of drug action.[38] Interestingly, we found that the polymer thickness could be easily modified from 330 nm to 770 nm depending on the pH of the polymerization medium. This property could be optimized for controlled drug release. In this study, PFOB was

used as a reference agent. The theranostic potential of these microcapsules will be investigated in the near future.

As previous studies, we found that Fuco-MCs shown low value of zeta potential compare to MCs. Flow cytometry experiments demonstrated that microcapsules were functionalized by fucoidan. Although the weight content of fucoidan in microcapsules was very low, it was stable at least for one month without obvious release. SEM and TEM analysis along with size measurements showed that the functionalization of microcapsules with fucoidan did not affect the spherical shape or the diameter distribution. Charoenphol et al. indicated that spheres exhibiting a diameter of 2.5 μm are optimal for targeting purposes in medium to large vessel walls, which are affected in numerous cardiovascular diseases.[8, 39] The size of our microcapsules from 2.2 μm to 5.8 μm appeared therefore adapted for vascular targeting purposes.

Cell viability assay is a powerful toll in providing valuable information regarding the safety of biomaterials. In this study, the *in vitro* cytotoxicity of microcapsules was evaluated by a colorimetric MTT assay on reference 3T3 cells. Results indicated that both types of microcapsules did not present obvious detrimental effects on 3T3 cells proliferation even at high concentration. Moreover, there was no significant difference between MCs and Fuco-MCs, as both of them had no cytotoxicity and good biocompatibility.

Using flow cytometry, we evidenced that the Fuco-MCs exhibited a stronger affinity for human activated platelets than MCs and that this binding could be inhibited by a P-selectin antibody. Similar results had been published by Bonnard T. et al. using fucoidan functionalized polysaccharide microparticles.[40]

Up to now, the design of carrier systems targeting specific molecules and able to bind them under high velocity blood flow conditions remains a challenge. In this study, an *in vitro* flow adhesion assay onto recombinant selectins confirmed that fucoidan functionalized microcapsules/Fuco-MCs rapidly and specifically bound to P-selectin compared to MCs even under high shear rate conditions (1,500 s⁻¹). Moreover, the number of attached Fuco-MCs was dependent on P-selectin concentration and free fucoidan in solution inhibited the binding of Fuco-MCs to P-selectin. Previous reports

indicated that the sulfate ester groups of fucoidan could be recognized by P-selectin and L-selectin,[41] but not by E-selectin.[42, 43] Our results indicated that Fuco-MCs could bind P-selectin but not L/E-selectins. Moreover, Fuco-MCs revealed a higher ability as compared to MCs to adhere to the surface of activated platelet aggregates under arterial flow conditions. The interaction between the fucoidan coated onto microcapsules and the P-selectin was strong enough to overcome kinetic energy of microcapsules even with their high density (close to 1.3 g/mL) that comes from the presence of liquid PFOB into their core.

Histological and semi-quantitative analysis revealed that Fuco-MCs were localized inside the media layer of the thrombotic AAA wall in rats, whereas very low binding was observed on AAA injected with MCs or on the artery wall of healthy rats injected with Fuco-MCs. Biodistribution studies showed that both types of microcapsules were present in the Mononuclear Phagocyte System (MPS), which is consistent with what is described in the literature, that they tended to be eliminated over 24 hours and that they had no obvers effect on the health of rats. In fact, some of the injected rats were still alive after 3 months. Since microcapsules functionalized with fucoidan accumulated in the inner wall of the AAA, a promising strategy to treat AAA could be to inhibit the proteolytic activity which occurs within the medial layer and lead to the arterial wall degradation.[44] The ability of Fuco-MCs to target the AAA could be associated with the loading of a proteolytic inhibitor in this microcarrier. Preliminary *in vitro* experiments also indicated that the loading of microcapsules with PFOB allowed ultrasound imaging. Such microcapsules loaded with a drug and functionalized with fucoidan appear therefore as promising molecular theranostic systems.

Conclusion

Microcapsules functionalized with fucoidan were developed here for the targeting of activated platelets in thrombotic abdominal aorta aneurysm using biodegradable and biocompatible polymer membrane composed of poly(isobutyl cyanoacrylate) and polysaccharides. In this work, we described their elaboration with a new alkaline solvent emulsion-evaporation polymerization process and we confirmed their hydrodynamic

diameter distribution, the microcapsule structure and the presence of the targeting agent, fucoidan, at the surface. This work gave the first evidence that functionalized microcapsules can be obtained according to an easy one-step polymerization process of isobutyl cyanoacrylate in neutral and alkaline conditions. *In vitro* cytotoxicity assay showed that the microcapsules exhibited excellent compatibility with cells *in vitro*. Subsequently, we demonstrated *in vitro* by flow cytometry that these fucoidan functionalized microcapsules could specifically bind to the P-selectin expressed by human activated platelets. Flow chamber experiments further confirmed that Fuco-MCs bind to P-selectin and to activated platelet aggregates even at high shear rate. Finally, we showed *in vivo* on rats the ability of Fuco-MCs to bind to thrombotic AAA and evidenced their presence in the AAA wall by histology. Future works are required to study the loading of contrast agents or therapeutics to achieve molecular diagnosis and/or treatment of cardiovascular pathologies overexpressing P-selectin.

Acknowledgments

This study was supported by Inserm, Paris Diderot University, Paris 13 University and Sorbonne Paris Cité. Bo LI is a recipient of the China Scholarship Council (CSC, No. 201206180031). The authors would like to thank C. Dong (CNRS UMR 7086, ITODYS, Paris Diderot University) for NMR measurements and F. Nadaud (UTC Compiègne, France) for SEM and TEM images. This work was also support by grants from ANR (ANR-12-EMMA-0020-01 “MicroSound”, ANR-13-LAB1-0005-01 “Fuco-Chem”) and EU project NanoAthero FP7-NMP-2012-LARGE-6-309820.

References

1. Yokoyama, S., et al., *Platelet P-selectin plays an important role in arterial thrombogenesis by forming large stable platelet-leukocyte aggregates*. Journal of the American College of Cardiology, 2005. **45**(8): p. 1280-6.
2. Hannawa, K.K., et al., *Attenuation of experimental aortic aneurysm formation in P-selectin knockout mice*. Annals of the New York Academy of Sciences, 2006. **1085**: p. 353-9.
3. Barber, P.A., et al., *MR molecular imaging of early endothelial activation in focal ischemia*. Annals of Neurology, 2004. **56**(1): p. 116-20.
4. Villanueva, F.S., et al., *Myocardial ischemic memory imaging with molecular echocardiography*. Circulation, 2007. **115**(3): p. 345-52.
5. McAteer, M.A., et al., *Magnetic resonance imaging of endothelial adhesion molecules in mouse atherosclerosis using dual-targeted microparticles of iron oxide*. Arterioscler Thromb Vasc Biol, 2008. **28**(1): p. 77-83.
6. Kaufmann, B.A., et al., *Detection of recent myocardial ischaemia by molecular imaging of P-selectin with targeted contrast echocardiography*. European heart journal, 2007.
7. Haverslag, R., G. Pasterkamp, and I.E. Hoefer, *Targeting adhesion molecules in cardiovascular disorders*. Cardiovascular & Haematological Disorders-Drug Targets, 2008. **8**(4): p. 252-260.
8. Charoenphol, P., et al., *Targeting therapeutics to the vascular wall in atherosclerosis--carrier size matters*. Atherosclerosis, 2011. **217**(2): p. 364-70.
9. Saboural, P., et al., *Purification of a low molecular weight fucoidan for SPECT molecular imaging of myocardial infarction*. Marine Drugs, 2014. **12**(9): p. 4851-67.
10. Rouzet, F., et al., *Radiolabeled fucoidan as a p-selectin targeting agent for in vivo imaging of platelet-rich thrombus and endothelial activation*. Journal of Nuclear Medicine, 2011. **52**(9): p. 1433-40.
11. Bonnard, T., et al., *Leukocyte mimetic polysaccharide microparticles tracked in vivo on activated endothelium and in abdominal aortic aneurysm*. Acta Biomaterialia, 2014. **10**(8): p. 3535-45.
12. Bachelet-Violette, L., et al., *Strong and specific interaction of ultra small superparamagnetic iron oxide nanoparticles and human activated platelets mediated by fucoidan coating*. RSC Advances, 2014. **4**(10): p. 4864-4871.
13. Suzuki, M., et al., *Ultrasmall superparamagnetic iron oxide nanoparticles coated with fucoidan for molecular MRI of intraluminal thrombus*. Nanomedicine (Lond), 2014: p. 1-15.
14. Couvreur, P., et al., *Polycyanoacrylate nanocapsules as potential lysosomotropic carriers: preparation, morphological and sorptive properties*. Journal of Pharmacy and Pharmacology, 1979. **31**(1): p. 331-332.
15. Bertholon, I., et al., *Characterization of Dextran-Poly(isobutylcyanoacrylate) Copolymers Obtained by Redox Radical and Anionic Emulsion Polymerization*. Macromolecules, 2006. **39**(10): p. 3559-3567.
16. Chauvierre, C., et al., *Radical Emulsion Polymerization of Alkylcyanoacrylates Initiated by the Redox System Dextran-Cerium(IV) under Acidic Aqueous Conditions*. Macromolecules, 2003. **36**(16): p. 6018-6027.
17. Chauvierre, C., et al., *Novel Polysaccharide-Decorated Poly(Isobutyl Cyanoacrylate) Nanoparticles*. Pharmaceutical Research, 2003. **20**(11): p. 1786-1793.
18. Langer, K., et al., *Characterisation of polybutylcyanoarylate nanoparticles: I. Quantification of PCBA polymer and dextrans*. International Journal of Pharmaceutics, 1994. **110**(1): p. 21-27.
19. Chauvierre, C., et al., *Enhancing the tolerance of poly(isobutylcyanoacrylate) nanoparticles with a modular surface design*. International Journal of Pharmaceutics, 2007. **338**(1-2): p. 327-332.
20. Lambert, G., et al., *Polyisobutylcyanoacrylate nanocapsules containing an aqueous core as a novel colloidal carrier for the delivery of oligonucleotides*. Pharmaceutical Research, 2000. **17**(6): p. 707-14.
21. Yordanov, G., *Poly (alkyl cyanoacrylate) nanoparticles as drug carriers: 33 years later*. Bulgarian Journal of Chemistry, 2012. **1**(2).
22. Bagad, M. and Z.A. Khan, *Poly(n-butylcyanoacrylate) nanoparticles for oral delivery of quercetin: preparation, characterization, and pharmacokinetics and biodistribution studies in Wistar rats*. International Journal of Nanomedicine, 2015. **10**: p. 3921-35.
23. Vauthier, C., et al., *Drug delivery to resistant tumors: the potential of poly(alkyl cyanoacrylate) nanoparticles*. Journal of Controlled Release, 2003. **93**(2): p. 151-60.

24. Kisich, K.O., et al., *Encapsulation of moxifloxacin within poly(butyl cyanoacrylate) nanoparticles enhances efficacy against intracellular Mycobacterium tuberculosis*. International Journal of Pharmaceutics, 2007. **345**(1-2): p. 154-62.
25. Soma, C.E., et al., *Reversion of multidrug resistance by co-encapsulation of doxorubicin and cyclosporin A in polyalkylcyanoacrylate nanoparticles*. Biomaterials, 2000. **21**(1): p. 1-7.
26. Chauvierre, C., et al., *Heparin coated poly(alkylcyanoacrylate) nanoparticles coupled to hemoglobin: a new oxygen carrier*. Biomaterials, 2004. **25**(15): p. 3081-3086.
27. Liang, M., N.M. Davies, and I. Toth, *Increasing entrapment of peptides within poly(alkyl cyanoacrylate) nanoparticles prepared from water-in-oil microemulsions by copolymerization*. International Journal of Pharmaceutics, 2008. **362**(1-2): p. 141-6.
28. Lambert, G., *Polyalkylcyanoacrylate Nanospheres and Nanocapsules for the Delivery of Antisense Oligonucleotides*. Journal of Dispersion Science and Technology, 2003. **24**(3-4): p. 439-452.
29. Yordanov, G. and C. Dushkin, *Preparation of poly(butylcyanoacrylate) drug carriers by nanoprecipitation using a pre-synthesized polymer and different colloidal stabilizers*. Colloid and Polymer Science, 2010. **288**(9): p. 1019-1026.
30. Yordanov, G., R. Skrobanska, and A. Evangelatov, *Entrapment of epirubicin in poly(butyl cyanoacrylate) colloidal nanospheres by nanoprecipitation: formulation development and in vitro studies on cancer cell lines*. Colloids and Surface. B Biointerfaces, 2012. **92**: p. 98-105.
31. Yordanov, G., A. Evangelatov, and R. Skrobanska, *Epirubicin loaded to pre-polymerized poly(butyl cyanoacrylate) nanoparticles: preparation and in vitro evaluation in human lung adenocarcinoma cells*. Colloids and Surface. B Biointerfaces, 2013. **107**: p. 115-23.
32. Yordanov, G., R. Skrobanska, and A. Evangelatov, *Colloidal formulations of etoposide based on poly(butyl cyanoacrylate) nanoparticles: preparation, physicochemical properties and cytotoxicity*. Colloids and Surface. B Biointerfaces, 2013. **101**: p. 215-22.
33. Evangelatov, A., et al., *Epirubicin loading in poly(butyl cyanoacrylate) nanoparticles manifests via altered intracellular localization and cellular response in cervical carcinoma (HeLa) cells*. Drug Deliv, 2015: p. 1-10.
34. Li, S., et al., *In vitro release of protein from poly(butylcyanoacrylate) nanocapsules with an aqueous core*. Colloid and Polymer Science, 2005. **283**(5): p. 480-485.
35. Lira, M.C.B., et al., *Cytotoxicity and cellular uptake of newly synthesized fucoidan-coated nanoparticles*. European Journal of Pharmaceutics and Biopharmaceutics, 2011. **79**(1): p. 162-170.
36. Vauthier, C., et al., *Poly(alkylcyanoacrylates) as biodegradable materials for biomedical applications*. Adv Drug Deliv Rev, 2003. **55**(4): p. 519-48.
37. Jiao, Y., et al., *Synthesis of discrete and dispersible hollow mesoporous silica nanoparticles with tailored shell thickness for controlled drug release*. Journal of Materials Chemistry, 2012. **22**(34): p. 17636-17643.
38. Chan, J.M., et al., *Spatiotemporal controlled delivery of nanoparticles to injured vasculature*. Proceedings of the National Academy of Sciences, 2010. **107**(5): p. 2213-2218.
39. Charoenphol, P., R.B. Huang, and O. Eniola-Adefeso, *Potential role of size and hemodynamics in the efficacy of vascular-targeted spherical drug carriers*. Biomaterials, 2010. **31**(6): p. 1392-402.
40. Bonnard, T., et al., *Abdominal Aortic Aneurysms Targeted by Functionalized Polysaccharide Microparticles: a new Tool for SPECT Imaging*. Theranostics, 2014. **4**(6): p. 592-603.
41. Thorlacius, H., et al., *The polysaccharide fucoidan inhibits microvascular thrombus formation independently from P- and L-selectin function in vivo*. European Journal of Clinical Investigation, 2000. **30**(9): p. 804-10.
42. Foxall, C., et al., *The three members of the selectin receptor family recognize a common carbohydrate epitope, the sialyl Lewis(x) oligosaccharide*. The Journal of Cell Biology, 1992. **117**(4): p. 895-902.
43. Silva, A.K., D. Letourneau, and C. Chauvierre, *Polysaccharide nanosystems for future progress in cardiovascular pathologies*. Theranostics, 2014. **4**(6): p. 579-91.
44. Klink, A., et al., *Diagnostic and therapeutic strategies for small abdominal aortic aneurysms*. Nature Reviews. Cardiology, 2011. **8**(6): p. 338-47.
45. Pisani, E., et al., *Polymeric nano/microcapsules of liquid perfluorocarbons for ultrasonic imaging: physical characterization*. Langmuir, 2006. **22**(9): p. 4397-402.
46. Gustafsson, L., *Determination of ultramicro amounts of sulphate as methylene blue—I*. Talanta, 1960. **4**(4): p. 227-235.
47. Delbosc, S., et al., *Porphyromonas gingivalis participates in pathogenesis of human abdominal aortic aneurysm by neutrophil activation. Proof of concept in rats*. PLoS One, 2011. **6**(4): p. e18679.

Conclusion

Des microcapsules fonctionnalisées ont été synthétisées par un nouveau procédé simple et reproductible. Sous cette forme, les matériaux n'induisent pas de cytotoxicité à 24 heures. Ces systèmes apparaissent comme très prometteurs pour l'imagerie moléculaire de l'AAA. Ils lient spécifiquement la P-sélectine et présentent une affinité très importante pour les plaquettes activées sous conditions de flux artériel. Une accumulation des microcapsules fonctionnalisées est observée dans la paroi anévrismale dans un modèle préclinique d'AAA. L'utilisation de ces microcapsules comme outils fonctionnels pour l'échographie reste à démontrer en étudiant leur échogénicité *in vitro* et *in vivo*.

2. Nanoparticules copolymères pour la thrombolyse ciblée

Publication:

Thrombolytic therapy based on fucoidan-functionalized polymer nanoparticles targeting P-selectin

*Maya Juenet, Rachida Aid-Launais, Alice Berger, Bo Li, Joël Aerts,
Véronique Ollivier, Didier Letourneur, Cédric Chauvierre*

Theranostics – currently under revision

Keywords: nanomedicine, thrombolysis, fucoidan, P-selectin, drug delivery

Introduction

Le rt-PA est le traitement standard des AVC ischémiques. Des études cliniques ont montré que ce traitement avait une efficacité limitée avec l'induction d'une recanalisation totale chez moins de 50% des patients qui en bénéficient. Les complications hémorragiques liées à son utilisation font qu'il n'est en pratique injecté qu'à moins de 10% des patients. Plusieurs études précliniques ont démontré le potentiel de la nanomédecine pour augmenter l'efficacité thrombolytique. La nanomédecine permet d'assurer une délivrance ciblée au thrombus. Parmi les différentes stratégies à l'étude, le ciblage moléculaire semble prometteur en vue d'une simple injection. L'interaction forte entre le fucoïdane et la P-sélectine exprimée par les plaquettes activées n'a pas, à notre connaissance, encore été mise à profit dans ce cadre. Des nanoparticules copolymères polysaccharides-PIBCA présentant du fucoïdane dans leur couronne de polysaccharides sont chargées en rt-PA par adsorption. Ces systèmes sont évalués *in vitro* et *in vivo*.

Résumé de l'article

Les références en italique désignent les figures de l'article qui suit.

Des nanoparticules copolymères polysaccharides-PIBCA sont synthétisées par le mécanisme de RREP illustré **Figure 18**. Deux types de nanoparticules sont formulées, avec les proportions suivantes de polysaccharides : 10% fucoïdane/40% dextrane-NH₂/50% dextrane (Fuco-NPs) et 10% Carboxyméthyle-dextrane/40% dextrane-NH₂/50% dextrane (Control-NPs). Le fucoïdane utilisé est le même que celui du projet présenté dans l'article précédent. Les Fuco-NPs et Control-NPs sont sphériques et présentent une taille hydrodynamique similaire (136 nm et 130 nm respectivement) et un potentiel zéta proche (-4,9 mV et -2,5 mV respectivement). Le fucoïdane est présent dans les Fuco-NPs à hauteur de 1,56% du poids total de la nanoparticule (**Figure 1**). La biodistribution des Fuco-NPs est évaluée chez la souris après marquage des nanoparticules au ^{99m}Tc. L'imagerie TEMP et la biodistribution tissulaire, réalisées à 80 minutes après injection, montrent une élimination rénale suivie d'une accumulation dans le foie (**Figure 2**).

Le modèle en flux décrit au précédent chapitre est utilisé pour comparer l'interaction des Fuco-NPs et Control-NPs avec la P-sélectine et avec des agrégats plaquettaires activés. Pour cette étude, du Nile Red, un fluorophore hydrophobe, est chargé au cœur de la nanoparticule. Le fucoïdane permet de multiplier par un facteur 10 le nombre de clusters de nanoparticules visibles à la surface de la P-sélectine recombinante en conditions veineuses et artérielles (**Figure 3**). Aussi, les Fuco-NPs s'accumulent davantage que les Control-NPs à la surface des agrégats plaquettaires activés en flux, même une fois chargées en rt-PA (**Figure 5**). Ce test est réalisé en condition veineuse pour simuler les conditions du modèle *in vivo* testé ensuite.

Afin de garder l'affinité du rt-PA pour la fibrine et ainsi conserver la totalité de son activité enzymatique, le rt-PA est chargé sur les nanoparticules par adsorption dans un tampon PBS-Tween 20 0,01% w/v. Après 3 cycles d'ultrafiltration, l'activité amidolytique du rt-PA restant est légèrement affectée. Une diminution de 14% est mesurée dans le cas des rt-PA-Fuco-NPs par rapport à la même quantité d'actif seul préparé dans le même tampon. Cette observation est probablement liée à un changement

de conformation de l'enzyme au contact des nanoparticules. Néanmoins, l'activité fibrinolytique, mesurée par une méthode classique de lyse d'un réseau de fibrine dans un gel d'agar, est entièrement conservée (**Figure 4**).

Un modèle de thrombose murin est obtenu par apposition de FeCl_3 à 10% sur une veine mésentérique pendant 1 minute (**Figure 22**). Une injection de rhodamine 6G (Rh6G) dans la circulation est effectuée pour marquer les plaquettes et suivre l'évolution du thrombus par microscopie intravitale. 5 groupes sont définis ; rt-PA-Fuco-NPs, rt-PA-Control-NPs, rt-PA, Fuco-NPs et tampon. Les différents traitements sont injectés en moyenne 7 minutes après induction du modèle et entrent en compétition avec la formation du thrombus. L'intensité de fluorescence du thrombus est enregistrée à intervalles réguliers jusqu'à 30 minutes après injection. À 30 minutes, seules les Fuco-NPs associées au rt-PA (rt-PA-Fuco-NPs) induisent une recanalisation significative par rapport à l'injection du tampon (**Figure 6**).

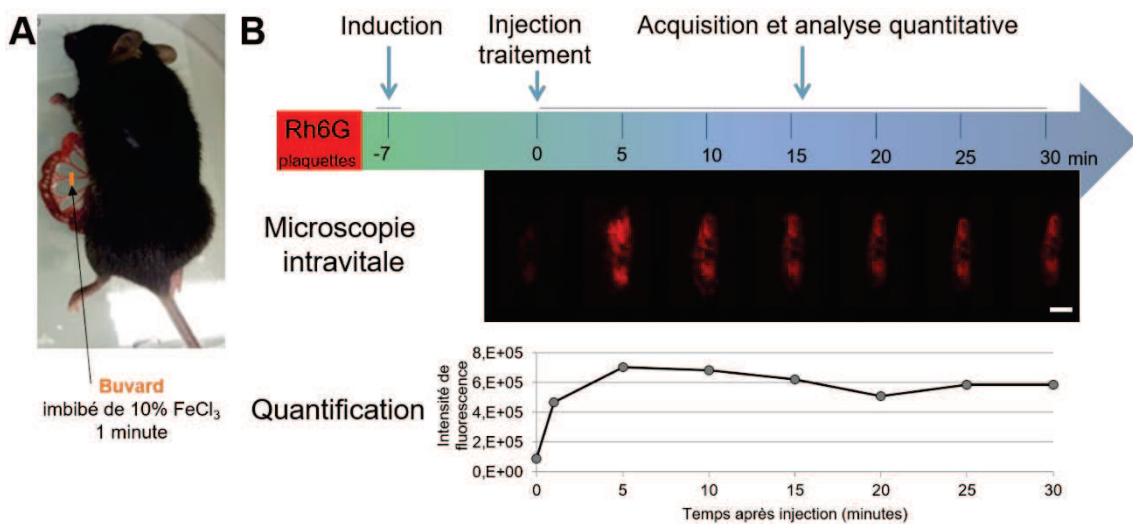
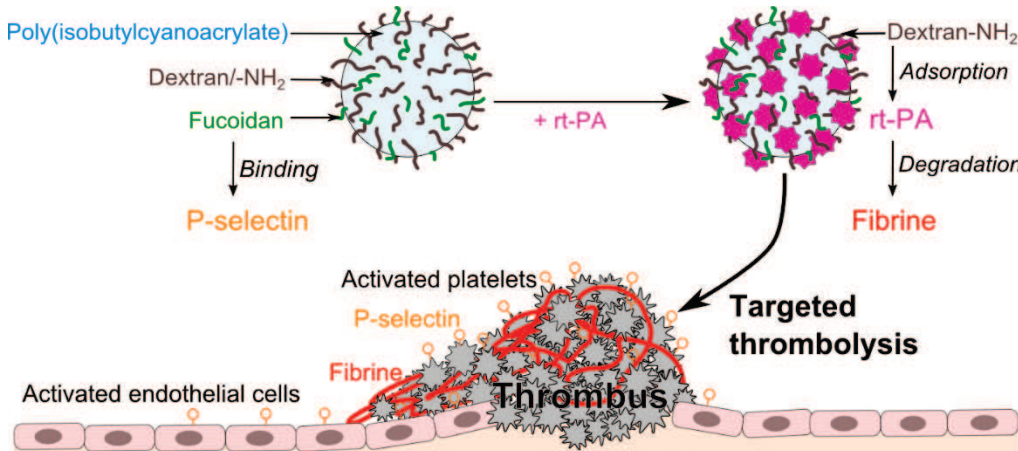


Figure 22. Modèle préclinique pour l'évaluation des nanoparticules copolymères.

A) Exposition du mésentère et induction du thrombus. B) Protocole pour l'induction du thrombus, l'injection du traitement et la visualisation de l'évolution du thrombus. Exemple d'images et signal correspondant dans le cas de l'injection d'un tampon (groupe contrôle). Une injection de Rhodamine 6G (Rh6G) dans la circulation est réalisée pour marquer les plaquettes. Le thrombus est visualisé en temps réel par microscopie intravitale. Le traitement est injecté quand une agrégation plaquettaire est enclenchée (en moyenne 7 minutes après induction). L'intensité de fluorescence totale du thrombus est mesurée. Enfin, la réduction relative entre le maximum d'intensité et l'intensité à 30 minutes est calculée pour comparer les différents traitements.

Thrombolytic therapy based on fucoidan-functionalized polymer nanoparticles targeting P-selectin



Abstract

Acute thrombotic events, such as ischemic stroke, are major causes of death and long-term disability. Injection of recombinant tissue plasminogen activator (rt-PA) remains the standard non-invasive drug treatment to induce thrombolysis and restore the blood flow. However, rt-PA shows a limited efficiency even at high doses and is associated to subsequent risk of intracranial hemorrhages. In this study, polysaccharide-poly(isobutylcyanoacrylate) nanoparticles functionalized with fucoidan and loaded with rt-PA were investigated to improve the thrombolytic efficiency of rt-PA by specifically accumulating this drug on the thrombus. Fucoidan, a natural sulfated polysaccharide, has indeed a nanomolar affinity for the P-selectin expressed by activated platelets in the thrombus.

Solid spherical fluorescent nanoparticles with a hydrodynamic diameter of 136 ± 4 nm were synthesized by redox radical emulsion polymerization. rt-PA in its clinical formulation (Actilyse®) was loaded by adsorption on aminated nanoparticles. We found that loaded rt-PA kept its full fibrinolytic potential *in vitro*. The binding efficiency of the functionalized nanoparticles to recombinant P-selectin and to activated platelet aggregates

under flow was validated *in vitro*. The thrombolysis efficiency of rt-PA associated to fucoidan-nanoparticles was demonstrated in a mouse model of venous thrombosis by monitoring the platelet density with intravital microscopy.

This study supports the hypothesis that fucoidan-nanoparticles improve the rt-PA efficiency by promoting its specific accumulation. This work establishes the first proof-of-concept of the potential of fucoidan-based nanocarriers for targeted thrombolysis. Future development will focus on the nanoparticle interactions *in vivo* using several animal models of thrombosis.

Introduction

Since the 1990's, intravenous injection of recombinant tissue plasminogen activator (rt-PA) has remained the recommended treatment to induce vessel recanalization in acute thrombotic events such as ischemic stroke [1, 2]. rt-PA is a serine protease that catalyzes the conversion of plasminogen to plasmin. Plasmin degrades the fibrin network of the thrombus and therefore generates thrombolysis. rt-PA preferentially acts by forming a ternary complex in which both rt-PA and plasminogen are bound to fibrin. However, because of its short half-life, high doses of rt-PA need to be injected which generate a cascade of events in the circulation leading to serious side effects. Intracranial hemorrhages are indeed observed in 6% of the treated patients causing 50% of subsequent mortality [3]. In consequence of these bleeding complications and of reported neurotoxic effects, the benefit-to-risk ratio of rt-PA administration rapidly decreases with time and less than 10% of patients end up receiving treatment [4].

The most significant improvements in interventional management of stroke include the association of rt-PA with endovascular methods [5]. These strategies have enabled to increase the therapeutic window from 3.5 to 6 hours after the first symptoms onset. However, the use of endovascular devices is limited to "easy-to-reach" thrombi and requires highly trained neuro-interventionist as well as specific clinical facilities [6]. Thus, there is still an urgent need for safe and non-invasive treatments. In addition to the development of other fibrinolytic agents [2, 7], nanomedical approaches for local or

targeted delivery of thrombolytic drugs arouse a growing interest [8-10]. Lipid and/or PEGylated nanostructures encapsulating a thrombolytic drug were first reported and showed benefit from increasing the drug half-life [11-14]. More recently, this strategy was combined with active targeting approaches, mostly based on magnetic guidance [15-19]. Once accumulated on the thrombus, nano-carriers improve thrombolytic efficiency while reducing hemorrhagic complications, in preclinical models of thrombosis. Yet, the use of an external magnet makes these nanostructures hardly scalable in general clinical setting. Another approach to promote the specific accumulation of the drug relies on functionalizing nanocarriers with antibodies and/or peptides directed against the fibrin network [20-22] or against the glycoprotein IIb/IIIa (GPIIb/IIIa) expressed by activated platelets [23-25]. Unlike GPIIb/IIIa, P-selectin has been poorly explored with respect to targeted thrombolysis, although this transmembrane glycoprotein is not expressed by resting platelets in the circulation and is extensively expressed by activated platelets localized in the thrombus [26]. In addition, P-selectin is overexpressed by activated endothelial cells, in diseases with vascular activation such as ischemic events [27].

In this work, P-selectin was chosen as the molecular target. It has been previously demonstrated *in vivo* that fucoidan-functionalized nanoparticles or microparticles targeting P-selectin can be used for the diagnosis of endothelial activation and intraluminal thrombosis [28, 29]. Fucoidan refers to a type of highly sulfated polysaccharide containing L-fucose groups [30]. This natural compound exhibits a high affinity for P-selectin, mimicking its main ligand the P-selectin Glycoprotein Ligand 1 (PSGL-1) [31]. To the best of our knowledge, no nanoparticle combining fucoidan and a thrombolytic drug has been developed yet.

Polymer nanoparticles, and especially polysaccharide-based nanoparticles, are promising for the combination of fucoidan with rt-PA [32]. The nanoparticles (NPs) designed in this study were based on polysaccharide-poly(isobutylcyanoacrylate) NPs produced by redox radical emulsion polymerization (RREP). In contrast to the anionic emulsion polymerization, RREP produces stealth NPs with polysaccharides located at the surface in a brush-like structure [33, 34]. The drug was loaded by adsorption on the polysaccharide shell to promote its direct availability at the thrombus site and the full

retention of its activity. Dextran modified with amino groups was incorporated into the nanoparticle formulation, to mimic the free primary amines present in L-arginine used to stabilize rt-PA in Actilyse® [35]. After demonstrating that the presence of fucoidan can effectively improve *in vitro* the interaction of fucoidan-functionalized NPs (Fuco-NPs) with P-selectin under flow, rt-PA-Fuco-NPs were evaluated *in vitro* and *in vivo*.

Methods and Materials

Materials

Isobutylcyanoacrylate (IBCA) monomers were provided by Orapi (Saint Vulbas, France). Several polysaccharides were used: dextran 40 was purchased from PharmaCosmos (Holbaek, Denmark) and carboxymethyl-dextran 40 (carboxyl content of 5% w/w) from TdB Consultancy (Uppsala, Sweden). Medium molecular weight fucoidan ($M_n = 18 \text{ kDa} / M_w = 104 \text{ kDa}$) was a gift from Algues & Mer (Ouessant, France). NPs were mixed with commercially available rt-PA provided by Boehringer Ingelheim (Ingelheim am Rhein, Germany) in its Actilyse® form. It was reconstituted according to the manufacturer's recommendations and then aliquoted and stored at -80°C for up to 12 months.

Chemical modification of dextran with amino groups

Amino groups were grafted to dextran chains according to a method described by Prigent-Richard et al. [36]. Dextran was dissolved in an aqueous basic solution, cooled at 4°C during 40 minutes and 3-Bromopropylamine hydrobromide (Sigma-Aldrich, Saint-Quentin Fallavier, France) was added at an equivalent of 0.5 molecules per glucose unit. The solution was left to react 4 hours at room temperature under stirring and then neutralized. Modified dextran chains were precipitated in ethanol, solubilized in distilled water and extensively dialyzed against water using a Biotech CE tubing dialysis tubing (MWCO 1,000 Da, Spectrum Europe B.V., Breda, The Netherlands). The polysaccharide was finally freeze-dried before use. The amine content was determined by elemental analysis of nitrogen.

Polysaccharide-poly(isobutylcyanoacrylate) nanoparticle synthesis

Polysaccharides were dissolved in a nitric acid solution (0.2 M) and kept 10 minutes at 40°C under nitrogen bubbling and magnetic stirring. To synthesize fucoidan-functionalized NPs (Fuco-NPs), 137.5 mg of polysaccharides were introduced in the following proportions: 10% w/w fucoidan, 40% w/w amino-dextran and 50% w/w dextran. For control-NPs, the anionic fucoidan was replaced by anionic carboxymethylated dextran. Ammonium nitrate cerium (IV) ions at 0.08 M in nitric acid 0.2 M were added to the polysaccharide solution, which initiated the formation of radicals. 500 µL of IBCA monomers were consequently added, according to the method described by Chauvierre et al. [33]. Nile Red, a hydrophobic fluorescent dye (Sigma Aldrich, Saint Quentin Fallavier, France), dissolved in acetone at 0.5 mg/mL was incorporated in the medium just after the IBCA to label the hydrophobic core based on the work of Lira et al. [37]. To synthesize similar non-fluorescent NPs, acetone alone was added. The medium was left to react for 50 minutes. A trisodium citrate solution was added dropwise to inhibit the reaction and the medium was neutralized by NaOH 1 M. The final suspension was centrifuged at 2,500 g to remove any large aggregates coming from the block polymerization of IBCA and further dialyzed against water (MWCO 100 kDa).

Physico-chemical nanoparticle characterization

Size and Zeta potential were measured by dynamic light scattering (DLS) and electrophoretic light scattering (ELS) respectively (Zetasizer NanoZS, Malvern Instruments SARL, Orsay, France). Samples were dissolved in distilled water and KCl 1 mM for size and zeta potential determination respectively. Particles morphology was visualized by Scanning Electron Microscopy (SEM) (Philips XL 30 ESEM-FEG, Amsterdam, The Netherlands). For all experiments described in this study, NPs were normalized by mass concentration determined after freeze-drying.

Finally, the fucoidan content was determined by a semi-quantitative solid-phase colorimetric assay described by Lee et al. [38]. Briefly, NPs were fixed on Whatman

chromatography paper (Sigma-Aldrich) and put in contact with methylene blue. After extraction with Sodium Dodecyl Sulfate at 2% w/v in methanol 15 minutes at 50°C, the amount of adsorbed dye was determined by absorbance reading at 663 nm on an Infinite® 200 PRO microplate reader (TECAN Group Ltd., Männedorf, Switzerland). Standard curves were obtained from fucoidan in solution with known concentrations.

Nanoparticle radiolabeling for biodistribution study

Fuco-NPs were radiolabeled with ^{99m}Tc to assess their biodistribution. The radiolabeling protocol for SPECT was adapted from the one developed by our team to label polysaccharide microparticles [28]. 200 MBq of sodium pertechnetate [^{99m}Tc]Na was mixed with 2.8 µg of stannous chloride and 500 µg of Fuco-NPs in NaCl 0.9%. Stannous chloride is required to reduce pertechnetate and enable an interaction of the reduced radioactive species with the polysaccharide shell of the nanoparticles [39]. The suspension was incubated for 7 minutes at room temperature. Instant thin-layer chromatography (ITLC) was performed to control that the amount of free ^{99m}Tc was \leq 5%. 2 µL of the suspension were dropped off a silica gel layer (ITLC-SG Varian) and migration was allowed to occur with methyl-ethyl-ketone (minimum 7 cm). Thus, no supplementary purification step was performed to eliminate free pertechnetate from radiolabeled Fuco-NPs before injection. In parallel, 1 mL of the radiolabeled nanoparticles was centrifuged at 6,400 g for 5 minutes to remove any technetium aggregates. The activities of the supernatant (containing the radiolabeled nanoparticles) and of the pellet (containing large aggregates) were measured with an ionization chamber (Medi 40, Medisystem, Guyancourt, France).

In vivo SPECT/CT imaging

The animal study was performed in respect of the applicable regulation for animal experimentation and with approval of the animal care and use committee of the Claude Bernard Institute (Autor. APAFIS #8724, Paris, France).

C57BL/6 male mice (weight 20-23 g) (Elevage Janvier, CERJ, Laval, France) were used for *in vivo* imaging studies. Mice were kept fully sedated with 1.5-2% isoflurane during the injection step and the SPECT/CT imaging. 200 µL of the radiolabeled suspension (30 MBq) corresponding to 100 µg of nanoparticles was injected through the retro-orbital route. SPECT/CT images were acquired 80 minutes after injection, using a nanoSPECT/CT apparatus (Mediso medical imaging systems, Hungary) with 4 detectors. Ultra-high resolution (0.5 mm) multi-pinhole whole body mouse collimators were used. In addition, 20 angular projections with 50 s/projection and a peak energy window of 140 keV ± 20% were used. Data were reconstructed using the TeraTomo software (Mediso medical imaging systems, Hungary) and a 3D Monte Carlo-based algorithm (64×64 matrix, voxel size of 0.47×0.47×0.47 mm³, 3 subsets and 48 iterations). Finally, slides were visualized in 3 planes: sagittal, coronal and axial. A 3D movie was also reconstructed.

Tissue biodistribution

Biodistribution of radiolabeled nanoparticles was performed in 3 mice C57Bl/6 (20–23 g, Elevage Janvier, CERJ, Laval, France). Mice were anesthetized with intraperitoneal injection of ketamine (Vétoquinol SA, Lure, France) and xylazine (Bayer SAS, La Garenne-Colombes, France) at 100 mg/kg and 10 mg/kg respectively. Mice were injected through the retro-orbital route, with an activity of 10 MBq, corresponding to 100 µg of radiolabeled nanoparticles. Mice were sacrificed on average 80 minutes after injection with an overdose of anesthesia. Liver, spleen, kidneys, heart, lungs, brain, testis, a sample of skin (plus hairs), skeletal muscle, bone (femur), blood and urine, were sampled. All samples, as well as the injected solution, were put in pre-weighed plastic vials. The samples were weighed, and their radioactivity was measured in an automated gamma counter (PerkinElmer 1480 Wizard™3'', Villebon-sur-Yvette, France) collecting 171 and 245 keV gamma rays (window width: 135-300 keV). The results were calculated as percent injected dose per gram of organ (% ID/g). It is worth highlighting that after 80 minutes, urine had been partially excreted. Therefore the % ID/g value associated to it is an underestimate of what had been eliminated by this way.

Flow binding assay of nanoparticles on recombinant P-selectin

To evaluate the interaction of unloaded NPs with their molecular target, an *in vitro* binding assay under flow was developed [40]. Micro-channels of Vena8 Fluoro+ chambers (Cellix Ltd, Dublin, Ireland) were coated overnight with recombinant human P-selectin (R&D systems France, Lille, France) at 50 µg/mL and rinsed with NaCl 0.9% just before use.

NPs diluted at 1 mg/mL in NaCl 0.9% were perfused through channels for 5 minutes either at venous or arterial flow with an ExiGo™ pump (Cellix Ltd, Dublin, Ireland). Venous and arterial conditions corresponded to a shear stress of 6.75 dyne/cm² and of 67.5 dyne/cm², respectively. The binding of NPs was visualized in real time under fluorescence microscopy (Axio Observer, Carl Zeiss Microimaging GmbH, Iena, Germany). The quantitative analysis was limited to NP clusters that formed onto the coated channel because of the resolving power of the fluorescence microscope. After rinsing with NaCl 0.9%, 10 fields per channel (area of 1230 µm x 105 µm) were imaged and analyzed with the image analysis software ImageJ (NIH, Bethesda, U.S.) to quantify the number of fluorescent NPs clusters. Unspecific binding was controlled on uncoated channels and on channels coated with Bovine Serum Albumin at 50 µg/mL.

rt-PA loading onto nanoparticles

rt-PA at 0.4 mg/mL was put in contact with NPs at 0.3 mg/mL for 2 hours at 4°C under gentle agitation in PBS buffer with 0.01% v/v Tween 20. The suspensions were then purified by ultrafiltration at 15,000 g with Vivaspin 500 device (Sartorius France SAS, Dourdan, France). A Molecular Weight Cut Off of 300 kDa was chosen to eliminate free rt-PA (68 kDa). Three cycles of washes were performed with the Tween-PBS buffer. The protein content of the purified suspensions was determined by Pierce BCA protein assay (Life Technologies SAS, Courtaboeuf, France). A supplementary step to eliminate any artifact coming from the NPs was applied according to the manufacturer's protocol for eliminating interfering substances.

***In vitro* amidolytic and fibrinolytic activities of rtPA-loaded-nanoparticles**

After normalizing the amount of rt-PA loaded onto the NPs and free rt-PA based on the Pierce BCA protein assay, amidolytic and fibrinolytic activities were measured.

Amidolytic activity of rt-PA loaded NPs was assessed with the fluorogenic substrate PefaFluor® tPA (Cryopep, Montpellier, France). After addition of Pefafuor®, a kinetic profile was obtained by measuring the fluorescence level every 30 seconds during 80 minutes at 37°C with Infinite® 200 PRO microplate reader. Increase of fluorescence corresponded to the formation of a fluorescent product coming from the substrate hydrolysis by rt-PA. Enzymatic velocity was determined from the initial slope of the resulting kinetic profile and compared to that of free rt-PA at the same concentration.

Fibrinolytic activity was assessed with a fibrin lysis assay adapted from the work of Liang et al. [40]. Low melting agarose (Carl Roth GmbH + Co. KG, Karlsruhe, Germany) solution at 3% w/v in TRIS buffer was heated at 65°C. The solution was cooled at 37°C and 2.5 U of thrombin (Sigma-Aldrich) were added. 5 mL of a fibrinogen (Sigma-Aldrich) solution in TRIS buffer were heated at 37°C and added. The reaction mixture was poured into 9 cm culture dish and cooled at 4°C for 30 min. On the solidified agar plate, 3 mm wells were created as sample reservoir. 5 µl of samples were added into the wells and incubated overnight at 37°C in a humid atmosphere. After incubation, the lysis area was quantified with ImageJ and compared to that of free rt-PA at the same concentration.

Flow binding assay of nanoparticles on activated platelet aggregates

To further investigate the binding efficiency of unloaded and loaded NPs to activated platelets, channels of Vena8 Fluoro+ chambers were coated with 50 µg/mL of fibrillar type I collagen Horm® (Takeda, Linz, Austria) overnight and rinsed with NaCl 0.9% before use. Human whole blood (EFS, Hôpital Bichat, Paris, France) collected on 75 µM PPACK (Cryopep, Montpellier, France) was perfused at arterial shear rate for 3.5 to 5 minutes to induce platelet activation and aggregation.

In a first set of experiments, the expression of P-selectin by platelet aggregates was controlled by perfusing whole blood containing 20 µg/mL of a FITC-labeled anti-P-

selectin antibody or a FITC-labeled matched isotype IgG (Ancell, Bayport, U.S.). After rinsing, 10 fields per channel were imaged and analyzed with the image analysis software ImageJ to compare the fluorescence uptake of aggregates.

In a second set of experiments, PPACK-anticoagulated whole human blood was mixed with 5 µM of DIOC₆ (Life Technologies SAS, Saint-Aubin, France), a green fluorescent dye that label mitochondria of live cells, and perfused at arterial shear stress (67.5 dyne/cm²) to allow platelet aggregation. After rinsing, suspensions of Nile Red-NPs at 1 mg/mL were then perfused over preformed platelet aggregates at venous shear stress (6.75 dyne/cm²) for 5 minutes. Their accumulation onto activated aggregates was monitored by fluorescence microscopy in real time. After rinsing, 10 fields per channel (area of 1230 µm x 105 µm) were imaged and analyzed with ImageJ to quantify the level of fluorescent NPs bound to aggregates. Intensity settings were kept the same for both types of NPs. Aggregates were detected using ImageJ by thresholding the green fluorescence level generated by the platelets. The Mean Fluorescence Intensity (MFI) of the NPs on these selected areas was determined using ImageJ. One MFI value was obtained per channel averaged over more than 25 aggregates.

In a third set of experiments, rt-PA was loaded onto Nile Red Fuco-NPs and Control-NPs in PBS as previously described. Loaded NPs were resuspended in PBS just before being perfused at venous shear rate onto activated platelets aggregates marked with DIOC₆. Channels were rinsed after 12 minutes of NPs perfusion and 10 fields per channel were imaged and analyzed with ImageJ. One MFI value was obtained per channel by averaging the NPs fluorescence intensity on several aggregates.

***In vivo* model of thrombosis on mouse mesenteric vein**

FeCl₃-induced thrombosis model on mouse mesenteric vein was developed based on the work of Bonnard et al. [42]. C57BL/6 male mice (Elevage Janvier, CERJ, Laval, France) aged from 5 to 8 weeks were chosen for the study. Mice were anesthetized with intraperitoneal injection of ketamine (Vétoquinol SA, Lure, France) and xylazine (Bayer SAS, La Garenne-Colombes, France) at 100 mg/kg and 10 mg/kg respectively. A midline

abdominal incision was performed to expose the mesentery. The mesentery was gently laid out over a transparent Petri dish lid and vessels were visualized by intravital microscopy (Leica MacroFluo™, Leica Microsystems SAS, Nanterre Cedex, France) using Orca Flash 4.0 scientific CMOS camera (Hamamatsu Photonics France SARL, Massy, France). Retro-orbital injection of 30 µL of Rhodamine 6G (Sigma-Aldrich) prepared at 0.3% w/v was performed. Rhodamine 6G fluorescently labeled the platelets and the leukocytes.

A 1 mm large Whatman chromatography paper soaked into a 10% w/v iron chloride (Sigma-Aldrich) solution prepared in saline was then left 1 minute on one of the mesentery veins. After the paper was removed, the vein was washed twice with a saline solution. The veins were measured to have a mean diameter of $171 \pm 31 \mu\text{m}$ (mean \pm SD, n = 50 mice). The thrombus formation was monitored in real-time by fluorescence microscopy by following the accumulation of fluorescently labeled platelets.

Evaluation of *in vivo* thrombolysis by fluorescence microscopy

55 mice were randomly set into 5 groups for the study receiving buffer, Fuco-NPs, reconstituted Actilyse® at 2.5 mg/kg (rt-PA), Control-NPs associated with Actilyse® normalized to a dose of 2.5 mg/kg (rt-PA-Control-NPs), and Fuco-NPs associated with Actilyse® normalized to a dose of 2.5 mg/kg (rt-PA-Fuco-NPs).

Samples were prepared on the day of animal experiments. Non-fluorescent Fuco-NPs and Control-NPs at 0.3 mg/mL in Tween-PBS were mixed with Actilyse® at 0.4 mg/mL during 2 hours at 4°C under gentle agitation as previously detailed. Suspensions were washed 3 times by ultrafiltration using Vivaspin 500 devices (MWCO 300 kDa, Sartorius France SAS, Dourdan, France). After the third ultrafiltration cycle, concentrated samples were used for injection. Amidolytic activity of the concentrated samples was consequently measured with the fluorogenic substrate Peflafuor® tPA and used to normalize the injected dose. Samples were stored on ice and used within 2 hours.

Retro-orbital injection of the different treatments and controls was performed once fluorescently labeled platelets started to aggregate in the injured site and formed a visible

thrombus, on average 7 ± 3 minutes after thrombosis induction (mean \pm SD, n = 55 mice). This injection method was chosen because it is fast, simple, does not require moving the mouse and ensures a distribution in the circulation similar to that obtained with standard intravenous injection [43]. The injected volumes were of $125 \pm 36 \mu\text{L}$ (mean \pm SD), which has been reported to be adapted to the mouse [44]. The thrombus evolution was monitored in real-time by fluorescence imaging (excitation 545 nm – emission 610 nm). Images were acquired just before injection and regularly during the first 15 minutes after injection, then every 5 minutes up to 30 minutes. The thrombus was detected over time using ImageJ by thresholding the fluorescence level. The thrombus density was defined as the total intensity of the detected area. The thrombus relative density was normalized to the peak platelet accumulation for each animal. This parameter was used to assess the benefit of the different treatments compared to the group receiving buffer. It allowed to alleviate the variability between thrombi and was a better estimate of the global thrombolysis trend.

On few additional mice, images were taken continuously over 40 minutes (one image every 10 seconds) to provide typical examples of thrombus formation followed by thrombolysis. In these mice, DIOC₆ (Life Technologies SAS, Saint-Aubin, France) was injected at 25 μM instead of Rhodamine 6G. These movies were taken for the following groups: rt-PA, rt-PA-Control-NPs, and rt-PA-Fuco-NPs. The nanoparticles used were fluorescently labeled in red with Nile Red and dual fluorescence imaging was performed (excitation 480 nm – emission 527 nm / excitation 545 nm – emission 610 nm).

Statistics

Results are presented as mean \pm standard error of the mean (n \geq 3). Statistical significance between experimental groups was assessed using the software GraphPad Prism (GraphPad Software, Inc., La Jolla, U.S.) with 95% confidence level: ns non-significant, *p < 0.05, **p < 0.01. For all tests, data were assumed to be normally distributed. Unpaired non-parametric test (Mann Whitney) was used for samples that contain ≤ 6 elements. One-way ANOVA with following Post hoc Turkey's test was applied for the *in vivo* experiments.

Results

Nanoparticle synthesis and characterization

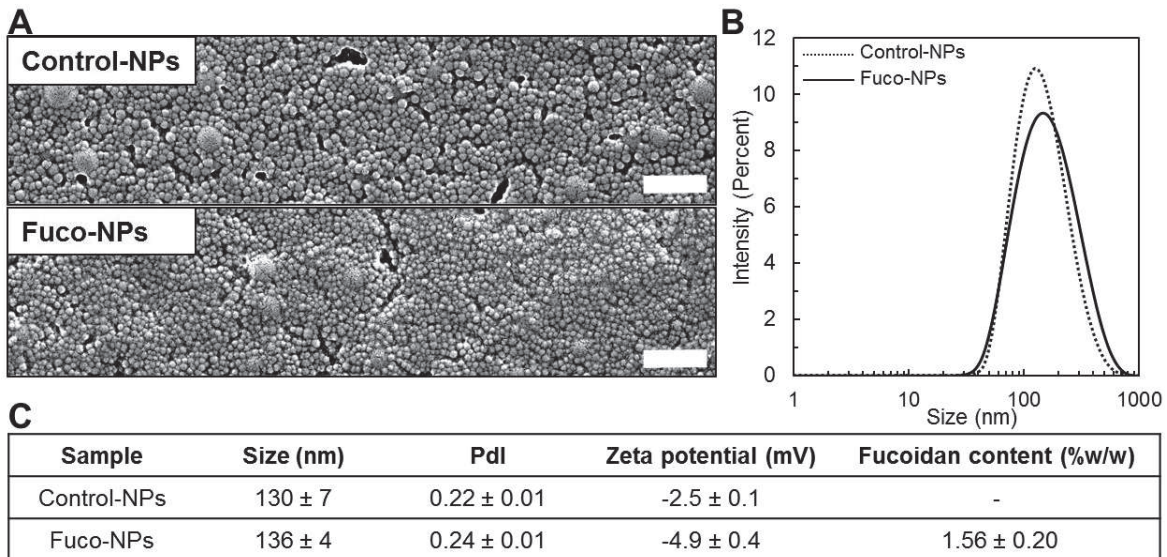


Figure 1. Physico-chemical characterization of Control-NPs and Fuco-NPs.

A) Scanning Electron Microscopy (SEM) (scale bar = 500 nm). **B)** Diffusion Light Scattering (DLS) measurement in intensity. **C)** Size values and Polydispersity Index (Pdl) determined by DLS and zeta potential values measured by Electrophoretic Light Scattering (ELS) ($n = 5$ independent batches per type of nanoparticle; mean \pm standard error of the mean). Fucoidan content of Fuco-NPs in mass percent of the total nanoparticle weight determined by a colorimetric assay ($n = 3$).

NPs made of dextran, aminated dextran and IBCA were synthesized by redox radical emulsion polymerization in the presence of either fucoidan (Fuco-NPs) or carboxymethyl-dextran (Control-NPs). Solid spherical NPs were obtained, as shown in SEM images (Figure 1A). The size distribution determined by DLS was similar for both types of NPs, with an average size in intensity of 130 ± 7 nm for Control-NPs and 136 ± 4 nm for Fuco-NPs (Figures 1B, 1C). Samples exhibited polydispersity index numbers of 0.22 ± 0.01 for Control-NPs and of 0.24 ± 0.01 for Fuco-NPs. ELS measurements provided slightly negative zeta potential values of -2.5 ± 0.1 mV for Control-NPs and of -4.9 ± 0.4 mV for Fuco-NPs (Figure 1C). The N content of the aminated dextran was determined to be 0.4% w/w. Physico-chemical properties of Control-NPs were therefore close to those of Fuco-NPs. Fuco-NPs were composed of 1.56 ± 0.20 % of fucoidan in mass percent of the total nanoparticle weight (Figure 1C).

Fucoidan-functionalized nanoparticle biodistribution

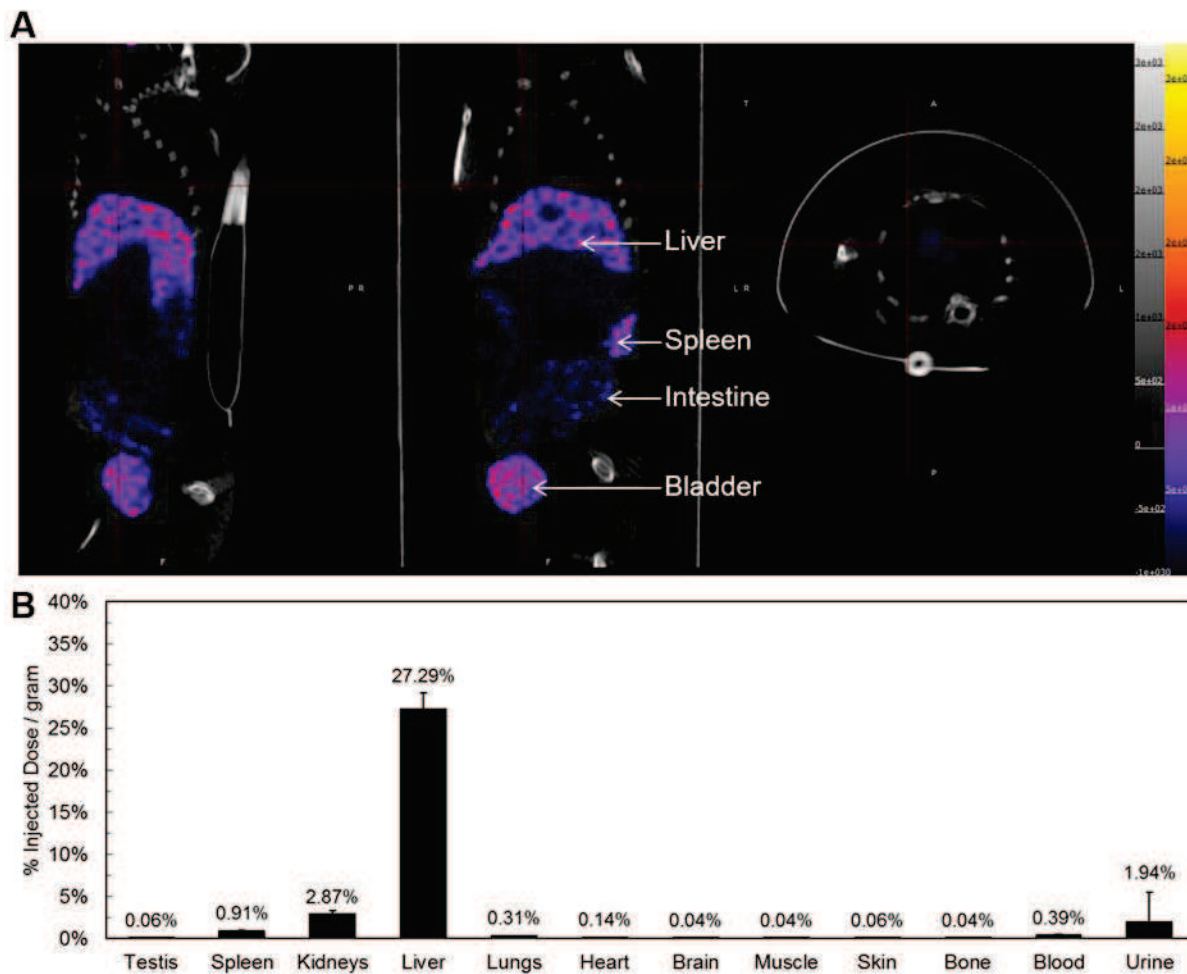


Fig 2. SPECT/CT imaging and tissue biodistribution in mice determined 80 minutes after injection of Fuco-NPs labeled with ^{99m}Tc .

A) Representative whole body SPECT/CT imaging: from left to right: sagittal, coronal and axial planes. **B)** Tissue biodistribution determined by tissue activity measurement normalized to the tissue weight and expressed as a percentage of the injected dose ($n=3$ mice).

Fuco-NPs were radiolabeled with ^{99m}Tc and injected in mice for SPECT/CT imaging and tissue biodistribution. SPECT/CT profiles at 80 minutes illustrated in Figure 2A showed a major nanoparticle accumulation in the bladder as well as a high uptake by the liver. Normalized activity values associated to each organ depicted in Figure 2B validated that Fuco-NPs were mainly taken by the liver. Some activity was also detected in kidneys and in urine. No signal was detected on SPECT/CT images in the stomach wall and in the thyroid corroborating a stable nanoparticle labeling. No significant accumulation was noticed in the lungs, the heart and the brain (Figure 2).

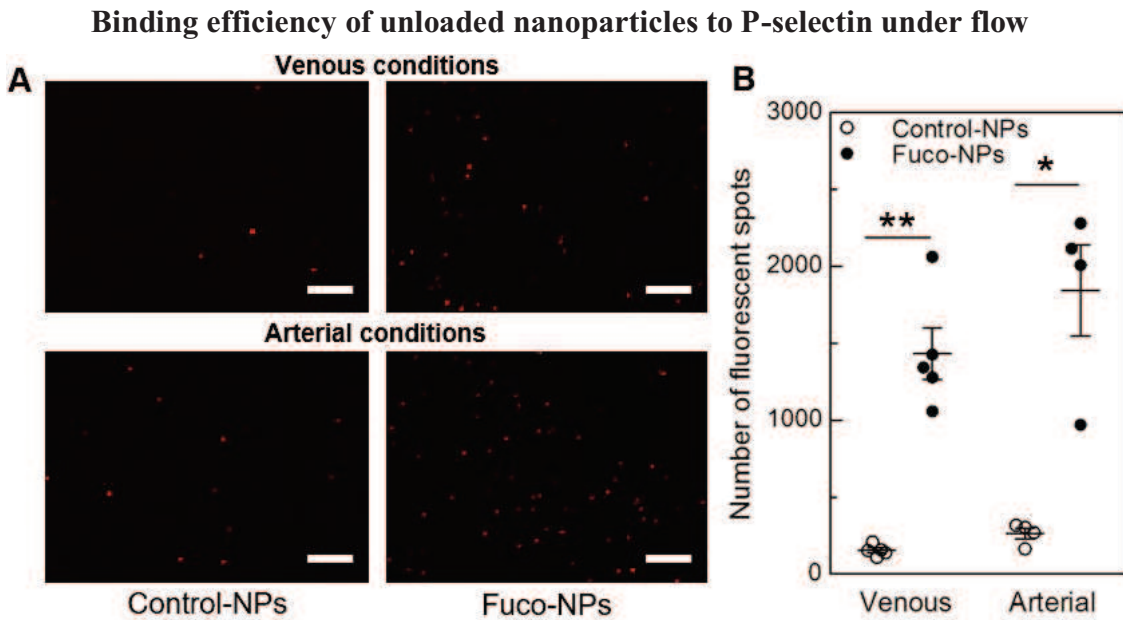


Figure 3. Evaluation of NPs binding on recombinant P-selectin.

A) Adhesion of fluorescent clusters on a P-selectin coated at 50 µg/mL. Nile Red-labelled Fuco-NPs and Control-NPs were infused in micro-channels at either venous or arterial shear stress for 5 minutes (6.75 and 67.50 dyne/cm², respectively) (scale bar = 10 µm). B) Corresponding quantitative analysis of the number of fluorescent spots corresponding to NP clusters on a surface of 1230 µm x 105 µm (*p<0.05; **p<0.01; n=5 channels in venous conditions; n=4 channels in arterial conditions).

The nanoparticle binding efficiency to P-selectin *in vitro* is illustrated in Figure 3A. Unloaded NPs were evaluated to first control the capacity of fucoidan to interact with its molecular target. Under venous and arterial conditions, Fuco-NPs bound significantly more to P-selectin than Control-NPs, with 1434 ± 169 clusters versus 154 ± 17 clusters under venous shear stress, and 1844 ± 297 clusters versus 264 ± 34 clusters under arterial shear stress (Figure 3B).

***In vitro* activity of rt-PA-loaded nanoparticles**

Quantification of rt-PA adsorbed on the NPs showed that the same amount of drug was retained in rt-PA-Fuco-NPs and in rt-PA-Control-NPs corresponding to 0.35 ± 0.02 mg of protein per mg of NPs. Results of the loaded protein enzymatic activity and its activity in contact with fibrin are presented in Figure 4.

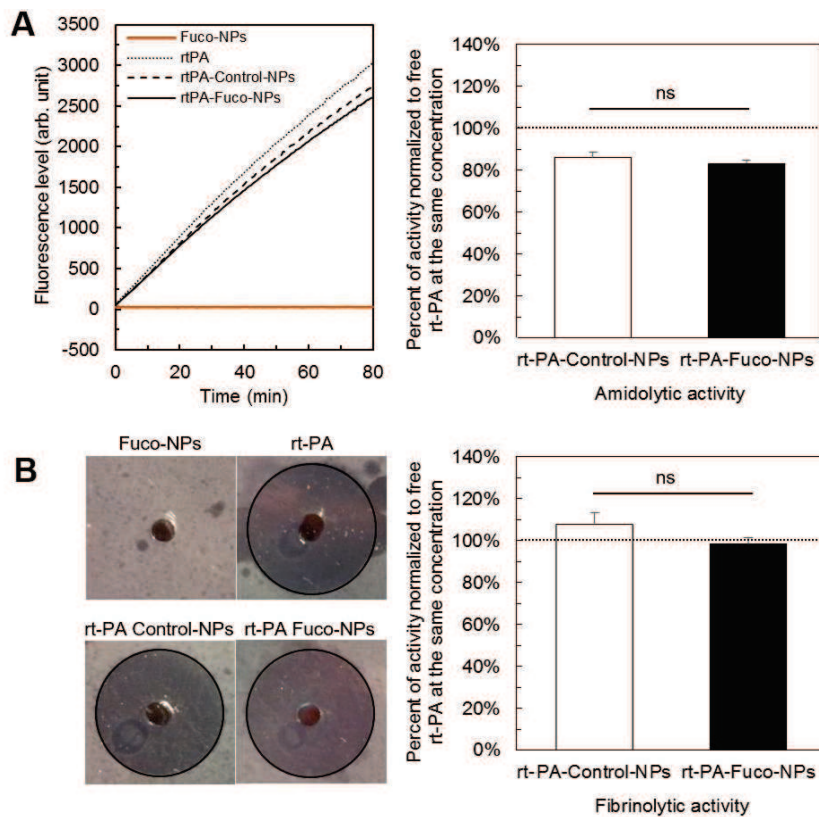


Figure 4. Amidolytic and fibrinolytic activities.

A) Amidolytic activities of Fuco-NPs, free rt-PA, rt-PA-Control-NPs and rt-PA-Fuco-NPs measured by the Pefluor® fluorogenic assay. Left; the tangent gradient is correlated to the enzymatic velocity. Right; corresponding quantitative analysis normalized to free rt-PA at the same concentration ($n \geq 3$ experiments; ns non-significant). **B)** Fibrinolytic activities of the same samples determined by a fibrin-plate agarose assay. Left; the fibrinolytic potential is obtained by measuring the lysed zone area after overnight incubation at 37°C. Right; corresponding quantitative analysis normalized to free rt-PA at the same concentration ($n \geq 3$ experiments; ns non-significant).

The amidolytic activity of the rt-PA in contact with Control-NPs and Fuco-NPs decreased by $14\% \pm 3\%$ and $17\% \pm 2\%$ respectively (Figure 4A). The capacity of loaded rt-PA to induce fibrinolysis in the fibrin plate assay was maintained, with values of $108\% \pm 6\%$ for Control-NPs and of $99\% \pm 3\%$ for Fuco-NPs (Figure 4B). Thus, rt-PA loaded onto the NPs kept its full activity in contact with fibrin. No significant difference was observed between both types of NPs enabling to compare them in following experiments. In addition, unloaded Fuco-NPs induced no effect (Figures 4A, 4B).

Binding efficiency of unloaded and loaded nanoparticles to activated platelets aggregates under flow

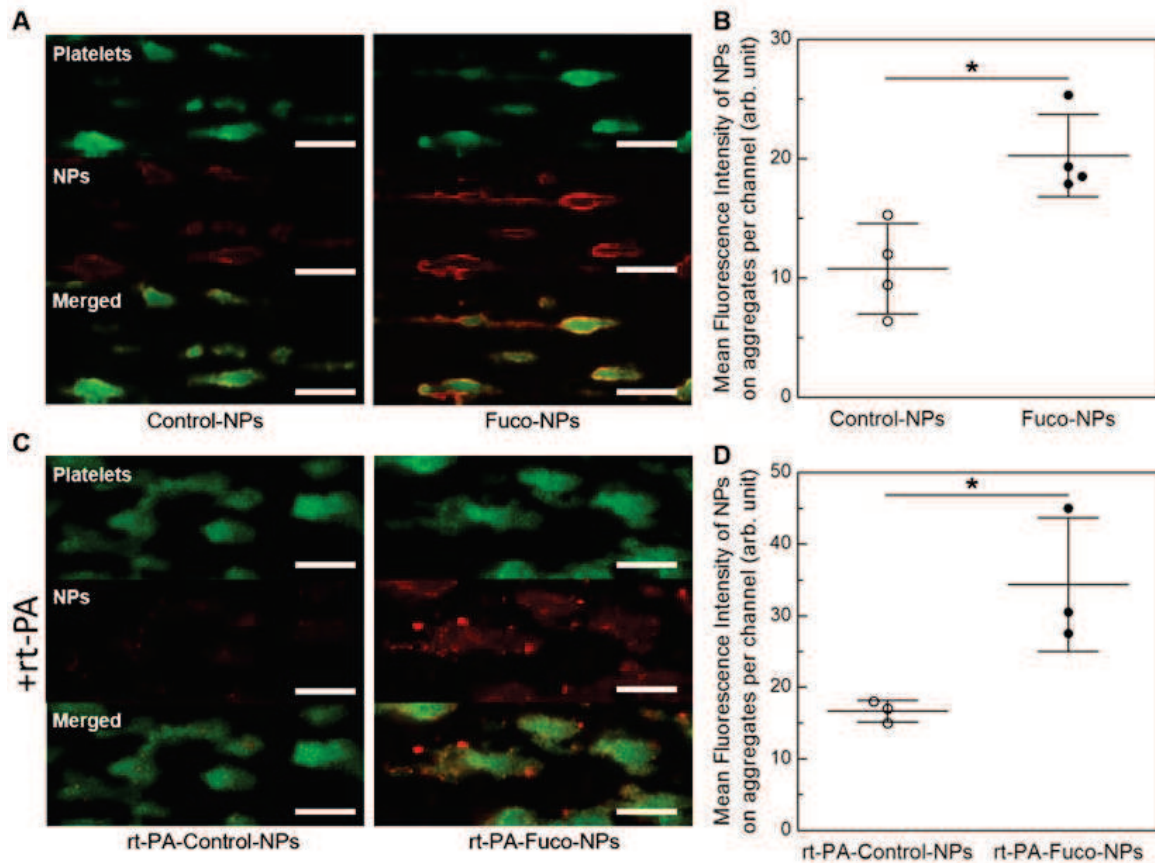


Figure 3. Evaluation of NPs binding on activated platelet aggregates under flow.

A) Fluorescence uptake after infusion for 5 minutes of Nile Red-nanoparticles (red) onto activated platelets aggregates in venous conditions. Human whole blood mixed with 5 μ M of DIOC₆ (green) was previously infused during 3.5 minutes in collagen coated micro-channels to induce platelet aggregates (scale bar = 50 μ m) B) Corresponding quantitative analysis of the Mean Fluorescence Intensity averaged on platelet aggregates. One MFI value was obtained per channel averaged over more than 25 aggregates. Values of 4 independent experiments are reported (*p<0.05). C) Fluorescence uptake after infusion for 12 minutes of Nile Red-nanoparticles (red) loaded with rt-PA under similar conditions (scale bar = 50 μ m) D) Corresponding quantitative analysis of rt-PA-loaded nanoparticles on platelet aggregates (*p<0.05).

The NPs binding efficiency to P-selectin expressed by activated human platelets is illustrated in Figure 5. Perfusion of whole blood on collagen at arterial shear stress induced formation of platelet aggregates that expressed P-selectin (supplementary data Figure S1). After perfusion of either Nile Red-Fuco-NPs or Nile Red-Control-NPs on preformed aggregates at venous shear rate, an uptake of red fluorescence over time was observed at the surface of the platelets related to the accumulation of NPs. After perfusion, the fluorescence uptake induced by Fuco-NPs was two-fold higher than that of

Control-NPs showing that Fuco-NPs accumulated significantly more onto activated platelets ($p<0.05$) (Figures 5A, 5B). As shown in Figures 5C and 5D, NPs loaded with rt-PA showed the same trend. After perfusion, a strong fluorescence uptake was observed on the platelet aggregates with rt-PA-Fuco-NPs (Figure 5C). Their accumulation was significantly higher than that of rt-PA-Control-NPs ($p<0.05$) (Figure 5D).

***In vivo* thrombolytic efficiency**

All treatments were injected during thrombus formation. After injection, all thrombi encountered a growing phase. In 68% of mice, the maximum intensity was reached in the first 10 minutes after injection. Figure 6A gives representative examples of thrombus evolution with the different treatments. The thrombus density normalized to the peak intensity for each animal was similar for mice that received buffer as a control ($n = 10$) and for mice receiving unloaded Fuco-NPs ($n = 11$), as shown by the quantitative analysis depicted in Figure 6B. In both groups, the thrombus became rapidly stable after reaching a peak and the relative thrombus density at 30 minutes was around 70% ($72\% \pm 6\%$ for Buffer and $71\% \pm 6\%$ for Fuco-NPs). In mice receiving rt-PA-based treatments (rt-PA, rt-PA-Control-NPs and rt-PA-Fuco-NPs), a competition between thrombosis and thrombolysis was observed in the first 15 minutes. However, the overall trend was a fast platelet recruitment followed by a decrease and a stabilization at 30 minutes. Three illustrations are depicted in Figure 6A. Other examples can be found in supplementary data for these groups (supplementary figure S3). rt-PA injection alone at a dose of 2.5 mg/kg ($n = 12$) decreased the thrombus density down to $59\% \pm 6\%$, which was not significantly different from the control group. At this dose, free rt-PA was thus not sufficient to generate a pronounced thrombolytic effect. rt-PA-Control-NPs were injected in 10 mice. The thrombus density was on average $60\% \pm 8\%$ at 30 minutes, which is similar to the value induced by rt-PA alone. Injection of rt-PA-Fuco-NPs ($n = 12$) at a similar dose generated a significant thrombus reduction. The density decreased down to $43\% \pm 7\%$ after 30 minutes. Furthermore, rt-PA-Fuco-NPs were the only treatment to induce more than 70% of reduction (density <30%) in 5 mice out of 12.

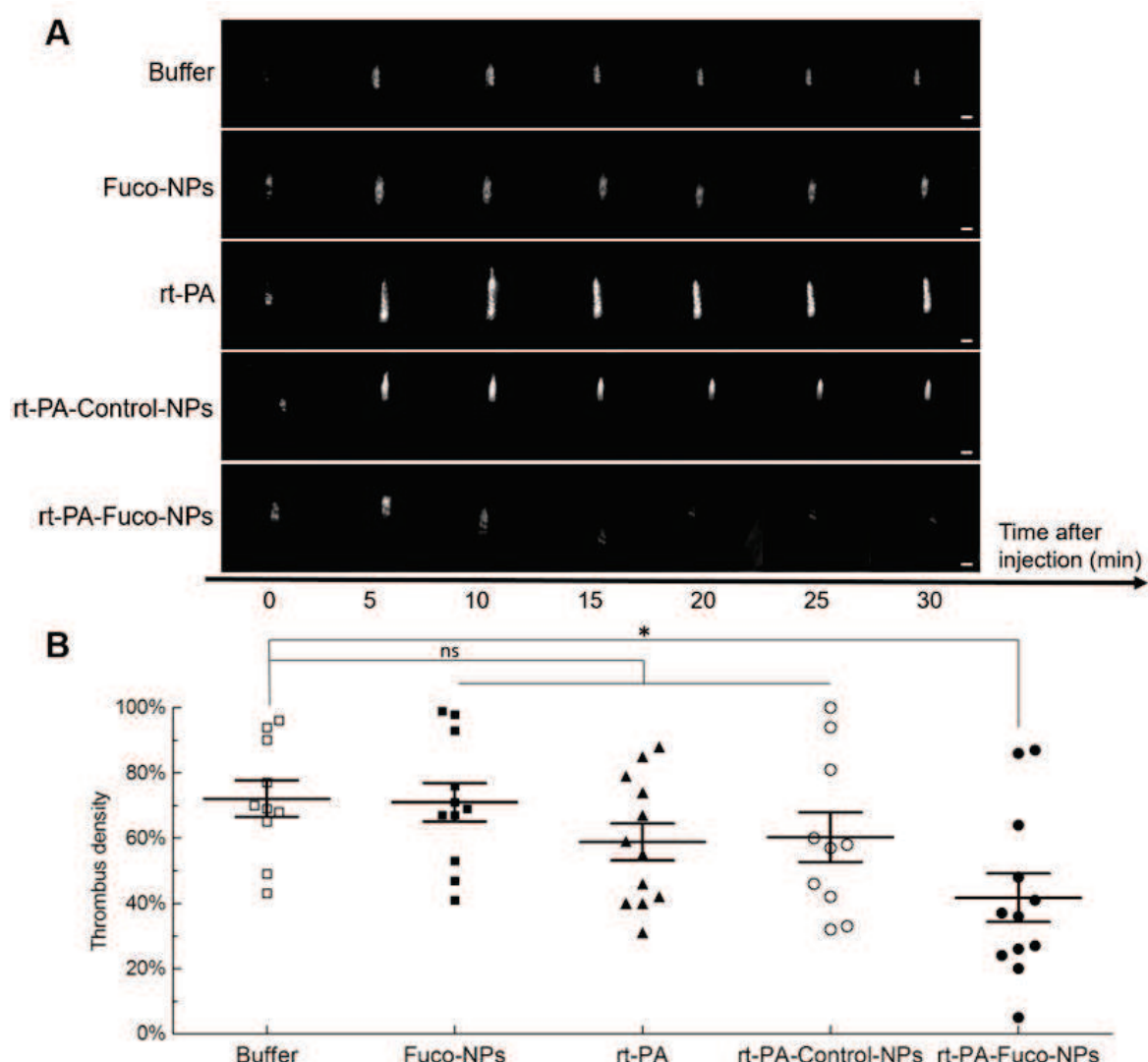


Figure 5. Evaluation of thrombolysis efficiency in a mouse model of venous thrombosis.
A) Thrombosis was obtained by leaving a FeCl₃-soaked paper for 1 minute on a mesenteric vein. Rhodamine 6G-labeled platelets accumulation was followed in real time by fluorescence macroscopy for 30 minutes. Examples of thrombus evolution after treatment of five mice that were injected with: buffer, Fuco-NPs, rt-PA, rt-PA-Control-NPs and rt-PA-Fuco-NPs (scale bar = 200 μm). B) Thrombus density at 30 minutes after injection. The thrombus density was defined as the fluorescence intensity of the thrombus area normalized to the peak platelet accumulation after injection. Five groups were analyzed (n = 55 mice). The dose of rt-PA was normalized by the protein amount. The significance is defined with respect to the control group receiving buffer (ns non-significant; *p<0.05).

Discussion

In this study, a new strategy for targeted thrombolysis based on polymer NPs functionalized with fucoidan was evaluated. The preclinical study demonstrated the potential of such NPs in acute thrombosis. Fucoidan is a cheap and natural polysaccharide that presents no immunogenic risk. It is therefore of great interest in comparison with P-selectin antibodies and recombinant PSGL-1 used to functionalize nano- and microsystems [45, 46]. Fucoidan-based NPs are highly promising nanocarriers to be used in pathologies overexpressing P-selectin, such as thrombosis. In addition, injection of rt-PA to induce thrombolysis has a limited efficiency and is associated to serious side effects. Fucoidan-functionalized NPs were therefore developed as carriers for rt-PA to improve the drug efficiency by promoting its specific accumulation.

Spherical NPs with a hydrodynamic diameter of around 130 nm were obtained (Figure 1). Similar but unspecific NPs (Control-NPs) were synthesized with a negatively charged polysaccharide instead of fucoidan to assess the benefit of using targeted NPs (Figure 1). Carboxymethyl-dextran was chosen to obtain NPs with a slightly negative surface charge but without the sulfate groups of fucoidan that are involved in its interaction with P-selectin [26, 39]. The physico-chemical properties of Control-NPs and Fuco-NPs were similar. The NPs size was in the range of other types of NPs developed for thrombolysis [13-16]. Although the size could be an important parameter to study, no work has investigated the optimal NP size for interaction with a fibrin network, to the best of our knowledge. The Fuco-NPs biodistribution profile in mice shown by both SPECT images and tissue biodistribution in Figure 2 highlighted a partial elimination by the kidneys with a high adsorbed dose in the bladder, followed by a capture of Fuco-NPs by the reticuloendothelial system in the liver. These results were relevant with a study performed with nanoparticles synthesized by RREP but with a different polysaccharide coating [47]. In our case, no signal was found in the heart and in the lungs.

The *in vitro* binding assay performed on recombinant P-selectin confirmed that fucoidan could efficiently recognize and bind P-selectin, even when incorporated in the polysaccharide shell (Figure 3). Interestingly, this experiment showed that the affinity of Fuco-NPs for P-selectin was observed both at low shear stress (6.75 dyne/cm^2) and at

high shear stress (67.5 dyne/cm^2), whereas most *in vitro* affinity assays described in the literature are performed in static conditions [21, 23] or at very low ($<6.75 \text{ dyne/cm}^2$) or uncontrolled shear stress [48, 49]. The *in vitro* results described in Figure 4 revealed that Fuco-NPs interacted significantly more with activated platelet aggregates than Control-NPs. In addition, adsorption of rt-PA did not seem to impair the Fuco-NPs binding efficiency. Thus, these results suggested that more rt-PA could accumulate into the thrombus and were promising for the potential use of rt-PA-Fuco-NPs.

Fucoidan-functionalized NPs associated with rt-PA were therefore tested *in vivo* in a mouse model of venous thrombosis induced by iron chloride. This method shows the advantage to create a dense and reproducible thrombus within several minutes, in comparison with other standard venous models that require hours or days to develop, and lack of reproducibility [50]. Buffer alone was injected in 10 mice to evaluate thrombosis standard evolution. In all mice, the maximum platelet accumulation was reached within the first 15 minutes after injection. At 30 minutes the thrombus was therefore considered stable. Figure 6 summarized the preclinical study results. Fuco-NPs did not improve the outcome compared with buffer. This result confirmed that naked Fuco-NPs have no effect on the thrombosis process even if they potentially accumulate on the thrombus. Free rt-PA and rt-PA-Control-NPs were not significantly different from the control group. Interestingly, they both induced similar recanalization rates (remaining thrombus density of 59% for free rt-Pa and of 60% for rt-PA-Control-NPs at 30 minutes). In this design, associating rt-PA with a non-targeted nanocarrier had therefore no significant effect on the drug efficiency. In our work, rt-PA is loaded by adsorption post-synthesis, whereas entrapment strategies during the NP synthesis process have mainly been described with non-targeted nanocarriers [12-14]. Covalent binding strategies could avoid premature drug release but enhance the risk to decrease the protein fibrinolytic activity once on site [51]. In our design, the presence of NPs only slightly affected the drug amidolytic activity and full fibrinolytic activity of the protein was recovered in contact with fibrin, as shown in Figure 5. Positively charged aminated dextran (N content of 0.4% w/w) was incorporated into the polysaccharide shell to mimic L-arginine used to stabilize rt-PA and promote electrostatic interaction [14, 52]. Some functional groups such as lysine could be

explored in future studies to load the drug [53, 54]. Targeted nanoparticles loaded with rt-PA (rt-PA-Fuco-NPs) significantly improved the outcome at 30 minutes as the mean thrombus density decreased down to 42%. In addition, 5 mice out of 12 showed a decrease >70%. Despite the risk of desorption [55], this suggested that the protein remained loaded and active onto the NPs. Together, these results evidenced that rt-PA and Fuco-NPs had a synergic effect. In addition, a short time point of 30 minutes post induction was sufficient to demonstrate a beneficial effect of the targeting strategy, whereas other targeted nanocarriers described in the literature required more time to improve the drug efficiency [24, 25].

The results of this preclinical study suggested that the fucoidan present on the surface of the NPs increases the thrombolytic efficiency. The *in vitro* binding assay results supported the hypothesis that this is achieved by promoting the accumulation of the NPs on the platelet surface. Injection of 100 µg of fluorescent NPs did not allow us to observe any uptake with the limited detection of the imaging technique. Once injected at a 20 times higher dose, Fuco-NPs were clearly identified on the edge of the thrombus from the first minute and accumulated over more than 30 minutes (supplementary figure S2). This observation is in accordance with other targeting studies and is promising for future developments of Fuco-NPs [21, 56].

Although the developed animal model is far from the complexity and variety of human thrombi and remains limited by the number of animals, it is a first proof-of-concept for the association of rt-PA with fucoidan-functionalized nanocarriers. The nanocarriers that were used were chosen according to the presence of polysaccharides at the surface and to their stealth properties [57]. The concentration at injection was calculated to be about 50 µg NPs per mL of blood. Their cytocompatibility and biodegradability need to be considered for future development [58, 59]. Even if intravital microscopy is a powerful and precise technique to assess thrombosis evolution in terms of platelet recruitment [60], complementary techniques to monitor the blood flow, to evaluate treatment side effects, like bleeding time, and to assess the targeting capacity of rt-PA-Fuco-NPs *in vivo*, would be of great interest to implement [23, 49].

Conclusion

An efficient thrombolytic agent based on fucoidan-functionalized polymer nanoparticles targeting P-selectin was developed. A flow assay was designed to validate the role of fucoidan at the surface of the nanoparticle. As compared to other strategies that involve grafting antibodies or using external magnetic force, fucoidan is of great interest for promoting the specific accumulation of nanocarriers at site of thrombosis. An *in vivo* proof-of-concept showed that rt-PA loaded fucoidan-nanoparticles improved the thrombolysis efficiency of the drug in thrombosis acute phase. These results highlighted for the first time the relevance of targeting P-selectin for the treatment of thrombosis. Optimization steps of the drug-nanoparticles interaction and in-depth studies of the *in vivo* behavior of loaded nanoparticles should be performed before moving towards larger animal models and clinical implementation.

Acknowledgments

This study was supported by Inserm, Paris Diderot University, Paris 13 University. This work received the financial support of the ANR-13-LAB1-0005-01 “Fuco-Chem” and the EU project FP7-NMP-2012-LARGE-6-309820 “NanoAthero”. Bo Li is grateful to the China Scholarship Council for the PhD grant No. 201206180031. The authors are most grateful to PLATIN’ (PLATEAU d’Isotopie de Normandie, France) core facility for all elemental analysis used in this study and to Frédéric Nadaud (SAPC, UTC Compiègne, France) for SEM analysis. The authors are thankful to members of the LVTS: Dr M Jandrot-Perrus and S Loyau for advice about rt-PA use, Dr B Ho-Tin-Noe for his expertise in the *in vivo* model, Dr J C Antunes for advice about protein quantification, and L Louedec for her help with the *in vivo* procedure. The authors gratefully acknowledge Dr G Almer (Medical University of Graz, Austria) for discussions on fucoidan quantitative analysis.

Supplementary material

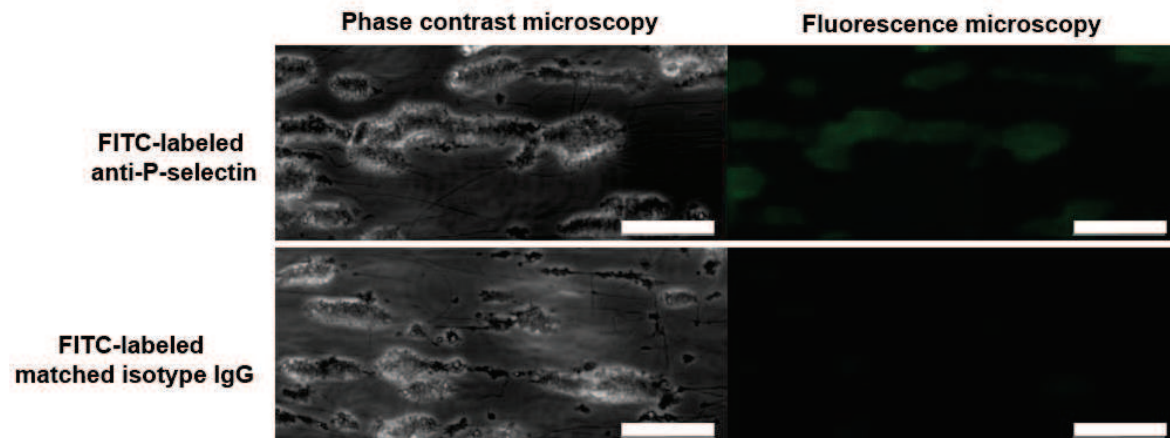


Figure 1S. Expression of P-selectin by activated platelet aggregates evidenced by perfusion of FITC-labeled anti-P-selectin. FITC-labeled anti-P-selectin or FITC-labeled IgG with matched isotype were mixed with human whole blood. Blood was perfused in collagen coated micro-channels at arterial shear stress (67.5 dyne/cm^2). Activation and aggregation of platelets were visualized by phase contrast microscopy and fluorescence microscopy (scale bar = $50 \mu\text{m}$).

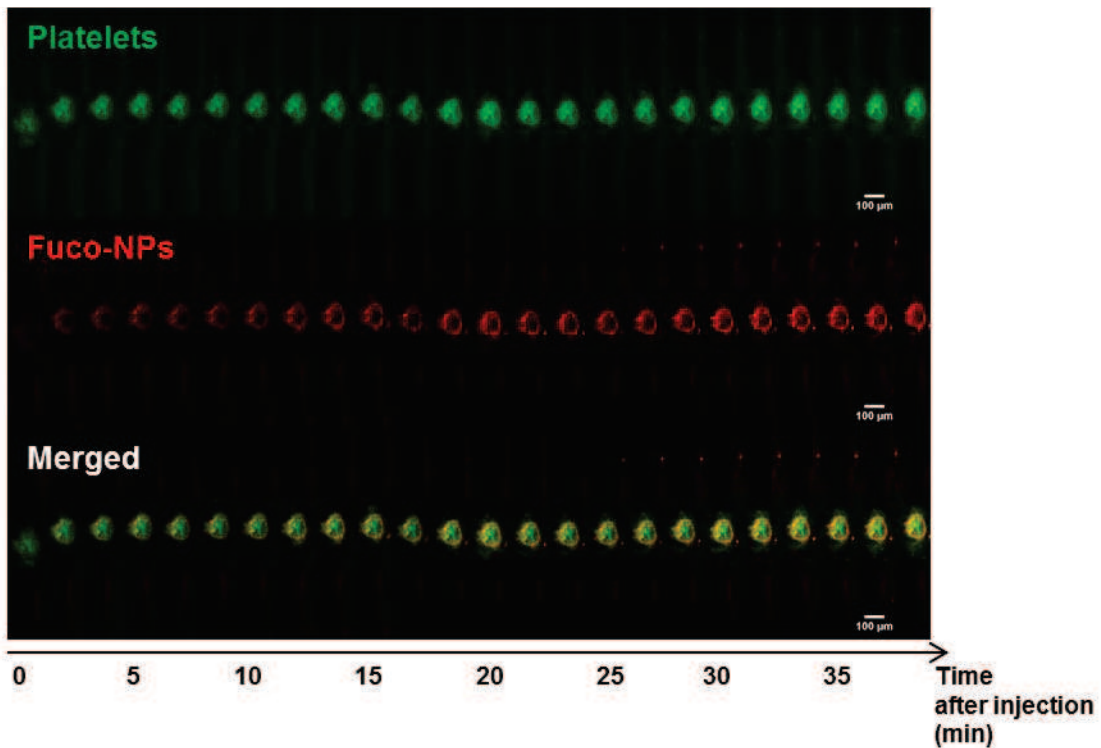


Figure 2S. Accumulation of Fuco-NPs in the thrombus monitored by intravital microscopy. 2 mg of Nile Red-labelled Fuco-NPs were injected in mice where thrombosis was previously induced and platelets were labeled in green with DIOC₆. Platelet and NP accumulation at site of injury was monitored in real-time up to 40 minutes. Images shown here were taken every 100 seconds.

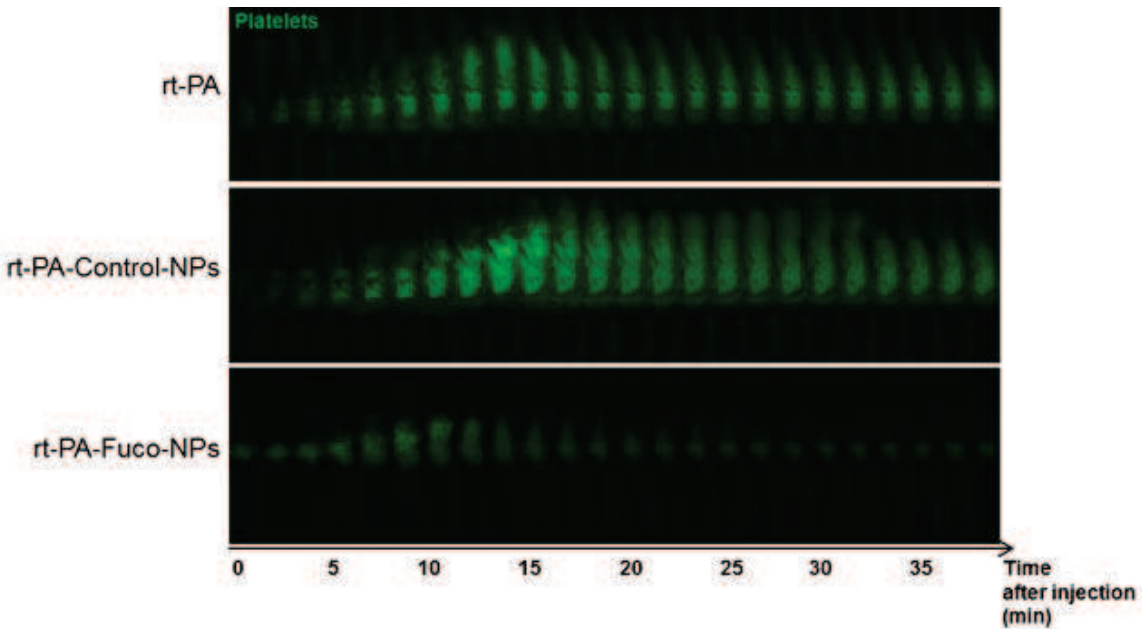


Figure 3S. Examples of thrombolysis efficiency of three treatments: rt-PA, rt-PA-Control-NPs and rt-PA-Fuco-NPs. Treatments were injected in mice where thrombosis was previously induced and platelets were labeled in green with DIOC₆. Platelet accumulation at site of injury was monitored in real-time up to 40 minutes. Images shown here were taken every 100 seconds.

References

1. Marler, J.R., et al., *Tissue-plasminogen activator for acute ischemic stroke*. New England Journal of Medicine, 1995. **333**(24): p. 1581-1587.
2. Bonaventura, A., F. Montecucco, and F. Dallegrì, *Update on the effects of treatment with recombinant tissue-type plasminogen activator (rt-PA) in acute ischemic stroke*. Expert Opinion on Biological Therapy, 2016. **16**(11): p. 1323-1340.
3. Yaghi, S., A. Eisenberger, and J.Z. Willey, *Symptomatic Intracerebral Hemorrhage in Acute Ischemic Stroke After Thrombolysis With Intravenous Recombinant Tissue Plasminogen Activator A Review of Natural History and Treatment*. Jama Neurology, 2014. **71**(9): p. 1181-1185.
4. Jaffer, H., et al., *Advances in stroke therapy*. Drug Delivery and Translational Research, 2011. **1**(6): p. 409-419.
5. Fiehler, J., et al., *European Recommendations on Organisation of Interventional Care in Acute Stroke (EROICAS)*. International Journal of Stroke, 2016. **11**(6): p. 701-716.
6. Wahlgren, N., et al., *Mechanical thrombectomy in acute ischemic stroke: Consensus statement by ESO-Karolinska Stroke Update 2014/2015, supported by ESO, ESMINT, ESNR and EAN*. International Journal of Stroke, 2016. **11**(1): p. 134-147.
7. Piechowski-Jozwiak, B. and J. Bogousslavsky, *The use of desmoteplase (bat saliva) in the treatment of ischaemia*. Expert Opinion on Biological Therapy, 2013. **13**(3): p. 447-453.
8. Cicha, I., *Thrombosis: Novel nanomedical concepts of diagnosis and treatment*. World Journal of Cardiology, 2015. **7**(8): p. 434-441.
9. Silva, A.K., D. Letourneur, and C. Chauvierre, *Polysaccharide nanosystems for future progress in cardiovascular pathologies*. Theranostics, 2014. **4**(6): p. 579-91.
10. Varna, M., et al., *Nanomedicine as a strategy to fight thrombotic diseases*. Future Sci OA, 2015. **1**(4): p. FSO46.
11. Nguyen, P.D., et al., *Accelerated thrombolysis and reperfusion in a canine model of myoacardial-infarction by liposomal encapsulation of streptokinase*. Circulation Research, 1990. **66**(3): p. 875-878.

12. Leach, J.K., E. Patterson, and E.A. O'Rear, *Encapsulation of a plasminogen activator speeds reperfusion, lessens infarct and reduces blood loss in a canine model of coronary artery thrombosis*. Thrombosis and Haemostasis, 2004. **91**(6): p. 1213-1218.
13. Kim, J.Y., et al., *The use of PEGylated liposomes to prolong circulation lifetimes of tissue plasminogen activator*. Biomaterials, 2009. **30**(29): p. 5751-6.
14. Uesugi, Y., et al., *An ultrasound-responsive nano delivery system of tissue-type plasminogen activator for thrombolytic therapy*. Journal of Controlled Release, 2010. **147**(2): p. 269-277.
15. Ma, Y.H., et al., *Magnetically targeted thrombolysis with recombinant tissue plasminogen activator bound to polyacrylic acid-coated nanoparticles*. Biomaterials, 2009. **30**(19): p. 3343-51.
16. Bi, F., et al., *Chemical conjugation of urokinase to magnetic nanoparticles for targeted thrombolysis*. Biomaterials, 2009. **30**(28): p. 5125-30.
17. Yang, H.W., et al., *Bioconjugation of recombinant tissue plasminogen activator to magnetic nanocarriers for targeted thrombolysis*. International Journal of Nanomedicine, 2012. **7**: p. 5159-73.
18. Chen, J.P., et al., *Magnetically controlled release of recombinant tissue plasminogen activator from chitosan nanocomposites for targeted thrombolysis*. Journal of Materials Chemistry B, 2016. **4**(15): p. 2578-2590.
19. Hu, J.N., et al., *Magnetically active Fe₃O₄ nanorods loaded with tissue plasminogen activator for enhanced thrombolysis*. Nano Research, 2016. **9**(9): p. 2652-2661.
20. Marsh, J.N., et al., *A fibrin-specific thrombolytic nanomedicine approach to acute ischemic stroke*. Nanomedicine, 2011. **6**(4): p. 605-615.
21. McCarthy, J.R., et al., *Multifunctional nanoagent for thrombus-targeted fibrinolytic therapy*. Nanomedicine, 2012. **7**(7): p. 1017-1028.
22. Kim, J.Y., et al., *Direct Imaging of Cerebral Thromboemboli Using Computed Tomography and Fibrin-targeted Gold Nanoparticles*. Theranostics, 2015. **5**(10): p. 1098-114.
23. Absar, S., et al., *Thrombus-targeted nanocarrier attenuates bleeding complications associated with conventional thrombolytic therapy*. Pharmaceutical Research, 2013. **30**(6): p. 1663-76.
24. Vaidya, B., G.P. Agrawal, and S.P. Vyas, *Platelets directed liposomes for the delivery of streptokinase: development and characterization*. Eur J Pharm Sci, 2011. **44**(5): p. 589-94.
25. Zhou, J., et al., *Construction and evaluation of Fe(3)O(4)-based PLGA nanoparticles carrying rtPA used in the detection of thrombosis and in targeted thrombolysis*. ACS Applied Materials & Interfaces, 2014. **6**(8): p. 5566-76.
26. Ley, K., *The role of selectins in inflammation and disease*. Trends in Molecular Medicine, 2003. **9**(6): p. 263-268.
27. Porter, T.R., *Cardiovascular imaging of remote myocardial ischemia: detecting a molecular trace of evidence left behind*. Circulation, 2007. **115**(3): p. 292-3.
28. Bonnard, T., et al., *Abdominal aortic aneurysms targeted by functionalized polysaccharide microparticles: a new tool for SPECT imaging*. Theranostics, 2014. **4**(6): p. 592-603.
29. Suzuki, M., et al., *Ultrasmall superparamagnetic iron oxide nanoparticles coated with fucoidan for molecular MRI of intraluminal thrombus*. Nanomedicine, 2015. **10**(1): p. 73-87.
30. Chollet, L., et al., *Fucoidans in Nanomedicine*. Marine Drugs, 2016. **14**(8).
31. Bachelet, L., et al., *Affinity of low molecular weight fucoidan for P-selectin triggers its binding to activated human platelets*. Biochim Biophys Acta, 2009. **1790**(2): p. 141-6.
32. Silva, A.K., et al., *Polysaccharide-based strategies for heart tissue engineering*. Carbohydr Polym, 2015. **116**: p. 267-77.
33. Chauvierre, C., et al., *Radical emulsion polymerization of alkylcyanoacrylates initiated by the redox system dextran-cerium(IV) under acidic aqueous conditions*. Macromolecules, 2003. **36**(16): p. 6018-6027.
34. Bertholon-Rajot, I., D. Labarre, and C. Vauthier, *Influence of the initiator system, cerium-polysaccharide, on the surface properties of poly(isobutylcyanoacrylate) nanoparticles*. Polymer, 2005. **46**(4): p. 1407-1415.
35. Urano, T., Y. Takada, and A. Takada, *Stimulation of the amidolytic activity of single chain tissue-type plasminogen activator by fibrinogen degradation products: possible fibrin binding sites on single chain tissue-type plasminogen activator molecule*. Biochim Biophys Acta, 1991. **1077**(3): p. 245-52.
36. Prigent-Richard, S., et al., *Fluorescent and radiolabeling of polysaccharides: Binding and internalization experiments on vascular cells*. Journal of Biomedical Materials Research, 1998. **40**(2): p. 275-281.

37. Lira, M.C., et al., *Cytotoxicity and cellular uptake of newly synthesized fucoidan-coated nanoparticles*. Eur J Pharm Biopharm, 2011. **79**(1): p. 162-70.
38. Lee, J.M., et al., *Solid-Phase Colorimetric Method for the Quantification of Fucoidan*. Applied Biochemistry and Biotechnology, 2012. **168**(5): p. 1019-1024.
39. Saboural, P., et al., *Purification of a low molecular weight fucoidan for SPECT molecular imaging of myocardial infarction*. Marine Drugs, 2014. **12**(9): p. 4851-67.
40. Li, B., et al., *Development of Polymer Microcapsules Functionalized with Fucoidan to Target P-Selectin Overexpressed in Cardiovascular Diseases*. Adv Health Mater, 2016.
41. Liang, J.F., et al., *A novel heparin/protamine-based pro-drug type delivery system for proteases drugs*. Journal of Pharmaceutical Sciences, 2000. **89**(5): p. 664-673.
42. Bonnard, T. and C.E. Hagemeyer, *Ferric Chloride-induced Thrombosis Mouse Model on Carotid Artery and Mesentery Vessel*. Jove-Journal of Visualized Experiments, 2015(100).
43. Steel, C.D., et al., *Comparison of the lateral tail vein and the retro-orbital venous sinus as routes of intravenous drug delivery in a transgenic mouse model*. Lab Anim (NY), 2008. **37**(1): p. 26-32.
44. Yardeni, T., et al., *Retro-orbital injections in mice*. Lab Anim (NY), 2011. **40**(5): p. 155-60.
45. McAtee, M.A., et al., *Magnetic resonance imaging of endothelial adhesion molecules in mouse atherosclerosis using dual-targeted microparticles of iron oxide*. Arterioscler Thromb Vasc Biol, 2008. **28**(1): p. 77-83.
46. Mott, B., et al., *Echocardiographic Ischemic Memory Imaging Through Complement-Mediated Vascular Adhesion of Phosphatidylserine-Containing Microbubbles*. JACC Cardiovasc Imaging, 2016. **9**(8): p. 937-46.
47. Alhareth, K., et al., *Conformation of surface-decorating dextran chains affects the pharmacokinetics and biodistribution of doxorubicin-loaded nanoparticles*. Eur J Pharm Biopharm, 2012. **81**(2): p. 453-7.
48. Wu, Z., et al., *Rhodamine-loaded intercellular adhesion molecule-1-targeted microbubbles for dual-modality imaging under controlled shear stresses*. Circ Cardiovasc Imaging, 2013. **6**(6): p. 974-81.
49. Wang, X., et al., *Thrombus-Targeted Theranostic Microbubbles: A New Technology towards Concurrent Rapid Ultrasound Diagnosis and Bleeding-free Fibrinolytic Treatment of Thrombosis*. Theronostics, 2016. **6**(5): p. 726-38.
50. Diaz, J.A., et al., *Critical review of mouse models of venous thrombosis*. Arterioscler Thromb Vasc Biol, 2012. **32**(3): p. 556-62.
51. Friedrich, R.P., et al., *Tissue Plasminogen Activator Binding to Superparamagnetic Iron Oxide Nanoparticle-Covalent Versus Adsorptive Approach*. Nanoscale Res Lett, 2016. **11**(1): p. 297.
52. Jin, H.J., et al., *Urokinase-coated chitosan nanoparticles for thrombolytic therapy: preparation and pharmacodynamics in vivo*. Journal of Thrombosis and Thrombolysis, 2013. **36**(4): p. 458-68.
53. Hebert, M., et al., *The story of an exceptional serine protease, tissue-type plasminogen activator (tPA)*. Revue Neurologique, 2016. **172**(3): p. 186-97.
54. Tang, Z.C., et al., *A t-PA/nanoparticle conjugate with fully retained enzymatic activity and prolonged circulation time*. Journal of Materials Chemistry B, 2015. **3**(6): p. 977-982.
55. Rana, S., Y.C. Yeh, and V.M. Rotello, *Engineering the nanoparticle-protein interface: applications and possibilities*. Curr Opin Chem Biol, 2010. **14**(6): p. 828-34.
56. Korin, N., et al., *Shear-Activated Nanotherapeutics for Drug Targeting to Obstructed Blood Vessels*. Science, 2012. **337**(6095): p. 738-742.
57. Chauvierre, C., et al., *Novel polysaccharide-decorated poly(isobutyl cyanoacrylate) nanoparticles*. Pharmaceutical Research, 2003. **20**(11): p. 1786-93.
58. Chauvierre, C., et al., *Enhancing the tolerance of poly(isobutylcyanoacrylate) nanoparticles with a modular surface design*. International Journal of Pharmaceutics, 2007. **338**(1-2): p. 327-32.
59. Matuszak, J., et al., *Nanoparticles for intravascular applications: physicochemical characterization and cytotoxicity testing*. Nanomedicine, 2016. **11**(6): p. 597-616.
60. Boulaftali, Y., et al., *The mouse dorsal skinfold chamber as a model for the study of thrombolysis by intravital microscopy*. Thromb Haemost, 2012. **107**(5): p. 962-71

Conclusion

Des nanoparticules copolymères polysaccharides-PIBCA fonctionnalisées avec du fucoïdane ont été synthétisées. *In vitro*, le fucoïdane favorise l'interaction de ces nanoparticules avec la P-sélectine et les agrégats plaquettaires activés. Le mode de chargement du rt-PA permet de conserver son activité fibrinolytique. *In vivo*, l'association de ces nanoparticules avec le rt-PA est efficace pour réduire la densité plaquettaire du thrombus dès 30 minutes après injection du traitement. Cette étude démontre le potentiel de la vectorisation d'un actif thrombolytique par une nanoparticule capable d'interagir avec la P-sélectine par le fucoïdane. Les effets secondaires liés à un tel système devront être évalués.

3. Formulation de nanogels polysaccharides

Article en préparation sur la base de résultats préliminaires :

**New synthesis process of cross-linked polysaccharide nanogel
for the molecular imaging of thrombotic pathologies**

Keywords: nanoprecipitation, cross-linking, polysaccharide, molecular imaging

Introduction

Les polysaccharides, tels que le dextrane et le pullulane, sont biocompatibles et biodégradables. Ils ont été largement utilisés dans la conception d'hydrogels réticulés chimiquement pour l'ingénierie tissulaire et la médecine régénérative. De plus, le fucoïdane, un polysaccharide naturel extrait d'algues brunes, présente une affinité très forte pour la P-sélectine exprimée par les plaquettes et les cellules endothéliales activées. Synthétiser des vecteurs à partir de ces matériaux est donc très intéressant pour le domaine cardiovasculaire. Des microparticules (300 nm – 10 µm) formulées à partir de dextrane, de pullulane et de fucoïdane réticulées chimiquement par du trimétaphosphate de sodium (STMP) ont montré une affinité particulière pour le 99m Technétium (99m Tc) et ont ainsi permis de détecter *in vivo* des anévrismes de l'aorte abdominale chez le rat par TEMP. Des suspensions colloïdales faites de ces mêmes matériaux, mais de taille inférieure et avec une distribution en taille plus étroite, pourraient présenter des interactions différentes avec les cellules cibles et offrir de nouvelles perspectives d'applications. La méthode d'émulsion utilisée pour synthétiser les microparticules est limitante pour diminuer leur taille et leur dispersion. Une nouvelle méthode par précipitation-réticulation est donc développée et optimisée. La capacité des nanovecteurs obtenus à lier le 99m Tc et à détecter des zones d'activation endothéliale et plaquettaire *in vivo* est évaluée.

Résumé

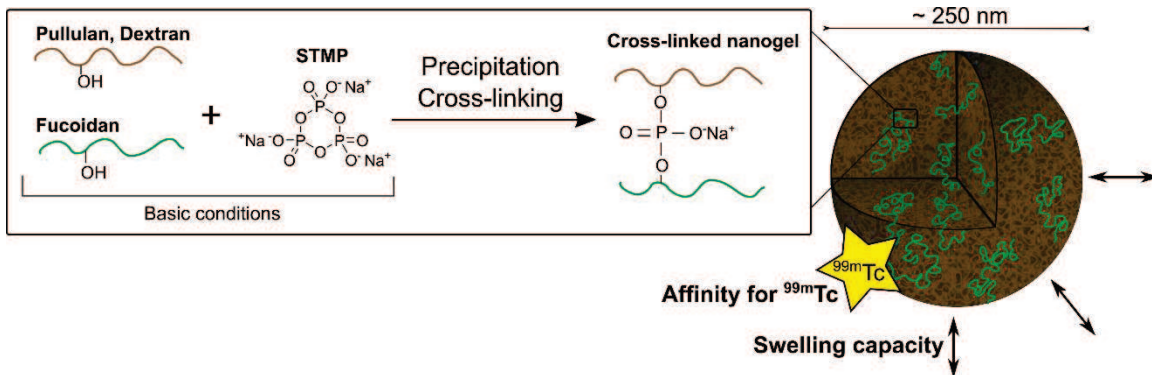
Les références *en italique* désignent les figures de l'article qui suit.

La précipitation des polysaccharides et du STMP dans l'éthanol est ici exploitée pour obtenir des nanoparticules réticulées chimiquement. Du STMP est ajouté à un mélange de pullulan, dextrane et fucoidane préparé en solution basique. Cette solution est versée goutte-à-goutte sous forte agitation dans un mélange composé de 93% d'éthanol et de 7% d'eau en volume. Du Triton X100 est utilisé pour favoriser la dispersion des polysaccharides sous forme de nanostructures. Les précipités obtenus sont remis en suspension dans l'eau et purifiés par dialyse. Des particules sphériques d'une taille de 330 nm dans l'eau sont d'abord formulées par ce procédé (*Figure 1*). Ces particules présentent une taille de 253 nm dans du tampon phosphate salin (PBS). Elles montrent en effet un taux de gonflement plus faible dans un milieu de force ionique plus élevée et sont donc qualifiées de "nanogels". Ces nanogels ne montrent aucune cytotoxicité à l'égard de cellules endothéliales primaires issues d'artères coronaires humaines (*Figures 2 et 3*).

Le taux de Triton X100 utilisé est diminué par un facteur 9 et le procédé est optimisé pour synthétiser des particules homogènes avec moins de surfactant. Des nanostructures réticulées contenant 0.6% w/w de groupements phosphates sont obtenues (*Figure 4A*). Elles ont une taille similaire aux précédentes nanoparticules dans l'eau et dans du PBS, et une taille de 258 nm dans du NaCl 0.9% (*Figure 4B*). Elles peuvent être stockées à 4°C ou à 37°C dans du NaCl 0.9% pendant plusieurs semaines (*Figure 4C*). Comme attendu, elles sont rapidement (< 1 heure) dégradées par la pullulanase et la dextranase, des enzymes spécifiques du pullulan et du dextrane (*Figure 4D*).

Enfin, de façon similaire aux microparticules faites des mêmes polymères réticulés également par du STMP, les nanogels sont marqués de façon efficace et stable au ^{99m}Tc (*Figure 5*). Ils s'accumulent rapidement (< 1 heure) au site d'activation dans un modèle de thrombose et dans un modèle d'ischémie-reperfusion myocardique chez le rat et restent sur site pendant au moins 5 heures 30 après injection (*Figures 6 et 7*).

New synthesis process of cross-linked polysaccharide nanogel for the molecular imaging of thrombotic pathologies



Abstract

A new process for synthesizing nanogels of about 250 nm composed of cross-linked polysaccharides including fucoidan is described. Nanogels are obtained by co-precipitation of the polysaccharides and of a chemical cross-linker, sodium trimetaphosphate, in ethanol followed by purification steps in aqueous solution. They are designed as tools for the molecular imaging of thrombosis by scintigraphy. Fucoidan has indeed a high affinity for P-selectin expressed by activated platelets and activated endothelial cells. The nanogels are evaluated *in vitro* and *in vivo*. They show a full compatibility with endothelial cells even at high concentration (400 µg/mL). They are made of biodegradable materials that can swell in aqueous conditions. In addition, they are easily radiolabeled with ^{99m}Tc for SPECT. In two preclinical models of platelet and endothelial activation, an uptake of radioactivity is observed in the injured vascular area as soon as 1 hour after injection of ^{99m}Tc -nanoparticles. In conclusion, nanovectors made of such biocompatible and biodegradable materials are very interesting for the molecular imaging and the treatment of cardiovascular pathologies expressing P-selectin.

Introduction

Chemical cross-linking has been largely used in the formulation of biocompatible and biodegradable polysaccharide hydrogels for tissue engineering and regenerative medicine [1-3]. Sodium trimetaphosphate (STMP) is a common cross-linking agent used

in food industry that acts by forming phosphate bounds between polysaccharide hydroxyl groups in basic conditions [4]. Our group previously synthesized microparticles made of dextran, pullulan and fucoidan cross-linked with STMP. These microparticles were obtained by emulsifying an aqueous phase of polysaccharides and STMP in oil. They had great potential in imaging cardiovascular pathologies overexpressing P-selectin [5, 6]. Fucoidan shows indeed a high affinity for P-selectin, a glycoprotein expressed by activated platelets and activated endothelial cells present at site of thrombus formation [7]. In addition, dextran and fucoidan are ligands of ^{99m}Tc (Technetium), a very common medical radioisotope for SPECT [8, 9]. These microparticles were therefore radiolabeled and functionalized for molecular imaging [6].

A water-in-oil macroemulsion is easy to produce. It leads to particles in the micrometer range with a broad size distribution (from 300 nm to 10 μm in one batch) that can be further separated by centrifugation. However, keeping the size at the nanoscale (< 500 nm) and promoting a narrower size distribution requires huge energy input and large quantity of surfactants with the water-in-oil emulsion technique [10]. Similar particles but with a hydrodynamic size in the nanometer range are still of interest for cardiovascular pathologies, as they would show a higher specific surface of interaction. Their behavior towards target cells and their biodistribution are also expected to be different. Therefore, other methods to synthesize nanoparticles made of the same materials are needed.

Several techniques have been described to synthesize polysaccharide nanoparticles [11]. These nanoparticles are usually referred to as nanogels. The term “nanogel” applies indeed to polymer networks assembled into nanostructures that exhibit swelling properties and that can load a large amount of water [12]. In particular, nanoparticles composed of dextran and/or pullulan have mainly been synthesized by coupling hydrophobic moieties to the polysaccharide chain. This induces the spontaneous formation of nanoparticles such as hydrophobized dextran-cyclodextrin self-assembly systems [13] and cholesterol-bearing pullulan nanoparticles [14]. These systems have interesting properties for the controlled release of hydrophobic drugs [15]. However, keeping a chemical cross-linking process as in the microparticles formulation would

ensure the full compatibility of the systems. Furthermore, totally hydrophilic nanoparticles could be of interest for the specific delivery of hydrophilic proteins, such as tissue plasminogen activator. This enzyme is the standard thrombolytic drug used to induce thrombus degradation in acute clinical events such as ischemic stroke [16].

Kahn and Schneider have adapted a nanoprecipitation technique to form hydrophilic gelatin nanoparticles cross-linked with glutaraldehyde in ethanol [17]. Nanoprecipitation is a method commonly used for the synthesis of nanoparticles from hydrophobic polymer chains in water [18]. The polymer is dissolved in a specific solvent and added in an antisolvent in which it precipitates. The solvent and the antisolvent must be miscible so that the solvent can diffuse into the antisolvent. This allows the polymer to assemble into nanostructures. Using such method is promising in the development of polysaccharides nanogels cross-linked with STMP. Ethanol has indeed been used for many years in the purification of polysaccharides by precipitation [19]. STMP precipitates also in ethanol. A co-precipitation of a polysaccharide blend and STMP in ethanol is therefore investigated in this study to form hydrophilic polysaccharide nanogels. The nanogels are characterized in terms of *in vitro* biocompatibility and biodegradability. In a similar manner to microparticles made of the same materials, their potential for the diagnosis of pathologies overexpressing P-selectin is evaluated *in vivo*.

Methods and Materials

Materials

Three types of polysaccharides were used: pullulan 100 was purchased from Hayashibara (Okayama, Japan), dextran 70 was purchased from PharmaCosmos (Holbaek, Denmark) and medium molecular weight fucoidan ($M_n = 18 \text{ kDa} / M_w = 104 \text{ kDa}$) was a gift from Algues & Mer (Ouessant, France). Some samples were synthesized by incorporating 1% w/w of FITC-dextran 70 bought from TdB Consultancy (Uppsala, Sweden).

Nanoparticles synthesis and physico-chemical characterization

Synthesis

Polysaccharides (75% pullulan, 12.5% dextran, 12.5% fucoidan) at 10 mg/mL were activated in 1 M NaOH. 10 mg of STMP (Sigma-Aldrich, Saint-Quentin Fallavier, France) were mixed with the polysaccharides. 760 µL of the solution was added dropwise in 93% v/v ethanol / 7% v/v water containing 6% w/v Triton X100 (Sigma-Aldrich) under agitation at 13,500 rpm with a homogenizer (Ultra-turrax® Ika, Sigma-Aldrich). The suspension was left 2 more minutes under agitation and then 30 minutes at room temperature without agitation. Precipitate material was removed by centrifugation (3,000 g 15 minutes 25°C) and resuspended in 5 mL of distilled water. The suspension was extensively dialyzed against water (Molecular Weight Cut-Off 300 kDa, Spectrum Europe B.V., Breda, The Netherlands). The purified suspension was finally put 5 minutes in an ultrasonic bath (Transsonic T080 Prolabo, Elma Schmidbauer GmbH, Singen, Germany). Mass concentration of each sample was determined by freeze-drying.

Physico-chemical characterization

Size and zeta potential were measured by dynamic light scattering (DLS) and electrophoretic light scattering (ELS) respectively (Zetasizer NanoZS, Malvern Instruments SARL, Orsay, France). Samples were dissolved in distilled water and KCl 1 mM for size and zeta potential determination respectively. Particle morphology in water was visualized by Scanning Electron Microscopy (SEM) (Philips XL 30 ESEM-FEG, Amsterdam, The Netherlands).

Swelling properties

Nanoparticles were suspended in either PBS 1x or distilled water, two solutions with different ionic strength. Their hydrodynamic diameter was measured by DLS.

Compatibility testing on primary Human Coronary Artery Endothelial Cells

Nanoparticles synthesized with 1% w/w FITC-dextran were used. They were suspended at 1 mg/mL in water and they were left 15 minutes under UV radiation to avoid contamination of the cell culture by other living microorganisms, such as bacteria, yeast, fungi and viruses. Based on DLS measurement, this step did not affect the physico-chemical properties of the samples.

Primary Human Coronary Artery Endothelial Cells (HCAECs, PromoCell, ref. C-12221) at passage number 4 were seeded at 20,000 cells/well onto fibronectin (PromoCell, ref. C-43060; coated at 50 µg/mL) pre-coated 96-well plates (Corning®, Sigma-Aldrich). Cells were incubated at 37°C in a humidified atmosphere of 5% CO₂. Cell culture medium (Endothelial Cell Basal Medium MV 2, ref. C22221, and supplemental pack, ref. C-39221, PromoCell; plus 1% penicillin-streptomycin, ref. 15240-062, Life Technologies; plus 0.2% Primocin, ref. ant-pm-2, InvivoGen; plus 0.02% Plasmocin, ref. ant-mpt, InvivoGen) was changed every 2-3 days. After reaching confluence, HCAECs were incubated with nanoparticles diluted in cell culture medium at two different concentrations: 400 µg/mL and 100 µg/mL. Cells with medium but without nanoparticles were chosen as controls.

Cell metabolic activity was assessed after 24 hours of contact with the different culture conditions by resazurin conversion. Cells were incubated with medium containing 10% resazurin (Sigma-Aldrich) for 4 hours at 37°C. Fluorescence intensity (530 nm / 590 nm) of the cell culture supernatants was measured with an Infinite® 200 PRO microplate reader (TECAN Group Ltd., Männedorf, Switzerland). A blank control comprising only medium was also included. Cells were imaged by light microscopy (EVOSTM XL Core, Life Technologies SAS) to infer simultaneously on their morphology.

In addition, phase contrast and fluorescence images of the cells were taken using an inverted microscope (Axio Observer, Carl Zeiss Microimaging GmbH, Iena, Germany), also after 24 hours of incubation with nanoparticles. The medium was changed just before cell imaging to remove any nanoparticle in suspension.

Optimized synthesis process and complementary characterization

Synthesis

An optimized protocol to get monodisperse and reproducible batches with a lower amount of Triton X100 was developed. Polysaccharides (75% pullulan, 12.5% dextran, 12.5% fucoidan) at 10 mg/mL were activated in 1 M NaOH. 10 mg of STMP were mixed with the polysaccharides. 760 µL of the solution was added dropwise in 93% v/v ethanol / 7% v/v water containing 0.66% w/v Triton X100 (Sigma-Aldrich) under agitation at 13,500 rpm with a homogenizer (Ultra-turrax® Ika, Sigma-Aldrich). The suspension was left 2 more minutes under agitation and then 15 minutes at room temperature under gentle magnetic agitation. Precipitate material was removed by centrifugation (3,000 g 3 minutes 25°C) and resuspended in 5 mL of distilled water. The resuspension step was performed by pipetting thoroughly during 3 minutes to induce strong local shear stress on the centrifuged pellet. The suspension was extensively purified by dialysis against NaCl 0.9% (Molecular Weight Cut-Off 300 kDa, Spectrum Europe B.V., Breda, The Netherlands). The mass concentration of each sample was determined by freeze-drying.

Swelling properties

Nanoparticles were suspended in either NaCl 0.9%, PBS 1x or distilled water. Their hydrodynamic diameter was measured by DLS.

Stability on storage

Nanoparticles at 1 mg/mL were left at either 4°C or 37°C in NaCl 0.9%. The samples left at 37°C were first put 15 minutes under UV radiation to avoid bacterial growth. The size and zeta potential in both conditions were measured by DLS and ELS respectively at different time points (Day 0, 1, 7, 14, 21, 28). Nanoparticles were kept in NaCl 0.9% for size determination and were diluted in KCl 1 mM for zeta potential measurement. Measurement parameters were kept the same for all time points.

Sodium trimetaphosphate quantitative analysis

The phosphate content, directly related to the STMP content, was determined by a spectrophotometric titration assay based on the colored complex formed by phosphate and metavanadate-molybdate in acidic conditions. The protocol was adapted from a

method developed for the characterization of hydrogel made of dextran and pullulan cross-linked with STMP [20]. Nanoparticles at 2.5 mg/mL were degraded in 10% nitric acid at 105°C for 15 minutes. A solution of ammonium metavanadate (NH_4VO_3) prepared at 21 mM in 13% nitric acid and a solution of ammonium heptamolybdate ($(\text{NH}_4)_6\text{Mo}_7\text{O}_{24}$) prepared at 43 mM in water were then added to the degraded polysaccharides. After 15 minutes at room temperature, the absorbance of the samples at 405 nm was determined with an Infinite® 200 PRO microplate reader. The total phosphate content was determined by using a standard curve prepared in parallel with phosphoric acid. A polysaccharide solution prepared at the same concentration than the nanoparticles was used as blank.

In vitro enzymatic degradation

Nanoparticles were suspended at 4 mg/mL in PBS 1x containing pullulanase (Sigma-Aldrich) and dextranase (Sigma-Aldrich) in excess. The suspensions were left at 37°C and their hydrodynamic size was measured by DLS with fixed measurement parameters. The count rate, related to the number of events detected by DLS, and the polydispersity index (PDI) were measured each hour and up to 5 hours.

In vivo application for molecular imaging by SPECT

Nanoparticle radiolabeling

The radiolabeling protocol for SPECT was adapted from the one developed by our team to radiolabeled polysaccharide microparticles [6]. Sodium pertechnetate ($\text{Na}(\text{TcO}_4)$) with an activity of 200 to 300 MBq (volume < 200 µL) was mixed with 3 µg of stannous chloride and 1.3 mg of nanoparticles in NaCl 0.9%. Stannous chloride was required to reduce TcO_4^- to enable its interaction with the polysaccharides [21]. After 15 minutes of incubation at room temperature, radiolabeled nanoparticles were centrifuged at 18,000 g for 8 minutes to separate them from free ^{99m}Tc . The activities of the supernatant and the pellet were measured with an activimeter (Medi 40, Medisystem, Guyancourt, France) to determine the radiolabeling efficiency. The efficiency was defined as the percentage of activity associated to the pellet normalized to the introduced activity.

The nanoparticle pellet was resuspended in NaCl 0.9% at a nanoparticle concentration of 5.2 mg/mL and left at room temperature. To assess the amount of released ^{99m}Tc and then the radiolabeling stability, instant thin-layer chromatography (ITLC) was performed at different time points and up to 3 hours and 20 minutes. One drop of the suspension was dropped off a chromatography paper. Free ^{99m}Tc was allowed to migrate for a few minutes in methyl-ethyl-ketone solvent.

Preclinical models

Wistar adult rats (400 g) were purchased from Elevage Janvier (Le Genest, St-Berthevin, France). The animal study was performed in respect of the applicable regulation for animal experimentation and with approval of the animal care and use committee of the Claude Bernard Institute.

FeCl₃ model: Animals were anesthetized by intra-peritoneal injection of sodium pentobarbital (1 $\mu\text{L/g}$, Ceva Santé Animale SA, La Ballastiere, France). The infrarenal abdominal aorta was exposed and isolated. A chromatography paper soaked into a 10% FeCl₃ solution was left on the aorta for 5 minutes. The vessel surface was rinsed and the vessel was put back in place. This model was done on 1 rat. The nanoparticles were injected via the penis vein just after thrombus induction.

Myocardial ischemia-reperfusion. Rats were anesthetized by intra-peritoneal injection of ketamine at 100 mg/kg (Vétoquinol SA, Lure, France). The proximal left anterior descending coronary artery was occluded using a suture made around a catheter. After 20 minutes, the suture was cut and the vessel was reperfused. This model was done on 2 rats. The injection of the nanoparticles was performed via the penis vein after 2 hours of reperfusion.

SPECT/CT imaging

During the whole imaging phase, rats were maintained under isoflurane and positive pressure ventilation. In both models, 70 to 80 MBq of the radiolabeled nanoparticle suspension corresponding to less than 500 μg of nanoparticles was administrated via the penis vein. Helical SPECT/CT scans were performed with 4-head

camera multiplexing multipinhole camera (NanoSPECT/CT plus, Bioscan Inc, Paris, France).

Whole body CT and SPECT acquisitions were performed at 1 and 3 hours after injection. The SPECT acquisition was performed with the following parameters: helical scan with 28 projections per rotation plus circular scan at the beginning and at the end of the scan range, matrix size = 256 x 256, zoom 1.14 (pixel size: 1 mm²). SPECT data were reconstructed using HiSPECT (Bioscan Inc., Washington D.C., USA) iterative reconstruction software. Images were visualized using the Bioscan InVivoScope software with co-registration of SPECT and CT images.

To validate the imaging potential of injected nanoparticles, reconstructed slices were visualized in 3 planes: sagittal, coronal and axial planes centered on the injured area. Finally, these regions of interest were explanted at 5h30 after injection and imaged by SPECT to assess the remaining radioactivity.

Results

Nanoparticle synthesis by nanoprecipitation-cross-linking

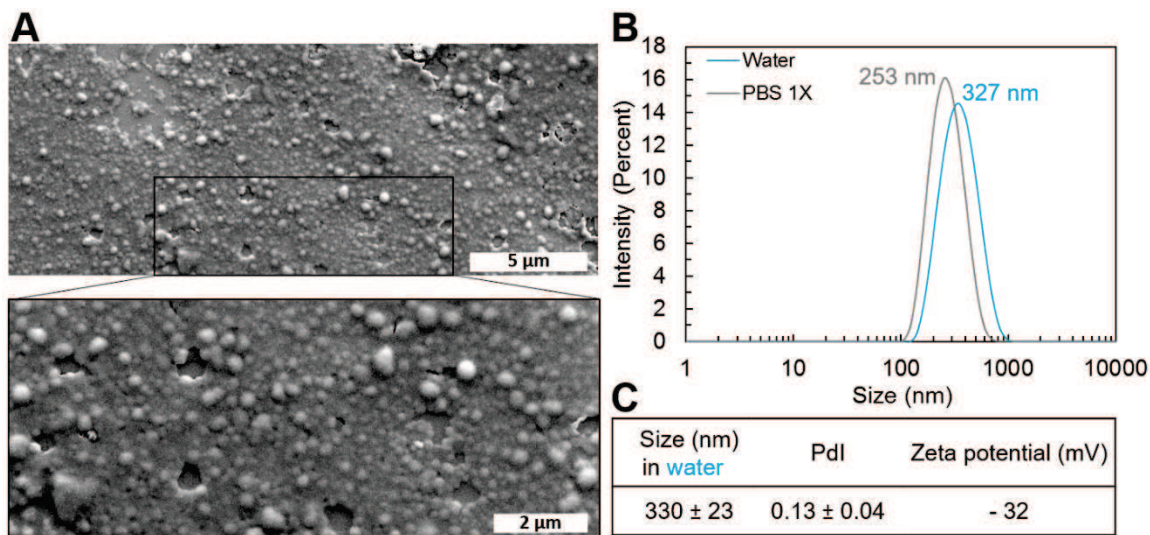


Figure 1. Physico-chemical characterization of nanoparticles.

A) Scanning Electron Microscopy (SEM). **B)** Diffusion Light Scattering (DLS) measurement in intensity in water and in PBS1x. **C)** Size values in water and Polydispersity Index (PdI) determined by DLS ($n = 3$ independent batches; mean \pm standard deviation). Zeta potential values measured by ELS ($n = 1$).

A new process was set up to synthesize cross-linked hydrophilic nanoparticles made of dextran, pullulan and fucoidan. The nanoprecipitates that formed by addition of polysaccharides and STMP in 93% v/v ethanol were highly unstable and aggregated rapidly after the agitation phase. The precipitates were therefore easily removed from the ethanol phase by centrifugation. After resuspension in distilled water, the pH was > 10 and some foam indicated the presence of residual Triton X100 in the aqueous solution. After purification by dialysis, the nanoparticles were suspended in distilled water at pH 5-7. Dialysis seemed efficient to remove Triton X100 and avoided multiple resuspension steps compare to centrifugation. The absence of Triton X100 was validated by the absence of foam in the suspension. The morphology of the nanoparticles was assessed by SEM. Solid spherical nanostructures were obtained (Figure 1A). Their hydrodynamic size in water was determined to be 330 ± 23 nm with a polydispersity index of 0.13 ± 0.04 (Figures 1B &1C). No aggregate and/or larger particle was detected by DLS. The nanoparticles showed a negative surface charge (Figure 1C).

One interesting properties of cross-linked hydrogel relies on their capacity to swell in aqueous solutions and therefore to load a high amount of liquid. Hydrogel swelling rate usually depends on the ionic strength of the medium [22]. Here, the hydrodynamic size of the nanoparticles decreased by 23% (averaged size) once the particles were suspended in PBS 1x (Figure 1B). Therefore, the term nanogel appeared appropriate to characterize this structure.

Cytocompatibility of polysaccharide nanoparticles

The particles were made of biocompatible materials. However, the size and the structure of the nanoparticles could influence their cytocompatibility. To evaluate potential deleterious effects, nanoparticles were directly incubated with HCAECs at high concentrations of 100 $\mu\text{g}/\text{mL}$ and 400 $\mu\text{g}/\text{mL}$. The viability of HCAECs was not affected by 24 hours of incubation with nanoparticles at both concentrations as shown by their metabolic activity (Figure 2A). The cells show no major morphological change compared to control cells as visualized by bright-field microscopy (Figure 2B).

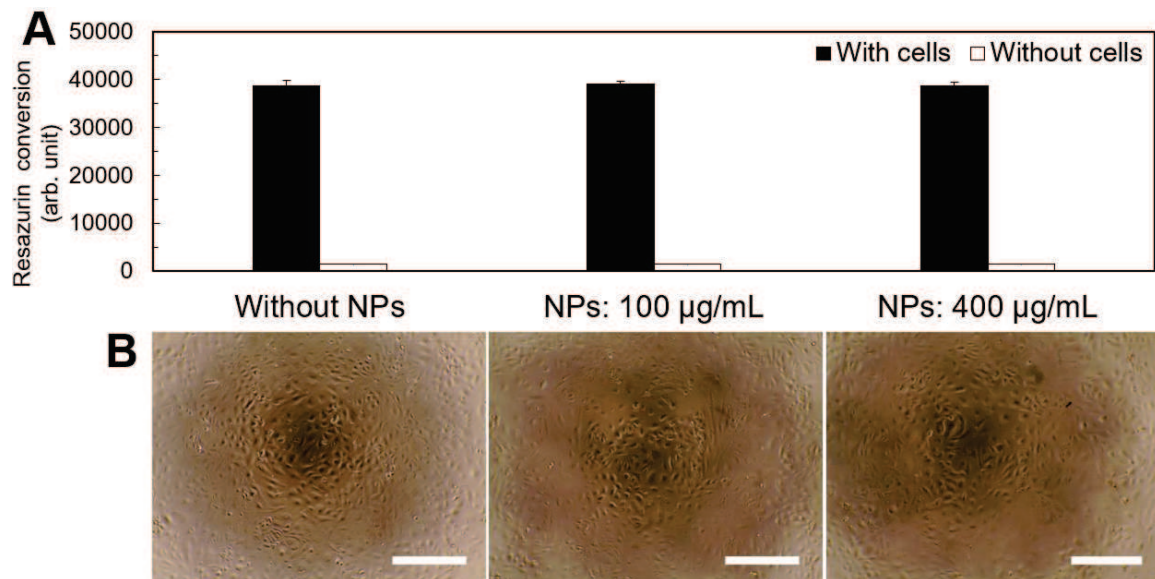


Figure 2. Viability of primary Human Coronary Artery Endothelial Cells after 24 hours of incubation with nanoparticles (NPs) at different concentrations.

A) Resazurin assay; the signal is correlated to the number of viable cells. B) Corresponding bright field imaging of the cells (scale bar = 500 µm).

In addition, an uptake of green fluorescence in the cell cytoplasm was observed in cells incubated with nanoparticles, suggesting that the fluorescent nanoparticles were able to enter the cells. The fluorescent signal intensity was correlated to the nanoparticle concentration (Figure 3).

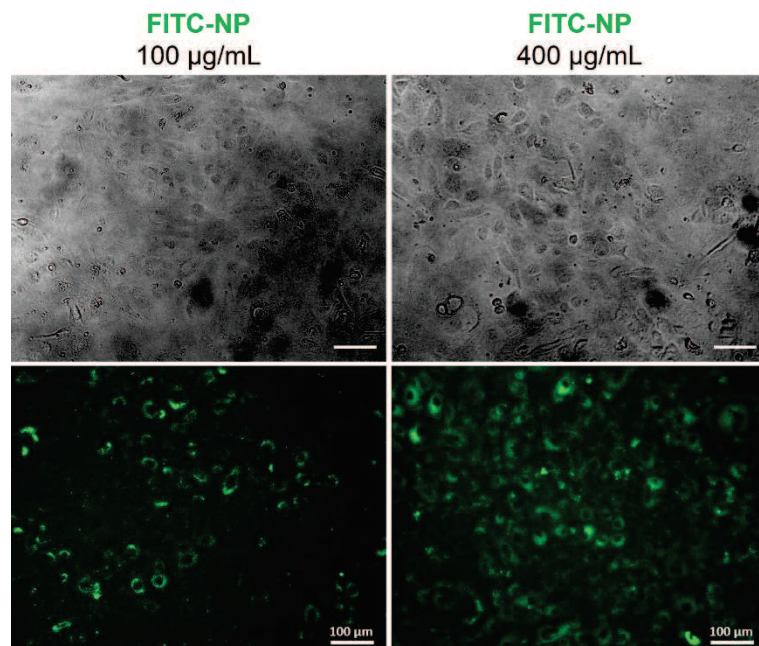


Figure 3. Phase contrast and fluorescence microscopy images of Primary Human Coronary Artery Endothelial Cells after 24 hours of incubation with FITC-labeled nanoparticles (FITC-NPs) at different concentrations.

Optimized synthesis process and *in vitro* enzymatic degradation

The amount of Triton X100 introduced in ethanol was reduced by 90%. The resuspension step was critical. After resuspension in water, less foam was observed than with previous parameters. The residual Triton X100 was removed by dialysis. Homogeneous suspensions were synthesized (Figure 4A). They showed similar hydrodynamic size and similar swelling properties than the nanoparticles synthesized with more Triton X100 (Figure 4B & Figure 1B). In particular, the hydrodynamic size of the nanoparticles in NaCl 0.9% measured by DLS was 258 ± 13 nm with a polydispersity index of 0.16 ± 0.03 (Figure 4A). Their behavior in NaCl 0.9% and PBS 1x were very close. Their zeta potential value was -19 ± 2 mV. The nanoparticles were stable in NaCl 0.9% at 37°C and 4°C for at least 4 weeks, as shown by the DLS and ELS measurements (Figure 4C).

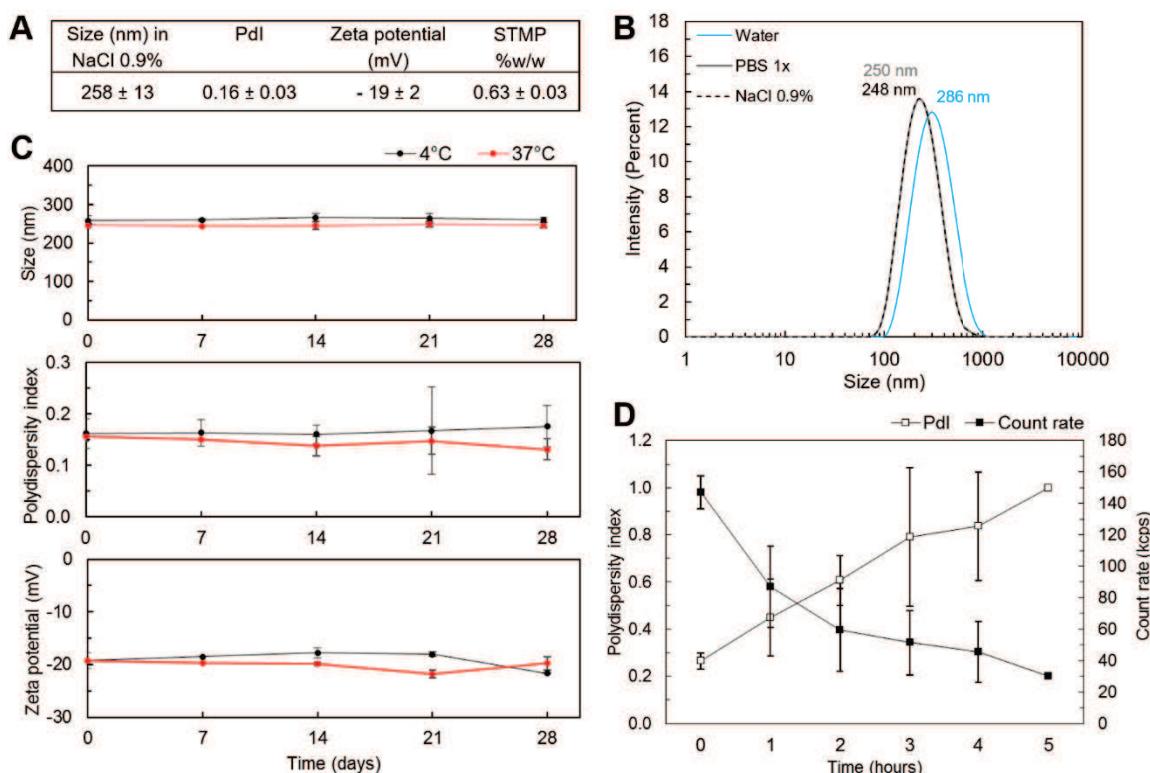


Figure 4. Physico-chemical characterizations of the optimized nanoparticle formulation.
A) Size values and Polydispersity Index (Pdl) determined by DLS and zeta potential values measured by ELS ($n = 4$ independent batches; mean \pm standard deviation). STMP content in weight as determined by phosphate quantitative analysis. **B)** Stability on storage; at 4°C and 37°C in NaCl 0.9% over 28 days. **C)** Swelling properties; DLS measurement in intensity of one batch of nanoparticle in NaCl 0.9% and in water. **D)** Degradation; Pdl and count rate determined by DLS after incubation with specific enzymes.

The phosphate quantitative analysis highlighted the presence of phosphate bonds in the structure. This result validated the cross-linking mechanism. The amount of STMP represented $0.63\% \pm 0.03\%$ of the total nanoparticle weight (Figure 4A).

To evaluate the nanoparticle degradability in contact with specific enzymes (pullulanase and dextranase), the count rate and the polydispersity index of nanoparticle suspensions were determined by DLS after putting the nanoparticles in contact with the enzymes. After the first hour, the count rate had already decreased from 147 to 87 kcps (Figure 4D). Under 100 kcps, the NanoZS does not detect enough particle to perform robust measurement. Non-surprisingly, the polydispersity index increase up to 1 over time showing that the monodisperse suspension of nanoparticles was transformed into a mixture of polydisperse structures (Figure 4D).

Nanoparticle radiolabeling with ^{99m}Tc

$89\% \pm 3\%$ of the activity put in contact with the nanoparticles was recovered in the nanoparticle pellet. After resuspension, the proportion of bound ^{99m}Tc determined by ITLC was of $81\% \pm 2\%$ (Figure 5). The radiolabeling was stable over time at room temperature at least up to 50 minutes. No dramatic decrease was noticed at later time points and the activity associated to bound ^{99m}Tc remained around 70% up to 3 hours and 20 minutes.

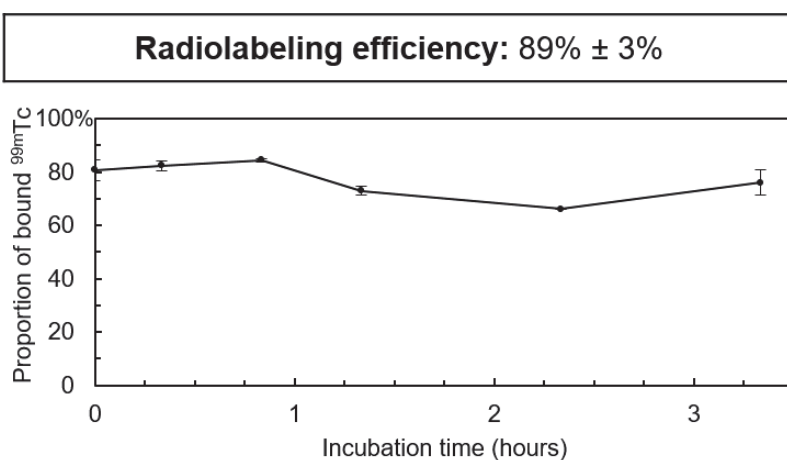


Figure 5. Radiolabeling efficiency and stability *in vitro*.

Radiolabeling efficiency as measured by the activity of the nanoparticle pellet after nanoparticle labeling and centrifugation ($n = 3$ independent experiments, mean \pm standard deviation). Plot: percentage of bound ^{99m}Tc as determined by instant thin-layer chromatography over time after nanoparticle resuspension in NaCl 0.9% ($n = 2$).

In vivo application for thrombosis imaging

Two different preclinical models were performed. The first one consisted in inducing thrombosis with FeCl₃. This model generates platelet recruitment and formation of an important platelet aggregate that may be stabilized by a fibrin network onto the denuded endothelium [23]. 1 hour after injection of ^{99m}Tc-nanoparticles, a strong uptake was observed along the abdominal aorta (Figure 6A). The second model consisted in temporarily reducing the blood supply of the myocardium. Under such ischemic conditions, the endothelium becomes activated. Once the flow is re-established, a cascade of events is generated which drives the recruitment of inflammatory cells and the activation of platelets at the surface of the activated endothelium [24]. These processes cause an important inflammation. 1 hour after injection of ^{99m}Tc-nanoparticles, an accumulation of radiolabeled nanoparticles was observed at the myocardium (Figure 6B).

In both models, the signal was still visible at 3 hours after injection (data not shown). These results were confirmed by the remaining radioactivity associated to explanted aorta and myocardium 5h30 after injection (Figures 7A & 7B). Both regions associated with activity corresponded to the location of vascular injury.

Qualitative analysis of the relative organ retention showed a trend towards fast renal elimination. Also, a strong liver uptake of the radiolabeled compounds was observed at 1 hour but decreased from 1 to 3 hours. No signal was seen in the lungs. The injection was associated to limited release of free ^{99m}Tc, as was assessed by the low accumulation in the thyroid and on the stomach wall (data not shown).

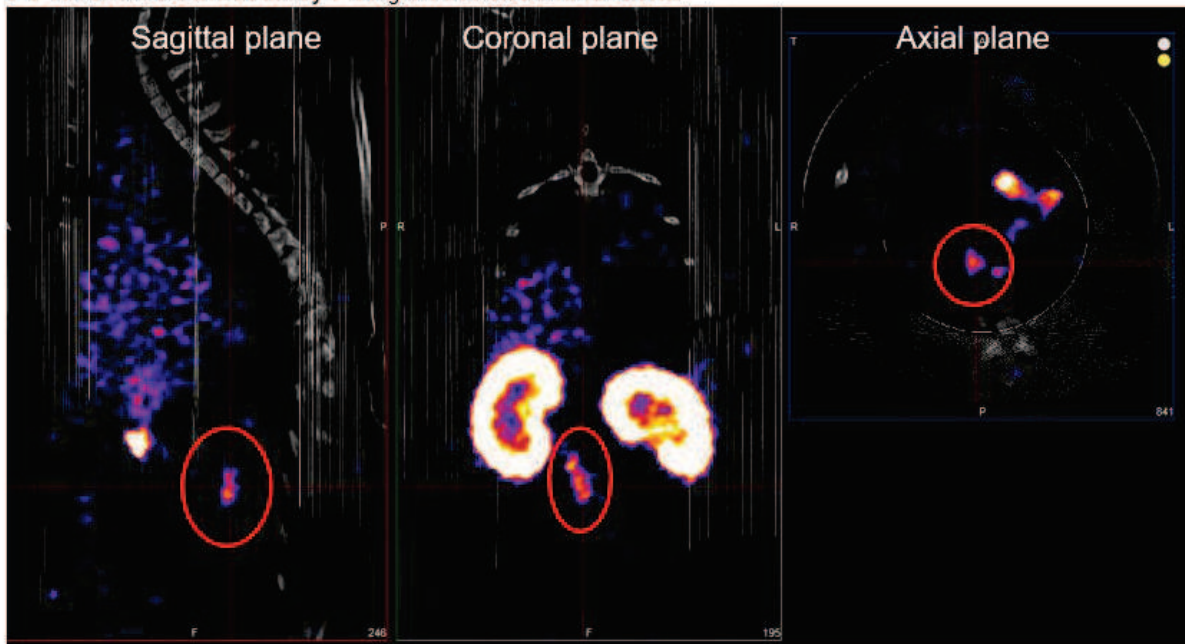
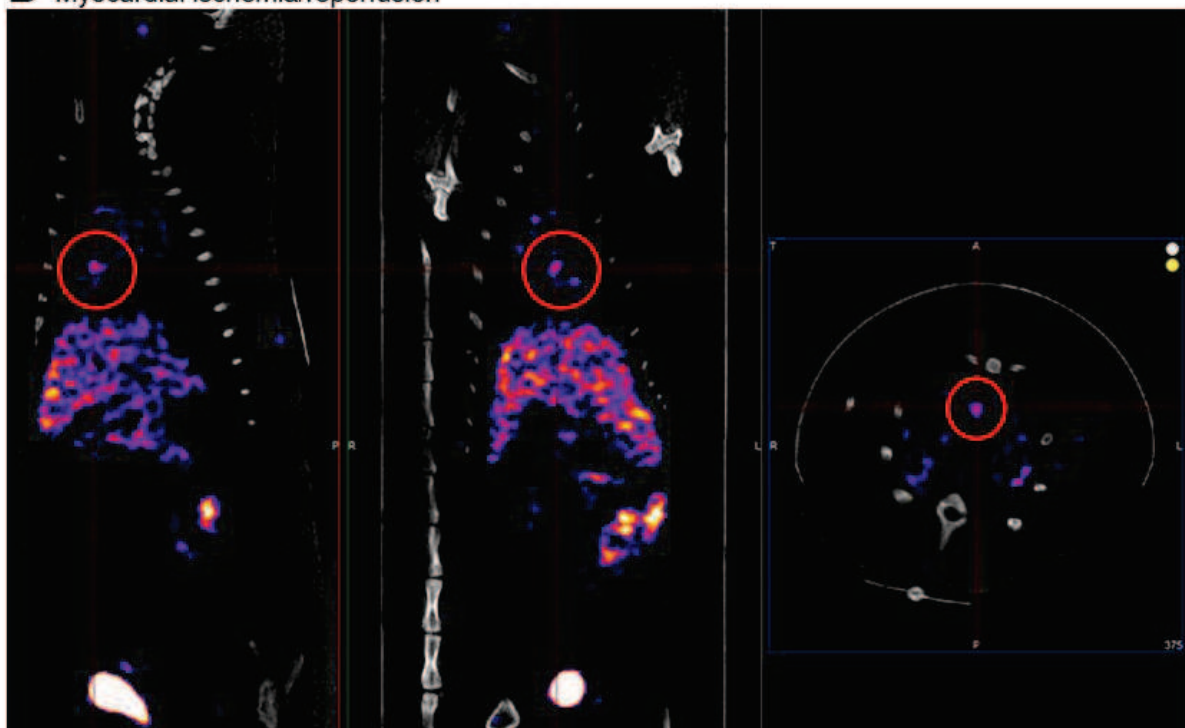
A Thrombosis induced by FeCl_3 on the abdominal aorta**B** Myocardial ischemia/reperfusion

Figure 6. SPECT/CT of 2 rats with a different injury model 1 hour after injection of $^{99\text{m}}\text{Tc}$ -nanoparticles.

A) FeCl_3 -induced thrombus. A strong uptake of activity is visible along the aorta on the three planes (circled in red). **B)** Myocardial ischemia-reperfusion. An uptake of activity, localized at the myocardium, is observed on the three planes (circled in red).



Figure 7. Radioactivity associated with explanted regions of interest.

The animals were sacrificed at 5h30 after ^{99m}Tc -nanoparticles injection. The areas were immediately imaged after explantation. **A)** Adbominal aorta from the FeCl_3 model. **B)** Myocardium from the ischemia-reperfusion model.

Discussion

A new synthesis process of hydrophilic nanogel was developed and optimized. Spherical structures of around 250 nm were obtained with a simple, fast and reproducible technique. These nanogels were made of a mix of 75% w/w pullulan, 12.5% w/w dextran and 12.5% w/w fucoidan. The final composition of these nanogels was not assessed but will be done in future work. The negative value of the surface charge supported the presence of some anionic fucoidan at the surface [6]. The phosphate groups that come from the cross-linker are also negatively charged but were present in a lesser extent (0.63% w/w). The fucoidan content will be quantitatively analyzed by elemental analysis of the sulfur content in future work.

The method described in this study requires equilibrium between chain precipitation (contraction and local accumulation) and the solvation of reactive hydroxyl groups to allow them to react with STMP. Indeed, it was observed in preliminary experiments that the cross-linking process did not happen when adding the aqueous solution to absolute ethanol (data not shown). A mix of 93% v/v ethanol / 7% v/v water was therefore chosen here to get STMP cross-linked nanogels. Among several surfactants (Poloxamer 407, Tween 80, Span 80), Triton X100 was the only one to promote the formulation of a homogeneous suspension. However, above a concentration of about 0.1 mg/mL, Triton X100 was shown to be cytotoxic and cause permeation of cell

membranes [25]. In our study, its initial concentration in ethanol was decreased down to 6.7 mg/mL with the optimized protocol. The major part of it was expected to be retained in the ethanol phase when removing the nanoprecipitates and the rest was eliminated by dialysis. Nevertheless, a quantitative analysis is required to confirm the final concentration.

The nanoparticles showed a full biocompatibility and biodegradability. They did not affect cell viability at a concentration as high as 400 µg/mL, which is comparable to biocompatible lipid-based nanosystems [26]. The nanogels were degraded by pullulanase and dextranase. Future studies will focus on earlier degradation time points, as the results of this report showed that the samples were mostly degraded at 1 hour. As for hydrogels, the degradation time is expected to increase with increasing amount of cross-linker and to depend on the pullulan/dextran ratio [20].

Finally, similarly to microparticles made of the same materials, the nanoparticles interacted with ^{99m}Tc which enabled to inject them in models of vascular activation where P-selectin is expressed. Obviously, nanoparticles without fucoidan must be tested as controls to complete the study. In addition, the expression of P-selectin at site of injury and its co-localization with fluorescent nanogels will be assessed by histological analysis. Furthermore, the biodistribution of the systems will be studied by counting the radioactivity of each organ [27]. Hydrophilic compounds can potentially be loaded by resuspending the freeze-dried structure in a solution in which the compound is dissolved.

In conclusion, a simple and fast synthesis process has been developed and optimized to form cross-linked polysaccharide nanogels. These structures hold a lot of promises for future applications in the cardiovascular field.

References

1. Coviello, T., et al., *Polysaccharide hydrogels for modified release formulations*. Journal of Controlled Release, 2007. **119**(1): p. 5-24.
2. Silva, A.K., et al., *Polysaccharide-based strategies for heart tissue engineering*. Carbohydrate Polymers, 2015. **116**: p. 267-77.
3. Guerrero, J., et al., *Cell interactions between human endothelial cells and mesenchymal stem cells in a three dimensional macroporous polysaccharide-based scaffold*. Journal of Tissue Engineering and Regenerative Medicine, 2012. **6**: p. 309-309.

4. Wattanachant, S., et al., *Effect of crosslinking reagents and hydroxypropylation levels on dual-modified sago starch properties*. Food Chemistry, 2003. **80**(4): p. 463-471.
5. Bonnard, T., et al., *Leukocyte mimetic polysaccharide microparticles tracked in vivo on activated endothelium and in abdominal aortic aneurysm*. Acta Biomaterialia, 2014. **10**(8): p. 3535-45.
6. Bonnard, T., et al., *Abdominal aortic aneurysms targeted by functionalized polysaccharide microparticles: a new tool for SPECT imaging*. Theranostics, 2014. **4**(6): p. 592-603.
7. Bachelet, L., et al., *Affinity of low molecular weight fucoidan for P-selectin triggers its binding to activated human platelets*. Biochimica et Biophysica Acta, 2009. **1790**(2): p. 141-6.
8. Rouzet, F., et al., *Radiolabeled Fucoidan as a P-Selectin Targeting Agent for In Vivo Imaging of Platelet-Rich Thrombus and Endothelial Activation*. Journal of Nuclear Medicine, 2011. **52**(9): p. 1433-1440.
9. Bhatnagar, A., et al., *Technetium-99m dextran: A promising new protein-losing enteropathy imaging agent*. European Journal of Nuclear Medicine, 1996. **23**(5): p. 575-578.
10. Tadros, T.F., *Emulsion Formation, Stability, and Rheology*, in *Emulsion Formation and Stability* (ed T. F. Tadros). 2013, Wiley-VCH Verlag GmbH & Co. KGaA, Weinheim, Germany. .
11. Debele, T.A., S.L. Mekuria, and H.C. Tsai, *Polysaccharide based nanogels in the drug delivery system: Application as the carrier of pharmaceutical agents*. Materials Science & Engineering C-Materials for Biological Applications, 2016. **68**: p. 964-981.
12. Soni, K.S., S.S. Desale, and T.K. Bronich, *Nanogels: An overview of properties, biomedical applications and obstacles to clinical translation*. Journal of Controlled Release, 2016. **240**: p. 109-126.
13. Daoud-Mahammed, S., et al., *Cyclodextrin and Polysaccharide-Based Nanogels: Entrapment of Two Hydrophobic Molecules, Benzophenone and Tamoxifen*. Biomacromolecules, 2009. **10**(3): p. 547-554.
14. Kobayashi, H., et al., *Effects of Cholesterol-Bearing Pullulan (CHP)-Nanogels in Combination with Prostaglandin E1 on Wound Healing*. Journal of Biomedical Materials Research Part B-Applied Biomaterials, 2009. **91B**(1): p. 55-60.
15. Wasiak, I., et al., *Dextran Nanoparticle Synthesis and Properties*. Plos One, 2016. **11**(1).
16. Varna, M., et al., *Nanomedicine as a strategy to fight thrombotic diseases*. Future Sci OA, 2015. **1**(4).
17. Khan, S.A. and M. Schneider, *Improvement of Nanoprecipitation Technique for Preparation of Gelatin Nanoparticles and Potential Macromolecular Drug Loading*. Macromolecular Bioscience, 2013. **13**(4): p. 455-463.
18. Rao, J.P. and K.E. Geckeler, *Polymer nanoparticles: Preparation techniques and size-control parameters*. Progress in Polymer Science, 2011. **36**(7): p. 887-913.
19. Neuchl, C. and A. Mersmann, *Fractionation of polydisperse dextran using ethanol*. Chemical Engineering Science, 1995. **50**(6): p. 951-958.
20. Abed, A., et al., *Influence of polysaccharide composition on the biocompatibility of pullulan/dextran-based hydrogels*. Journal of Biomedical Materials Research Part A, 2011. **96A**(3): p. 535-542.
21. Saboural, P., et al., *Purification of a low molecular weight fucoidan for SPECT molecular imaging of myocardial infarction*. Marine Drugs, 2014. **12**(9): p. 4851-67.
22. Maire, M., et al., *Retention of transforming growth factor beta 1 using functionalized dextran-based hydrogels*. Biomaterials, 2005. **26**(14): p. 1771-1780.
23. Eckly, A., et al., *Mechanisms underlying FeCl₃-induced arterial thrombosis*. Journal of Thrombosis and Haemostasis, 2011. **9**(4): p. 779-789.
24. Eltzschig, H.K. and T. Eckle, *Ischemia and reperfusion-from mechanism to translation*. Nature Medicine, 2011. **17**(11): p. 1391-1401.
25. Koley, D. and Bard, A. J., *Triton X-100 concentration effects on membrane permeability of a single HeLa cell by scanning electrochemical microscopy (SECM)*. Proceedings of the National Academy of Sciences U S A, 2010. **107**(39): p. 16783-16787
26. Matuszak, J., et al., *Nanoparticles for intravascular applications: physicochemical characterization and cytotoxicity testing*. Nanomedicine, 2016. **11**(6): p. 597-616.
27. Desbree, A., et al., *Evaluation of Functionalized Polysaccharide Microparticles Dosimetry for SPECT Imaging Based on Biodistribution Data of Rats*. Molecular imaging and biology : MIB : the official publication of the Academy of Molecular Imaging, 2014.

Conclusion

Un nouveau procédé a été mis en place pour synthétiser des nanovecteurs à partir de matériaux entièrement biocompatibles et biodégradables. Ce procédé permet d'obtenir de façon simple et très rapide (<30 minutes) des structures réticulées de 250 nm environ dans du NaCl 0.9%. Ces nanogels de polysaccharides ont la capacité de gonfler selon la force ionique du milieu. Un mélange éthanol/eau est utilisé pour provoquer la création de nanoprécipités concentrés en polysaccharides et en STMP, qui sont capables de réticuler. Le mécanisme repose sur l'hypothèse que la contraction des chaînes de polysaccharides dans l'éthanol augmente localement leur concentration et favorise leur agrégation, ce qui rend les groupements hydroxyles suffisamment proches pour réagir avec le STMP. Au vu des propriétés des microparticules et des hydrogels développés précédemment au sein de l'équipe de *Bio-ingénierie cardiovasculaire* à partir des mêmes matériaux, ces nanogels sont prometteurs pour l'imagerie moléculaire et le traitement de la thrombose.

Discussion et perspectives

Ce travail de thèse a permis d'explorer l'utilisation de nano et microparticules polymères fonctionnalisées avec du fucoïdane pour l'imagerie moléculaire et le traitement de la thrombose. Ces vecteurs sont formulés à partir de polysaccharides et/ou de PIBCA. Dans le **projet expérimental 1**, un test *in vitro* en flux est mis au point pour valider l'interaction des vecteurs développés avec leur cible moléculaire, la P-sélectine, et leur cible cellulaire, les plaquettes activées. Il valide l'interaction forte entre ces cibles et des microcapsules polymères fonctionnalisées avec le fucoïdane. Dans le **projet expérimental 2**, des nanoparticules copolymères fonctionnalisées avec du fucoïdane sont chargées avec du rt-PA. Dans un modèle murin de thrombose, ces nanoparticules augmentent significativement l'efficacité thrombolytique de l'actif. Ces résultats sont prometteurs pour le développement de vecteurs dirigés contre la P-sélectine à des fins thérapeutiques. Dans le **projet expérimental 3**, des nanoparticules composées exclusivement de polysaccharides et entièrement hydrophiles, dites nanogels, sont synthétisées par un procédé innovant. Ces nanogels ne montrent aucune cytotoxicité *in vitro* même à forte concentration. Ils peuvent être radiomarqués au ^{99m}Tc pour la détection du thrombus par TEMP. Les résultats de ces trois parties expérimentales sont analysés sur la base des points suivants :

- l'évaluation du couple fucoïdane/P-sélectine,
- l'évaluation de la vectorisation du rt-PA par les nanoparticules copolymères et les perspectives pour le développement de nanovecteurs pour la thrombolyse ciblée,
- l'évaluation des nanovecteurs synthétisés d'un point de vue physico-chimique et biologique.

Évaluation du couple fucoïdane/P-sélectine

Les vecteurs décrits dans ce manuscrit sont fonctionnalisés avec le fucoïdane selon différents procédés : i) dans le cas des microcapsules, le fucoïdane est incorporé dans la coque polymère pendant la synthèse, ii) dans le cas des nanoparticules copolymères, il est greffé à la surface du cœur hydrophobe, enfin iii) dans les nanogels, il

est réticulé dans la matrice de polysaccharides. Selon le mode de fixation du fucoïdane aux vecteurs, la conformation de ce ligand et donc ses interactions avec la P-sélectine peuvent être modifiées. C'est dans ce contexte qu'a été développé le test d'adhésion en flux présenté **Figure 20**. Les trois vecteurs ont été évalués tour à tour.

Dans un premier temps, nous avons utilisé ce test d'adhésion pour étudier les microcapsules. Les résultats sont détaillés dans le **projet expérimental 1**. Du fait de leur taille, les microcapsules sont parfaitement visibles et quantifiables en microscopie à fluorescence, ce qui permet de développer et d'optimiser le design expérimental. Les résultats montrent que le fucoïdane permet aux microcapsules d'adhérer en nombre à la P-sélectine et de s'accumuler sur les agrégats plaquettaires activés. Ces observations valident donc l'efficacité du ciblage par le fucoïdane. Aussi, les microcapsules contrôles synthétisées avec un revêtement 100% dextrane ne présentent quasiment aucune affinité pour la P-sélectine et pour les agrégats plaquettaires activés. Cependant, la comparaison des microcapsules fonctionnalisées 10% fucoïdane / 90% dextrane avec des microcapsules contrôles 100% dextrane a des limites du fait que la charge de surface des systèmes est différente : - 52 mV pour les microcapsules-fucoïdane contre -9 mV pour les microcapsules contrôles. Il serait intéressant d'évaluer le comportement de microcapsules formulées avec un autre polysaccharide anionique que le fucoïdane, comme le dextrane carboxyméthylé [152]. La forte adhésion des microcapsules-fucoïdane aux agrégats plaquettaires valident tout de même qu'il se produit une interaction forte entre ces vecteurs et leurs cellules cibles et que cette interaction est stable sous flux artériel. Ces résultats sont similaires à ceux observés avec des microbulles fonctionnalisées en surface avec un anticorps anti-P-sélectine [126, 181]. Utiliser le fucoïdane comme agent de ciblage permet donc de s'affranchir du coût et/ou du risque immunogène lié à l'utilisation d'anticorps, sans perdre en efficacité. Toutefois, en plus de présenter une forte interaction avec sa cible, un vecteur ciblé doit en être spécifique. Le passage des microcapsules-fucoïdane sur un revêtement de E- et L-sélectines montre que les microcapsules-fucoïdane adhèrent 6,5 fois moins à la E-sélectine qu'à la P-sélectine et n'adhèrent pas à la L-sélectine. La fonctionnalisation de ces vecteurs par le fucoïdane les rend donc sélectifs de la P-sélectine. Élucider la relation structure-fonction du fucoïdane permettrait

d'identifier les groupements spécifiquement responsables des interactions du fucoïdane avec les différentes sélectines et d'optimiser davantage cet agent de ciblage pour arriver à une spécificité équivalente à celle des anticorps (voir **section 2.3.1.b**) [132].

Nous avons ensuite utilisé ce test d'adhésion en flux pour caractériser l'interaction des nanoparticules copolymères avec la P-sélectine et avec des agrégats plaquettaires activés. Les résultats sont détaillés dans le **projet expérimental 2**. Ce test démontre que les nanoparticules-fucoïdane sont retenues sous flux à la surface de la P-sélectine et qu'elles s'accumulent en masse sur les bords des agrégats plaquettaires activés. Lors du passage des nanoparticules sur les agrégats plaquettaires, une prise de contraste progressive, corrélée à l'accumulation des nanoparticules sur les plaquettes, est visualisée en temps réel. Cette prise de contraste est fonction du nombre de nanoparticules qui se lient aux agrégats plaquettaires. La résolution de la microscopie à fluorescence étant limitée à environ 1 μm , le nombre de nanoparticules doit être conséquent avant de générer un signal détectable. Dans cette étude, les nanoparticules-fucoïdane sont comparées à des nanoparticules contrôles présentant du dextrane carboxyméthylé et qui ont donc un potentiel zêta proche : -4,9 mV pour les nanoparticules-fucoïdane et -2,5 mV pour les nanoparticules contrôles. L'utilisation de ces nanoparticules contrôles est d'autant plus justifiée qu'à l'échelle nanométrique, la surface spécifique d'interaction est très importante et la charge de surface a un rôle clé dans les interactions des nanoparticules avec leur environnement [193]. Les résultats valident donc bien l'effet du fucoïdane sur les interactions des nanoparticules avec la P-sélectine et avec les plaquettes activées. Cependant, le test en flux sur P-sélectine est limité aux agglomérats de nanoparticules qui se forment à la surface du revêtement, du fait de la résolution du microscope. Cette méthode n'est donc pas adaptée pour évaluer l'interaction d'une nanoparticule individuelle avec le biomarqueur. Des mesures complémentaires de l'affinité d'une nanoparticule avec la P-sélectine pourraient par exemple être obtenues par résonance plasmonique de surface [135]. En conclusion, du fucoïdane avait déjà été chargé avec succès par RREP [194], mais cette étude démontre pour la première fois que cette méthode de synthèse de nanoparticules copolymères permet au fucoïdane de conserver sa fonction de ciblage. Cette observation est en accord avec les études publiées sur des

nanoparticules copolymères fonctionnalisées avec d'autres polysaccharides [189, 190, 195]. De ce fait, ces nanoparticules se placent comme des vecteurs potentiels pour la thrombose.

Pour finir, nous avons réalisé des tests préliminaires en injectant les nanogels polysaccharides développés dans le **projet expérimental 3** dans les microcanaux utilisés pour le test d'adhésion afin de contrôler dans un premier temps les interactions non spécifiques de ces nanogels pour le matériau. Les premiers essais sur canaux non recouverts montrent une interaction non spécifique relativement élevée des nanogels avec le matériau. Le protocole devra donc être adapté pour évaluer spécifiquement l'interaction nanogel/P-sélectine. L'interaction pour la P-sélectine d'un autre système chargé en fucoïdane, non décrit dans ce manuscrit, a également été évaluée. Ainsi, dans le cadre d'une collaboration avec l'unité mixte *UTCBS* de l'université Paris Descartes, des microbulles lipidiques chargées positivement ont été fonctionnalisées avec du fucoïdane par interaction électrostatique. Ces microbulles sont stables une fois chargées avec le polysaccharide anionique. Néanmoins aucune adhésion des microbulles-fucoïdane n'est observée sur la P-sélectine. Ce résultat soutient l'hypothèse que les groupements impliqués dans l'interaction du fucoïdane avec la P-sélectine ne sont pas disponibles dans cette configuration, du fait de leur interaction électrostatique avec les groupements positifs des lipides. En conclusion, ce test d'adhésion a été développé comme un indicateur de la capacité du fucoïdane chargé à la surface de vecteurs à lier efficacement sa cible. Il a été conçu comme un test de routine pour évaluer différents types de vecteurs et est plus proche des contraintes physiologiques que les tests d'adhésion standards où le vecteur est simplement incubé avec ses cellules cibles [171, 173]. Il a validé que les microcapsules et les nanoparticules copolymères formulées avec du fucoïdane interagissent fortement avec la P-sélectine et sont capables de s'accumuler sur des agrégats plaquettaires activés. Ces résultats confirment l'efficacité et la sélectivité du fucoïdane comme agent de ciblage de la P-sélectine et soulignent le potentiel de ces particules comme vecteurs.

Vectorisation du rt-PA et perspectives pour la thrombolyse

Dans le **projet expérimental 2**, nous avons mis en place une nouvelle stratégie pour promouvoir l'accumulation spécifique et améliorer l'efficacité locale du rt-PA à l'aide de nanoparticules copolymères. Comme détaillé dans le paragraphe précédent, nous avons d'abord validé que le fucoïdane chargé dans la couronne de polysaccharides permet d'augmenter l'affinité des nanoparticules pour la P-sélectine et les plaquettes activées. Cette étude a ensuite porté sur l'évaluation de ces nanoparticules, chargées en rt-PA, dans un modèle *in vivo* de thrombose veineuse. Dans le modèle préclinique utilisé, les traitements sont injectés pendant la phase de croissance du thrombus, en moyenne 7 minutes après l'induction (**Figure 22**). Leurs effets sur le recrutement plaquettaire et la stabilisation du thrombus sont suivis en temps réel par microscopie intravittale. Lors de l'injection de rt-PA associé aux nanoparticules-fucoïdane, une réduction significative de la densité plaquettaire est observée à 30 minutes. Un effet similaire n'est pas observé avec l'actif seul suggérant que sa vectorisation améliore effectivement son efficacité thrombolytique. Cet effet n'est pas non plus observé avec les nanoparticules non chargées en fucoïdane, confirmant que la présence de fucoïdane potentialise l'action du rt-PA *in vivo*. À notre connaissance, aucun système n'avait été développé contre la P-sélectine pour la thrombolyse ciblée. Cette expérience valide ainsi la stratégie de ciblage de la P-sélecine par le fucoïdane. La dose de rt-PA vectorisé est relativement élevée par rapport aux systèmes décrits dans la littérature, qui sont en moyenne injectés à une dose 2,5 à 10 fois plus faible [167, 171, 173, 177, 178] (voir **Tableau 4**). Toutefois, l'induction du thrombus au FeCl₃ mise en place dans notre étude favorise la formation d'un thrombus dense en plaquettes et soumis à une activation endothéliale permanente qui favorise un recrutement plaquettaire continu [140, 196]. L'efficacité de ces systèmes sur un thrombus plus fibrineux que plaquettaire, donc plus "facile" à lyser avec un actif fibrinolytique comme le rt-PA, complèterait cette étude préclinique [197]. Aussi, pour quantifier plus directement l'action fibrinolytique, il serait possible de marquer le réseau de fibrine en pré-injectant du fibrinogène fluorescent pour avoir une évaluation directe et plus précise de la fibrinolyse [198]. De plus, nous avons formé le thrombus *in vivo*, alors que la plupart de ces études insèrent des thrombi formés *in vitro* à partir de sang total humain,

sur lequel le rt-PA est plus réactif [141]. Ce projet fournit donc la preuve de concept pour le ciblage de la P-sélectine par le fucoïdane pour favoriser l'efficacité du rt-PA. D'autres modèles, et notamment des modèles artériels, devront être mis en place pour se rapprocher des conditions cliniques et définir l'efficacité de ces vecteurs sur différents types de thrombi. Les perspectives pour développer une stratégie plus efficace et plus sûre sur la base de ces nanovecteurs prometteurs sont maintenant discutées.

Tout d'abord, la méthode de chargement de l'actif thrombolytique décrite dans le **projet expérimental 2** est évaluée. L'hypothèse faite dans cette étude est que l'adsorption favorise la conservation à court terme de l'activité fibrinolytique du rt-PA. Cette hypothèse est validée *in vitro* par la conservation de l'activité fibrinolytique et *in vivo* par la démonstration de l'efficacité thrombolytique. Pour optimiser le chargement par adsorption, nous avions en amont réalisé une étude préliminaire en mettant en contact le rt-PA sous sa forme Actilyse® avec différentes compositions de nanoparticules, dans les mêmes conditions que celles décrites dans le **projet 2**. Les résultats du **Tableau 6** montrent que la présence de groupements NH₂ semble améliorer la rétention de l'actif dans la suspension de nanoparticules, probablement en mimant l'action de l'arginine, excipient utilisé dans la formulation de l'Actilyse®. Cette étude pourra être complétée en quantifiant la quantité de protéine retenue et non l'activité amidolytique retenue, qui peut être modifiée au contact de la nanoparticule et est donc un moins bon indicateur du taux effectif de rétention de la protéine. D'autres groupements, comme la lysine, pourraient être avantageux pour favoriser la rétention du rt-PA sans modifier son activité [199].

Composition en polysaccharides	Potentiel zêta (mV)	Rétention (%activité amidolytique introduite)
90% Dextran-COOH 10% Fucoïdane	-34,1 ± 0,7	9%
90% Dextrane 10% Fucoïdane	-18,5 ± 0,2	20%
50% Dextrane 40% Dextrane-NH ₂ 10% Fucoïdane	-12,5 ± 0,6	26 ± 2%
50% Dextrane 50% Dextrane-DEAE	+ 39,0 ± 0,4	12%

Tableau 6. Rétention de l'activité amidolytique du rt-PA au contact de différentes compositions de nanoparticules copolymères.
Étude préliminaire.

Charger l'actif par adsorption présente toutefois un risque de désorption incontrôlée. Dans les études présentées dans la **section 3.2** de l'état de l'art et résumées dans le **Tableau 4**, l'actif thrombolytique est soit greffé de manière covalente sur la nanoparticule, soit encapsulé en son sein. Un lien covalent permet effectivement de s'assurer que le rt-PA chargé reste immobilisé sur la nanoparticule *in vivo* pour éviter son relargage incontrôlé. Une étude menée par une autre équipe du consortium *NanoAthero* a de plus démontré que le greffage covalent permet de conserver l'activité amidolytique du rt-PA dans le temps par rapport à l'adsorption [179]. Toutefois, cette étude démontre également que l'activité fibrinolytique mesurée par la méthode du gel d'agar est réduite lorsque le rt-PA est greffé par rapport à lorsque cet actif est simplement adsorbé, probablement parce que le rt-PA greffé n'est plus capable de diffuser dans le réseau de fibrine. Un chargement par adsorption aurait donc l'avantage de permettre au rt-PA de diffuser localement dans le thrombus. Aussi, plusieurs études ont montré *in vivo* sur différents vecteurs que les systèmes ciblés contre le thrombus ont tendance à adhérer aux bords des thrombi sans s'y infiltrer [171, 182, 200]. Cette observation est liée au fait que le flux à l'intérieur du thrombus est quasi nul. Une adsorption de l'actif est donc favorable pour lui permettre d'agir dans le thrombus une fois que les vecteurs se sont accumulés en surface. Dans le modèle d'adhésion *in vitro* en flux, nous avons également observé que les nanoparticules copolymères s'accumulent en masse sur les bords des agrégats mais qu'il n'y a pas de prise de contraste au sein de l'agrégat. Pour compléter l'étude et valider ce mécanisme avec nos vecteurs, deux expériences complémentaires vont être menées. Dans un premier temps, l'adhésion des nanoparticules-fucoïdane chargées en rt-PA sera évaluée en flux sur les agrégats. Dans un second temps, les nanoparticules-fucoïdane ou les nanoparticules contrôles fluorescentes seront injectées *in vivo* dans le modèle préclinique décrit et la prise de contraste en fluorescence sur le thrombus sera enregistrée. Une étude préliminaire a été menée avec les mêmes paramètres d'injection que ceux utilisés dans le **projet 2**, et les nanoparticules n'étaient pas suffisamment concentrées pour qu'une prise de contraste puisse être détectée sur le thrombus par microscopie intravitaire. Ces expériences doivent donc être optimisées. Un chargement par adsorption est donc intéressant pour garder l'activité du rt-PA au contact

du réseau de fibrine du thrombus. Les interactions nanoparticules-rt-PA peuvent être optimisées pour mieux maîtriser la rétention de l'actif au contact des nanoparticules.

Le second aspect à discuter avant d'envisager une application clinique est l'effet de ces nanovecteurs chargés en rt-PA sur les risques hémorragiques associés à cet actif (voir **section 1.5.2.b** de l'état de l'art). Étant donné que les HIS constituent le risque le plus grave, un système validé pour son efficacité doit par la suite être testé dans des modèles précliniques plus complexes d'ischémie cérébrale où des hémorragies intracrâniennes ont été observées. La majorité des études citées en **section 3.2**, ainsi que celle présentée dans ce manuscrit, n'évaluent pas ces risques. Quelques études ont mesuré le taux de fibrinogène plasmatique [158, 159, 173] et/ou quantifié la durée de saignement après induction d'une blessure à la queue ou au point d'injection [158, 159, 169]. Avec une stratégie d'adsorption, l'actif sous sa forme libre va s'accumuler en masse au niveau du thrombus. C'est effectivement ce qui est recherché pour augmenter l'efficacité, mais une telle approche peut favoriser les effets secondaires locaux du rt-PA : neurotoxicité et risque accru d'HIS. Ainsi, des études cliniques menées avec délivrance du rt-PA en intra-artériel, donc localement, ont globalement montré une amélioration du taux de recanalisation mais également une augmentation du taux d'HIS [84]. De plus, du polysorbate (Tween) est utilisé dans la formulation de l'Actilyse® et a été utilisé dans la formulation du complexe nanoparticule-rt-PA. Or, plusieurs études ont montré que le polysorbate favorisait l'extravasation des nanoparticules par la BHE [201-203]. Des études supplémentaires sont donc nécessaires pour évaluer les interactions nanoparticules-BHE.

En conclusion, cette étude démontre le potentiel de l'adsorption d'un thrombolytique à la surface de nanoparticules copolymères fonctionnalisées avec du fucoïdane. D'autres modèles précliniques seront mis en place pour confirmer ce potentiel et évaluer les effets secondaires associés. Le rt-PA a été choisi parce qu'il est l'actif de référence. La stratégie développée dans ce manuscrit alliée à un actif non toxique, comme le desmoteplase ou des formes modifiées du rt-PA, serait grandement prometteuse (voir **section 1.5.3.a**). D'autres pistes reposant sur la vectorisation d'actifs présentant des modes d'action thérapeutique différents sont également à explorer pour améliorer la prise

en charge des évènements thrombotiques. Des actifs qui inhibent des récepteurs engagés dans le recrutement plaquettaire et la formation d'un thrombus stable (**Figure 3**), comme la GPVI, pourraient être choisis [204]. Il serait également très intéressant d'étudier l'effet de la co-vectorisation d'actifs thrombolytiques et neuroprotecteurs, comme des antioxydants, dans des modèles d'ischémie [87]. La nanomédecine tient justement sa force dans le fait de pouvoir combiner plusieurs actifs au sein d'un même vecteur, par rapport aux stratégies où le ligand est directement combiné à l'actif (voir **sections 1.4.2.b** et **1.5.3.a**). Pour finir, les nanoparticules copolymères développées dans ce projet ont pu être chargées avec un actif hydrophobe fluorescent pour les rendre détectables par microscopie à fluorescence. D'autres agents de contraste pourraient être incorporés dans le cœur hydrophobe de la nanoparticule afin de créer des outils d'imagerie moléculaire pour les techniques implantées en clinique, comme la CT ou l'IRM (voir **section 1.4**). Entre autres, des essais préliminaires ont été menés pour incorporer un composé iodé et obtenir un système fonctionnel pour l'imagerie CT, modalité standard pour la prise en charge des AVC ischémiques [41].

Évaluation des nanovecteurs

Les trois études présentées dans ce manuscrit justifient le développement de vecteurs pour une prise en charge plus efficace des évènements thrombotiques. Deux types de nanovecteurs polymères ont été synthétisés : des nanoparticules copolymères polysaccharides-PIBCA et des nanogels polysaccharides. Une translation vers la clinique nécessite de s'interroger sur les deux points suivants : i) le mode de synthèse des nanovecteurs et les caractéristiques physico-chimiques qui en résultent, doivent être bien définis et facilement implantables à grande échelle, et ii) le comportement des nanovecteurs au contact de l'organisme doit leur permettre d'être injectés en IV sans générer de toxicité et en garantissant leur élimination.

Dans un premier temps, les caractéristiques physico-chimiques des nanovecteurs sont discutées. Les nanoparticules copolymères ont été choisies pour la thrombolyse du fait de leur structure bien définie, de leur couronne de polysaccharides et de leur potentiel

à charger des protéines (voir **section 4.3.1** de l'état de l'art). Les nanoparticules copolymères synthétisées dans le **projet expérimental 2** présentent un indice de polydispersité légèrement plus élevé que les nanoparticules copolymères synthétisées par RREP présentées dans la littérature [205]. Cette polydispersité provient de la méthode d'incorporation du fluorophore dans le cœur hydrophobe de la nanoparticule. Le fluorophore est d'abord dilué dans de l'acétone, puis ce solvant est ajouté au milieu réactionnel au cours de la synthèse [194]. Nous avons observé par DLS que les nanoparticules ainsi obtenues sont plus petites et présentent un indice de polydispersité supérieur à des nanoparticules synthétisées avec les mêmes polymères mais sans l'ajout d'acétone (non présenté dans le **projet 2**). Ces observations sont indépendantes du fluorophore utilisé. En remplaçant notamment l'acétone par de l'éthanol, nous avons depuis pu obtenir des nanoparticules fluorescentes qui conservent les mêmes propriétés physico-chimiques que les nanoparticules classiques formulées sans solvant organique. Des nanoparticules fluorescentes synthétisées par cette méthode, donc formées de populations très homogènes, sont désormais à privilégier pour la suite des travaux. En parallèle, un nouveau procédé qui s'inspire des méthodes standards de formulation de nanoparticules polymères a été mis au point pour former des particules à partir de fucoïdane, de dextrane et de pullulane. La méthode est détaillée dans le **projet expérimental 3**. Elle a été développée dans le but de s'affranchir des contraintes liées à l'utilisation d'huile pour la formulation de microparticules faites à partir de ces mêmes polysaccharides et ainsi de diminuer la taille et la polydispersité des particules obtenues [153, 154]. Cette méthode permet de synthétiser des populations homogènes et reproductibles. Les deux méthodes de synthèse de nanovecteurs sont totalement indépendantes de l'expérimentateur, rapides et peuvent donc être facilement transposables à plus grande échelle.

Dans un second temps, le comportement de ces nanovecteurs au contact des cellules a été observé. La cytocompatibilité de nanoparticules copolymères polysaccharide-PIBCA a ainsi été évaluée dans le cadre d'un travail commun réalisé au sein du consortium *NanoAthero*. Dans cette étude, des nanoparticules copolymères sont synthétisées avec deux revêtements différents de polysaccharides :

- PM-NP1 : 90% carboxyméthyle-dextrane / 10% fucoïdane. Elles présentent un potentiel zêta de - 51 mV,
- PM-NP2 : 80% dextrane / 10% diéthylaminoéthyle-dextrane / 10% fucoïdane. Elles présentent un potentiel zêta de + 3 mV.

Ces nanoparticules sont incubées à différentes concentrations avec des cellules endothéliales (Human Umbilical Vein Endothelial Cells) pour évaluer leur effet sur la viabilité cellulaire. Les nanoparticules montrent un effet délétère à partir d'une concentration de 50 µg/mL pour les PM-NP1 et de 100 µg/mL pour les PM-NP2 dès 24 heures d'incubation. Ce travail a donné lieu à une publication jointe en **Annexe B**. Il donne des indications sur la cytotoxicité des nanoparticules utilisées dans le **projet expérimental 2**. De part leur composition en polysaccharides, celles-ci sont plus similaires aux PM-NP2. Dans le modèle préclinique, elles ont été injectées à une concentration initiale dans la circulation de l'ordre de 50 µg/mL. Cette valeur est donc dans une gamme de compatibilité acceptable mais des expériences de biocompatibilité sur ces nanoparticules en particulier seront mises en place pour confirmer cette hypothèse. Dans le cadre de la mise au point de vecteurs pour le domaine cardiovasculaire, des systèmes entièrement biocompatibles sont toutefois à privilégier et les résultats de l'**Annexe B** ont été un moteur pour développer les nanogels polysaccharides. Un test de viabilité sur cellules endothéliales primaires (HCAEC) a montré que ce type de nanovecteur n'induit pas d'effets délétères à 24 heures à une concentration élevée de 400 µg/mL. L'utilisation de Triton X100 dans la synthèse peut toutefois être un frein au développement de cette technique, bien qu'il soit éliminé par des cycles de dialyse. Des essais sans Triton X100 ont donné des synthèses moins reproductibles, mais ont tout de même permis la formulation de suspensions colloïdales. Les paramètres de synthèse sont donc encore en cours d'optimisation pour s'affranchir de ce surfactant.

En conclusion, deux types de nanovecteurs ont été formulés. Ces deux structures se distinguent par leurs propriétés physico-chimiques : rigidité, configuration des polysaccharides à la surface et hydrophilicité. Les deux méthodes de synthèse permettent d'obtenir de façon simple et rapide des nanovecteurs fonctionnels. Ces nanovecteurs

peuvent potentiellement être synthétisés avec différents polysaccharides, ce qui permet de moduler leurs fonctions. Tous deux peuvent être envisagés pour une injection IV à faible concentration (50 µg/mL), mais les nanogels sont supérieurs aux nanoparticules copolymères polysaccharides-PIBCA en termes de biocompatibilité. La biodistribution de ces deux nanovecteurs sera évaluée par TEMP sur des animaux sains dans la suite du projet après marquage des nanoparticules au ^{99m}Tc [206]. Leur biodégradabilité sera également un élément décisif pour évaluer leur potentiel clinique.

Conclusion générale

La thrombose est le point culminant du développement de plaques d'athérosclérose vulnérables. Elle est à l'origine d'évènements cliniques aigus, comme les AVC ischémiques, qui sont associés à un fort taux de mortalité. La prise en charge clinique de ces évènements reste un problème actuel majeur. D'une part, le traitement standard par injection IV de rt-PA présente une efficacité limitée et est associé à des risques hémorragiques élevés. D'autre part, les méthodes d'imagerie disponibles actuellement ne permettent pas de quantifier avec certitude le bénéfice qu'engendrerait l'injection de rt-PA par rapport aux risques encourus.

La compréhension des mécanismes moléculaires impliqués dans la formation d'un thrombus offre de nouvelles perspectives pour améliorer l'imagerie et le traitement de la thrombose. La mise en place d'une médecine personnalisée passe par le développement d'une médecine "moléculaire". Idéalement, l'état moléculaire de la pathologie est mis en évidence par l'expression de biomarqueurs connus, puis le traitement est délivré de façon ciblée et contrôlée.

La nanomédecine est un domaine de recherche prometteur pour le développement d'approches moléculaires. Ce projet de recherche s'est spécifiquement focalisé sur une molécule fortement exprimée dans le thrombus, la P-sélectine, et a permis la formulation de vecteurs polymères capables de se lier à cette cible moléculaire. Le fucoïdane, polysaccharide naturel extrait d'algues brunes, a été utilisé pour promouvoir ce ciblage.

Trois types de vecteurs polymères fonctionnalisés avec du fucoïdane ont été présentés dans ce travail : des microcapsules copolymères, des nanoparticules copolymères et des nanogels polysaccharides. Ils ont été chargés en agents de contraste (PFOB et ^{99m}Tc) ou en rt-PA, et ont le potentiel d'incorporer d'autres actifs.

D'autres vecteurs présentant du fucoïdane ont déjà démontré leur efficacité pour l'imagerie moléculaire *in vivo* de pathologies surexprimant la P-sélectine. Dans ce projet, des nanoparticules copolymères composées d'une couronne de polysaccharides renfermant du fucoïdane ont été chargées avec du rt-PA à des fins thérapeutiques. À notre connaissance, ces nanoparticules sont les premiers vecteurs à augmenter l'efficacité thrombolytique du rt-PA en ciblant la P-sélectine. Ce travail de thèse valide ainsi que : i) la P-sélectine est une cible d'intérêt dans les stratégies moléculaires développées pour améliorer le traitement de la thrombose, ii) ce ciblage peut être réalisé par le fucoïdane. Ce projet a également abordé les problématiques liées au développement clinique des nanoparticules en s'interrogeant sur les matériaux les plus adaptés pour le domaine cardiovasculaire. Une nouvelle méthode de synthèse de nanoparticules formées uniquement de polysaccharides biocompatibles et biodégradables est proposée.

La conception de vecteurs sûrs et efficaces se situe à la croisée de plusieurs domaines : de la physico-chimie à l'évaluation biologique *in vitro* et *in vivo* des matériaux. Alliée au développement de nouveaux agents thérapeutiques et aux progrès effectués dans le domaine de l'imagerie médicale, la nanomédecine peut prendre une place importante dans la médecine de demain.

Bibliographie

1. OMS www.who.int/mediacentre/factsheets/fs317/fr/. [cited.
2. Jackson, S.P., *Arterial thrombosis-insidious, unpredictable and deadly*. Nature Medicine, 2011. **17**(11): p. 1423-1436.
3. Michel, J.B., et al., *Novel aspects of the pathogenesis of aneurysms of the abdominal aorta in humans*. Cardiovascular Research, 2011. **90**(1): p. 18-27.
4. Lusis, A.J., *Atherosclerosis*. Nature, 2000. **407**(6801): p. 233-41.
5. Ross, R., *Mechanisms of disease - Atherosclerosis - An inflammatory disease*. New England Journal of Medicine, 1999. **340**(2): p. 115-126.
6. Davies, M.J., *Stability and instability: Two faces of coronary atherosclerosis - The Paul Dudley White Lecture 1995*. Circulation, 1996. **94**(8): p. 2013-2020.
7. Bentzon, J.F., et al., *Mechanisms of Plaque Formation and Rupture*. Circulation Research, 2014. **114**(12): p. 1852-1866.
8. Falk, E., et al., *Update on acute coronary syndromes: the pathologists view*. European Heart Journal, 2013. **34**(10): p. 719-+.
9. Libby, P., P.M. Ridker, and G.K. Hansson, *Progress and challenges in translating the biology of atherosclerosis*. Nature, 2011. **473**(7347): p. 317-325.
10. Libby, P. and P. Theroux, *Pathophysiology of coronary artery disease*. Circulation, 2005. **111**(25): p. 3481-3488.
11. Davies, M.J., et al., *Risk of thrombosis in human atherosclerotic plaques - Role of extracellular lipid, macrophage, and smooth-muscle cell content*. British Heart Journal, 1993. **69**(5): p. 377-381.
12. Wang, J.L., et al., *Vascular Smooth Muscle Cell Senescence Promotes Atherosclerosis and Features of Plaque Vulnerability*. Circulation, 2015. **132**(20): p. 1909-1919.
13. Libby, P., M. DiCarli, and R. Weissleder, *The vascular biology of atherosclerosis and imaging targets*. Journal of Nuclear Medicine, 2010. **51 Suppl 1**: p. 33S-37S.
14. Michel, J.B., et al., *Pathology of human plaque vulnerability: Mechanisms and consequences of intraplaque haemorrhages*. Atherosclerosis, 2014. **234**(2): p. 311-319.
15. Clarke, M.C.H., et al., *Chronic apoptosis of vascular smooth muscle cells accelerates atherosclerosis and promotes calcification and medial degeneration*. Circulation Research, 2008. **102**(12): p. 1529-1538.

16. Libby, P., *Collagenases and cracks in the plaque*. Journal of Clinical Investigation, 2013. **123**(8): p. 3201-3203.
17. Libby, P., *The molecular mechanisms of the thrombotic complications of atherosclerosis*. J Intern Med, 2008. **263**(5): p. 517-27.
18. Lippi, G., M. Franchini, and G. Targher, *Arterial thrombus formation in cardiovascular disease*. Nature Reviews Cardiology, 2011. **8**(9): p. 502-512.
19. Kumar, A. and C.P. Cannon, *Acute Coronary Syndromes: Diagnosis and Management, Part I*. Mayo Clinic Proceedings, 2009. **84**(10): p. 917-938.
20. Burke, A.P., et al., *Healed plaque ruptures and sudden coronary death - Evidence that subclinical rupture has a role in plaque progression*. Circulation, 2001. **103**(7): p. 934-940.
21. Rittersma, S.Z.H., et al., *Plaque instability frequently occurs days or weeks before occlusive coronary thrombosis - A pathological thrombectomy study in primary percutaneous coronary intervention*. Circulation, 2005. **111**(9): p. 1160-1165.
22. Kramer, M.C.A., et al., *Relationship of Thrombus Healing to Underlying Plaque Morphology in Sudden Coronary Death*. Journal of the American College of Cardiology, 2010. **55**(2): p. 122-132.
23. Bassand, J.P. and C. Hamm, *Guidelines for the diagnosis and treatment of non-ST-segment elevation acute coronary syndromes: The task force for the diagnosis and treatment of non-ST-segment elevation acute coronary syndromes of the European Society of Cardiology: reply*. European Heart Journal, 2008. **29**(2): p. 278-279.
24. Aggarwal, S., et al., *Abdominal aortic aneurysm: A comprehensive review*. Experimental & Clinical Cardiology, 2011. **16**(1): p. 11-15.
25. Kent, K.C., *Abdominal Aortic Aneurysms*. New England Journal of Medicine, 2014. **371**(22): p. 2101-2108.
26. Klink, A., et al., *Diagnostic and therapeutic strategies for small abdominal aortic aneurysms*. Nature Reviews. Cardiology, 2011. **8**(6): p. 338-47.
27. Huang, Y., et al., *High Structural Stress and Presence of Intraluminal Thrombus Predict Abdominal Aortic Aneurysm F-18-FDG Uptake Insights From Biomechanics*. Circulation-Cardiovascular Imaging, 2016. **9**(11).
28. Kazi, M., et al., *Influence of intraluminal thrombus on structural and cellular composition of abdominal aortic aneurysm wall*. Journal of Vascular Surgery, 2003. **38**(6): p. 1283-1292.
29. Martufi, G., et al., *Local Diameter, Wall Stress, and Thrombus Thickness Influence the Local Growth of Abdominal Aortic Aneurysms*. Journal of Endovascular Therapy, 2016. **23**(6): p. 957-966.
30. Denis, C. and P. Frenette, *Plaquette et endothélium: un mariage de raison*. 2001, Médecine Sciences (French). p. 252-255.
31. Loscalzo, J., *Nitric oxide insufficiency, platelet activation, and arterial thrombosis*. Circulation Research, 2001. **88**(8): p. 756-762.
32. Aird, W.C., *Spatial and temporal dynamics of the endothelium*. Journal of Thrombosis and Haemostasis, 2005. **3**(7): p. 1392-1406.
33. Gimbrone, M.A. and G. Garcia-Cardena, *Endothelial Cell Dysfunction and the Pathobiology of Atherosclerosis*. Circulation Research, 2016. **118**(4): p. 620-636.
34. McEver, R.P., *Adhesive interactions of leukocytes, platelets, and the vessel wall during hemostasis and inflammation*. Thrombosis and Haemostasis, 2001. **86**(3): p. 746-756.
35. Gibbins, J.M., *Platelet adhesion signalling and the regulation of thrombus formation*. Journal of Cell Science, 2004. **117**(16): p. 3415-3425.

36. Furie, B. and B.C. Furie, *Mechanisms of disease: Mechanisms of thrombus formation*. New England Journal of Medicine, 2008. **359**(9): p. 938-949.
37. Merten, M. and P. Thiagarajan, *P-selectin expression on platelets determines size and stability of platelet aggregates*. Circulation, 2000. **102**(16): p. 1931-1936.
38. Furie, B. and B.C. Furie, *Role of platelet P-selectin and microparticle PSGL-1 in thrombus formation*. Trends in Molecular Medicine, 2004. **10**(4): p. 171-178.
39. Silvain, J., et al., *Composition of Coronary Thrombus in Acute Myocardial Infarction*. Journal of the American College of Cardiology, 2011. **57**(12): p. 1359-1367.
40. Mizuno, K., et al., *Angioscopic evaluation of coronary-artery thrombi in acute coronary syndromes*. New England Journal of Medicine, 1992. **326**(5): p. 287-291.
41. Birenbaum, D., L.W. Bancroft, and G.J. Felsberg, *Imaging in Acute Stroke*. 2011, Western Journal of Emergency Medicine. p. 67-76.
42. Tansy, A.P. and D.S. Liebeskind, *Imaging Acute Ischemic Stroke: Mapping Present and Future Clinical Practice*. Current Atherosclerosis Reports, 2015. **17**(9).
43. Fayad, Z.A. and V. Fuster, *Clinical imaging of the high-risk or vulnerable atherosclerotic plaque*. Circulation Research, 2001. **89**(4): p. 305-316.
44. Huang, P.Y., et al., *Clinical applications of susceptibility weighted imaging in patients with major stroke*. Journal of Neurology, 2012. **259**(7): p. 1426-1432.
45. Ezzeddine, M.A., et al., *CT angiography with whole brain perfused blood volume imaging - Added clinical value in the assessment of acute stroke*. Stroke, 2002. **33**(4): p. 959-966.
46. Ois, A., et al., *High Risk of Early Neurological Recurrence in Symptomatic Carotid Stenosis*. Stroke, 2009. **40**(8): p. 2727-2731.
47. Purroy, F., et al., *Patterns and predictors of early risk of recurrence after transient ischemic attack with respect to etiologic subtypes*. Stroke, 2007. **38**(12): p. 3225-3229.
48. Riedel, C.H., et al., *The Importance of Size Successful Recanalization by Intravenous Thrombolysis in Acute Anterior Stroke Depends on Thrombus Length*. Stroke, 2011. **42**(6): p. 1775-1777.
49. Molina, C.A., et al., *Differential pattern of tissue plasminogen activator-induced proximal middle cerebral artery recanalization among stroke subtypes*. Stroke, 2004. **35**(2): p. 486-490.
50. Kim, J., et al., *Direct Thrombus Imaging in Stroke*. Journal of Stroke, 2016. **18**(3): p. 286-296.
51. Blasi, F., et al., *Multisite Thrombus Imaging and Fibrin Content Estimation With a Single Whole-Body PET Scan in Rats*. Arteriosclerosis Thrombosis and Vascular Biology, 2015. **35**(10): p. 2114-2121.
52. Weisstanner, C., et al., *Thrombus imaging in acute stroke: correlation of thrombus length on susceptibility-weighted imaging with endovascular reperfusion success*. European Radiology, 2014. **24**(8): p. 1735-1741.
53. Naggara, O., et al., *T2*"Susceptibility Vessel Sign" Demonstrates Clot Location and Length in Acute Ischemic Stroke*. Plos One, 2013. **8**(10).
54. Chu, B.C., et al., *Hemorrhage in the atherosclerotic carotid plaque: A high-resolution MRI study*. Stroke, 2004. **35**(5): p. 1079-1084.
55. Saam, T., et al., *Comparison of symptomatic and asymptomatic atherosclerotic carotid plaque features with in vivo MR imaging*. Radiology, 2006. **240**(2): p. 464-472.
56. Fuster, V., F. Lois, and M. Franco, *Early identification of atherosclerotic disease by noninvasive imaging*. Nature Reviews Cardiology, 2010. **7**(6): p. 327-333.
57. Tarkin, J.M., et al., *Imaging Atherosclerosis*. Circulation Research, 2016. **118**(4): p. 750-769.

58. Tarkin, J.M., F.R. Joshi, and J.H. Rudd, *PET imaging of inflammation in atherosclerosis*. Nature Reviews. Cardiology, 2014. **11**(8): p. 443-57.
59. Tahara, N., et al., *Simvastatin attenuates plaque inflammation: evaluation by fluorodeoxyglucose positron emission tomography*. J Am Coll Cardiol, 2006. **48**(9): p. 1825-31.
60. Taillefer, R., et al., *Acute thromboscintigraphy with Tc-99m-apcitide: Results of the phase 3 multicenter clinical trial comparing Tc-99m-apcitide scintigraphy with contrast venography for imaging acute DVT*. Journal of Nuclear Medicine, 2000. **41**(7): p. 1214-1223.
61. *Assessment of radiolabeled rhAnnexin V-128 in infective endocarditis (AnnIE)* www.clinicaltrials.gov/ct2/show/NCT02459613. 2015 [cited].
62. Rouzet, F., et al., *Radiolabeled Fucoidan as a P-Selectin Targeting Agent for In Vivo Imaging of Platelet-Rich Thrombus and Endothelial Activation*. Journal of Nuclear Medicine, 2011. **52**(9): p. 1433-1440.
63. Saboural, P., et al., *Purification of a low molecular weight fucoidan for SPECT molecular imaging of myocardial infarction*. Marine Drugs, 2014. **12**(9): p. 4851-67.
64. Rouzet, F., et al., *Molecular imaging of platelet activation in thrombus*. Journal of Nuclear Cardiology, 2009. **16**(2): p. 277-286.
65. Vymazal, J., et al., *Thrombus imaging with fibrin-specific gadolinium-based MR contrast agent EP-2104R: results of a phase II clinical study of feasibility*. Invest Radiol, 2009. **44**(11): p. 697-704.
66. Nahrendorf, M., et al., *Multimodality Cardiovascular Molecular Imaging, Part II*. Circulation-Cardiovascular Imaging, 2009. **2**(1): p. 56-70.
67. Spuentrup, E., et al., *MR imaging of thrombi using EP-2104R, a fibrin-specific contrast agent: initial results in patients*. European Radiology, 2008. **18**(9): p. 1995-2005.
68. Stacy, M.R., W. Zhou, and A.J. Sinusas, *Radiotracer imaging of peripheral vascular disease*. Journal of Nuclear Medicine, 2013. **54**(12): p. 2104-10.
69. Lippi, G., C. Mattiuzzi, and E.J. Favaloro, *Novel and Emerging Therapies: Thrombus-Targeted Fibrinolysis*. Seminars in Thrombosis and Hemostasis, 2013. **39**(1): p. 48-58.
70. Van de Craen, B., P.J. Declerck, and A. Gils, *The Biochemistry, Physiology and Pathological roles of PAI-1 and the requirements for PAI-1 inhibition in vivo*. Thrombosis Research, 2012. **130**(4): p. 576-585.
71. Murray, V., et al., *The molecular basis of thrombolysis and its clinical application in stroke*. Journal of Internal Medicine, 2010. **267**(2): p. 191-208.
72. Hoylaerts, M., et al., *Kinetics of the activation of plasminogen by human-tissue plasminogen-activator - Role of fibrin*. Journal of Biological Chemistry, 1982. **257**(6): p. 2912-2919.
73. Collen, D., *Fibrin-selective thrombolytic therapy for acute myocardial infarction*. Circulation, 1996. **93**(5): p. 857-865.
74. Collen, D. and H.R. Lijnen, *The Tissue-Type Plasminogen Activator Story*. Arteriosclerosis Thrombosis and Vascular Biology, 2009. **29**(8): p. 1151-1155.
75. Mueller, R.L. and S. Scheidt, *History of drugs for thrombotic disease - Discovery, development, and directions for the future*. Circulation, 1994. **89**(1): p. 432-449.
76. Collen, D. and H.R. Lijnen, *Tissue-type plasminogen activator: a historical perspective and personal account*. Journal of Thrombosis and Haemostasis, 2004. **2**(4): p. 541-546.
77. Topol, E., et al., *An international randomized trial comparing 4 thrombolytic strategies for acute myocardial infarction*. New England Journal of Medicine, 1993. **329**(10): p. 673-682.

78. Emberson, J., et al., *Effect of treatment delay, age, and stroke severity on the effects of intravenous thrombolysis with alteplase for acute ischaemic stroke: a meta-analysis of individual patient data from randomised trials*. Lancet, 2014. **384**(9958): p. 1929-1935.
79. Rha, J.H. and J.L. Saver, *The impact of recanalization on ischemic stroke outcome - A meta-analysis*. Stroke, 2007. **38**(3): p. 967-973.
80. Wardlaw, J.M., et al., *Recombinant tissue plasminogen activator for acute ischaemic stroke: an updated systematic review and meta-analysis*. Lancet, 2012. **379**(9834): p. 2364-2372.
81. Wardlaw, J.M., et al., *Thrombolysis for acute ischaemic stroke*. Cochrane Database of Systematic Reviews, 2014(7).
82. Whiteley, W.N., et al., *Risk of intracerebral haemorrhage with alteplase after acute ischaemic stroke: a secondary analysis of an individual patient data meta-analysis*. Lancet Neurology, 2016. **15**(9): p. 925-933.
83. Vivien, D., et al., *Impact of tissue plasminogen activator on the neurovascular unit: from clinical data to experimental evidence*. Journal of Cerebral Blood Flow and Metabolism, 2011. **31**(11): p. 2119-2134.
84. Alvarez-Sabin, J., et al., *Factors influencing haemorrhagic transformation in ischaemic stroke*. Lancet Neurology, 2013. **12**(7): p. 689-705.
85. Chevilly, A., et al., *Impacts of tissue-type plasminogen activator (tPA) on neuronal survival*. Frontiers in Cellular Neuroscience, 2015. **9**.
86. Wechsler, L.R., *Intravenous Thrombolytic Therapy for Acute Ischemic Stroke*. New England Journal of Medicine, 2011. **364**(22): p. 2138-2146.
87. Jaffer, H., et al., *Advances in stroke therapy*. Drug Delivery and Translational Research, 2011. **1**(6): p. 409-419.
88. Bhatia, R., et al., *Low Rates of Acute Recanalization With Intravenous Recombinant Tissue Plasminogen Activator in Ischemic Stroke Real-World Experience and a Call for Action*. Stroke, 2010. **41**(10): p. 2254-2258.
89. Karaszewski, B., et al., *What causes intracerebral bleeding after thrombolysis for acute ischaemic stroke? Recent insights into mechanisms and potential biomarkers*. Journal of Neurology Neurosurgery and Psychiatry, 2015. **86**(10): p. 1127-1136.
90. Nordt, T.K. and C. Bode, *Thrombolysis: Newer thrombolytic agents and their role in clinical medicine*. Heart, 2003. **89**(11): p. 1358-1362.
91. Hebert, M., et al., *The story of an exceptional serine protease, tissue-type plasminogen activator (tPA)*. Revue Neurologique, 2016. **172**(3): p. 186-197.
92. Bivard, A., L.T. Lin, and M.W. Parsons, *Review of Stroke Thrombolytics*. Journal of Stroke, 2013. **15**(2): p. 90-98.
93. Haley, E.C., et al., *Phase IIB/III Trial of Tenecteplase in Acute Ischemic Stroke Results of a Prematurely Terminated Randomized Clinical Trial*. Stroke, 2010. **41**(4): p. 707-711.
94. Runge, M.S., et al., *Enhanced thrombolytic and antithrombotic potency of a fibrin-targeted plasminogen activator in baboons*. Circulation, 1996. **94**(6): p. 1412-1422.
95. Runge, M.S., et al., *Antibody-enhanced thrombolysis - Targeting of tissue plasminogen-activator in vivo*. Proceedings of the National Academy of Sciences of the United States of America, 1987. **84**(21): p. 7659-7662.
96. Bode, C., et al., *Platelet-targeted fibrinolysis enhances clot lysis and inhibits platelet-aggregation*. Circulation, 1991. **84**(2): p. 805-813.
97. Liberatore, G.T., et al., *Vampire bat salivary plasminogen activator (desmoteplase) - A unique fibrinolytic enzyme that does not promote neurodegeneration*. Stroke, 2003. **34**(2): p. 537-543.

98. von Kummer, R., et al., *Desmoteplase 3 to 9 Hours After Major Artery Occlusion Stroke The DIAS-4 Trial (Efficacy and Safety Study of Desmoteplase to Treat Acute Ischemic Stroke)*. Stroke, 2016. **47**(12): p. 2880-2887.
99. Wahlgren, N., et al., *Mechanical thrombectomy in acute ischemic stroke: Consensus statement by ESO-Karolinska Stroke Update 2014/2015, supported by ESO, ESMINT, ESNR and EAN*. International Journal of Stroke, 2016. **11**(1): p. 134-147.
100. Rubiera, M. and A.V. Alexandrov, *Sonothrombolysis in the Management of Acute Ischemic Stroke*. American Journal of Cardiovascular Drugs, 2010. **10**(1): p. 5-10.
101. Molina, C.A., et al., *Transcranial ultrasound in clinical sonothrombolysis (TUCSON) trial*. Ann Neurol, 2009. **66**(1): p. 28-38.
102. Havel, H.A., *Where Are the Nanodrugs? An Industry Perspective on Development of Drug Products Containing Nanomaterials*. Aaps Journal, 2016. **18**(6): p. 1351-1353.
103. Mura, S. and P. Couvreur, *Nanotheranostics for personalized medicine*. Adv Drug Deliv Rev, 2012. **64**(13): p. 1394-416.
104. Cicha, I., C. Garlich, and C. Alexiou, *Cardiovascular therapy through nanotechnology - how far are we still from bedside?* Eur J Nanomed, 2014.
105. Gref, R., et al., *Biodegradable long-circulating polymeric nanospheres*. Science, 1994. **263**(5153): p. 1600-3.
106. Allen, T.M., et al., *Liposomes containing synthetic lipid derivatives of poly(ethylene glycol) show prolonged circulation half-lives in vivo*. Biochimica Et Biophysica Acta, 1991. **1066**(1): p. 29-36.
107. Mulder, W.J., et al., *Lipid-based nanoparticles for contrast-enhanced MRI and molecular imaging*. NMR in Biomedicine, 2006. **19**(1): p. 142-64.
108. Ruiz-Esparza, G.U., et al., *The physiology of cardiovascular disease and innovative liposomal platforms for therapy*. International Journal of Nanomedicine, 2013. **8**: p. 629-640.
109. Akbarzadeh, A., et al., *Liposome: classification, preparation, and applications*. Nanoscale Research Letters, 2013. **8**.
110. Tassa, C., S.Y. Shaw, and R. Weissleder, *Dextran-Coated Iron Oxide Nanoparticles: A Versatile Platform for Targeted Molecular Imaging, Molecular Diagnostics, and Therapy*. Accounts of Chemical Research, 2011. **44**(10): p. 842-852.
111. Kooi, M.E., et al., *Accumulation of ultrasmall superparamagnetic particles of iron oxide in human atherosclerotic plaques can be detected by in vivo magnetic resonance imaging*. Circulation, 2003. **107**(19): p. 2453-2458.
112. Richards, J.M., et al., *Abdominal aortic aneurysm growth predicted by uptake of ultrasmall superparamagnetic particles of iron oxide: a pilot study*. Circ Cardiovasc Imaging, 2011. **4**(3): p. 274-81.
113. De La Vega, J.C. and U.O. Hafeli, *Utilization of nanoparticles as X-ray contrast agents for diagnostic imaging applications*. Contrast Media Mol Imaging, 2014.
114. Connor, E.E., et al., *Gold nanoparticles are taken up by human cells but do not cause acute cytotoxicity*. Small, 2005. **1**(3): p. 325-327.
115. Giljohann, D.A., et al., *Gold Nanoparticles for Biology and Medicine*. Angewandte Chemie-International Edition, 2010. **49**(19): p. 3280-3294.
116. Rao, J.P. and K.E. Geckeler, *Polymer nanoparticles: Preparation techniques and size-control parameters*. Progress in Polymer Science, 2011. **36**(7): p. 887-913.
117. Danhier, F., et al., *PLGA-based nanoparticles: an overview of biomedical applications*. Journal of Controlled Release, 2012. **161**(2): p. 505-22.

118. Silva, A.K., D. Letourneur, and C. Chauvierre, *Polysaccharide nanosystems for future progress in cardiovascular pathologies*. Theranostics, 2014. **4**(6): p. 579-91.
119. Porter, T.R., *Improving the evaluation of left ventricular systolic function with intravenous perfluorocarbon ultrasound contrast: will suboptimal echocardiograms become an endangered species?* J Am Coll Cardiol, 2000. **35**(2): p. 491-2.
120. Diaz-Lopez, R., N. Tsapis, and E. Fattal, *Liquid perfluorocarbons as contrast agents for ultrasonography and (19)F-MRI*. Pharmaceutical Research, 2010. **27**(1): p. 1-16.
121. Wagner, C.L., et al., *Analysis of GPIIb/IIIa receptor number by quantification of 7E3 binding to human platelets*. Blood, 1996. **88**(3): p. 907-914.
122. Bennett, J.S., *Structure and function of the platelet integrin alpha(IIb)beta(3)*. Journal of Clinical Investigation, 2005. **115**(12): p. 3363-3369.
123. Ruoslahti, E., *RGD and other recognition sequences for integrins*. Annual Review of Cell and Developmental Biology, 1996. **12**: p. 697-715.
124. Coller, B.S., *alpha IIb3: structure and function*. Journal of Thrombosis and Haemostasis, 2015. **13**: p. S17-S25.
125. Zhou, Y., S. Chakraborty, and S. Liu, *Radiolabeled Cyclic RGD Peptides as Radiotracers for Imaging Tumors and Thrombosis by SPECT*. Theranostics, 2011. **1**: p. 58-82.
126. Wang, X., et al., *Novel single-chain antibody-targeted microbubbles for molecular ultrasound imaging of thrombosis: validation of a unique noninvasive method for rapid and sensitive detection of thrombi and monitoring of success or failure of thrombolysis in mice*. Circulation, 2012. **125**(25): p. 3117-26.
127. Blann, A.D., S.K. Nadar, and G.Y.H. Lip, *The adhesion molecule P-selectin and cardiovascular disease*. European Heart Journal, 2003. **24**(24): p. 2166-2179.
128. Vestweber, D. and J.E. Blanks, *Mechanisms that regulate the function of the selectins and their ligands*. Physiological Reviews, 1999. **79**(1): p. 181-213.
129. Ohmori, K., et al., *P- and E-selectins recognize sialyl 6-sulfo Lewis X, the recently identified L-selectin ligand*. Biochemical and Biophysical Research Communications, 2000. **278**(1): p. 90-96.
130. Kannagi, R. *Selectin mediated cell recognition and its structural basis* www.glycoforum.gr.jp/science/glycogenes/02/02E.html. 2002 [cited].
131. Stahli, B.E., et al., *Effects of the P-Selectin Antagonist Inclacumab on Myocardial Damage After Percutaneous Coronary Intervention According to Timing of Infusion: Insights From the SELECT-ACS Trial*. Journal of the American Heart Association, 2016. **5**(11).
132. Schmitt, C., et al., *First-in-man Study With Inclacumab, a Human Monoclonal Antibody Against P-selectin*. Journal of Cardiovascular Pharmacology, 2015. **65**(6): p. 611-619.
133. Ley, K., *The role of selectins in inflammation and disease*. Trends in Molecular Medicine, 2003. **9**(6): p. 263-268.
134. Varki, A., *Selectin ligands*. Proc Natl Acad Sci U S A, 1994. **91**(16): p. 7390-7.
135. Bachelet, L., et al., *Affinity of low molecular weight fucoidan for P-selectin triggers its binding to activated human platelets*. Biochim Biophys Acta, 2009. **1790**(2): p. 141-6.
136. Berteau, O. and B. Mulloy, *Sulfated fucans, fresh perspectives: structures, functions, and biological properties of sulfated fucans and an overview of enzymes active toward this class of polysaccharide*. Glycobiology, 2003. **13**(6): p. 29R-40R.
137. Chollet, L., et al., *Fucoidans in Nanomedicine*. Marine Drugs, 2016. **14**(8).
138. Chaubet, F., et al. *Relationships between chemical characteristics and anticoagulant activity of low molecular weight fucans from marine algae*. in *International Symposium of the Phytochemical-Society-of-Europe on Bioactive Carbohydrate Polymers*. 1998. Sundoya, Norway.

139. Foxall, C., et al., *The 3 members of the selectin receptor family recognize a common carbohydrate epitope, the Sialyl Lewis oligosaccharide*. Journal of Cell Biology, 1992. **117**(4): p. 895-902.
140. Sachs, U.J.H. and B. Nieswandt, *In vivo thrombus formation in murine models*. Circulation Research, 2007. **100**(7): p. 979-991.
141. Korninger, C. and D. Collen, *Studies on the specific fibrinolytic effect of human extrinsic (tissue-type) plasminogen-activator in human-blood and in various animal species in vitro*. Thrombosis and Haemostasis, 1981. **46**(2): p. 561-565.
142. Eltzschig, H.K. and T. Eckle, *Ischemia and reperfusion-from mechanism to translation*. Nature Medicine, 2011. **17**(11): p. 1391-1401.
143. Delbos, S., et al., *Porphyromonas gingivalis Participates in Pathogenesis of Human Abdominal Aortic Aneurysm by Neutrophil Activation. Proof of Concept in Rats*. Plos One, 2011. **6**(4).
144. Guo, S.C., et al., *Detection of High-Risk Atherosclerotic Plaques with Ultrasound Molecular Imaging of Glycoprotein IIb/IIIa Receptor on Activated Platelets*. Theranostics, 2015. **5**(4): p. 418-430.
145. Flacke, S., et al., *Novel MRI contrast agent for molecular imaging of fibrin: implications for detecting vulnerable plaques*. Circulation, 2001. **104**(11): p. 1280-5.
146. Wu, W., et al., *In vivo ultrasound molecular imaging of inflammatory thrombosis in arteries with cyclic Arg-Gly-Asp-modified microbubbles targeted to glycoprotein IIb/IIIa*. Invest Radiol, 2013. **48**(11): p. 803-12.
147. Hu, G., et al., *Ultrasound molecular imaging of arterial thrombi with novel microbubbles modified by cyclic RGD in vitro and in vivo*. Thrombosis and Haemostasis, 2012. **107**(1): p. 172-83.
148. McAteer, M.A., et al., *A leukocyte-mimetic magnetic resonance imaging contrast agent homes rapidly to activated endothelium and tracks with atherosclerotic lesion macrophage content*. Arterioscler Thromb Vasc Biol, 2012. **32**(6): p. 1427-35.
149. Kaufmann, B.A., et al., *Molecular imaging of the initial inflammatory response in atherosclerosis: implications for early detection of disease*. Arterioscler Thromb Vasc Biol, 2010. **30**(1): p. 54-9.
150. Villanueva, F.S., et al., *Myocardial ischemic memory imaging with molecular echocardiography*. Circulation, 2007. **115**(3): p. 345-52.
151. Davidson, B.P., et al., *Detection of antecedent myocardial ischemia with multiselectin molecular imaging*. J Am Coll Cardiol, 2012. **60**(17): p. 1690-7.
152. Suzuki, M., et al., *Ultrasmall superparamagnetic iron oxide nanoparticles coated with fucoidan for molecular MRI of intraluminal thrombus*. Nanomedicine (Lond), 2015. **10**(1): p. 73-87.
153. Bonnard, T., et al., *Leukocyte mimetic polysaccharide microparticles tracked in vivo on activated endothelium and in abdominal aortic aneurysm*. Acta Biomater, 2014. **10**(8): p. 3535-45.
154. Bonnard, T., et al., *Abdominal aortic aneurysms targeted by functionalized polysaccharide microparticles: a new tool for SPECT imaging*. Theranostics, 2014. **4**(6): p. 592-603.
155. Song, Y., et al., *Multimodal SPION-CREKA peptide based agents for molecular imaging of microthrombus in a rat myocardial ischemia-reperfusion model*. Biomaterials, 2014. **35**(9): p. 2961-70.
156. Kim, D.E., et al., *Hyperacute direct thrombus imaging using computed tomography and gold nanoparticles*. Ann Neurol, 2013. **73**(5): p. 617-25.
157. Kim, J.Y., et al., *Direct Imaging of Cerebral Thromboemboli Using Computed Tomography and Fibrin-targeted Gold Nanoparticles*. Theranostics, 2015. **5**(10): p. 1098-1114.
158. Leach, J.K., et al., *Accelerated thrombolysis in a rabbit model of carotid artery thrombosis with liposome-encapsulated and microencapsulated streptokinase*. Thrombosis and Haemostasis, 2003. **90**(1): p. 64-70.

159. Leach, J.K., E. Patterson, and E.A. O'Rear, *Encapsulation of a plasminogen activator speeds reperfusion, lessens infarct and reduces blood loss in a canine model of coronary artery thrombosis*. Thrombosis and Haemostasis, 2004. **91**(6): p. 1213-1218.
160. Leach, J.K., E. Patterson, and E.A. O'Rear, *Distributed intraclot thrombolysis: mechanism of accelerated thrombolysis with encapsulated plasminogen activators*. Journal of Thrombosis and Haemostasis, 2004. **2**(9): p. 1548-55.
161. Kim, J.Y., et al., *The use of PEGylated liposomes to prolong circulation lifetimes of tissue plasminogen activator*. Biomaterials, 2009. **30**(29): p. 5751-5756.
162. Jin, H.J., et al., *Urokinase-coated chitosan nanoparticles for thrombolytic therapy: preparation and pharmacodynamics in vivo*. Journal of Thrombosis and Thrombolysis, 2013. **36**(4): p. 458-68.
163. Korin, N., et al., *Shear-Activated Nanotherapeutics for Drug Targeting to Obstructed Blood Vessels*. Science, 2012. **337**(6095): p. 738-742.
164. Ma, Y.H., et al., *Magnetically targeted thrombolysis with recombinant tissue plasminogen activator bound to polyacrylic acid-coated nanoparticles*. Biomaterials, 2009. **30**(19): p. 3343-51.
165. Chen, J.P., et al., *Characterization of chitosan magnetic nanoparticles for in situ delivery of tissue plasminogen activator*. Carbohydrate Polymers, 2011. **84**(1): p. 364-372.
166. Yang, H.W., et al., *Bioconjugation of recombinant tissue plasminogen activator to magnetic nanocarriers for targeted thrombolysis*. Int J Nanomedicine, 2012. **7**: p. 5159-73.
167. Chen, J.P., et al., *Magnetically controlled release of recombinant tissue plasminogen activator from chitosan nanocomposites for targeted thrombolysis*. Journal of Materials Chemistry B, 2016. **4**(15): p. 2578-2590.
168. Kempe, M., et al., *The use of magnetite nanoparticles for implant-assisted magnetic drug targeting in thrombolytic therapy*. Biomaterials, 2010. **31**(36): p. 9499-510.
169. Bi, F., et al., *Chemical conjugation of urokinase to magnetic nanoparticles for targeted thrombolysis*. Biomaterials, 2009. **30**(28): p. 5125-30.
170. Marsh, J.N., et al., *A fibrin-specific thrombolytic nanomedicine approach to acute ischemic stroke*. Nanomedicine (Lond), 2011. **6**(4): p. 605-15.
171. McCarthy, J.R., et al., *Multifunctional nanoagent for thrombus-targeted fibrinolytic therapy*. Nanomedicine (Lond), 2012. **7**(7): p. 1017-28.
172. Vaidya, B., G.P. Agrawal, and S.P. Vyas, *Platelets directed liposomes for the delivery of streptokinase: development and characterization*. Eur J Pharm Sci, 2011. **44**(5): p. 589-94.
173. Absar, S., et al., *Thrombus-Targeted Nanocarrier Attenuates Bleeding Complications Associated with Conventional Thrombolytic Therapy*. Pharmaceutical Research, 2013. **30**(6): p. 1663-1676.
174. Laing, S.T., et al., *Ultrasound-enhanced thrombolytic effect of tissue plasminogen activator-loaded echogenic liposomes in an in vivo rabbit aorta thrombus model--brief report*. Arterioscler Thromb Vasc Biol, 2011. **31**(6): p. 1357-9.
175. Laing, S.T., et al., *Thrombolytic efficacy of tissue plasminogen activator-loaded echogenic liposomes in a rabbit thrombus model*. Thrombosis Research, 2012. **130**(4): p. 629-35.
176. Haga, K., et al., *Thrombus-targeted perfluorocarbon-containing liposomal bubbles for enhancement of ultrasonic thrombolysis: in vitro and in vivo study*. Journal of Thrombosis and Haemostasis, 2013. **11**(8): p. 1565-73.
177. Uesugi, Y., et al., *An ultrasound-responsive nano delivery system of tissue-type plasminogen activator for thrombolytic therapy*. Journal of Controlled Release, 2010. **147**(2): p. 269-77.
178. Kawata, H., et al., *A new drug delivery system for intravenous coronary thrombolysis with thrombus targeting and stealth activity recoverable by ultrasound*. J Am Coll Cardiol, 2012. **60**(24): p. 2550-7.

179. Friedrich, R.P., et al., *Tissue Plasminogen Activator Binding to Superparamagnetic Iron Oxide Nanoparticle-Covalent Versus Adsorptive Approach*. *Nanoscale Research Letters*, 2016. **11**.
180. Yumura, K., et al., *Mutations for decreasing the immunogenicity and maintaining the function of core streptavidin*. *Protein Science*, 2013. **22**(2): p. 213-221.
181. Wang, X.W., et al., *Thrombus-Targeted Theranostic Microbubbles: A New Technology towards Concurrent Rapid Ultrasound Diagnosis and Bleeding-free Fibrinolytic Treatment of Thrombosis*. *Theranostics*, 2016. **6**(5): p. 726-738.
182. Zhou, J., et al., *Construction and evaluation of Fe(3)O(4)-based PLGA nanoparticles carrying rtPA used in the detection of thrombosis and in targeted thrombolysis*. *ACS Appl Mater Interfaces*, 2014. **6**(8): p. 5566-76.
183. Chauvierre, C., et al., *Novel polysaccharide-decorated poly(isobutyl cyanoacrylate) nanoparticles*. *Pharmaceutical Research*, 2003. **20**(11): p. 1786-93.
184. Vauthier, C., et al., *Poly(alkylcyanoacrylates) as biodegradable materials for biomedical applications*. *Advanced Drug Delivery Reviews*, 2003. **55**(4): p. 519-548.
185. Lenaerts, V., et al., *Degradation of poly(isobutyl cyanoacrylate) nanoparticles*. *Biomaterials*, 1984. **5**(2): p. 65-68.
186. *Efficacy and safety doxorubicin transdrug study in patients suffering from advanced hepatocellular carcinoma (ReLive)* www.clinicaltrials.gov/ct2/show/NCT01655693. 2012 [cited].
187. Sulheim, E., et al., *Cellular uptake and intracellular degradation of poly(alkyl cyanoacrylate) nanoparticles*. *Journal of Nanobiotechnology*, 2016. **14**.
188. Passirani, C., et al., *Long-circulating nanoparticles bearing heparin or dextran covalently bound to poly(methyl methacrylate)*. *Pharmaceutical Research*, 1998. **15**(7): p. 1046-1050.
189. Chauvierre, C., et al., *Heparin coated poly(alkylcyanoacrylate) nanoparticles coupled to hemoglobin: a new oxygen carrier*. *Biomaterials*, 2004. **25**(15): p. 3081-6.
190. Labarre, D., et al., *Interactions of blood proteins with poly(isobutylcyanoacrylate) nanoparticles decorated with a polysaccharidic brush*. *Biomaterials*, 2005. **26**(24): p. 5075-84.
191. Tadros, T.F., *Emulsion Formation, Stability, and Rheology*, in *Emulsion Formation and Stability* (ed T. F. Tadros). 2013, Wiley-VCH Verlag GmbH & Co. KGaA, Weinheim, Germany. .
192. Alany, R.G., et al., *Effects of alcohols and diols on the phase behaviour of quaternary systems*. *International Journal of Pharmaceutics*, 2000. **196**(2): p. 141-145.
193. Frohlich, E., *The role of surface charge in cellular uptake and cytotoxicity of medical nanoparticles*. *International Journal of Nanomedicine*, 2012. **7**: p. 5577-5591.
194. Lira, M.C., et al., *Cytotoxicity and cellular uptake of newly synthesized fucoidan-coated nanoparticles*. *Eur J Pharm Biopharm*, 2011. **79**(1): p. 162-70.
195. Chauvierre, C., et al., *Enhancing the tolerance of poly(isobutylcyanoacrylate) nanoparticles with a modular surface design*. *International Journal of Pharmaceutics*, 2007. **338**(1-2): p. 327-32.
196. Diaz, J.A., et al., *Critical Review of Mouse Models of Venous Thrombosis*. *Arteriosclerosis Thrombosis and Vascular Biology*, 2012. **32**(3): p. 556-562.
197. Cooley, B.C., *Murine Arterial Thrombus Induction Mechanism Influences Subsequent Thrombodynamics*. *Thrombosis Research*, 2015. **135**(5): p. 939-943.
198. Boulaftali, Y., et al., *The mouse dorsal skinfold chamber as a model for the study of thrombolysis by intravital microscopy*. *Thrombosis and Haemostasis*, 2012. **107**(5): p. 962-971.
199. Tang, Z.C., et al., *A t-PA/nanoparticle conjugate with fully retained enzymatic activity and prolonged circulation time*. *Journal of Materials Chemistry B*, 2015. **3**(6): p. 977-982.

200. Jaffer, F.A., et al., *Molecular imaging of factor XIIIa activity in thrombosis using a novel, near-infrared fluorescent contrast agent that covalently links to thrombi*. Circulation, 2004. **110**(2): p. 170-176.
201. Kreuter, J., et al., *Passage of peptides through the blood-brain-barrier with colloidal polymer particles (nanoparticles)*. Brain Research, 1995. **674**(1): p. 171-174.
202. Tian, X.H., et al., *Enhanced brain targeting of temozolomide in polysorbate-80 coated polybutylcyanoacrylate nanoparticles*. International Journal of Nanomedicine, 2011. **6**: p. 445-452.
203. Kreuter, J., *Influence of the surface properties on nanoparticle-mediated transport of drugs to the brain*. Journal of Nanoscience and Nanotechnology, 2004. **4**(5): p. 484-488.
204. Mammadova-Bach, E., et al., *Platelet glycoprotein VI binds to polymerized fibrin and promotes thrombin generation*. Blood, 2015. **126**(5): p. 683-691.
205. Chauvierre, C., et al., *Radical emulsion polymerization of alkylcyanoacrylates initiated by the redox system dextran-cerium(IV) under acidic aqueous conditions*. Macromolecules, 2003. **36**(16): p. 6018-6027.
206. Desbree, A., et al., *Evaluation of Functionalized Polysaccharide Microparticles Dosimetry for SPECT Imaging Based on Biodistribution Data of Rats*. Molecular imaging and biology : MIB : the official publication of the Academy of Molecular Imaging, 2014.

Annexe A - Chapitre de livre et revues

A.1. Nanotheranostics in cardiovascular diseases

Chapitre du livre :

Nanotheranostics for Personalized Medicine, **2016 Jan.** World Scientific Publishing, Singapore, and Imperial College Press, London. Couvreur P, Mura S
Juenet M, Varna M, Chauvierre C, Letourneur D

A.2. Nanomedicine for the molecular diagnosis of cardiovascular pathologies

Biochemical Biophysical Research Communications, **2015 Dec.** 18;468(3): 476-484

Juenet M, Varna M, Aid-Launais R, Chauvierre C, Letourneur D

A.3. Nanomedicine as a strategy to fight thrombotic diseases

Future Science OA, **2015 Nov.** 1;1(4)

Varna M, Juenet M, Bayles R, Mazighi M, Chauvierre C, Letourneur D

Réédité comme chapitre du livre :

Handbook of Clinical Nanomedicine: From Bench to Bedside, **2016.** Pan Stanford Publishing, Singapore. Bawa R, Audette G and Rubinstein I

A.4. Polysaccharide-based strategies for heart tissue engineering

Carbohydrate Polymers, **2015 Feb**, 13;116: 267-277

Silva AKA, Juenet M, Meddahi-Pellé A, Letourneur D

Nanotheranostics for Personalized Medicine, 2016 Jan.
 World Scientific Publishing, Singapore, and Imperial College Press, London. *Couvreur P, Mura S*

CHAPTER

NANOTHERANOSTICS IN CARDIOVASCULAR DISEASES

Maya Juenet, Mariana Varna, Cédric Chauvierre and Didier Letourneur

*Inserm, U1148, Cardiovascular Bio-Engineering, X. Bichat Hospital
 Université Paris Diderot, Université Paris 13, Sorbonne Paris Cité, France
 didier.letourneur@inserm.fr*

Cardiovascular diseases (CVD) are the primary cause of death in the world. This chapter describes the potential of lipid-based, polymer-based and inorganic nano- and microplatforms as new tools for diagnosis and therapy of CVD. The detailed systems are in preclinical development and a few of them have been tested in clinical trials. The developed nano- and microparticles act as carriers for contrast agents and/or drugs, associating ligands to target specific biomarkers at cellular and molecular levels. The particles loaded with contrast agents provide molecular imaging of pathological events. Molecular imaging for all main types of modalities greatly completes morphological information provided by traditional imaging methods. A targeted and controlled drug release using carriers loaded with thrombolytic drugs for thrombus breakdown helps reducing the injected dose. It addresses therefore current therapeutic limitations by decreasing undesirable side effects. Hence, nanomedicine appears as a suitable tool to fight CVD, allowing for a personalized care and risk management.

1. Introduction

Cardiovascular diseases (CVD) are the major cause of death in the world with 17.3 million deaths per year and they represent major medical and economic issues. Among CVD, ischemic heart disease and stroke caused by atherosclerosis are responsible for 12.5 million deaths every year.¹

Atherosclerosis is a multifactorial and slowly progressing patho-physiological process.² It is characterized by the penetration of Low-Density Lipoproteins (LDL) into the intima resulting in the formation of lipid-rich plaques on the internal wall of large and mid-arteries and is often located at arterial bifurcations where the flow is the most perturbed. Risk factors include hypercholesterolemia, hypertension, diabetes, obesity, high fat diet, stress and cigarette smoking. Complications induced by atherosclerotic plaque are either caused by the growing of the plaque itself generating vessel stiffness and occlusion, or by its disruption. In response to plaque disruption, thrombogenic substances are released inducing platelets activation and adhesion to the endothelium and formation of a thrombus composed of fibrin and platelets. The thrombus or part of it can be dislodged, taken by blood flow leading to occlusion of another vessel in the body which could suddenly then generate an acute clinical event (ACE), such as myocardial infarct or ischemic stroke. Significant progress in biological understanding of CVD evolution established a correlation between plaque progression to rupture and expression of specific biomarkers at the molecular scale. Combining the targeting of these biomarkers with contrast agents opens the way to an exciting field of research: molecular imaging for personalized care.

Imaging methods performed to assess atherosclerosis development mostly provide morphological information, looking for vessel occlusion at site of plaque (stenosis). Angiography (X-ray Computed Tomography (CT)) with radiocontrast agent and Doppler Ultrasonography (Ultrasound imaging (US)) allow for visualizing lumen size and local flow perturbations on vessel walls. Magnetic Resonance Imaging (MRI) stands as the tool of choice for visualizing cerebral inflow with a good spatial resolution. However, beyond these morphological data, physicians lack tools to better define risks and adapt follow-up treatment. It has indeed been observed that unstable plaques are not necessarily associated with an advanced degree of stenosis and are most often diagnosed further to an ACE.³ Therefore, a personalized medicine is required to better characterize atherosclerotic lesions and predict their progression.

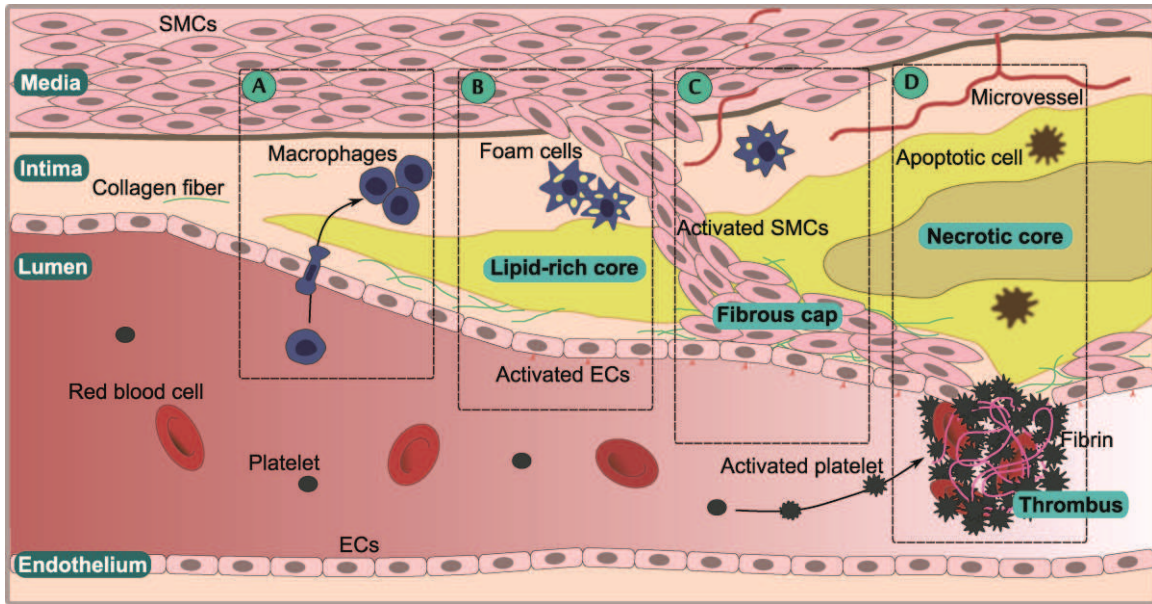


Fig. 1. Atherosclerotic plaque development showing molecular and cellular mechanisms as targets by nano- or microplatforms. **A)** Lipid accumulation (yellow) in the intima is associated with macrophage infiltration and accumulation. **B)** Activated Endothelial cells (ECs) express specific markers such as P- and E-selectins, VECAM-1 and ICAM-1. In the plaque, foam cells and a lipid-rich core are generated. **C)** Smooth muscle cells (SMCs) migrate into the intima and become activated, losing their stretching phenotype. A fibrous cap forms made of SMCs and collagen fibers. Remodeling affects intima size outwards the vessel wall. **D)** Apoptotic events and necrotic areas appear in a hypoxic environment inducing micro-vessels. In case of plaque rupture, the activated endothelium is broken allowing platelet activation through contact with the fibrous cap. A fibrin mesh forms and platelets and red blood cells accumulate at the site of injury.

Many biological mechanisms of plaque evolution and molecular markers are now described.⁴ For instance the mechanisms contributing to rupture-prone plaques are described to be associated with accumulation of macrophages, presence of foam cells, apoptotic events hypoxia and new microvessel development (angiogenesis) (Figure 1).³ Different molecular markers have been identified, among which: endothelial targets (PECAM-1, VECAM-1, ICAM-1, E- and P-selectins, integrins $\alpha_v\beta_5$, $\alpha_v\beta_3$, $\alpha_v\beta_1$)⁵, macrophage targets (Scavenger receptor class A (SR-A) or integrin MAC-1), inflammation (CD204), fibrous cap and extracellular matrix (collagen types I, III, IV), apoptosis (phosphatidylserine), angiogenesis (VEGFR, integrin $\alpha_v\beta_3$, CD13) and thrombus (activated platelets, activated factor XIII, fibrin).⁶ Other pathologies which would benefit from molecular imaging are for instance Abdominal Aortic Aneurysms (AAA). In clinic, the size of the aneurysm is the only criterion to predict its evolution and to assess risk for rupture. However, its expansion rate could be better predicted with complementary information about its activation state.⁷

As regards therapy, the inflammation, the reduction of cholesterol level, the smooth muscle cell proliferation, the angiogenesis or the thrombus were principally treated.⁸⁻¹² However a major issue is administration of high doses of therapeutic drugs. After being administered to patients, the drugs undergo cell metabolism and are distributed into the body. In order to obtain a therapeutic effect, high doses have to be injected, which may lead to undesirable side effects.¹³ Directing the drug against a specific biomarker expressed at the surface of activated endothelial cells or in the thrombus could enhance its therapeutic effect. However, this does not prevent drug degradation by enzymes into the blood. For that purpose, nano- and micro-carriers appear to be the dedicated tools. We choose here to focus on thrombolytic drugs and the usefulness of the different types of carriers to overcome the limitations of conventional therapy.

Thrombolytic drugs used in clinical practice are mainly recombinant-based tissue plasminogen activators (rtPA), which are the recombinant forms of tissue plasminogen activator (tPA).^{14,15} Other thrombolytic drugs exist but, because of their expensive price, or of allergic reactions development (uPA: urokinase, SK: streptokinase) they are not currently administrated. These agents convert inactive plasminogen into active plasmin which digests fibrin in clots. Because of their short half-lives and rapid inactivation by circulating inhibitors such as plasminogen activator inhibitor-1 (PAI-1), it is necessary to administer high doses to obtain a therapeutic response. Major drawbacks of thrombolytic therapy are a low treatment efficacy and intracranial hemorrhages.⁸⁸⁻⁹¹ In addition, tPA is able to cross blood brain barrier (BBB) due to an abnormal permeability of capillaries within the ischemic zone¹⁶ and promotes neuronal death. tPA increases also matrix metalloproteinase (MMPs) activity which degrade matrix proteins and breakdown the BBB integrity.

In next sections, we describe nano/micro platforms in preclinical development and in clinical use in cardiovascular field. We detail molecular imaging applications as well as the therapeutic opportunities.

2. Design of platforms for cardiovascular diseases

Three main types of platform have been developed for CVD imaging and/or therapy: lipid-based, polymer-based and inorganic particles. They are versatile systems. Their surface can be functionalized by grafting bioactive molecules. In addition, hydrophobic or hydrophilic compounds can be incorporated in the core of the particles during their synthesis.

2.1. Lipid-based platforms

Lipid-based nanoparticles mostly rely on a phospholipids assembly, mimicking the cellular membrane. Phospholipids are amphiphilic. Under certain conditions, they organize into micelles or liposomes. Different forms of lipid-based systems for molecular imaging were reviewed in details by Mulder *et al.*¹⁷ Micelles show a hydrophobic core and their size is generally less than 50 nm. On the contrary, liposomes are made of a double layer of lipids that surrounds a hydrophilic core. Their size can reach several hundreds of nanometers. Another lipid-based vector consists in micelle containing hydrophobic nanodroplets. They are named micro-emulsions and are larger than previously described systems (few hundreds of nm). In particular, micro-emulsions made of liquid perfluorocarbon (PFC) droplets are good candidates for CVD molecular imaging since PFC are inert, non-toxic and naturally eliminated from the body through the lungs. These chemicals are exclusively composed of atoms of carbon and fluorine. They were extensively studied in the 70s/80s for their capacity to dissolve oxygen in their liquid form and were first tested in clinic as blood substitute¹⁸ and for liquid breathing.¹⁹ Furthermore, they are compatible with Ultrasound (US) and Magnetic Resonance (MR) imaging.^{20,21}

Natural High-Density Lipoproteins (HDL) or HDL-like synthetic particles were also investigated as vectors for therapy and diagnosis.²² There are micelles made of extracted or synthesized lipoproteins, mainly apolipoproteins apo A-I and apo A-II. Their size stands around 5-17 nm. They are naturally entering LDL-rich plaques and show the advantages of being endogenous and entirely biodegradable. According to their biocompatibility and their versatility, lipid-based nanosystems have led to numerous formulations.

2.2. Polymer-based platforms

Synthetic or natural polymers are also of great interest to design nano- or micro-structures more resistant to mechanical constraints than lipid-based ones. Functional agents can be embedded into the polymer matrix during synthesis. Besides core loading, polymer surface generally enhances protein adsorption. Polymer particles are synthesized by different mechanisms, like nanoprecipitation, emulsion-reticulation and ionic gelation. According to the polymer nature and to the synthesis parameters, polymer platforms can be tuned in terms of size, porosity and hydrophobicity. Polymers offering good biocompatibility and biodegradability should of course be preferred. Polysaccharides show promising properties for CVD.²³ In particular chitosan and fucoidan present affinity for fibrin and P-selectin respectively. Poly(lactic-co-glycolic acid) (PLGA), a biodegradable FDA-approved polymer, and Polyvinyl alcohol (PVA) have also been formulated into nanoparticles.²⁴ Natural polymers, such as gelatin, have been considered for therapeutics loading too. Beyond their potential as vectors, polymers and especially poly(ethyleneglycol) (PEG), an hydrophilic biocompatible and biodegradable polymer, are also widely used to coat all types of particles in order to prevent their aggregation. In addition, by steric inhibition, PEG delays the opsonic recognition and thus macrophage uptake prolonging the circulation time of nanoparticles into whole blood. Moreover PEG can be easily modified to attach different ligands for a specific delivery.

2.3. Inorganic platforms

Inorganic nanoparticles are composed of an inorganic core with imaging properties, generally coated with a polymer shell. The polymer coating improves colloidal stability and particle biocompatibility. This type of platform includes magnetic nanoparticles, metal nanocrystals and quantum dots. Magnetic nanoparticles are usually composed of a paramagnetic iron oxide core, either made of magnetite (Fe_3O_4) or maghemite ($\gamma-Fe_2O_3$) or a mixture of both, surrounded by a shell made of dextran or derivatives.²⁵ Magnetic particles are biodegradable, participating in the iron homeostasis in the body.²⁶ They can be formulated into ultrasmall superparamagnetic iron oxides (USPIO), which hydrodynamic size is defined as inferior to 50 nm (coating including), or into superparamagnetic iron oxides (SPIO) particles, which

hydrodynamic size stands between 50 and a few hundreds of nanometers. Under a uniform and strong magnetic field (1.5 to 3 Tesla), these nanoparticles are used as contrast agents for MRI. Under local application of a magnet, they are promising candidates for magnetic guided thrombolytic therapy. Metal nanocrystals developed for CVD molecular imaging concern especially gold (Au). This element show good properties for Computed Tomography (CT), because of its high atomic number and its high K-edge energy. Quantum dots are nanocrystals of semiconductors, such as Cadmium Selenide (CdSe), with a size of a few nanometers. They emit light when illuminated at a given wavelength related to their size and their composition. As they are known to be toxic and carcinogenic, they are only used for preclinical development, along with an appropriate coating to be tolerated by the cells. Alternatively to polymer coating, other coatings developed for inorganic nanoparticles include small molecules, as bisphosphonates, and phospholipids.

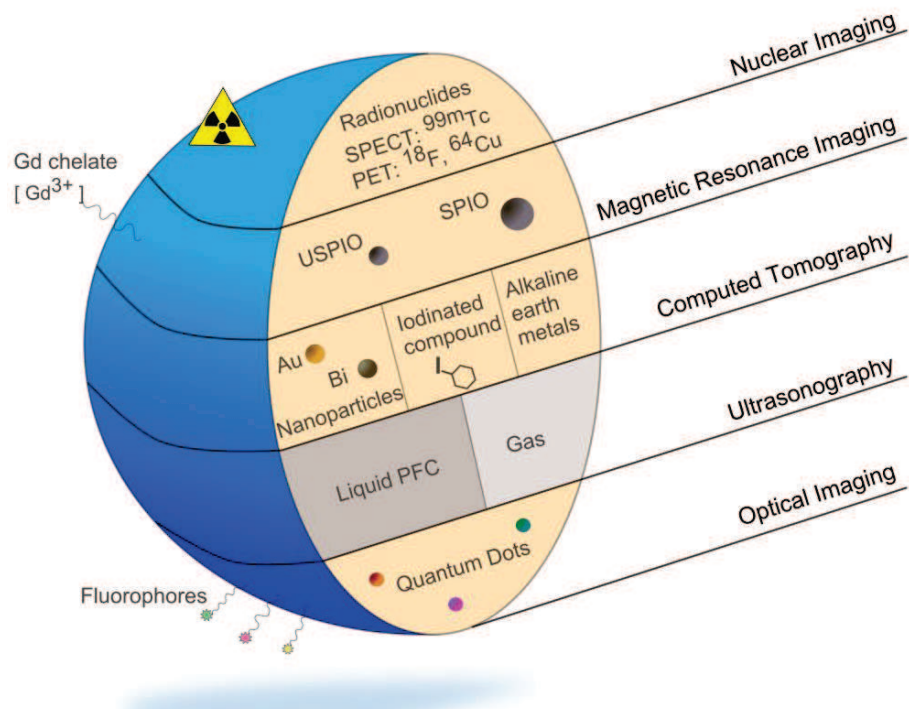


Fig. 2. Illustration of nano/microplatforms for various imaging modalities in preclinical molecular imaging of CVD.

3. Imaging modalities and corresponding contrast agents

CVD diagnosis may be based on several exams relying on different physical phenomena. The imaging modalities have to be chosen according to the type of pathology and to its location. Molecular imaging platforms are in development for all modalities described below (Figure 2).

3.1. Nuclear Imaging

Single-photon emission computed tomography (SPECT) and positron emission tomography (PET) provide functional imaging of the body, highlighting for example cell metabolic activity. These two techniques require the intra-venous (IV) injection of a radionuclide (also called radioactive nuclide or radioisotope). In clinic, most machines perform a CT-scan at the same time to localize in two or three dimensions the accumulation of radionuclides in the body. Nuclear imaging is the most sensitive technique and is therefore at an advanced stage for CVD molecular imaging. In particular, macrophages uptake has been exploited for atherosclerosis imaging.²⁷ This glucose analog is trapped into metabolically active macrophages where it accumulates. ^{18}F -FDG imaging has been set up in humans for imaging high-risk plaques²⁷ and is now employed as an

endpoint in most clinical trials²⁸ testing new therapeutics. ¹⁸F-FDG PET scans provide an image 2 to 3 hours after injection. The main limitation is that it does not interact exclusively with macrophages. ¹⁸F-FDG unspecific uptake is especially an issue for imaging coronary diseases as myocardial assimilation is very important. Other radioisotopes, such as Technetium-99m (^{99m}Tc) and Copper-64 (⁶⁴Cu) were associated to molecules for targeting. For instance, radiolabeled ^{99m}Tc-fucoidan proved its efficacy in detecting the intra-arterial thrombi in different models of vessel injury in rats (Figure 3).^{29,30} More generally, radiotracers combined with targeting agents forming molecular assembly were reviewed by Stacy *et al.* in case of peripheral vascular disease.³¹ Combining these molecular probes into nanoplatforms would enable to improve their specificity and avoid their rapid clearance.³² Nuclear imaging is also frequently used in preclinical development to study biodistribution of newly developed platforms.

3.2. Magnetic Resonance Imaging

Magnetic Resonance Imaging (MRI) relies on the nuclear magnetic resonance of hydrogen atoms of water molecules present in abundance in tissues. Hydrogen nuclei behave as small magnet exhibiting an intrinsic magnetic moment. A strong and uniform magnetic field is applied to the body via a superconducting magnet, in order to align magnetic moment of all hydrogen atoms. An oscillating magnetic field is then switched on temporarily at a given frequency that makes the magnetic moments deviate from their equilibrium position. This phenomenon is called resonance. When the oscillating field is switched off, magnetic moments return to their equilibrium position at a given rate called relaxation. Two different relaxation times characterize a nucleus; its longitudinal relaxation time (T1) and its transversal one (T2). The relaxation intensity coming from a precise scanned area is directly correlated to the density of hydrogen atoms, varying from one tissue to another. MRI offers a very good spatial resolution (25 µm to 1 mm) and precise morphological localization in the body. Recently, improvements in MRI sequences and parameters (multiparameters-MRI) enable to distinguish plaque components, like necrotic core, fibrous cap and lipid-rich area, without requiring nanoparticles. To complete this information, molecular imaging tools based on MRI contrast agents are developed.

MRI contrast agents are classified in two types according to the way they influence their magnetic environment: Gadolinium chelates (T1-shortening agents) and iron oxide based particles (T2-shortening agents). Relaxivity is defined as the capacity of contrast agents to modify the relaxation rate of surrounding protons. Gadolinium(III) (Gd³⁺) complexes are small paramagnetic compounds commonly used in MR angiography as blood pool enhancers. They are usually hydrophilic but can easily be grafted onto lipids.³³ Gd-chelates have been covalently bound to targeting peptides, leading to systems such as the fibrin specific EP-2104R (EPIX Pharmaceuticals, Inc.). This molecular probe has been proved to successfully target thrombus in humans³⁴ and penetrate plaque in animals.³⁵ The proof-of-concept was achieved in a phase II clinical trial of feasibility on 52 patients. However, its poor relaxivity limited its translation to clinic. Gd chelates are now studied to be concentrated into nanostructures. Iron oxides based contrast agents are USPIOs and SPIOS detailed in the previous section. They show a great potential for molecular imaging as their relaxivity is much higher than that of Gd-chelates. In T2 imaging, iron oxides generate a signal loss (hyposignal).

3.3. X-Ray Computed Tomography

Computed Tomography scan (CT-scan) is based on the capacity of tissues to absorb X-rays. One major application of CT-scan for CVD diagnosis is angiography performed with intra-venous injection of radiocontrasts. These radiocontrasts are small iodine-based molecules working as blood pool enhancers. They are strongly radiopaque and enable to draw a map of the vessels with a very good spatial resolution (50 - 200 µm) in only few minutes. As iodinated compounds may cause severe adverse effects, research is going on to decrease the dose by incorporating them into more complex structures, such as PEGylated nanoemulsions. Additionally, new radiopaque agents are investigated.^{36,37} In particular, elements with higher atomic number have a better X-ray attenuation capacity. Furthermore k-edge imaging with multicolor CT (more commonly referred to as spectral CT) is an emerging technique that provides elemental characterization of a tissue with an enhanced sensitivity, detecting for example calcium phosphate in atherosclerotic lesions. Contrast agents for k-edge imaging should be composed of elements with high k-edge energy. Metal nanoparticles, in particular gold and bismuth are good candidates as they have high atomic numbers and high k-edge energy levels. Although their toxicity has to be studied in depth, they are believed to be better tolerated than iodine-based agents. For preclinical studies with micro-CT, development of alkaline earth-based nanoparticles seems promising, as they generated strong contrast enhancement of vessels.^{38,39}

3.4. Ultrasonography

Ultrasound imaging (or Ultrasonography (US)) is the least sensitive method but an accessible and lower cost technique that stands as the tool of choice for bedside patient management. An ultrasonic pulse is sent to the body via a transducer. In standard modes, the contrast is based on the ability of tissues to reflect ultrasonic waves according to their acoustic impedance.

Contrast-enhanced ultrasound (CEUS) imaging has been developed in the 1990s. Gas microbubbles (1 - 5 μm) emerged as very good scatters due to their impedance difference with surrounding blood and tissue. They were developed in order to enhance blood pool signal and visualize flow even in the capillaries. Most importantly, they allowed visualizing left ventricle endocardial borders and quantifying myocardial perfusion.⁴⁰ The first generation consisted in air bubbles, which dissolve rapidly in blood. Gaseous PFC bubbles appeared to be more stable leading to a longer circulating time and less artefacts. These kinds of systems are stabilized by shell made of lipids, proteins or polymer. Today, three types of microbubbles are FDA-approved and routinely used in clinic: SonoVue® (Bracco), Definity® (Lantheus Medical Imaging) and Optison™ (GE Healthcare). Their main application is echocardiography for the diagnosis of left ventricular systolic dysfunction which stands as one major type of heart failure. Some PFC show echogenic properties into their liquid form too. Micro-emulsions made of liquid PFC droplets are often stabilized with a lipid coating, but protein and polymer coatings are under investigation. Gas or liquid PFC stand as platforms for molecular imaging tools for US imaging.

3.5. Fluorescence Optical Imaging

Fluorescence optical imaging performed with fluorescence microscopy is of great importance for pre-clinical development. Due to low penetration of light through biological tissues and to the toxicity of some contrast agents, this technique cannot be translated to clinic for CVD. However, it is easily compatible with laboratory practice. Fluorescent compounds (fluorophores) are injected into the animal bloodstream. The tissue of interest is illuminated at an appropriate wavelength depending on the fluorescent elements. The excited compound will emit light back at another wavelength. Optical imaging exhibits a high sensitivity.

Contrast agents are either small fluorescent probes or quantum dots. Quantum dots were described in the previous section. They are known to be toxic and carcinogenic, requiring therefore a coating in order to be tolerated by cells.

4. Nano- and Micro-platforms for molecular imaging

This section reviews several systems with a clinical potential or already in clinical trials for molecular imaging of CVD. All systems described below have been tested in animal models, the most common one being Apolipoprotein E-deficient mouse (ApoE-/-).

4.1. Preclinical development

4.1.1. Lipid-based platforms

Numerous contrast agents were loaded into lipid-based platforms to image atherosclerotic lesions. The most studied ones have been systems incorporating Gd diethylene triamine pentaacetic acid (Gd-DTPA) and Gd 1,4,7,10-tetraazacyclododecane-1,4,7,10-tetraacetic acid (Gd-DOTA) based lipids for MRI.¹¹ Lipid platforms can concentrate up to several thousands of Gd³⁺ ions per NP.^{41,42} Gd-labeled lipids were integrated with success in discoidal reconstituted HDL and native spherical HDL,⁴³ in fibrin-targeted PFC micro-emulsion,⁴² in liposomes and in micelles.^{33,44} Surface modification to make these systems specific to a biomarker was further achieved by grafting targeting agents, either directly to lipids or via a PEG spacer. Among others, systems that ensure targeting via an antibody are defined as immuno-micelles or immuno-liposomes. They were shown to significantly increase plaque uptake compared to naked systems. For example, adding an antibody targeted towards the macrophage scavenger receptor improved signal intensity of Gd-loaded micelles from 34% to 79% in atherosclerotic aortas of ApoE-/- mice.⁴⁵ More recently, HDL-like particles were functionalized with a peptide via a PEG spacer targeted towards collagen present in the extracellular matrix.⁴⁶ As plaque regression is associated with collagen degradation, they were able to assess plaque evolution with MRI in a regression model of mouse atherosclerosis. Biologically active proteins were also grafted for targeting. Van

Tilborg *et al.*⁴⁴ developed small Gd-loaded PEGylated micelles (15 nm) with covalently bound Annexin A5 to target intra-plaque apoptotic events via phosphatidylserine exposed at cell surface. Their size allows for extravasation and detection of extravascular events. No significant difference in MRI signal compared to untargeted micelles was observed but a heterogeneous distribution of targeted micelles was shown to be more consistent with plaque composition.

Other contrast agents were also successfully loaded into all types of lipid-based platforms. They are detailed by types of particles in the next paragraphs.

Liposomes

Insertion of contrast agents into the liposomal bilayer led to imaging tools for US imaging and MRI. As regards US imaging, echogenic liposomes (ELIP) have been developed in the nineties by McPherson's team.⁴⁷ A freeze-drying process combined with specific lipids formulation allowed for incorporating air nanobubbles into the bilayer, making it echogenic. Since then, the group has improved the formulation and developed targeted immuno-ELIP, even combined with drug delivery.⁴⁸ ELIP show longer circulating time than microbubbles usually used for US but their echogenic properties need still to be improved.

Gadolinium chelates were also inserted into the liposomal bilayer instead of being grafted through Gd-labelled lipids. Dellinger *et al.*⁴⁹ managed to load a fullerene cage holding Gadolinium. This liposome was functionalized with a peptide to target selectively foam cells by their scavenger receptor CD36 present in atherosclerotic plaques in ApoE-/- mice. Lesions were visualized at 7 Tesla after 30 minutes post-injection. The toxicity of this system and its activity in clinically relevant conditions have to be further validated. Liposomes that allow in addition incorporation of hydrophilic component in their core for therapy will be described later.

Micelles and HDL-like particles

In 2010, Skajaa *et al.*⁵⁰ reviewed the potential of HDL-like particles to be loaded with inorganic compounds, such as gold nanocrystals, quantum dots and SPIOs. In particular, Au-HDL combined with spectral CT were tested *in vivo* in ApoE-/- mice. They were shown to accumulate in macrophage-rich plaques and to give a good contrast with micro-CT.⁵¹ Furthermore, combining such systems with multicolor CT allowed distinguishing at once macrophages accumulation and calcification.⁵² More recently, Jung *et al.*⁵³ studied the biodistribution and *in vivo* plaques uptake of SPIO-HDL, showing promising results for the use of such recombinant HDL nanopartitions.

Micro-emulsions

Ding *et al.*⁵⁴ developed a bimodal platform where quantum dots were dispersed in an iodinated oil (Lipiodol®, Guerbet). Lipophilic nanodroplets were stabilized in water by PEGylated lipids. This system underwent passive uptake by macrophages in a rabbit model of atherosclerosis. Only 2 hours after administration, lumen signal was decreased to its value before injection whereas a significant uptake was observed in macrophages-rich plaques, compared to 24h to 72h with USPIOs.

Liquid PFCs were also incorporated into micelles leading to micro-emulsions. PFCs are interesting for molecular imaging due to their intrinsic properties of being visualized by both ultrasound and MRI.⁵⁵ Fluor ¹⁹F has indeed a nonzero spin. It is present in negligible amount in the body. Therefore, direct imaging of the compound accumulation is possible by MRI, but this technique cannot be easily implemented in clinic. PFC nanodroplets stabilized by lipid shell are much smaller than microbubbles made of gaseous PFC. Hence they can extravagate into vascular walls. They ensure also a better accessibility to diseased organs, as they are not affected by pulmonary passage.²¹ In 1996, Lanza *et al.*⁵⁶ established a three steps approach using biotin/streptavidin bond to link microbubbles to thrombus *in vivo* in dogs. The nanodroplets appeared far less echogenic in the circulation but give a strong signal enhancement while accumulating at their targeting site. Since then and beyond their imaging potential, PFC liquids with lipid coating have rather been used as vectors for loading lipophilic therapeutics⁵⁷ and amphiphilic targeting agents.⁵⁵

Micro-bubbles

As previously indicated, gaseous perfluorocarbons were mostly developed as blood pool agents for ultrasound imaging. Integration of targeting moieties in their shell makes them interesting tools for real time therapeutic effect monitoring.⁶¹ Due to their size, they cannot be considered for imaging molecular events happening inside vascular walls. However, in

early stage of thrombus formation or in post-ischemic area, endothelial cells exposed to the flow express specific markers, such as P- or E-selectins and VECAM-1. Microbubbles targeted towards P-selectin through its natural ligand Sialyl Lewis^X⁶² or through specific anti-P-selectin antibody⁶³ were evaluated in different animal models of thrombus or ischemia.⁶⁴ Correlation with histological results showed that area of signal enhancement, observed on average after two hours, corresponded to activated endothelium. Other microbubbles were shown to target successfully glycoprotein IIb/IIIa expressed in thrombi.^{65,66} One should be careful of the reliability of *in vitro* and *in vivo* models, as first systems were tested at low shear rate, which is not consistent with arterial pathologies. Furthermore, the synthesis was achieved via a biotin/streptavidin linkage and covalent binding should be investigated to avoid immunogenic potential. Finally lipid-based microbubbles are easily destroyed in the body. One strategy could be to use polymeric shell.⁶⁷

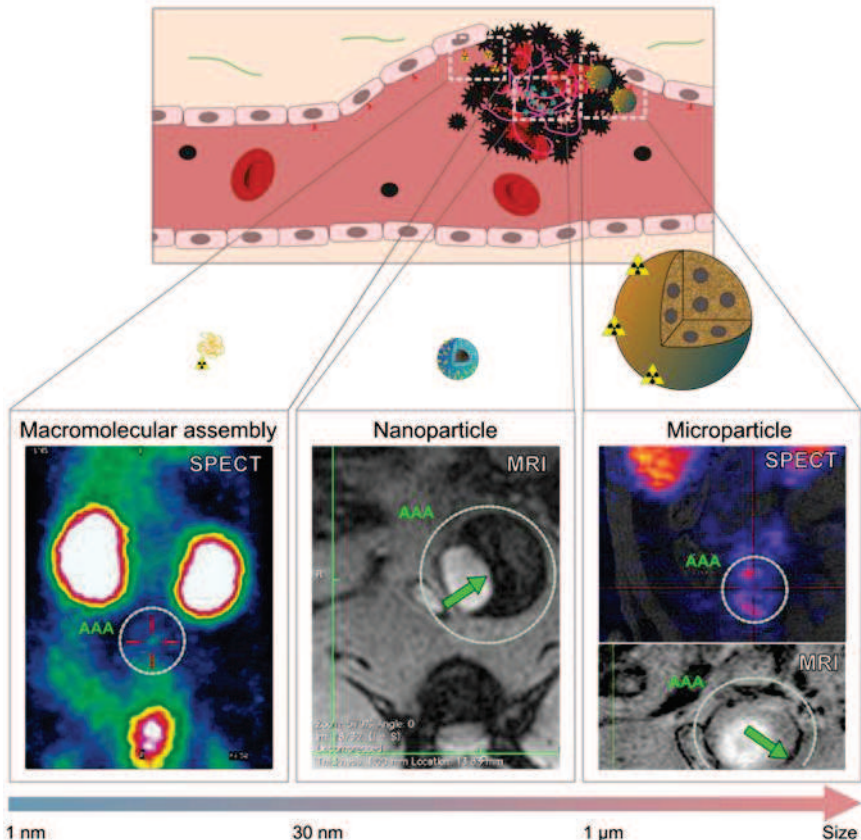


Fig. 3. Illustration of P-selectin targeting using different types of carriers as examples of molecular imaging in preclinical diagnosis of CVD. P-selectin is expressed by activated endothelial cells and activated platelets. All images were taken in rat models of Abdominal Aortic Aneurysm (AAA). From left to right: a macromolecular system made of fucoidan radiolabeled with ^{99m}Tc was injected to image intra-arterial thrombus with SPECT.²⁹ A dextran-coated USPIO grafted with fucoidan allowed to detect thrombus and activated endothelium by MRI.⁵⁸ Microparticles made of cross-linked dextran, pullulan and fucoidan were either radiolabeled with ^{99m}Tc for SPECT⁵⁹ or contained USPIOS for MRI⁶⁰, and enable thrombus detection.

4.1.2. Polymer-based platforms

Polysaccharides-based platforms

Polymer nanoparticles of a few nanometers (13 nm) were obtained by cross-linking short chain dextran with epichlorohydrin.⁶⁸ These nanoparticles were radiolabelled with Zirconium-89 (⁸⁹Zr) via desferoxamine for PET. PET/CT imaging was performed 48 hours after injection of 354 ± 13 μCurie/mouse. A significant activity was detected in the aortic root of ApoE-/ mice compared to wild-type controls, which was consistent with the development of atherosclerotic lesions. However, epichlorohydrin raises an issue for translation to clinic as it is not biodegradable. Bonnard *et al.*^{59,60} used STMP to cross-link dextran, pullulan and fucoidan to form targeted biodegradable microparticles (MP). These particles were either loaded with USPIOS (Sinerem®, Guerbet) for MRI⁶⁰ or labelled with ^{99m}Tc for SPECT (Figure 3).⁵⁹ *In vivo* results were promising, as MP accumulated onto the affected endothelium in a rat model of AAA. MRI was performed at 7.4 T after injection of an iron dose of 0.56 mg Fe/kg. A contrast uptake was observed after 30

minutes. Similarly, contrast enhancement in the abdominal aortic region was registered after 30 minutes with SPECT after injection of radiolabelled MP (at a dose of 37 MBq/rat). Interestingly, their size ($< 4\mu\text{m}$) and their behavior make them mimic rolling of leukocytes, which could be of great importance for drug release.

Other polymer platforms

Another type of iron oxide MP, tosyl-activated polystyrene-coated superparamagnetic colloids (Dynabeads®, Life Technologies) with a covalent grafting of P-selectin antibody were shown to accumulate onto activated endothelium.⁶⁹ Over several weeks of injection in ApoE-/- mice, the highest accumulation was obtained at the initial stage where the leukocytes were recruited, before apparition of a necrotic core. Although this system is not biodegradable, it remains interesting for basic studies in CVD understanding.

Poly(methyl methacrylate) (PMMA), which is not biodegradable either, was also studied for pre-clinical investigation. Luehmann *et al.*⁷⁰ developed PMMA nanoparticles covered with a functionalized PEG shell targeted towards chemokine receptor 5. NPs were radiolabelled with ^{64}Cu for PET. NPs were compared to ^{64}Cu -chelate directly coupled to the targeting unit. Using a nanoplatform greatly improved ^{64}Cu -chelate imaging potential.

PLGA seems more promising as regards its degradability and biocompatibility. It has been used with success for atherosclerosis as the core matrix of targeted systems⁷¹ even combined with drug release.⁷² Zhou *et al.*⁷² developed HDL mimicking polymer-lipid nanoparticle platform where iron oxides (Fe_3O_4) were embedded in a PLGA matrix. The polymer core was covered by a shell of chitosan bound to cyclic RGD peptides. The PLGA matrix encapsulated a thrombolytic drug (see section 5). These nanoparticles showed a good affinity for thrombi and induced a hyposignal at site of injury in a rat model of ferric chloride induced thrombus.

Hyafil *et al.*⁷³ demonstrated that a colloidal suspension of crystalline iodinated particles (N1177, Nanoscan Imaging LCC) allowed detecting high risk plaques with CT in a rabbit model of atherosclerotic lesions. Nanoparticles were obtained by precipitation of an iodinated ester and stabilized by PEG and surfactants. Detection relied on macrophage uptake.

4.1.3. Inorganic platforms

Magnetic particles for MRI

Most iron oxide based particles are coated with dextran or derivatives and dextran-coated USPIO and SPIO undergo spontaneous uptake by macrophages and can therefore be injected to image high-risk plaques. A few systems already reached the clinic (see next section). However, macrophage detection remains non-specific. In consequence, high doses are required and the time from injection to imaging is generally more than 24 hours. Therefore, grafting of ligands was investigated to improve the particles specificity. For instance fucoidan has been covalently grafted onto synthesized dextran-coated USPIOs. USPIO-fucoidan led to a strong hyposignal only one hour after injection in area of thrombus formation in a rat model of AAA (Figure 3). *In vivo* MRI experiments were performed at 4.7T before and after injection of 0.2 mmol Fe/kg.⁵⁸ Iron oxide based particles were also studied to image thrombus formed in a rat model of myocardial ischemia-reperfusion by adding a clot-binding peptide sequence to a dextran-coated SPIO.⁷⁴ 4 hours after injection, targeted SPIO generate a significant signal loss in the heart where microthrombi were formed, compared to untargeted systems.

Other coatings have also been investigated to replace dextran. Mannan coating has been set up to enhance macrophage uptake of SPIO and USPIO via mannose receptors.⁷⁵ Mannan-coated SPIO and USPIO were significantly more internalized by phagocytic cells than carboxydextran-coated systems in a rabbit model of atherosclerosis (after injection of 0.8 mmol Fe/kg). Mulhen *et al.*⁷⁶ constructed another iron oxide based structure targeted toward the integrin MAC-1 via an anti-CD11b, as CD11b is believed to participate in the phagocytosis of USPIO. The coating consisted in a PVA and a Vinyl alcohol-vinyl amine copolymer. After injection of 1 mg/kg, an uptake was observed in atherosclerotic plaques of ApoE-/- mice but quantification assessment showed no significant difference between control and targeted particles. Another system under investigation consists in a core made of maghemite and magnetite coated with a copolymer of gem-bisphosphonate. Functionalized with a PEG spacer, it allowed for grafting peptides targeted towards VECAM-1.^{77,78} This system enabled to decrease the recommended dose of 1 mmol Fe/kg with available unspecific USPIOs to 0.1 mmol Fe/kg at 4.7 T to image atherosclerotic lesions in mice. Most importantly, only 6 hours were necessary to obtain a good contrast.

Magnetic particles as platforms for PET/CT

Cross-linked iron oxide nanoparticles (CLIO) have been developed as a platform that can concentrate one or several monocrystalline iron oxides.⁷⁹ In these systems, the dextran coating is cross-linked via epichlorohydrin and is aminated, what makes the surface easily tunable. As they constitute accessible experimental platforms, such superparamagnetic particles were used by the Weissleder team as PET imaging tools radiolabelled with ⁶⁴Cu and ¹⁸F, to overcome issues relative to ¹⁸F-FDG imaging.⁸⁰⁻⁸² As PET is the most sensitive modality, it enabled to decrease the amount of particles injected (4.5 mg of iron oxide/kg that is less than the recommended dose of current FDA-approved iron oxides based particles). In addition, the biodistribution of such nanotools depends greatly on the size of the particle which can be tuned and adapted to the radionuclide half-life. Another team showed the potential for such bimodal platform by injecting ⁶⁴Cu radiolabelled CLIO in several mouse and rat models of CVD.⁸³

Gold nanoparticles

In addition to Au-HDL described in the lipid-based section, glycol chitosan (GC) coating has also been demonstrated to enhance retention and compatibility of gold nanoparticles (Au-NPs).⁸⁴ Furthermore, its affinity for fibrin makes it a coating of choice for thrombus targeting. Injection of 0.5 mg GC-AuNPs/mouse allowed to immediately image the thrombus and monitored the response to thrombolytic therapy in real time.

4.2. Clinical use

Apart from microbubbles detailed in the section 3 used as blood pool enhancers, dextran-coated USPIO and SPIO have already led to clinical trials for the diagnosis of several pathologies including pelvic and carotid atherosclerosis, AAA and acute ischemic events. Dextran-coated iron oxide based particles without targeting agents have been shown to spontaneously accumulate in macrophage-rich area allowing to detect inflammatory-like processes expressed in CVD. Pilot studies using iron oxide based nanoparticles were recently reviewed in details by Cicha *et al.*⁸⁵ The main results will be briefly described below. Macrophages detection relies on what is called passive targeting; particles are phagocytized by macrophages via physiological mechanisms. FDA-approved Ferumoxtran-10 (Sinerem, Guerbet/Combidex, AMAG Pharma) has been proved more than a decade ago to undergo spontaneous uptake by macrophages in high-risk plaques.⁸⁶ Ferumoxtran-10 is coated with dextran T10 and shows a long circulating time due to its small hydrodynamic size (30 nm). Kooi *et al.*⁸⁶ injected Ferumoxtran-10 to eleven patients suffering from advanced stage carotid stenosis. USPIOS significant uptake by rupture-prone plaques was observed after 24h by MRI at 1.5 Tesla and validated by histological analysis after endarterectomy. A significant hyposignal in rupture-prone plaques compared to stable plaques was further validated in several clinical trials for carotid atherosclerosis. More recently, Ferumoxtran-10 injection in patients after ischemic stroke suggested inflammatory variability in post-ischemic areas, underlining the need for personalized post-traumatic therapy.⁸⁷ This USPIO was also used in the ATHEROMA trial to monitor the effects of atorvastatin therapy for reducing plaque progression.⁸⁸ Post-analytical results were not significantly conclusive in predicting statistical risk for ACE. Two other iron oxide-based contrast agents were FDA-approved: SPIO Ferumoxides (Feridex IV, Berlex Laboratories/Endorem, Guerbet) which size is much larger (50-180 nm) and SPIO Ferucarbotran (Resovist®, Bayer Healthcare) (55-65 nm) coated with carboxymethyldextran.⁸⁹ Both were tested for CVD application. A correlation was found between Ferumoxides uptake (observed at 24h and 36h after injection) and rapidly progressive AAA expansion, independently from the initial size of the aneurysm.⁹⁰

However, these three types of particles are now totally or partially withdrawn from the market as regards their initial application, what make them less accessible. More recently, ferumoxytol (Feraheme), an USPIO (20-40 nm) coated with polyglucose sorbital carboxymethylether emerged as a promising tool. In the recent NIMINI-2 clinical trial ferumoxytol injection combined with mutiparameters MRI successfully delimited infarction area, as well as the peri-infarct zone in patients suffering from acute myocardial infarction.⁹¹ This is currently confirmed in another clinical trial.⁹² One limitation of imaging with these USPIOs is the time required after injection to get a signal in the region of interest. Significant passive accumulation requires 24h to 72h after injection. Another drawback is the dose of particles required (generally 1 - 20 mg of iron oxide/kg).⁸⁰ As detailed in the previous section, researchers work on increasing the affinity of iron oxides for plaques and activated area by incorporating targeting moieties.

5. Nano- and Micro-platforms for thrombolytic therapy

Another application of nano and micro-platforms is based on the delivery of therapeutic drugs. This strategy shows several advantages such as: i) Protection of active compounds (AC) from inhibitors in the circulation and their degradation. ii) Increase of circulating time: the circulating time of encapsulated drugs is much higher than this of not encapsulated drugs. Moreover the coating with hydrophilic compounds such as poly(ethylene) glycol (PEG) avoid the macrophage uptake and increase thus the circulation time. iii) The possibility for a targeted delivery which induce the concentration of AC into a specific site (Figure 4). In this section, we detail the preclinical and clinical applications of thrombolytic drug delivery using nano- and micro-platforms.

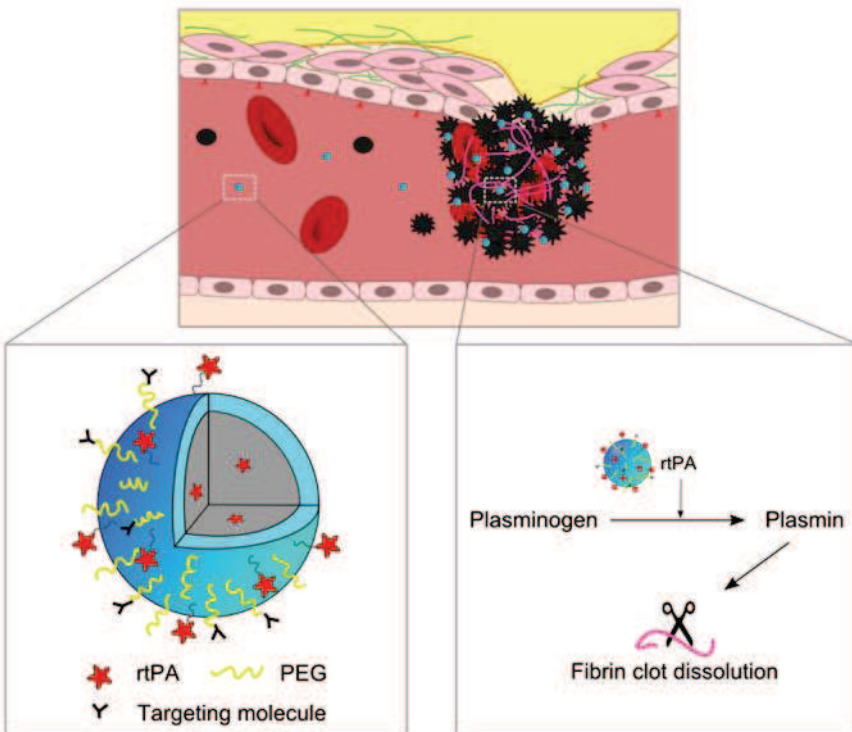


Fig. 4. Schematic representation of thrombolysis induced by nanocarriers. Most of developed nanocarriers loaded with thrombolytic agents (rtPA) are protected with a PEG shell. A targeting molecule can be used in order to enhance accumulation of the particles into the thrombus. Inside the thrombus, the rtPA activates plasminogen into plasmin which dissolves the fibrin clot.

5.1. Preclinical development

5.1.1. Polymer-based platforms

Among polymer materials, PEGylated polyvinyl-alcohol (PVA) nanocapsules encapsulating streptokinase were developed by Leach *et al.* The same quantity of streptokinase, free or loaded into nanocapsules, was injected into dogs with coronary artery thrombosis. The authors observed that dogs receiving streptokinase loaded in nanocapsules, showed an enhanced thrombolytic activity with a reduction of clot size and also a reduction of bleeding complications.⁹³ This enhancement of thrombolysis was explained by the greater penetration of encapsulated agent into clots compared to un-encapsulated streptokinase.⁹⁴ Nanoparticles composed of a polymer mixture made by chitosan and tripolyphosphate and coated with urokinase with a final size of 236 nm, were prepared by Jin *et al.* The authors obtained a high drug encapsulation efficiency of urokinase ($94.8 \pm 2.1\%$). When injected into rabbits with jugular thrombosis, an increased capacity of clot lysis compared to free urokinase was observed.⁹⁵ One possible reason could be that the encapsulation protects urokinase from degradation and induces also a slow release of the encapsulated drug.

Uesugi *et al.* have developed PEGylated gelatin nanoparticles (192 nm) loaded with rtPA. When injected into a rabbit with femoral artery thrombosis, the half-life of rtPA was enhanced by a factor of three, due to its complexation with gelatin. Despite the fact that rtPA activity was 45% lower than the original rtPA, the application of ultrasound (1MHz, up for 60 minutes) induced a complete re-canalization compared to nanoparticles-rtPA alone. This

recanalization can be explained by the fact that the rtPA activity was fully recovered after the dissociation of rtPA from gelatin.⁹⁶ Later, the same team tested gelatin nanoparticles (100 to 150 nm) loaded with rtPA in swine with acute myocardial infarction with a thrombotic occlusion of left coronary artery. They applied trans-thoracic ultrasound (1.0 MHz, 40 minutes) after administration of either nanoparticles containing rtPA (55 000 UI/kg) or rtPA alone. A re-canulation in 9 of the 10 animals was observed in swine receiving rtPA nanoparticles. When rtPA alone was administered, only one out of ten animals showed complete re-canulation (Table 1).⁹⁷

Composition/ Coating/Drug	Advantages	Drawbacks	Ref
Gelatin-zinc acetate/rtPA	Enhanced thrombolytic activity	45% suppression of rtPA activity when complexed with nanoparticles	96,97
Poly viny-alcool/PEG/ streptokinase	Enhancement of thrombolytic activity High accumulation into clot		93,94
Chitosan and tripolyphosphate/ urokinase	Drug encapsulation efficiency of urokinase		95
	Increased thrombolytic efficacy		

Table 1. Examples of thrombolytic drug delivery using polymer-based (nano)carriers in preclinical models.

5.1.2. Magnetic platforms

Magnetic nanoparticles are equally promising candidates for therapy. Under a non-uniform magnetic field obtained with a magnet, the nanoparticles have the tendency to approach the magnet. This property was largely used in order to attract and retain the magnetic nanoparticles at a specific site. Thus, cells labelled with magnetic nanoparticles were used in the tissue engineering and regenerative medicine for cardiovascular applications.⁹⁸ Substitutes of vessels were coated with a uniform layer of endothelial progenitor cells through the use of magnetic forces on the cells labeled by the nanomagnets.^{99,100} Another study showed a therapeutic benefit of the magnetic targeting of stem cells in cardiac cell therapy. Autologous cardiac stem cells labeled with magnetic particles were attracted toward the magnet and accumulated in the ischemic area of a mouse's heart.¹⁰¹

Magnetic nanoparticles conjugated with thrombolytic agents show interesting theranostic properties (Table 2). Bi *et al.* synthesized dextran coated magnetic nanoparticles conjugated with urokinase, with a final size of 116 nm. These nanoparticles were injected into rats with carotid artery and left jugular vein thrombosis. Using two discal permanent magnets around the site of the thrombus, the nanoparticles were concentrated at the thrombotic site. The thrombolytic activity was 5 times higher in rats receiving urokinase-coated nanoparticles than in rats receiving only urokinase.¹⁰²

Composition/ Coating/Drug	Advantages	Drawbacks	Ref
Dextran/urokinase	Enhancement of thrombolytic activity		102
PEG/rtPA	Reduced amounts of rtPA necessary to obtain the restauration of blood flow	Low amounts of rtPA loaded	103
Poly [aniline-co-N-(1-one-butyric acid) aniline]/rtPA	High amount of rtPA loaded; no haematological toxicity		104
PEG/rtPA	Very low amounts of rtPA necessary to the restoration of blood flow	Reduced number of animals	105
Dextran/PEG spacer/ FXIIIa target/rtPA	Thrombus targeted with FXIIIa factor	Steric hindrance ; reduced activity of rtPA	106

Table 2. Examples of thrombolytic drug delivery using magnetic (nano)carriers in preclinical models.

Ma *et al.* used magnetic nanoparticles (246 nm size) coated with polyacrylic acid and covalently coupled with rtPA (PAA-MNP-rtPA), for a targeted thrombolysis. After injection into rats with iliac artery embolisms and concentration into thrombus under external magnetic guidance, the blood flow was restored 75 minutes later. This effect was obtained with an equivalent of 0.2 mg/kg of rtPA coupled with magnetic nanoparticles. Free rtPA administration of a dose of 0.5 mg/kg did not show any effect in rats, while with a dose of 1 mg/kg, the blood flow restoration occurred within 30 minutes.¹⁰³ Similar results were obtained with rtPA immobilized on chitosan-coated nanoparticles.¹⁰⁷ In order to improve the drug-carrying capacities, magnetic nanoparticles (with a size of 12 - 14.8 nm) were developed with a shell of poly [aniline-co-N-(1-one-butyric acid) aniline]. The amount of rtPA loaded with this polymer was 50% higher than that obtained previously with PAA-MNP. These magnetic nanocarriers were injected into rats with iliac embolism and guided using an external magnet into the clot. The authors observed a restoration of blood flow within 15–25 minutes of treatment without hematological toxicity.¹⁰⁴ However a limitation of this method is that the magnetic field generated by an external magnet decreases with the deep localization into the body, leading to difficulties to target a specific area.

A strategy for improving magnetic force is to use ferromagnetic stents. Along these lines, a recombinant tissue plasminogen activator covalently coupled with PEGylated magnetic nanoparticles (rtPA-NP) was tested for the treatment of in-stent thrombosis. The amount of drug loaded on the surface of the nanoparticles was between 63 and 71 µg/mg, with an enzyme activity yield between 41-45 %. These nanoparticles were injected to treat thrombosis in pigs with ferromagnetic stents in the coronary artery and an external magnet. The restoration of blood flow was reached with an amount of rtPA-NP corresponding to 0.38 mg of free rtPA. This dose is lower than the dose administered in humans (100 mg for 90 minutes).¹⁰⁵ However, a limitation of this study is the low number of animals used (n=2) and the fact that the authors did not compare with the animals receiving only rtPA (control group). The McCarthy team designed magnetic nanoparticles for thrombus targeting without an external magnetic field but targeted with a peptide. They used cross-linked dextran-coated iron oxide nanoparticles (CLIO) with a size between 10 and 30 nm and coupled with rtPA. A PEG spacer moiety was added to minimize the steric interactions and to increase the distance between the fibrinolytic drug and the particles. The nanoparticles targeted a component of thrombi named activated factor XIII (FXIIIa) via peptide affinity ligands. These nanoparticles were injected in mice with pulmonary embolisms obtained with human clots. The injection of the same amount of rtPA loaded or not to CLIO showed a similar or slightly lower efficacy as compared with free rtPA. This study represents the proof of principle of thrombus targeted fibrinolytic agent using a peptide without an external magnetic field.¹⁰⁶ Zhou *et al.* developed magnetic nanocarriers loaded with rtPA and a peptide for a specific accumulation in abdominal aorta thrombi in rats.⁷²

These studies showed that thrombolytic drugs loaded to magnetic nanoparticles, directed to a specific site with an external magnetic field or with peptides, could enhance thrombolysis with a smaller quantity of the drug and thus circumvent the undesirable side effects.

5.1.3. Lipid-based platforms

Liposomes are largely used for therapy. Since the works in 1960 by the Bangham team^{108,109}, liposome technology continues to be developed and improved. The first liposomes developed were uncoated and rapidly cleared by the reticuloendothelial system. Stealth liposomes, obtained after incorporation of a hydrophilic polymer, such as poly (ethylene)-glycol (PEG) at the surface, showed an increased circulation time into the body¹¹⁰ while targeting liposomes can improve the specific delivery of therapeutics.¹¹¹ These nanocarriers protect thrombolytic drugs, reducing their side effects.

Leach *et al.* have encapsulated streptokinase into naked liposomes and injected them in rabbits with carotid artery thrombosis. The efficacy of encapsulation of streptokinase into liposomes was 30%. They compared the thrombolytic effect of 6000 UI/kg free streptokinase with streptokinase encapsulated into liposomes. Two hours after drug administration, they showed that the thrombolytic effect was improved with liposome-loaded streptokinase.¹¹² Encapsulation into liposomes protects the drug from premature inactivation into the blood. However, the authors noted some difficulties with the stability of the liposomes and low encapsulation efficacy.

Streptokinase encapsulation into liposomes, with 18% efficacy of entrapment, was carried out by Vaidya *et al.* The authors loaded the liposomes with arginine-glycine-aspartic acid (RGD) peptide. These liposomes, with a size between 100 and 200 nm, were injected into rats with carotid thrombosis obtained with a human clot. Thirty minutes after treatment, a higher thrombolytic activity was observed in rats receiving liposomes encapsulating streptokinase compared to streptokinase alone (28 % versus 17 % respectively). This thrombolytic effect was explained by a higher accumulation of liposomes in the thrombus area.¹¹³

Tissue plasminogen activator encapsulated into PEGylated (173nm) and non PEGylated (150nm) liposomes showed an entrapment efficacy of approximately 20%. When injected into rats, encapsulated rtPA showed a prolonged circulation time (21 and 16 fold respectively).¹¹⁴ Targeted stealth liposomes were developed by Absar *et al.* They loaded rtPA with PEGylated or non PEGylated liposomes decorated with a peptide sequence (CQQHHLGGAKQAGDV) of fibrinogen gamma-chain targeting GPIIb/IIIa on activated platelets. The entrapment efficacy of the non PEGylated liposomes was between 12 and 26%, whereas for PEGylated liposomes was higher, between 36 and 52%. When injected into rats with inferior vena cava thrombosis, an increased half-life was observed for rtPA loaded into PEGylated and not PEGylated liposomes (141 and 103 minutes respectively). Compared to native rtPA, an enhancement of 35% of thrombolytic activity was observed in rtPA-loaded into the peptide-linked pegylated liposomes.¹¹⁵

In order to target thrombolytic activity, perfluorocarbon (PFC) nanoparticles loaded with urokinase were used by different research teams.¹¹⁶ Marsh *et al.* have developed PFC nanoparticles covalently coupled with an anti-fibrin antibody and urokinase. The nanoparticles had 20 antibody and 200 urokinase molecules attached to their surface for a final size of 240 nm. When injected into dogs with femoral thrombosis, the authors showed that the dissolution of plasma clots was higher in animals receiving urokinase-functionalized PFC nanoparticles compared to the control group receiving irrelevant IgG targeted urokinase nanoparticles (Table 3).¹¹⁷

Composition/ Coating/Drug	Advantages	Drawbacks	Ref
Liposome/PEG/peptide (CQQHHLGGAKQAGDV)/rtPA	Enhanced thrombolytic activity; reduced haemorrhagic risk		¹¹⁵
Perfluorocarbon/anti-fibrin antibody/ urokinase	Enhanced thrombolytic activity	Possible steric inhibition of urokinase activity by the anti-fibrin antibody	¹¹⁷
ELIP/rtPA	Prolonged circulation time for rtPA ; enhanced thrombolytic activity for ELIP/rtPA associated with ultrasound	Low amounts of rtPA encapsulated	¹¹⁸
Perfluorocarbon/RGD peptide	High recanalization rate when PFC/RGD peptide is associated with iv rtPA and ultrasound	Low recanalization rate for PFC and ultrasound	¹¹⁹
Microbubbles±ultrasounds	Equivalent to rtPA for restoration of blood flow		¹²⁰
Microbubbles/±rtPA/ ultrasounds	High recanalization rate for microbubble, rtPA associated to ultrasound		¹²¹
Microbubbles/urokinase/±ultrasounds	High recanalization rate for microbubble, urokinase associated with ultrasound		^{122,123}

Table 3. Examples of thrombolytic drug delivery using lipid-based (nano)carriers in preclinical models.

5.1.4. Sonothrombolysis associated to microbubbles as adjuvant therapy

In experimental preclinical studies, ultrasound was used as an adjuvant to enhance re-canalisation rate (sonothrombolysis). Excellent reviews summarized sonothrombolysis in preclinical studies.^{124,125} The added value of ultrasounds was demonstrated using different types of lipid-based carriers.

Echogenic liposomes (ELIP) composed by phospholipids bilayer vesicles with both gas and fluid were synthesized by Laing *et al.* These liposomes were loaded with rtPA, with 15% entrapment in the core and 35% associated with the bilayer.¹¹⁸ In order to compare the thrombolytic activity of these carriers, they injected them into rabbits with an aorta thrombus. Their results showed that encapsulated tPA had an enhanced circulation time into the blood. Moreover, the efficacy for thrombus dissolution of encapsulated rtPA was similar to the free drug. The addition of 5.7 MHz ultrasound for two minutes, significantly enhanced lytic treatment efficacy for both rtPA and rtPA ELIP.¹²⁶

Echogenic liposomes (with a size < 200 nm) grafted or not with RGD peptides were developed by Hagisawa *et al.* When injected into rabbits with iliac artery occlusion, they showed a higher re-canalisation rate (9 of 10 rabbits) when ultrasounds were applied, compared to the animals receiving not targeted liposomes (2 of 10 rabbits) or receiving rtPA monotherapy (27 500 IU kg⁻¹).¹¹⁹

Microbubbles (MBs), with a size between 2 and 8 µm, composed by a phospholipid, a polymer or an albumin shell, and air or high molecular weight gas in the core, were already used as contrast agents in echography.¹²⁴ Alone or with rtPA, they have been combined with ultrasounds in order to enhance re-canalisation rate.¹²⁷ In rats with acute cerebral ischemia, Moumouh *et al.* showed that the treatment with intravenous rtPA (n=5) or microbubbles and ultrasound (n=5) were equivalent in the restoration of blood flow.¹²⁰ Nedelmann *et al.* have worked on a larger number of rats (n=25 per group) with occlusion of the right middle cerebral artery. They showed that rtPA alone partially improved hemispheric perfusion, while the association of rtPA, microbubbles and ultrasounds completely restored the blood flow.¹²¹ A better re-canalisation rate was also obtained with urokinase, microbubbles and transcranial Doppler ultrasounds (2MHz) when compared with the results obtained on rabbits receiving only urokinase.¹²² Similar results were observed in pigs with coronary thrombotic occlusion.¹²³

A smaller quantity of r tPA was necessary to obtain a beneficial effect on rabbits with carotid artery clot when microbubbles and trans-cutaneous pulsed ultrasound (1MHz) were applied.¹²⁸ Several mechanisms have been proposed to explain the phenomenon of ultrasound enhanced thrombolysis including acoustic cavitation,¹²⁹⁻¹³¹ thermal effects¹³² and micro-streaming.¹³³

These preclinical results showed on one hand that sonothrombolysis could be equivalent to the efficacy of thrombolytic drugs. On the other hand, the association of ultrasound, microbubbles and thrombolytics enhanced the re-canalisation rate.

5.2. Clinical use

Only microbubbles were tested in clinics for thrombolytic therapy with or without ultrasound (Table 4). Microbubbles and ultrasound, associated or not with thrombolytics, showed encouraging results.¹³⁴ Molina *et al.* in their clinical trial, included 111 patients with middle cerebral artery occlusions. 38 patients received tPA and galactose-based microbubbles plus 2 hours continuous 2 MHz pulsed waves transcranial Doppler (TCD) monitoring and another 73 patients received either tPA and ultrasound or only tPA. This study showed that a high re-canalization rate was observed in the group with tPA, continuous 2 MHz TCD and microbubbles when compared with groups receiving tPA and ultrasounds or tPA alone.¹³⁵ Later, they showed in the TUCSON trial (Transcranial Ultrasound in Clinical Sonothrombolysis), conducted on 35 patients receiving either intravenously (*iv*) tPA, 2MHz TCD and perflutren lipid (MRX-801) or standard *iv* tPA, that the complete re-canalisation rates at the end of TCD monitoring were 67% and 46% respectively.¹³⁶

Another clinical trial was carried out by Alexandrov *et al.*, on 15 patients receiving tPA, 2MHz continuous TCD monitoring and perflutren-lipid based microbubbles (n=12) or only tPA and ultrasound (n=3). The authors observed a complete recanalization rate in 50% of patients (6/12) while none reached complete recanalization in the control group.¹³⁷ Perren *et al.*, evaluated the recanalization rate in 26 patients receiving intravenous rtPA and phospholipid encapsulated sulphur hexafluoride microbubbles combined with 60 minutes of transcranial color-coded duplex (TCCD) ultrasound monitoring (n=11). They compared with patients receiving only rtPA and ultrasound (n=15). This study showed a higher recanalization rate in patients receiving microbubbles (64%) compared to patients without microbubbles (53%). This could be explained by the fact that the streaming of microbubbles under ultrasound pulses induces mechanical damages at the surface of the thrombus allowing a higher penetration of rtPA into the thrombus.¹³⁸ Pagola *et al.* have determined the time of recanalization rate in patients with stroke with basilar artery occlusion. All 20 patients have received *iv* tPA with two hours continuous ultrasound and galactose based microbubbles. They observed a difference between the recanalization rates in these patients. Only 10 patients showed a progressive recanalization rate while 10 others do not show any recanalization rate at 24 hours.¹³⁹ On 138 patients with stroke with middle cerebral artery occlusion, Rubiera *et al.* compared the outcome of patients receiving rtPA, and one of two different types of microbubbles galactose based and phospholipid encapsulated sulphur-hexafluoride based and underwent 2 MHz transcranial Doppler. The recanalization was similar in both groups despite the different characteristics of microbubbles.¹⁴⁰

These clinical trials showed that microbubbles associated with ultrasounds could be an interesting tool for increasing recanalization rates in patients with stroke. Another advantage could be the reduction of the drug quantity administered to obtain a beneficial effect, thus limiting intracranial bleeding.

Patients (n=)	Therapy procedures	Outcomes	Ref
111	Group 1: tPA/US 2MHz TCD 2 hours monitoring (n=73) Group 2: tPA/US 2MHz TCD 2 hours monitoring/Galactose-based MBs (n=38)	Group 1: 38% recanalization rate Group 2: 55% recanalization rate	135
15	Group 1: tPA/US 2MHz TCD 2 hours monitoring/Perflutren-based MBs (n=12)	Group 1: complete recanalization rate 6/12	137
	Group 2: tPA/US 2MHz TCD 2 hours monitoring (n=3)	Group 2: none reached complete recanalization rate	
35	Group 1: tPA/2MHz TCD/Perflutren lipid microspheres MRX-801 (n = 23) Group 2: tPA/Brief TCD assessments (n= 12)	Rate of recanalization higher in group 1 without statistical significance	136
26	Group 1: rtPA/60 min TCCD pulsed-wave monitoring/Phospholipid MBs encapsulating sulphur hexafluoride (n=11)	Group 1: recanalization rate (53 %)	138
	Group 2: rtPA/60 min TCCD pulsed-wave monitoring (n=15)	Group 2: recanalization rate (64%)	
20	rtPA/2 hours TCD monitoring/Galactose-based MBs	10 patients with progressive recanalization: 10% raised at 1 hour, 50% raised at 24 hours 10 patients showed no recanalization	139
138	Group 1: rtPA/Galactose-based air filled MBs (n=91)	Similar recanalization rate at 6 hours	140
	Group 2: rtPA/Sulphur hexafluoride-filled MBs (n=47)		

Table 4. Clinical trials in patients with stroke receiving thrombolytic drug associated or not with microbubbles (MBs) and/or ultrasound.

5. Conclusions and Outlook

Molecular imaging with nano- and microsystems provides precise information on the expression of specific biomarkers compared to conventional imaging. This allows an improved understanding and a better management of the cardiovascular diseases. Materials have been validated for the development of micro- and nanocarriers *in vitro* and in animal models. Despite development of several versatile platforms in preclinical research, only two types of systems have been tested in clinical trials for cardiovascular imaging; microbubbles and iron oxide based particles. For therapy, no system loaded with a therapeutic drug exists yet in clinics in the cardiovascular domain. It would be of a great importance to improve existing preclinical systems that are biocompatible, biodegradable and of low toxicity for clinical applications. The actual limitations are linked to the amount of drug encapsulated, the possibility to control the release, and the specific targeting. When these limitations will be overwhelmed a new era will be open for personalized cardiovascular medicine.

Acknowledgments

This study was supported by Inserm, University Paris 13 and University Paris Diderot, France. This work was also supported in part by the EU project NanoAthero FP7-NMP-2012-LARGE-6-309820, Lefoulon – Delalande scholarship (to MV), IMOVA project (FUI/OSEO, CG93), and ANR-13-LAB1-0005-01 “FucoChem”.

References

1. A. S. Go, D. Mozaffarian, V. L. Roger, E. J. Benjamin, J. D. Berry, W. B. Borden, D. M. Bravata, S. Dai, E. S. Ford, C. S. Fox, S. Franco, H. J. Fullerton, C. Gillespie, S. M. Hailpern, J. A. Heit, V. J. Howard, M. D. Huffman, B. M. Kissela, S. J. Kittner, D. T. Lackland, J. H. Lichtman, L. D. Lisabeth, D. Magid, G. M. Marcus, A. Marelli, D. B. Matchar, D. K. McGuire, E. R. Mohler, C. S. Moy, M. E. Mussolini, G. Nichol, N. P. Paynter, P. J. Schreiner, P. D. Sorlie, J. Stein, T. N. Turan, S. S. Virani, N. D. Wong, D. Woo and M. B. Turner, *Circulation*, **e6** (2013).
2. A. J. Lusis, *Nature*, **233** (2000).
3. P. Libby, M. DiCarli and R. Weissleder, *J. Nucl. Med.*, **33S** (2010).
4. P. Libby, *J. Lipid Res.*, **S352** (2009).
5. E. D. Hood, M. Chorny, C. F. Greineder, S. A. I, R. J. Levy and V. R. Muzykantov, *Biomaterials*, **3708** (2014).
6. K. Douma, L. Prinzen, D. W. Slaaf, C. P. Reutelingsperger, E. A. Biessen, T. M. Hackeng, M. J. Post and M. A. van Zandvoort, *Small*, **544** (2009).
7. A. Klink, F. Hyafil, J. Rudd, P. Faries, V. Fuster, Z. Mallat, O. Meilhac, W. J. Mulder, J. B. Michel, F. Ramirez, G. Storm, R. Thompson, I. C. Turnbull, J. Egido, J. L. Martin-Ventura, C. Zaragoza, D. Letourneur and Z. A. Fayad, *Nat. Rev. Cardiol.*, **338** (2011).
8. V. J. Dzau, R. C. Braun-Dullaeus and D. G. Sedding, *Nat. Med.*, **1249** (2002).
9. J. E. Feig, B. Hewing, J. D. Smith, S. L. Hazen and E. A. Fisher, *Circ. Res.*, **205** (2014).
10. L. N. Marzec and T. M. Maddox, *Curr. Cardiol. Rep.*, **418** (2013).
11. D. J. Rader and G. K. Hovingh, *Lancet*, **618** (2014).
12. C. Weber and H. Noels, *Nat. Med.*, **1410** (2011).
13. C. R. Sirtori, *Pharmacol. Res.*, **3** (2014).
14. D. Collen and H. R. Lijnen, *Thromb. Haemost.*, **627** (2005).
15. G. Lippi, R. Rossi, L. Ippolito, V. Zobbi, D. Azzi, S. Pipitone, E. J. Favoloro and D. M. Funk, *Semin. Thromb. Hemost.*, **834** (2013).
16. J. Alvarez-Sabin, O. Maisterra, E. Santamarina and C. S. Kase, *Lancet Neurol.*, **689** (2013).
17. W. J. Mulder, G. J. Strijkers, G. A. van Tilborg, A. W. Griffioen and K. Nicolay, *NMR Biomed.*, **142** (2006).
18. N. S. Faithfull, C. E. King and S. M. Cain, *Microvasc. Res.*, **183** (1987).
19. U. Kaisers, K. P. Kelly and T. Busch, *Br. J. Anaesth.*, **143** (2003).
20. J. Chen, H. Pan, G. M. Lanza and S. A. Wickline, *Adv. Chronic Kidney Dis.*, **466** (2013).
21. R. Diaz-Lopez, N. Tsapis and E. Fattal, *Pharm. Res.*, **1** (2010).
22. J. C. Frias, K. J. Williams, E. A. Fisher and Z. A. Fayad, *J. Am. Chem. Soc.*, **16316** (2004).
23. A. K. Silva, D. Letourneur and C. Chauvierre, *Theranostics*, **579** (2014).
24. F. Danhier, E. Ansorena, J. M. Silva, R. Coco, A. Le Breton and V. Preat, *J. Control. Release*, **505** (2012).
25. M. Di Marco, C. Sadun, M. Port, I. Guibert, P. Couvreur and C. Dubernet, *Int. J. Nanomedicine*, **609** (2007).
26. Y. Javed, L. Lartigue, P. Hugounenq, Q. L. Vuong, Y. Gossuin, R. Bazzi, C. Wilhelm, C. Ricolleau, F. Gazeau and D. Alroyeau, *Small*, **3325** (2014).
27. J. M. Tarkin, F. R. Joshi and J. H. Rudd, *Nat. Rev. Cardiol.*, **443** (2014).
28. N. Tahara, H. Kai, M. Ishibashi, H. Nakaura, H. Kaida, K. Baba, N. Hayabuchi and T. Imaizumi, *J. Am. Coll. Cardiol.*, **1825** (2006).
29. F. Rouzet, L. Bachelet-Violette, J. M. Alsac, M. Suzuki, A. Meulemans, L. Louedec, A. Petiet, M. Jandrot-Perrus, F. Chaubet, J. B. Michel, D. Le Guludec and D. Letourneur, *J. Nucl. Med.*, **1433** (2011).
30. P. Saboural, F. Chaubet, F. Rouzet, F. Al-Shoukr, R. B. Azzouna, N. Bouchemal, L. Picton, L. Louedec, M. Maire, L. Rolland, G. Potier, D. L. Guludec, D. Letourneur and C. Chauvierre, *Mar. Drugs*, **4851** (2014).
31. M. R. Stacy, W. Zhou and A. J. Sinusas, *J. Nucl. Med.*, **2104** (2013).
32. C. J. Anderson, J. W. Bulte, K. Chen, X. Chen, B. A. Khaw, M. Shokeen, K. L. Wooley and H. F. VanBrocklin, *J. Nucl. Med.*, **3S** (2010).
33. A. Beilvert, D. P. Cormode, F. Chaubet, K. C. Briley-Saebo, V. Mani, W. J. Mulder, E. Vucic, J. F. Toussaint, D. Letourneur and Z. A. Fayad, *Magn. Reson. Med.*, **1195** (2009).
34. J. Vymazal, E. Spuentrup, G. Cardenas-Molina, A. J. Wiethoff, M. G. Hartmann, P. Caravan and E. C. Parsons, Jr., *Investig. Radiol.*, **697** (2009).
35. M. R. Makowski, S. C. Forbes, U. Blume, A. Warley, C. H. Jansen, A. Schuster, A. J. Wiethoff and R. M. Botnar, *Atherosclerosis*, **43** (2012).
36. J. C. De La Vega and U. O. Hafeli, *Contrast Media Mol. Imaging*, (2014).
37. E. Jin and Z. R. Lu, *Biomaterials*, **5822** (2014).
38. H. Boll, S. Nittka, F. Doyon, M. Neumaier, A. Marx, M. Kramer, C. Groden and M. A. Brockmann, *PLoS One*, **e25692** (2011).
39. B. Trachet, R. A. Fraga-Silva, A. Piersigilli, A. Tedgui, J. Sordet-Dessimoz, A. Astolfo, C. Van der Donckt, P. Modregger, M. F. Stampanoni, P. Segers and N. Stergiopoulos, *Cardiovasc. Res.*, **213** (2015).
40. T. R. Porter, *J. Am. Coll. Cardiol.*, **491** (2000).
41. S. Hak, H. M. Sanders, P. Agrawal, S. Langereis, H. Grull, H. M. Keizer, F. Arena, E. Terreno, G. J. Strijkers and K. Nicolay, *Eur. J. Pharm. Biopharm.*, **397** (2009).
42. S. Flacke, S. Fischer, M. J. Scott, R. J. Fuhrhop, J. S. Allen, M. McLean, P. Winter, G. A. Sicard, P. J. Gaffney, S. A. Wickline and G. M. Lanza, *Circulation*, **1280** (2001).
43. J. C. Frias, Y. Ma, K. J. Williams, Z. A. Fayad and E. A. Fisher, *Nano Lett.*, **2220** (2006).
44. G. A. van Tilborg, E. Vucic, G. J. Strijkers, D. P. Cormode, V. Mani, T. Skajaa, C. P. Reutelingsperger, Z. A. Fayad, W. J. Mulder and K. Nicolay, *Bioconjug. Chem.*, **1794** (2010).

45. V. Amirbekian, M. J. Lipinski, K. C. Briley-Saebo, S. Amirbekian, J. G. Aguinaldo, D. B. Weinreb, E. Vucic, J. C. Frias, F. Hyafil, V. Mani, E. A. Fisher and Z. A. Fayad, *Proc. Natl. Acad. Sci. U. S. A.*, **96**1 (2007).
46. W. Chen, D. P. Cormode, Y. Vengrenyuk, B. Herranz, J. E. Feig, A. Klink, W. J. Mulder, E. A. Fisher and Z. A. Fayad, *JACC Cardiovasc. Imaging*, **3**73 (2013).
47. S. M. Demos, H. Alkan-Onyuksel, B. J. Kane, K. Ramani, A. Nagaraj, R. Greene, M. Klegerman and D. D. McPherson, *J. Am. Coll. Cardiol.*, **8**67 (1999).
48. H. Kim, P. H. Kee, Y. Rim, M. R. Moody, M. E. Klegerman, D. Vela, S. L. Huang, D. D. McPherson and S. T. Laing, *Atherosclerosis*, **2**52 (2013).
49. A. Dellinger, J. Olson, K. Link, S. Vance, M. G. Sandros, J. Yang, Z. Zhou and C. L. Kepley, *J. Cardiovasc. Magn. Reson.*, **7** (2013).
50. T. Skajaa, D. P. Cormode, E. Falk, W. J. Mulder, E. A. Fisher and Z. A. Fayad, *Arterioscler. Thromb. Vasc. Biol.*, **1**69 (2010).
51. D. P. Cormode, T. Skajaa, M. M. van Schooneveld, R. Koole, P. Jarzyna, M. E. Lobatto, C. Calcagno, A. Barazza, R. E. Gordon, P. Zanzonicco, E. A. Fisher, Z. A. Fayad and W. J. Mulder, *Nano Lett.*, **3**715 (2008).
52. D. P. Cormode, E. Roessl, A. Thran, T. Skajaa, R. E. Gordon, J. P. Schlomka, V. Fuster, E. A. Fisher, W. J. Mulder, R. Proksa and Z. A. Fayad, *Radiology*, **7**74 (2010).
53. C. Jung, M. G. Kaul, O. T. Bruns, T. Ducic, B. Freund, M. Heine, R. Reimer, A. Meents, S. C. Salmen, H. Weller, P. Nielsen, G. Adam, J. Heeren and H. Ittrich, *Circ. Cardiovasc. Imaging*, **3**03 (2014).
54. J. Ding, Y. Wang, M. Ma, Y. Zhang, S. Lu, Y. Jiang, C. Qi, S. Luo, G. Dong, S. Wen, Y. An and N. Gu, *Biomaterials*, **2**09 (2013).
55. T. D. Tran, S. D. Caruthers, M. Hughes, J. N. Marsh, T. Cyrus, P. M. Winter, A. M. Neubauer, S. A. Wickline and G. M. Lanza, *Int. J. Nanomedicine*, **5**15 (2007).
56. G. M. Lanza, K. D. Wallace, M. J. Scott, W. P. Cacheris, D. R. Abendschein, D. H. Christy, A. M. Sharkey, J. G. Miller, P. J. Gaffney and S. A. Wickline, *Circulation*, **3**334 (1996).
57. P. M. Winter, A. M. Neubauer, S. D. Caruthers, T. D. Harris, J. D. Robertson, T. A. Williams, A. H. Schmieder, G. Hu, J. S. Allen, E. K. Lacy, H. Zhang, S. A. Wickline and G. M. Lanza, *Arterioscler. Thromb. Vasc. Biol.*, **2**103 (2006).
58. M. Suzuki, L. Bachelet-Violette, F. Rouzet, A. Beilvert, G. Autret, M. Maire, C. Menager, L. Louedec, C. Choqueux, P. Saboural, O. Haddad, C. Chauvierre, F. Chaubet, J. B. Michel, J. M. Serfaty and D. Letourneau, *Nanomedicine (Lond)*, **1** (2014).
59. T. Bonnard, G. Yang, A. Petiet, V. Ollivier, O. Haddad, D. Arnaud, L. Louedec, L. Bachelet-Violette, S. M. Derkaoui, D. Letourneau, C. Chauvierre and C. Le Visage, *Theranostics*, **5**92 (2014).
60. T. Bonnard, J. M. Serfaty, C. Journe, B. Ho Tin Noe, D. Arnaud, L. Louedec, S. M. Derkaoui, D. Letourneau, C. Chauvierre and C. Le Visage, *Acta Biomater.*, **3**535 (2014).
61. X. Wang, C. E. Hagemeyer, J. D. Hohmann, E. Leitner, P. C. Armstrong, F. Jia, M. Olschewski, A. Needles, K. Peter and I. Ahrens, *Circulation*, **3**117 (2012).
62. F. S. Villanueva, E. Lu, S. Bowry, S. Kilic, E. Tom, J. Wang, J. Gretton, J. J. Pacella and W. R. Wagner, *Circulation*, **3**45 (2007).
63. B. P. Davidson, B. A. Kaufmann, J. T. Belcik, A. Xie, Y. Qi and J. R. Lindner, *J. Am. Coll. Cardiol.*, **1**690 (2012).
64. B. A. Kaufmann, C. L. Carr, J. T. Belcik, A. Xie, Q. Yue, S. Chadderton, E. S. Caplan, J. Khangura, S. Bullens, S. Bunting and J. R. Lindner, *Arterioscler. Thromb. Vasc. Biol.*, **5**4 (2010).
65. W. Wu, Y. Wang, S. Shen, J. Wu, S. Guo, L. Su, F. Hou, Z. Wang, Y. Liao and J. Bin, *Investig. Radiol.*, **8**03 (2013).
66. G. Hu, C. Liu, Y. Liao, L. Yang, R. Huang, J. Wu, J. Xie, K. Bundhoo, Y. Liu and J. Bin, *Thromb. Haemost.*, **1**72 (2012).
67. S. Fokong, A. Fragoso, A. Rix, A. Curaj, Z. Wu, W. Lederle, O. Iranzo, J. Gatjens, F. Kiessling and M. Palmowski, *Investig. Radiol.*, **8**43 (2013).
68. M. D. Majmudar, J. Yoo, E. J. Keliher, J. J. Truelove, Y. Iwamoto, B. Sena, P. Dutta, A. Borodovsky, K. Fitzgerald, M. F. Di Carli, P. Libby, D. G. Anderson, F. K. Swirski, R. Weissleder and M. Nahrendorf, *Circ. Res.*, **7**55 (2013).
69. M. A. McAteer, K. Mankia, N. Ruparelia, A. Jefferson, H. B. Nugent, L. A. Stork, K. M. Channon, J. E. Schneider and R. P. Choudhury, *Arterioscler. Thromb. Vasc. Biol.*, **1**427 (2012).
70. H. P. Luehmann, E. D. Pressly, L. Detering, C. Wang, R. Pierce, P. K. Woodard, R. J. Gropler, C. J. Hawker and Y. Liu, *J. Nucl. Med.*, **6**29 (2014).
71. S. Marrache and S. Dhar, *Proc. Natl. Acad. Sci. U. S. A.*, **9**445 (2013).
72. J. Zhou, D. Guo, Y. Zhang, W. Wu, H. Ran and Z. Wang, *ACS Appl. Mater. Interfaces*, **5**566 (2014).
73. F. Hyafil, J. C. Cornily, J. E. Feig, R. Gordon, E. Vucic, V. Amirbekian, E. A. Fisher, V. Fuster, L. J. Feldman and Z. A. Fayad, *Nat. Med.*, **6**36 (2007).
74. Y. Song, Z. Huang, J. Xu, D. Ren, Y. Wang, X. Zheng, Y. Shen, L. Wang, H. Gao, J. Hou, Z. Pang, J. Qian and J. Ge, *Biomaterials*, **2**961 (2014).
75. K. Tsuchiya, N. Nitta, A. Sonoda, H. Otani, M. Takahashi, K. Murata, M. Shiomi, Y. Tabata and S. Nohara, *Eur. J. Radiol.*, **1**919 (2013).
76. C. von zur Muhlen, A. Fink-Petri, J. Salaklang, D. Paul, I. Neudorfer, V. Berti, A. Merkle, K. Peter, C. Bode and D. von Elverfeldt, *Contrast Media Mol. Imaging*, **2**68 (2010).
77. C. Burtea, S. Ballet, S. Laurent, O. Rousseaux, A. Dencausse, W. Gonzalez, M. Port, C. Corot, L. Vander Elst and R. N. Muller, *Arterioscler. Thromb. Vasc. Biol.*, **e3**6 (2012).
78. M. Michalska, L. Machtoub, H. D. Manthey, E. Bauer, V. Herold, G. Krohne, G. Lykowsky, M. Hildenbrand, T. Kampf, P. Jakob, A. Zernecke and W. R. Bauer, *Arterioscler. Thromb. Vasc. Biol.*, **2**350 (2012).
79. L. Josephson, C. H. Tung, A. Moore and R. Weissleder, *Bioconjug. Chem.*, **1**86 (1999).
80. M. Nahrendorf, H. Zhang, S. Hembrador, P. Panizzi, D. E. Sosnovik, E. Aikawa, P. Libby, F. K. Swirski and R. Weissleder, *Circulation*, **3**79 (2008).

81. W. J. Mulder, F. A. Jaffer, Z. A. Fayad and M. Nahrendorf, *Sci. Transl. Med.*, **239sr1** (2014).
82. M. Nahrendorf, E. Keliher, B. Marinelli, F. Leuschner, C. S. Robbins, R. E. Gerszten, M. J. Pittet, F. K. Swirski and R. Weissleder, *Arterioscler. Thromb. Vasc. Biol.*, **750** (2011).
83. B. R. Jarrett, C. Correa, K. L. Ma and A. Y. Louie, *PLoS One*, **e13254** (2010).
84. D. E. Kim, J. Y. Kim, I. C. Sun, D. Schellingerhout, S. K. Lee, C. H. Ahn, I. C. Kwon and K. Kim, *Ann. Neurol.*, **617** (2013).
85. I. Cicha, C. Garlichs and C. Alexiou, *Eur. J. Nanomed.*, (2014).
86. M. E. Kooi, V. C. Cappendijk, K. Cleutjens, A. G. H. Kessels, P. Kitslaar, M. Borgers, P. M. Frederik, M. Daemen and J. M. A. van Engelshoven, *Circulation*, **2453** (2003).
87. A. Saleh, M. Schroeter, A. Ringelstein, H. P. Hartung, M. Siebler, U. Modder and S. Jander, *Stroke*, **2733** (2007).
88. A. J. Degnan, A. J. Patterson, T. Y. Tang, S. P. Howarth and J. H. Gillard, *Cerebrovasc. Dis.*, **169** (2012).
89. Y. X. Wang, *Quant. Imaging Med. Surg.*, **35** (2011).
90. J. M. Richards, S. I. Semple, T. J. MacGillivray, C. Gray, J. P. Langrish, M. Williams, M. Dweck, W. Wallace, G. McKillop, R. T. Chalmers, O. J. Garden and D. E. Newby, *Circ. Cardiovasc. Imaging*, **274** (2011).
91. A. Yilmaz, S. Rosch, H. Yildiz, S. Klumpp and U. Sechtem, *Circulation*, **1932** (2012).
92. S. R. Alam, A. S. Shah, J. Richards, N. N. Lang, G. Barnes, N. Joshi, T. MacGillivray, G. McKillop, S. Mirsadraee, J. Payne, K. A. Fox, P. Henriksen, D. E. Newby and S. I. Semple, *Circ. Cardiovasc. Imaging*, **559** (2012).
93. J. K. Leach, E. Patterson and E. A. O'Rear, *Thromb. Haemost.*, **1213** (2004).
94. J. K. Leach, E. Patterson and E. A. O'Rear, *J. Thromb. Haemost.*, **1548** (2004).
95. H. J. Jin, H. Zhang, M. L. Sun, B. G. Zhang and J. W. Zhang, *J. Thromb. Thrombolysis*, **458** (2013).
96. Y. Uesugi, H. Kawata, J. Jo, Y. Saito and Y. Tabata, *J. Control. Release*, **269** (2010).
97. H. Kawata, Y. Uesugi, T. Soeda, Y. Takemoto, J. H. Sung, K. Umaki, K. Kato, K. Ogiwara, K. Nogami, K. Ishigami, M. Horii, S. Uemura, M. Shima, Y. Tabata and Y. Saito, *J. Am. Coll. Cardiol.*, **2550** (2012).
98. E. A. Lee, H. Yim, J. Heo, H. Kim, G. Jung and N. S. Hwang, *Arch. Pharmacal Res.*, **120** (2014).
99. D. Robert, D. Fayol, C. Le Visage, G. Frasca, S. Brule, C. Menager, F. Gazeau, D. Letourneau and C. Wilhelm, *Biomaterials*, **1586** (2010).
100. D. Fayol, N. Luciani, L. Lartigue, F. Gazeau and C. Wilhelm, *Adv. Healthc. Mater.*, **313** (2013).
101. K. Cheng, T. S. Li, K. Malliaras, D. R. Davis, Y. Zhang and E. Marban, *Circ. Res.*, **1570** (2010).
102. F. Bi, J. Zhang, Y. Su, Y. C. Tang and J. N. Liu, *Biomaterials*, **5125** (2009).
103. Y. H. Ma, S. Y. Wu, T. Wu, Y. J. Chang, M. Y. Hua and J. P. Chen, *Biomaterials*, **3343** (2009).
104. H. W. Yang, M. Y. Hua, K. J. Lin, S. P. Wey, R. Y. Tsai, S. Y. Wu, Y. C. Lu, H. L. Liu, T. Wu and Y. H. Ma, *Int. J. Nanomedicine*, **5159** (2012).
105. M. Kempe, H. Kempe, I. Snowball, R. Wallen, C. R. Arza, M. Gotberg and T. Olsson, *Biomaterials*, **9499** (2010).
106. J. R. McCarthy, I. Y. Sazonova, S. S. Erdem, T. Hara, B. D. Thompson, P. Patel, I. Botnaru, C. P. Lin, G. L. Reed, R. Weissleder and F. A. Jaffer, *Nanomedicine (Lond)*, **1017** (2012).
107. J. P. Chen, P. C. Yang, Y. H. Ma and T. Wu, *Carbohydr. Polym.*, **364** (2011).
108. D. Deamer and A. D. Bangham, *Biochim. Biophys. Acta*, **629** (1976).
109. S. M. Johnson, A. D. Bangham, M. W. Hill and E. D. Korn, *Biochim. Biophys. Acta*, **820** (1971).
110. S. M. Moghimi and J. Szebeni, *Prog. Lipid Res.*, **463** (2003).
111. S. Gurudevan, R. K. Kanwar, R. N. Veedu, S. Sasidharan, R. L. Kennedy, K. Walder, N. Prasad and J. R. Kanwar, *Curr. Gene Ther.*, **322** (2013).
112. J. K. Leach, E. A. O'Rear, E. Patterson, Y. Miao and A. E. Johnson, *Thromb. Haemost.*, **64** (2003).
113. B. Vaidya, G. P. Agrawal and S. P. Vyas, *Eur. J. Pharm. Sci.*, **589** (2011).
114. J. Y. Kim, J. K. Kim, J. S. Park, Y. Byun and C. K. Kim, *Biomaterials*, **5751** (2009).
115. S. Absar, K. Nahar, Y. M. Kwon and F. Ahsan, *Pharm. Res.*, **1663** (2013).
116. G. M. Lanza, P. M. Winter, S. D. Caruthers, M. S. Hughes, G. Hu, A. H. Schmieder and S. A. Wickline, *Angiogenesis*, **189** (2010).
117. J. N. Marsh, G. Hu, M. J. Scott, H. Zhang, M. J. Goette, P. J. Gaffney, S. D. Caruthers, S. A. Wickline, D. Abendschein and G. M. Lanza, *Nanomedicine (Lond)*, **605** (2011).
118. S. T. Laing, M. R. Moody, H. Kim, B. Smulevitz, S. L. Huang, C. K. Holland, D. D. McPherson and M. E. Klegerman, *Thromb. Res.*, **629** (2012).
119. K. Hagisawa, T. Nishioka, R. Suzuki, K. Maruyama, B. Takase, M. Ishihara, A. Kurita, N. Yoshimoto, Y. Nishida, K. Iida, H. Luo and R. J. Siegel, *J. Thromb. Haemost.*, **1565** (2013).
120. A. Moumouh, L. Barentin, F. Tranquart, S. Serriére, I. Bonnaud and J. P. Tasu, *Ultrasound Med. Biol.*, **51** (2010).
121. M. Nedelmann, N. Ritschel, S. Doenges, A. C. Langheinrich, T. Acker, P. Reuter, M. Yeniguen, J. Pukropski, M. Kaps, C. Mueller, G. Bachmann and T. Gerriets, *J. Cereb. Blood Flow Metab.*, **1712** (2010).
122. W. S. Liu, Z. Z. Huang, X. W. Wang and J. Zhou, *Thromb. Res.*, **547** (2012).
123. F. Xie, J. Lof, T. Matsunaga, R. Zutshi and T. R. Porter, *Circulation*, **1378** (2009).
124. M. de Saint Victor, C. Crake, C. C. Coussios and E. Stride, *Expert Opin. Drug Deliv.*, **187** (2014).
125. S. Ricci, L. Dinia, M. Del Sette, P. Anzola, T. Mazzoli, S. Cenciarelli and C. Gandolfo, *Cochrane Database Syst. Rev.*, **CD008348** (2012).
126. S. T. Laing, M. Moody, B. Smulevitz, H. Kim, P. Kee, S. Huang, C. K. Holland and D. D. McPherson, *Arterioscler. Thromb. Vasc. Biol.*, **1357** (2011).

127. F. Kiessling, S. Fokong, P. Koczera, W. Lederle and T. Lammers, *J. Nucl. Med.*, **34** (2012).
128. A. T. Brown, R. Flores, E. Hamilton, P. K. Roberson, M. J. Borrelli and W. C. Culp, *Investig. Radiol.*, **202** (2011).
129. E. A. Brujan, *Med. Eng. Phys.*, **742** (2009).
130. E. C. Everbach and C. W. Francis, *Ultrasound Med. Biol.*, **1153** (2000).
131. E. Unger, T. Porter, J. Lindner and P. Grayburn, *Adv. Drug Delivery. Rev.*, **110** (2014).
132. D. V. Sakharov, R. T. Hekkenberg and D. C. Rijken, *Thromb. Res.*, **333** (2000).
133. C. W. Francis, A. Blinc, S. Lee and C. Cox, *Ultrasound Med. Biol.*, **419** (1995).
134. G. Tsivgoulis, W. C. Culp and A. V. Alexandrov, *Ultrasonics*, **303** (2008).
135. C. A. Molina, M. Ribo, M. Rubiera, J. Montaner, E. Santamarina, R. Delgado-Mederos, J. F. Arenillas, R. Huertas, F. Purroy, P. Delgado and J. Alvarez-Sabin, *Stroke*, **425** (2006).
136. C. A. Molina, A. D. Barreto, G. Tsivgoulis, P. Sierzenski, M. D. Malkoff, M. Rubiera, N. Gonzales, R. Mikulik, G. Pate, J. Ostrem, W. Singleton, G. Manvelian, E. C. Unger, J. C. Grotta, P. D. Schellinger and A. V. Alexandrov, *Ann. Neurol.*, **28** (2009).
137. A. V. Alexandrov, R. Mikulik, M. Ribo, V. K. Sharma, A. Y. Lao, G. Tsivgoulis, R. M. Sugg, A. Barreto, P. Sierzenski, M. D. Malkoff and J. C. Grotta, *Stroke*, **1464** (2008).
138. F. Perren, J. Loulidi, D. Poglia, T. Landis and R. Sztajzel, *J. Thromb. Thrombolysis*, **219** (2008).
139. J. Pagola, M. Ribo, J. Alvarez-Sabin, M. Lange, M. Rubiera and C. A. Molina, *Stroke*, **2931** (2007).
140. M. Rubiera, M. Ribo, R. Delgado-Mederos, E. Santamarina, O. Maisterra, P. Delgado, J. Montaner, J. Alvarez-Sabin and C. A. Molina, *Ultrasound Med. Biol.*, **1573** (2008).



Contents lists available at ScienceDirect

Biochemical and Biophysical Research Communications

journal homepage: www.elsevier.com/locate/ybbrc

Review

Nanomedicine for the molecular diagnosis of cardiovascular pathologies

Maya Juenet ^{a,b,1}, Mariana Varna ^{a,b,1}, Rachida Aid-Launais ^{a,b}, Cédric Chauvierre ^{a,b,*}, Didier Letourneur ^{a,b}^a Inserm, U1148, Cardiovascular Bio-Engineering, X. Bichat Hospital, 75018, Paris, France^b Université Paris 13, Institut Galilée, Sorbonne Paris Cité, 75018, Paris, France

ARTICLE INFO

Article history:

Received 27 May 2015

Accepted 20 June 2015

Available online 27 June 2015

Keywords:

Nanomedicine

Atherosclerosis

Molecular imaging

Targeting

ABSTRACT

Predicting acute clinical events caused by atherosclerotic plaque rupture remains a clinical challenge. Anatomic mapping of the vascular tree provided by standard imaging technologies is not always sufficient for a robust diagnosis. Yet biological mechanisms leading to unstable plaques have been identified and corresponding biomarkers have been described. Nanosystems charged with contrast agents and targeted towards these specific biomarkers have been developed for several types of imaging modalities. The first systems that have reached the clinic are ultrasmall superparamagnetic iron oxides for Magnetic Resonance Imaging. Their potential relies on their passive accumulation by predominant physiological mechanisms in rupture-prone plaques. Active targeting strategies are under development to improve their specificity and set up other types of nanoplateforms. Preclinical results show a huge potential of nanomedicine for cardiovascular diagnosis, as long as the safety of these nanosystems in the body is studied in depth.

© 2015 Elsevier Inc. All rights reserved.

1. Introduction

Atherosclerosis is a slowly progressing pathophysiological process characterized by the formation of lipid-rich plaques in the intima of medium and large arteries. It is a major burden in Western societies principally induced by sedentism and rich fat diets [1]. Genetic factors play also an important role in the evolution of this disease [2]. The development of atherosclerosis itself is generally not fatal. However, atherosclerotic lesions became dangerous when they develop a thin fibrous cap and a large necrotic core [3]. In these conditions, plaques may break exposing thrombogenic substances to the circulation driving the formation of an intraluminal thrombus. Complications induced by thrombosis, such as ischemic stroke and myocardial infarction (also referenced as acute clinical events (ACE)), are and will remain the

Abbreviations: ACE, acute clinical event; MRA, magnetic resonance angiography; CT, computed tomography; AAA, Abdominal Aortic Aneurysm; MRI, Magnetic Resonance Imaging; ox-LDL, oxidized Low Density Lipoproteins; SMC, smooth muscle cell; ApoE^{-/-} mice, Apolipoprotein E Knockout mice; HDL, High Density Lipoprotein; PLGA, Poly(lactic-co-glycolic acid); PVA, polyvinyl alcohol; PEG, polyethylene glycol; MP, microparticle; MI/R, myocardial ischemia/reperfusion

* Corresponding author. Inserm U 1148, X. Bichat Hospital, 46 rue Henri Huchard, 75018, Paris, France.

E-mail address: cedric.chauvierre@inserm.fr (C. Chauvierre).

¹ Equal contribution.

leading cause of death in the world with more than 17 million of deaths per year [4].

Identifying people at risk to develop rupture-prone atherosclerotic plaques and predicting the rupture are therefore essential for a better care. Clinical methods performed to assess plaque evolution, such as Magnetic Resonance Angiography (MRA) and Angiography performed with Computed Tomography (CT) imaging, provide morphological information about the intraluminal stenosis generated by plaque growing. However, it has been observed that an advanced degree of stenosis is not necessarily characterizing unstable plaques.

Progresses have been made in biological understanding of phenomena leading to plaque rupture. Molecular markers more likely to be expressed in high-risk plaques have been identified, as well as some of their specific ligands. Targeting and imaging these biomarkers with contrast agents would enable to better identify plaque components and to provide information about the activation state conducive to plaque rupture.

Technological improvements in the field of medical imaging provide equipment with better resolution and sensitivity. Molecular imaging is now conceivable, as far as the specificity of the targeting method and the sensitivity of the imaging modality ensure injection of safe doses of contrast agents. To that end, nanoplateforms combining existing contrast agents with targeting units have been developed. They show exciting properties related

to their nanometric scale and to their potential for functionalization. Furthermore, they have great surface properties and can be tuned to interact preferentially with specific cells and plaque components.

This review highlights the relevance of nanomedicine for a personalized and robust diagnosis of atherosclerosis as well as for other types of lesions, such as Abdominal Aortic Aneurysms (AAA) and transient ischemic events. It describes the nanosystems in preclinical development and in clinical use for Magnetic Resonance Imaging (MRI), Nuclear Imaging and X-ray Computed Tomography (CT).

2. Molecular targets of cardiovascular pathologies

Among the different molecular and cellular targets identified in cardiovascular pathologies, some have been used for molecular imaging and are represented in Fig. 1.

Biological mechanisms of plaque evolution to rupture have been largely described [5]. Cholesterol charged Low-Density Lipoproteins (LDL) enter the intima where they become oxidized (ox-LDL). Activated endothelial cells express specific markers such as P- and E-selectins, VCAM-1 and ICAM-1 that allow for recognition and infiltration of monocytes. Monocytes differentiate into macrophages and accumulate in the plaque. Smooth muscle cells (SMCs) migrate into the intima and become activated, losing their stretching phenotype. Macrophage and SMCs become charged in ox-LDL generating foam cells. In active plaques, a fibrous cap forms made of SMCs and collagen fibers. Remodeling happens affecting the size of the intima outwards the vessel wall, which cannot be assessed by conventional imaging techniques. Apoptotic events and necrotic core appear in a hypoxic environment inducing micro-vessels development (angiogenesis) [6].

The mechanisms of plaque development being understood, different molecular markers have been identified, among which: endothelial targets (VCAM-1, ICAM-1, E- and P- selectins) [7], macrophage targets (scavenger receptor class A (SR-A) and integrin MAC-1), fibrous cap and extracellular matrix (collagen types I, III, IV), apoptosis (expression of phosphatidylserine) and angiogenesis [8]. For preclinical studies, animal models have been developed to mimic the atherosclerotic lesions, such as Apolipoprotein E deficient mice (ApoE^{-/-} mice) [9]. This model is the most common one but it shows some limitations. Although plaques become highly activated, their rupture is not observed.

E- and P- selectins expressed by activated endothelial cells are also relevant as molecular targets for the diagnosis of AAA and transient ischemic events. These pathologies would also benefit from molecular imaging. In clinic, the size of an aneurysm is the only criterion to predict its evolution and to assess risk for rupture. However, its expansion could be better predicted with complementary information about its activation state [10]. In addition to endothelial activation, the presence of a forming thrombus is especially worth detecting. Circulating platelets become activated and accumulate onto the affected endothelium. A fibrin mesh forms and platelets and red blood cells accumulate at site of injury. Detection can be achieved by targeting fibrin, activated factor XIII and P-selectin expressed by activated platelets. In case of transient ischemic event, physicians lack tools to precisely evaluate the extent of the damage. Yet the endothelium remains highly activated for a few hours after the event [11]. This phenomenon is referred to as ischemic memory.

A promising strategy to achieve the detection of the described biomarkers is the design of nanoplaforms through their high potential for functionalization and their compatibility with existing imaging technologies.

3. Nanoplaforms for molecular imaging of cardiovascular pathologies

Three main types of platforms have been developed for molecular imaging of cardiovascular pathologies: lipid-based, polymer-based and inorganic nanoparticles.

Lipid-based nanoparticles are composed of a phospholipid assembly. Phospholipids are amphiphilic components. Under aqueous conditions, they organize into structures, such as micelles, liposomes and micro-emulsions. Micelles are made of a monolayer of lipids surrounding a hydrophobic core. They are generally smaller than 50 nm. Liposomes are made of a phospholipid bilayer enclosing a hydrophilic core. Their size may reach several hundreds of nm. Micro-emulsions consist in micelles containing hydrophobic nanodroplets and are usually of a few hundreds of nm. Natural High-Density Lipoproteins (HDL) or HDL-like synthetic particles are also of great interest as they are naturally entering LDL-rich plaques and show the advantages of being endogenous and entirely biodegradable [12]. They are micelles made of extracted or synthesized lipoproteins, mainly apolipoproteins apo A-I and apo A-II. Their size stands around 5–17 nm. According to their biocompatibility and their versatility, lipid-based nanosystems have led to numerous formulations.

Synthetic and natural polymers have also been studied for the design of nanostructures more resistant to mechanical constraints than lipid-based systems. Different techniques, such as nanoprecipitation [13] and emulsion polymerization [14], enable to formulate polymer nanoparticles. According to the polymer nature and to the synthesis parameters, polymer platforms can be tuned in terms of size, porosity and hydrophobicity. Poly(lactic-co-glycolic acid) (PLGA), FDA-approved polymer, and Polyvinyl alcohol (PVA) are biodegradable polymers widely studied for nanomedical research [15,16]. Polysaccharides show also promising properties for cardiovascular applications. Among them, chitosan and fucoidan present affinity for fibrin and P-selectin respectively [17].

Inorganic nanoparticles are composed of an inorganic core with imaging properties, generally coated with a polymer shell. In particular, magnetic nanoparticles have been developed for MRI and metal nanoparticles for CT. The polymer coating improves colloidal stability and particle biocompatibility. Alternatively, other coatings include small molecules, as bisphosphonates, and phospholipids. For these three types of platforms, Poly(ethyleneglycol) (PEG), a hydrophilic biocompatible and biodegradable polymer, has been widely used as a coating in order to prevent nanoparticles aggregation and improve their pharmacokinetic properties [18].

4. Magnetic Resonance Imaging

4.1. Imaging modality and corresponding contrast agents

Magnetic Resonance Imaging (MRI) provides images with a very good resolution (from 25 μm to 1 mm) and a precise localization in the body while ensuring no exposure to ionizing radiations. MRI relies on the relaxation of hydrogen nuclei present in abundance in tissues. Under a strong and uniform magnetic field, typically from 1.5 to 3 T, the intrinsic magnetic moments of hydrogen nuclei of scanned tissues align. Resonance of hydrogen nuclei is then obtained via the application of an oscillating magnetic field. Each time the oscillating field is switched off, magnetic moments return to their equilibrium position at a given rate called relaxation. Two different relaxation times characterize a nucleus: its longitudinal relaxation time (T1) and its transversal one (T2 or T2*). Recording these relaxation times give information about

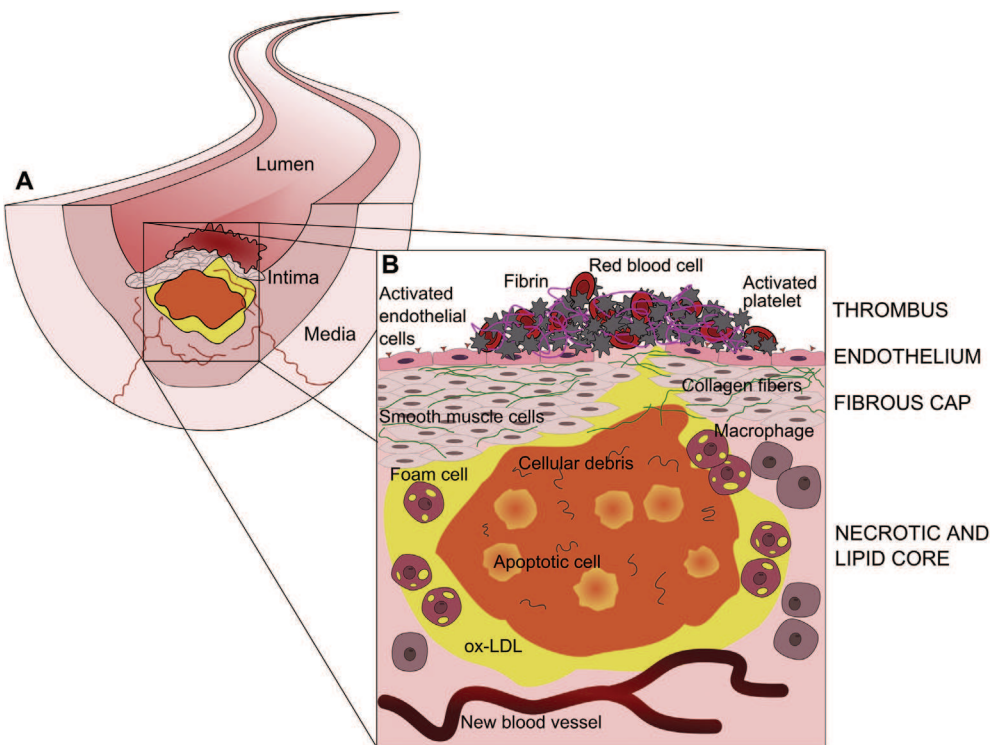


Fig. 1. Cross-sectional illustration of a rupture-prone atherosclerotic plaque showing potential cellular targets for molecular imaging. A) Illustration of an artery affected by atherosclerosis. A plaque has grown generating an intraluminal stenosis. Remodeling has happened affecting the size of the intima. B) A thrombus has formed. It is mainly made of activated platelets and red blood cells embedded in a fibrin mesh. Endothelial cells are highly activated expressing specific markers such as P- and E-selectins. Smooth muscle cells have migrated through the intima and have formed a fibrous cap rich in collagen fibers and extracellular matrix. At the site prone to rupture the fibrous cap is thinner and the endothelium is disrupted. During plaque progression, LDL are oxidized (ox-LDL) and are found in the intima. Macrophages and smooth muscle cells become charged in ox-LDL generating foam cells. Apoptotic events and development of new micro-vessels happen in this environment.

hydrogen density varying from one tissue to another and about their environment.

As regards cardiovascular diagnosis, MRI mostly provides information about tissue vascularization. Contrast agents are used as blood pool enhancers to detect stenosis and non-vascularized area. Recently, improvements in MRI sequences and parameters (multiparameter-MRI) enabled to distinguish plaque components, like necrotic core, fibrous cap and lipid-rich area. Nanoparticles based on existing contrast agents are developed in parallel in order to offer complementary information about tissue activation. One advantage of MRI is to image the accumulation of nanoparticles at the same time as their precise localization in the body.

MRI contrast agents are classified in two types according to the way they influence their magnetic environment: Gadolinium(III) (Gd^{3+}) chelates (T1-shortening agents) and iron oxide based particles (T2*-shortening agents). Relaxivity is defined as the capacity of contrast agents to modify the relaxation rate of surrounding protons. Both types of contrast agents have been integrated into nanoparticle systems in preclinical development (Fig. 2). Iron oxide based nanoparticles have already led to several clinical trials for plaque imaging. According to its good resolution and to the potential for contrast agents' functionalization, the use of nanomedicine for MRI appears possible in clinic.

4.2. Preclinical development

4.2.1. Gd^{3+} -based nanosystems

Gd^{3+} complexes, such as Gd diethylene triamine pentaacetic acid (Gd-DTPA) and Gd 1,4,7,10-tetraazacyclododecane-1,4,7,10-tetraacetic acid (Gd-DOTA), are small paramagnetic compounds commonly used in Magnetic Resonance Angiography as blood pool enhancers. They can be grafted onto lipids and easily integrated in

lipid nanoparticle systems [19]. Lipid-based nanoparticle systems enable to concentrate up to several thousands of Gd^{3+} ions per nanoparticle [20,21], greatly enhancing their relaxivity. Gd-labeled lipids were integrated with success in discoidal reconstituted HDL and native spherical HDL [22], in perfluorocarbon micro-emulsion [21], in liposomes [23] and in micelles [24,25].

Surface modification to make these systems specific to a biomarker was further achieved by grafting targeting agents, either directly to lipids or via a PEG spacer. Immuno-micelles, which ensure targeting via an antibody, were shown to penetrate plaques significantly more than naked systems. The signal intensity associated to accumulation of Gd-loaded micelles targeted towards the macrophage scavenger receptor was increased from 34% to 79% in atherosclerotic aortas of $\text{ApoE}^{-/-}$ mice [26]. Other strategies using small molecules were also set up. Tyrosine residues grafted on PEGylated micelles enhanced their affinity for lipid deposits allowing for plaque detection at 9.4 T 6 h after injection in $\text{ApoE}^{-/-}$ mice [24]. More recently, HDL-like particles were functionalized with a peptide targeted towards collagen present in the extracellular matrix [27]. As plaque regression is associated with collagen degradation, they were able to assess plaque evolution with MRI in a regression model of mouse atherosclerosis. Biologically active proteins were also grafted for targeting. Van Tilborg et al. [28] developed small Gd-loaded PEGylated micelles (15 nm) with covalently bound Annexin A5 to target intra-plaque apoptotic events via phosphatidylserine exposed at cell surface. Their size allows for extravasation and detection of extravascular events. No significant difference in MRI signal compared to untargeted micelles was observed but a heterogeneous distribution of targeted micelles was shown to be more consistent with plaque composition.

4.2.2. Iron-oxide based nanosystems

Iron oxide based contrast agents are ultrasmall superparamagnetic iron oxides (USPIO), which hydrodynamic size is defined as inferior to 50 nm (coating including), and superparamagnetic iron oxides (SPIO) particles, which hydrodynamic size stands between 50 and a few hundreds of nanometers. These magnetic nanoparticles are usually composed of a paramagnetic iron oxide core, either made of magnetite (Fe_3O_4) or maghemite ($\gamma\text{-Fe}_2\text{O}_3$) or a mixture of both, surrounded by a polymer shell [29]. Dextran-coated USPIO and SPIO were shown to undergo spontaneous uptake by intraplaque macrophages and have already been tested in clinical trials to image high-risk plaques. However, this passive accumulation process requires high doses (from 1 to 20 mg Fe/kg) and a time from injection to imaging generally higher than 24 h.

Preclinical research aims to associate USPIO and SPIO with targeting ligands to ensure a quicker specific accumulation and decrease the injected dose. They show indeed a great potential for molecular imaging as their relaxivity is much higher than that of Gd^{3+} chelates. For instance fucoidan has been covalently grafted onto synthesized dextran-coated USPIO. USPIO-fucoidan led to a strong hypointensity only 1 h after injection in area of thrombus formation in a rat model of AAA with *in vivo* MRI experiments performed at 4.7 T before and after injection of 0.2 mmol Fe/kg (Fig. 3) [30]. In another study, dextran-coated SPIO loaded with a peptide clot binding were also studied to image thrombus in a rat model of myocardial ischemia-reperfusion [31]. 4 h after injection, targeted SPIO induced a significant signal loss in the heart where microthrombi were formed, compared to untargeted systems. Other coatings have also been investigated. Mannan, a polysaccharide, has been set up to enhance macrophage uptake of SPIO and USPIO via mannose receptors [32]. Mannan-coated SPIO and USPIO were significantly more internalized by phagocytic cells than carboxydextrans-coated nanosystems in a rabbit model of atherosclerosis after injection of 0.8 mmol Fe/kg. Mulhen et al. [33] constructed another iron oxide based structure coated with PVA and a Vinyl alcohol-vinyl amine copolymer and targeted towards the monocyte integrin MAC-1 via an anti-CD11b, as CD11b is believed to participate in the phagocytosis of USPIO. After injection of 1 mg Fe/kg, an uptake was observed in atherosclerotic

plaques of ApoE^{-/-} mice. However quantification assessment showed no significant difference between control and targeted nanoparticles. Another system under investigation consists in a core made of maghemite and magnetite coated with a copolymer of gem-bisphosphonate. Functionalized with a PEG spacer, it allowed for grafting peptides targeted towards VCAM-1 [34,35]. This system enabled to image atherosclerotic lesions in mice at 4.7 T with a dose of 0.1 mmol Fe/kg compared to the recommended dose of 1 mmol Fe/kg with available unspecific USPIO. Most importantly, only 6 h were necessary to obtain a sufficient and reliable contrast.

Another strategy to enhance plaque penetration is the inclusion of these systems in HDL-like systems for detection of macrophages [36]. Not only SPIO, but also other inorganic compounds, such as gold nanocrystals, were loaded with success in such versatile nanoplateform [37].

Iron oxides based particles have also been embedded in polymer matrix forming targeting microparticles. Bonnard et al. [38,39] used sodium trimetaphosphate (STMP) to cross-link dextran, pullulan and fucoidan to form targeted biodegradable microparticles (MP). These microparticles were loaded with USPIOS (Sinerem®, Guerbet) [38]. When injected in a rat model of AAA, these MP accumulated onto the intraluminal thrombus. After injection of an iron dose of 0.56 mg Fe/kg, MRI was performed at 7.4 T. A contrast uptake was observed after 30 min. Non-biodegradable tosyl-activated polystyrene-coated superparamagnetic MP (Dynabeads®, Life Technologies) with a covalent grafting of P-selectin antibody were shown to accumulate onto activated endothelium at most during fibrous cap formation [40].

4.3. Clinical applications

Dextran-coated USPIO and SPIO have already led to clinical trials for the diagnosis of several pathologies including pelvic and carotid atherosclerosis, AAA and acute ischemic events. They have been shown to be spontaneously phagocytized by macrophages enabling to detect inflammatory-like processes expressed in atherosclerotic lesions. Pilot studies using iron oxide based nanoparticles were recently reviewed in detail by Cicha et al. [41]. Three types of particles were already tested in clinic. The efficacy

	Sensitivity	Spatial resolution	Time from injection to imaging
Magnetic Resonance Imaging	++	+++	+
Nuclear Imaging	+++	+	++
X-ray Computed Tomography	+	+++	++

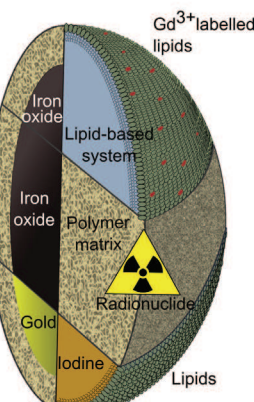


Fig. 2. Schematic representation of three types of nanostructure developed in preclinical or clinical stage for molecular imaging using Magnetic Resonance Imaging (MRI), Nuclear Imaging and X-ray Computed Tomography (CT). The modalities are compared according to the most important parameters for molecular imaging: sensitivity, spatial resolution and time from injection of contrast agents to imaging. MRI has a very good spatial resolution (250 μm – 1 mm) but most systems required at least 24 h before contrast enhancement. Two main types of nanosystems have been developed for MRI: iron oxides covered by a polymer shell, and lipid-based systems incorporating Gadolinium chelates. Nuclear imaging is the most sensitive technique but lacks of spatial resolution (few mm). It is often associated with CT to complete the diagnosis with morphological data. Two platforms from iron oxides based systems and polymer systems have been set up in preclinical studies with radionuclides. CT has the best resolution (25 μm – 250 μm) and requires at the most a few hours for contrast uptake but high concentrations of contrast agents. New contrast agents are under development to alleviate its poor sensitivity. Iodine-based systems, most often stabilized by a lipid shell and new contrast agents, such as gold nanocrystals stabilized by a polymer shell, are in preclinical development for molecular imaging of cardiovascular pathologies. In all cases, functionalization for targeting purposes is achieved by grafting targeting moieties (antibodies, peptides, polysaccharides ...) at the surface of the particles. Hybrid contrast agents for dual imaging modalities are also under investigation.

of Ferumoxtran-10 (Sinerem, Guerbet/Combidex, AMAG Pharma) has been validated more than 10 years ago [42–44]. Ferumoxtran-10 is coated with dextran T10 and shows a long circulating time due to its small hydrodynamic size (30 nm). The SPIO Ferumoxides (Feridex IV, Berlex Laboratories/Endorem, Guerbet) which size is much larger (50–180 nm) and the SPIO Ferucarbotran (Resovist®, Bayer Healthcare) (55–65 nm) coated with carboxymethylated dextran [45] were also clinically tested for cardiovascular application. A correlation was found between Ferumoxides uptake (observed at 24 h and 36 h after injection) and rapidly progressive AAA expansion, independently from the initial size of the aneurysm [46]. However, these three types of particles are now totally or partially withdrawn from the market as regards their initial application, making them less accessible. More recently, ferumoxytol (Feraheme), an USPIO (20–40 nm) coated with poly-glucose sorbital carboxymethylether emerged. In the recent NIMINI-2 clinical trial ferumoxytol injection combined with multiparameter-MRI successfully delimited infarction area, as well as the peri-infarct zone in patients suffering from acute myocardial infarction [47]. This should be confirmed with the results of another clinical trial [48]. Generally, significant passive accumulation requires 24–72 h after injection. Another drawback is the dose of particles required, from 1 to 20 mg of iron oxide/kg [49]. As detailed in the previous section, researchers work on increasing the affinity of iron oxides for plaques and activated area by incorporating targeting moieties.

5. Nuclear imaging

5.1. Imaging modality and corresponding contrast agents

Nuclear imaging refers to single-photon emission computed tomography (SPECT) and positron emission tomography (PET). These techniques provide functional imaging of the body. They require the intra-venous (IV) injection of a radionuclide (also called radioactive nuclide or radioisotope). The most commonly used radionuclides in cardiovascular diagnosis with PET are Fluorine-18 (¹⁸F) and Gallium-68 (⁶⁸Ga). Both have relatively short half-life, 110 and 68 min respectively. As regards SPECT, Technetium-99m (^{99m}Tc), with a 6 h half-life, is widely used.

Among the described modalities, nuclear imaging has the highest sensitivity and therefore the biggest potential for detecting molecular events while injecting safe doses. However, its application in nanomedicine could be limited by its resolution of a few millimeters. Most clinically used machines perform a CT-scan at the same time to localize in two or three dimensions the accumulation of the radionuclides in the body exposing patients to supplementary ionizing radiations.

Radiolabeled small molecules are already employed in clinic to perform metabolic imaging. ¹⁸F-fluorodeoxyglucose (FDG) is a commonly used radiopharmaceutical for PET imaging [50]. This glucose analog is trapped into metabolically active macrophages where it accumulates. ¹⁸F-FDG imaging has been set up in humans for imaging high-risk plaques and is now employed as an endpoint in most clinical trials testing new therapeutics [51]. ¹⁸F-FDG PET scans provide an image 2–3 h after injection of typically 185–300 MBq [50]. The main limitation is that it does not interact exclusively with macrophages. ¹⁸F-FDG unspecific uptake is especially an issue for imaging coronary diseases as myocardial assimilation is very important.

Other macromolecular assemblies with targeting moieties are in preclinical development for cardiovascular diagnosis [52–55]. Combining these molecular probes into nanoparticle platforms (Fig. 2) would enable to improve their specificity and avoid their rapid clearance from the body [56].

5.2. Preclinical development

5.2.1. Polymer-based systems

Polymer nanoparticles of a few nanometers (13 nm) were obtained by cross-linking short chain dextran with epichlorohydrin [57]. These nanoparticles were radiolabeled with Zirconium-89 (⁸⁹Zr) via desferoxamine for PET. PET/CT imaging was performed 48 h after injection of $354 \pm 13 \mu\text{Ci}/\text{mouse}$ (13 MBq/mouse). A significant activity was detected in the aortic root of ApoE^{-/-} mice compared to wild-type controls, which was consistent with the development of atherosclerotic lesions. However, the toxicity of epichlorohydrin raises an issue for its translation. In addition, ⁸⁹Zr is not recommended in clinic. Bonnard et al. used STMP to cross-link dextran, pullulan and fucoidan to form targeted biodegradable microparticles (MP). These

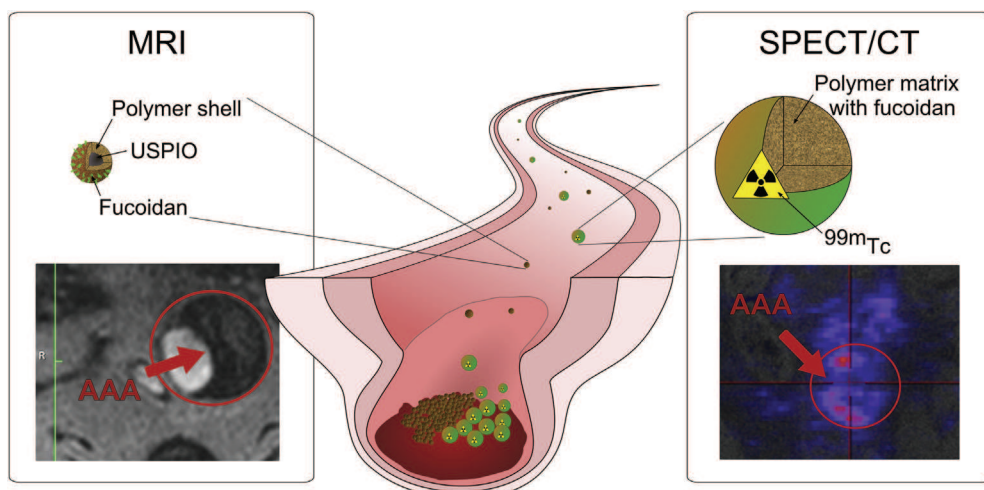


Fig. 3. Illustrated examples of targeted structures developed for molecular imaging of thrombus in Abdominal Aortic Aneurysm in rat. **Left**) Ultrasmall superparamagnetic iron oxides coated with a shell of dextran were functionalized with a covalent grafting of fucoidan [30]. Their size was less than 30 nm. A strong hypointense (red arrow) at site of thrombus was observed only 1 h after injection of 200 μmol of Fe/kg. **Right**) Polymer microparticles with a size below 4 μm were synthesized by chemical cross-linking of dextran, pullulan and fucoidan. They were radiolabeled with ^{99m}Tc. 30 min after injection of a dose of 37 MBq, the thrombus was visualized with SPECT and anatomic location obtained by parallel CT scans [39]. (For interpretation of the references to color in this figure legend, the reader is referred to the web version of this article.)

Table 1
Active targeting strategies set up in preclinical research. Systems are classified according to their cellular target.

Targets	Targeting strategy	Nanoplatform	Contrast agent	Imaging modality	Animal model	Ref
<i>Thrombus & activated endothelial cells</i>						
P-Selectin	Antibody Fucoidan	Polymer MP Polymer MP	USPIO ^{99m} Tc	MRI SPECT	ApoE-/- mice Rat AAA Rat AAA	[40] [38] [39]
VCAM-1	Peptide	Inorganic	USPIO	MRI	Rat AAA	[30]
Fibrin	Antibody Peptide Chitosan	Inorganic Lipid Lipid Inorganic	USPIO Gd ³⁺ USPIO Au	MRI MRI MRI CT	ApoE-/- mice Thrombus canine model Rat model of MI/R Thrombus model in C57BL/6 mice	[34,35] [21] [31] [72]
<i>Macrophages</i>						
MSR-A	Antibody	Lipid	Gd ³⁺	MRI	ApoE-/- mice	[26]
Mannose receptor	Mannan	Inorganic	USPIO	MRI	WHHL rabbit	[32]
CCR5 receptor	Peptide	Polymer	⁶⁴ Cu	PET	ApoE-/-	[58]
<i>Lipid core</i>						
Lipoproteins	Tyrosine residues	Lipid	Gd ³⁺	MRI	ApoE-/- mice	[24]
<i>Extracellular matrix</i>						
Collagen	Peptide	Lipid	Gd ³⁺	MRI	Reversa mice	[27]
<i>Apoptotic cells</i>						
Phosphatidylserine	Annexin 5 Peptide	Lipid Inorganic	Gd ³⁺ USPIO	MRI MRI	ApoE-/- mice ApoE-/- mice	[28] [34]

microparticles were labeled with ^{99m}Tc for SPECT [39]. Significant contrast enhancement *in vivo* in the abdominal aortic region in a rat model of AAA was registered after 30 min with SPECT after injection of radiolabeled MP at a dose of 37 MBq/rat (Fig. 3).

Poly(methyl methacrylate) (PMMA), which is not biodegradable, was also studied for pre-clinical investigation. Luehmann et al. [58] developed PMMA nanoparticles covered with a functionalized PEG shell targeted towards chemokine receptor 5. These nanoparticles were radiolabeled with ⁶⁴Cu for PET. In comparison to ⁶⁴Cu-chelate directly coupled to the targeting unit, using a nanoplatform greatly improved ⁶⁴Cu-chelate imaging potential. The potential development of this strategy is highly dependent on the degradability of the polymer nanosystems, since organ accumulation could be a main limitation.

5.2.2. Inorganic systems as platforms for PET imaging

Cross-linked iron oxide nanoparticles (CLIO) have been developed as a platform that concentrates one or several monocrystalline iron oxides [59]. In these systems, the dextran coating is cross-linked via epichlorohydrin and is aminated. Such superparamagnetic nanoparticles were used by the Weissleder's team as PET imaging agents radiolabeled with either ⁶⁴Cu or ¹⁸F [49,60,61]. Injection of 4.5 mg of Fe/kg was sufficient to image macrophage-rich atherosclerosis lesions with a PET/CT machine. Jarrett et al. [62] injected a dose of 18–20 mg Fe/kg of ⁶⁴Cu radiolabeled iron oxide nanoparticles in ApoE-/- mice. The nonspecific uptake of iron oxide nanoparticles by macrophages enabled to locate active plaques with PET imaging. Further analysis was performed with 7 T MRI to provide complementary anatomical information. Multimodal platforms are promising for future development as they combine the benefits of both modalities. Hybrid PET/MRI devices have already been set up in clinic.

6. X-ray computed tomography

6.1. Imaging modality and corresponding contrast agents

Computed Tomography scan (CT-scan) is based on the capacity of tissues to absorb X-rays. One major application of CT-scan for cardiovascular diseases diagnosis is angiography performed with intra-venous injection of radiocontrasts. It provides an image in a few minutes with a good resolution (from 25 to 250 μm) but

exposes patients to ionizing radiations. In addition, current radiocontrast agents may cause strong allergic effects.

The most common radiocontrasts are small iodine-based molecules as blood pool enhancers. Research aims to decrease the injected dose by incorporating them into more complex structures, such as PEGylated nanoemulsions. Additionally, new radiopaque agents are investigated [63,64]. In particular, elements with high atomic number have a good X-ray attenuation capacity. Furthermore k-edge imaging with multicolor CT (more commonly referred to as spectral CT) is an emerging technique that provides elemental characterization of a tissue with an enhanced sensitivity, detecting for example calcium phosphate in atherosclerotic lesions. Contrast agents for k-edge imaging should be composed of elements with high k-edge energy. Metal nanoparticles, in particular gold and bismuth are good candidates as they have high atomic numbers and high k-edge energy levels. Although their toxicity has to be studied, they are supposed to be better tolerated than iodine-based agents. For preclinical studies with micro-CT, development of alkaline earth-based nanoparticles seems promising [65], as they generated strong contrast enhancement of vessels [66,67]. At the best of our knowledge, no clinical application of nanotechnologies for diagnosis of cardiovascular pathologies with CT has been described yet, but preclinical research led to nanosystems based on iodine and on metal nanocrystals (Fig. 2).

6.2. Preclinical research

6.2.1. Iodine-based systems

Quantum dots dispersed in an iodinated oil (Lipiodol®, Guerbet) have been employed as a bimodal platform for optical and micro-CT imaging of macrophages accumulation [68]. Oil nanodroplets were stabilized in water by PEGylated lipids. 2 h after administration of 100 mg iodine/kg in a rabbit model of atherosclerosis, the background signal returned to its pre-injection value and a significant uptake was observed in macrophages-rich plaques.

Hyafil et al. [69] demonstrated that a colloidal suspension of crystalline iodinated particles (N1177, Nanoscan Imaging LCC) allowed detecting high risk plaques with CT in a rabbit model of atherosclerotic lesions. Nanoparticles were obtained by precipitation of an iodinated ester and stabilized by PEG and surfactants. They were injected at an equivalent dose of 250 mg iodine/kg.

Although encapsulated into nanosystems, the required dose of iodine for imaging remains high.

6.2.2. Gold nanoparticles

Gold nanoparticles were evaluated in preclinical models of cardiovascular pathologies. Au-HDL combined with spectral CT were tested *in vivo* in ApoE^{-/-} mice. They were shown to accumulate in macrophage-rich plaques and to give a good contrast with micro-CT [70]. Furthermore, combining such systems with multicolor CT allowed distinguishing at once macrophages accumulation and calcification [71]. Glycol chitosan (GC) coating has also been demonstrated to enhance retention and compatibility of gold nanoparticles (Au-NPs) [72]. Furthermore, its affinity for fibrin makes it a coating of choice for thrombus targeting. Injection of 0.5 mg GC-AuNPs/mouse allowed to immediately image the thrombus and monitored the response to thrombolytic therapy in real time.

7. Discussion and perspectives

Current limitations in diagnosis mostly regard the ability for assessing evolution of long-term pathologies. Atherosclerosis diagnosis is especially affected by this issue, as atherosclerosis is a silent disease developing over a life-time. Plaque rupture prediction remains difficult with a high patient-to-patient variability. Standard imaging modalities provide anatomical information about stenosis development and flow perturbation but do not translate how affected the arteries are at molecular and cellular scales. Nanomedicine has the potential to answer clinical need for a personalized diagnosis.

The first clinically tested nanoparticles, USPIO for MRI, rely on their nonspecific physiological uptake by macrophages present in abundance in active plaques. They showed a great potential but the first FDA-approved systems have been withdrawn from the market, making them less accessible. New generations are still under clinical testing.

In parallel, preclinical research using targeted nanotools with enhanced specificity is under development. Targeting is achieved by grafting either specific antibodies or small molecules to the surface of the particles, most often via a PEG spacer. Promising results showed the potential of developed nanosystems for identifying affected area using several types of imaging modalities. In particular, endothelial activation is of great importance in the detection of ischemic events, rapidly evolving AAA or active plaques. For that reason, most systems have been designed to interact with endothelial biomarkers (Table 1).

Each modality shows its own advantages and it is worth developing nanosystems for all types of imaging technologies. Furthermore, each modality is not associated with the same types of systems, and therefore not with the same targets. According to its good resolution and to the potential for contrast agents' functionalization, the use of nanomedicine for MRI appears promising for plaque imaging. Several lipid-based systems with Gd³⁺-chelates have been developed to image intraplaque events. USPIO are studied in depth for their spontaneous accumulation by macrophages in high-risk plaques. Nuclear imaging is compatible with a lot of systems and requires minimal doses. For these reasons, it is often used in preclinical development to study the biodistribution of newly developed nanoparticle platforms. CT imaging allows for short time detection. It evolves significantly with metal nanocrystals, a new type of contrast agents. Interesting nanotools for cardiovascular imaging should therefore be designed in the near future.

A remarkable trend is the design of multimodal systems. In light of the progresses in imaging technologies, we could anticipate the routine use of multimodal imaging in a few years. PET/CT

is commonly used and PET/MRI machines have already been set up. Developing multimodal nanoparticle platforms would enable to get a wide range of anatomic and functional information.

Nanosystems developed for molecular diagnosis have to be entirely safe without side effect. A rapid elimination and a controlled biodegradability have to be ensured. Concerning the pharmacokinetics of newly created systems, several fundamental steps are still required before a safe translation into clinic. Numerous techniques are under development in preclinical research to study the clearance of the nanosystems in the body. For this new area of diagnosis, the specificity is also one of the main criteria. In parallel, campaign for healthy life-styles and awareness of risk factors should be continued. In that sense, research in this field provides not only promising nanotools but also a better understanding of the diseases.

Acknowledgments

This study was supported by Inserm, University Paris 13 and University Paris Diderot, France. This work was also supported in part by the EU project NanoAthero FP7-NMP-2012-LARGE-6-309820, Lefoulon – Delalande post-doctoral scholarship (to MV), IMOVA project (FUI/OSEO, CG93), and ANR-13-LAB1-0005-01 “FucoChem”.

Transparency document

Transparency document related to this article can be found online at <http://dx.doi.org/10.1016/j.bbrc.2015.06.138>.

References

- [1] A.J. Lusis, Atherosclerosis, *Nature* 407 (2000) 233–241.
- [2] E. Incalcaterra, G. Accardi, C.R. Balistreri, G. Caimi, G. Candore, M. Caruso, C. Caruso, Pro-inflammatory genetic markers of atherosclerosis, *Curr. Atheroscler. Rep.* 15 (2013) 329.
- [3] D.J. Rader, A. Daugherty, Translating molecular discoveries into new therapies for atherosclerosis, *Nature* 451 (2008) 904–913.
- [4] C.D. Mathers, D. Loncar, Projections of global mortality and burden of disease from 2002 to 2030, *PLoS Med.* 3 (2006) e442.
- [5] P. Libby, Molecular and cellular mechanisms of the thrombotic complications of atherosclerosis, *J. Lipid Res.* 50 (Suppl.) (2009) S352–S357.
- [6] P. Libby, M. DiCarli, R. Weissleder, The vascular biology of atherosclerosis and imaging targets, *J. Nucl. Med.* 51 (Suppl. 1) (2010) 33S–37S.
- [7] E.D. Hood, M. Chorny, C.F. Greineder, S.A. I., R.J. Levy, V.R. Muzykantov, Endothelial targeting of nanocarriers loaded with antioxidant enzymes for protection against vascular oxidative stress and inflammation, *Biomaterials* 35 (2014) 3708–3715.
- [8] K. Douma, L. Prinzen, D.W. Slaaf, C.P. Reutelingsperger, E.A. Biessen, T. M. Hackeng, M.J. Post, M.A. van Zandvoort, Nanoparticles for optical molecular imaging of atherosclerosis, *Small* 5 (2009) 544–557.
- [9] K.J. Moore, F.J. Sheedy, E.A. Fisher, Macrophages in atherosclerosis: a dynamic balance, *Nat. Rev. Immunol.* 13 (2013) 709–721.
- [10] A. Klink, F. Hyafil, J. Rudd, P. Farries, V. Fuster, Z. Mallat, O. Meilhac, W.J. Mulder, J.B. Michel, F. Ramirez, G. Storm, R. Thompson, I.C. Turnbull, J. Egido, J. L. Martin-Ventura, C. Zaragoza, D. Letourneur, Z.A. Fayad, Diagnostic and therapeutic strategies for small abdominal aortic aneurysms, *Nat. Rev. Cardiol.* 8 (2011) 338–347.
- [11] F.S. Villanueva, E. Lu, S. Bowry, S. Kilic, E. Tom, J. Wang, J. Gretton, J.J. Pacella, W.R. Wagner, Myocardial ischemic memory imaging with molecular echocardiography, *Circulation* 115 (2007) 345–352.
- [12] J.C. Frias, K.J. Williams, E.A. Fisher, Z.A. Fayad, Recombinant HDL-like nanoparticles: a specific contrast agent for MRI of atherosclerotic plaques, *J. Am. Chem. Soc.* 126 (2004) 16316–16317.
- [13] S. Galindo-Rodriguez, E. Allemann, H. Fessi, E. Doelker, Physicochemical parameters associated with nanoparticle formation in the salting-out, emulsification-diffusion, and nanoprecipitation methods, *Pharm. Res.* 21 (2004) 1428–1439.
- [14] C. Chauvierre, D. Labarre, P. Couvreur, C. Vauthier, Novel polysaccharide-decorated poly(isobutyl cyanoacrylate) nanoparticles, *Pharm. Res.* 20 (2003) 1786–1793.

- [15] F. Danhier, E. Ansorena, J.M. Silva, R. Coco, A. Le Breton, V. Preat, PLGA-based nanoparticles: an overview of biomedical applications, *J. Control. Release* 161 (2012) 505–522.
- [16] U. Westedt, M. Kalinowski, M. Wittmar, T. Merdan, F. Unger, J. Fuchs, S. Schaller, U. Bakowsky, T. Kissel, Poly(vinyl alcohol)-graft-poly(lactide-co-glycolide) nanoparticles for local delivery of paclitaxel for restenosis treatment, *J. Control. Release* 119 (2007) 41–51.
- [17] A.K. Silva, D. Letourneur, C. Chauvierre, Polysaccharide nanosystems for future progress in cardiovascular pathologies, *Theranostics* 4 (2014) 579–591.
- [18] R. Gref, Y. Minamitake, M.T. Peracchia, V. Trubetskoy, V. Torchilin, R. Langer, Biodegradable long-circulating polymeric nanospheres, *Science* 263 (1994) 1600–1603.
- [19] W.J. Mulder, G.J. Strijkers, G.A. van Tilborg, A.W. Griffioen, K. Nicolay, Lipid-based nanoparticles for contrast-enhanced MRI and molecular imaging, *NMR Biomed.* 19 (2006) 142–164.
- [20] S. Hak, H.M. Sanders, P. Agrawal, S. Langereis, H. Grull, H.M. Keizer, F. Arena, E. Terreno, G.J. Strijkers, K. Nicolay, A high relaxivity Gd(III)DOTA-DSPE-based liposomal contrast agent for magnetic resonance imaging, *Eur. J. Pharm. Biopharm.* 72 (2009) 397–404.
- [21] S. Flacke, S. Fischer, M.J. Scott, R.J. Fuhrhop, J.S. Allen, M. McLean, P. Winter, G. A. Sicard, P.J. Gaffney, S.A. Wickline, G.M. Lanza, Novel MRI contrast agent for molecular imaging of fibrin: implications for detecting vulnerable plaques, *Circulation* 104 (2001) 1280–1285.
- [22] J.C. Frias, Y. Ma, K.J. Williams, Z.A. Fayad, E.A. Fisher, Properties of a versatile nanoparticle platform contrast agent to image and characterize atherosclerotic plaques by magnetic resonance imaging, *Nano Lett.* 6 (2006) 2220–2224.
- [23] W.J. Mulder, K. Douma, G.A. Koning, M.A. van Zandvoort, E. Lutgens, M. J. Daemen, K. Nicolay, G.J. Strijkers, Liposome-enhanced MRI of neointimal lesions in the ApoE-KO mouse, *Magn. Reson. Med.* 55 (2006) 1170–1174.
- [24] A. Beilvert, D.P. Cormode, F. Chaubet, K.C. Briley-Saebo, V. Mani, W.J. Mulder, E. Vucic, J.F. Toussaint, D. Letourneur, Z.A. Fayad, Tyrosine polyethylene glycol (PEG)-micelle magnetic resonance contrast agent for the detection of lipid rich areas in atherosclerotic plaque, *Magn. Reson. Med.* 62 (2009) 1195–1201.
- [25] G.A. van Tilborg, W.J. Mulder, N. Deckers, G. Storm, C.P. Reutelingsperger, G. J. Strijkers, K. Nicolay, Annexin A5-functionalized bimodal lipid-based contrast agents for the detection of apoptosis, *Bioconjug. Chem.* 17 (2006) 741–749.
- [26] V. Amirbekian, M.J. Lipinski, K.C. Briley-Saebo, S. Amirbekian, J.G. Aguinaldo, D.B. Weinreb, E. Vucic, J.C. Frias, F. Hyafil, V. Mani, E.A. Fisher, Z.A. Fayad, Detecting and assessing macrophages in vivo to evaluate atherosclerosis noninvasively using molecular MRI, *Proc. Natl. Acad. Sci. U S A* 104 (2007) 961–966.
- [27] W. Chen, D.P. Cormode, Y. Vengrenyuk, B. Herranz, J.E. Feig, A. Klink, W. J. Mulder, E.A. Fisher, Z.A. Fayad, Collagen-specific peptide conjugated HDL nanoparticles as MRI contrast agent to evaluate compositional changes in atherosclerotic plaque regression, *JACC Cardiovasc. Imaging* 6 (2013) 373–384.
- [28] G.A. van Tilborg, E. Vucic, G.J. Strijkers, D.P. Cormode, V. Mani, T. Skajaa, C. P. Reutelingsperger, Z.A. Fayad, W.J. Mulder, K. Nicolay, Annexin A5-functionalized bimodal nanoparticles for MRI and fluorescence imaging of atherosclerotic plaques, *Bioconjug. Chem.* 21 (2010) 1794–1803.
- [29] M. Di Marco, C. Sadun, M. Port, I. Guibert, P. Couvreur, C. Dubernet, Physicochemical characterization of ultrasmall superparamagnetic iron oxide particles (USPIO) for biomedical application as MRI contrast agents, *Int. J. Nanomedicine* 2 (2007) 609–622.
- [30] M. Suzuki, L. Bachelet-Violette, F. Rouzet, A. Beilvert, G. Autret, M. Maire, C. Menager, L. Louedec, C. Choqueux, P. Saboural, O. Haddad, C. Chauvierre, F. Chaubet, J.B. Michel, J.M. Serfaty, D. Letourneur, Ultrasmall superparamagnetic iron oxide nanoparticles coated with fucoidan for molecular MRI of intraluminal thrombus, *Nanomedicine* 10 (2015) 73–87.
- [31] Y. Song, Z. Huang, J. Xu, D. Ren, Y. Wang, X. Zheng, Y. Shen, L. Wang, H. Gao, J. Hou, Z. Pang, J. Qian, J. Ge, Multimodal SPION-CREKA peptide based agents for molecular imaging of microthrombus in a rat myocardial ischemia-reperfusion model, *Biomaterials* 35 (2014) 2961–2970.
- [32] K. Tsuchiya, N. Nitta, A. Sonoda, H. Otani, M. Takahashi, K. Murata, M. Shiomi, Y. Tabata, S. Nohara, Atherosclerotic imaging using 4 types of superparamagnetic iron oxides: new possibilities for mannan-coated particles, *Eur. J. Radiol.* 82 (2013) 1919–1925.
- [33] C. von zur Muhlen, A. Fink-Petri, J. Salaklang, D. Paul, I. Neudorfer, V. Berti, A. Merkle, K. Peter, C. Bode, D. von Elverfeldt, Imaging monocytes with iron oxide nanoparticles targeted towards the monocyte integrin MAC-1 (CD11b/CD18) does not result in improved atherosclerotic plaque detection by in vivo MRI, *Contrast Media Mol. Imaging* 5 (2010) 268–275.
- [34] C. Burtea, S. Ballet, S. Laurent, O. Rousseaux, A. Dencausse, W. Gonzalez, M. Port, C. Corot, L. Vander Elst, R.N. Muller, Development of a magnetic resonance imaging protocol for the characterization of atherosclerotic plaque by using vascular cell adhesion molecule-1 and apoptosis-targeted ultrasmall superparamagnetic iron oxide derivatives, *Arterioscler. Thromb. Vasc. Biol.* 32 (2012) e36–48.
- [35] M. Michalska, L. Machtoub, H.D. Manthey, E. Bauer, V. Herold, G. Krohne, G. Lykowsky, M. Hildenbrand, T. Kampf, P. Jakob, A. Zernecke, W.R. Bauer, Visualization of vascular inflammation in the atherosclerotic mouse by ultrasmall superparamagnetic iron oxide vascular cell adhesion molecule-1-specific nanoparticles, *Arterioscler. Thromb. Vasc. Biol.* 32 (2012) 2350–2357.
- [36] C. Jung, M.G. Kaul, O.T. Bruns, T. Ducic, B. Freund, M. Heine, R. Reimer, A. Meents, S.C. Salmen, H. Weller, P. Nielsen, G. Adam, J. Heeren, H. Ittrich, Intrapерitoneal injection improves the uptake of nanoparticle-labeled high-density lipoprotein to atherosclerotic plaques compared with intravenous injection: a multimodal imaging study in ApoE knockout mice, *Circ. Cardiovasc. Imaging* 7 (2014) 303–311.
- [37] T. Skajaa, D.P. Cormode, E. Falk, W.J. Mulder, E.A. Fisher, Z.A. Fayad, High-density lipoprotein-based contrast agents for multimodal imaging of atherosclerosis, *Arterioscler. Thromb. Vasc. Biol.* 30 (2010) 169–176.
- [38] T. Bonnard, J.M. Serfaty, C. Journe, B. Ho Tin Noe, D. Arnaud, L. Louedec, S. M. Derkaoui, D. Letourneur, C. Chauvierre, C. Le Visage, Leukocyte mimetic polysaccharide microparticles tracked in vivo on activated endothelium and in abdominal aortic aneurysm, *Acta Biomater.* 10 (2014) 3535–3545.
- [39] T. Bonnard, G. Yang, A. Petiet, V. Ollivier, O. Haddad, D. Arnaud, L. Louedec, L. Bachelet-Violette, S.M. Derkaoui, D. Letourneur, C. Chauvierre, C. Le Visage, Abdominal aortic aneurysms targeted by functionalized polysaccharide microparticles: a new tool for SPECT imaging, *Theranostics* 4 (2014) 592–603.
- [40] M.A. McAteer, K. Mankia, N. Ruparelia, A. Jefferson, H.B. Nugent, L.A. Stork, K. M. Channon, J.E. Schneider, R.P. Choudhury, A leukocyte-mimetic magnetic resonance imaging contrast agent homes rapidly to activated endothelium and tracks with atherosclerotic lesion macrophage content, *Arterioscler. Thromb. Vasc. Biol.* 32 (2012) 1427–1435.
- [41] I. Cicha, C. Garlichs, C. Alexiou, Cardiovascular therapy through nanotechnology - how far are we still from bedside? *Eur. J. Nanomed.* 6 (2014) 63–87.
- [42] M.E. Kooi, V.C. Cappendijk, K. Cleutjens, A.G.H. Kessels, P. Kitslaar, M. Borgers, P.M. Frederik, M. Daemen, J.M.A. van Engelshoven, Accumulation of ultrasmall superparamagnetic particles of iron oxide in human atherosclerotic plaques can be detected by in vivo magnetic resonance imaging, *Circulation* 107 (2003) 2453–2458.
- [43] A. Saleh, M. Schroeter, A. Ringelstein, H.P. Hartung, M. Siebler, U. Modder, S. Jander, Iron oxide particle-enhanced MRI suggests variability of brain inflammation at early stages after ischemic stroke, *Stroke* 38 (2007) 2733–2737.
- [44] A.J. Degnan, A.J. Patterson, T.Y. Tang, S.P. Howarth, J.H. Gillard, Evaluation of ultrasmall superparamagnetic iron oxide-enhanced MRI of carotid atherosclerosis to assess risk of cerebrovascular and cardiovascular events: follow-up of the ATHEROMA trial, *Cerebrovasc. Dis.* 34 (2012) 169–173.
- [45] Y.X. Wang, Superparamagnetic iron oxide based MRI contrast agents: current status of clinical application, *Quant. Imaging Med. Surg.* 1 (2011) 35–40.
- [46] J.M. Richards, S.I. Semple, T.J. MacGillivray, C. Gray, J.P. Langrish, M. Williams, M. Dweck, W. Wallace, G. McKillop, R.T. Chalmers, O.J. Garden, D.E. Newby, Abdominal aortic aneurysm growth predicted by uptake of ultrasmall superparamagnetic particles of iron oxide: a pilot study, *Circ. Cardiovasc. Imaging* 4 (2011) 274–281.
- [47] A. Yilmaz, S. Rosch, H. Yildiz, S. Klumpp, U. Sechtem, First multiparametric cardiovascular magnetic resonance study using ultrasmall superparamagnetic iron oxide nanoparticles in a patient with acute myocardial infarction: new vistas for the clinical application of ultrasmall superparamagnetic iron oxide, *Circulation* 126 (2012) 1932–1934.
- [48] S.R. Alam, A.S. Shah, J. Richards, N.N. Lang, G. Barnes, N. Joshi, T. MacGillivray, G. McKillop, S. Mirsadraee, J. Payne, K.A. Fox, P. Henriksen, D.E. Newby, S. I. Semple, Ultrasmall superparamagnetic particles of iron oxide in patients with acute myocardial infarction: early clinical experience, *Circ. Cardiovasc. Imaging* 5 (2012) 559–565.
- [49] M. Nahrendorf, H. Zhang, S. Hembrador, P. Panizzi, D.E. Sosnovik, E. Aikawa, P. Libby, F.K. Swirski, R. Weissleder, Nanoparticle PET-CT imaging of macrophages in inflammatory atherosclerosis, *Circulation* 117 (2008) 379–387.
- [50] J.M. Tarkin, F.R. Joshi, J.H. Rudd, PET imaging of inflammation in atherosclerosis, *Nat. Rev. Cardiol.* 11 (2014) 443–457.
- [51] N. Tahara, H. Kai, M. Ishibashi, H. Nakaura, H. Kaida, K. Baba, N. Hayabuchi, T. Imaizumi, Simvastatin attenuates plaque inflammation: evaluation by fluorodeoxyglucose positron emission tomography, *J. Am. Coll. Cardiol.* 48 (2006) 1825–1831.
- [52] F. Rouzet, L. Bachelet-Violette, J.M. Alsac, M. Suzuki, A. Meulemans, L. Louedec, A. Petiet, M. Jandrot-Perrus, F. Chaubet, J.B. Michel, D. Le Guludec, D. Letourneur, Radiolabelled fucoidan as a p-selectin targeting agent for in vivo imaging of platelet-rich thrombus and endothelial activation, *J. Nucl. Med.* 52 (2011) 1433–1440.
- [53] X. Li, W. Bauer, I. Israel, M.C. Kreissl, J. Weirather, D. Richter, E. Bauer, V. Herold, P. Jakob, A. Buck, S. Frantz, S. Samnick, Targeting P-selectin by gallium-68-labeled fucoidan positron emission tomography for noninvasive characterization of vulnerable plaques: correlation with in vivo 17.6T MRI, *Arterioscler. Thromb. Vasc. Biol.* 34 (2014) 1661–1667.
- [54] P. Saboural, F. Chaubet, F. Rouzet, F. Al-Shoukr, R.B. Azzouna, N. Bouchemal, L. Picton, L. Louedec, M. Maire, L. Rolland, G. Potier, D.L. Guludec, D. Letourneur, C. Chauvierre, Purification of a low molecular weight fucoidan for SPECT molecular imaging of myocardial infarction, *Mar. Drugs* 12 (2014) 4851–4867.
- [55] S. Isobe, S. Tsimikas, J. Zhou, S. Fujimoto, M. Sarai, M.J. Branks, A. Fujimoto, L. Hofstra, C.P. Reutelingsperger, T. Murohara, R. Virmani, F.D. Kolodgie, N. Narula, A. Petrov, J. Narula, Noninvasive imaging of atherosclerotic lesions in apolipoprotein E-deficient and low-density-lipoprotein receptor-deficient mice with annexin A5, *J. Nucl. Med.* 47 (2006) 1497–1505.
- [56] C.J. Anderson, J.W. Bulte, K. Chen, X. Chen, B.A. Khaw, M. Shokeen, K.L. Wooley, H.F. VanBrocklin, Design of targeted cardiovascular molecular imaging probes, *J. Nucl. Med.* 51 (Suppl. 1) (2010) 3S–17S.
- [57] M.D. Majmudar, J. Yoo, E.J. Kelher, J.J. Truelove, Y. Iwamoto, B. Sena, P. Dutta, A. Borodovsky, K. Fitzgerald, M.F. Di Carli, P. Libby, D.G. Anderson, F.K. Swirski, R. Weissleder, M. Nahrendorf, Polymeric nanoparticle PET/MR imaging allows

- macrophage detection in atherosclerotic plaques, *Circ. Res.* 112 (2013) 755–761.
- [58] H.P. Luehmann, E.D. Pressly, L. Detering, C. Wang, R. Pierce, P.K. Woodard, R.J. Gropler, C.J. Hawker, Y. Liu, PET/CT imaging of chemokine receptor CCR5 in vascular injury model using targeted nanoparticle, *J. Nucl. Med.* 55 (2014) 629–634.
- [59] L. Josephson, C.H. Tung, A. Moore, R. Weissleder, High-efficiency intracellular magnetic labeling with novel superparamagnetic-Tat peptide conjugates, *Bioconjug. Chem.* 10 (1999) 186–191.
- [60] W.J. Mulder, F.A. Jaffer, Z.A. Fayad, M. Nahrendorf, Imaging and nanomedicine in inflammatory atherosclerosis, *Sci. Transl. Med.* 6 (2014) 239sr231.
- [61] M. Nahrendorf, E. Keliher, B. Marinelli, F. Leuschner, C.S. Robbins, R.E. Gerszten, M.J. Pittet, F.K. Swirski, R. Weissleder, Detection of macrophages in aortic aneurysms by nanoparticle positron emission tomography-computed tomography, *Arterioscler. Thromb. Vasc. Biol.* 31 (2011) 750–757.
- [62] B.R. Jarrett, C. Correa, K.L. Ma, A.Y. Louie, In vivo mapping of vascular inflammation using multimodal imaging, *PLoS One* 5 (2010) e13254.
- [63] J.C. De La Vega, U.O. Hafeli, Utilization of nanoparticles as X-ray contrast agents for diagnostic imaging applications, *Contrast Media Mol. Imaging* 10 (2015) 81–95.
- [64] E. Jin, Z.R. Lu, Biodegradable iodinated polydisulfides as contrast agents for CT angiography, *Biomaterials* 35 (2014) 5822–5829.
- [65] N. Lee, S.H. Choi, T. Hyeon, Nano-sized CT contrast agents, *Adv. Mater.* 25 (2013) 2641–2660.
- [66] H. Boll, S. Nittka, F. Doyon, M. Neumaier, A. Marx, M. Kramer, C. Groden, M.A. Brockmann, Micro-CT based experimental liver imaging using a nanoparticulate contrast agent: a longitudinal study in mice, *PLoS One* 6 (2011) e25692.
- [67] B. Trachet, R.A. Fraga-Silva, A. Piersigilli, A. Tedgui, J. Sordet-Dessimoz, A. Astolfo, C. Van der Donckt, P. Modregger, M.F. Stampanoni, P. Segers, N. Stergiopoulos, Dissecting abdominal aortic aneurysm in Ang II-infused mice: suprarenal branch ruptures and apparent luminal dilatation, *Cardiovasc. Res.* 105 (2015) 213–222.
- [68] J. Ding, Y. Wang, M. Ma, Y. Zhang, S. Lu, Y. Jiang, C. Qi, S. Luo, G. Dong, S. Wen, Y. An, N. Gu, CT/fluorescence dual-modal nanoemulsion platform for investigating atherosclerotic plaques, *Biomaterials* 34 (2013) 209–216.
- [69] F. Hyafil, J.C. Cornily, J.E. Feig, R. Gordon, E. Vucic, V. Amirkopian, E.A. Fisher, V. Fuster, L.J. Feldman, Z.A. Fayad, Noninvasive detection of macrophages using a nanoparticulate contrast agent for computed tomography, *Nat. Med.* 13 (2007) 636–641.
- [70] D.P. Cormode, T. Skajaa, M.M. van Schooneveld, R. Koole, P. Jarzyna, M.E. Lobatto, C. Calcagno, A. Barazzza, R.E. Gordon, P. Zanzonico, E.A. Fisher, Z.A. Fayad, W.J. Mulder, Nanocrystal core high-density lipoproteins: a multimodality contrast agent platform, *Nano Lett.* 8 (2008) 3715–3723.
- [71] D.P. Cormode, E. Roessl, A. Thran, T. Skajaa, R.E. Gordon, J.P. Schломка, V. Fuster, E.A. Fisher, W.J. Mulder, R. Proksa, Z.A. Fayad, Atherosclerotic plaque composition: analysis with multicolor CT and targeted gold nanoparticles, *Radiology* 256 (2010) 774–782.
- [72] D.E. Kim, J.Y. Kim, I.C. Sun, D. Schellingerhout, S.K. Lee, C.H. Ahn, I.C. Kwon, K. Kim, Hyperacute direct thrombus imaging using computed tomography and gold nanoparticles, *Ann. Neurol.* 73 (2013) 617–625.

Review

For reprint orders, please contact reprints@future-science.com



Nanomedicine as a strategy to fight thrombotic diseases

This review highlights the preclinical and clinical research based on the use of nano- and micro-carriers in thrombolytic drug delivery. Ischemic heart and stroke caused by thrombosis are the main causes of death in the world. Because of their inactivation in the blood, high doses of thrombolytics are administered to patients, increasing the risk of intracranial hemorrhage. Preclinical research conducted with lipid, polymer or magnetic nanoparticles loaded with thrombolytic drugs showed an enhancement of thrombolysis and a reduction of undesirable side effects. Targeted nanocarriers exhibited an increased accumulation into clot. Clinical trials were already conducted with lipid-based microbubbles combined with ultrasound and thrombolytic drug and showed thrombolysis improvement. Future validation of nanosystems is awaited in clinic. This research opens new strategies for the management of thrombotic diseases.

To dissolve a thrombus, thrombolytic drugs are administered, but they are rapidly inactivated in the blood. High amounts are thus injected to patients with the risk to develop intracranial hemorrhages. Nanocarriers and microbubbles have been tested in preclinical models to deliver thrombolytic drugs. These systems have the advantage to protect the drug from the degradation. In clinical trials, galactose and lipid-based microbubbles associated to ultrasound and thrombolytic drugs showed an enhancement of thrombolysis. Other systems are also expected with new drugs combined or not with endovascular intervention to treat ischemic heart or stroke.

Keywords: animal models • drug delivery • ischemic heart • microbubbles • nanocarriers • stroke • thrombolytic

Atherosclerosis is a multifactorial and slowly progressing pathophysiological disease. It is responsible for 17.3 million deaths per year. Among these, myocardial infarction and ischemic stroke are, and will remain the principal cause of death in the world [1]. The development of atherosclerosis is linked to some risk factors among which diabetes, hypertension, smoking, high total cholesterol, high BMI and physical inactivity [1].

The stages of this disease are now understood in detail. Atherosclerotic lesions begin as fatty streaks in lesion-prone areas in aortic bifurcations. These regions exposed to a disturbed flow may develop an activated endothelium. Low-density lipopro-

teins (LDLs) derived cholesterol extravasate through the defective endothelium into the subendothelial space. There, LDLs are oxidized (oxLDLs) by enzymes such as myeloperoxidase, 15-lipoxygenase or nitric oxide synthase. The recruitment of monocytes is stimulated in part by oxLDLs and is regulated by adhesion molecules expressed on the surface of endothelial cells (VCAM-1, ICAM-1). Monocytes are subsequently differentiated into macrophages (Figure 1A). The macrophages express scavenger receptors (SR-A and CD36) which recognize oxLDLs. In an advanced lesion, smooth muscle cells (SMCs) present in media, proliferate, express scavenger receptors and can also take up

Mariana Varna^{‡,1,2}, Maya Juenet^{‡,1,2}, Richard Bayles¹, Mikael Mazighi^{1,3}, Cédric Chauvierre^{1,2} & Didier Letourneur^{*1,2}

¹Inserm, U1148, Cardiovascular Bio-Engineering, X. Bichat Hospital, 75018, Paris, France

²Institut Galilée, Université Paris 13, Sorbonne Paris Cité, 93430, Villejuif, France

³AP-HP, Lariboisière Hospital, 75010, Paris, France

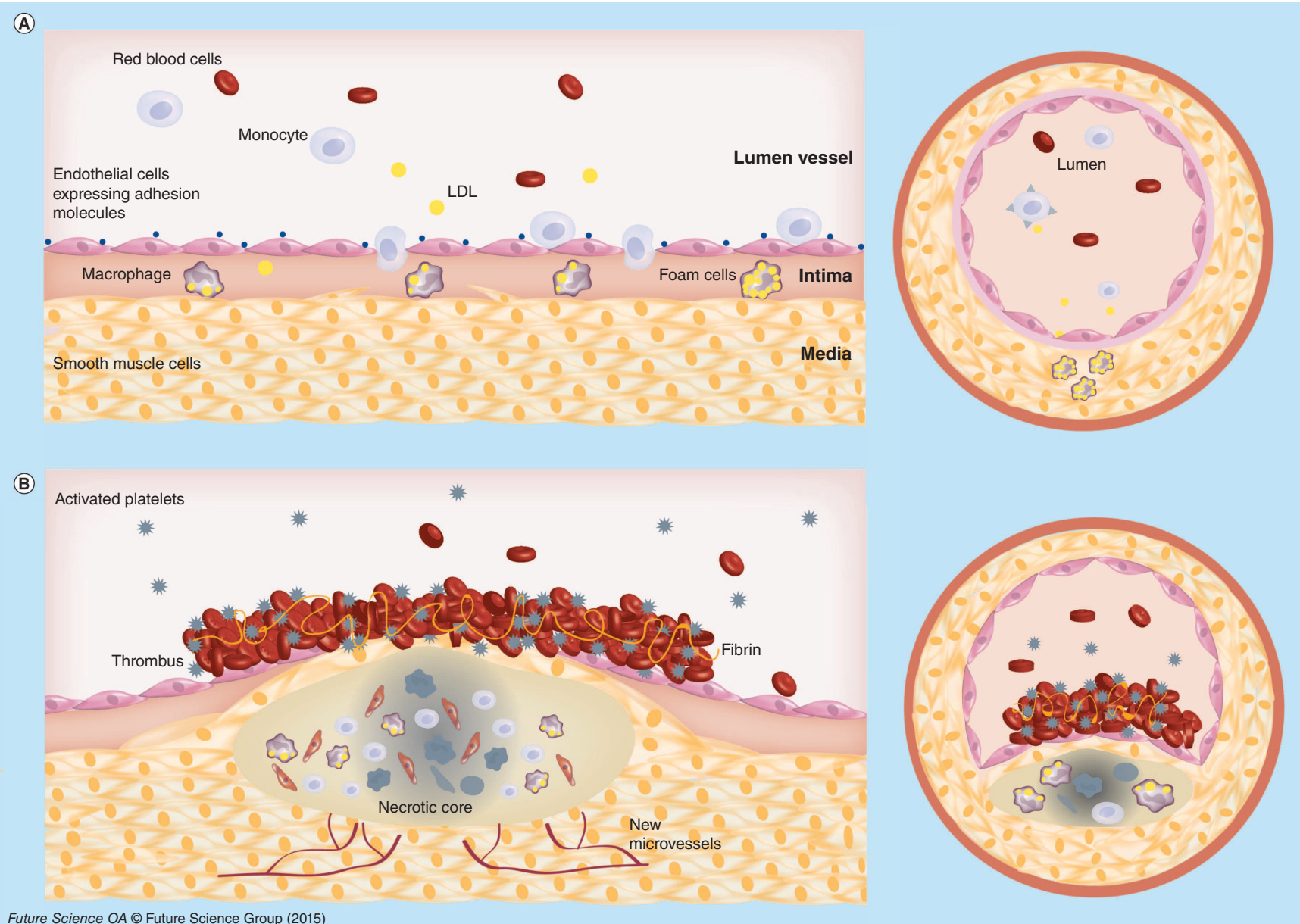
*Author for correspondence:

Tel.: +33 140 257 539

Fax: +33 149 403 008

didier.letourneur@inserm.fr

[‡]Authors contributed equally



Future Science OA © Future Science Group (2015)

Figure 1. Atherosclerotic plaque development. (A) Cholesterol derived low-density lipoproteins extravasate in the intima where they are oxidized low-density lipoproteins. Endothelial cells are activated and express specific adhesion molecules. These phenomena drive the recruitment of monocytes which differentiate into macrophages expressing scavenger receptors, and the uptake oxidized low-density lipoproteins. Smooth muscle cells migrate into the intima, proliferate and contribute to foam cell formation. (B) In advanced stages, a fibrous cap made of smooth muscle cells and collagen fibers is formed. Apoptotic events and necrotic zones appear in a hypoxic environment inducing new microvessel development. With plaque rupture thrombogenic substances are released into the circulation and promote platelet activation and adhesion to endothelium and thrombus formation.

oxLDLs contributing to foam cell formation. SMCs also synthesize extracellular matrix proteins leading to fibrous cap development. During the progression of atherosclerosis, endothelial cells, macrophages and smooth muscle cells die by apoptosis or necrosis contributing to necrotic core formation within the plaque [2,3]. Focal calcifications, neovascularization and intraplaque hemorrhages characterize high-risk plaques with a thin fibrous cap [4]. The development of atherosclerosis begins in childhood. Sometimes, growing plaques become suddenly complicated and could break inducing a luminal thrombosis (Figure 1B). Some factors have been identified to cause plaques rupture. It is recognized the key role of the thickness of the fibrous cap and intraplaque hemorrhages induced by neovascularization. Plaque rupture exposes thrombogenic substances of the plaque to the circulating blood, promoting platelet activation and adhesion to endothelium and thrombus formation [5]. The thrombus development is initiated by tissue factor, and culminates with the circulating platelet recruitment with concomitant generation of thrombin and fibrin [6]. The thrombus is composed of fibrin monomers cross-linked through lysine side chains [5].

Atherosclerosis alone is rarely fatal, but the complications induced by thrombosis, myocardial ischemia and stroke, are the most common causes of death in western societies [3]. Arterial thrombosis differs from venous thrombosis and is therefore treated in a different way. The arterial thrombi formed after plaque rupture are rich in activated platelets, while thrombi formed in veins are rather rich in fibrin and trapped red blood cells [7]. Arterial thrombosis is thus treated with drugs targeting platelets whereas venous thrombosis is treated with antithrombotic drugs.

Therapeutic drugs & side effects

Thrombolytic agents are able to induce thrombus lysis by the degradation of fibrin contained in clots [8]. Clot dissolution (fibrinolysis or thrombolysis) is enzymatically driven by a serine protease named plasmin, which is obtained from plasminogen. The conversion of plasminogen into plasmin is made by tissue plasminogen activators (tPAs). There are two groups of thrombolytic drugs: those which are able to bind both free circulating and/or clot bound plasminogen, and those which bind only clot bound plasminogen (Figure 2). Few plasminogen activators [5,9,10] have been approved by the US FDA for clinical applications: urokinase (UK), streptokinase (SK), alteplase (tPA), tenecteplase (TNK-tPA), reteplase (rPA) (Table 1). Natural inhibitors of plasminogen activators have been described such as α -2-antiplasmin, α -2-macroglobuline, anti-C1 esterase, α -1 antitrypsin and PAI-1 [11,12]. Because of their

relatively short half-life, high quantities of thrombolytic drugs need to be administered into patients. After being administered to patients, the drugs undergo cell metabolism and are distributed throughout the body. In order to obtain a therapeutic effect, high doses have to be injected, which may lead to undesirable risk of hemorrhagic transformation after thrombolytic therapy [8]. On one hand, the degradation of the components of neurovascular unit (endothelial cells, basal membrane, perivascular astrocytes and neurons) induced by ischemia leads to the passage of fluids from intravascular space into the brain, with formation of edema and intracranial hemorrhages. In these conditions, tPA can also pass the blood–brain barrier and through interaction with the NMDA-type-glutamate receptor can potentially amplify excitotoxic calcium currents. On the other hand, indirect upregulation by tPA of MMP9 activity, which degrades extracellular matrix integrity, increases the risk of neurovascular cell death and blood–brain barrier disruption [13].

The development of new formulation of these drugs gains more and more interest. A promising strategy consists of the use of nano- and micro-carriers [14,15]. The most important advantages of these platforms are the prevention of the degradation of the drugs by enzymes in the blood and the possibility to target a thrombus using specific ligands leading to increase the drug amount into the clot. In the next section we detail the different categories of nano- and micro-carriers used to deliver thrombolytic drugs.

Composition of nano- and micro-carriers used in thrombolytic therapy

Several types of materials, polymeric, lipid or metallic based, can be employed to deliver thrombolytic drugs (Figure 3). These materials are well-tolerated *in vivo*, possess low toxicity, and are easy to biofunctionalize. Depending on their composition, hydrophobic or hydrophilic drugs can be incorporated or attached. The formulations of nano- and micro-carriers include spheres, capsules and vesicles.

Some factors such as the size, the surface charge and the presence or not of a polymer coating, affect the clearance and the biodistribution of nano- and micro-carriers. The size can be modulated during the synthesis of nanoparticles. The charge and the composition of the surface determine the clearance by the monocyte macrophage system (MPS). Following intravenous administration, the naked nano- and micro-carriers are cleared by the MPS and the recognition is induced by the attachment on the surface of the carriers of plasma proteins named opsonins (C3b, iC3, IgG, IgM) [16]. To avoid this and to prolong the circulation time in the body, poly(ethylene glycol) (PEG), a hydrophilic

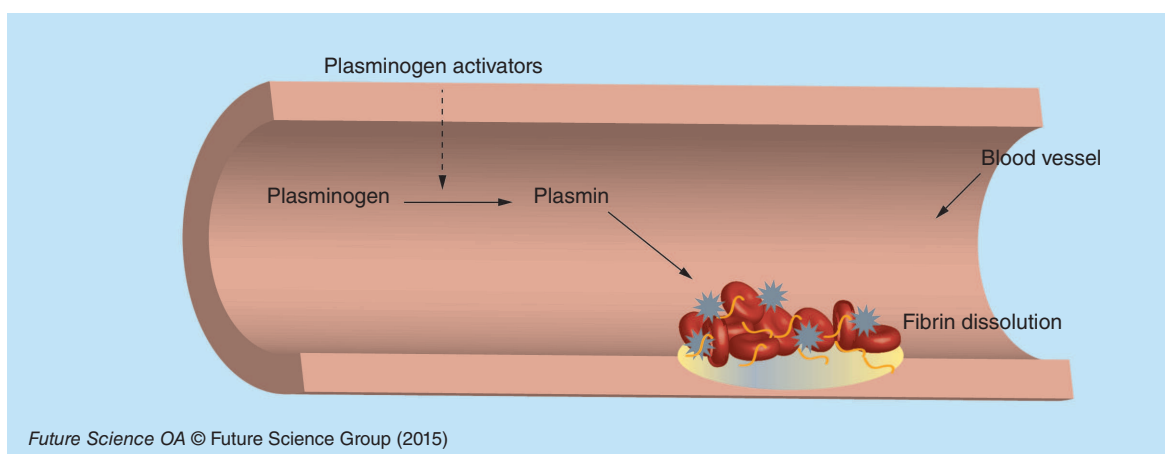


Figure 2. Schematic representation of fibrin clot thrombolysis induced by thrombolytic agents in blood vessels.

biocompatible and biodegradable polymer, has been commonly used in the coating. PEG is approved by the FDA for clinical use. PEG, either adsorbed or covalently attached to the surface of nano- and micro-carriers, induces steric inhibition of opsonins and thus their attachment at the surface of the carrier [17]. Moreover PEG is easy to functionalize. Another advantage provided by the coating of nano- and micro-carriers with PEG is the possibility to attach different ligands on the surface of the carriers, in order to target a tissue or cells of interest [18,19].

Lipid-based nanoparticles

Among the lipid-based, only liposomes and some types of microbubbles have been used in thrombo-therapy. Described 50 years ago by Bangham, liposomes represent the most used carriers to deliver active drugs. Liposomes are defined as bilayer phospholipid vesicles, mimicking the cellular membrane, enclosing an aqueous core. Since their discovery the preparation methods were diversified [20]. The choice of the method and subsequent processing steps are important because it determines the loading efficacy as well as the size. The lack of toxicity of liposomes and their biodegradation represent a significant advantage in their use as carriers to deliver thrombolytic drugs [21]. However, one of the limitations of liposomes is their poor stability in the blood flow.

Polymer-based carriers

Synthetic and natural polymers are used in the design of nano- and micro-carriers charged with thrombolytic drugs. The polymers have the advantage of being more resistant to mechanical constraints than lipid-based ones. In addition to their biocompatibility and biodegradability, polymer carriers can be tuned in terms of size, porosity and hydrophobicity. Polymers are either functionalized with reactive groups, such as primary amines, for reaction with the drug further to the

nanoparticle synthesis or are designed to directly interact with the therapeutic agent during the nanoparticle formulation. The first strategy leads to systems where the drug is charged at the surface of the particle. It has especially been applied to magnetic particles coated with a polymer shell (Figure 3). The most common is dextran which is a polysaccharide composed of α -D-glycose units that bind to each other through glycosidic bonds. Because of its affinity for iron, dextran is largely used in the coating of iron oxide nanoparticles [22]. With this strategy, the drug covalent binding is often achieved via a functionalized PEG spacer. The second method results in drug encapsulation and has been set up with different polymer types. For example, polyvinyl alcohol (PVA), a biodegradable synthetic polymer, has been formulated into a porous material to encapsulate the drug. Poly(lactic-co-glycolic acid) (PLGA), an FDA and EMA-approved polymer, is another promising candidate for drug encapsulation. It is largely used in medical research because of its good biodegradability and biocompatibility.

Another mechanism of nanoparticle formation is the ionic gelation process. Chitosan nanoparticles are obtained by this method allowing for drug entrapment during the assembly process. Chitosan is a natural water soluble polysaccharide. It possesses cationic and hydrophilic properties as well as good biodegradability and biocompatibility, low toxicity and immunogenicity [23]. In some cases drug retention is enhanced by ionic interaction between the drug and the polymer chains. Gelatin, a natural polymer that shows the advantage to be biodegradable and easily tunable have been modified for an enhanced interaction [24].

Inorganic nanocarriers

Inorganic nanocarriers used in the delivery of thrombolytic drugs are principally represented by magnetic nanoparticles. They are composed of a paramag-

netic iron oxide core, made of magnetite (Fe_3O_4) or maghemite ($\gamma\text{-Fe}_2\text{O}_3$) or a mixture of both, surrounded by a shell made of polymers, to improve colloidal stability (Figure 3). Depending on the size, magnetic nanoparticles are divided into two categories: ultrasmall superparamagnetic iron oxides (USPIO), with a hydrodynamic size less than 50 nm and superparamagnetic iron oxides (SPIO) particles, with hydrodynamic size between 50 and a few hundred nanometers. Magnetic nanoparticles are biodegradable, participating in the iron homeostasis in the body [22].

One important aspect of the use of magnetic nanoparticles in the delivery of drugs is linked to their magnetic capabilities. Under the local application of a magnet generating a strong magnetic field, magnetic nanoparticles tend to accumulate into a specific site. This property was evaluated in regenerative medicine for cardiovascular applications [25–27].

In the next section, we describe the preclinical uses of nanosystems in the delivery of thrombolytic drugs.

Thrombolytic therapy using nanocarriers & microbubbles in preclinical development

The use of nano- and micro-carriers to deliver thrombolytic drugs shows several advantages such as protection from inhibitors present in the blood and concentration of drugs at the thrombus. The nanocarriers have a size between a few nanometers to a few hundred of nanometers. Microbubbles have a size between 2 and 8 μm and are composed of a shell made of phospholipid, polymer or albumin, and a core loaded with air or high molecular weight gas [28]. Only three thrombolytic drugs have been loaded into nano- and micro-carriers and tested *in vivo*. These aspects will be detailed in this section dedicated to preclinical development.

Streptokinase

The history of thrombolytic therapy began in 1933, with the discovery, by Tillett and Garner, that certain strains of *Streptococcus* were able to dissolve fibrin clots [10,29]. SK is a single chain protein produced by different strains of streptococcal bacteria [30]. This protein has a molecular weight of 47 kDa and contains 414 amino acids. SK indirectly catalyses the activation of plasminogen [31] by binding with free circulating plasminogen and thus forming a complex that converts plasminogen to plasmin [9]. SK activates not only fibrin-bound plasminogen but also the free plasminogen inducing serious bleeding complications [30]. This protein shows a biphasic half-life, a first one rapid (16 min) and a second one longer (90 min). The first initial half-life is linked to the complexation of anti-SK antibodies while the second half-life is due to biological elimination of the protein. SK is inexpensive but shows

Table 1. Examples of clinically used thrombolytic drugs.

Thrombolytic agent	Abbreviation	Molecular weight (kDa)	Indication	US FDA status	Structure (domains)	Half-life (min)	Fibrin selective	Elimination
Urokinase (Abbokinase [®] , Abbot Laboratories, TX, USA)	UK	2 polypeptides chains (32/54)	AMI, PE	Approved	P/K/EGF	15–20	No	Kidney
Streptokinase (Streptase)	SK	47	AMI, PE, DVT, PAO	Approved	α, β, γ	10–16	No	Kidney
Alteplase (Activase [®] , Genentech, CA, USA; Actilyse [®] , Boehringer Ingelheim, Germany)	tPA	68	AMI, PE, IS	Approved	F/EGF/K1/K2/S	4–6	Yes	Liver
Tenecteplase (TNKase [®] , Genentech, USA; Metalyse [®] , Boehringer Ingelheim, Germany)	TNK-tPA	70	AMI	Approved	F/EGF/K1	20	Yes	Kidney
Reteplase (Retavase [®] , Chiesi Farmaceutici S.p.A., Italy; RapiLyse [®] , Actavis, NJ, USA)	rPA	40	AMI, DVT, PAO	Phase II	K2/SP	18	Yes	Kidney
Staphylokinase	SAK	16.5	AMI	Phase II	2 chains: a, b	6	Yes	Liver
Lanoteplase	nPA	53.5	AMI	Phase II	F/K1/K2/SP	37	Yes	Liver
Desmoteplase	batPA	52	IS	Phase III	F/EGF/K1/SP	240	Yes	Liver

AMI: Acute myocardial infarction; DVT: Deep-vein thrombosis; EGF: EGF domain; F: Finger domain; IS: Ischemic stroke; K1: Kringle 1 domain; K2: Kringle 2 domain; PAO: Peripheral arterial occlusion; PE: Pulmonary embolism; SP: Serine protease domain.

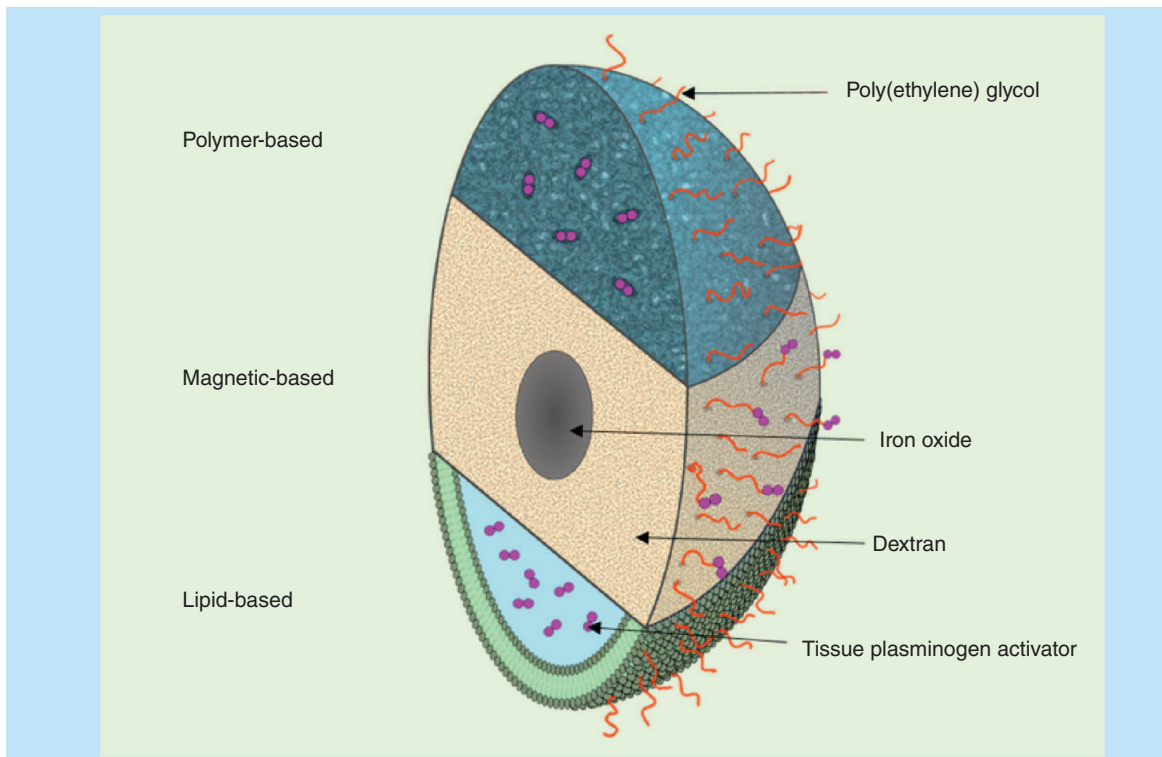


Figure 3. Schematic representation of polymer-, magnetic- and lipid-based stealth nanocarriers loaded with thrombolytic drugs.

an immunogenic effect and his activity is affected by the presence of antibodies [9,10].

Nanocarriers loaded with SK

In order to reduce side effects induced by SK (Streptase[®]) treatment, Leach *et al.* encapsulated the enzyme into naked liposomes and into a water-soluble double emulsion polymer (PEG and PVA). The authors noted some difficulties with the stability of the liposomes. Only 30% of the initial SK was entrapped within liposomes. The SK yield into polymeric porous particles was 82%. When injected into rabbits with autologous carotid artery thrombosis, the time necessary for reperfusion was significantly reduced: on average 7.3 min were necessary for SK loaded into polymers, 19.3 min for SK-liposome and 74.5 min for free SK [32]. Later, the same team tested these polymer-based nanoparticles in dogs with autologous coronary thrombus. The polymer-based nanoparticles showed a greater reduction in the time required to achieve reperfusion than free SK. In parallel, a reduction of infarct size and less hemorrhage were observed. These results were probably due to the enhanced transport of the encapsulated drug into the core of the thrombus. This accumulation was associated with the polymer dissolution and the release of protected SK [33,34].

Vaidya *et al.* obtained 18% of SK entrapment efficacy into liposomes. The SK was loaded into liposomes

during hydration of the lipid film. The liposomes were moreover loaded with RGD (arginine-glycine-aspartic acid) peptide in order to target GPIIb/IIIa receptor expressed at the surface of the activated platelets in thrombi (Figure 4). The liposomes were injected into rats with carotid thrombosis generated by a human clot. Thirty minutes after treatment, a better thrombolytic activity was observed in rats receiving liposomes encapsulating SK compared with SK alone (28 vs 17%, respectively). This thrombolytic effect was explained by the protection of the SK simultaneous to the accumulation of targeted liposomes into clot [35].

Taken together these preclinical results show that loading the SK into nanocarriers protects it from premature inactivation in the blood and improves its accumulation into the clot leading to an enhanced thrombolysis.

Urokinase

UK is a serine protease that activates plasminogen into plasmin thus degrading fibrin clots [36]. It is a protein with two polypeptide chains of 32 kDa and 54 kDa, respectively. Originally obtained from human urine, UK is now produced from human renal cell lines. Into whole blood, UK has a half-life from 15 to 20 min. High amounts are necessary to obtain a significant thrombolytic effect, inducing undesirable side effects such as hemorrhages [9]. Like SK, UK

activates both the circulating and the fibrin-bound plasminogen [10].

Nanocarriers loaded with urokinase

Jin *et al.* prepared UK-loaded in water-soluble chitosan nanoparticles using an ionic cross-linking method. The final size was 236 nm with a drug encapsulation efficiency of 95%. They injected these nanocarriers into rabbits with jugular thrombosis obtained after administration of thrombin. An increased capacity of clot lysis was observed when compared with free UK. *In vivo*, free UK was metabolized rapidly with a half-life <20 min while the UK loaded inside the NPs showed a slow release rate [37].

Dextran-coated magnetic nanoparticles were used for covalent bioconjugation with UK via primary amine. The nanoparticles with 116-nm size were injected into rats with autologous carotid artery and left jugular vein thrombosis. When applying permanent magnets in the thrombus area, the nanoparticles were concentrated into the thrombotic site, showing a fivefold higher thrombolytic activity than free UK [38].

In an interesting approach, Marsh *et al.* developed perfluorocarbon (PFC) nanoparticles covalently coupled with UK. In order to target femoral thrombi

generated in dogs, they coupled antifibrin antibody on the surface of the nanoparticles. When injected into the animals, the thrombus dissolution was higher in animals receiving PFC-UK loaded and antifibrin functionalized nanoparticles than in control animals receiving irrelevant IgG targeted UK PFC nanoparticles [39]. This thrombus specificity was achieved by fibrin monoclonal antibodies allowing an enhanced delivery of UK.

Mu *et al.* have successfully loaded UK and RGD to the surface of a microbubble-based ultrasound contrast agent. They observed an aggregation at the surface of femoral arterial thrombi in rabbits. However, the authors did not quantify the *in vivo* thrombolytic activity [40]. In rabbits with middle cerebral artery occlusion receiving UK and sulfur hexafluoride microbubbles, the addition of transcranial Doppler ultrasounds (2MHz) showed an enhancement of the recanalization rate compared with animals receiving only UK [41].

Tissue plasminogen activator & its recombinant forms (tPA, rtPA)

tPA is encoded in humans by a gene on chromosome 8 and is produced by endothelial cells. tPA has two

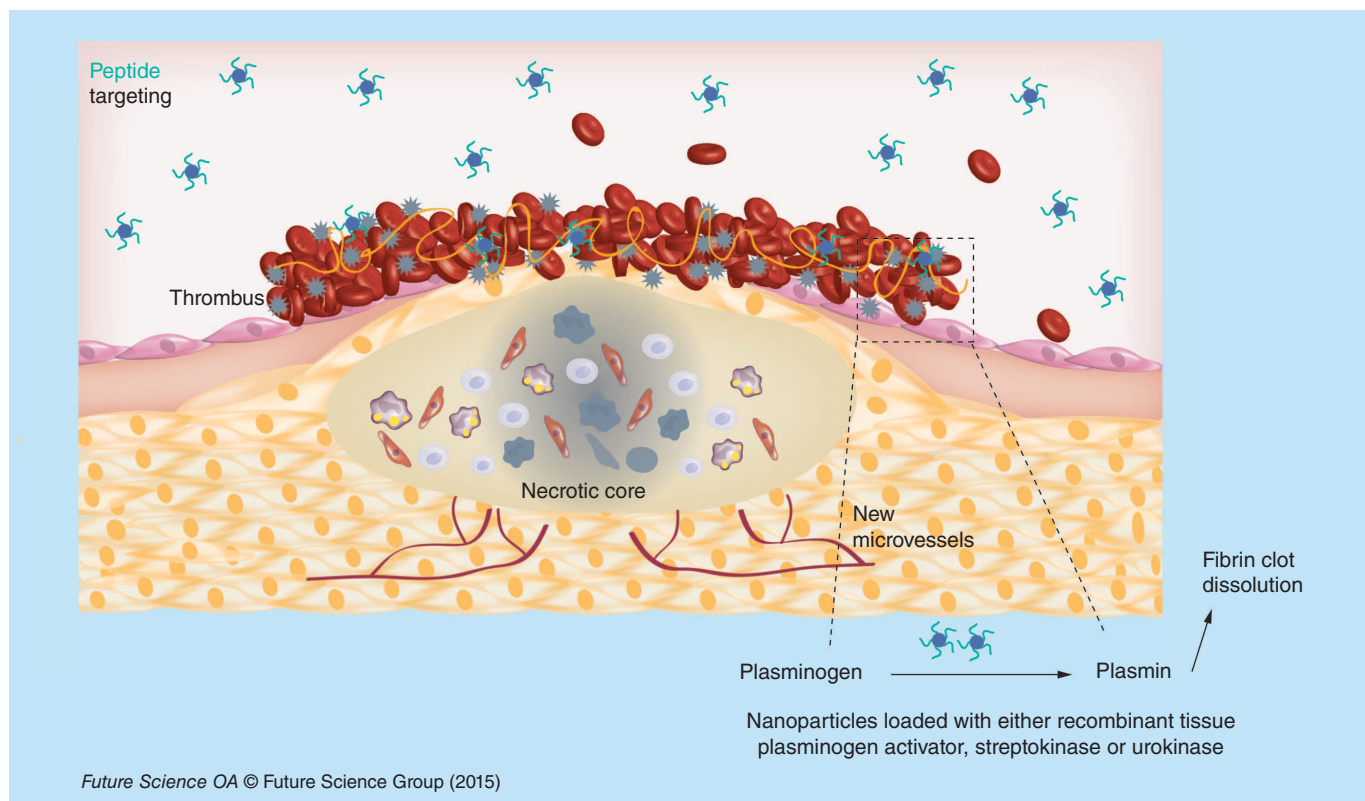


Figure 4. Targeting modality by peptides. Nanocarriers loaded with thrombolytic drugs and decorated with RGD peptides that recognize GPIIb/IIIa receptor at the surface of activated platelets, show an accumulation in the thrombus and leading to an enhancement of thrombus lysis.

inhibitors, PAI-1 and PAI-2, which belong to the serpin superfamily. The tPA residues 296–304 are critical for the interaction with PAI-1. It shows a limited half-life of about 4–6 min [9]. Recombinant tPA (rtPA, Alteplase) is a serine protease with a molecular weight of 68 kDa. This recombinant form is produced by Chinese hamster ovary (CHO) cell lines by cDNA technology. This enzyme cleaves the Arg–Val bond, inducing the plasminogen conversion into plasmin [10].

Nanocarriers loaded with rtPA

Uesugi *et al.* have loaded rtPA (Cleactor[®]) on cationized gelatin and PEG-grafted nanoparticles. When injected into rabbits with balloon injury of right femoral artery, the half-life of rtPA was three times enhanced due to its complexation with gelatin. In order to induce thrombolysis they applied ultrasound (1MHz, 0.75 W/cm²) for up to 60 min [24]. A complete recanalization was observed, which was probably linked to the dissociation of rtPA from gelatin and maybe to the effects of ultrasound on thrombus. Similar results were obtained on swine with acute myocardial infarction with a thrombotic occlusion of left coronary artery. A high recanalization rate was observed in 9 out of 10 swines when receiving nanoparticles, whereas only 1 out of 10 showed complete recanalization in a group with rtPA alone [42].

Zhou *et al.* developed PLGA nanocarriers loaded with rtPA (Alteplase). In order to enhance the accumulation in a rat model of abdominal aortic thrombi induced using ferric chloride, they covered the nanoparticles with a chitosan shell and targeted it with cyclic RGD peptide via a carbodiimide bond. The rtPA loaded into the nanoparticles showed a prolonged half-life. The authors reported some limitations such as the encapsulation efficacy of the rtPA (between 54 and 64%) simultaneously to a partial loss of rtPA activity [43].

Magnetic nanoparticles coated with polyacrylic acid (PAA) were covalently coupled with an amine group of rtPA (Alteplase). Magnetic nanoparticles show the advantage of being made of a magnetite (Fe_3O_4) core that responds to an external magnetic field with superparamagnetic properties. The nanoparticles were concentrated into a thrombus under external magnetic guidance after injection into rats with iliac artery embolisms (Figure 5). The blood flow restoration was observed 75 min later with an equivalent of 0.2 mg/kg of rtPA coupled with magnetic nanoparticles. With a dose of 1 mg/kg, the blood flow restoration was obtained within only 30 min [44]. The same team later developed magnetic nanoparticles coated with a shell of poly(aniline-co-N-[1-one-butrylic acid] aniline) and loaded with rtPA. With this strategy the amount of

rtPA loaded was 50% higher than the amount loaded previously into PAA-coated nanoparticles. After injection into rats with iliac embolisms, the nanoparticles were guided towards the clots using an external magnetic field [45]. rtPA (Alteplase) was covalently immobilized on chitosan-coated magnetic nanoparticles and injected into rats with iliac artery embolisms. The administration of rtPA loaded on chitosan magnetic nanoparticles associated with a magnetic guidance resulted in 70–80% blood flow recovery with a five-fold lower dosage, 0.2 mg/kg compared with 1 mg/kg required for thrombolysis with free rtPA [23].

These nanocarriers reduce the effective dose of active principle injected but also increase the local concentration and prevent side effects. A limitation of this method could be linked to the fact that the external magnetic field decreases with the tissue depth, and thus makes it difficult to target a site deeper in the body. Kempe *et al.*, implanted ferromagnetic stents for the treatment of in-stent thrombosis. In their approach, they used PEGylated magnetic nanoparticles loaded with rtPA (Alteplase). The nanoparticles were injected in pigs with ferromagnetic stents in their coronary artery. The restoration of blood flow with rtPA loaded nanoparticles was reached with a lower amount of drug compared with free rtPA [46].

The McCarthy team coupled rtPA (Alteplase) to cross-linked dextran-coated iron oxide nanoparticles (CLIO). In order to increase the distance between the fibrinolytic drug and the particles and to minimize the steric interactions they added a PEG spacer moiety. The nanoparticles were moreover functionalized by covalent grafting of activated factor XIII (FXIIIa) via peptide affinity ligands. They injected these targeted nanoparticles (CLIO-FXIII-PEG-rtPA) into mice with pulmonary embolisms obtained with human clots. This choice was based on the facts that the murine plasminogen system is tenfold less sensitive to human tPA. The authors concluded that the targeted nanoagent displayed similar thrombolytic potential as free tPA [47]. These studies showed that magnetic nanoparticles have a potential for local delivery of thrombolytic drugs either by an external magnetic field or with peptides.

The loading of rtPA (Alteplase) into liposomes obtained using the freeze-thawing preparation method, did not alter the fibrinolytic activity of the drug. The rtPA loaded into PEGylated liposomes showed 21-fold prolonged circulation time compared with free rtPA [17]. Absar *et al.* developed liposomes, either coated with PEG or not, and decorated with a peptide sequence of fibrinogen gamma-chain targeting GPIIb/IIIa. Entrapment efficacy of rtPA (Alteplase) varied from 12 to 26% for non-PEGylated liposomes and from 36 to 52% for

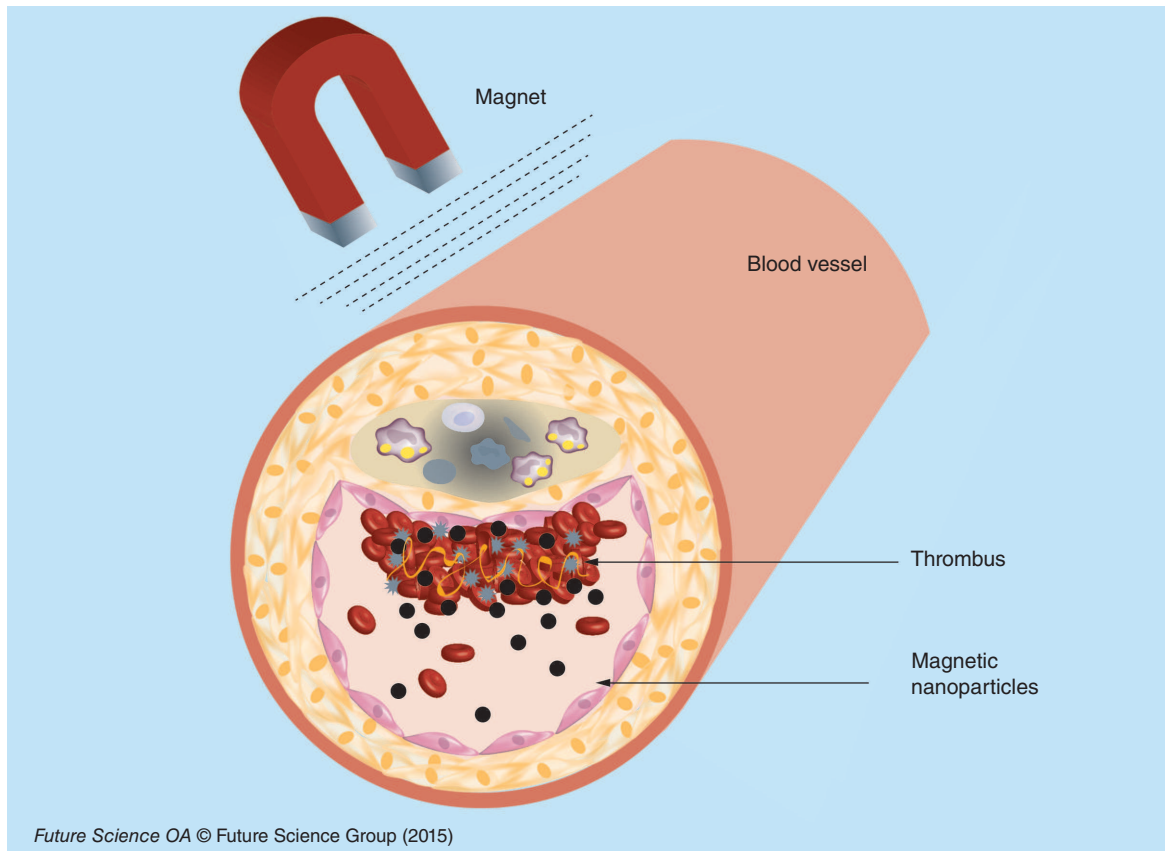


Figure 5. Targeting modality by magnet. Ultrasmall paramagnetic iron oxide nanocarriers loaded with thrombolytic drugs are concentrated by an external magnet in the thrombus to enhance its lysis.

PEGylated liposomes. These nanoparticles were injected into rats with inferior vena cava thrombosis induced with a FeCl_3 solution. An enhancement of 35% of thrombolytic activity was observed for rtPA-loaded into targeted liposomes when compared with native rtPA. Tested *ex vivo* on human clot, liposomal rtPA showed a slightly lower activity compared with native rtPA, this being probably linked to the incomplete release of the drug from liposomes [48].

An interesting approach to enhance the thrombolysis is the use of ultrasound as adjuvant therapy. This strategy was developed with echogenic liposomes as well as with microbubbles. Echogenic liposomes (ELIP) are composed of a phospholipid bilayer enclosing both gas and liquid. The advantage of this system is the follow-up by echography of thrombus evolution before, during and after thrombolysis. Moreover, ELIP are not only ultrasound contrast agents but also potential vectors for thrombolysis. Laing *et al.* developed ELIP loaded with rtPA (Alteplase) in the core (15%) or associated with the phospholipid bilayer (35%). The rtPA solution was loaded into liposomes during the hydration of lipid film. ELIP loaded with rtPA were injected into rabbits with abdominal aortic thrombi exposed to ultrasound (pulsed ultrasound 5.7 MHz

for 2 min). The degree of recanalization determined by Doppler flow measurements, showed that ELIP charged with rtPA had similar efficacy to free rtPA for thrombus dissolution *in vivo*. Injection of saline (control), empty ELIP, or empty ELIP associated with ultrasound did not show any thrombolytic effect [49]. The recanalization rate was variable in the absence of ultrasound, showing that ultrasound therapy enhance thrombolytic effect [50]. This enhancement could be explained by acoustic cavitation, thermal effects or microstreaming (Figure 6) [51–53].

In order to enhance accumulation into thrombus, Higisawa *et al.* developed perfluorocarbon based echogenic liposomes targeted with a RGD peptide loaded or not with rt-PA (Monteplase). They injected them intravenously into rabbits with thrombus in ilio-femoral arteries and applied ultrasound. A higher recanalization rate (nine out of ten rabbits) was observed when ultrasound were applied, compared with that of animals receiving nontargeted liposomes (two out of ten rabbits) or rtPA monotherapy (four out of ten rabbits) [54].

Microbubbles with a size from 2 to 8 μm represent another class of lipid based carriers used in thrombolytic strategies. They are composed of a shell made of phospholipids, polymers or albumin, and a core of air or

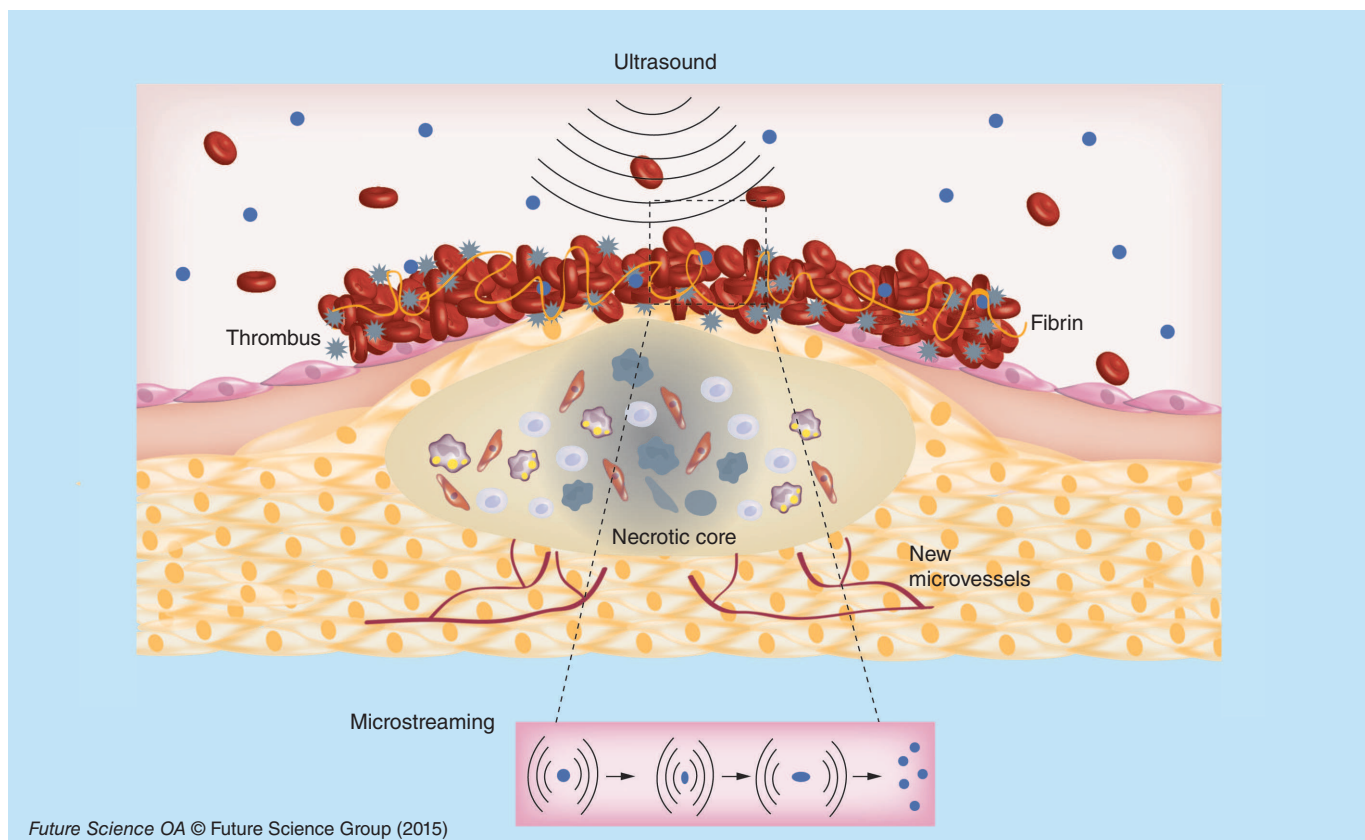


Figure 6. Schematic representation of thrombus dissolution by ultrasound.

high molecular weight gas [28]. The effect of sulfur hexafluoride lipid based microbubbles associated with ultrasound was compared with intravenous administration of rtPA (10 mg/kg) into rats with acute cerebral ischemia obtained after autologous thrombus injection into carotid artery. The two modalities of treatment showed equivalent result in the restoration of blood flow [55].

Nedelmann *et al.* showed on rats with filament occlusion of the right middle cerebral artery that the association of rtPA (Alteplase) with microbubbles and ultrasounds completely restored the blood flow, while rtPA alone partially improved hemispheric perfusion [56]. In a rabbit model of embolic stroke obtained with a clot from a donor rabbit, the combination of microbubbles with rtPA and pulsed ultrasound (1MHz) showed a good recanalization rate [57]. These studies demonstrated that ultrasound could be associated with microbubbles and/or thrombolytic drugs to enhance the recanalization effect.

Microbubbles associated with thrombolytic drugs and/or ultrasound for clinical applications

Microbubbles are the only platform tested in the clinic for thrombolytic therapy. In clinical trials, they were associated or not with ultrasound and showed encour-

aging results. Molina *et al.* included 111 patients with middle cerebral artery occlusions. The 38 patients who received galactose-based microbubbles, rtPA and 2 MHz ultrasound pulse showed a better recanalization rate than the other 73 patients who received either rtPA and ultrasound or rtPA only [58,59]. Later, they associated in another clinical trial, perflutren lipid (MRX-801) microbubbles with rtPA and ultrasound and obtained 67% of recanalization rate compared with 46% for the group receiving only rtPA [60]. Alexandrov *et al.* showed that half of patients receiving rtPA, 2 MHz continuous TCD monitoring and perflutren-lipid based microbubbles demonstrated a complete recanalization rate (six patients out of 12) while none of the patients receiving only rtPA reached a complete recanalization [61]. Microbubbles based on phospholipids encapsulating sulfur hexafluoride combined with transcranial ultrasound and rtPA showed a better recanalization rate compared with patients receiving rtPA and ultrasound [62].

Another clinical trial was made by Pagola *et al.* in patients with stroke with basilar artery occlusion. All the 20 patients received intravenous rtPA, ultrasound and galactose based microbubbles. At 24 h, only 50% of patients showed a progressive recanalization while the other 50% did not show any recanalization [63].

Rubiera *et al.* showed that the recanalization was similar in patients receiving either galactose-based microbubbles or phospholipid-based microbubbles encapsulating sulfur-hexafluoride, and rtPA associated with 2 MHz transcranial Doppler [64].

One possible explanation of thrombolysis enhancement when microbubbles and ultrasound are associated with rtPA, is the mechanical damage induced by the streaming of microbubbles at the surface of the thrombus allowing a higher diffusion of rtPA. This opens new perspectives for clinical thrombolytic therapy with the aim to reduce the dose and, therefore, hemorrhagic side effects.

Discussion & conclusion

Nano- and micro-carriers are able to replace the systemic therapy of whole body with a local therapy reducing significantly undesirable side effects. Although ischemic heart and stroke caused by thrombosis are the main causes of death in the world, there is no existing nanocarrier loaded with thrombolytic drug in clinic. Currently, only galactose or lipid-based microbubbles associated to ultrasound with or without rtPA systemic injection have been evaluated in clinical trials and showed an enhancement of thrombolytic effect. In other pathologies such as cancer or infectious diseases, different therapeutic drugs loaded to nanocarriers have already reached the market. This gap could be partly explained by the distinctive features of thrombosis and of the thrombolytic drugs.

In the case of heart ischemia or stroke it is necessary to act rapidly within the first minutes or hours (<4.30 h) after the appearance of the symptoms. Thrombolytic drugs administered by systemic way are quickly inactivated by inhibitors in blood. Nanocarriers have the advantage to protect the drug, enhancing its half-life in the blood. Encouraging results were thus obtained on preclinical models with lipid or polymer systems loaded with thrombolytic drugs.

The drugs loaded into nanocarriers must keep their therapeutic capacities. The therapeutic drugs are either charged on the surface of the nanoparticles, as for magnetic nanoparticles, or loaded inside nanocarriers, which is the case of polymer or lipid based systems. Another critical point is linked to the amount of drug loaded into nanocarriers. The loading capacity must be maximal in order to reduce the injected quantity of carriers. The preclinical results obtained with liposomes showed a low entrapment efficacy, while a better efficacy was usually obtained with polymer based nanoparticles.

An interesting aspect linked to the use of nanocarriers loaded with therapeutic drugs is the capacity to achieve an active targeting of the thrombus, improving

the therapeutic efficacy. This was for instance possible by using targeting peptides on the surface of nanocarriers. Another modality of targeting tested on preclinical models was based on the use of magnetic nanoparticles. Although encouraging results were obtained in small animals, this method seems difficult to apply in patients because of the deep localization of the thrombus. Maybe, the use of large and ultrastrong magnets would be a possibility to overcome this limitation in the near future.

For all systems, a common limitation is linked to the difficulty to obtain a controlled release. The use of ultrasound can partially control the release into thrombus of therapeutics loaded into echogenic liposomes. However, the ultrasound have a limited penetration into the body, and the use of high frequencies could induce blood vessel lesions. Again, improvements of ultrasound equipment may increase its efficacy.

Another important aspect is linked to the thrombus itself in preclinical studies. Some preclinical models are made on animals with an autologous thrombus. However, the affinity of thrombolytics used in clinics for the animal clot is not similar to the affinity for the human one. The use of animal models obtained with a human clot would thus be more relevant. The aging of the used thrombus is also relevant.

In conclusion, more in depth preclinical research and developments are necessary to improve the targeted delivery of thrombolytic drugs before their translation into clinical practice.

Future perspective

Nanomedicine offers an opportunity and a challenge in the management of a targeted thrombolytic therapy. There are some specific features to take into account for thrombus therapy using nanocarriers. The nanocarrier should load a maximum amount of drug while keeping the thrombolytic efficacy, protect the drug from enzymatic degradation and ensure a rapid release in the thrombus. A balance between all these aspects is mandatory for a better patient care. The development of new materials for nanocarriers and the discovery of new thrombolytic drugs are also considered in the development of nanothrombolysis.

Financial & competing interests disclosure

This work was supported by Lefoulon-Delalande scholarships (to M Varna and R Bayles), EU project NanoAthero FP7-NMP-2012-LARGE-6-309820, IMOVA project (FUI/OSEO, CG93), and ANR-13-LAB1-0005-01 'FucoChem,' University Paris 13 and Inserm. The authors have no other relevant affiliations or financial involvement with any organization or entity with a financial interest in or financial conflict with the subject mat-

ter or materials discussed in the manuscript apart from those disclosed.

No writing assistance was utilized in the production of this manuscript.

Open Access

This work is licensed under the Creative Commons Attribution 4.0 License. To view a copy of this license, visit <http://creativecommons.org/licenses/by/4.0>

Executive summary

- Heart ischemia and stroke are the main causes of death in the world.
- Tissue plasminogen activator but also urokinase and streptokinase are the thrombolytic drugs used in clinic. These drugs are inactivated by circulating inhibitors. Therefore, high amounts are injected to patients in order to obtain a therapeutic effect but with a risk of undesirable side effects such as intracranial hemorrhages.
- Polymer-, lipid- or magnetic-based nano- and micro-carriers are able to deliver thrombolytic drugs according to their size and structure.
- In preclinical studies, nanoparticles loaded with either urokinase, streptokinase or recombinant tissue plasminogen activator (rtPA) have been evaluated. As compared with free drug, a lower amount of drug loaded into nanoparticles was necessary to induce a thrombolytic effect. In parallel, a reduction of intracranial hemorrhages was observed.
- In clinical trials, only galactose and lipid-based microbubbles were evaluated. They were associated to ultrasound and/or rtPA. Enhancement of thrombolytic efficacy was observed with microbubbles associated to ultrasound and rtPA. However, further validation is necessary before a daily clinical use.
- In conclusion, loading thrombolytic drugs into nanocarriers opens new perspectives for thrombotic diseases therapy.

References

Papers of special note have been highlighted as:
•• of considerable interest

- 1 Go AS, Mozaffarian D, Roger VL *et al*. Heart disease and stroke statistics – 2013 update: a report from the american heart association. *Circulation* 127(1), e6–e245 (2013).
- 2 Hilgendorf I, Swirski FK, Robbins CS. Monocyte fate in atherosclerosis. *Arterioscler. Thromb. Vasc. Biol.* 35(2), 272–279 (2015).
- 3 Falk E. Pathogenesis of atherosclerosis. *J. Am. Coll. Cardiol.* 47(8 Suppl.), C7–C12 (2006).
- 4 Fuster V, Fayad ZA, Moreno PR, Poon M, Corti R, Badimon JJ. Atherothrombosis and high-risk plaque: part ii: approaches by noninvasive computed tomographic/magnetic resonance imaging. *J. Am. Coll. Cardiol.* 46(7), 1209–1218 (2005).
- 5 Bivard A, Lin L, Parsons MW. Review of stroke thrombolytics. *J. Stroke* 15(2), 90–98 (2013).
- 6 Furie B, Furie BC. Mechanisms of thrombus formation. *N. Engl. J. Med.* 359(9), 938–949 (2008).
- 7 Mackman N. Triggers, targets and treatments for thrombosis. *Nature* 451(7181), 914–918 (2008).
- 8 Mazighi M, Serfaty JM, Labreuche J *et al*. Comparison of intravenous alteplase with a combined intravenous–endovascular approach in patients with stroke and confirmed arterial occlusion (recanalise study): a prospective cohort study. *Lancet Neurol.* 8(9), 802–809 (2009).
- 9 Baruah DB, Dash RN, Chaudhari MR, Kadam SS. Plasminogen activators: a comparison. *Vascul. Pharmacol.* 44(1), 1–9 (2006).
- Concise review on plasminogen activators.
- 10 Kotb E. The biotechnological potential of fibrinolytic enzymes in the dissolution of endogenous blood thrombi. *Biotechnol. Prog.* 30(3), 656–672 (2014).
- 11 Van De Craen B, Declerck PJ, Gils A. The biochemistry, physiology and pathological roles of pai-1 and the requirements for pai-1 inhibition *in vivo*. *Thromb. Res.* 130(4), 576–585 (2012).
- 12 Fortenberry YM. Plasminogen activator inhibitor-1 inhibitors: a patent review (2006–present). *Expert Opin. Ther. Pat.* 23(7), 801–815 (2013).
- 13 Copin JC, Bengualid DJ, Da Silva RF, Kargiotis O, Schaller K, Gasche Y. Recombinant tissue plasminogen activator induces blood–brain barrier breakdown by a matrix metalloproteinase-9-independent pathway after transient focal cerebral ischemia in mouse. *Eur. J. Neurosci.* 34(7), 1085–1092 (2011).
- Description of recombinant tissue plasminogen activator (rtPA) and secondary effects.
- 14 Klink A, Hyafil F, Rudd J *et al*. Diagnostic and therapeutic strategies for small abdominal aortic aneurysms. *Nat. Rev. Cardiol.* 8(6), 338–347 (2011).
- 15 Silva AK, Letourneur D, Chauvierre C. Polysaccharide nanosystems for future progress in cardiovascular pathologies. *Theranostics* 4(6), 579–591 (2014).
- 16 Ricklin D, Hajishengallis G, Yang K, Lambris JD. Complement: a key system for immune surveillance and homeostasis. *Nat. Immunol.* 11(9), 785–797 (2010).
- 17 Kim JY, Kim JK, Park JS, Byun Y, Kim CK. The use of pegylated liposomes to prolong circulation lifetimes of tissue plasminogen activator. *Biomaterials* 30(29), 5751–5756 (2009).
- 18 Koshkaryev A, Sawant R, Deshpande M, Torchilin V. Immunoconjugates and long circulating systems: Origins, current state of the art and future directions. *Adv. Drug Deliv. Rev.* 65(1), 24–35 (2013).
- 19 Rabanel JM, Hildgen P, Banquy X. Assessment of peg on polymeric particles surface, a key step in drug carrier translation. *J. Control. Release* 185, 71–87 (2014).

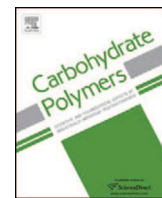
- 20 Bowey K, Tanguay JF, Tabrizian M. Liposome technology for cardiovascular disease treatment and diagnosis. *Expert Opin. Drug Deliv.* 9(2), 249–265 (2012).
- Review of liposome systems in the cardiovascular field.
- 21 Ruiz-Esparza GU, Flores-Arredondo JH, Segura-Ibarra V *et al.* The physiology of cardiovascular disease and innovative liposomal platforms for therapy. *Int. J. Nanomedicine* 8, 629–640 (2013).
- 22 Tassa C, Shaw SY, Weissleder R. Dextran-coated iron oxide nanoparticles: a versatile platform for targeted molecular imaging, molecular diagnostics, and therapy. *Acc. Chem. Res.* 44(10), 842–852 (2011).
- 23 Chen JP, Yang PC, Ma YH, Wu T. Characterization of chitosan magnetic nanoparticles for *in situ* delivery of tissue plasminogen activator. *Carbohydrate Polymers* 84(1), 364–372 (2011).
- Study demonstrating *in vivo* delivery of tPA using magnetic nanoparticles.
- 24 Uesugi Y, Kawata H, Jo J, Saito Y, Tabata Y. An ultrasound-responsive nano delivery system of tissue-type plasminogen activator for thrombolytic therapy. *J. Control. Release* 147(2), 269–277 (2010).
- 25 Robert D, Fayol D, Le Visage C *et al.* Magnetic micro-manipulations to probe the local physical properties of porous scaffolds and to confine stem cells. *Biomaterials* 31(7), 1586–1595 (2010).
- 26 Cheng K, Li TS, Malliaras K, Davis DR, Zhang Y, Marban E. Magnetic targeting enhances engraftment and functional benefit of iron-labeled cardiosphere-derived cells in myocardial infarction. *Circ. Res.* 106(10), 1570–1581 (2010).
- 27 Silva AK, Luciani N, Gazeau F *et al.* Combining magnetic nanoparticles with cell derived microvesicles for drug loading and targeting. *Nanomedicine* 11(3), 645–655 (2015).
- 28 De Saint Victor M, Crake C, Coussios CC, Stride E. Properties, characteristics and applications of microbubbles for sonothrombolysis. *Expert Opin. Drug Deliv.* 11(2), 187–209 (2014).
- Review on sonothrombolysis.
- 29 Collen D, Lijnen HR. Thrombolytic agents. *Thromb. Haemost.* 93(4), 627–630 (2005).
- 30 Butcher K, Shuaib A, Saver J *et al.* Thrombolysis in the developing world: is there a role for streptokinase? *Int. J. Stroke* 8(7), 560–565 (2013).
- 31 Kunamneni A, Abdelghani TT, Ellaiah P. Streptokinase – the drug of choice for thrombolytic therapy. *J. Thromb. Thrombolysis* 23(1), 9–23 (2007).
- 32 Leach JK, O'Rear EA, Patterson E, Miao Y, Johnson AE. Accelerated thrombolysis in a rabbit model of carotid artery thrombosis with liposome-encapsulated and microencapsulated streptokinase. *Thromb. Haemost.* 90(1), 64–70 (2003).
- 33 Leach JK, Patterson E, O'Rear EA. Encapsulation of a plasminogen activator speeds reperfusion, lessens infarct and reduces blood loss in a canine model of coronary artery thrombosis. *Thromb. Haemost.* 91(6), 1213–1218 (2004).
- 34 Leach JK, Patterson E, O'Rear EA. Distributed intraclot thrombolysis: mechanism of accelerated thrombolysis with encapsulated plasminogen activators. *J. Thromb. Haemost.* 2(9), 1548–1555 (2004).
- 35 Vaidya B, Agrawal GP, Vyas SP. Platelets directed liposomes for the delivery of streptokinase: development and characterization. *Eur. J. Pharm. Sci.* 44(5), 589–594 (2011).
- 36 Kunamneni A, Ravuri BD, Saisha V, Ellaiah P, Prabhakhar T. Urokinase – a very popular cardiovascular agent. *Recent Pat. Cardiovasc. Drug Discov.* 3(1), 45–58 (2008).
- 37 Jin HJ, Zhang H, Sun ML, Zhang BG, Zhang JW. Urokinase-coated chitosan nanoparticles for thrombolytic therapy: preparation and pharmacodynamics *in vivo*. *J. Thromb. Thrombolysis*, 36(4), 458–468 (2013).
- 38 Bi F, Zhang J, Su Y, Tang YC, Liu JN. Chemical conjugation of urokinase to magnetic nanoparticles for targeted thrombolysis. *Biomaterials* 30(28), 5125–5130 (2009).
- 39 Marsh JN, Hu G, Scott MJ *et al.* A fibrin-specific thrombolytic nanomedicine approach to acute ischemic stroke. *Nanomedicine (Lond.)* 6(4), 605–615 (2011).
- 40 Mu Y, Li L, Ayoubi G. Experimental study of the preparation of targeted microbubble contrast agents carrying urokinase and rgds. *Ultrasonics* 49(8), 676–681 (2009).
- 41 Liu WS, Huang ZZ, Wang XW, Zhou J. Effects of microbubbles on transcranial doppler ultrasound-assisted intracranial urokinase thrombolysis. *Thromb. Res.* 130(3), 547–551 (2012).
- 42 Kawata H, Uesugi Y, Soeda T *et al.* A new drug delivery system for intravenous coronary thrombolysis with thrombus targeting and stealth activity recoverable by ultrasound. *J. Am. Coll. Cardiol.* 60(24), 2550–2557 (2012).
- 43 Zhou J, Guo D, Zhang Y, Wu W, Ran H, Wang Z. Construction and evaluation of $\text{Fe}_{(3)}\text{O}_{(4)}$ -based PLGA nanoparticles carrying rtPA used in the detection of thrombosis and in targeted thrombolysis. *ACS Appl. Mater. Interfaces* 6(8), 5566–5576 (2014).
- 44 Ma YH, Wu SY, Wu T, Chang YJ, Hua MY, Chen JP. Magnetically targeted thrombolysis with recombinant tissue plasminogen activator bound to polyacrylic acid-coated nanoparticles. *Biomaterials* 30(19), 3343–3351 (2009).
- 45 Yang HW, Hua MY, Lin KJ *et al.* Bioconjugation of recombinant tissue plasminogen activator to magnetic nanocarriers for targeted thrombolysis. *Int. J. Nanomedicine* 7, 5159–5173 (2012).
- 46 Kempe M, Kempe H, Snowball I *et al.* The use of magnetite nanoparticles for implant-assisted magnetic drug targeting in thrombolytic therapy. *Biomaterials* 31(36), 9499–9510 (2010).
- 47 McCarthy JR, Sazonova IY, Erdem SS *et al.* Multifunctional nanoagent for thrombus-targeted fibrinolytic therapy. *Nanomedicine (Lond.)* 7(7), 1017–1028 (2012).
- 48 Absar S, Nahar K, Kwon YM, Ahsan F. Thrombus-targeted nanocarrier attenuates bleeding complications associated with conventional thrombolytic therapy. *Pharm. Res.* 30(6), 1663–1676 (2013).
- 49 Laing ST, Moody M, Smulevitz B *et al.* Ultrasound-enhanced thrombolytic effect of tissue plasminogen

- activator-loaded echogenic liposomes in an *in vivo* rabbit aorta thrombus model – brief report. *Arterioscler. Thromb. Vasc. Biol.* 31(6), 1357–1359 (2011).
- Study showing *in vivo* delivery of tPA using echogenic liposomes with an enhancement of thrombolytic effect.
- 50 Laing ST, Moody MR, Kim H *et al.* Thrombolytic efficacy of tissue plasminogen activator-loaded echogenic liposomes in a rabbit thrombus model. *Thromb. Res.* 130(4), 629–635 (2012).
- 51 Brujan EA. Cardiovascular cavitation. *Med. Eng. Phys.* 31(7), 742–751 (2009).
- 52 Unger E, Porter T, Lindner J, Grayburn P. Cardiovascular drug delivery with ultrasound and microbubbles. *Adv. Drug Deliv. Rev.* 72, 110–126 (2014).
- Review on ultrasound, microbubbles and drug delivery in the cardiovascular field.
- 53 Chen X, Leeman JE, Wang J, Pacella JJ, Villanueva FS. New insights into mechanisms of sonothrombolysis using ultra-high-speed imaging. *Ultrasound Med. Biol.* 40(1), 258–262 (2014).
- 54 Hagisawa K, Nishioka T, Suzuki R *et al.* Thrombus-targeted perfluorocarbon-containing liposomal bubbles for enhancement of ultrasonic thrombolysis: *in vitro* and *in vivo* study. *J. Thromb. Haemost.* 11(8), 1565–1573 (2013).
- 55 Mounouh A, Barentin L, Tranquart F, Serrierre S, Bonnau I, Tasu JP. Fibrinolytic effects of transparietal ultrasound associated with intravenous infusion of an ultrasound contrast agent: study of a rat model of acute cerebral stroke. *Ultrasound Med. Biol.* 36(1), 51–57 (2010).
- 56 Nedelmann M, Ritschel N, Doenges S *et al.* Combined contrast-enhanced ultrasound and rt-pa treatment is safe and improves impaired microcirculation after reperfusion of middle cerebral artery occlusion. *J. Cereb. Blood Flow Metab.* 30(10), 1712–1720 (2010).
- 57 Brown AT, Flores R, Hamilton E, Roberson PK, Borrelli MJ, Culp WC. Microbubbles improve sonothrombolysis *in vitro* and decrease hemorrhage *in vivo* in a rabbit stroke model. *Invest. Radiol.* 46(3), 202–207 (2011).
- 58 Tsivgoulis G, Culp WC, Alexandrov AV. Ultrasound enhanced thrombolysis in acute arterial ischemia. *Ultrasound* 48(4), 303–311 (2008).
- 59 Molina CA, Ribo M, Rubiera M *et al.* Microbubble administration accelerates clot lysis during continuous 2-MHz ultrasound monitoring in stroke patients treated with intravenous tissue plasminogen activator. *Stroke* 37(2), 425–429 (2006).
- Clinical study on microbubbles, ultrasound and rtPA.
- 60 Molina CA, Barreto AD, Tsivgoulis G *et al.* Transcranial ultrasound in clinical sonothrombolysis (tucson) trial. *Ann. Neurol.* 66(1), 28–38 (2009).
- 61 Alexandrov AV, Mikulik R, Ribo M *et al.* A pilot randomized clinical safety study of sonothrombolysis augmentation with ultrasound-activated perflutren-lipid microspheres for acute ischemic stroke. *Stroke* 39(5), 1464–1469 (2008).
- 62 Perren F, Loulidi J, Poglia D, Landis T, Sztajzel R. Microbubble potentiated transcranial duplex ultrasound enhances iv thrombolysis in acute stroke. *J. Thromb. Thrombolysis* 25(2), 219–223 (2008).
- 63 Pagola J, Ribo M, Alvarez-Sabin J, Lange M, Rubiera M, Molina CA. Timing of recanalization after microbubble-enhanced intravenous thrombolysis in basilar artery occlusion. *Stroke* 38(11), 2931–2934 (2007).
- 64 Rubiera M, Ribo M, Delgado-Mederos R *et al.* Do bubble characteristics affect recanalization in stroke patients treated with microbubble-enhanced sonothrombolysis? *Ultrasound Med. Biol.* 34(10), 1573–1577 (2008).



Contents lists available at ScienceDirect

Carbohydrate Polymers

journal homepage: www.elsevier.com/locate/carbpol

Polysaccharide-based strategies for heart tissue engineering

Amanda K. A. Silva ^{a,b}, Maya Juenet ^{b,c}, Anne Meddahi-Pellé ^{b,c}, Didier Letourneur ^{b,c,*}^a Laboratoire Matière et Systèmes Complexes, UMR 7057 CNRS, Université Paris 7, 10 rue Alice Domon et Léonie Duquet, F-75205 Paris Cedex 13, France^b Inserm, U1148, Cardiovascular Bio-Engineering, X. Bichat Hospital, 46 rue H. Huchard, F-75018 Paris, France^c Université Paris 13, Sorbonne Paris Cité, F-93430 Villejuif, France

ARTICLE INFO

Article history:

Received 9 January 2014

Received in revised form 6 June 2014

Accepted 7 June 2014

Available online 16 June 2014

Chemical compounds studied in this article:

Alginate (PubChem CID: 6850754)

Dextran (PubChem CID: 71315856)

Chitosan (PubChem CID: 71853)

Hyaluronic acid (PubChem CID: 24759)

RGD peptide (PubChem CID: 104802)

Fibroblast growth factor (PubChem CID: 5486993)

Keywords:

Polysaccharides

Heart tissue engineering

Scaffolds

Cardiac patch

ABSTRACT

Polysaccharides are abundant biomolecules in nature presenting important roles in a wide variety of living systems processes. Considering the structural and biological functions of polysaccharides, their properties have raised interest for tissue engineering. Herein, we described the latest advances in cardiac tissue engineering mediated by polysaccharides. We reviewed the data already obtained *in vitro* and *in vivo* in this field with several types of polysaccharides. Cardiac injection, intramyocardial *in situ* polymerization strategies, and scaffold-based approaches involving polysaccharides for heart tissue engineering are thus discussed.

© 2014 Elsevier Ltd. All rights reserved.

1. Introduction

Polysaccharides are long carbohydrate molecules which contain repeated monosaccharide units joined together by means of glycosidic bonds. Polysaccharides constitute the most abundant biomolecules in nature and they present essential roles in a wide variety of living systems processes (Muthana, Campbell, & Gildersleeve, 2012; Nitta & Numata, 2013; Oh, Lee, & Park, 2009). Polysaccharides are molecules that display high biocompatibility and biodegradability. They can be classified according to their origin: vegetal origin (e.g. pectin), algal origin (e.g. alginate), microbial origin (e.g. dextran, xanthan gum), and animal origin (chitosan, heparin) (Sinha & Kumria, 2001). Polysaccharides may also be classified as a function of their charge: cationic (chitosan), anionic (hyaluronic acid, heparin) and nonionic (dextran). Most natural polysaccharides present groups such as hydroxyl, carboxyl and

amino groups (Quignard, Di Renzo, & Guibal, 2010), which easily enable their chemical modifications.

Considering the structural and biological functions of polysaccharides, it is reasonable to consider the interest in exploiting them for cardiac tissue engineering. In fact, biomaterials exhibiting both mechanical and biochemical functions may contribute to tissue engineering and are worthy of development (Chi, Yang, Chung, Chou, & Wang, 2013). Additionally, polysaccharides meet several criteria for an eligible biomaterial for tissue engineering, which include biocompatibility, biodegradation, and the ability to deliver and foster cells (Silvestri, Boffito, Sartori, & Ciardelli, 2013). It is important to highlight that the concept of the ideal biomaterial relies not only on its chemical constitution but also on macroscopic structural features. The biomaterial scaffold should present a porous structure to enable mass transport (permeability and diffusion) (Hollister, 2005). Besides, the biomaterial design should attempt to reproduce the organizational, mechanical, and elastic properties of native tissues, which is even more important for vital and highly specialized tissues, such as the cardiac one (De Mulder, Buma, & Hannink, 2009; Engelmayr et al., 2008; McDevitt, Woodhouse, Hauschka, Murry, & Stayton, 2003). Therefore, the ideal biomaterial should consist of a structure that support

* Corresponding author at: Inserm, U1148, Cardiovascular Bio-Engineering, X. Bichat Hospital, 46 rue H. Huchard, F-75018 Paris, France. Tel.: +33 1 4025 8600; fax: +33 1 4025 8602.

E-mail address: didier.letourneur@inserm.fr (D. Letourneur).

cells' attachment and growth while facilitating their organization and possibly differentiation toward a highly ordered biomimetic construct (Sokolsky-Papkov, Agashi, Olaye, Shakesheff, & Domb, 2007). The biomaterial should be also a resistant structure prone to withstand the high and permanent mechanical stresses related to cardiac contraction and relaxation. Another major role concerns the integration within the host tissue and eventual progressive replacement by the host extracellular matrix (Giraud, Guex, & Tevaearai, 2012). Additionally, biomaterials should ideally present biological properties that enhance tissue repair. Functions such as angiogenesis, cell recruitment and cardiomyocyte protection may be promising assets to contribute to the treatment of heart disease (Nelson, Ma, Fujimoto, Hashizume, & Wagner, 2011). Last but not least, tissue engineering products must be both efficient and cost-effective by combining functionality and ease of production (Place, Evans, & Stevens, 2009).

Polysaccharides are promising materials for meeting many of the above mentioned criteria for eligible biomaterials for cardiac tissue engineering. In combination with appropriate cells and bioactive molecules, polysaccharides may represent an important asset to promote heart tissue regeneration. In this regard, it is important to mention that regeneration capacity varies between different cell types and also depends on the nature of the tissue as well as the extent of injury or insult. Tissues that are in constant renewing as the skin are capable of regrowth in an important extent. In comparison, the cardiac tissue lacks mechanisms of regeneration in adults (Sokolsky-Papkov et al., 2007). The aim of this paper is to provide an overview of polysaccharide-based approaches for heart tissue engineering. Initially, the general context of tissue engineering is disclosed. It is followed by heart tissue engineering strategies related to xylan, alginate, pullulan and dextran, chitosan and hyaluronan. Finally, challenges in the field are discussed and concluding remarks are presented.

2. The context of heart tissue engineering

Cardiac infarct is followed by a sequence of wound repair processes associated with cell death, inflammation, the formation of granulation tissue (constituted by myofibroblast, macrophage, and collagen), and finally fibrosis. In response to the loss of cardiomyocytes, there is a reorganization of the extracellular matrix for compensation. This remodeling will result in cardiac wall thinning, ventricle dilatation and heart failure (Ertl & Frantz, 2005; Gajara & Kloner, 2011; Stefanon et al., 2013; Vilahur et al., 2011). Cardiac cell death, depending on its extent, renders the heart unable to deliver sufficient blood to meet the body's metabolic requirements leading to cardiac failure. After myocardial injury such as following important myocardial infarction, the heart regenerative capacity is overwhelmed (Giraud et al., 2012). Cardiac cell loss requires strategies to repair and regenerate the infarcted area of the myocardium (Jawad et al., 2007). Treatment options may concern approaches ranging from medication to surgical interventions. Most surgical options mainly rely on heart transplants. However, there is a chronic shortage of sources for human donors (Lam & Wu, 2012). In fact, the complex series of events involved in myocardial cell loss, and the subsequent post-myocardial infarction remodeling that result in heart failure are inefficiently addressed by current clinical strategies (Martinez & Kofidis, 2011). Current cardiac tissue engineering research aims to design tissue constructs to support, repair, replace, or enhance the function of injured or diseased myocardial tissue (Venugopal et al., 2013). Initial studies focused on the direct injection of viable cells into the infarcted myocardium tissue, a technique which is termed cellular cardiomyoplasty (Christman & Lee, 2006). The aim was to replace necrotic cardiomyocytes via the direct administration of cells from an aqueous cell suspension. It

can be performed via intravenous, intracoronary or direct injection into the myocardium. Some improvement in cardiac performance has been observed by using cellular cardiomyoplasty. However, there are several hurdles associated with this technique. Indeed, the technique suffers from limited cell retention and poor cell survival. The results are quite disappointing considering an acute cell retention (within 24 h of delivery) in the heart that is generally <10%, irrespectively to the cell type or the administration route. In this regard, it would be important to gain deeper insight into the mechanisms underlying cell retention following coronary delivery as a function of the time (Dib et al., 2010). A main reason for that relies on the poor cell attachment ability due to the lack of extracellular matrix attached to them (Wang et al., 2008). Therefore, cells are soon washed out via the coronary venous system and mechanically ejected, as attested by retention rates in beating hearts markedly lower than in non-beating hearts (Malliaras & Marbán, 2011). It has been reported that cells injected into injured myocardium often relocate to the lungs, spleen, liver, kidneys and non-infarcted cardiac muscle (Hale, Dai, Dow, & Kloner, 2008; Zhang et al., 2007). The long-term engraftment of the remaining fraction of cells is also low. This raises the question concerning the real mechanisms at play. It seems difficult to state that the injected cells effectively contribute to the contractility capacity of the infarct zone. Alternatively, they seem to act mostly as a short-term reservoir of growth factors and cytokines that support the survival of host cells via a paracrine effect (Giraud et al., 2012; Nelson et al., 2011). In large panel of actions may be potentially induced via paracrine effect, such as angiogenesis (Zhou et al., 2011), pro-survival effect on cardiomyocytes (Kawaguchi et al., 2010), antifibrotic effects (Li et al., 2009), mobilization of endogenous stem cells (Bollini, Smart, & Riley, 2011) and cardioprotective action mediated by an anti-inflammatory effect (Premaratne et al., 2011).

Beyond the paracrine effect, some strategies have been developed in order to improve cell engraftment and enhance cell survival. They rely on the preconditioning of the cells prior to graft via heat shock, hypoxia approaches as well as exposition to pro-survival factors and enhancement of the expression of survival factors (Gerczuk & Kloner, 2012; Giraud et al., 2012).

Still concerning cell suspension injection approach, a main limitation is that such strategy relies mainly on the cells to improve cardiac function, without considering biomechanical factor that could be provided from a biomaterial (Wang & Guan, 2010). An alternative strategy involving the use of biomaterials seems to be very promising. This will be further discussed as follows.

Concerning the biomaterial approach, many of the investigated strategies for cardiac repair focused on the application of the biomaterial externally anchored to the myocardium in order to provide support. This is the case of cardiac restraint devices such as the CorCap (Acorn Cardiovascular Inc) and Heart Net (Paracor Medical Inc) that are based on Dacron and nitinol wraps, respectively, in order to mechanically support ventricular wall (Mann et al., 2007; Starling et al., 2007; Topkara, Kondareddy, & Mann, 2009). Additionally, devices such as CardioClasp (CardioClasp Inc) and Myosplint (Myocor Inc) reduce heart wall stress by constraining the dilated ventricle and decreasing intraventricular radius (Fukamachi & McCarthy, 2005; Kashem et al., 2003; Sabbah, 2003).

An alternative strategy to the cardiac restraint devices is the incorporation of the biomaterial within the heart wall in direct contact with cardiac cells. These approaches rely on natural or synthetic materials in an injectable form in combination or not with cells (Fig. 1, first, second and third panels), which are then directly injected *in vivo* (Christman et al., 2004; Zhang et al., 2010). By this way, the emerging field of tissue engineering has begun to provide promising alternatives to cellular cardiomyoplasty. The advantages of such an approach include providing a cell-friendly microenvironment to engrafted cells (Habib et al., 2011).

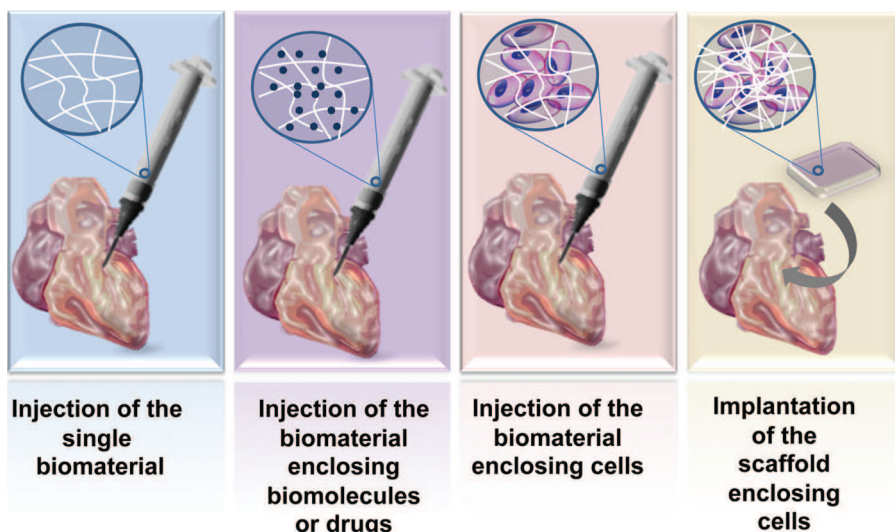


Fig. 1. Polymer-based strategies for cardiac tissue engineering.

Additionally, hydrogels can be tailored in order to deliver cells by minimally invasive catheter-based procedures while enabling high accuracy of the localization of cells at the area of interest (Vunjak-Novakovic, Lui, Tandon, & Chien, 2011). In fact, intramyocardial *in situ* polymerization represents a promising alternative to overcome both leakage and clearance-mediated cell loss and also to address the need for “conditioning” of the immediate cell environment (Davis et al., 2005; Martens et al., 2009). In a related approach, injectable acellular biomaterials can be a strategy to support the heart wall and also for preventing remodeling (Landa et al., 2008). Additionally, this approach may also be of interest for the controlled delivery of therapeutic genes and proteins to ischemic myocardium (Christman & Lee, 2006; Garbern, Minami, Stayton, & Murry, 2011; Wu et al., 2011). In spite of advances in the field, optimal design parameters, including degradation rate and profile, elastic modulus and injectability, largely remain to be fully elucidated. Another important parameter is the effect of the chemical constitution of the material itself (Nelson et al., 2011).

An alternative approach is related to the use of biomaterials to design patches *ex vivo* featuring adapted size and shape and implant them epicardially onto the infarcted tissue (Fig. 1 right panel). Such biomaterials can be loaded with cells and are expected to promote a mechanical reinforcement to the infarct scar to limit ventricular dilation (Leor & Cohen, 2004). It is interesting to highlight that patch-based strategies increase the thickness of the heart wall and by Laplace's law, this increase induces a reduction in the heart wall stress. Even if regeneration does not take place, such an effect may limit ventricular remodeling and improve disease management (Chen, Harding, Ali, Lyon, & Boccaccini, 2008). Although *in vitro*-engineered patches have demonstrated promising results, one main limitation concerns the invasiveness of the implanting technique, which requires surgical intervention. The injectable approach remains minimally invasive, and is therefore more clinically appealing (Christman & Lee, 2006).

In addition to the mechanical support, the biomaterial (in injected form or as a patch) may present intrinsic bioactivity promoting angiogenesis (Garbern et al., 2011) or cell homing (Tsur-Gang et al., 2009). In fact, the biomaterial may act as a niche favoring cellular infiltration of recruited endogenous cells that may potentially improve cardiac function (Johnson & Christman, 2013). Besides, the biomaterial may contribute to reduce border zone extension and limit infarct expansion by another mechanism. Depending on its physical properties, the biomaterial may trap necrotic and apoptotic cells originated from the

infarcted area preventing the dissemination of pro-inflammatory danger-associated molecular patterns (DAMPS) into the healthy surrounding tissue (Zouein, Zgheib, Liechty, & Booz, 2012). This mechanism would reduce infarct spread *via* a decrease in surrounding molecular stress, which is highly related to contractile dysfunction due to cardiomyocyte death (Arslan, de Kleijn, & Pasterkamp, 2011). In this regard, several parameters such as degradation time, polymer crosslink density and molecular affinity play an important role in the process of DAMPS retention and alleviation of infarct spread (Venugopal et al., 2012). These different mechanisms of biomaterial contribution to cardiac tissue repair in the context of cardiac infarct processes are shown in Fig. 2.

Biologically derived, synthetic and hybrid materials have been investigated in the context of heart tissue engineering (Nelson et al., 2011). In the next section, examples of these techniques will be detailed concerning polysaccharide materials. Research on other types of polymers falls outside the scope of this review. Herein, we intend to cover the latest advances in cardiac tissue engineering mediated by polysaccharides.

3. Polysaccharide-based strategies for heart tissue engineering

3.1. Xylan

Xylan is an abundant hemicellulose whose chemical structure is mainly composed of D-glucuronic acid, L-arabinose and D-xylose (Fig. 3) (Ebringerová, Hromádková, Kačuráková, & Antal, 1994; Silva et al., 2007). *Eucalyptus globulus* wood, corn cobs, rice husks and barley husks are frequent xylan sources (Parajó, Garrote, Cruz, & Dominguez, 2004). The structural diversity and complexity of xylan depend on the source. Several extraction procedures are suitable for the isolation of xylyans originated from diverse botanic sources (Ebringerová & Heinze, 2000). Naturally available xylan hydrogels are of interest considering their renewable character and nontoxic properties but also due to their biocompatibility and biodegradability. Additionally, xylyans may present immunomodulatory activity (Ebringerová, Kardošová, Hromádková, Malovíková, & Hříbalová, 2002).

Xylyans present special gelling properties for production of hydrogels that can be used as matrices for the controlled release of bioactive agents (Chimphango, van Zyl, & Görgens, 2012). Indeed, hydrogels in general possess a degree of flexibility due to their significant water content and they are promising biomaterials

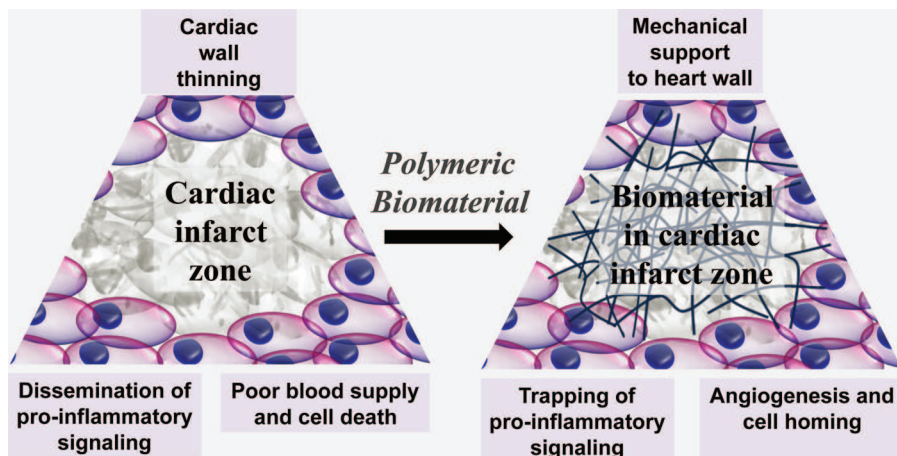


Fig. 2. Processes related to cardiac infarct (left) and the mechanisms of biomaterial interaction with these processes to promote cardiac tissue repair (right).

(Venugopal et al., 2013). Hydrogels are in fact three-dimensional polymer networks swollen by aqueous solvent, which is the major component of the gel system (Chimphango et al., 2012; Silva, Richard, Bessodes, Scherman, & Merten, 2008).

Besides forming hydrogels, xylan may be engineered to design nanofibrous scaffolds. Hybrid xylan/polyvinyl alcohol (PVA) nanofibrous electrospun scaffolds were fabricated and cross-linked with glutaraldehyde. Nanofibers were investigated for culturing rat cardiac cells for cardiac tissue engineering. Such scaffold mimicking cardiac tissue in both stiffness and anisotropy resulted in cardiac cells monolayer interconnection by intercellular junctions,

which were well aligned like in native heart tissue (Venugopal et al., 2013). Scaffolds have also been shown to improve cardiomyocytes electrical excitation and formation of gap junction (Black, Meyers, Weinbaum, Shvelidze, & Tranquillo, 2009). Indeed, biomimetic materials that mimic the fibrillar architecture of the extracellular matrix (ECM) can provide necessary guidance for orientating cells (Prabhakaran, Venugopal, Kai, & Ramakrishna, 2011). Fibers may provide low-resistance pathways for electrical signal propagation mimicking the native heart tissue (Kai, Prabhakaran, Jin, & Ramakrishna, 2013). Besides, tissue constructs that mimic the structural and mechanical properties of the myocardium may

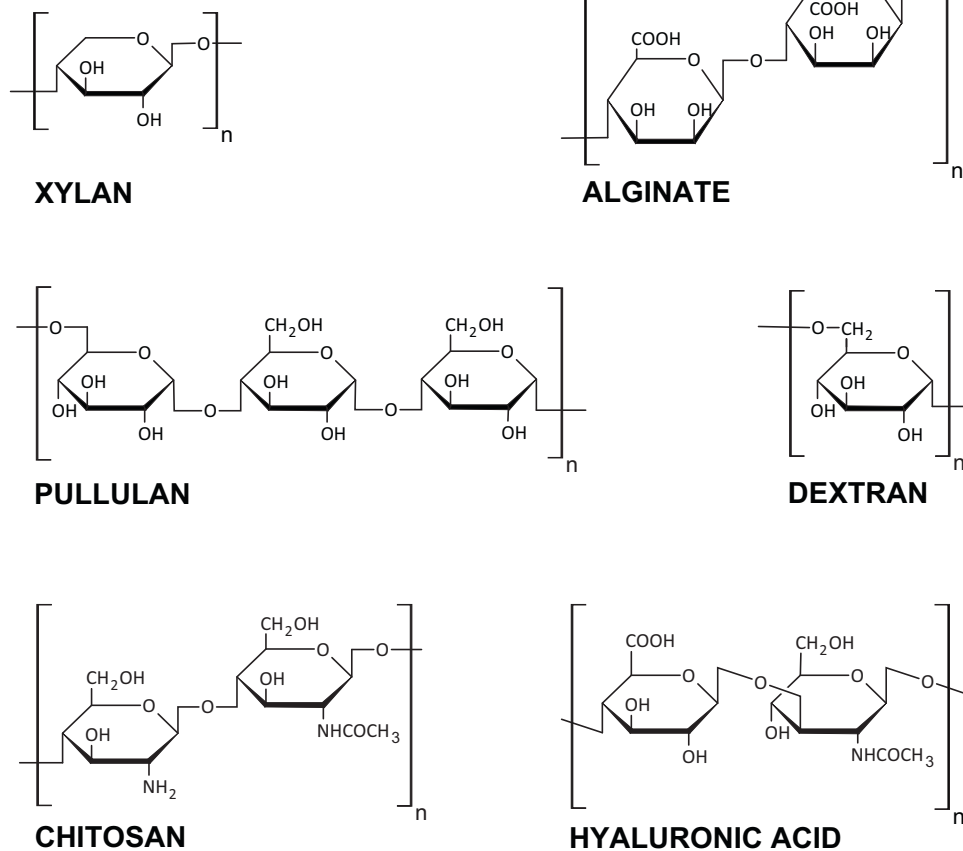


Fig. 3. Chemical structures of polysaccharides investigated for heart tissue engineering.

provide a native-like microenvironment for stimulating stem cell differentiation into a cardiac lineage (Guan et al., 2011). In the study of Venugopal et al. (2013), xylan-based nanofibers might be delivered directly into the myocardium considering their mechanical strength and swelling properties. This would avoid an open-heart surgery and the massive cell loss from the site of injection.

3.2. Alginate

Alginate is a natural polysaccharide obtained from brown seaweed. It has been widely investigated for several biomedical applications due to its biocompatibility, relatively low cost and low toxicity. Alginate is in fact a family of linear copolymers containing blocks of (1,4)-linked β -D-mannuronate (M) and α -L-guluronate (G) residues (Fig. 3). The blocks are composed of consecutive G residues (GGGGGG), consecutive M residues (MMMMMM), and alternating M and G residues (GMGMGM) (Lee & Mooney, 2012). Alginate main source is brown macroalgae, in which alginate represents the major structural component of intercellular matrix and of the cell wall (Yabur, Bashan, & Hernández-Carmona, 2007).

Although alginate presents many attractive properties, its slow and quite uncontrollable degradation can be an undesirable feature (Boontheekul, Kong, & Mooney, 2005). In order to control alginate gel degradation, partial periodate oxidation may be used. By means of oxidation, hydrolytically labile bonds in the polysaccharide were created (Boontheekul et al., 2005; Bouhadir et al., 2001).

An alternative approach to regulate alginate gel degradation is related to the control of molecular weight distribution of the polymer chains (Kong, Kaigler, Kim, & Mooney, 2004). In a combined approach, partial oxidation of alginate and the use of polymers with different molecular weight distributions is an interesting way to provide controlled degradation kinetics of gels (Boontheekul et al., 2005; Kong et al., 2004), allowing control of the release kinetics of incorporated factors (Hao et al., 2007; Silva & Mooney, 2007). Sustained growth factor delivery of vascular endothelial growth factor-A 165 and platelet-derived growth factor-BB from such alginate hydrogels enhanced the formation of mature vessels and was shown to improve cardiac function in rats (Hao et al., 2007).

Literature data has also indicated the benefits of alginate hydrogels via a mechanic effect. It has been described that injection in a rat model of *in situ* – forming, bioabsorbable acellular alginate hydrogel prevented cardiac remodeling and dysfunction in recent and old myocardial infarctions (Landa et al., 2008). Additionally, intracoronary injection of alginate was found to improve infarct repair and prevent adverse remodeling in a swine model (Leor et al., 2009). After implantation, the hydrogel gradually disappears, and the water-soluble alginate chains were excreted by the kidneys (Al-Shamkhani & Duncan, 1995). It was hypothesized that the injectable alginate biomaterial enabled mechanical/physical support to the infarcted cardiac tissue, a task usually fulfilled by the cardiac ECM, mainly by the collagen constituting the ECM (Brower et al., 2006). In fact, the cardiac ECM is damaged after infarction, as observed by collagen loss and reorganization. The replacement of ECM by the alginate biomaterial could be a strategy to compensate for collagen loss until cardiac healing progresses (Tsur-Gang et al., 2009).

Although mechanical effects are most commonly pointed out, the material-related biological response could potentially present a contributing effect (Nelson et al., 2011). For instance, an angiogenic effect concomitant to improved heart function was observed in rats after alginate injection alone. It indicates that the polymer itself may influence the tissue microenvironment and induce a potential therapeutic effect (Yu et al., 2009). Additionally, it was demonstrated that alginate hydrogel injection enhanced cell recruitment into the infarct, including the homing of myofibroblasts that take part in cardiac healing (Tsur-Gang et al., 2009).

In addition to the injection-based approach, the implantable scaffold-based approach was also tested for alginate. Fetal cardiac cells were cultured into 3D porous alginate scaffolds and implanted into the infarcted myocardium of rats. Following implantation, the scaffold stimulated neovascularization and attenuated heart wall dilatation and cardiac failure in treated rats when compared with controls. The approach improved the regeneration and healing of the infarcted myocardium and reduced wall stress and infarct expansion (Leor et al., 2000).

This strategy could be supplemented by the grafting of RGD peptide into alginate scaffolds. The RGD peptide is supposed to enhance cell attachment to the matrix, improved cell survival and facilitated the organization of the tissue. Indeed, the cardiomyocytes were able *in vitro* to reorganize their myofibrils and reconstructed myofibers constituted of several cardiomyocytes in a typical myofiber bundle in a way quite similar to the native cardiac tissue. In contrast, such structural organization could not be evidenced in the non-peptide grafted alginate scaffolds. In addition to cell morphology/organization results, data concerning expression levels of α -actinin, N-cadherin and connexin-43, indicated further improved *in vitro* features of the engineered cardiac tissue when RGD was grafted to alginate scaffolds (Shachar, Tsur-Gang, Dvir, Leor, & Cohen, 2011).

In a related approach, Sapir et al. investigated *in vitro* the combination of two matrix-attached peptides, the adhesion peptide G₄RGDY and heparin-binding peptide G₄SPPRRARVTV (HBP) attached to alginate for cardiac tissue regeneration. Neonatal rat cardiac cells were seeded into unmodified, single peptide or double peptide-attached alginate scaffolds. The cardiac tissue developed in the HBP/RGD-attached scaffolds demonstrated the best features of a functional muscle tissue considering data from immunostaining of cardiac cell markers, histology, Western blot of proteins and metabolic activity. Well-developed myocardial fibers could be observed by day 7. At 14 days, the HBP/RGD-attached constructs displayed an isotropic myofiber arrangement, which was not evidenced in the other constructs. The formation a contractile muscle tissue in the HBP/RGD-attached scaffolds was further demonstrated *via* the expression levels of α -actinin, N-cadherin and Connexin-43. Such strategy of attaching peptides representing different signaling in ECM-cell interactions proved to support the formation of a functional cardiac muscle tissue *in vitro* (Sapir, Kryukov, & Cohen, 2011).

3.3. Pullulan and dextran

Pullulan is a non-ionic exopolysaccharide of fungal origin. Indeed, pullulan is an exocellular homopolysaccharide produced by the strain of *Aureobasidium pullulans* (Wu, Jin, Kim, Tong, & Chen, 2009). It consists of a water-soluble, neutral linear polysaccharide consisting of α -1,6-linked maltotriose residues (Fig. 3). Pullulan is currently used in the food industry and in pharmaceuticals. Due to its non-toxic, non-immunogenic, non-mutagenic and non-carcinogenic nature, there are attempts to explore this polysaccharide for several biomedical applications (Autissier, Letourneau, & Le Visage, 2007; Rekha & Sharma, 2007; Wolf, Garleb, Choe, Humphrey, & Maki, 2003).

Dextran consists of a high molecular-weight polysaccharide of microbial origin composed of glucose molecules connected in α 1-6 glucosidic linkage, in which side chains are connected in α 1-4 linkage (Fig. 3). The exact structure of each type of dextran depends on the microbial strain (Ciardelli et al., 2005; Vu, Chen, Crawford, & Ivanova, 2009). Crosslinked dextran has been widely used as a molecular sieve for purification and separation of biomolecules. It has also been used as a soluble form for biomedical applications such as plasma expander considering its biocompatibility (Cai, Yang, Bei, & Wang, 2002). Dextran is biodegradable and

biocompatible and also available in a wide variety of molecular weights. These properties make it suitable for many biomedical applications including tissue engineering (Malafaya, Silva, & Reis, 2007).

Scaffolds made of crosslinked pullulan and dextran have been investigated for cardiovascular tissue engineering (Chaouat, Le Visage, Autissier, Chaubet, & Letourneur, 2006; Lavergne et al., 2012). The scaffolds consisted on a mixture of pullulan and dextran cross-linked with sodium trimetaphosphate, containing sodium carbonate as a porogen agent. Such scaffolds presented good compatibility with respect to blood–material interactions and no anticoagulant treatment was needed. Additionally, scaffolds made of cross-linked pullulan and dextran were able to withstand pressure under physiological flow conditions in a rat model (Chaouat et al., 2006). It was also demonstrated that such biomaterial preserved the viability and the proliferation of cord-blood endothelial colony-forming cells. Indeed, pullulan and dextran scaffold enabled endothelial cell delivery while preserving cell functions, namely the capacity to form vascular structures and ability to be activated by pro-inflammatory effectors. Such biomaterial was also tested to deliver cells for cardiac repair. *In vivo* effectiveness of mesenchymal stem cells (MSCs) engraftment in rat infarcted tissue was investigated in a comparative study by testing pullulan/dextran-based porous scaffold and endocardial injection approach. The delivery of MSCs to injured rat myocardium using a polysaccharide porous scaffold resulted in improved engraftment in comparison with the endocardial injection approach. The amount of residual cells was higher for the scaffold approach compared to the injection at 1 and 2 months. Additionally, there was an observable trend toward a lower left ventricular dilatation and a reduced fibrosis in the scaffold group (Le Visage et al., 2011).

3.4. Chitosan

Chitosan is a natural polymer originated from renewable resources. Chitosan is obtained from shell of shellfish and also from the wastes of the seafood industry (Kim et al., 2008). Chitin is the source material for chitosan and represents one of the most abundant organic materials, being an important constituent of the exoskeleton in animals, especially in crustacean, insects and molluscs (Kim et al., 2008). It consists of a linear polymer composed of glucosamine and N-acetyl glucosamine units linked by β (1–4) glycosidic bonds (Fig. 3). This polysaccharide presents interesting features such as biocompatibility, biodegradability, antibacterial as well as wound-healing properties (Kim et al., 2008).

Conjugation of hydroxybutyl groups to chitosan renders the polymer water soluble and thermally responsive (Brun-Graeppi, Richard, Bessodes, Scherman, & Merten, 2010). Below its lower critical solution temperature, a solution of hydroxybutyl chitosan (HBC) can be maintained in its solvated state. Upon exposure to the temperature of 37 °C, a 3.8 wt% HBC solution rapidly forms a gel. Upon cooling, the gel is reverted to its solvated state (Dang et al., 2006). Under physiological temperature, concentrated HBC aqueous solution becomes a hydrogel within 30 s after injection (Wang et al., 2013).

The thermal responsiveness of HBC renders it an eligible polymer for injection based-approach for tissue engineering. Temperature-responsive chitosan hydrogels constitute an attractive biomaterial to deliver cells as well as bioactive factors such as growth factors and genes relevant for the repair and tissue regeneration. Once the biomaterial experiences body temperature, the polymer solution polymerize rapidly *in situ*, trapping and retaining the cells and the bioactive factors (Wang, Zhou, Liu, & Wang, 2010).

Injection of basic fibroblast growth factor (bFGF) with temperature-responsive chitosan hydrogels enhanced arteriogenesis, ventricular remodeling and cardiac function in rat infarction

models (Wang, Zhang, et al., 2010). Liu et al. investigated the use of thermo-responsive chitosan hydrogel for adipose-derived MSC delivery into ischemic rat hearts. They demonstrated that chitosan hydrogel was able to improve injected cell microenvironment, enhance cell engraftment and survival, contributing to myocardial repair (Liu et al., 2012).

It is interesting to highlight that thermoresponsive chitosan itself exhibited interesting mechanical properties. This results in a beneficial effect *in vivo* that is also enhanced by the bioactivity of the polymer. In fact, injection of chitosan alone increased the microvesSEL density significantly within the infarcted scar (Wang et al., 2010b). Thermoresponsive chitosan in combination to embryonic stem cells was found to present supportive mechanical function, support angiogenesis and increase cardiac function after injection in a myocardial infarction rat model (Lu et al., 2008).

In a recent paper, thermoresponsive chitosan chloride was conjugated to glutathione in order to design a hydrogel able to reduce the oxidative stress injury for cardiomyocytes. In fact, myocardial infarction is associated to overproduction of reactive oxygen species, which is a hurdle for cardiac tissue engineering. The produced hydrogel was found to present antioxidant capacity and also excellent biocompatibility in order to favor the adhesion and survival of cardiomyocytes, representing then an interesting alternative to support heart tissue engineering by delivering cells while minimizing oxidative stress (Li et al., 2013).

3.5. Hyaluronan

Hyaluronan is a high-molecular-weight polysaccharide, which is an important constituent of the extracellular matrix (Laurent & Fraser, 1992). It is a linear polysaccharide constituted of a repeating disaccharide unit of (1,4)-glucuronic acid (GlcUA)- β (1,3)-N-acetylglucosamine (GlcNAc) (Fig. 3). Hyaluronan may have different sources. It can be produced by bacteria or extracted from animal tissues (Boeriu, Springer, Kooy, van den Broek, & Eggink, 2013). Large hyaluronan molecules are space filling polymers presenting regulatory as well as structural functions, while small hyaluronan fragments are involved in immunostimulation, angiogenesis and inflammation (Frenkel, 2012; Stern, Asari, & Sugahara, 2006). Hyaluronan hydrogels have the advantages of being formed in mild conditions and they enable the incorporation of angiogenic growth factors, plasmids, or cells to deliver them into ischemic tissues. Furthermore, the derivatives of hyaluronan hydrogels retain the polysaccharide angiogenic activity, which will enhance vascularization (Shen, Tanaka, & Takamori, 2009). Hyaluronan hydrogels grafted with thiols display faster degradation rates. This is assumed to be the result of relatively weak covalent cross-linking of disulfide bonds. Such faster degradation could facilitate neovascularization (Shen et al., 2009).

2-Iminothiolane grafted hyaluronan hydrogel and periodate oxidized hyaluronan hydrogel were implanted into rat adductor muscles. They showed rapid degradation rates, while inducing low inflammation and dense blood vessel formation in the areas surrounding the implanted hydrogels (Shen et al., 2009). Hyaluronan-mediated angiogenic effect *in vivo* is related to its degradation products, which stimulate endothelial cell proliferation and migration (Peattie et al., 2004).

An injectable hyaluronan-based hydrogel showed promising results when injected into mice model of myocardial infarction. Yoon and colleagues reported an increase in the thickness of the heart, a decrease in the infarcted area of the left ventricle, a higher number of arterioles and capillaries in the border zone, a reduction of apoptosis and an improvement of heart functions, such as ejection fraction (Yoon et al., 2009).

In a related study, hyaluronan-based hydrogels presenting differential moduli (~8 versus ~43 kPa) were injected into an ovine

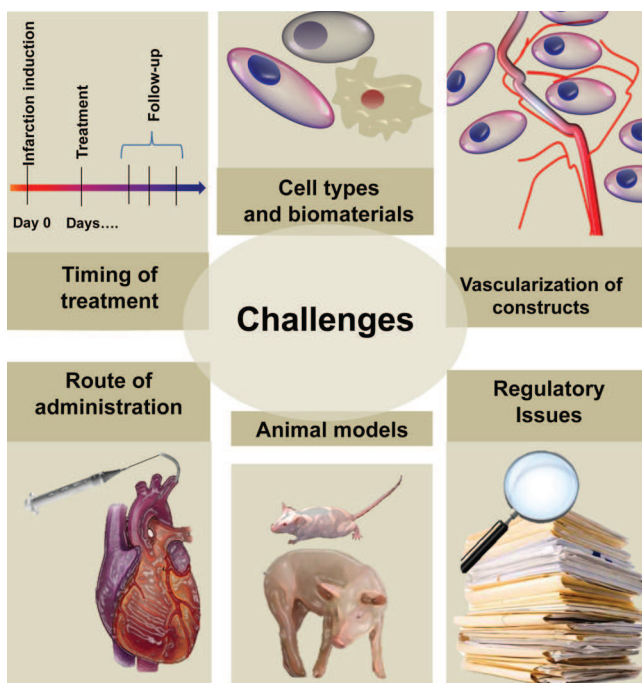


Fig. 4. Challenges in polysaccharide-based strategies for heart tissue engineering.

model of myocardial infarction. It was found that both hydrogels significantly increased the heart wall thickness compared with the control. The higher-modulus hydrogel induced a statistical reduction in the infarct area compared with the control group. The higher-modulus hydrogel also improved functional outcomes (cardiac output and ejection fraction) in a higher extent than the low-modulus and control groups (Ifkovits et al., 2010). The same team compared hyaluronan-based hydrogels presenting degradation time of about 3 weeks or 10 weeks. Both treatments resulted in increased vessel formation and cardiac output compared to controls. However, slow-degrading hyaluronan-based hydrogel was more effective at 8 weeks, implying that longer wall stabilization is needed for an improved cardiac repair (Tous et al., 2011).

In a combined approach, covalently *in situ* cross-linked hydrogels based on alginate and hyaluronic acid were designed. The mechanophysical properties of the resulting hydrogels were easily adjustable by varying degrees of derivatization, concentrations and composition of blends. *In vitro* tests with neonatal rat heart cells showed that the hydrogel allowed for the generation of a fine-tuning contractile bioartificial cardiac tissue (Dahmann et al., 2013).

Hyaluronan hydrogels were also combined with cells for cardiac repair. Hydrogels containing cardiosphere-derived cells were injected intra-myocardially or applied epicardially in rats following myocardial infarction. The encapsulation of cell into hyaluronan hydrogel markedly increased acute myocardial retention and an improved left ventricular ejection fraction was reported. Additionally, hydrogels were highly adhesive, biodegradable and promoted the survival of cardiosphere-derived cells after administration into the heart (Chang et al., 2012).

4. Challenges

Polysaccharide-based strategies for heart tissue engineering still face many challenges. They are depicted in Fig. 4 and commented as follows.

Concerning cell-based approaches, the choice of the cell type is an issue of paramount importance that is quite challenging. Regulatory aspects and clinical availability are important points to consider in the choice of the cell source as they critically impact on translational aspects. For instance, although neonatal cardiomyocytes have been largely investigated in preclinical studies, they do not represent a quite valuable option for clinical studies due to ethical concerns and low accessibility. There are also many research investigations on embryonic stem cells. However, teratogenicity and ethical issues may hamper safe clinical use. The same applies to induced pluripotent stem cells even if they overcome some major shortcomings such as accessibility and expansion. Considering skeletal myoblasts, adverse events such as arrhythmias may occur (Giraud et al., 2012; Siepe, Akhyari, Lichtenberg, Schlensak, & Beyersdorf, 2008). Cell sourcing is therefore a complex technical and regulatory obstacle.

The optimal time window for therapy is another important challenge to be considered. Indeed, the kinetics and timing to deliver cells/biomaterials have received little attention in preclinical studies. The ideal choice of this window seems to be situated between days 3 and 7 after the infarction (Dib et al., 2010). When transplantation is performed in the first week post myocardial infarction, reduced inflammation as well as early tissue remodeling facilitates transplanted cells integration (Hu et al., 2007).

The choice of the animal model is also a main concern. It is important to mention that experimental and preclinical investigations have widely been performed in small (rodent) models. Alternatively, swine model of myocardial infarction induced by either balloon inflation or coil placement in the left anterior descending artery is considered a robust and reproducible model that simulates quite well human myocardial infarction (Dib et al., 2010).

The way of administration is also a point that deserves further attention. The biomaterial may be administered in a single or multiple injections. The injection volume is also an important parameter to be determined as well as the location of the injection (Wall, Walker, Healy, Ratcliffe, & Guccione, 2006; Wenk et al., 2009). The administration of the biomaterial to the border zone may be more appropriate to encourage regeneration than an injection in the center of the infarct (Nelson et al., 2011). The route of administration also represents a key issue. Intramyocardial, transendocardial and epicardial delivery approaches are quite frequent. The epicardial approach brings along high risk related to its invasive nature. However, it offers the benefit to provide direct visualization of the heart enabling accurate administration. Transendocardial methods via the use of the 3D mapping systems allow increased accuracy although the risk of perforating the myocardium is the highest. The intracoronary method is also a usual procedure, but coronary sinus delivery is considered lower risk although limited by the variability in coronary sinus anatomy. Considering all this, intravenous delivery is regarded as the most straightforward and least invasive route of administration. However, it relies on cell homing even more than the other routes of administration (Dib, Khawaja, Varner, McCarthy, & Campbell, 2011).

Vascularization aspects are equally a main concern. The contractile activity related to myogenic function requires that effective metabolic resources are supplied appropriately. In infarcted areas, oxygen and nutrition supply may fall below the minimum required levels for cell survival. *In vivo* vascularization is quite needed to avoid ischemic cell damage especially in the core zone of the engineered tissue constructs. The addition of endothelial cells in the biomaterial might favor vascularization induction (Akhyari, Kamiya, Haverich, Karck, & Lichtenberg, 2008).

Last but not least, regulatory issues represent a main challenge. There are major regulatory hurdles in the translation of polysaccharide-based tissue engineered constructs in marketed

Table 1

Patents related to polysaccharide-based approaches for heart tissue engineering.

Polysaccharide-based approaches for heart tissue engineering	Patents	References
Polysaccharide biodegradable gel matrix containing a biologically active agent and stem cells for the treatment of heart failure	EP1730265A2 WO2005093047A2 WO2005093047A3 US 20080226726 A1	Jaconi and Zammaretti-Schaer (2005a, 2005b, 2006a, 2006b)
Alginate solution to be injected in the heart to be gelled <i>in situ</i> for cardiac tissue repair	WO2004098669 A1 EP2314327 B1	Cohen and Leor (2004, 2013)
Alginate matrices with nanowires and seeded with cardiomyocytes as cardiac patches	US 20130289687 A1 WO2012094208 A1	Dvir, Kohane, Langer, and Timko (2012, 2013)
Three-dimensional aligned scaffold to grow cells in predetermined orientations for regeneration and repair of cardiac tissue	US7579189 B2 US 20050042254 A1 US7384786 B2 EP 1649008 A2 WO 2005010172 A2	Freyman, Palasis, and Ungs (2005a, 2005b, 2006, 2008, 2009)
Alginate-based vascularized support matrix to mediate the controlled release of chemical or biological agents	US20070299508 A1 US20120209403 A1 US7998735 B2 US20050056291 A1	Morrison, Messina, Knight, and Pennington (2005, 2007, 2011, 2012)
Chitosan or hyaluronan-based nanofiber scaffold seeded with cells mimicking the structure of cardiac tissue	US20130183352 A1 WO2013109642 A1	Xie (2013a, 2013b)
Chitosan or hyaluronan-based anisotropic scaffold prepared by electrospinning for cardiac tissue engineering	WO2011149836 A1 US20130131830 A1	Lelkes, Senel, Brookstein, and Govindaraj (2011, 2013)
Textured surface of chitosan to align cells for generating a cardiac patch	WO2010108025 A2 WO2010108025 A3 US20120129209 A1	Khine and Luna (2010, 2011, 2012)

products. Currently, there are several patents on polysaccharide-based approaches for cardiac tissues engineering (Table 1). This indicates an interest in translating research into commercial products. In this regard, careful attention should be paid to regulatory concerns in order to design marketed products.

Thorough consideration of the challenges going from bench to bedside is paramount in maximizing the chances that a scientific approach becomes a treatment (Pashuck & Stevens, 2012). Products derived from an autologous source would provide a straightforward route to clinical translation by reducing regulatory concerns (Seif-Naraghi, Salvatore, Schup-Magoffin, Hu, & Christman, 2010). However, for cardiac tissue engineering using polysaccharides, the source is often algae, microbial, crustacean etc. In addition to that, the presence of cells increases the complexity of the product. As a general rule, the regulatory difficulties concerning a particular tissue engineering product increase with the complexity of the product. For instance, a polymeric scaffold is regarded as a device, while such a scaffold endowed with growth factors and containing cells might be considered and regulated as a combination product. As a consequence, it is important to minimize complexity in the

Table 2

Regulatory concerns related to the manufacture, preclinical investigation, and clinical evaluation of tissue engineered products (Hellman, 1997).

Manufacture	Preclinical investigation	Clinical evaluation
Product consistency	Structural and functional activity of the biomaterial	Indications
Product stability	Biomaterial compatibility testing	Efficacy endpoints
Material sourcing	<i>In vitro</i> /animal models used	Safety monitoring
Adventitious agents	Efficacy of the tissue engineered product	Post-market reporting
Testing		
Process validation		
Toxicity testing		
Carcinogenicity		
Immunogenicity		
Sterility		

pursuit of the simplest product sufficient to match the desired clinical need in order to reduce regulatory requirements (Atala, Kasper, & Mikos, 2012). Indeed, interactions and exchanges with the regulatory body should begin at the initial stages of development in order to facilitate identification of the appropriate regulatory pathway. This is also of interest to guide the selection of the most appropriate methods for preclinical and clinical investigations in order to support regulatory requirements (Atala et al., 2012). Such concerns regard the manufacture of the product, cell purity, preclinical issues, clinical investigation and post-market requirements (Condic & Rao, 2008; Hellman, 1997), as detailed in Table 2.

5. Conclusions

Heart tissue engineering intends to improve cardiac function by supporting, replacing or repairing the injured tissue. Notably, efforts have been done to propose a new alternative to cellular cardiomyoplasty, whose attempts so far have failed since most of the implanted cells die soon after transplantation or are not retained at the site of interest. Biomaterials including polysaccharides represent a new venue for cardiac repair. They may act by providing a mechanical support, by their intrinsic bioactivity and also by avoiding the spread of pro-inflammatory agents, which would induce further cardiomyocyte death and infarction expansion. Additionally, polysaccharide biomaterial may enclose cells and bioactive molecules, which have an additional contribution to for alleviation of myocardial infarction. Enclosing cells and signaling molecules such as growth factors into polysaccharide biomaterial provide an additional opportunity to enhance the effect of the biomaterial alone. Besides, in such a case, the polymer increases the cell residence time in the site of interest while improving cells survival by providing a friendly microenvironment. Several studies have been published based on polysaccharides such as xylan, alginate, pullulan and dextran, chitosan and hyaluronan and there are equally many patents on the field, as reviewed herein. However, there are still many challenges in the domain related to the choice of the cell type, the choice of the animal model, the way of administration (volume, route and timing), the angiogenic potential of the construct and also regulatory concerns. Critical issues in the near future will be the demonstration of safety and efficacy of polysaccharide-based approaches in large animal models, at long term and complying with regulatory requirements. This will ultimately lead to the transition of polysaccharide-based approaches toward clinical trials and also to the market, as a perspective.

Acknowledgements

The authors would like to thank the institutions of Inserm (National Institute for Health and Medical Research), Universities of Paris Diderot and Paris 13 for financial support, as well as the French Research National Agency (ANR TECSAN-2012-0011 Ineov), and the European Community for the NanoAthero FP-7 project (NMP-LA-2012 Grant agreement 309820).

References

- Akhya, P., Kamiya, H., Haverich, A., Karck, M., & Lichtenberg, A. (2008). *Myocardial tissue engineering: The extracellular matrix*. *European Journal of Cardio-Thoracic Surgery*, 34(2), 229–241.
- Al-Shamkhani, A., & Duncan, R. (1995). Radioiodination of alginate via covalently-bound tyrosinamide allows monitoring of its fate in vivo. *Journal of Bioactive and Compatible Polymers*, 10(1), 4–13.
- Arslan, F., de Kleijn, D., & Pasterkamp, G. (2011). Innate immune signaling in cardiac ischemia. *Nature Reviews Cardiology*, 8(5), 292–300.
- Atala, A., Kasper, F. K., & Mikos, A. G. (2012). Engineering complex tissues. *Science Translational Medicine*, 4(160), 160rv12.
- Autissier, A., Letourneur, D., & Le Visage, C. (2007). Pullulan-based hydrogel for smooth muscle cell culture. *Journal of Biomedical Materials Research Part A*, 82(2), 336–342.
- Black, L. D., III, Meyers, J. D., Weinbaum, J. S., Shvelidze, Y. A., & Tranquillo, R. T. (2009). Cell-induced alignment augments twitch force in fibrin gel-based engineered myocardium via gap junction modification. *Tissue Engineering Part A*, 15(10), 3099–3108.
- Boeriu, C. G., Springer, J., Kooy, F. K., van den Broek, L. A., & Eggink, G. (2013). Production methods for hyaluronan. *International Journal of Carbohydrate Chemistry*, 1–14.
- Bollini, S., Smart, N., & Riley, P. R. (2011). Resident cardiac progenitor cells: At the heart of regeneration. *Journal of Molecular and Cellular Cardiology*, 50(2), 296–303.
- Bontheekul, T., Kong, H.-J., & Mooney, D. J. (2005). Controlling alginate gel degradation utilizing partial oxidation and bimodal molecular weight distribution. *Biomaterials*, 26(15), 2455–2465.
- Bouhadir, K. H., Lee, K. Y., Alsberg, E., Damm, K. L., Anderson, K. W., & Mooney, D. J. (2001). Degradation of partially oxidized alginate and its potential application for tissue engineering. *Biotechnology Progress*, 17(5), 945–950.
- Brower, G. L., Gardner, J. D., Forman, M. F., Murray, D. B., Voloshenyuk, T., Levick, S. P., et al. (2006). The relationship between myocardial extracellular matrix remodeling and ventricular function. *European Journal of Cardio-Thoracic Surgery*, 30(4), 604–610.
- Brun-Graeppi, A. K., Richard, C., Bessodes, M., Scherman, D., & Merten, O.-W. (2010). Thermoresponsive surfaces for cell culture and enzyme-free cell detachment. *Progress in Polymer Science*, 35(11), 1311–1324.
- Cai, Q., Yang, J., Bei, J., & Wang, S. (2002). A novel porous cells scaffold made of polylacitide–dextran blend by combining phase-separation and particle-leaching techniques. *Biomaterials*, 23(23), 4483–4492.
- Chang, C. Y., Chan, A. T., Armstrong, P. A., Luo, H.-C., Higuchi, T., Strehin, I. A., et al. (2012). Hyaluronic acid–human blood hydrogels for stem cell transplantation. *Biomaterials*, 33(32), 8026–8033.
- Chaouat, M., Le Visage, C., Autissier, A., Chaubet, F., & Letourneur, D. (2006). The evaluation of a small-diameter polysaccharide-based arterial graft in rats. *Biomaterials*, 27(32), 5546–5553.
- Chen, Q.-Z., Harding, S. E., Ali, N. N., Lyon, A. R., & Boccaccini, A. R. (2008). Biomaterials in cardiac tissue engineering: Ten years of research survey. *Materials Science and Engineering: R: Reports*, 59(1–6), 1–37.
- Chi, N.-H., Yang, M.-C., Chung, T.-W., Chou, N.-K., & Wang, S.-S. (2013). Cardiac repair using chitosan-hyaluronan/silk fibroin patches in a rat heart model with myocardial infarction. *Carbohydrate Polymers*, 92(1), 591–597.
- Chimpango, A. F. A., van Zyl, W. H., & Görgens, J. F. (2012). In situ enzymatic aided formation of xylan hydrogels and encapsulation of horse radish peroxidase for slow release. *Carbohydrate Polymers*, 88(3), 1109–1117.
- Christman, K. L., & Lee, R. J. (2006). Biomaterials for the treatment of myocardial infarction. *Journal of the American College of Cardiology*, 48(5), 907–913.
- Christman, K. L., Vardanian, A. J., Fang, Q., Sievers, R. E., Fok, H. H., & Lee, R. J. (2004). Injectable fibrin scaffold improves cell transplant survival, reduces infarct expansion, and induces neovascularization formation in ischemic myocardium. *Journal of the American College of Cardiology*, 44(3), 654–660.
- Ciardelli, G., Chiono, V., Vozzi, G., Pracella, M., Ahluwalia, A., Barbani, N., et al. (2005). Blends of poly-(ϵ -caprolactone) and polysaccharides in tissue engineering applications. *Biomacromolecules*, 6(4), 1961–1976.
- Cohen, S., & Leor, J. (2004). Injectable cross-linked polymeric preparations and uses thereof. WO2004098669 A1.
- Cohen, S., & Leor, J. (2013). Injectable cross-linked polymeric preparations and uses thereof. EP2314327 B1.
- Codic, M. L., & Rao, M. (2008). Regulatory issues for personalized pluripotent cells. *Stem Cells*, 26(11), 2753–2758.
- Dahlmann, J., Krause, A., Möller, L., Kensah, G., Möwes, M., Diekmann, A., et al. (2013). Fully defined *in situ* cross-linkable alginate and hyaluronic acid hydrogels for myocardial tissue engineering. *Biomaterials*, 34(4), 940–951.
- Dang, J. M., Sun, D. D. N., Shin-Ya, Y., Sieber, A. N., Kostuik, J. P., & Leong, K. W. (2006). Temperature-responsive hydroxybutyl chitosan for the culture of mesenchymal stem cells and intervertebral disk cells. *Biomaterials*, 27(3), 406–418.
- Davis, M. E., Motion, J. P. M., Narmeneva, D. A., Takahashi, T., Hakuno, D., Kamm, R. D., et al. (2005). Injectable self-assembling peptide nanofibers create intramyocardial microenvironments for endothelial cells. *Circulation*, 111(4), 442–450.
- De Mulder, E. L., Buma, P., & Hannink, G. (2009). Anisotropic porous biodegradable scaffolds for musculoskeletal tissue engineering. *Materials*, 2(4), 1674–1696.
- Dib, N., Menasche, P., Bartunek, J. J., Zeiher, A. M., Terzic, A., Chronos, N. A., et al. (2010). Recommendations for successful training on methods of delivery of biologics for cardiac regeneration: A report of the international society for cardiovascular translational research. *JACC: Cardiovascular Interventions*, 3(3), 265–275.
- Dib, N., Khawaja, H., Varner, S., McCarthy, M., & Campbell, A. (2011). Cell therapy for cardiovascular disease: A comparison of methods of delivery. *Journal of Cardiovascular Translational Research*, 4(2), 177–181.
- Dvir, T., Kohane, D. S., Langer, R. S., & Timko, B. (2012). Nanowired three dimensional tissue scaffolds. WO2012094208 A1.
- Dvir, T., Kohane, D. S., Langer, R. S., & Timko, B. (2013). Nanowired three dimensional tissue scaffolds. US20130289687 A1.
- Ebringerová, A., & Heinze, T. (2000). Xylan and xylan derivatives—biopolymers with valuable properties. 1. Naturally occurring xyloans structures, isolation procedures and properties. *Macromolecular Rapid Communications*, 21(9), 542–556.
- Ebringerová, A., Hromádková, Z., Kačuráková, M., & Antal, M. (1994). Quaternized xyloans: Synthesis and structural characterization. *Carbohydrate Polymers*, 24(4), 301–308.
- Ebringerová, A., Kardošová, A., Hromádková, Z., Malov'ková, A., & Hříbalová, V. (2002). Immunomodulatory activity of acidic xyloans in relation to their structural and molecular properties. *International Journal of Biological Macromolecules*, 30(1), 1–6.
- Engelmayr, G. C., Cheng, M., Bettinger, C. J., Borenstein, J. T., Langer, R., & Freed, L. E. (2008). Accordion-like honeycombs for tissue engineering of cardiac anisotropy. *Nature Materials*, 7(12), 1003–1010.
- Ertl, G., & Frantz, S. (2005). Healing after myocardial infarction. *Cardiovascular Research*, 66(1), 22–32.
- Frenkel, J. S. (2012). The role of hyaluronan in wound healing. *International Wound Journal*, <http://dx.doi.org/10.1111/j.1742-1481X.2012.01057.x>
- Freyman, T., Palasis, M., & Ungs, M. (2005a). Aligned scaffolds for improved myocardial regeneration. US20050042254 A1.
- Freyman, T., Palasis, M., & Ungs, M. (2005b). Aligned scaffolds for improved myocardial regeneration. WO2005010172 A2.
- Freyman, T., Palasis, M., & Ungs, M. (2006). Aligned scaffolds for improved myocardial regeneration. EP1649008 A2.
- Freyman, T., Palasis, M., & Ungs, M. (2008). Aligned scaffolds for improved myocardial regeneration. US7384786 B2.
- Freyman, T., Palasis, M., & Ungs, M. (2009). Aligned scaffolds for improved myocardial regeneration. US7579189 B2.
- Fukamachi, K., & McCarthy, P. M. (2005). Initial safety and feasibility clinical trial of the myosplint device? *Journal of Cardiac Surgery*, 20(s6), S43–S47.
- Gajarsa, J. J., & Kloner, R. A. (2011). Left ventricular remodeling in the post-infarction heart: A review of cellular, molecular mechanisms, and therapeutic modalities. *Heart Failure Reviews*, 16(1), 13–21.
- Garbern, J. C., Minami, E., Stayton, P. S., & Murry, C. E. (2011). Delivery of basic fibroblast growth factor with a pH-responsive, injectable hydrogel to improve angiogenesis in infarcted myocardium. *Biomaterials*, 32(9), 2407–2416.
- Gerczuk, P. Z., & Kloner, R. A. (2012). An update on cardioprotection: review of the latest adjunctive therapies to limit myocardial infarction size in clinical trials. *Journal of the American College of Cardiology*, 59(11), 969–978.
- Giraud, M.-N., Guex, A. G., & Tevaearai, H. T. (2012). Cell therapies for heart function recovery: Focus on myocardial tissue engineering and nanotechnologies. *Cardiology Research and Practice*, 2012.
- Guan, J., Wang, F., Li, Z., Chen, J., Guo, X., Liao, J., et al. (2011). The stimulation of the cardiac differentiation of mesenchymal stem cells in tissue constructs that mimic myocardium structure and biomechanics. *Biomaterials*, 32(24), 5568–5580.
- Habib, M., Shapira-Schweitzer, K., Caspi, O., Gepstein, A., Arbel, G., Aronson, D., et al. (2011). A combined cell therapy and in-situ tissue-engineering approach for myocardial repair. *Biomaterials*, 32(30), 7514–7523.
- Hale, S. L., Dai, W., Dow, J. S., & Kloner, R. A. (2008). Mesenchymal stem cell administration at coronary artery reperfusion in the rat by two delivery routes: A quantitative assessment. *Life Sciences*, 83(13–14), 511–515.
- Hao, X., Silva, E. A., Månnsson-Broberg, A., Grinnemo, K.-H., Siddiqui, A. J., Dellgren, G., et al. (2007). Angiogenic effects of sequential release of VEGF-A165 and PDGF-BB with alginate hydrogels after myocardial infarction. *Cardiovascular Research*, 75(1), 178–185.
- Hellman, K. B. (1997). Bioartificial organs as outcomes of tissue engineering scientific and regulatory issues. *Annals of the New York Academy of Sciences*, 831(1), 1–9.
- Hollister, S. J. (2005). Porous scaffold design for tissue engineering. *Nature Materials*, 4(7), 518–524.
- Hu, X., Wang, J., Chen, J., Luo, R., He, A., Xie, X., et al. (2007). Optimal temporal delivery of bone marrow mesenchymal stem cells in rats with myocardial infarction. *European Journal of Cardio-Thoracic Surgery*, 31(3), 438–443.
- Ifkovits, J. L., Tous, E., Minakawa, M., Morita, M., Robb, J. D., Koomalsingh, K. J., et al. (2010). Injectable hydrogel properties influence infarct expansion and extent

- of postinfarction left ventricular remodeling in an ovine model. *Proceedings of the National Academy of Sciences of the United States of America*, 107(25), 11507–11512.
- Jaconi, M. E., & Zammaretti-Schaer, P. (2005a). 3D-cardiac tissue engineering for the cell therapy of heart failure. WO2005093047 A2.
- Jaconi, M. E., & Zammaretti-Schaer, P. (2005b). 3D-cardiac tissue engineering for the cell therapy of heart failure. US20080226726 A1.
- Jaconi, M. E., & Zammaretti-Schaer, P. (2006a). 3D-cardiac tissue engineering for the cell therapy of heart failure. EP1730265 A2.
- Jaconi, M. E., & Zammaretti-Schaer, P. (2006b). 3D-cardiac tissue engineering for the cell therapy of heart failure. WO2005093047 A3.
- Jawad, H., Ali, N. N., Lyon, A. R., Chen, Q. Z., Harding, S. E., & Boccaccini, A. R. (2007). Myocardial tissue engineering: A review. *Journal of Tissue Engineering and Regenerative Medicine*, 1(5), 327–342.
- Johnson, T. D., & Christman, K. L. (2013). Injectable hydrogel therapies and their delivery strategies for treating myocardial infarction. *Expert Opinion on Drug Delivery*, 10(1), 59–72.
- Kai, D., Prabhakaran, M. P., Jin, G., & Ramakrishna, S. (2013). Biocompatibility evaluation of electrically conductive nanofibrous scaffolds for cardiac tissue engineering. *Journal of Materials Chemistry B*, 1(17), 2305–2314.
- Kashem, A., Kashem, S., Santamore, W. P., Crabbe, D. L., Margulies, K. B., Melvin, D. B., et al. (2003). Early and late results of left ventricular reshaping by passive cardiac-support device in canine heart failure. *Journal of Heart and Lung Transplantation*, 22(9), 1046–1053.
- Kawaguchi, N., Smith, A. J., Waring, C. D., Hasan, M. K., Miyamoto, S., Matsuoka, R., et al. (2010). c-kitpos GATA-4 high rat cardiac stem cells foster adult cardiomyocyte survival through IGF-1 paracrine signalling. *PLoS ONE*, 5(12), e14297.
- Khine, M., & Luna, J. I. (2010). Aligning cells on wrinkled surface. WO2010108025 A2.
- Khine, M., & Luna, J. I. (2011). Aligning cells on wrinkled surface. WO2010108025 A3.
- Khine, M., & Luna, J. I. (2012). Aligning cells on wrinkled surface. US20120129209 A1.
- Kim, I.-Y., Seo, S.-J., Moon, H.-S., Yoo, M.-K., Park, I.-Y., Kim, B.-C., et al. (2008). Chitosan and its derivatives for tissue engineering applications. *Biotechnology Advances*, 26(1), 1–21.
- Kong, H. J., Kaigler, D., Kim, K., & Mooney, D. J. (2004). Controlling rigidity and degradation of alginate hydrogels via molecular weight distribution. *Biomacromolecules*, 5(5), 1720–1727.
- Lam, M. T., & Wu, J. C. (2012). Biomaterial applications in cardiovascular tissue repair and regeneration. *Expert Review of Cardiovascular Therapy*, 10(8), 1039.
- Landa, N., Miller, L., Feinberg, M. S., Holbova, R., Shachar, M., Freeman, I., et al. (2008). Effect of injectable alginate implant on cardiac remodeling and function after recent and old infarcts in rat. *Circulation*, 117(11), 1388–1396.
- Laurent, T. C., & Fraser, J. (1992). Hyaluronan. *FASEB Journal*, 6(7), 2397–2404.
- Lavergne, M., Derkaoui, M., Delmau, C., Letourneau, D., Uzan, G., & Le Visage, C. (2012). Porous polysaccharide-based scaffolds for human endothelial progenitor cells. *Macromolecular Bioscience*, 12(7), 901–910.
- Le Visage, C., Gournay, O., Benguirat, N., Hamidi, S., Chaussumier, L., Mougenot, N., et al. (2011). Mesenchymal stem cell delivery into rat infarcted myocardium using a porous polysaccharide-based scaffold: A quantitative comparison with endocardial injection. *Tissue Engineering Part A*, 18(1–2), 35–44.
- Lee, K. Y., & Mooney, D. J. (2012). Alginate: Properties and biomedical applications. *Progress in Polymer Science*, 37(1), 106–126.
- Leiknes, P. I., Senel, G. H., Brookstein, D., & Govindaraj, M. (2011). Textile-templated electrospun anisotropic scaffolds for tissue engineering and regenerative medicine. WO2011149836 A1.
- Lelkes, P. I., Senel, G. H., Brookstein, D., & Govindaraj, M. (2013). Textile-templated electrospun anisotropic scaffolds for tissue engineering and regenerative medicine. US20130131830 A1.
- Leor, J., & Cohen, S. (2004). Myocardial tissue engineering: Creating a muscle patch for a wounded heart. *Annals of the New York Academy of Sciences*, 1015(1), 312–319.
- Leor, J., Aboulafia-Etzion, S., Dar, A., Shapiro, L., Barbash, I. M., Battler, A., et al. (2000). Bioengineered cardiac grafts a new approach to repair the infarcted myocardium? *Circulation*, 102(3), 56–61.
- Leor, J., Tuvia, S., Guetta, V., Manczur, F., Castel, D., Willenz, U., et al. (2009). Intra-coronary injection of in situ forming alginate hydrogel reverses left ventricular remodeling after myocardial infarction in swine. *Journal of the American College of Cardiology*, 54(11), 1014–1023.
- Li, L., Zhang, S., Zhang, Y., Yu, B., Xu, Y., & Guan, Z. (2009). Paracrine action mediate the antifibrotic effect of transplanted mesenchymal stem cells in a rat model of global heart failure. *Molecular Biology Reports*, 36(4), 725–731.
- Li, J., Shu, Y., Hao, T., Wang, Y., Qian, Y., Duan, C., et al. (2013). A chitosan–glutathione based injectable hydrogel for suppression of oxidative stress damage in cardiomyocytes. *Biomaterials*, 34(36), 9071–9081.
- Liu, Z., Wang, H., Wang, Y., Lin, Q., Yao, A., Cao, F., et al. (2012). The influence of chitosan hydrogel on stem cell engraftment, survival and homing in the ischemic myocardial microenvironment. *Biomaterials*, 33(11), 3093–3106.
- Lu, W.-N., Lü, S.-H., Wang, H.-B., Li, D.-X., Duan, C.-M., Liu, Z.-Q., et al. (2008). Functional improvement of infarcted heart by co-injection of embryonic stem cells with temperature-responsive chitosan hydrogel. *Tissue Engineering Part A*, 15(6), 1437–1447.
- Malafaya, P. B., Silva, G. A., & Reis, R. L. (2007). Natural-origin polymers as carriers and scaffolds for biomolecules and cell delivery in tissue engineering applications. *Advanced Drug Delivery Reviews*, 59(4), 207–233.
- Malliaras, K., & Marbán, E. (2011). Cardiac cell therapy: Where we've been, where we are, and where we should be headed. *British Medical Bulletin*, 98(1), 161–185.
- Mann, D. L., Acker, M. A., Jessup, M., Sabbah, H. N., Starling, R. C., & Kubo, S. H. (2007). Clinical evaluation of the CorCap Cardiac Support Device in patients with dilated cardiomyopathy. *The Annals of Thoracic Surgery*, 84(4), 1226–1235.
- Martens, T. P., Godier, A. F., Parks, J. J., Wan, L. Q., Koeckert, M. S., Eng, G. M., et al. (2009). Percutaneous cell delivery into the heart using hydrogels polymerizing in situ. *Cell Transplantation*, 18(3), 297–304.
- Martinez, E. C., & Kofidis, T. (2011). Adult stem cells for cardiac tissue engineering. *Journal of Molecular and Cellular Cardiology*, 50(2), 312–319.
- McDevitt, T. C., Woodhouse, K. A., Hauschka, S. D., Murry, C. E., & Stayton, P. S. (2003). Spatially organized layers of cardiomyocytes on biodegradable polyurethane films for myocardial repair. *Journal of Biomedical Materials Research Part A*, 66A(3), 586–595.
- Morrison, W., Messina, A., Knight, K., & Pennington, A. (2005). Vascularized tissue graft. US20050056291 A1.
- Morrison, W., Messina, A., Knight, K., & Pennington, A. (2007). Vascularized tissue graft. US20070299508 A1.
- Morrison, W. A., Messina, A., Knight, K. R., & Pennington, A. J. (2011). Vascularized tissue graft. US7998735 B2.
- Morrison, W., Messina, A., Knight, K., & Pennington, A. (2012). Vascularized tissue graft. US20120209403 A1.
- Muthana, S. M., Campbell, C. T., & Gildersleeve, J. C. (2012). Modifications of glycans: Biological significance and therapeutic opportunities. *ACS Chemical Biology*, 7(1), 31–43.
- Nelson, D. M., Ma, Z., Fujimoto, K. L., Hashizume, R., & Wagner, W. R. (2011). Intramyocardial biomaterial injection therapy in the treatment of heart failure: Materials, outcomes and challenges. *Acta Biomaterialia*, 7(1), 1–15.
- Nitta, S. K., & Numata, K. (2013). Biopolymer-based nanoparticles for drug/gene delivery and tissue engineering. *International Journal of Molecular Sciences*, 14(1), 1629–1654.
- Oh, J. K., Lee, D. I., & Park, J. M. (2009). Biopolymer-based microgels/nanogels for drug delivery applications. *Progress in Polymer Science*, 34(12), 1261–1282.
- Parajó, J., Garrote, G., Cruz, J., & Dominguez, H. (2004). Production of xylooligosaccharides by autohydrolysis of lignocellulosic materials. *Trends in Food Science & Technology*, 15(3), 115–120.
- Pashuck, E. T., & Stevens, M. M. (2012). Designing regenerative biomaterial therapies for the clinic. *Science Translational Medicine*, 4(160), 160sr164.
- Peattie, R. A., Nayate, A. P., Firpo, M. A., Shelby, J., Fisher, R. J., & Prestwich, G. D. (2004). Stimulation of in vivo angiogenesis by cytokine-loaded hyaluronic acid hydrogel implants. *Biomaterials*, 25(14), 2789–2798.
- Place, E. S., Evans, N. D., & Stevens, M. M. (2009). Complexity in biomaterials for tissue engineering. *Nature Materials*, 8(6), 457–470.
- Prabhakaran, M. P., Venugopal, J., Kai, D., & Ramakrishna, S. (2011). Biomimetic material strategies for cardiac tissue engineering. *Materials Science and Engineering C*, 31(3), 503–513.
- Premaratne, G. U., Ma, L.-P., Fujita, M., Lin, X., Bollano, E., & Fu, M. (2011). Stromal vascular fraction transplantation as an alternative therapy for ischemic heart failure: Anti-inflammatory role. *Journal of Cardiothoracic Surgery*, 6(43), 8090–8096.
- Quignard, F., Di Renzo, F., & Guibal, E. (2010). From natural polysaccharides to materials for catalysis, adsorption, and remediation. *Topics in Current Chemistry*, 294, 165–197.
- Rekha, M., & Sharma, C. P. (2007). Pullulan as a promising biomaterial for biomedical applications: A perspective. *Trends in Biomaterials and Artificial Organs*, 20(2), 116–121.
- Sabbah, H. N. (2003). The cardiac support device and the myosplint: Treating heart failure by targeting left ventricular size and shape. *The Annals of Thoracic Surgery*, 75(6), S13–S19.
- Sapir, Y., Kryukov, O., & Cohen, S. (2011). Integration of multiple cell-matrix interactions into alginate scaffolds for promoting cardiac tissue regeneration. *Biomaterials*, 32(7), 1838–1847.
- Seif-Naraghi, S. B., Salvatore, M. A., Schup-Magoffin, P. J., Hu, D. P., & Christman, K. L. (2010). Design and characterization of an injectable pericardial matrix gel: A potentially autologous scaffold for cardiac tissue engineering. *Tissue Engineering Part A*, 16(6), 2017–2027.
- Shachar, M., Tsur-Gang, O., Dvir, T., Leor, J., & Cohen, S. (2011). The effect of immobilized RGD peptide in alginate scaffolds on cardiac tissue engineering. *Acta Biomaterialia*, 7(1), 152–162.
- Shen, X., Tanaka, K., & Takamori, A. (2009). Coronary arteries angiogenesis in ischemic myocardium: Biocompatibility and biodegradability of various hydrogels. *Artificial Organs*, 33(10), 781–787.
- Siepe, M., Akhyari, P., Lichtenberg, A., Schlensak, C., & Beyersdorf, F. (2008). Stem cells used for cardiovascular tissue engineering. *European Journal of Cardio-Thoracic Surgery*, 34(2), 242–247.
- Silva, E., & Mooney, D. (2007). Spatiotemporal control of vascular endothelial growth factor delivery from injectable hydrogels enhances angiogenesis. *Journal of Thrombosis and Haemostasis*, 5(3), 590–598.
- Silva, A. K. A., da Silva, É. L., Oliveira, E. E., Nagashima, T., Jr., Soares, L. A. L., Medeiros, A. C., et al. (2007). Synthesis and characterization of xylan-coated magnetite microparticles. *International Journal of Pharmaceutics*, 334(1–2), 42–47.
- Silva, A. K. A., Richard, C., Bessodes, M., Scherman, D., & Merten, O.-W. (2008). Growth factor delivery approaches in hydrogels. *Biomacromolecules*, 10(1), 9–18.
- Silvestri, A., Boffito, M., Sartori, S., & Ciardelli, G. (2013). Biomimetic materials and scaffolds for myocardial tissue regeneration. *Macromolecular Bioscience*, 13(8), 984–1019.
- Sinha, V., & Kumria, R. (2001). Polysaccharides in colon-specific drug delivery. *International Journal of Pharmaceutics*, 224(1), 19–38.

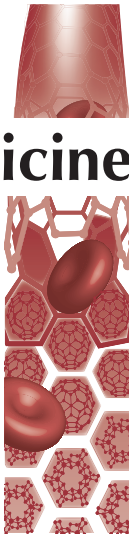
- Sokolsky-Papkov, M., Agashi, K., Olaye, A., Shakesheff, K., & Domb, A.J. (2007). *Polymer carriers for drug delivery in tissue engineering*. *Advanced Drug Delivery Reviews*, 59(4–5), 187–206.
- Starling, R. C., Jessup, M., Oh, J. K., Sabbah, H. N., Acker, M. A., Mann, D. L., et al. (2007). *Sustained benefits of the CorCap Cardiac Support Device on left ventricular remodeling: Three year follow-up results from the Acorn clinical trial*. *The Annals of Thoracic Surgery*, 84(4), 1236–1242.
- Stefanon, I., Valero-Muñoz, M., Fernandes, A. A., Ribeiro, R. F., Jr., Rodríguez, C., Miana, M., et al. (2013). *Left and right ventricle late remodeling following myocardial infarction in rats*. *PLoS ONE*, 8(5), e64986.
- Stern, R., Asari, A. A., & Sugahara, K. N. (2006). Hyaluronan fragments: An information-rich system. *European Journal of Cell Biology*, 85(8), 699–715.
- Topkara, V. K., Kondareddy, S., & Mann, D. L. (2009). Modulation of left ventricular dilation remodeling with epicardial restraint devices in postmyocardial infarction heart failure. *Current Heart Failure Reports*, 6(4), 229–235.
- Tous, E., Ifkovits, J. L., Koomalsingh, K. J., Shuto, T., Soeda, T., Kondo, N., et al. (2011). Influence of injectable hyaluronic acid hydrogel degradation behavior on infarction-induced ventricular remodeling. *Biomacromolecules*, 12(11), 4127–4135.
- Tsur-Gang, O., Ruvinov, E., Landa, N., Holbova, R., Feinberg, M. S., Leor, J., et al. (2009). The effects of peptide-based modification of alginate on left ventricular remodeling and function after myocardial infarction. *Biomaterials*, 30(2), 189–195.
- Venugopal, J. R., Prabhakaran, M. P., Mukherjee, S., Ravichandran, R., Dan, K., & Ramakrishna, S. (2012). *Biomaterial strategies for alleviation of myocardial infarction*. *Journal of the Royal Society Interface*, 9(66), 1–19.
- Venugopal, J., Rajeswari, R., Shayant, M., Sridhar, R., Sundarrajan, S., Balamurugan, R., et al. (2013). *Xylan polysaccharides fabricated into nanofibrous substrate for myocardial infarction*. *Materials Science and Engineering C*, 33(3), 1325–1331.
- Velahur, G., Juan-Babot, O., Peña, E., Oñate, B., Casaní, L., & Badimon, L. (2011). Molecular and cellular mechanisms involved in cardiac remodeling after acute myocardial infarction. *Journal of Molecular and Cellular Cardiology*, 50(3), 522–533.
- Vu, B., Chen, M., Crawford, R. J., & Ivanova, E. P. (2009). *Bacterial extracellular polysaccharides involved in biofilm formation*. *Molecules*, 14(7), 2535–2554.
- Vunjak-Novakovic, G., Lui, K. O., Tandon, N., & Chien, K. R. (2011). *Bioengineering heart muscle: A paradigm for regenerative medicine*. *Annual Review of Biomedical Engineering*, 13, 245–267.
- Wall, S. T., Walker, J. C., Healy, K. E., Ratcliffe, M. B., & Guccione, J. M. (2006). Theoretical impact of the injection of material into the myocardium a finite element model simulation. *Circulation*, 114(24), 2627–2635.
- Wang, F., & Guan, J. (2010). *Cellular cardiomyoplasty and cardiac tissue engineering for myocardial therapy*. *Advanced Drug Delivery Reviews*, 62(7–8), 784–797.
- Wang, C.-C., Chen, C.-H., Lin, W.-W., Hwang, S.-M., Hsieh, P. C. H., Lai, P.-H., et al. (2008). *Direct intramyocardial injection of mesenchymal stem cell sheet fragments improves cardiac functions after infarction*. *Cardiovascular Research*, 77(3), 515–524.
- Wang, H., Zhang, X., Li, Y., Ma, Y., Zhang, Y., Liu, Z., et al. (2010). *Improved myocardial performance in infarcted rat heart by co-injection of basic fibroblast growth factor with temperature-responsive chitosan hydrogel*. *Journal of Heart and Lung Transplantation*, 29(8), 881–887.
- Wang, H., Zhou, J., Liu, Z., & Wang, C. (2010). *Injectable cardiac tissue engineering for the treatment of myocardial infarction*. *Journal of Cellular and Molecular Medicine*, 14(5), 1044–1055.
- Wang, Q., Kong, M., An, Y., Liu, Y., Li, J., Zhou, X., et al. (2013). *Hydroxybutyl chitosan thermo-sensitive hydrogel: A potential drug delivery system*. *Journal of Materials Science*, 48(16), 5614–5623.
- Wenk, J. F., Sabbah, H. N., Burger, M., Ratcliffe, M. B., Guccione, J. M., Stander, N., et al. (2009). *A method for automatically optimizing medical devices for treating heart failure: Designing polymeric injection patterns*. *Journal of Biomechanical Engineering*, 131(12), 121011.
- Wolf, B. W., Garleb, K. A., Choe, Y. S., Humphrey, P. M., & Maki, K. C. (2003). *Pullulan is a slowly digested carbohydrate in humans*. *Journal of Nutrition*, 133(4), 1051–1055.
- Wu, S., Jin, Z., Kim, J. M., Tong, Q., & Chen, H. (2009). *Downstream processing of pullulan from fermentation broth*. *Carbohydrate Polymers*, 77(4), 750–753.
- Wu, J., Zeng, F., Huang, X.-P., Chung, J. C. Y., Konecny, F., Weisel, R. D., et al. (2011). *Infarct stabilization and cardiac repair with a VEGF-conjugated, injectable hydrogel*. *Biomaterials*, 32(2), 579–586.
- Xie, J. (2013a). *Nanofiber scaffolds and methods for repairing damaged cardiac tissue*. WO2013109642 A1.
- Xie, J. (2013b). *Nanofiber scaffolds and methods for repairing damaged cardiac tissue*. US20130183352 A1.
- Yabur, R., Bashan, Y., & Hernández-Carmona, G. (2007). *Alginate from the macroalgae *Sargassum sinicola* as a novel source for microbial immobilization material in wastewater treatment and plant growth promotion*. *Journal of Applied Phycology*, 19(1), 43–53.
- Yoon, S. J., Fang, Y. H., Lim, C. H., Kim, B. S., Son, H. S., Park, Y., et al. (2009). *Regeneration of ischemic heart using hyaluronic acid-based injectable hydrogel*. *Journal of Biomedical Materials Research Part B: Applied Biomaterials*, 91B(1), 163–171.
- Yu, J., Gu, Y., Du, K. T., Mihardja, S., Sievers, R. E., & Lee, R. J. (2009). *The effect of injected RGD modified alginate on angiogenesis and left ventricular function in a chronic rat infarct model*. *Biomaterials*, 30(5), 751–756.
- Zhang, H., Song, P., Tang, Y., Zhang, X.-L., Zhao, S.-H., Wei, Y.-J., et al. (2007). *Injection of bone marrow mesenchymal stem cells in the borderline area of infarcted myocardium: Heart status and cell distribution*. *Journal of Thoracic and Cardiovascular Surgery*, 134(5), 1234–1240, e1231.
- Zhang, X., Wang, H., Ma, X., Adila, A., Wang, B., Liu, F., et al. (2010). *Preservation of the cardiac function in infarcted rat hearts by the transplantation of adipose-derived stem cells with injectable fibrin scaffolds*. *Experimental Biology and Medicine*, 235(12), 1505–1515.
- Zhou, Y., Wang, S., Yu, Z., Hoyt, R. F., Jr., Qu, X., & Horvath, K. A. (2011). *Marrow stromal cells differentiate into vasculature after allogeneic transplantation into ischemic myocardium*. *The Annals of Thoracic Surgery*, 91(4), 1206–1212.
- Zouein, F. A., Zgheib, C., Liechty, K. W., & Booz, G. W. (2012). *Post-infarct biomaterials, left ventricular remodeling, and heart failure: Is good good enough?* *Congestive Heart Failure*, 18(5), 284–290.

Annexe B - Publication dans le cadre du consortium *NanoAthero*

B.1. Nanoparticles for intravascular applications: physicochemical characterization and cytotoxicity testing

Nanomedicine. 2016 Mar. 11(6): 597-616

Matuszak J, Baumgartner J, Zaloga J, Juenet M, da Silva AE, Franke D, Almer G, Texier I, Faivre D, Metselaar JM, Navarro FP, Chauvierre C, Prassl R, Dezsi L, Urbanics R, Alexiou C, Mangge H, Szebeni J, Letourneur D, Cicha I



Nanoparticles for intravascular applications: physicochemical characterization and cytotoxicity testing

Aim: We report the physicochemical analysis of nanosystems intended for cardiovascular applications and their toxicological characterization in static and dynamic cell culture conditions. **Methods:** Size, polydispersity and ζ -potential were determined in 10 nanoparticle systems including liposomes, lipid nanoparticles, polymeric and iron oxide nanoparticles. Nanoparticle effects on primary human endothelial cell viability were monitored using real-time cell analysis and live-cell microscopy in static conditions, and in a flow model of arterial bifurcations. **Results & conclusions:** The majority of tested nanosystems were well tolerated by endothelial cells up to the concentration of 100 $\mu\text{g}/\text{ml}$ in static, and up to 400 $\mu\text{g}/\text{ml}$ in dynamic conditions. Pilot experiments in a pig model showed that intravenous administration of liposomal nanoparticles did not evoke the hypersensitivity reaction. These findings are of importance for future clinical use of nanosystems intended for intravascular applications.

First draft submitted: 9 October 2015; Accepted for publication: 18 December 2015;
Published online: 22 March 2016

Keywords: atherosclerosis • endothelial cells • hypersensitivity reaction • live-cell analysis
• nanoparticle biocompatibility • nanoparticle stability

Atherosclerosis and consecutive cardiovascular events represent one of the biggest global health problems [1]. Rupture of vulnerable atherosclerotic plaques can lead to ischemia of the heart, brain or extremities [2], the predominant causes of morbidity and mortality worldwide. Although both the understanding of disease mechanisms and the imaging techniques for atherosclerotic plaque detection have considerably advanced during the last decades, effective approaches to early diagnosis and improved targeted therapies are still missing [3].

The potential of nanotechnology-based therapies to overcome the disadvantages of systemic drug administration has been well recognized in the field of oncology, but no specific nanoparticle-based system has yet been approved for diagnosis or therapy of cardiovascular diseases. By coating nanopar-

ticles with plaque-specific ligands, significantly increased accumulation of these agents at the sites of atherosclerotic lesions could be achieved, leading to improved detection and characterization of the plaques [4]. Furthermore, the treatment outcome can be dramatically improved if the drug-carrying nanoparticles were directly targeted at the diseased artery region, thus reducing the systemic side effects [5]. Hence, our goal is the development of effective, safe and innovative nanoparticle-based systems for the diagnosis and therapy of clinically relevant atherosclerosis. For this purpose, systematic analyses of the candidate nanosystems including their basic physicochemical characterization, their long-term stability and the biological effects of nanoparticles, for example, on the vascular cells, are necessary. So far, the majority of studies utilized fibroblasts, mesenchymal

Jasmin Matuszak¹, Jens Baumgartner², Jan Zaloga¹, Maya Juenet³, Acarília Eduardo da Silva⁴, Danielle Franke⁵, Gunter Almer⁶, Isabelle Texier⁷, Damien Faivre², Josbert M Metselaar^{4,8}, Fabrice P Navarro⁷, Cédric Chauvierre³, Ruth Prassi⁹, László Dézsi¹⁰, Rudolf Urbanics¹¹, Christoph Alexiou¹, Harald Mangge⁶, János Szébeni^{10,11}, Didier Letourneur³ & Iwona Cicha^{*1}

¹Cardiovascular Nanomedicine Unit, Section of Experimental Oncology and Nanomedicine (SEON), ENT-Department, University Hospital Erlangen, Glückstr. 10a, 91054 Erlangen, Germany

²Department of Biomaterials, Max Planck Institute of Colloids & Interfaces, Science Park Golm, Potsdam, Germany

³Inserm U1148, LVTS, Paris Diderot University, Paris 13 University, Sorbonne Paris Cité, X. Bichat Hospital, Paris, France

⁴Department of Targeted Therapeutics, MIRA Institute, University of Twente, Enschede, The Netherlands

⁵nanoPET Pharma GmbH, Berlin, Germany

⁶Clinical Institute of Medical & Chemical Laboratory Diagnostics, Medical University of Graz, Graz, Austria

⁷CEA-LETI MINATEC/DTBS, Université Grenoble Alpes, Grenoble, France

⁸Department of Experimental Molecular Imaging, University Clinic & Helmholtz Institute for Biomedical Engineering, RWTH-Aachen University, Aachen, Germany

⁹Institute of Biophysics, Medical University of Graz, Graz, Austria

¹⁰Nanomedicine Research & Education Center, Semmelweis University, Budapest, Hungary

¹¹SeroScience Ltd., Budapest, Hungary

*Author for correspondence:
Tel.: +49 9131 8543953
Fax: +49 9131 8534282
Iwona.Cicha@uk-erlangen.de

stem cells or cancer cells to investigate the biocompatibility of nanosystems. In the recent years, increased numbers of publications appeared concerning the possible interactions between nanoparticles and endothelial cells, which are the first contact cells in the vascular wall for circulating nanoparticles. However, these reports usually focus on one type of nanosystems in the context of endothelial viability, or barrier function [6–9]. Thus, the purpose of this work was to perform comparative physicochemical and biological analyses of different types of nanoparticles intended for intravascular applications.

The candidate nanosystems included in these analyses comprise lipid nanoparticles, liposomes, polymeric nanoparticles, as well as inorganic nanoparticles, that are briefly outlined below.

Lipid nanoparticles (LipidotsTM) can be considered as nano-oil droplets stabilized by a mixture of surfactants (oil-in-water emulsion). They are composed of a lipid core, herein a mixture of soybean oil and a wax, and a surfactant shell, containing a mixture of phospholipids and polyethylene glycol (PEG)-ylated surfactants [10]. Liposomes are composed of a lipid bilayer consisting of amphipathic phospholipids (primarily phosphatidylcholine) that enclose an interior aqueous space [11]. The head groups of phospholipids are often functionalized with polymerizable moieties to improve stability (e.g., PEGylated stealth liposomes [12]), or with molecular groups, which allow conjugation to antibodies or other ligands. Among the advantages of lipid nanoparticles and liposomes as drug-delivery platforms are the ease of preparation, and the reported low immunogenicity [13,14], which is expected to enable safe and repeated administration.

Polymeric nanoparticles are composed of polymers, most commonly poly(lactic-*co*-glycolic acid), poly(lactic acid), poly(caprolactone), poly(alkylcyanoacrylates) or chitosan. The core of the nanoparticles used in our studies (~80% of the total mass) is made of poly(isobutylcyanoacrylate) (PIBCA), which is covalently cross-linked with polysaccharides of the coating, forming a hydrophilic shell. Functionalization of these nanoparticles allows conjugation of targeting ligands, for example, fucoidan, a mimic of sialyl Lewis X, the natural ligand of P-selectin [15,16], a promising molecule to target processes upregulated during destabilization of vulnerable plaques. Inorganic nanoparticle systems included in this work comprised superparamagnetic iron oxide nanoparticles. These particles consist of an iron oxide core, which is coated with organic materials such as fatty acids, polysaccharides or polymers. Iron oxide nanoparticles have good biocompatibility and contrast-enhancing properties in MRI, enabling plaque detection and characterization [17–20]. Furthermore,

the magnetic properties of these particles could allow their remote targeting by means of external magnetic field [21–23].

Although the concept of nanomedicine encompasses a localized delivery of nanosystems to the diseased organs or target tissues and minimized systemic side effects, the extended circulation time, as well as multiple degradation products, may result in nanoparticle cytotoxicity [24], or immunogenicity [25]. Hence, in order to predict *in vivo* responses, the toxicity of any nanosystem should first be evaluated on cultured cells (e.g., endothelial cells in the case of intravenous application, and the target cells), preferably under conditions that resemble the physiological state. Although standard cytotoxicity assays have been commonly used to estimate the cellular responses to various nanosystems, many nanoparticles interfere with the available photometric assays, which may render the experimental results difficult to assess and interpret [26]. Here, we compare nanosystems' biological effects on primary human endothelial cells, using two complementary methods for long-term *in vitro* monitoring in static conditions (real-time cell analysis and live-cell microscopy), as well as an *in vitro* model of arterial bifurcation that allows observation of endothelial cells under physiologic-like flow conditions. Furthermore, we report the initial results of the pilot studies on the complement activation-related pseudoallergy (CARPA) upon the intravenous administration of liposomal nanoparticles in a pig model.

Materials & methods

In total, ten nanoparticle systems were synthesized and investigated, including two types of liposomes (LP-NPs), three types of lipid nanoparticles (LD-NPs), two types of polymeric nanoparticles (PM-NPs) and three types of iron oxide nanoparticles (IO-NPs). The detailed description of nanoparticle characterization is provided in the [Online Supplement](#).

Reagents

Soybean oil and MyrijTM s40 (PEGylated surfactant) were purchased from Croda, Chocques, France. Lipoid S75 and dipalmitoylphosphatidylcholine were from Lipoid GmbH, Ludwigshafen, Germany. Suppocire NB was from Gatefosse, Saint-Priest, France. 1-palmitoyl-2-oleoyl-sn-glycero-3-phosphocholine (POPC), cholesterol, 1,2-distearoyl-sn-glycero-3-phospho-ethanolamine-N-[methoxy (polyethylene glycol)-2000] (DSPE-PEG-2000) and 1,2-distearoyl-phosphatidyl-ethanolamine-methyl-polyethyleneglycol conjugate-550 (DSPE-PEG550) were purchased from Avanti Polar Lipids, Inc. (AL, USA).

Dextran T70 was from Roth (Karlsruhe, Germany), or from Amersham Pharmacia Biotech (Freiburg, Germany), and dextran T40 from PharmaCosmos (Holbaek, Denmark). Carboxymethyl-dextran sodium salt (CM-Dextran) was purchased from Sigma Aldrich (Saint Quentin Fallavier, France) and diethylaminoethyl-dextran 20 (DEAE-dextran) from TdB Consultancy (Uppsala, Sweden). Low molecular weight Fucoidan (3–8 kDa, Fucoidan Ascophyseient®) was from Algues et Mer (Ouessant, France). IBCA (isobutylcyanoacrylate, Glue 368) was from Orapi (Saint-Vulbas, France). Bovine serum albumin (BSA) and iron (II) chloride tetrahydrate were from Merck, Darmstadt, Germany. Lauric acid, epichlorohydrin and dextranT6 (Mw = 6 kDa) were from Sigma Aldrich, Munich, Germany. Ceric (IV) ammonium nitrate and tri-sodium citrate dihydrate were purchased from Fluka (Saint Quentin Fallavier, France). NaOH, HCl (25%), NH₃ (25%) and nitric acid (65% w/w) were from Roth. Iron (III) chloride hexahydrate was purchased from Sigma-Aldrich or from Roth. All compounds used were of pharmaceutical (Ph. Eur) or highly pure ($\geq 99\%$) grade and were used without any further purification.

Nanoparticle synthesis

Lipidots

Lipid nanoparticles (LD-NP) were prepared by the sonication method [10]. Briefly, the lipid phase was prepared by mixing Suppocire™ NB, soybean oil and lipoid S75. The aqueous phase, containing Myrj s40 (PEGylated surfactant) in phosphate buffered saline (PBS), was heated to 50°C to melt the surfactant and then mixed with the lipid phase. Following sonication for 5 min, the samples were dialyzed against PBS and sterilized by filtration through a 0.22 μ m filter. The batches of particles with specified diameter were obtained by altering the lipid and surfactants ratios. Three different sizes (diameters) were formulated: 50 nm (LD-NP1), 80 nm (LD-NP2) and 120 nm (LD-NP3).

Liposomes

For the synthesis of sterically stabilized PEGylated liposomes (LP-NP1), POPC, cholesterol (Avanti Polar Lipids) and DSPE-PEG-2000 were used. Lipids were dissolved in chloroform-methanol 2:1 (v/v) at molar ratios of 3:2:0.15. LP-NP1 were made using a dry film rehydration technique, followed by size extrusion, as described previously [12,27]. Briefly, the organic solvent was evaporated under a stream of nitrogen to obtain a lipid film. For complete removal of solvents the film was dried in a vacuum chamber overnight. Subsequently, the dry lipid film was hydrated in PBS and size-extruded using an Avanti Polar mini-extruder

(Avanti Polar Lipids, Inc.) and 100 nm polycarbonate membranes.

The LP-NP2 liposomes were prepared using the lipid injection method, by mixing the ethanolic lipid solution with the aqueous phase under magnetic stirring at 60°C. Briefly, dipalmitoylphosphatidylcholine, cholesterol (BUFA, Uitgeest, The Netherlands), and DSPE-PEG550 were dispersed in ethanol at molar ratios of 1.85:1:0.15. Subsequently, the lipid solution was transferred into PBS previously heated to 60°C. The resulting emulsion was downsized by multiple extrusion steps through polycarbonate filter membranes with decreasing pore sizes of (200–100 nm). Subsequently, ethanol and dissolved lipids were removed by dialysis against PBS.

Polymeric nanoparticles

Polymeric nanoparticles (PM-NP) were synthesized by a redox radical emulsion polymerization method. This method ensures the polysaccharides of the shell to assemble into a brush-like layer of coating. Here, two different coatings were used: 90% CM-Dextran/10% Fucoidan (PM-NP1); and 80% DextranT70 (Pharmacia Biotech)/10% DEAE-dextran/10% Fucoidan (PM-NP2). Briefly, polysaccharides (0.1375 g) were dissolved in a nitric acid solution (2×10^{-1} M) at 40°C and left under nitrogen bubbling for 10 min. Polymerization was initiated by adding 2 ml ceric (IV) ammonium nitrate solution (8×10^{-2} M) in nitric acid and 0.5 ml of IBCA monomers to the polysaccharide solution under nitrogen atmosphere and vigorous stirring. The reaction was then left for 40 min at 40°C under gentle stirring, followed by cooling to room temperature. Subsequently, 1.25 ml of a trisodium citrate dihydrate solution (1.02 M) was added to the suspension and the pH was adjusted to 7.0 with NaOH. PM-NPs were purified by dialysis (molecular weight cut-off 100 kDa) against water. One final dialysis was performed against NaCl 0.9%. Nanoparticles were sterilized by filtration through a 0.45 μ m filter, followed by 15 min exposure to UV radiation.

Iron oxide nanoparticles (IO-NP)

Lauric acid/BSA-coated magnetite nanoparticles (IO-NP1) were synthesized by coprecipitation, subsequent *in situ* coating with lauric acid and formation of an artificial albumin corona as previously described [28]. Briefly, Fe (II) and Fe (III) salts at a defined molar ratio ($\text{Fe}^{3+}/\text{Fe}^{2+} = 2$) were dissolved in 20 ml of water and stirred at 80°C under argon atmosphere, followed by addition of 20 ml of NH₃ solution (25%). The solution was heated to 90°C and 1.25 g lauric acid, dissolved in acetone, was added. The brownish suspension was left to homogenate for 30 min at 90°C. The suspen-

sion was then dialyzed multiple times against water. Subsequently, IO-NP1 were stabilized by incubation with a freshly prepared 20% BSA solution, purified by centrifugal ultrafiltration (molecular weight cut-off 100 kDa), and sterilized by filtration through a 0.22 µm filter.

For preparation of dextran-coated magnetite nanoparticles (IO-NP2), the synthesis method by Unterweger *et al.* was used [29]. Briefly, Fe (II) and Fe (III) salts in molar ratios ($\text{Fe}^{3+}/\text{Fe}^{2+} = 2$) as well as 1.75 g of dextranT6 were dissolved in water. After cooling to 4°C under continuous stirring and argon atmosphere, 5 ml of ice-cold 25% NH₃ was added. After 5 min, the reaction mixture was heated and kept at 75°C for a further 40 min, followed by cooling to RT and dialysis (molecular weight cut-off 8 kDa). The mixture was then cleared from excess dextran and concentrated to a total volume of 20 ml using ultrafiltration (molecular weight cut-off 100 kDa). To stabilize the dextran coating, crosslinking was performed by adding 4 ml of epichlorohydrine dropwise to the nanoparticle suspension after alkalization with NaOH under vigorous stirring for 24 h. The solution was then dialyzed against water, concentrated by ultrafiltration and sterile filtered through 0.22 µm membrane.

IO-NP3 nanoparticles were also synthesized by the coprecipitation method. Briefly, Fe (II) and Fe (III) salts at a defined molar ratio ($\text{Fe}^{3+}/\text{Fe}^{2+} = 2$) were dissolved in water under nitrogen atmosphere, followed by addition of a preheated strong alkali solution under continuous stirring. In the second step, the coating material (carboxydextran) was added to the aqueous suspension of iron oxide nanoparticles followed by heating under reflux. After cooling, the resulting material was filtered and dispersed in water, followed by dialysis against water, and sterile filtration using a 0.45 µm filter.

Physicochemical characterization & stability on storage

Z-averaged hydrodynamic diameter, polydispersity (PDI) and ζ-potential were determined with a Zetasizer Nano ZS (Malvern) using standard polystyrene cuvettes and disposable folded capillary cells (DTS1070), respectively. All samples were diluted prior to the measurement according to the producers' instructions: LD-NPs, LP-NP1 suspensions were diluted 10× in deionized and 0.2 µm-membrane filtered water, LP-NP2 were diluted 10× in PBS pH 7.4, and PM-NPs and IO-NPs were diluted between 50× and 100× in ultrapure water. Samples were equilibrated to 25°C and 3 × > 10 runs of 10 s performed in 173° backscatter mode. The employed refractive indices and absorption coefficients for the different particles

systems were: LD-NPs, 1.5, 0.1; LP-NP1, 1.4, 0.001; LP-NP2, PM-NPs, 1.59, 0.01; IO-NPs, 2.9, 5.18. To determine sample stability, the first time-point for physicochemical characterization was set at 1 month post synthesis date, followed by the subsequent measurements after 3 and 6 months of storage at 4°C. The detailed description of further characterization methods relevant for the respective nanoparticle types is provided in the [Online Supplement](#).

Real-time cell analysis

Human umbilical vein endothelial cells (HUVECs) were isolated from freshly collected umbilical cords (kindly provided by the Department of Gynaecology, University Hospital Erlangen) and cultured as described in the [Online Supplement](#). In all experiments, HUVECs at passage 1–2 were used. The use of human material was approved by the local ethics committee at the University Hospital Erlangen (review number 237_12B from 19.09.2012). For monitoring the effects of nanoparticles on HUVEC viability, the xCELLigence system (RTCA DP Analyzer, Roche Diagnostics, Mannheim, Germany) was used [30]. Experiments were performed in 16-well E-plates (ACEA Bioscience, CA, USA), in which the impedance is measured with the help of microelectrodes localized at the bottom of the wells (for detailed description, see [Online Supplement](#)).

For the background measurement, 100 µl of cell-free endothelial cell growth medium was added to the wells. Afterwards, 50 µl of media from each well were replaced with 50 µl of cell suspension containing 1×10^3 HUVECs. About 30 min after seeding of the cells, monitoring of impedance by the xCELLigence system was initiated. At 24 h after seeding, an additional 100 µl of media containing different concentrations of nanoparticles were added to the wells, as follows: (a) for controls, 100 µl of pure medium without nanoparticles, and (b) for the treatment samples, 100 µl of medium containing nanoparticles at concentrations 2× higher than the required final nanoparticle concentration. The final nanoparticle concentrations were as follows: 0, 12.5, 25, 50, 100, 200 and 400 µg/ml. Concentrations for iron oxide nanoparticles were calculated as total iron (Fe) concentration. The concentrations for lipid nanoparticles, liposomes and polymeric nanoparticles were calculated as total dry mass weight per volume. Cell growth was monitored every 10 min for 96 h. The experiments were performed in hexuplicate.

Live-cell microscopy

HUVECs were seeded in 96-well plates at 2×10^3 cells/well in 100 µl medium. At 24 h after seeding, additional 100 µl of media containing different con-

centrations of nanoparticles were added to the wells, as described in detail above. Cell growth was monitored for 72 h using a live cell-imager (IncuCyte FLR microscope system, Essen Bioscience, MI, USA). The experiments were performed in hexuplicate.

Flow experiments

Flow experiments were performed as previously described (see [31] and [Online Supplement](#)). For the perfusion with nanoparticles, two different concentrations were used (100 µg/ml and 400 µg/ml). Subsequently, HUVECs were stained with Alexa488-phalloidin (PromoKine, Heidelberg, Germany). Cell nuclei were counterstained with DAPI (Molecular Probes, Darmstadt, Germany). Images were obtained using fluorescence microscope Zeiss Axio Observer. Z1 (Carl Zeiss AG, Oberkochen, Germany). The confluence was determined on ×10 objective magnification images using ImageJ software.

Pig model of complement activation-related pseudoallergy (CARPA)

Pilot studies in a pig model of infusion reaction to LP-NP1 were performed as described by Szebeni [32]. Briefly, domestic male Yorkshire pigs (20–25 kg) were anesthetized with isoflurane (2–3% in O₂). Intubation was performed with endotracheal tubes to maintain free airways. Oxygen saturation was monitored using a pulse-oximeter fixed on the tail, and body temperature was monitored rectally. A capnograph was connected to the tracheal tube to monitor EtCO₂ and the respiratory rate (CAP10, Medlab GmbH, Karlsruhe, Germany). To measure the pulmonary arterial blood pressure (PAP), a Swan-Ganz catheter (AI-07124, 5 Fr. 110 cm, Arrow International, Inc., Teleflex, Athlone, Ireland) was introduced into the pulmonary artery via the right external jugular vein – right atrium – right ventricle, while systemic arterial blood pressure (SAP) was measured in the femoral artery. LP-NP1 and zymosan were injected in the animals in bolus (<10 s) via the left external jugular vein. The amount of test material injected is given as mg phospholipids/kg, unless otherwise indicated. Hemodynamic changes were continuously monitored at 1000 Hz sampling rate, using an AD Instruments PowerLab System with LabChart Pro v6 software. From the mean PAP, SAP and heart rate (HR) data about 20 s intervals were averaged and evaluated by AD Instruments LabChart Pro v6 software modules. The usual evaluated periods were: before the test material injection, then 20 s in every minute for 10 min, and every 5 min until the end of the reaction. Plasma levels of thromboxane B2 (TXB₂, the stable metabolite of TXA₂) were measured with a commercially available ELISA kit (Cayman Chemi-

cals, MI, USA). The study was approved by the local ethics committee for animal experimentation.

Statistical analyses

The differences between the *in vitro* treatment groups were calculated using ANOVA on Ranks. Data were expressed as mean ± SEM, unless stated otherwise. *In vivo* changes in SAP and HR, as well as TXB₂ were compared with time 0 (baseline) values using one-way ANOVA with Dunnett's post hoc test. p < 0.05 was considered statistically significant.

Results

Nanoparticle characterization & stability on storage

The detailed description of physicochemical properties of respective nanoparticles is provided in the [Online Supplement](#) ([Supplementary Figures 1–16](#), see also [10,12,27–29]). To validate the stability of physicochemical parameters upon prolonged storage, the Z-averaged hydrodynamic diameter, the polydispersity (expressed as polydispersity index, PDI) and the ζ-potential of the investigated nanoparticles were determined at different time points. The first collective analysis time-point was set at 1-month post synthesis date. The detailed characteristics of the nanoparticles are shown in [Table 1](#). To ensure the long-term particle stability, subsequent measurements were performed on the various nanoparticles after 3 and 6 months of storage at 4°C in their respective dilution media. As shown in [Table 2](#), no significant changes in hydrodynamic diameter, PDI and ζ-potential of the nanoparticles were found, indicating a good stability with time.

Real-time cell analysis of nanoparticle cytotoxicity

Endothelial cells are the first-contact vascular cells for any nanosystems designed for intravascular applications. A suitable *in vitro* method to investigate the potential toxicity of intravenously applied nanosystems is to test their effect on HUVECs, which serve as a model system of the human endothelium. Real-time cell analysis using xCELLigence is a well-established method used, among others, for nanotoxicity studies [33]. As described in detail in [Online Supplement](#), cell index measured with this technique reflects cell viability, number, morphology and adhesion strength. To ensure that the tested nanoparticles do not interfere with the impedance measurements, a series of control experiments was performed. Importantly, the presence of nanoparticles alone (without cells) did not affect the impedance measured by the electrodes, as shown in [Supplementary Figures 17–20](#). In studies with HUVECs, a steady increase in cell index was observed

Table 1. Physicochemical characterization of nanoparticles.

Nanoparticle type	Z-avg d(nm)	PDI	ζ (mV)	SD ζ (mV)
LD-NP1	53.3	0.156	-7.0	14.5
LD-NP2	82.8	0.191	-9.0	14.6
LD-NP3	120.1	0.151	-8.8	8.4
LP-NP1	138.6	0.104	-16.3	7.4
LP-NP2	108.8	0.034	-9.0	4.7
PM-NP1	145.1	0.072	-51.0	5.6
PM-NP2	226.9	0.194	3.3	5.7
IO-NP1	78.7	0.145	-37.3	12.9
IO-NP2	79.6	0.173	13.7	9.3
IO-NP3	57.5	0.217	-24.9	8.4

Physicochemical characterizations were performed for various nanosystems 1 month after particle synthesis. Z-avg d: Z-averaged hydrodynamic diameter; PDI: Polydispersity ($PDI = SD^2/d^2$); ζ : Zeta-potential; SD ζ : Standard deviation of zeta-potential; NP: Nanoparticles; LD: Lipidots; LP: Liposomes; PM: Polymeric NPs; IO: Superparamagnetic iron oxide nanoparticles.

over time in control (untreated) endothelial cells, but also in the cells treated with LP-NPs up to the highest tested concentration (400 μ g/ml, Figure 1). There were no significant differences in the growth curves of the liposome-treated cells versus control samples, showing a similar increase of cell index until the end of the measurement at 72 h post-application. In cells treated with 100 μ g/ml LD-NP1 (Figure 2A), a decrease in cell index at 48 and 72 h was observed in comparison to control, indicative of cell growth inhibition or loss of adherence. Interestingly, the decrease in cell indices became obvious at the concentration of 100 μ g/ml for LD-NP1, 200 μ g/ml for LD-NP2 and above 200 μ g/ml for LD-NP3, suggesting that the larger lipid nanoparticles may be better tolerated by endothelial cells (Figure 2). For polymeric nanoparticles (Figure 3), the decrease in endothelial cell index rela-

tive to the preapplication values, which was indicative of cytostatic or cytotoxic effects, was induced from the concentration of 50 μ g/ml for PM-NP1, and from 100 μ g/ml for PM-NP2.

In cells treated with 50 μ g/ml IO-NP1 (Figure 4), a significantly lower cell-index in comparison to control was observed at 48 and 72 h, indicative of cell growth inhibition. The decrease in endothelial cell index relative to preapplication values, indicative of negative effects on cell viability or adherence was induced from the concentration of 100 μ g/ml IO-NP1 (Figure 4A). There were no significant differences in the growth curves of the cells treated with IO-NP2 versus control samples, showing a similar increase of cell index until the end of the measurement at 72 h post-application (Figure 4B). Since IO-NP3 were no longer stable upon dilution in the serum-containing endothelial cell

Table 2. Nanoparticle stability on storage.

Nanoparticle type	1 month				3 months				6 months			
	Z-avg d (nm)	PDI	ζ (mV)	SD ζ (mV)	Z-avg d (nm)	PDI	ζ (mV)	SD ζ (mV)	Z-avg d (nm)	PDI	ζ (mV)	SD ζ (mV)
LD-NP1	53.3	0.156	-7.0	14.5	52.5	0.142	-8.5	11.5	53.3	0.193	-7.7	4.6
LD-NP2	82.8	0.191	-9.0	14.6	83.0	0.173	-8.6	6.9	84.3	0.213	-8.2	5.9
LD-NP3	120.1	0.151	-8.8	8.4	125.7	0.161	-9.0	7.3	123.5	0.156	-8.4	5.3
LP-NP1	138.6	0.104	-16.3	7.4	143.2	0.110	-10.7	8.7	165.5	0.199	-11.5	7.4
LP-NP2	108.8	0.034	-9.0	4.7	108.6	0.016	-7.4	9.7	107.6	0.040	*	
PM-NP1	145.1	0.072	-51.0	5.6	135.7	0.087	-53.4	8.4	139.1	0.108	-47.6	10.1
PM-NP2	226.9	0.194	3.3	5.7	237.5	0.235	9.4	5.7	215.2	0.126	11.4	5.6
IO-NP1	78.7	0.145	-37.3	12.9	84.4	0.258	-44.3	11.6	71.1	0.160	-43.4	10.7
IO-NP2	79.6	0.173	13.7	9.3	80.6	0.150	-17.0	11.1	81.1	0.140	-0.65	6.6
IO-NP3	57.5	0.217	-24.9	8.4	68.9	0.252	-35.0	9.6	58.8	0.228	-26.6	7.2

Physicochemical parameters were obtained for the various nanosystems at 1, 3 and 6 months after particle synthesis. Z-avg d: Z-averaged hydrodynamic diameter; PDI: Polydispersity ($PDI = SD^2/d^2$); ζ : Zeta-potential; SD ζ : Standard deviation of zeta-potential; NP: Nanoparticles; LD: Lipidots; LP: Liposomes; PM: Polymeric NPs; IO: Superparamagnetic iron oxide nanoparticles. * No steady values could be obtained due to foaming during measurement.

medium, yielding significant nanoparticle agglomeration at concentrations above 50 µg/ml, the effect of IO-NP3 on HUVECs could not be investigated.

Live cell imaging of nanoparticle-treated endothelial cells

The results of real-time cell analysis were validated using live-cell microscopy. In contrast to real-time cell analysis, which estimates cell numbers, attachment and viability based on the impedance measurements, live-cell microscopy allows the observation of cell morphology, and the measurement of confluence at the same time (see also *Supplementary Figures 21–24*). Using this method, no differences were observed in confluence (*Supplementary Figure 21*) or morphology between untreated cells and the cells treated with different concentrations of LP-NPs, confirming the real-time analysis data (*Figure 1A–C*). Upon treatment with LD-NP1, endothelial cell numbers were only slightly affected at 100 µg/ml, but the morphology of the cells changed, starting at around 24 h of incubation, leading to an elongated phenotype at 28 h post-application. At 200 µg/ml, stronger cell elongation, and reduced number of adherent cells were observed at 24 h (*Figure 2A*, *Supplementary Figure 22*). For LD-NP2, slight morphological changes became apparent at 100 µg/ml after 30 h of incubation, which were more strongly pronounced at 200 µg/ml, in parallel with reduced cell numbers after 48 h of incubation (*Figure 2B*). In LD-NP3-treated cells, reduced proliferation and strong elongation were detectable at 100 µg/ml after 72 h and at 200 µg/ml after 48 h incubation (*Figure 2C*). Cytotoxicity was apparent for LD-NP2 at 400 µg/ml after 24 h incubation, for LD-NP3 at 400 µg/ml after 48 h of incubation and for the smallest LD-NP1 at 200 µg/ml after 24 h of incubation.

Upon treatment with PM-NP1, strong reduction in cell number (reflected by decreased confluence, see *Supplementary Figure 23*) was visible at 50 µg/ml, whereas the presence of dead cells was observed at 100 µg/ml (*Figure 3A*). Treatment with 50 µg/ml PM-NP2 did not significantly affect cell numbers or morphology. Cytotoxic effects were observable from 100 µg/ml (*Figure 3B*). In the case of iron oxide nanoparticles, decreased cell numbers were observed upon treatment with 100 µg/ml IO-NP1, and a strong growth inhibition accompanied by cell shape change was induced at 200 µg/ml (*Figure 4A*, *Supplementary Figure 24*). In contrast, up to 400 µg/ml of IO-NP2 were well tolerated by endothelial cells and did not affect the morphology or confluence of cells as compared with untreated controls (*Figure 4B*).

Taken together, the results of real-time cell analysis and live-cell microscopy indicated that for the major-

ity of the tested nanosystems, there were no significant toxic effects on HUVECs up to the concentration of 100 µg/ml. Because of the biological/cytotoxic effects observed at and above 100 µg/ml for LD-NPs, PM-NPs and IO-NPs, subsequent studies under flow conditions were performed to investigate the effects of circulating nanosystems in physiological-like settings.

Nanoparticle effects on ECs in dynamic cell culture conditions

In physiological conditions, endothelial cells are constantly exposed to shear stress induced by the flow of blood and its viscosity, and their responses to stimuli are determined by the patterns of shear stress. Whereas laminar flow protects endothelial cells from harmful stimuli, nonuniform shear stress induces endothelial activation [31]. Furthermore, recent studies showed that the endothelial uptake on untargeted nanoparticles greatly depends on the presence and magnitude of shear stress [34–36]. Therefore, experiments under flow conditions are necessary to estimate the cell responses in physiological-like settings. *In vitro*, the toxic effects of circulating substances manifest themselves as endothelial cell shrinking and detachment. Consequently, the viability and confluence of the cells upon treatment with nanoparticles, as well as their morphology and cell–cell contacts can be assessed by immunofluorescent staining. We therefore perfused a HUVEC monolayer with medium containing 100 or 400 µg/ml of nanoparticles for 18 h and subsequently compared the nanoparticle effects on cells exposed to different types of shear stress (laminar vs non-uniform shear stress). In contrast to static conditions, all LD-NPs (*Figure 5*) and IO-NP1 (*Figure 6*) were well tolerated by the cells up to 400 µg/ml and did not affect endothelial cell viability and morphology, nor induced cell detachment due to shear stress exposure. In the case of PM-NP1, the circulating nanoparticles induced endothelial cell rounding at 100 µg/ml, and resulted in massive cell detachment both in the laminar and nonuniform shear stress region at 400 µg/ml (*Figure 6A*). The negative effects of circulating PM-NP2 on HUVECs remained observable at 100 µg/ml (*Figure 6B*), similar as seen in static conditions.

Reaction to liposomal nanoparticles in a pig model of CARPA

Evaluation of cardiovascular changes upon intravenous bolus injection of LP-NP1 at two different doses (0.1 and 0.5 mg phospholipid/kg) was done in domestic pigs. After the negative control injection (5 ml saline), the first test dose (0.1 mg phospholipid/kg) was diluted in 5 ml of sterile PBS and injected as a

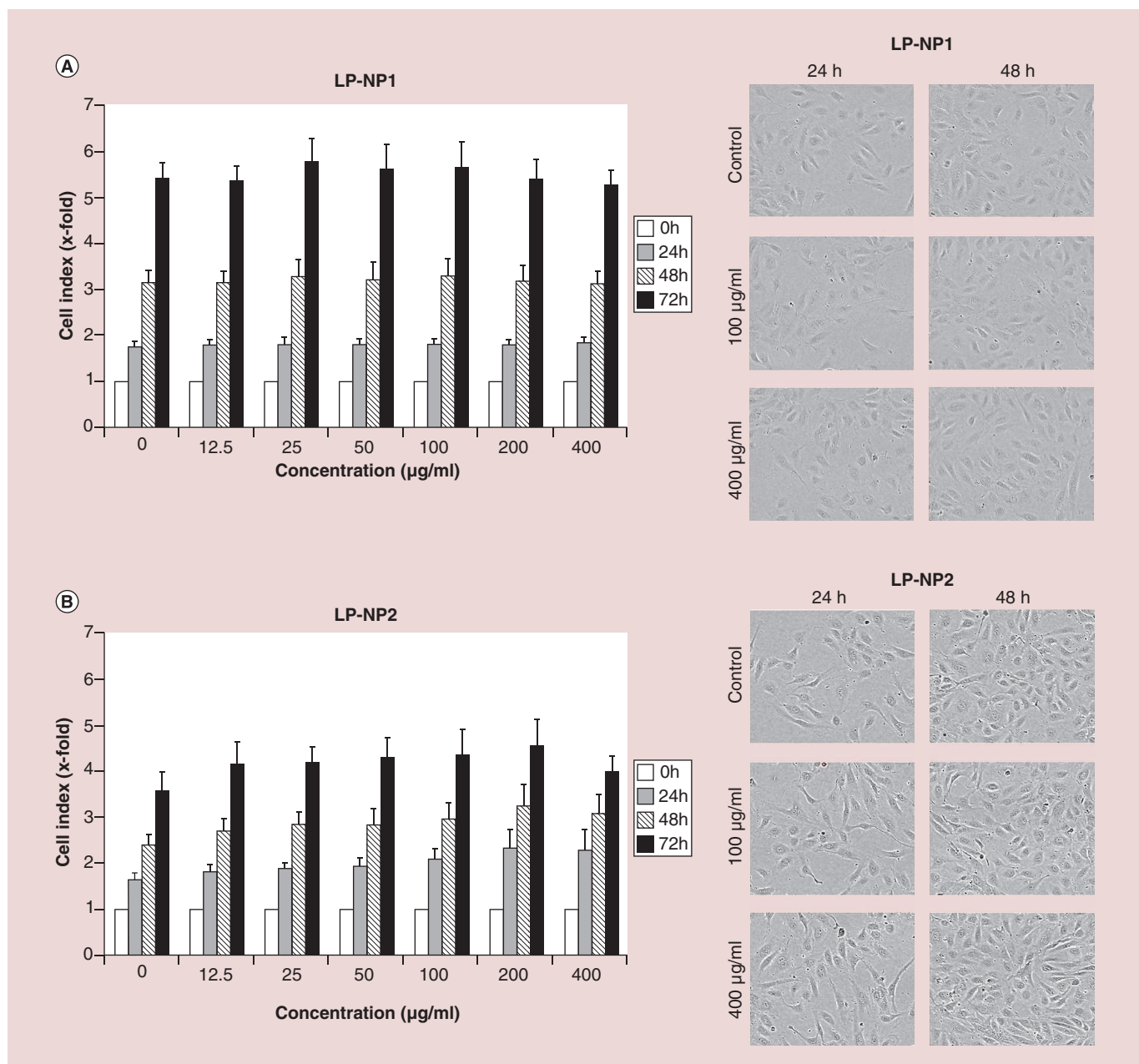


Figure 1. Biological effects of liposomes on endothelial cells grown in static conditions. HUVECs were treated with (A) LP-NP1 and (B) LP-NP2 for up to 72 h. Left panel: Real-time cell analysis. Cell index is displayed as x-fold of untreated controls. Right panel: Live-cell microscopy images at $\times 10$ objective magnification. Data are expressed as mean \pm SEM.

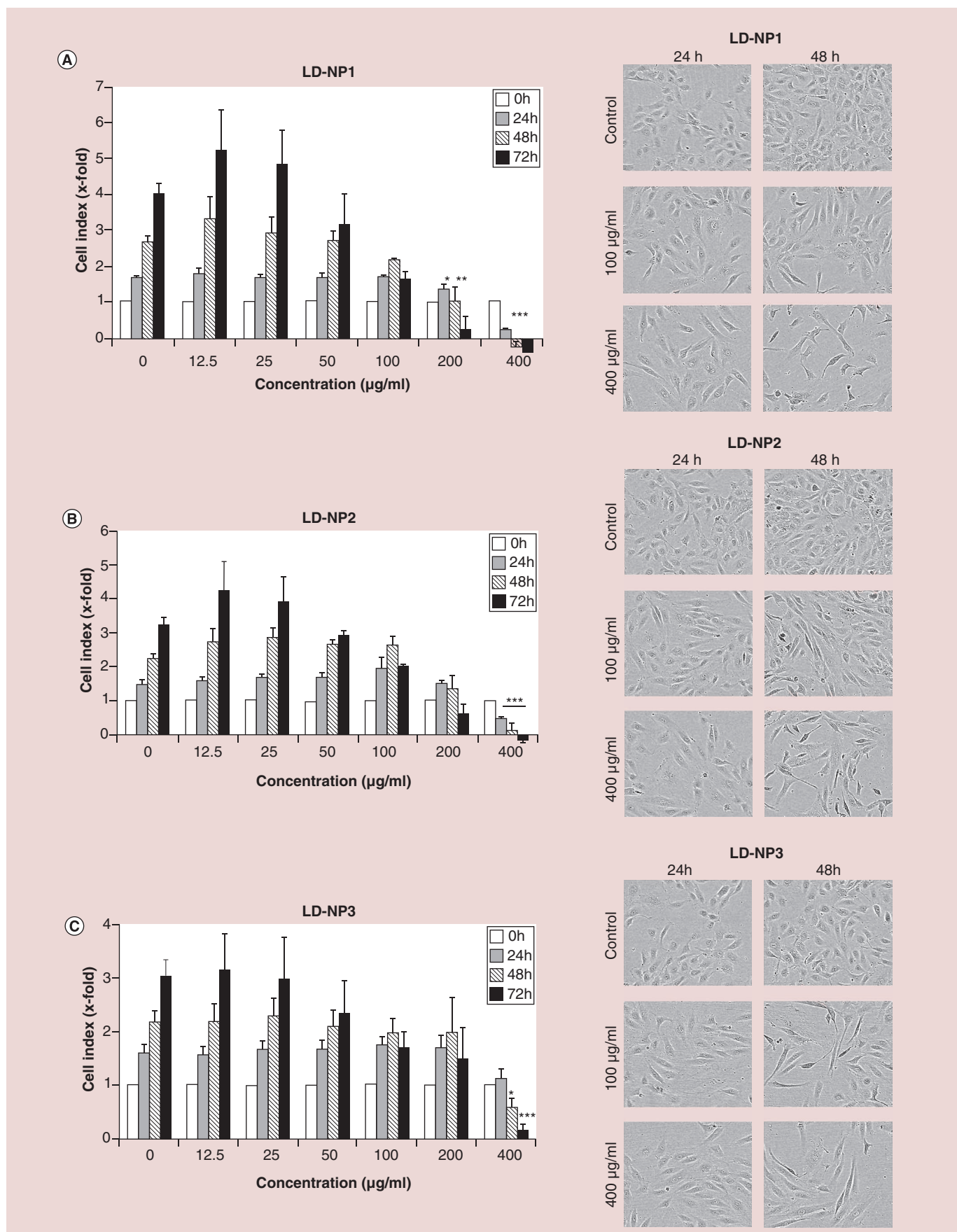
* $p < 0.05$, ** $p < 0.01$, *** $p < 0.001$ vs control (one-way ANOVA); $n = 4$.

bolus in the external jugular vein of anesthetized animal (see online supplement for the outline of the pig model). The saline injection caused no cardiovascular changes. Following the injection of LP-NP1 at 0.1 mg/kg dose, mild PAP increase was observed (from 16.6 to 20.9 mmHg), without any other changes (Figure 7A).

The steady increase of HR was not nanoparticle-related. To test for the presence of tachyphylaxis (desensitization), the same dose was repeatedly injected 30 min later. This repeated 0.1 mg/kg bolus injection caused no reaction, just like the subsequent injection of 5× higher dose (0.5 mg/kg LP-NP1), indicating that there

Figure 2. See facing page. Biological effects of lipid nanoparticles on endothelial cells grown in static conditions. HUVECs were treated with (A) LD-NP1, (B) LD-NP2 and (C) LD-NP3 for up to 72 h. Left panel: Real-time cell analysis. Cell index is displayed as x-fold of untreated controls. Right panel: Live-cell microscopy images at $\times 10$ objective magnification. Data are expressed as mean \pm SEM.

* $p < 0.05$, ** $p < 0.01$, *** $p < 0.001$ vs control (one-way ANOVA); $n = 3$.



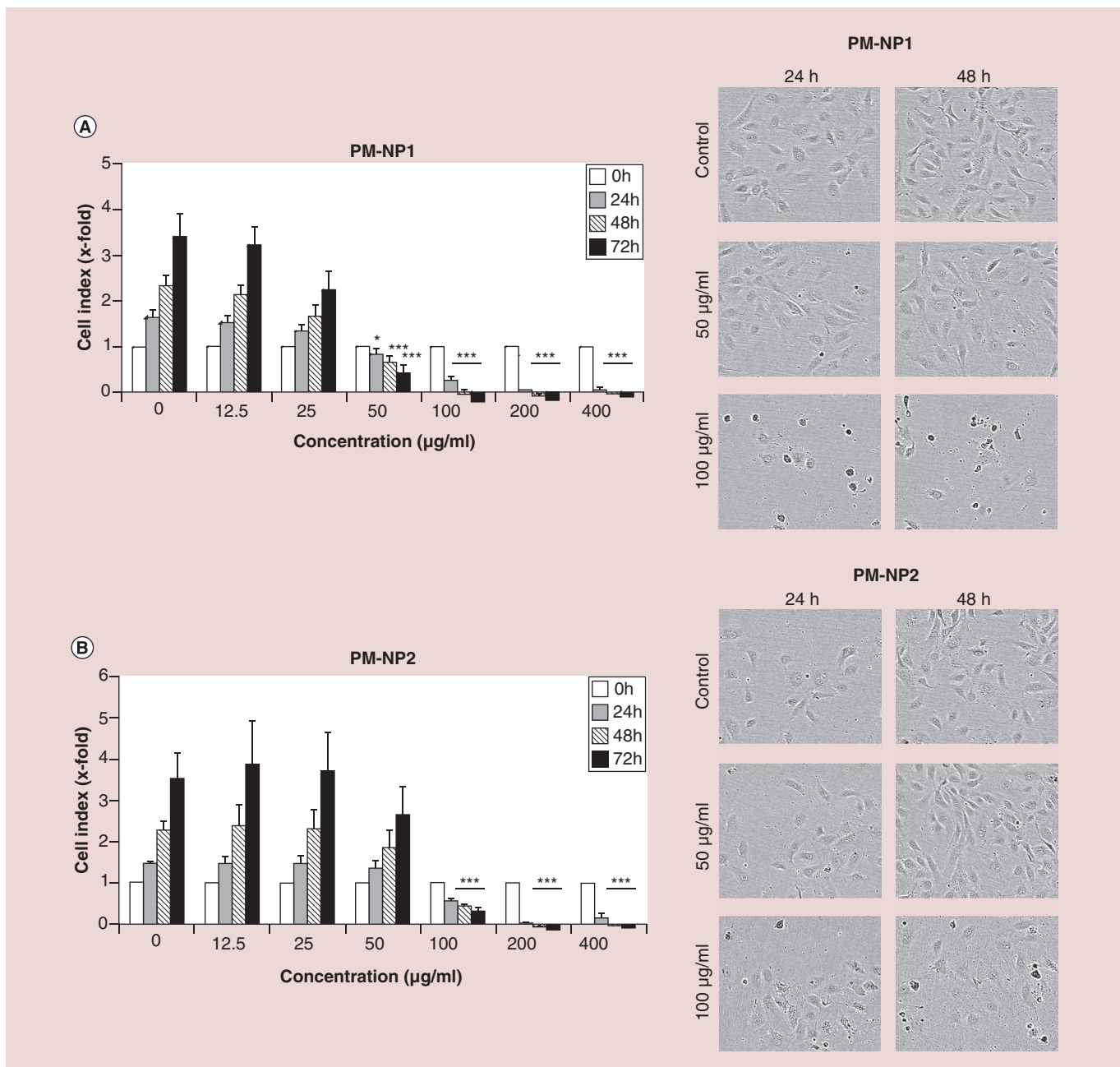


Figure 3. Biological effects of polymeric nanoparticles on endothelial cells grown in static conditions. HUVECs were treated with (A) PM-NP1 and (B) PM-NP2 for up to 72 h. Left panel: Real-time cell analysis. Cell index is displayed as x-fold of untreated controls. Right panel: Live-cell microscopy images at $\times 10$ objective magnification. Data are expressed as mean \pm SEM. * $p < 0.05$, ** $p < 0.01$, *** $p < 0.001$ vs control (one-way ANOVA); n = 5 for PM-NP1; n = 3 for PM-NP2.

was full tachyphylaxis. The positive control, zymosan at 0.1 mg/kg evoked severe PAP increase and a short lasting SAP decrease. The most characteristic PAP changes during the three LP-NP1 and zymosan injections, expressed as the % of the preinjection values, are shown in Figure 7B.

Pulmonary hypertension is closely associated with elevations of plasma thromboxane in response to zymo-

san-induced complement activation [37,38]. TXB2 measurement in blood samples collected before injections and during the reactions showed an approximate 40% TXB2 elevation in the later phase (10 min) following the first 0.1 mg/kg LP-NP1 injection (Figure 7C). Upon repeated injection, the same dose caused neither PAP nor TXB2 elevation (not shown), which confirmed the presence of tachyphylaxis.

Discussion

Detailed *in vitro* characterization facilitates the prediction of nanoparticle behavior in more complex physiological conditions, and is a prerequisite for human use [39]. We therefore investigated 10 nanoparticle systems, including lipid nanoparticles (Lipidots), liposomes, polymeric nanoparticles and iron oxide

nanoparticles with regard to their physicochemical features, stability and biological effects. Important parameters affecting nanoparticle properties include size, charge and PDI [40]. Size is one of the critical factors that affect the circulation time and bioavailability of nanoparticles. Surface charge, indicated by the ζ -potential, has a strong influence on nanoparticle sta-

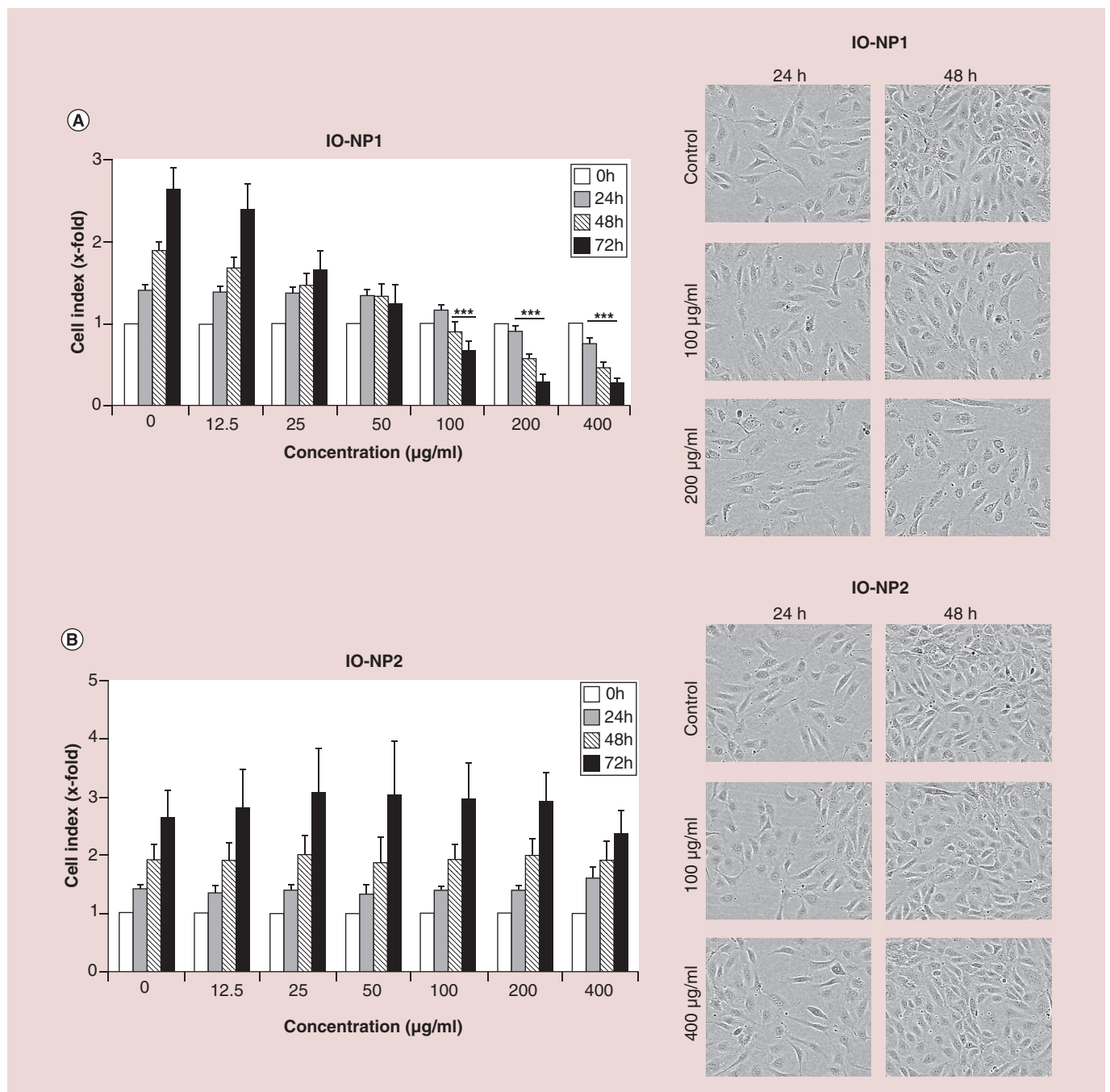


Figure 4. Biological effects of iron oxide nanoparticles on endothelial cells grown in static conditions. HUVECs were treated with (A) IO-NP1 and (B) IO-NP2 for up to 72 h. Left panel: Real-time cell analysis. Cell index is displayed as x-fold of untreated controls. Right panel: Live-cell microscopy images at $\times 10$ objective magnification. Data are expressed as mean \pm SEM.

* $p < 0.05$, ** $p < 0.01$, *** $p < 0.001$ vs control (one-way ANOVA); $n = 6$ for IO-NP1; $n = 3$ for IO-NP2.

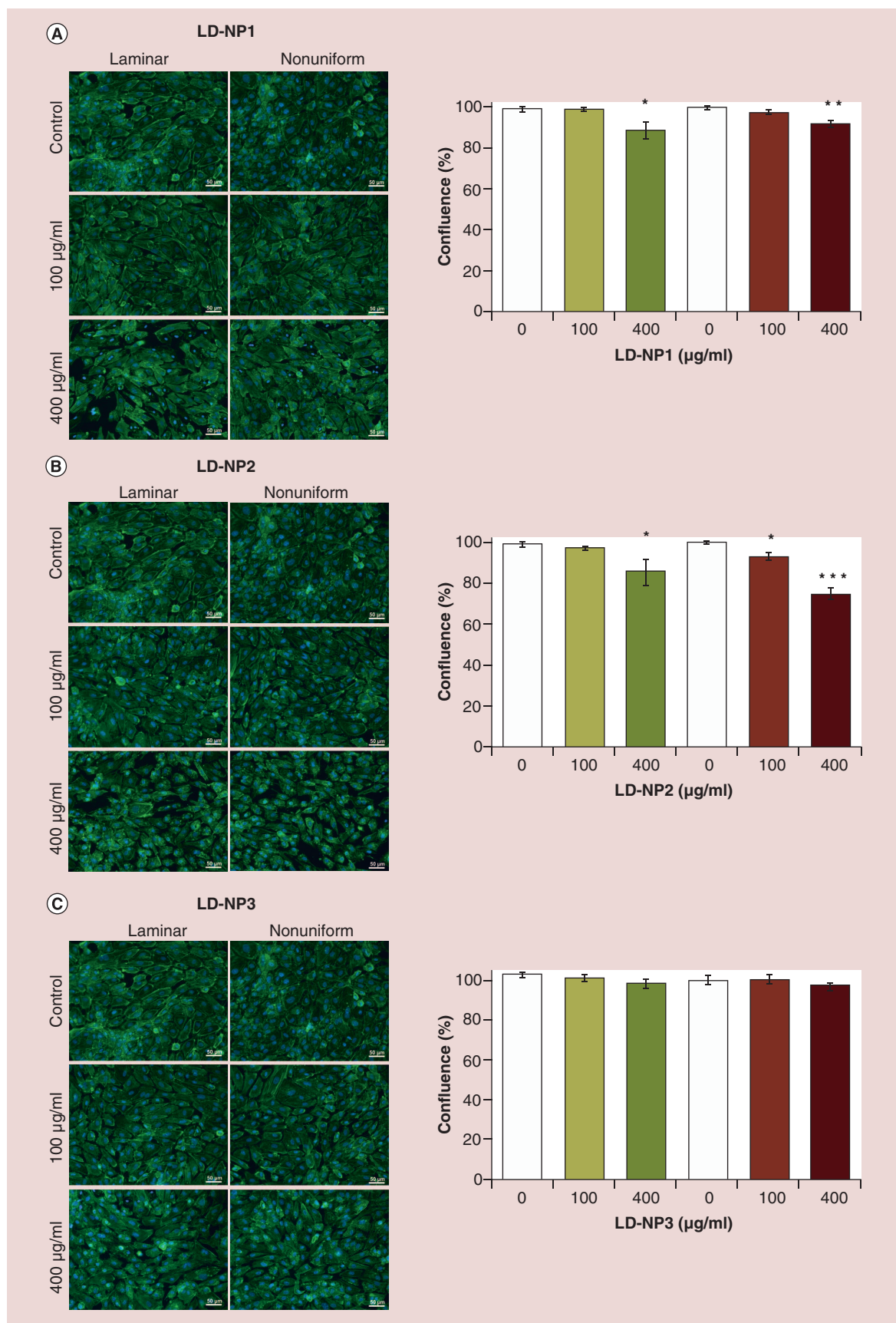


Figure 5. See facing page. Biological effects of circulating lipid nanoparticles on endothelial cells grown under flow conditions.

HUVECs were grown in bifurcating slides until confluence and perfused for 18 h with medium containing LD-NP1 (**A**), LD-NP2 (**B**), or LD-NP3 (**C**) at 100 and 400 µg/ml. Left panel: Fluorescent images of representative laminar and nonuniform regions at 20x objective magnification are shown. F-actin was visualized with Alexa 488-conjugated 488 (green) and nucleus with Hoechst 33342 (blue). Right panel: The graphs show a semiquantitative analysis of the confluence in laminar (green bars) and nonuniform region (red bars), determined on ×10 objective magnification images using ImageJ software. Nanoparticle-untreated controls (white columns) were set to 100%. Data are expressed as mean ± SEM.

*p < 0.05, **p < 0.01, ***p < 0.001 vs corresponding control.

bility in biological fluids. Moreover, positively charged nanoparticles enhance cellular uptake and can induce cytotoxicity [40,41]. Nanoparticles with a ζ -potential above (+/-) 30 mV are usually considered as colloidally stable, since the surface charge prevents their aggregation, but ζ -potential cannot be regarded as an absolute predictor of nanoparticle stability, especially in biological fluids as the ζ -potential is dependent on solvent composition. Steric repulsion, such as the hindrance provided by a PEGylated coating of the nanoparticle surface, can also provide high colloidal stability despite a nearly neutral ζ -potential [42].

Nanoparticle agglomeration is thus influenced by their physicochemical properties, but also by extrinsic factors, for example, temperature, as well as pH, osmotic strength and the presence of serum in the dispersion media. For clinical applications, nanoparticle agglomeration may be a key factor limiting their use in patients, as it affects bioavailability, and thus efficacy. Aggregated nanoparticles are no longer nanosized, and undergo a rapid recognition by the reticuloendothelial system followed by the clearance via liver or spleen. Moreover, the presence of agglomerates in circulation may cause serious undesirable side effects, such as clogging blood or lymphatic vessels [41]. In our study, although the results of physicochemical characterization of all investigated nanosystems in their respective dilution media indicated a good colloidal stability also upon prolonged storage, one type of nanoparticles (IO-NP3) was prone to agglomeration in serum-containing media, and was therefore excluded from biocompatibility testing. This underlines that only a careful nanoparticle analysis enables the design of a stable, clinically safe nanosystem.

The potential toxicity of nanoparticles is a major concern that must be excluded prior to their application in humans [39]. As nanoparticles may interfere with the available photometric methods for testing cell viability and/or metabolic activity [26,43–44], it is important to use in parallel at least two different methods for toxicity testing, to enable the verification of the results. In our studies, the biological effects of nanoparticles on endothelial cells were analysed *in vitro* using two real-time cell-monitoring methods. The obtained data underscore the importance of applying different methods to assess the toxicity of nanoparticles, as one single

method may increase the risk of bias. For example, the impedance measurements indicated a negative effect of LD-NP1 at 100 µg/ml on HUVECs (cell-index significantly lower in comparison to control), hinting to a reduced endothelial cell numbers, whereas the results of live-cell microscopy indicated a change in cell morphology, possibly resulting in weaker adherence of the cells, that is responsible for the measured impedance differences. Smaller lipid nanoparticles (LD-NP1) had more pronounced effect on cell elongation and adherence of the cells than larger lipid nanoparticles. This could be due both to the effect of higher surfactant concentration and the small size facilitating the uptake. Concerning the mechanisms of nanoparticle-induced toxicity, we did not observe acute cell death accompanied by the rupture of plasma membrane, which would be indicative of necrosis. Based on the morphological features, including blebbing and cell shrinkage occurring over longer incubation periods, most probably the apoptotic processes were responsible for cell death induced at the concentrations of, and above, 100 µg/ml of the tested nanoparticles. To gain a more detailed insight into the mechanisms of toxicity, future studies including annexin V and caspases staining would be necessary.

Compared with iron oxide nanoparticles, which have been extensively investigated for their effects on endothelial cells, very scarce information are available regarding the endothelial toxicity of solid lipid nanoparticles or polymeric nanoparticles composed of PIBCA. Lipid particles composed of cetyl palmitate and polysorbate 80 have been well tolerated by human cerebral microvascular endothelial cell line up to 1500 µg/ml [6], although the selected exposure time was very short (4 h). Polymeric nanoparticles coated with fucoidan and dextran have previously been tested by Lira *et al.* [45] on macrophage and fibroblast cell lines, showing the IC₅₀ of 9.6 µg/ml after 48 h incubation, but no data are available in the literature concerning their endothelial effects. Stealth liposomes of various compositions are generally well tolerated by endothelial cells [46,47], which is in agreements with our present observations. The largest pool of data related to endothelial toxicity is thus far available for iron oxide nanoparticles (reviewed in [48,49]). Based on the existing literature, the presence and the type of coating is a

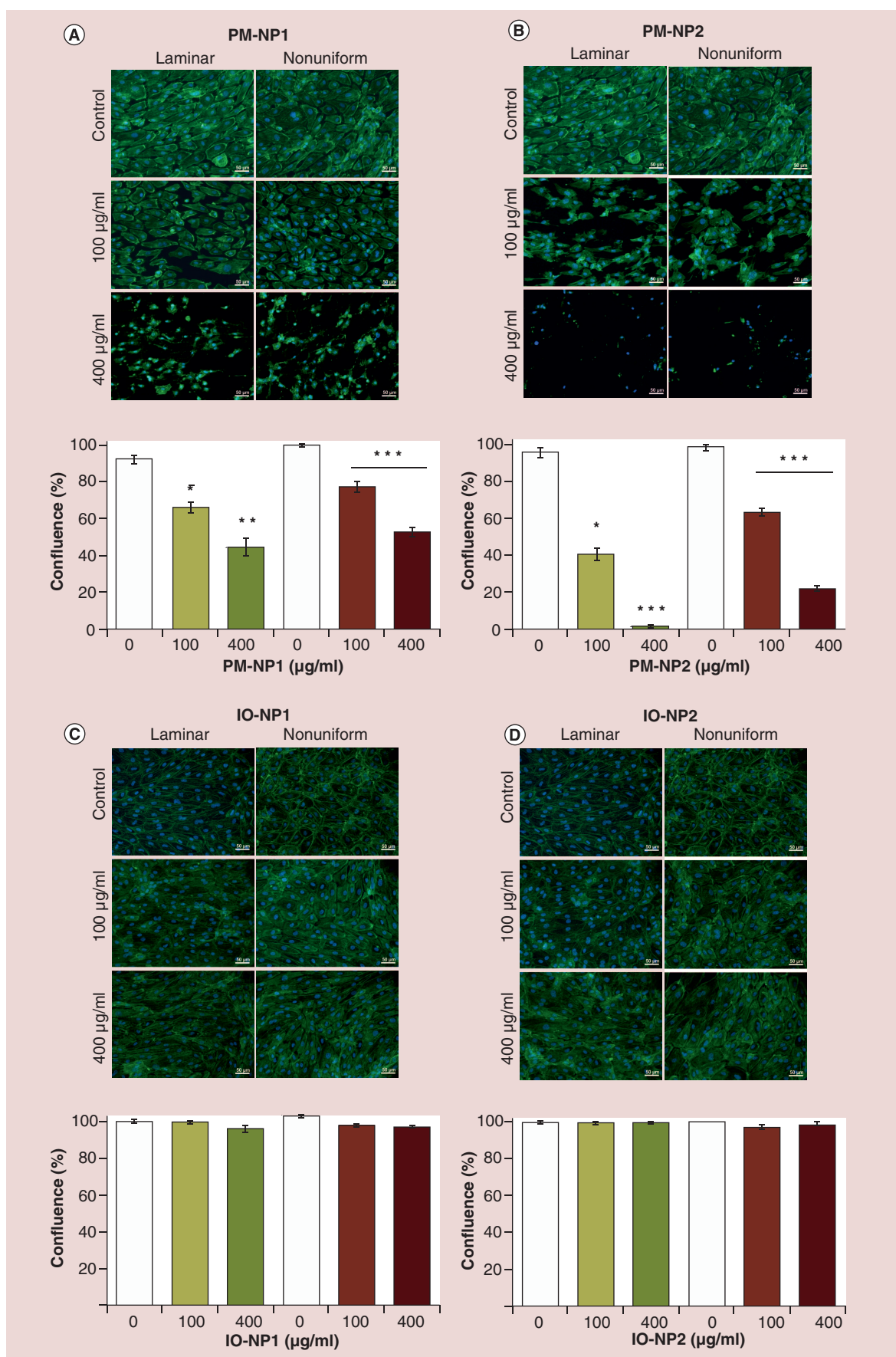


Figure 6. See facing page. Biological effects of circulating PM-NPs and IO-NPs on endothelial cells grown under flow conditions. HUVECs were grown in bifurcating slides until confluence and perfused for 18 h with medium containing PM-NP1 (A), PM-NP2 (B), IO-NP1 (C), or IO-NP2 (D) at 100 and 400 µg/ml. Upper panel: Fluorescent images of representative laminar and nonuniform regions at 20x objective magnification are shown. F-actin was visualized with Alexa 488-conjugated 488 (green) and nucleus with Hoechst 33342 (blue). Lower panel: The graphs show a semiquantitative analysis of the confluence in laminar (green bars) and nonuniform region (red bars), determined on ×10 objective magnification images using ImageJ software. Nanoparticle-untreated controls (white columns) were set to 100%. Data are expressed as mean ± SEM.
*p < 0.05, **p < 0.01, ***p < 0.001 vs corresponding control.

decisive factor for the biocompatibility of these particles [50,51], with good endothelial compatibility of dextran- and PEG-coated iron oxide nanoparticles up to 500 µg/ml over 24 h, as reported by Yu *et al.* [50]. The net effect of iron oxide nanoparticles was also related to the amount of cellular uptake, which differs strongly among different formulations [51,52]. These data are in accordance with our observations, indicating very good biocompatibility of dextran-coated IO-NP2 at all tested concentrations, and little endothelial toxicity of lauric acid/albumin-coated IO-NP1 below 100 µg/ml.

It must be noted that the nanoparticle toxicity was tested up to a very high concentration (400 µg/ml). Such high doses (above 100 µg/ml) are not expected to occur in the systemic circulation *in vivo*, but may be encountered locally at the region of administration and should therefore be considered in analyses. Caution is also necessary when interpreting the results obtained with iron oxide nanoparticles versus other nanoparticle types, as the concentrations of the former are normalized to the total iron content, which corresponds to a much higher total dry mass weight. We have applied long-term monitoring techniques instead of single-point measurements, to ensure the toxicity readouts over extended time. Although some nanoparticles, particularly those intended for imaging applications will be expected to circulate for relatively short time, thus far no detailed pharmacokinetics and clearance data are available. Hence, the long-term effects must be investigated both for intended imaging and therapeutic nanosystems to ensure their safety also over extended periods of time.

In endothelial cells, constantly exposed to the blood flow, shear stress-activated mechanisms are one of the major modulators of the physiologic functions, but little is known about the influence of hemodynamic factors on the endothelial responses to circulating nanoparticles. *In vitro* assays in dynamic conditions corresponding to the physiological environment of endothelial cells are thus of critical importance, as the susceptibility to atherosclerosis is governed by the specific patterns of shear stress. In general, our data indicate that in case of nanoparticles, the cell culture assays under static conditions may overestimate the potential toxicity. This results from the inherent prop-

erty of nanoparticles, namely their sedimentation, which occurs over time and leads to increased effective concentrations of nanoparticles in the nearest vicinity of cell monolayer. As shown in our studies, this effect is responsible for the majority of the cytostatic and cytotoxic effects observed below the concentration of 200 µg/ml. Only for one nanoparticle type (PM-NP2), the concentrations affecting cell growth and viability in static conditions (100 µg/ml) also induced cell detachment under flow conditions, other nanosystems being well-tolerated under flow up to 400 µg/ml. This may be related to the fact that except IO-NP2, PM-NP2 are the only positively charged nanoparticles, characterized furthermore by a relatively large Z-average size and a tendency to aggregate. Collectively, these features may negatively affect endothelial cell growth and viability at concentrations of 100 µg/ml and higher. Moreover, the recently reported data as well as our present studies indicate that physiologic flow is one of the important factors that must be considered when designing drug delivery nanosystems, as the internalization of untargeted nanoparticles by endothelial cells differs greatly between static and dynamic conditions [34–36].

Due to their size, nanoparticles may remain in the circulation for several hours or more, and their *in vivo* behavior and interactions with cellular and extracellular substrates may induce undesired effects, including hemolytic reactions, and/or complement activation. Apart from clinical efficacy and safety, diagnostic and therapeutic nanosystems should therefore offer the possibility of repeated intravenous/intra-arterial administration without inducing anaphylactoid (hypersensitivity) reactions. In this context, the clinical significance of CARPA-genic reaction upon the intravenous administration of nanosystems lies not only in the severe, occasionally lethal cardiopulmonary distress but also in a heightened risk that the nanomedicines become immunogenic, preventing their multiple applications [32]. In order to minimize such risks, the nanoparticles included in our analyses are currently entering the CARPA tests in the pig model [53]. The results of a pilot study involving the intravenous bolus administration of LP-NP1 confirmed the *in vitro* data, indicating a favorable safety profile and low immunogenicity of these nanoparticles. In the next stage of the

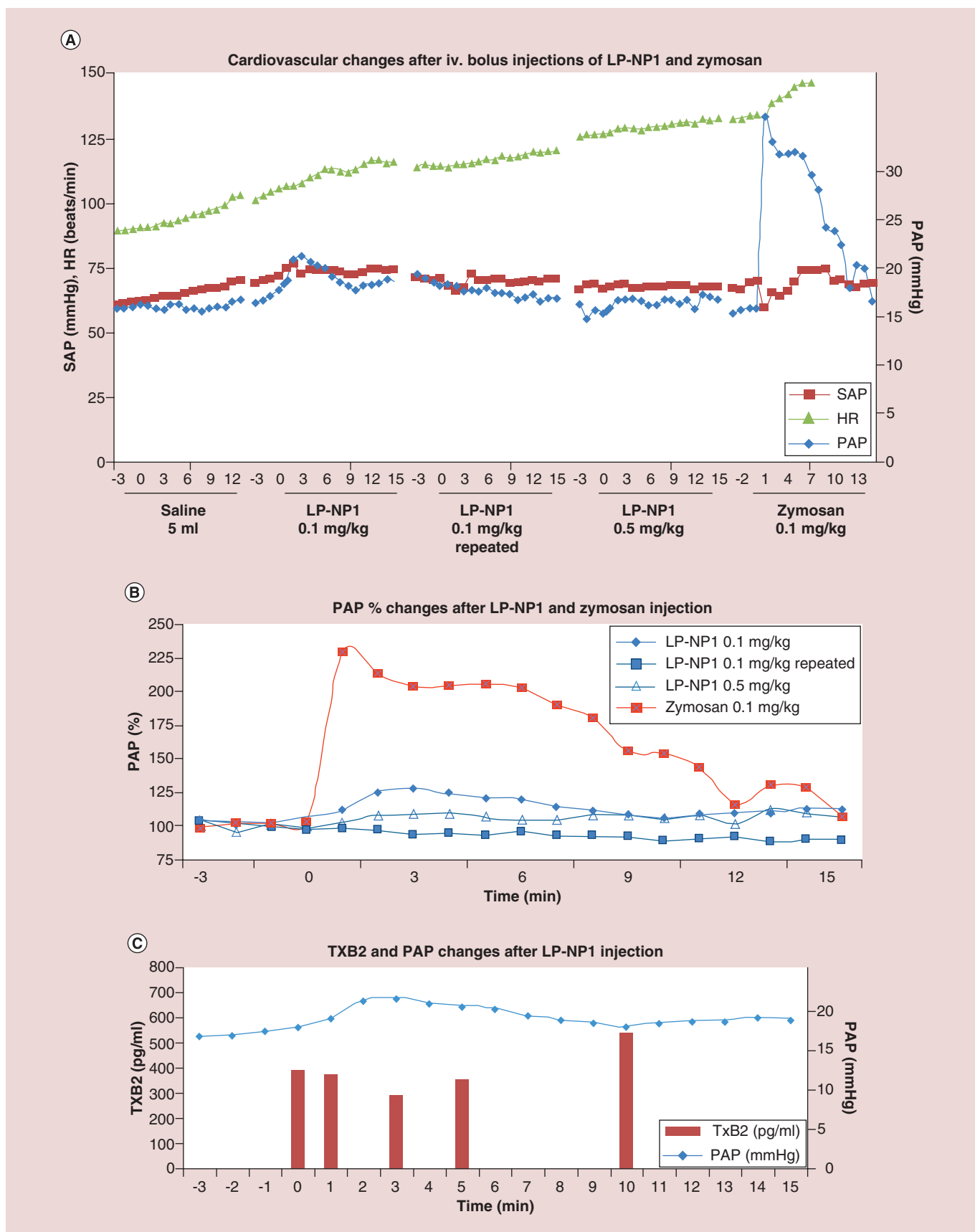


Figure 7. Cardiovascular reaction to LP-NP1 in a pig model of CARPA. LP-NP1 (0.1 mg/kg or 0.5 mg/kg) were administered intravenously as a bolus injection. Saline and zymosan (0.1 mg/kg) were used as negative and positive controls, respectively. **(A)** Changes in SAP, HR and PAP upon iv. injection of NP-LP1. **(B)** Percentage changes in PAP after LP-NP1 injection. **(C)** Plasma concentrations of TXB2 in relation to PAP changes following LP-NP1 injection are shown.

project, *in vivo* tests of other nanosystems selected for further development, as well as the determination of pharmacokinetics will be performed.

Conclusion

In this study we report the results of systematic physicochemical and biological analysis of diverse nanosystems intended for intravascular applications. The majority of nanosystems were well tolerated by endothelial cells, and did not induce major toxic effects *in vitro* up to the concentration of 100 µg/ml in static, and up to 400 µg/ml in dynamic cell culture conditions. These findings indicate an overall favorable biocompatibility profile of the tested nanosystems and their potential for cardiovascular imaging and drug targeting applications.

Future perspective

The potential clinical impact of nanotechnology in terms of detection and management of cardiovascular diseases is enormous. But in spite of the promising results obtained in the vast number of bench investigations that have been published in the recent years [4], no specific nanoparticle-based system has been approved for diagnosis or therapy of atherosclerosis in humans. The reasons for that are mainly the safety requirements related to nanoparticulate medicines, the lacking regulatory guidelines and insufficient standardization in the matters of particle characterization and nanotoxicity testing. To ensure clinical safety, the intravascular diagnostic and drug-delivery systems must first be subject to a close toxicologic scrutiny *in vitro*. Our studies represent an attempt to advance this field by utilizing a systematic approach to the comparative analysis of nanoparticle effects on primary human endothelial cells. Importantly, no interference resulting from the presence nanoparticles was observed in real-time cell analysis method, indicating the suitability of this technique for the future nanotoxicology studies. Furthermore, the comparison of nanoparticle effects on cell viability in static culture conditions and the effects of circulating nanoparticles on endothelial monolayer under physiologic-like shear stress allowed the conclusion that the majority of tested nanosystems have very good biocompatibility profiles. To understand how the physicochemical features of nanoparticles can affect the specific cellular responses, we are currently investigating the functional effects of the described nanosystems in endothelial and monocytic cells. These studies are expected to provide further important information concerning the mechanisms of nanoparticle-elicited cellular effects. Our pilot studies

in the pig model confirmed the safety of liposomal formulation (LP-NP1) *in vivo*, and constitute an important step toward further development and functionalization of these particles for the purpose of intravascular imaging and targeted drug delivery. In the future, substantial amount of *in vivo* studies will be necessary before the nanosystems with proven *in vitro* safety and efficacy can be translated into clinical trials. But despite multiple safety and regulatory constraints, the future progress in diagnosis and treatment of cardiovascular disorders is expected to benefit strongly from the development of novel nanotechnology-based strategies.

It must also be noted that cardiovascular disease, including various clinical manifestations of atherosclerosis and thrombosis, is but an example of the disease the therapy of which may profit from intravascular application of nanoparticulate drug carriers. In fact, the majority of the clinically-relevant nanocarriers, such as anticancer and anti-inflammatory nano-drugs, are expected to require intravascular administration. Although the main focus of our work is the diagnosis and therapy of atherosclerosis, the nanosystems investigated in this study constitute a versatile platform, adjustable also for the intravascular drug-delivery in other disease conditions.

Financial & competing interests disclosure

This work was supported by the EU ('NanoAthero' project FP7-NMP-2012-LARGE-6-309820), the DFG (CI 162/2-1), and received the financial support from ANR-13-LAB1-0005-01 'Fuc-oChem.' LETI/DTBS is part of the Arcane Labex program, funded by the French National Research Agency (ARCANE project n° ANR-12-LABX-003). The authors thank Prof. M. Beckmann (Department of Gynaecology, University Hospital Erlangen, Germany) for providing umbilical cords, N Jaziri for help with HUVEC isolation and P Dörfler for help with flow experiments. The authors have no other relevant affiliations or financial involvement with any organization or entity with a financial interest in or financial conflict with the subject matter or materials discussed in the manuscript apart from those disclosed.

No writing assistance was utilized in the production of this manuscript.

Ethical conduct of research

The authors state that they have obtained appropriate institutional review board approval or have followed the principles outlined in the Declaration of Helsinki for all human or animal experimental investigations. In addition, for investigations involving human subjects, informed consent has been obtained from the participants involved.

Executive summary

Background

- Detailed physicochemical and biological characterization of nanosystems *in vitro* is necessary to ensure their safety in more complex physiological conditions.

Methods

- We investigated 10 diverse nanosystems, comprising liposomes, lipid nanoparticles, polymeric and iron oxide nanoparticles to assess their long-term stability and biological effects on endothelial cells (ECs).
- EC viability in static conditions was monitored using real-time cell analysis and live-cell microscopy.
- A flow model of arterial bifurcations was used to assess the effect of circulating nanoparticles on EC monolayer under physiologic-like shear stress.

Results

- The majority of tested nanosystems were well tolerated by ECs up to the concentration of 100 µg/ml in static, and up to 400 µg/ml in dynamic conditions.
- In static conditions, nanoparticle sedimentation was responsible for the majority of the cytostatic and cytotoxic effects observed below nanoparticle concentration of 200 µg/ml.
- The results of a pilot study in a pig model showed that intravenous administration of liposomal nanoparticles did not evoke the hypersensitivity reaction, indicating a low immunogenicity of these nanoparticles.

Conclusion

- The majority of tested nanosystems had an overall favorable biocompatibility profile, constituting good candidates for cardiovascular imaging and drug targeting applications.

References

- Papers of special note have been highlighted as:
- of interest
 - of considerable interest
- 1 Lozano R, Naghavi M, Foreman K *et al.* Global and regional mortality from 235 causes of death for 20 age groups in 1990 and 2010: a systematic analysis for the Global Burden of Disease Study 2010. *Lancet* 380(9859), 2095–2128 (2012).
 - 2 Libby P, Theroux P. Pathophysiology of coronary artery disease. *Circulation* 111(25), 3481–3488 (2005).
 - The in-depth review of the pathophysiology of atherosclerosis as an inflammatory disease.
 - 3 Mangge H, Almer G, Stelzer I, Reininghaus E, Prassl R. Laboratory medicine for molecular imaging of atherosclerosis. *Clin. Chim. Acta* 437 19–24 (2014).
 - 4 Cicha I, Garlich CD, Alexiou C. Cardiovascular therapy through nanotechnology – how far are we still from bedside? *Eur. J. Nanomed.* 6(2), 63–87 (2014).
 - This review highlights the recent advances in the preclinical and clinical applications of nanoparticulate agents for cardiovascular diagnostics and therapy.
 - 5 Cicha I, Lyer S, Alexiou C, Garlich CD. Nanomedicine in diagnostics and therapy of cardiovascular diseases: beyond atherosclerotic plaque imaging. *Nanotechnol. Rev.* 2(4), 449–472 (2013).
 - 6 Neves AR, Queiroz JF, Weksler B, Romero IA, Couraud PO, Reis S. Solid lipid nanoparticles as a vehicle for brain-targeted drug delivery: two new strategies of functionalization with apolipoprotein E. *Nanotechnology* 26(49), 495103 (2015).
 - 7 Kennedy IM, Wilson D, Barakat AI, Committee HEIHR. Uptake and inflammatory effects of nanoparticles in a human vascular endothelial cell line. *Research Rep.* (136), 3–32 (2009).
 - 8 Battaglia L, Gallarate M, Peira E *et al.* Bevacizumab loaded solid lipid nanoparticles prepared by the coacervation technique: preliminary *in vitro* studies. *Nanotechnology* 26(25), 255102 (2015).
 - 9 Dan M, Scott DF, Hardy PA *et al.* Block copolymer cross-linked nanoassemblies improve particle stability and biocompatibility of superparamagnetic iron oxide nanoparticles. *Pharmaceut. Res.* 30(2), 552–561 (2013).
 - 10 Gravier J, Navarro FP, Delmas T *et al.* Lipidots: competitive organic alternative to quantum dots for *in vivo* fluorescence imaging. *J. Biomed. Opt.* 16(9), 096013 (2011).
 - 11 Puri A, Loomis K, Smith B *et al.* Lipid-based nanoparticles as pharmaceutical drug carriers: from concepts to clinic. *Crit. Rev. Therapeut. Drug Carrier Syst.* 26(6), 523–580 (2009).
 - 12 Almer G, Frascione D, Pali-Scholl I *et al.* Interleukin-10: an anti-inflammatory marker to target atherosclerotic lesions via PEGylated liposomes. *Mol. Pharmaceut.* 10(1), 175–186 (2013).
 - 13 Huwyler J, Drewe J, Krahenbuhl S. Tumor targeting using liposomal antineoplastic drugs. *Int. J. Nanomedicine* 3(1), 21–29 (2008).
 - 14 Muller RH, Shegokar R, Keck CM. 20 years of lipid nanoparticles (SLN and NLC): present state of development and industrial applications. *Curr. drug Discov. Technol.* 8(3), 207–227 (2011).
 - 15 Bachelet L, Bertholon I, Lavigne D *et al.* Affinity of low molecular weight fucoidan for P-selectin triggers its binding to activated human platelets. *Biochim. Biophys. acta* 1790(2), 141–146 (2009).
 - 16 Rouzet F, Bachelet-Violette L, Alsac JM *et al.* Radiolabeled fucoidan as a p-selectin targeting agent for *in vivo* imaging of platelet-rich thrombus and endothelial activation. *J. Nucl. Med.* 52(9), 1433–1440 (2011).

- 17 Trivedi RA, Mallavarachi C, Jm UK-I *et al.* Identifying inflamed carotid plaques using *in vivo* USPIO-enhanced MR imaging to label plaque macrophages. *Arterioscl. Thromb. Vasc. Biol.* 26(7), 1601–1606 (2006).
- 18 Howarth SP, Tang TY, Trivedi R *et al.* Utility of USPIO-enhanced MR imaging to identify inflammation and the fibrous cap: a comparison of symptomatic and asymptomatic individuals. *Eur. J. Radiol.* 70(3), 555–560 (2009).
- 19 Tang TY, Muller KH, Graves MJ *et al.* Iron oxide particles for atheroma imaging. *Arterioscl. Thromb. Vasc. Biol.* 29(7), 1001–1008 (2009).
- 20 Sadat U, Howarth SP, Usman A, Tang TY, Graves MJ, Gillard JH. Sequential imaging of asymptomatic carotid atherosclerosis using ultrasmall superparamagnetic iron oxide-enhanced magnetic resonance imaging: a feasibility study. *J. Stroke Cerebrovasc. Dis.* 22(8), e271–276 (2013).
- 21 Janko C, Durr S, Munoz LE *et al.* Magnetic drug targeting reduces the chemotherapeutic burden on circulating leukocytes. *Int. J. Mol. Sci.* 14(4), 7341–7355 (2013).
- 22 Lyer S, Tietze R, Jurgons R *et al.* Visualisation of tumour regression after local chemotherapy with magnetic nanoparticles – a pilot study. *Anticancer Res.* 30(5), 1553–1557 (2010).
- 23 Tietze R, Lyer S, Durr S *et al.* Efficient drug-delivery using magnetic nanoparticles – biodistribution and therapeutic effects in tumour bearing rabbits. *Nanomedicine* 9(7), 961–971 (2013).
- This article presents the results of the world's largest animal study to date, investigating the efficacy of magnetic drug targeting using mitoxantrone-loaded SPIONs in tumor-bearing rabbits.
- 24 Kumar A, Dhawan A. Genotoxic and carcinogenic potential of engineered nanoparticles: an update. *Arch. Toxicol.* 87(11), 1883–1900 (2013).
- 25 Zolnik BS, Gonzalez-Fernandez A, Sadrieh N, Dobrovolskaia MA. Nanoparticles and the immune system. *Endocrinology* 151(2), 458–465 (2010).
- 26 Ong KJ, MacCormack TJ, Clark RJ *et al.* Widespread nanoparticle-assay interference: implications for nanotoxicity testing. *PLoS ONE* 9(3), e90650 (2014).
- Important contribution to the issue of nanoparticle interference with toxicity assays. This article also provides guidance on controlling for such interference to improve the accuracy of nanotoxicity assessments.
- 27 Almer G, Wernig K, Saba-Lepke M *et al.* Adiponectin-coated nanoparticles for enhanced imaging of atherosclerotic plaques. *Int. J. Nanomedicine* 6, 1279–1290 (2011).
- 28 Zaloga J, Janko C, Nowak J *et al.* Development of a lauric acid/albumin hybrid iron oxide nanoparticle system with improved biocompatibility. *Int. J. Nanomedicine* 9, 4847–4866 (2014).
- 29 Unterweger H, Tietze R, Janko C *et al.* Development and characterization of magnetic iron oxide nanoparticles with a cisplatin-bearing polymer coating for targeted drug delivery. *Int. J. Nanomedicine* 9, 3659–3676 (2014).
- 30 Matuszak J, Zaloga J, Friedrich RP *et al.* Endothelial biocompatibility and accumulation of SPION under flow conditions. *J. Magn. Magn. Mater.* 380, 20–26 (2015).
- 31 Cicha I, Beronov K, Ramirez EL *et al.* Shear stress preconditioning modulates endothelial susceptibility to circulating TNF-alpha and monocytic cell recruitment in a simplified model of arterial bifurcations. *Atherosclerosis* 207(1), 93–102 (2009).
- 32 Szebeni J. Complement activation-related pseudoallergy: a stress reaction in blood triggered by nanomedicines and biologicals. *Mol. Immunol.* 61(2), 163–173 (2014).
- This review provides basic information on complement activation-related pseudoallergy (CARPA), including a short history, incidence, classification of CARPA-genic drugs and symptoms, and the mechanisms of C activation via different pathways.
- 33 Durr S, Lyer S, Mann J *et al.* Real-time cell analysis of human cancer cell lines after chemotherapy with functionalized magnetic nanoparticles. *Anticancer Res.* 32(5), 1983–1989 (2012).
- 34 Fede C, Fortunati I, Weber V *et al.* Evaluation of gold nanoparticles toxicity towards human endothelial cells under static and flow conditions. *Microvasc. Res.* 97, 147–155 (2015).
- 35 Rinkenauer AC, Press AT, Raasch M *et al.* Comparison of the uptake of methacrylate-based nanoparticles in static and dynamic *in vitro* systems as well as *in vivo*. *J. Control. Release* 216, 158–168 (2015).
- 36 Klingberg H, Loft S, Oddershede LB, Moller P. The influence of flow, shear stress and adhesion molecule targeting on gold nanoparticle uptake in human endothelial cells. *Nanoscale* 7(26), 11409–11419 (2015).
- 37 Cooper JD, McDonald JWD, Ali M, Menkes E, Masterson J, Clement P. Prostaglandin production associated with the pulmonary vascular-response to complement activation. *Surgery* 88(2), 215–221 (1980).
- 38 Szebeni J, Fontana JL, Wassef NM *et al.* Hemodynamic changes induced by liposomes and liposome-encapsulated hemoglobin in pigs - A model for pseudoallergic cardiopulmonary reactions to liposomes: role of complement and inhibition by soluble CR1 and anti-C5a antibody. *Circulation* 99(17), 2302–2309 (1999).
- 39 Desai N. Challenges in development of nanoparticle-based therapeutics. *AAPS J.* 14(2), 282–295 (2012).
- 40 Aillon KL, Xie Y, El-Gendy N, Berkland CJ, Forrest ML. Effects of nanomaterial physicochemical properties on *in vivo* toxicity. *Adv. Drug Deliv. Rev.* 61(6), 457–466 (2009).
- 41 Oberdorster G. Safety assessment for nanotechnology and nanomedicine: concepts of nanotoxicology. *J. Intern. Med.* 267(1), 89–105 (2010).
- 42 Hirsjärvi S, Dufort S, Gravier J *et al.* Influence of size, surface coating and fine chemical composition on the *in vitro* reactivity and *in vivo* biodistribution of lipid nanocapsules versus lipid nanoemulsions in cancer models. *Nanomedicine* 9(3), 375–387 (2013).
- 43 Keene AM, Allaway RJ, Sadrieh N, Tyner KM. Gold nanoparticle trafficking of typically excluded compounds

- across the cell membrane in JB6 Cl 41–5a cells causes assay interference. *Nanotoxicology* 5(4), 469–478 (2011).
- 44 Monteiro-Riviere NA, Inman AO, Zhang LW. Limitations and relative utility of screening assays to assess engineered nanoparticle toxicity in a human cell line. *Toxicol. Appl. Pharmacol.* 234(2), 222–235 (2009).
- 45 Lira MCB, Santos-Magalhaes NS, Nicolas V et al. Cytotoxicity and cellular uptake of newly synthesized fucoidan-coated nanoparticles. *Eur. J. Pharmaceut. Biopharmaceut.* 79(1), 162–170 (2011).
- 46 Coimbra M, Banciu M, Fens MH et al. Liposomal pravastatin inhibits tumor growth by targeting cancer-related inflammation. *J. Control. Release* 148(3), 303–310 (2010).
- 47 Orlando A, Re F, Sesana S et al. Effect of nanoparticles binding beta-amyloid peptide on nitric oxide production by cultured endothelial cells and macrophages. *Int. J. Nanomedicine* 8, 1335–1347 (2013).
- 48 Soenen SJ, De Cuyper M. Assessing iron oxide nanoparticle toxicity *in vitro*: current status and future prospects. *Nanomedicine (Lond.)* 5(8), 1261–1275 (2010).
- This work presents an overview of different types of iron oxide nanoparticles developed for biomedical research with particular focus on their internalization and cytotoxicity.
- 49 Mahmoudi M, Hofmann H, Rothen-Rutishauser B, Petri-Fink A. Assessing the *in vitro* and *in vivo* toxicity of superparamagnetic iron oxide nanoparticles. *Chemical Rev.* 112(4), 2323–2338 (2012).
- 50 Yu M, Huang S, Yu KJ, Clyne AM. Dextran and polymer polyethylene glycol (PEG) coating reduce both 5 and 30 nm iron oxide nanoparticle cytotoxicity in 2D and 3D cell culture. *Int. J. Mol. Sci.* 13(5), 5554–5570 (2012).
- 51 Buyukhatipoglu K, Clyne AM. Superparamagnetic iron oxide nanoparticles change endothelial cell morphology and mechanics via reactive oxygen species formation. *J. Biomed. Mater. Res. A* 96A(1), 186–195 (2011).
- 52 Li M, Kim HS, Tian L, Yu MK, Jon S, Moon WK. Comparison of two ultrasmall superparamagnetic iron oxides on cytotoxicity and MR imaging of tumors. *Theranostics* 2(1), 76–85 (2012).
- 53 Szebeni J, Bedocs P, Csukas D, Rosivall L, Bunger R, Urbanics R. A porcine model of complement-mediated infusion reactions to drug carrier nanosystems and other medicines. *Adv. Drug Deliv. Rev.* 64(15), 1706–1716 (2012).

Résumé

Les pathologies de la paroi artérielle, et notamment l'athérosclérose, sont responsables de plus de 25% des décès dans le monde. Ces pathologies sont à l'origine de la thrombose, caractérisée par l'occlusion d'une artère par un caillot, ou thrombus. Ce travail de thèse explore l'utilisation de nanoparticules et microparticules polymères pour améliorer le diagnostic et le traitement de la thrombose. Ce type de particules permet en effet d'associer des agents de contraste et des actifs thérapeutiques à des agents de ciblage pour favoriser leur accumulation spécifique au niveau du thrombus. Les particules sont formulées à partir de polysaccharides et/ou de poly(cyanoacrylate d'isobutyle). Elles sont fonctionnalisées en surface avec du fucoïdane, un polysaccharide naturel extrait d'algues brunes. Le fucoïdane présente une affinité très forte pour la P-sélectine, molécule exprimée par les plaquettes activées qui constituent en partie le thrombus. Au cours de ce projet, un test *in vitro* d'adhésion en flux a été mis au point pour valider l'interaction des systèmes développés avec leur cible moléculaire, la P-sélectine, et leur cible cellulaire, les plaquettes activées. L'agent thérapeutique standard utilisé pour induire la dégradation du thrombus est l'activateur tissulaire du plasminogène. Celui-ci a été chargé sur des nanoparticules copolymères fonctionnalisées avec du fucoïdane. L'efficacité de ces systèmes a ensuite été validée dans un modèle murin de thrombose. Enfin, des nanoparticules composées exclusivement de polysaccharides et entièrement hydrophiles, dites "nanogels", ont été synthétisées par un procédé innovant. Les résultats obtenus dans ce travail de thèse confirment le fort potentiel des approches ciblées pour le diagnostic et le traitement de la thrombose. Ils contribuent d'une manière plus générale au développement de la médecine personnalisée dans le domaine cardiovasculaire.

Mots clés : nanomédecine, thrombose, P-sélectine, polymère, polysaccharide, fucoïdane

Abstract

Arterial wall diseases, including atherosclerosis, are responsible for more than 25% of all deaths worldwide. These pathologies are at the origin of thrombotic events, characterized by the occlusion of an artery by a clot, called a thrombus. This thesis explores the use of polymer nanoparticles and microparticles for thrombosis imaging and therapy. This type of particles combines contrast agents and therapeutic agents with targeting moieties to promote their specific accumulation at the thrombus. The particles are composed of polysaccharides and/or poly(isobutyl cyanoacrylate). They are functionalized with fucoidan, a polysaccharide extracted from brown algae. Fucoidan shows a very strong affinity for P-selectin, a molecule expressed by activated platelets which form part of the thrombus. In this study, an *in vitro* flow adhesion assay was set up to validate the interaction of developed systems with their molecular target, the P-selectin, and with their cellular target, the activated platelets. Tissue plasminogen activator is the standard therapeutic agent used to induce thrombus degradation. This agent was loaded onto copolymer nanoparticles functionalized with fucoidan. Their efficiency was then validated in a murine model of thrombosis. Finally, nanoparticles exclusively composed of polysaccharides and entirely hydrophilic, called "nanogels", were synthesized by an innovative process. The results of this work confirm the high potential of using targeted approach for thrombosis diagnosis and treatment and pave the way towards the development of personalized cardiovascular medicine.

Keywords: nanomedicine, thrombosis, P-selectin, polymer, polysaccharide, fucoidan

